Computational Intelligence & Neuroscience

Brain-Computer Interfaces: Towards Practical Implementations and Potential Applications

Guest Editors: Fabio Babiloni, Andrzej Cichocki, and Shangkai Gao

Brain-Computer Interfaces: Towards Practical Implementations and Potential Applications

Computational Intelligence and Neuroscience

Brain-Computer Interfaces: Towards Practical Implementations and Potential Applications

Guest Editors: Fabio Babiloni,
Andrzej Cichocki, and Shangkai Gao

Contents

Hindawi Publishing Corporation
Computational Intelligence and Neuroscience
Volume 2007, Article ID 62637, 2 pages
doi:10.1155/2007/62637

Editorial

Brain-Computer Interfaces: Towards Practical Implementations and Potential Applications

F. Babiloni,[1] A. Cichocki,[2] and S. Gao[3]

[1] *Dipartimento di Fisiologia Umana e Farmacologia "Vittorio Erspamer", Università delgi Studi di Roma "La Sapienza", Piazzale Aldo Moro 5, 00185 Roma, Italy*
[2] *Laboratory for Advanced Brain Signal Processing (ABSP), RIKEN Brain Science Institute, 2-1 Hirosawa, Wako-shi, Saitama 351-0198, Japan*
[3] *Department of Biomedical Engineering, Tsinghua University, Beijing 100084, China*

Correspondence should be addressed to A. Cichocki, a.cichocki@riken.jp

Received 3 December 2007; Accepted 3 December 2007

Brain-computer interfaces (BCIs) are systems that use brain signals (electric, magnetic, metabolic) to control external devices such as computers, switches, wheelchairs, or neuroprosthesis. While BCI research hopes to create new communication channels for disabled or elderly persons using their brain signals, recently efforts have been focused on developing potential applications in rehabilitation, multimedia communication, and relaxation (such as immersive virtual reality control). The various BCI systems use different methods to extract the user's intentions from her/his brain activity. Many researchers world wide are actually investigating and testing several promising BCI paradigms, including (i) measuring the brain activities over the primary motor cortex that results from imaginary limbs and tongue movements, (ii) detecting the presence of EEG periodic waveforms, called steady-state visual evoked potentials (SSVEPs), elicited by flashing light sources (e.g., LEDs or phase-reversing checkerboards), and (iii) identifying event-related potentials (ERPs) in EEG that follow an event noticed by the user (or his/her intention), for example, P300 peak waveforms after a target/rare (oddball) stimulus among a sequence the user pay attention to. One promising extension of BCI is to incorporate various neurofeedbacks to train subjects to modulate EEG brain patterns and parameters such as event-related potentials (ERPs), event-related desynchronization (ERD), sensorimotor rhythm (SMR), or slow cortical potentials (SCPs) to meet a specific criterion or to learn self-regulation skills. The subject then changes their brain patterns in response to some feedbacks. Such integration of neurofeedback in BCI is an emerging technology for rehabilitation, but we believe it is also a new paradigm in neuroscience that might reveal previously unknown brain activities associated with behavior or self-regulated mental states. The possibility of automatic context-awareness as a new interface goes far beyond the standard BCI with simple feedback control. BCI relies increasingly on findings from other disciplines, especially, neuroscience, information technology, biomedical engineering, machine learning, and clinical rehabilitation.

This special issue covers the following topics:

(i) noninvasive BCI systems (EEG, MEG, fMRI) for decoding and classification neural activity in humans;
(ii) comparisons of linear versus nonlinear signal processing for decoding and classifying neural activity;
(iii) multimodal neural imaging methods for BCI;
(iv) systems for monitoring brain mental states to enable cognitive user interfaces;
(v) online and offline algorithms for decoding brain activity;
(vi) signal processing and machine learning methods for handling artifacts and noise in BCI systems;
(vii) neurofeedback and BCI;
(viii) applications of BCI, especially, in therapy and rehabilitation;
(ix) new technologies for BCI, especially, multielectrode technologies interfacing, telemetry, wireless communication for BCI.

This special issue includes 23 contributions which cover a wide range of techniques and approaches for BCI and related problems.

ACKNOWLEDGMENTS

The guest editors of this special issue are much indebted to their authors and reviewers who put a tremendous amount of effort and dedication to make this issue a reality.

F. Babiloni
A. Cichocki
S. Gao

Hindawi Publishing Corporation
Computational Intelligence and Neuroscience
Volume 2007, Article ID 94561, 9 pages
doi:10.1155/2007/94561

Research Article

Fully Online Multicommand Brain-Computer Interface with Visual Neurofeedback Using SSVEP Paradigm

Pablo Martinez, Hovagim Bakardjian, and Andrzej Cichocki

Laboratory for Advanced Brain Signal Processing, Brain Science Institute RIKEN, Wako-Shi, Saitama 351-0198, Japan

Correspondence should be addressed to Pablo Martinez, pablo.martinez@brain.riken.jp

Received 22 December 2006; Accepted 22 May 2007

Recommended by Fabio Babiloni

We propose a new multistage procedure for a real-time brain-machine/computer interface (BCI). The developed system allows a BCI user to navigate a small car (or any other object) on the computer screen in real time, in any of the four directions, and to stop it if necessary. Extensive experiments with five young healthy subjects confirmed the high performance of the proposed online BCI system. The modular structure, high speed, and the optimal frequency band characteristics of the BCI platform are features which allow an extension to a substantially higher number of commands in the near future.

1. INTRODUCTION

A brain-computer interface (BCI), or a brain-machine interface (BMI), is a system that acquires and analyzes brain signals to create a high-bandwidth communication channel in real time between the human brain and the computer or machine [1–5]. In other words, brain-computer interfaces (BCI) are systems that use brain activity (as reflected by electric, magnetic, or metabolic signals) to control external devices such as computers, switches, wheelchairs, or neuroprosthetic extensions [6–12]. While BCI research hopes to create new communication channels for disabled or elderly persons using their brain signals [1, 2], recent efforts have been focused on developing potential applications in rehabilitation, multimedia communication, and relaxation (such as immersive virtual reality control) [13, 14]. Today, BCI research is an interdisciplinary endeavor involving neuroscience, engineering, signal processing, and clinical rehabilitation, and lies at the intersection of several emerging technologies such as machine learning (ML) and artificial intelligence (AI). BCI is considered as a new frontier in science and technology, especially in multimedia communication [1–18].

The various BCI systems use different methods to extract the user's intentions from her/his brain-electrical activity, for example:

(i) measuring the brain activity over the primary motor cortex that results from imaginary limbs and tongue movements [3, 5],

(ii) detecting the presence of EEG periodic waveforms, called steady-state visual evoked potentials (SSVEP), elicited by multiple flashing light sources (e.g., LEDs or phase-reversing checkerboards) [6–18],

(iii) identifying characteristic event-related potentials (ERP) in EEG that follow an event noticed by the user (or his/her intention), for example, P300 peak waveforms after a flash of a character the user focused attention on [1–3].

In the first approach, the usually exploited features of the brain signals are their temporal/spatial changes and/or the spectral characteristics of the SMR (sensorimotor rhythm) oscillations, or the mu-rhythm (8–12 Hz), and the beta rhythm (18–25 Hz). These oscillations typically decrease during movement or when preparing for movement (event-related desynchronization, ERD) and increase after movement and in relaxation (event-related synchronization, ERS). ERD and ERS help identify those EEG features associated with the task of motor imagery EEG classification [3, 5].

While the first example (i) relies on imaginary actions to activate the corresponding parts of the motor cortex, the

second (ii) and third (iii) examples involve actual selective stimulation in order to increase the information transfer bit rates [3].

Steady-state visual evoked potentials are the elicited exogenous responses of the brain under visual stimulations at specific frequencies. Repetitive stimulation evokes responses of constant amplitude and frequency. Each potential overlaps another so that no individual response can be related to any particular stimulus cycle. It is presumed therefore that the brain has achieved a steady state of excitability [19].

Applications of SSVEP on BCI were proposed by Middendorf et al. [6] and applied later by other groups [7–18, 20]. Previously cited BCI systems, except the approach done by Materka and Byczuk [10], have in common that they are based on spectrum techniques for feature extraction instead of time domain techniques. And all of them use sources of the stimuli (flickering patterns, LED…) in a fixed spatial position.

Comparing to previous SSVEP BCI, our system is based mainly on the temporal domain combining of a blind source separation (BSS) algorithm for artifact rejection and tuned microbatch filtering to estimate the features to be used with a classifier, in our case a fuzzy neural network classifier.

Also, in our design, the sources of stimulus are moving (adding extra complexity), and we have shown that it is possible to perform also a robust BCI for moving flickering targets.

In general, the SSVEP-BCI paradigm has the following potential advantages and perspectives.

(1) It offers the possibility of high performance (information rate) with minimal training time and low requirements from the subject.

(2) The carefully designed SSVEP-BCI system can be relatively robust in respect to noise and artifacts. Artifacts may cause performance degradation; however they can be removed or reduced using advanced signal processing techniques like BSS. Also, blink movement and electrocardiographic artifacts are confined to much lower frequencies and do not make serious problem to accurate feature extraction.

(3) SSVEP-BCI systems are relatively easy to extend to more commands.

(4) Usually BCI systems have higher information transfer rates.

(5) Short training phase is required and application almost does not require special training.

However, SSVEP-BCI may have also some disadvantages.

(1) The flickering visual stimuli may cause some fatigue or tiredness if subjects use it for a long time. This fatigue is caused from the stimulation, while other BCI systems as P300 can cause fatigue due to the required concentration, while SSVEP does not.

(2) The flickering stimuli at some frequencies, patterns, colors, and so forth may not be appropriate for subjects with photosensitive neurological disorders

(3) SSVEP-based BCIs depend on muscular control of gaze direction for their operation, whereas other kinds of BCI systems do not depend on the brain's normal output pathways of peripheral nerves and muscles. Due to this reason, this paradigm may not work for some seriously disable patients. In other words, evoked potentials, especially SSVEP, require stable control of the eye muscles so that such an approach may not be applicable to all users.

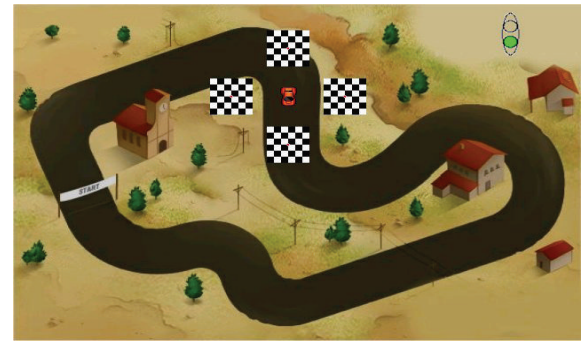

Figure 1: Four small checkerboards flickering at different but fixed frequencies move along with a navigated car. The subject is able to control the direction of movement of the car by focusing her/his attention on a specific checkerboard. Two sets of flickering frequencies were used: (i) low-frequency range {UP: 5 Hz, LEFT: 6 Hz, DOWN: 7 Hz, RIGHT: 8 Hz}, and (ii) medium-frequency range {UP: 12 Hz, LEFT: 13.3 Hz, DOWN: 15 Hz, RIGHT: 17 Hz}.

In this paper, we present a BCI platform based on the SSVEP paradigm. Although the SSVEP paradigm has been exploited in a number of studies [4, 6–18, 20], our design of experiments and signal preprocessing and classification tools are innovative, moreover they are suitable for real-time applications with visual neurofeedback.

2. BCI SYSTEM BASED ON SSVEP PARADIGM: DESIGN AND IMPLEMENTATION

2.1. Stimulator design

In this paper, we present a new BCI system with a visual stimulation unit designed as a smart multiple choice table in the form of an array of four small checkerboard images flickering with different frequencies and moving along with the controlled object (see Figure 1). When a BCI user focuses his/her attention or gazes on a specific flickering image, a corresponding periodic component (SSVEP) can be observed in the EEG signals notably over the occipital (visual) cortex [19].

When a BCI user focuses his/her attention or gaze on a specific flickering image, its corresponding weak quasi-periodic component (SSVEP) is elicited mainly over the occipital (visual) cortex [19]. In addition, they are buried in a large noise, and therefore it is a challenge to extract them reliably in real time. For this purpose, we developed and applied multistage online (real-time) signal processing tools described in detail below.

2.2. Analysis system overview

The signal analysis unit of our BCI system consists (see Figure 2) of a data acquisition module, an enhanced signal

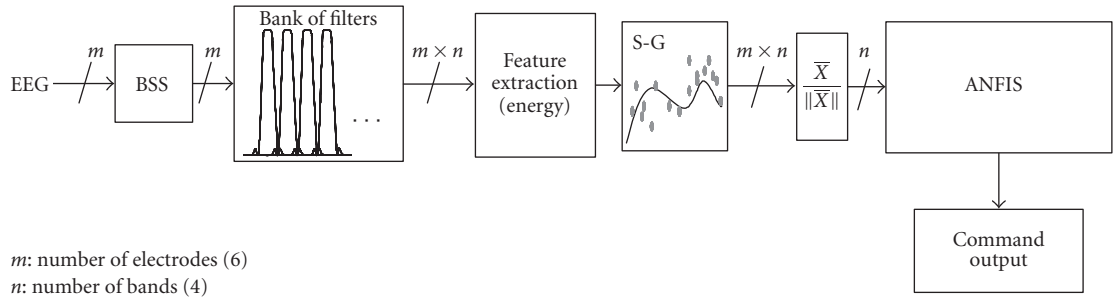

Figure 2: Conceptual scheme of the proposed real-time BCI system. The system consists of a BSS (blind source separation) module for automatic rejection of artifacts and noise, a bank of (narrow band-pass) filters to enhance the first harmonics of the SSVEP responses, a Feature Extraction block with S-G (Sawitzky-Golay) smoothing and energy normalization, and ANFIS (adaptive network fuzzy inference system) for a final classification.

preprocessing unit including online blind source separation (BSS) for artifact rejection and noise reduction, a bank of narrow band-pass filters, a multiple-feature extraction system with Savitzky-Golay (S-G) smoothing, energy normalization and an adaptive-network fuzzy inference system (ANFIS) [21].

To perform all signal processing tasks in real time, the analysis unit was implemented in LabVIEW® and C/C++, while the stimulation unit was based on speed-optimized matlab code.

A general platform overview of our BCI system is shown in Figure 3.

The system is currently able to use EEG input both from the Biosemi (active-electrodes) and from the Neuroscan commercial EEG devices and is fully adaptive, accounting for the well-known large intersubject variability in the brain responses. We used only six EEG channels sampled at 256 Hz. After a very short training, two modes of operation were possible: experimental assessment mode using comparison of command requests and responses in which the success rate and the transfer rates were determined, and a free-roaming mode for overall command and control estimation. By applying BSS and a bank of subband filters, we showed that is possible to decompose and discriminate in real time at least four SSVEP waveforms with very high reliability.

In this study, we applied a set of five electrodes placed over the occipital area {CPZ, PZ, POZ, P1, P2} and one electrode placed over the frontal cortex {FZ}, as illustrated in Figure 4 (left).

2.3. Artifact rejection by blind source separation

A second-order blind source separation (BSS) algorithm was applied to enhance the signal and to attenuate artifacts [22]. It was characterized by a continuous working system in microbatch mode with sliding time window of four seconds and with a discrete time shifts of 120 milliseconds. This means that the system was able to refresh the incoming data every 120 milliseconds and to take into account the EEG signals from the last 4 seconds. The presence of artifacts, especially eye movement-related artifacts, can decrease the performance of the system substantially. In the case of SSVEP stimulation and analysis, their very specific response frequencies (corresponding to the observed pattern flicker frequencies) could be erroneously detected in the presence of artifacts if online BSS is not applied.

For the BSS procedure, we applied a modified and improved real-time AMUSE algorithm with time sliding windows, since such an algorithm allows a very fast (few milliseconds) and reliable estimate of the independent components with automatic ranking (sorting) according to their increasing frequency contents and/or decreased linear predictability. The implemented BSS-AMUSE algorithm can be considered as consisting of two consecutive PCA (principal component analysis) blocks. First, PCA is applied to the input data; and then a second PCA (SVD) is applied to the time-delayed covariance matrix (in our case, the delay is set to one sample or four milliseconds) of the output from the previous stage. In the first step standard or robust prewhitening (sphering) is applied as a linear transformation [22]

$$\mathbf{z}(t) = \mathbf{Q}\mathbf{x}(t), \tag{1}$$

where $\mathbf{Q} = \mathbf{R}_x^{-1/2}$ of the standard covariance matrix

$$\mathbf{R}_x = E\{\mathbf{x}(t)\mathbf{x}^T(t)\} \tag{2}$$

and $\mathbf{x}(t)$ is a vector of observed data for time instant t. Next, SVD is applied to a time-delayed covariance matrix of prewhitened data:

$$\mathbf{R}_z = E\{\mathbf{z}(t)\mathbf{z}^T(t-1)\} = \mathbf{U}\mathbf{S}\mathbf{V}^T, \tag{3}$$

where $\mathbf{S}$ is a diagonal matrix with decreasing singular values and $\mathbf{U}$, $\mathbf{V}$ are matrices of eigenvectors. Then, an unmixing (separating) matrix is estimated as

$$\mathbf{W} = \widehat{\mathbf{A}}^{-1} = \mathbf{U}^T\mathbf{Q}. \tag{4}$$

The estimated independent components are obtained as

$$\mathbf{Y} = \mathbf{W}\mathbf{X}, \tag{5}$$

where $\mathbf{X} = [\mathbf{x}(1), \mathbf{x}(2), \ldots, \mathbf{x}(N)]$.

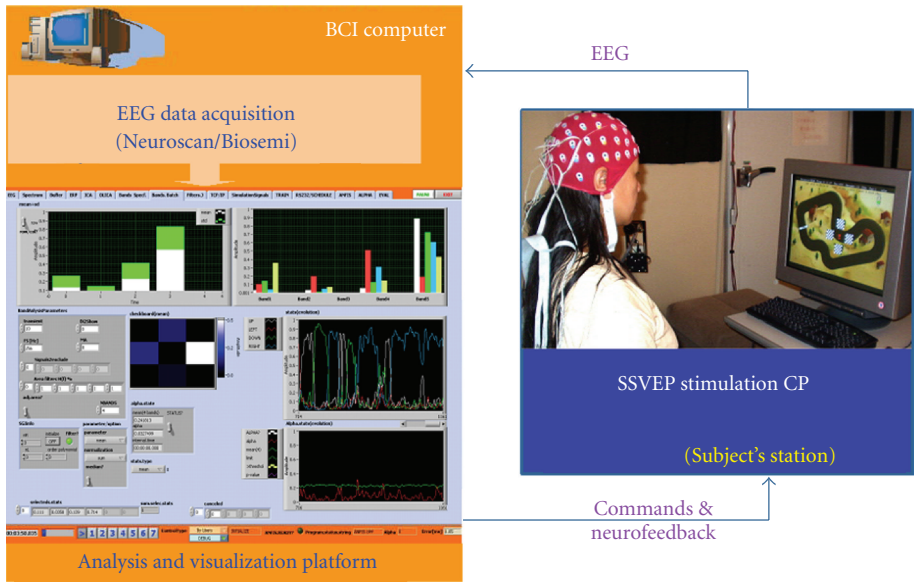

Figure 3: Our BCI platform consists of two PC computers. One for EEG data acquisition, stimuli generation, and a second machine for online processing of data in microbatch mode.

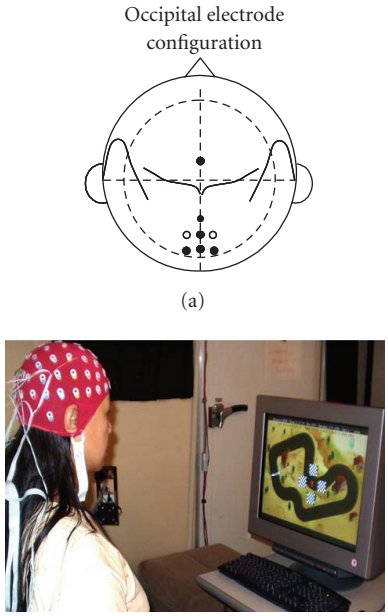

Figure 4: Electrode configuration. Five electrodes placed over the occipital area {CPZ, PZ, POZ, P1, P2} and one over the frontal cortex {FZ}.

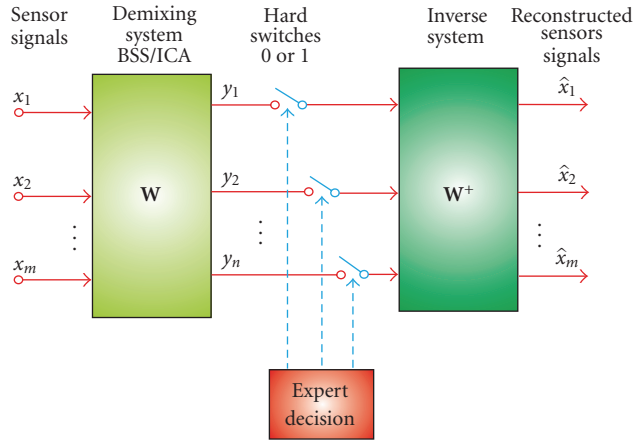

Figure 5: Enhancement of EEG via BSS. First, the raw EEG data (sensor signals) is decomposed and ranked as independent or spatially decorrelated components; in the next step, only the useful components are projected back to the scalp level, while undesirable components containing artifacts and noise are removed from the signal. The main advantage of our approach is that we do not need any expert decision to select significant components, since the AMUSE algorithm automatically ranks the components as illustrated in Figure 6.

The AMUSE BSS algorithm allowed us to automatically rank the EEG components. The undesired components corresponding to artifacts were removed and the rest of the useful (significant) components were projected back to scalp level using the pseudo inverse of $\mathbf{W}$, see Figure 5

$$\hat{\mathbf{X}} = \mathbf{W}^{+}\mathbf{X}. \tag{6}$$

The six EEG channels were high-pass-filtered with a cutoff frequency of 2 Hz before the AMUSE algorithm was applied.

The rejection of the first and the last components had two implications: (1) the EEG signal was enhanced as some oscillations were removed which were due to ocular and other artifacts but included frequencies similar to the target flicker responses. Without this procedure, the performance of the system would have deteriorated substantially since blinking could not be avoided by the experimental subjects; (2) at the

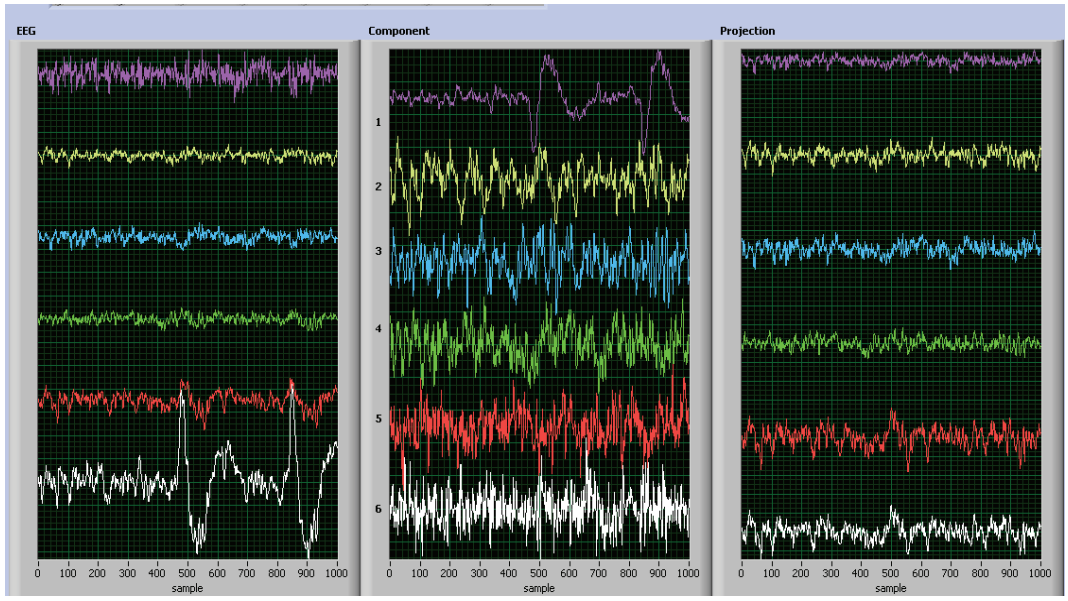

Figure 6: Illustration of the online preprocessing module—artifact rejection: actual EEG data (left), estimated automatically ranked independent components—the first and the last components were rejected as artifacts (center), back-projected (enhanced) EEG signals (right) which serve as the input for the bank of band-pass filters. (Four seconds window.)

same time, we ensured that the control of the car in our BCI system was strictly due to the SSVEP responses elicited by the cortex, and not simply due to eye movements.

2.4. Bank of band-pass filters and features extractions

We designed a bank of third-order elliptic IIR (infinite impulse response) filters with bandwidth 0.5 Hz and with center frequencies corresponding to the flickering frequencies of the checkerboards. The fundamental frequencies of the SSVEP responses were detected by estimating the power of the output signals of the filters. We should mention here that using another type of filters could also be appropriate under the assumption that the overlap of the bandwidths of the subbands would be small enough. As we were interested only in the power of signals, their phase had no relevance in this case.

Four-time series representing the fluctuations of the energies over time were obtained and subsequently smoothed by means of a Savitzky-Golay(S-G) filter [23].

Instead of smoothing each time series' power contents in each subband with a standard moving average (MA) filter, we propose using a Savitzky-Golay filter with a second-order polynomial smoothing. The main advantage of this approach is that it tends to preserve fundamental features such as relative maxima, minima, and width of the peaks, which are usually distorted by other filtering methods, like MA. The S-G smoother approximates the time series within the moving average window not by a constant (estimate of which is the average, as in MA), but by a polynomial of higher order. In other words, this method essentially performs a local polynomial regression (of degree $M = 2$) on a distribution, of at least $k = nR+nL+1$ points, to determine the smoothed value for each point.

The general mathematical expression of the Savitzky-Golay smoothing filter can be described as follows:

$$y[n] = \sum_{k=-nL}^{nR} c_n x[n+k], \tag{7}$$

$$c_n = \sum_{m=0}^{M} \left[\left(A^T A\right)^{-1}\right]_{0,m} n^m, \tag{8}$$

where

$$A_{ij} = i^j, \quad i = -nL, \ldots, nR, \; j = 0, \ldots, M. \tag{9}$$

The signal is smoothed by nL points before, and by nR points after each considered time point—according to (7), where the weighting coefficients c_n are obtained by means of (8). If the filter is casual, then $nR = 0$. We set $nR > 0$ to enhance the smoothing, although it introduced a small delay. For online purposes, $nR \ll nL$. A moving average filter MA is a S-G filter with $M = 0$.

In Figure 7, it is shown as an example that the performance of the S-G filter is compared with a moving average filter for a simulated signal with added noise.

The S-G was applied separately for each band-pass filter and electrode.

After S-G filtering, we performed also a standard normalization of the smoothed energy as follows:

$$E_j = \frac{\sum_{i=1}^{M} e_{ij}}{\sum_{j=1}^{N} \sum_{i=1}^{M} e_{ij}}, \quad i = 1 \cdots M, \; j = 1 \cdots N, \tag{10}$$

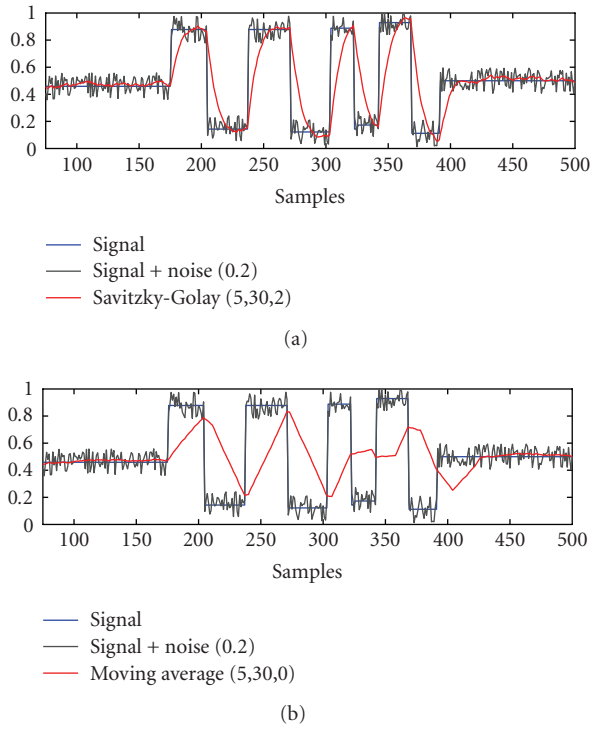

FIGURE 7: Simulated data was used in this example to show a comparison of (a) moving average smoothing ($nR = 30$, $nL = 5$) versus (b) an S-G filter ($nR = 30$, $nL = 5$, order 2). MA is not able to track short time changes having high time response. S-G moving average has similar no-noise cancellation but better track of changes. In BCI, it is important to find a good balance between enhanced smoothing and, at the same time, to be able to follow fast changes in the signal.

where M is the number of the electrodes, N is the number of the band-pass filters, and e_{ij} is the estimated energy of electrode i and band-pass filter j,

$$\sum_{j=1}^{M} E_j = 1. \tag{11}$$

As the stimulation frequencies are close to each other, there is no need of compensation for each frequency. In case of using more frequencies, it is better to send to the classifier normalized values, although this is not the case in this paper.

Therefore, E_j was the relative energy per band and these energy values were used as input parameters for the ANFIS classifier, see Figure 8.

2.5. ANFIS classifier

One of the most complicated problems with the BCI systems is the classification of very noisy EEG signals. For this purpose, we have applied an adaptive, subject-specific classifier to recognize different SSVEPs.

The standard adaptive network based fuzzy inference system (ANFIS) architecture network was used. This system consists of a fuzzy inference system (FIS) whose membership function parameters are tuned (adjusted) using a back propagation algorithm alone in combination with a least-squares type of method (Jang, 1993) [21]. Using a hybrid learning procedure, the ANFIS can learn an input-output mapping based on some a priori knowledge (in the form of if-then fuzzy rules).

The applied ANFIS has four inputs consisted in a Sugeno-type FIS with two membership functions (generalized bell function) per input and output as a constant membership function [21]

$$f(x \mid a, b, c) = \frac{1}{(1 + |x - c|/a)^{2b}}. \tag{12}$$

Four features of EEG signals were used as input patterns (normalized energy values) for the ANFIS system, corresponding to each checkerboard.

3. OPERATING MODES

To overcome the problem of the intersubject variability, some short-term preparatory activities were necessary for the BCI system before the final real-time practical evaluations or applications could be initiated. For this purpose, our BCI system was implemented to work in three separate modes.

(i) Training mode.
(ii) Evaluation (testing) mode.
(iii) Free racing (unsupervised) mode.

The training—and if necessary the evaluation modes, allowed us to find the optimal parameters for each specific subject. In this way, these parameters could be used later in the free racing (unsupervised) mode.

3.1. Training mode

In order to train the classifier, the computer requested the subject to fix their attention on each checkerboard {UP, LEFT, RIGHT, LEFT} during time intervals of six-seconds duration each, using voice-message requests. These requests to execute specific directions were presented in random order.

A fifth, additional, request required no stimulus and involved removing all checkerboard patterns from the screen during the six-seconds interval to measure the control non-SSVEP responses.

The corresponding values of the normalized energies were extracted for each command in the time interval between three and six seconds after each command request. In this time interval, it was considered that the subject was reaching a stable steady state for each corresponding event.

During the training mode, the neurofeedback was disconnected and the car was fixed in the center of the screen to facilitate the subject to focus her/his attention to each flickering checkerboard.

3.2. Evaluation mode

After the training, we asked the subject first to move the car as their own in order to confirm that he or she had the full

Table 1: Experimental results for occipital configuration (mean values).

Subject	#1	#2	#3	#4	#5
	LF (5–8 Hz)				
Success (%)	100	77.5	94.8	92.3	100
Delay Time [s]	3.6 ± 0.4	3.8 ± 1.7	3.3 ± 1	3.3 ± 1.1	4.8 ± 1
	MF (12–17 Hz)				
Success (%)	100	100	100	100	82.3
Delay Time [s]	3.6 ± 0.3	3.9 ± 0.8	3.2 ± 0.4	3.1 ± 1.1	3.7 ± 1.3

Table 2: Experimental results for occipital configuration (mean values and mean bit rate).

Flicker range (Frequency)	LF (5–8 Hz)	MF (12–17 Hz)
Success rate	93%	96.5%
Execution delay	3.7 ± 1.0 s	3.5 ± 0.8 s
Bit rate	26 bits/min	30 bits/min

ability to control the car in any direction. Then, to evaluate the BCI performance for this subject, including time responses and percentage of success (see results bellow), the computer generated in random order requests for movement in each direction using voice messages, similarly to the training mode. The subject was asked to move the car in one of the four directions at intervals of nine seconds in 32 trials (eight trials per direction). It was assumed that the subject successfully performed a task if she/he moved the car properly in a time window between one second and up to a maximum of six seconds after the onset of the voice-request command. During the evaluation mode, the neurofeedback was fully enabled and the car was able to move freely, responding to the subject's commands.

3.3. *Free race (unsupervised) mode*

In this mode, the user could move the car freely within the racing course (Figure 1), and we asked all the subjects to complete at least one lap to evaluate their overall control of the car by performing this task without any external voice commands. This typically took from each subject between 90 to 150 seconds to achieve this complex goal, also depending on the flicker frequency range.

4. EXPERIMENTAL SETTING AND RESULTS

We tested our SSVEP-based BCI system with five subjects (two females and three males) and for two different ranges of flicker frequencies: low-frequency (LF) range—5, 6, 7, 8 Hz and medium-frequency (MF) range—12, 13.3, 15, 17 Hz.

The subjects sat on a chair approximately 90 cm from the center of a 21-inch cathode-ray tube (CRT) monitor screen using a refresh rate of 120 Hz.

Six electrodes were used: five placed over the occipital cortex {CPZ, PZ, POZ, P1, P2} and one over the frontal cortex {Fz}, see Figure 2.

The performance of the BCI system was measured during the evaluation mode, as described in the previous section.

The results are shown in Table 1 (subject-specific results) and Table 2 (mean results). The data obtained in this study indicated that the performance for the medium-frequency range flicker was slightly higher when compared to the low-frequency range flicker responses, in terms of controllability of the car and execution-time delay.

Only one of the subjects was more comfortable with, and felt that his car control was better when using the low-frequency range flicker.

The subjects performed the BCI experiments just a single time for each frequency range (LF, MF), including classifier training and evaluation (results) modes. After the experiment, each subject was asked to demonstrate her/his overall control of the car for each frequency range by completing a full lap as quickly as possible in free racing mode.

5. CONCLUSION AND DISCUSSIONS

Although the SSVEP paradigm is well known in the BCI community since the studies performed by several research groups [6–18, 20], especially Shangkai Gao group at Tshinghua University [8–10, 18] and NASA research group of Trejo et al. [7], we believe that our system offers several novel points for improved usability and efficiency, such as the integrated moving checkerboard patterns to maximize selective attention and to minimize eye movements in respect to the controlled target, as well as an online BSS module to reduce automatically artifacts and noise, improved feature selection algorithm with efficient smoothing and filtering and an adaptive fuzzy neural network classifier ANFIS. All of our EEG signal processing modules and algorithms are carefully optimized to work online in real time. This proposed method and BCI platform could be easily extended for various BCI paradigms, as well as for other types of brain analysis in which real-time processing and dynamic visualization of features are crucial.

Paradigms based on steady-state visual and other evoked potentials are among the most reliable modes of communication for implementation of a fast noninvasive EEG-BCI system that can discriminate in near real time a very high number of unique commands or symbols. The capability of a BCI system to issue more commands in a more reliable way has significant advantages such as allowing better control of semiautonomous remote navigation devices in hazardous environments, or navigating precisely a cursor on a computer screen (or the realization of a virtual joystick). However, in our experimental design, we have incorporated a number of original elements and ideas as compared to the typical SSVEP paradigm. In addition to our new dynamic visual stimulation approach, we have developed and implemented novel and efficient real-time signal preprocessing tools and feature extraction algorithms. Although using our dynamic pattern movement design may require some eye movement control by the subjects, as well as sustained short-term attention, the

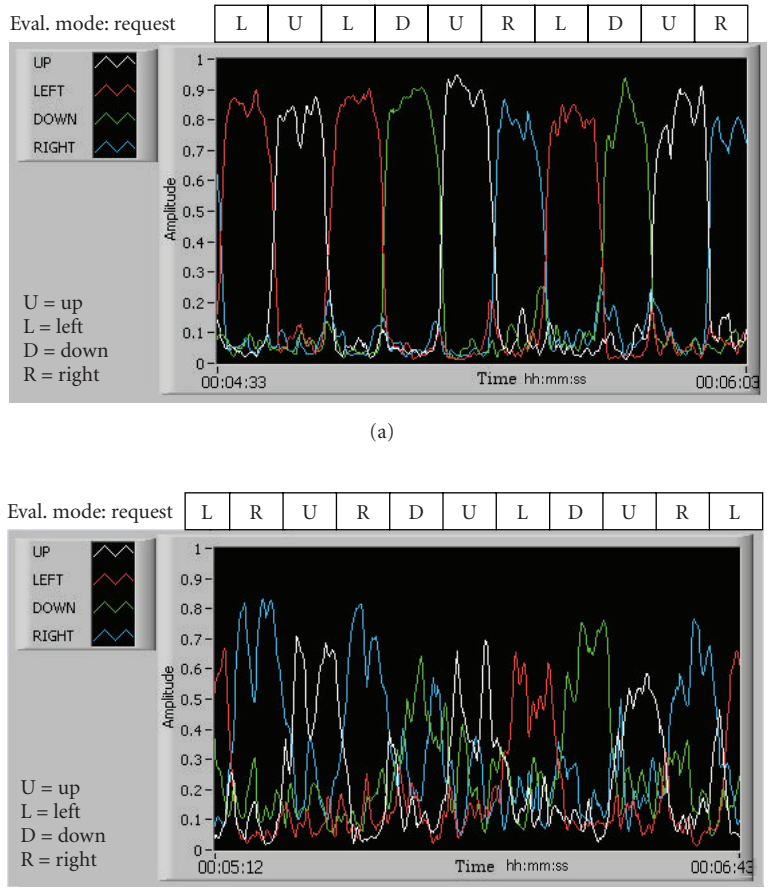

Figure 8: Normalized multiband signals Ej during evaluation mode: (a) a good example case with one of the subjects, and (b) a suboptimal example in another subject, where ANFIS was essential in enhancing the final performance of the system.

control of the object (car) could be easily changed to static for completely disabled subjects. According to our tests and to previous reports Müeller and Hillyard [24] and Kelly et al. [9], eye movement could be avoided altogether in SSVEP (possibly at some performance cost) so that selective attention (with a fixed gaze between the flicker patterns) could be used for flicker response gating/enhancement corresponding to the requested commands.

The ability of our SSVEP-BCI system to operate not only in the medium-frequency range flicker, but also in the low-frequency range, shows its advantages in comparison to the traditionally used FFT-based methods, which usually require the usage of the higher harmonics when the visual stimulation is in the low-frequency range. In contrast, our algorithm estimates the normalized energy of each flickering frequency directly by using a dedicated tuned filter, allowing us to discriminate easily between a stimulation-driven frequency and its higher harmonics. In multiple-command BCI experimental designs, the flickering pattern frequencies could be set to be very close and limited by the minimal overlapping band-pass filters of the applied filters under the physiological constraints of discerning between cortical responses to two close stimulation frequencies.

In summary, we successfully demonstrated the application of a fast online BSS algorithm for automatic rejection of artifacts and noise reduction, a bank of band-pass filters with nonstationary smoothing, and an adaptive fuzzy classifier.

REFERENCES

[1] N. Birbaumer, A. Kubler, N. Ghanayim, et al., "The thought translation device (TTD) for completely paralyzed patients," *IEEE Transactions on Rehabilitation Engineering*, vol. 8, no. 2, pp. 190–193, 2000.

[2] J. R. Wolpaw, N. Birbaumer, D. J. McFarland, G. Pfurtscheller, and T. M. Vaughan, "Brain-computer interfaces for communication and control," *Clinical Neurophysiology*, vol. 113, no. 6, pp. 767–791, 2002.

[3] G. Pfurtscheller, C. Neuper, C. Guger, et al., "Current trends in Graz brain-computer interface (BCI) research," *IEEE Transactions on Rehabilitation Engineering*, vol. 8, no. 2, pp. 216–219, 2000.

[4] G. R. Müller-Putz, R. Scherer, C. Brauneis, and G. Pfurtscheller, "Steady-state visual evoked potential (SSVEP)-based communication: impact of harmonic frequency components," *Journal of Neural Engineering*, vol. 2, no. 4, pp. 123–130, 2005.

[5] H. Lee, A. Cichocki, and S. Choi, "Nonnegative matrix factorization for motor imagery EEG classification," in *Proceedings of the 16th International Conference on Artificial Neural Networks (ICANN '06)*, vol. 4132 of *Lecture Notes in Computer Science*, pp. 250–259, Springer, Athens, Greece, September 2006.

[6] M. Middendorf, G. McMillan, G. Calhoun, and K. S. Jones, "Brain-computer interfaces based on the steady-state visual-evoked response," *IEEE Transactions on Rehabilitation Engineering*, vol. 8, no. 2, pp. 211–214, 2000.

[7] L. J. Trejo, R. Rosipal, and B. Matthews, "Brain-computer interfaces for 1-D and 2-D cursor control: designs using volitional control of the EEG spectrum or steady-state visual evoked potentials," *IEEE Transactions on Neural Systems and Rehabilitation Engineering*, vol. 14, no. 2, pp. 225–229, 2006.

[8] M. Cheng, X. Gao, S. Gao, and D. Xu, "Design and implementation of a brain-computer interface with high transfer rates," *IEEE Transactions on Biomedical Engineering*, vol. 49, no. 10, pp. 1181–1186, 2002.

[9] S. P. Kelly, E. C. Lalor, R. B. Reilly, and J. J. Foxe, "Visual spatial attention tracking using high-density SSVEP data for independent brain-computer communication," *IEEE Transactions on Neural Systems and Rehabilitation Engineering*, vol. 13, no. 2, pp. 172–178, 2005.

[10] A. Materka and M. Byczuk, "Using comb filter to enhance SSVEP for BCI applications," in *Proceedings of the 3rd International Conference on Advances in Medical, Signal and Information Processing (MEDSIP '06)*, p. 33, Glasgow, UK, July 2006.

[11] Z. Lin, C. Zhang, W. Wu, and X. Gao, "Frequency recognition based on canonical correlation analysis for SSVEP-based BCIs," *IEEE Transactions on Biomedical Engineering*, vol. 53, no. 12, part 2, pp. 2610–2614, 2006.

[12] O. Friman, I. Volosyak, and A. Graser, "Multiple channel detection of steady-state visual evoked potentials for brain-computer interfaces," *IEEE Transactions on Biomedical Engineering*, vol. 54, no. 4, pp. 742–750, 2007.

[13] E. C. Lalor, S. P. Kelly, C. Finucane, et al., "Steady-state VEP-based brain-computer interface control in an immersive 3D gaming environment," *EURASIP Journal on Applied Signal Processing*, vol. 2005, no. 19, pp. 3156–3164, 2005.

[14] L. Piccini, S. Parini, L. Maggi, and G. Andreoni, "A wearable home BCI system: preliminary results with SSVEP protocol," in *Proceedings of the 27th Annual International Conference of the IEEE Engineering in Medicine and Biology Society (EMBS '05)*, pp. 5384–5387, Shanghai, China, September 2005.

[15] Y. Wang, R. Wang, X. Gao, B. Hong, and S. Gao, "A practical VEP-based brain-computer interface," *IEEE Transactions on Neural Systems and Rehabilitation Engineering*, vol. 14, no. 2, pp. 234–240, 2006.

[16] K. D. Nielsen, A. F. Cabrera, and O. F. do Nascimento, "EEG based BCI-towards a better control. Brain-computer interface research at Aalborg university," *IEEE Transactions on Neural Systems and Rehabilitation Engineering*, vol. 14, no. 2, pp. 202–204, 2006.

[17] V. Jaganathan, T. M. S. Mukesh, and M. R. Reddy, "Design and implementation of high performance visual stimulator for brain computer interfaces," in *Proceedings of the 27th Annual International Conference of the IEEE Engineering in Medicine and Biology Society (EMBS '05)*, pp. 5381–5383, Shanghai, China, September 2005.

[18] X. Gao, D. Xu, M. Cheng, and S. Gao, "A BCI-based environmental controller for the motion-disabled," *IEEE Transactions on Neural Systems and Rehabilitation Engineering*, vol. 11, no. 2, pp. 137–140, 2003.

[19] E. Niedermeyer and F. L. Lopes da Silva, *Electroencephalography: Basic Principles, Clinical Applications and Related Fields*, chapter 54, Lippincott Williams & Wilkins, Philadelphia, Pa, USA, 1982.

[20] F. Beverina, G. Palmas, S. Silvoni, F. Piccione, and S. Giove, "User adaptive BCIs: SSVEP and P300 based interfaces," *PsychNology Journal*, vol. 1, no. 4, pp. 331–354, 2003.

[21] J.-S. R. Jang, "ANFIS: adaptive-network-based fuzzy inference system," *IEEE Transactions on Systems, Man and Cybernetics*, vol. 23, no. 3, pp. 665–685, 1993.

[22] A. Cichocki and S. Amari, *Adaptive Blind Signal and Image Processing: Learning Algorithms and Applications*, John Wiley & Sons, Chichester, UK, 2003.

[23] A. Savitzky and M. J. E. Golay, "Smoothing and differentiation of data by simplified least squares procedures," *Analytical Chemistry*, vol. 36, no. 8, pp. 1627–1639, 1964.

[24] M. M. Müller and S. Hillyard, "Concurrent recording of steady-state and transient event-related potentials as indices of visual-spatial selective attention," *Clinical Neurophysiology*, vol. 111, no. 9, pp. 1544–1552, 2000.

Hindawi Publishing Corporation
Computational Intelligence and Neuroscience
Volume 2007, Article ID 91651, 7 pages
doi:10.1155/2007/91651

Research Article

The Estimation of Cortical Activity for Brain-Computer Interface: Applications in a Domotic Context

F. Babiloni,[1,2] F. Cincotti,[1] M. Marciani,[1] S. Salinari,[3] L. Astolfi,[1,2] A. Tocci,[1] F. Aloise,[1] F. De Vico Fallani,[1] S. Bufalari,[1] and D. Mattia[1]

[1] *Istituto di Ricovero e Cura a Carattere Scientifico, Fondazione Santa Lucia, Via Ardeatina, 306-00179 Rome, Italy*
[2] *Dipartimento di Fisiologia Umana e Farmacologia, Università di Roma "La Sapienza", Piazzale Aldo Moro 5, 00185 Rome, Italy*
[3] *Dipartimento di Informatica e Sistemistica, Università di Roma "La Sapienza", Piazzale Aldo Moro 5, 00185 Rome, Italy*

Correspondence should be addressed to D. Mattia, d.mattia@hsantalucia.it

Received 18 February 2007; Revised 8 June 2007; Accepted 4 July 2007

Recommended by Andrzej Cichocki

In order to analyze whether the use of the cortical activity, estimated from noninvasive EEG recordings, could be useful to detect mental states related to the imagination of limb movements, we estimate cortical activity from high-resolution EEG recordings in a group of healthy subjects by using realistic head models. Such cortical activity was estimated in region of interest associated with the subject's Brodmann areas by using a depth-weighted minimum norm technique. Results showed that the use of the cortical-estimated activity instead of the unprocessed EEG improves the recognition of the mental states associated to the limb movement imagination in the group of normal subjects. The BCI methodology presented here has been used in a group of disabled patients in order to give them a suitable control of several electronic devices disposed in a three-room environment devoted to the neurorehabilitation. Four of six patients were able to control several electronic devices in this domotic context with the BCI system.

1. INTRODUCTION

Brain-computer interface (BCI) is an area of research that is rapidly growing in the neuroscience and bioengineering fields. One popular approach to the generation of a BCI system consists in the recognition of the patterns of electrical activity on the scalp gathered from a series of electrodes by a computer. One of the problems related to the use of surface EEG is the blurring effect due to the smearing of the skull on the transmission of the potential distribution from the cerebral cortex toward the scalp electrodes. This happens since the skull has a very low electric conductivity when compared with the scalp or the brain one. The blurring effect makes the EEG data gathered from the scalp electrodes rather correlated, a problem not observed in the cortical EEG data recorded from the invasive implants in monkeys and man. Such correlation makes the work of the classifiers problematic, since the features extracted from the different scalp electrodes tend to be rather similar and this correlation is hard to be disentangled with blind methods like principal component analysis.

In this last decade, high-resolution EEG technologies have been developed to enhance the spatial information content of EEG activity [1, 2]. Furthermore, since the ultimate goal of any EEG recording is to provide useful information about the brain activity, a body of mathematical techniques, known as inverse procedures, has been developed to estimate the cortical activity from the raw EEG recordings. Examples of these inverse procedures are the dipole localization, the distributed source, and the cortical imaging techniques [1–4]. Inverse procedures could use linear and nonlinear techniques to localize putative cortical sources from EEG data by using mathematical models of the head as volume conductor.

More recently, it has been suggested that, with the use of the modern high-resolution EEG technologies, it could be possible to estimate the cortical activity associated with the mental imagery of the upper limbs movements in humans better than with the scalp electrodes [4–6]. We currently use this technology to estimate the cortical current

density in particular region of interest (ROI) on the modeled brain structures from high-resolution EEG recordings to provide high-quality signals for the extraction of the features useful to be employed in a BCI system.

In this paper, we would like to illustrate how, with the use of such advanced high-resolution EEG methods for the estimation of the cortical activity, it is possible to run a BCI system able to drive and control several devices in a domotic environment. In particular, we first describe a BCI system used on a group of normal subjects in which the technology of the estimation of the cortical activity is illustrated. Then, we used the BCI system for the command of several electronic devices within a three-room environment employed for the neurorehabilitation. The BCI system was tested by a group of six patients.

2. METHODOLOGY

Subjects

Two groups of subjects have been involved in the training with the BCI system. One was composed of normal healthy subjects while the second one was composed of disabled persons who used the BCI system in attempt to drive electronic devices in a three-room facility at the laboratory of the foundation of Santa Lucia in Rome. The first group was composed by fourteen healthy subjects that voluntarily participated to the study. The second group of subjects were formed by six patients affected by Duchenne muscular dystrophy. According to the Barthel index (BI) score for their daily activity, all patients depended almost completely on caregivers, having a BI score lower than 35. In general, all patients were unable to walk since they were adolescent, and their mobility was possible only by a wheelchair which was electric in all (except two) patients and it was driven by a modified joystick which could be manipulated by either the residual "fine" movements of the first and second fingers or the residual movements of the wrist. As for the upper limbs, all patients had a residual muscular strength either of proximal or distal arm muscles that was insufficient for carrying on any everyday life activity. The neck muscles were as weak as to require a mechanical support to maintain the posture in all of them. Finally, eye movements were substantially preserved in all of them. At the moment of the study, none of the patients was using technologically advanced aids.

2.1. Patient's preparation and training

Patients were admitted for a neurorehabilitation program that includes also the use of BCI system on a voluntary base. Caregivers and patients gave the informed consent for the recordings in agreement with the ethical committee rules adopted for this study. The rehabilitation programs aimed to allow to the patients the use of a versatile system for the control of several domestic devices by using different input devices, tailored on the disability level of the final user. One of the possible inputs for this system was the BCI by using the modulation of the EEG.

The first step of the clinical procedure consisted of an interview and a physical examination performed by the clinicians, wherein several levels of the variables of interest (and possible combinations) were addressed as follows: the degree of motor impairment and of reliance on the caregivers for everyday activities as assessed by current standardized scale, that is, the Barthel Index (BI) for ability to perform daily activities; the familiarity with transducers and aids (sip/puff, switches, speech recognition, joysticks) that could be used as the input to the system; the ability to speak or communicate, being understandable to an unfamiliar person; the level of informatics alphabetization measured by the number of hours per week spent in front of a computer. Information was structured in a questionnaire administered to the patients at the beginning and the end of the training. A level of system acceptance by the users was schematized by asking the users to indicate, with a number ranging from 0 (not satisfactory) to 5 (very satisfactory), their degree of acceptance relative to each of the controlled output devices. The training consisted of weekly sessions; for a period of time ranging from 3 to 4 weeks, the patient and (when required) her/his caregivers were practicing with the system. During the whole period, patients had the assistance of an engineer and a therapist in their interaction with the system.

2.2. Experimental task

Both normals and patients were trained by using the BCI system in order to control the movement of a cursor on the screen on the base of the modulation of their EEG activity. In particular, the description of the experimental task performed by all of them during the training follows. Each trial consisted of four phases.

(1) Target appearance: a rectangular target appeared on the right side of the screen, covering either the upper or the lower half of the side.
(2) Feedback phase: one second after the target, a cursor appeared in the middle of the left side of the screen and moved at a constant horizontal speed to the right. Vertical speed was determined by the amplitude of sensorimotor rhythms (see Section 2.6). A cursor sweep lasted about three seconds.
(3) Reward phase: if the cursor succesfully hit the target, the latter flashed for about one second. Otherwise, it just disappeared.
(4) Intertrial interval: the screen stayed blank for about two seconds, in which the subject was allowed to blink and swallow.

Subjects were aware that the increase or decrease of a specific rhythm in their EEG produces a movement of the cursor towards the top or the bottom of the screen. They were suggested to concentrate on kinesthetic imagination of upper limb movements (e.g., fist clenching) to produce a desynchronization of the μ rhythm on relevant channels (cursor up), and to concentrate on kinesthetic imagination of lower limb movements (e.g., repeated dorsiflexion of ankle joint) to produce a contrasting pattern (with possible desynchronization of μ/β rhythm over the mesial channels, cursor down).

Using this simple binary task as performance measure, training is meant to improve performances from 50–70% to 80–100% of correct hits.

2.3. Experimental training

The BCI training was performed using the BCI2000 software system [7]. An initial screening session was used to define the ideal locations and frequencies of each subject's spontaneous μ- and β-rhythm activity. During this session, the subject was provided with any feedback (any representation of her/his μ rhythm), and she/he had to perform motor tasks just in an open loop. The screening session consisted in the alternate and random presentation of cues on opposite sides of the screen (either up/down -vertical- or left/right -horizontal). In two subsequent runs, the subject was asked to execute (first run) or to image (second run) movements of her/his hands or feet upon the appearance of top or bottom target, respectively. This sequence was repeated three times. From the seventh run on, the targets appeared on the left or right side of the screen, and the subject was asked to move (odd trials) or to image (even trials) her/his hands for a total of 12 trials. The offline analysis based on pairs of contrasts for each task aimed at detecting two, possibly independent, groups of features which will be used to train the subject to control two independent dimensions in the BCI. Analysis was carried on by replicating the same signal conditioning and feature extraction that was also used in the online processing (training session). Datasets are divided into epochs (usually 1-second long) and spectral analysis is performed by means of a maximum entropy algorithm, with a resolution of 2 Hz.

Different from the online processing, when the system only computes the few features relevant for BCI control, all possible features in a reasonable range are extracted and analyzed simultaneously. A feature vector is extracted from each epoch composed by the spectral value at each frequency bin between 0 and 60 Hz for each spatially filtered channel. When all features in the two datasets under contrast have been extracted, a statistical analysis is performed to assess significant differences in the values (epochs) of each feature in the two conditions. Usually an r^2 analysis is performed, but in the case of 2-level-independent variables (such in case tasks $= \{T1, T2\}$, t-test, ANOVA, etc.) would provide the analogous results. At the end of this process, the results were available (channel-frequency matrix and head topography of r^2 values) and evaluated to identify the most promising set of features to be enhanced with training.

Using information gathered from the offline analysis, the experimenter set the online feature extractor so that a "control signal" was generated from the linear combination of time-varying value of these features, and then passed to a linear classifier. The latter's output controls how the position of the feedback cursor was updated. During the following training sessions, the subjects were thus fed back with a representation of their μ-rhythm activity, so that they could learn how to improve its modulation.

Each session lasted about 40 minutes and consisted of eight 3-minute runs of 30 trials. The task was increased in difficulty during the training, so mainly two different task classes can be defined.

During the training sessions, subjects were asked to perform the same kinaesthetic imagination movement they were asked during the screening session. An upward movement of the cursor was associated to the bilateral decrease of μ rhythm over the hand area (which usually occurs during imagination of upper limb movement). Consequently, the (de)synchroinization pattern correlated to imagination of lower limb movements made the cursor move downwards. With the same principle, the horizontal movement of the cursor to the left (right) was linked to the lateralization of μ rhythm due to imagination of movement of the left (right).

To do so, two different control signals were defined. The vertical control signal was obtained as the sum of the μ-rhythm amplitude over both hand motor areas; the value of μ-rhythm amplitude over the foot area was possibly subtracted (depending on the individual subject's pattern). The horizontal control channel was obtained as the difference between the μ-rhythm amplitudes over each hand motor areas.

During the first 5–10 training sessions, the user is trained to optimize modulation of one control signal at a time, that is, overall amplitude ("vertical control") or lateralization ("horizontal control") of the μ rhythm. Either control channel was associated with vertical or horizontal movement of a cursor on the screen, respectively.

For the training of "vertical" control, the cursor moved horizontally across the screen from left to right at a fixed rate, while the user controlled vertical movements towards appearing targets, justified to the right side of the screen. Analogously, for the training of "horizontal" control, the cursor moved vertically across the screen from top to bottom at a fixed rate, while the user controlled horizontal movements towards appearing targets justified to the bottom side of the screen.

This phase was considered complete when the healthy subjects reached a performance of 70–80% correct hits (60–65% for patients) on both monodimensional tasks. In case of bidimensional task that was performed only by the normal subjects, the cursor appeared in the center, and its movement was entirely controlled by the subject, using both control channels ("horizontal" and "vertical") simultaneously.

2.4. Domotic system prototype features

The system core that disabled patients attempted to use in order to drive electronic devices in a three-room laboratory was implemented as follows. It received the logical signals from several input devices (including the BCI system) and converted them into commands that could be used to drive the output devices. Its operation was organized as a hierarchical structure of possible actions, whose relationship could be static or dynamic. In the static configuration, it behaved as a "cascaded menu" choice system and was used to feed the feedback module only with the options available at the moment (i.e., current menu). In the dynamic configuration, an intelligent agent tried to learn from the use which would have been the most probable choice the user will make. The user could select the commands and monitor the system behavior

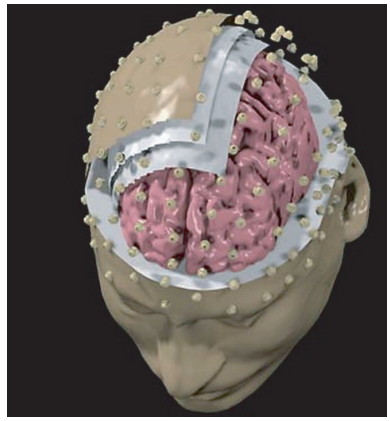

Figure 1: A realistic head model employed for the estimation of the cortical activity. Three layers are displayed, namely, representing dura mater, skull, and scalp. Also the electrode positions are visible on the scalp surface.

through a graphic interface. The prototype system allowed the user to operate remotely electric devices (e.g., TV, telephone, lights, motorized bed, alarm, and front door opener) as well as monitoring the environment with remotely controlled video cameras. While input and feedback signals were carried over a wireless communication, so that mobility of the patient was minimally affected, most of the actuation commands were carried via a powerline-based control system. As described above, the generated system admits the BCI as one possible way to communicate with it, being open to accept command by other signals related to the residual ability of the patient. However, in this study we report only the performance of these patients with the BCI system in the domotic applications.

2.5. Estimation of the cortical activity from the EEG recordings

For all normal subjects analyzed in this study, sequential MR images were acquired and realistic head models were generated. For all the patients involved in this study, due to the lack of their MR images, we used the Montreal average head model. Figure 1 shows realistic head models generated for a particular experimental subjects, together with the employed high-resolution electrode array. Scalp, skull, dura mater, and cortical surfaces of the realistic and averaged head models were obtained. The surfaces of the realistic head models were then used to build the boundary element model of the head as volume conductor employed in the present study. Conductivities values for scalp, skull, and dura mater were those reported in Oostendorp et al. [8]. A cortical surface reconstruction was accomplished for each subject's head with a tessellation of about 5000 triangles on average, while the average head model has about 3000 triangles.

The estimation of cortical activity during the mental imagery task was performed in each subject by using the depth-weighted minimum norm algorithm [9, 10]. Such estimation returns a current density estimate for each one of the thousand dipoles constituting the modeled cortical source space. Each dipole returns a time-varying amplitude representing the brain activity of a restricted patch of cerebral cortex during the entire task time course. This rather large amount of data can be synthesized by computing the ensemble average of all the dipoles magnitudes belonging to the same cortical region of interest (ROI). Each ROI was defined on each subject's cortical model adopted in accordance with its Brodmann areas (BAs). Such areas are regions of the cerebral cortex whose neurons sharing the same anatomical (and often also functional) properties. Actually, such areas are largely used in neuroscience as a coordinate system for sharing cortical activation patterns found with different neuroimaging techniques. In the present study, the activity in the following ROI was taken into account: the primary left and right motor areas, related to the BA 4, the left and right primary somatosensory and supplementary motor areas.

2.6. Online processing

Digitized EEG data were transmitted in real time to the BCI2000 software system [7] which performed all necessary signal processing and displayed feedback to the user. The processing pipe can be considered of several stages, which process the signal in sequence. Only the main ones will be mentioned below: spatial filter, spectral feature extraction, feature combination, and normalization.

Spatial filter

A general linear combination of data channels is implemented by defining a matrix of weights that is multiplied to each time sample of potentials (vector). This allowed implementation of different spatial filters, such for instance the estimation of cortical current density waveforms on the cortical ROIs.

Spectral feature extraction

It was performed every 40 milliseconds, using the latest 300 milliseconds of data. An autoregressive spectral estimator based on the maximum entropy algorithm yielded an amplitude spectrum with resolution of 2 Hz. Maximum frequency was limited to 60 Hz

Feature selection and combination

A small subset of those spectral features (frequency bins $\times$ EEG channels or ROIs) that were significantly modulated by the motor imagery tasks was linearly combined to form a single control signal. Selection of responsive channels and frequency bins and determination of combination weights were operated before each online session (see Section 2.7). In general, only two or three spectral amplitude values (depending on individual patterns) were generally used to obtain the control signal.

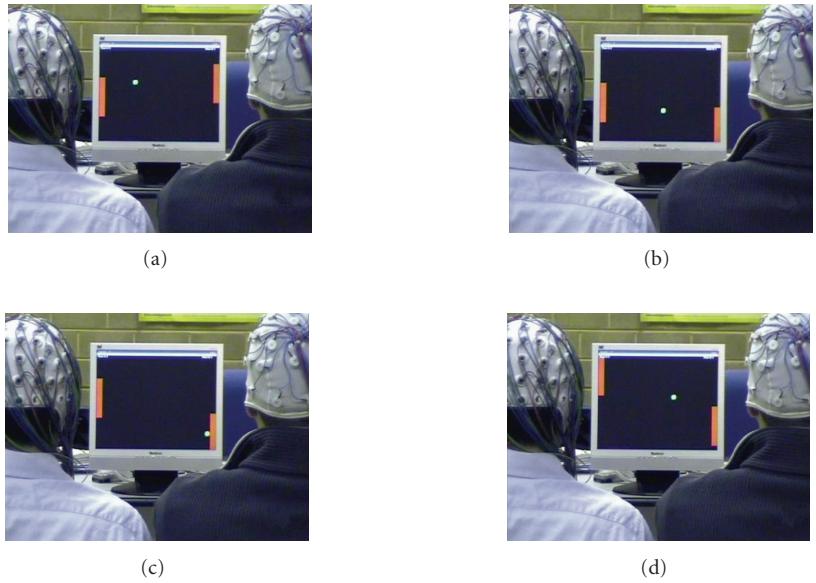

(a) (b)

(c) (d)

Figure 2: Sequence of two healthy subjects that play the ping-pong with the use of the BCI described in the text. Subjects control the cursor movement along the vertical directions. Sequence from (a) to (d).

Normalization

The control channel was detrended to avoid biases of the cursor and scaled so that the resulting vertical deflection of the feedback cursor was visible but not saturated. In fact, the vertical position of the cursor was updated every 40 milliseconds by a number of pixels (positive or negative) equal to the output by this stage. Normalization was adaptive and based on the estimate of the moving average and standard deviation of the control signal. During the very first session of each subject (screening session), since no offline analysis was available to guide feature selection and combination, the subject was given no online feedback (targets only).

2.7. Offline analysis

After artifact rejection, the EEG interval corresponding to the feedback phase were binned into two classes—up or down, depending on the target appeared in each trial. The spatial filtering and feature extraction stages of the online processing were replicated. Since no feedback delay issue had to be considered during the offline analysis, spectral estimation was computed on 1-second long epochs, overlapped by 50% (i.e., only five spectral estimates had to be computed for each 3-second long trial yielding about 600 spectral estimates per class for the whole session).

For each of the EEG channels or ROIs waveforms employed and for each one of the 30 frequency bins in which the EEG spectral interval was divided, a contrast was performed to assess statistically significant modulations induced on a specific feature. To this aim, we computed for each feature (dependent variable) the coefficient of determination (r^2) that is the proportion of the total variance of the feature samples accounted for by target position. This index had been previously utilized in literature for similar experimental setups [11] and allows direct comparison with published results. A fictitious independent variable was created, using values +1 or −1 in correspondence of "down" or "up" epochs, respectively. A negative sign was attributed to the r^2 value when dependent and independent variables were controvariant. Viewing statistical results from a different point of view, features characterized by a high r^2 value are those that maximize prediction of the current target. Higher values of r^2 indicate that the subject has gained steadier control of EEG rhythms (in fact they generally increase during the training, from values below 0.1 to values above 0.3).

3. RESULTS

By applying the mentioned signal processing techniques in the context of the proposed BCI setup, we used the r^2 as an index of reliability of the recognition of subject's mental activity. The comparisons between the maximum values of the r^2 that takes into account the best usable feature (frequency/ROI or scalp channel) were performed for the unprocessed EEG data as well as for the estimated cortical activity by using the procedure already described above. Mean r^2 is 0.20 ± 0.114 SD for the unprocessed EEG case, 0.55 ± 0.16 SD for the cortical current density estimation case. The differences are relatively constant across the subjects, and a paired student's t test returned a highly significant difference between the two conditions ($P < 10^{-5}$). Once all the normals have completed the training, we choose the two with the best performance and we train them to use a different BCI application, namely, the old game of electronic ping-pong.

Figure 2 shows a sequence with two subjects that played a ping-pong game with the use of the BCI system realized along the guidelines provided above. The subjects are able to control the movement of the vertical cursors while the white cursor, simulating the ball, moves across the screen.

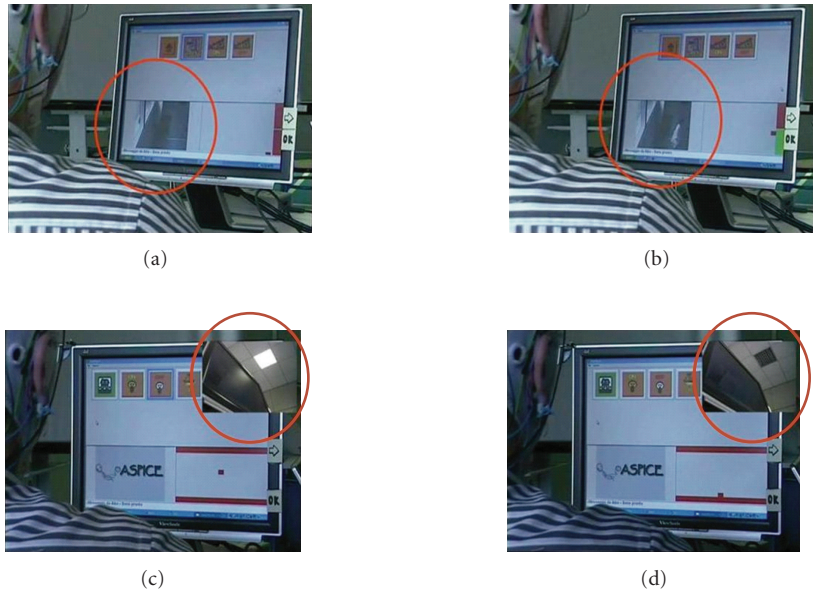

Figure 3: Two sequences of commands realized through the BCI systems at the foundation Santa Lucia in Rome. In the first row, foundations (a) and (b), there is a sequence with the BCI system that opens a door. In the red circles of the first row, a person enters through a door that was opened with the use of the BCI based on the EEG μ rhythm. The second row, (c) and (d), shows the closure of a light with the use of the same BCI system. The BCI system is controlled with the cursor at the right of the screen.

The sequence reads from (a) to (d). The two subjects are able to control the device by performing the 95 and 96% of successful hits during a game lasting several minutes, with a speed of about 5 correct hits per minute per subject.

3.1. Experimentation with the patients

As described previously in the methods section, all the patients underwent a standard BCI training. Over the 8–12 sessions of training, four out six patients were able to develop a sensorimotor reactivity sufficiently stable to control the cursor with performance as high as over 63%. They could image either foot or hand movements and the related sensorimotor modulation was mainly located at midline centroparietal electrode positions. Two patients were not able to control the cursor with a percentage superior to 55% and were not taken into consideration further here in the context of the use of BCI system. At the end of the training, the four patients were able to control the several system outputs, namely the domotic appliances. According to the early results of the questionnaire, these patients were independent in the use of the system at the end of the training and they experienced (as they reported) "the possibility to interact with the environment by myself." A schematic evaluation of the degree of the system acceptance revealed that amongst the several system outputs, the front door opener was the most accepted controlled device. Such application that controls the access to the domotic environment in the three-room facility rehabilitation laboratory is illustrated in the first row of Figure 3. In particular, the figure shows two sequences of commands realized through the BCI system. In the first row, (a) and (b), there is a sequence in which the BCI system was able to open a door. The red circles of the first row highlight a person that enters through the door that was opened by the successful modulation of the EEG μ rhythm. The second row, (c) and (d), shows the closure of a light with the use of the same BCI system. The feedback from the BCI system is displayed on the screen with the position of the cursor at the lower right of the screen.

4. DISCUSSION

The data reported here suggest that it is possible to retrieve the cortical activity related to the mental imagery by using sophisticated high-resolution EEG techniques, obtained by solving the linear inverse problem with the use of realistic head models. Of course, the analysis of the distribution of the potential fields associated to the motor imagery in humans has been already described [4–6, 11]. However, in the context of the brain-computer interface, it assumes importance if the activity related to the imagination of arm movement could be better detected by using such high-resolution EEG techniques than with the use of the unprocessed EEG. It is worth to note that the cortical estimation methodology illustrated above is suitable for the online applications needed for the BCI device. In fact, despite the use of sophisticated realistic head models for scalp, skull, dura mater, and cortical surface, the estimation of the instantaneous cortical distribution from the acquired potential measures required a limited amount of time necessary for a matrix multiplication. Such multiplication occurs between the data vector gathered and the pseudoinverse matrix that is stored offline before the start

of the EEG acquisition process. In the pseudoinverse matrix is enclosed with the complexity of the geometrical head modeling with the boundary element or with the finite element modeling techniques, as well as the priori constraints used for the minimum norm solutions.

The described methodologies were applied in the context of the neurorehabilitation in a group of six patients affected by the Duchenne muscular dystrophy. Four out of six were also able to control with the BCI system several electronic devices disposed in a three-room facility, we described previously. The devices guided by them with an average percentage score of 63% are as follows: (i) a simple TV remote commander, with the capabilities to switch on and off the device as well as the capability to change a TV channel; (ii) the opening and closing of the light in a room; (iii) the switch on and off of a mechanical engine for opening a door of the room. These devices can be, of course, also controlled with different inputs signals that eventually uses the residual degree of muscular control of such patients. This experiment was here reported because it demonstrates the capability for the patient to accept and adapt themselves to the use of the new technology for the control of their domestic environment.

There is a large trend in the modern neuroscience field to move toward invasive electrodes implants for the recording of cortical activity in both animals and humans for the realization of an efficient BCI device [12–14]. In this paper, we have presented evidences that suggest an alternative methodology for the estimation of such cortical activity in a noninvasive way, by using the possibilities offered by an accurate modeling of the principal head structures involved in the transmission of the cortical potential from the brain surface to the scalp electrodes.

ACKNOWLEDGMENTS

This work has been partially supported by the Italian Telethon Foundation (Grant GUP03562); Division for the Scientific and Technologic Development, the Minister for Foreign Affairs, in the framework of a bilateral project between Italy and China (Tsinghua University); the European Union through the MAIA project (IST Programme FET Project FP6-003758) and the COST granting scheme through the Action BM0601 NEUROMATH. It was also supported in part by a grant from NIH (EB006356) in the USA. This paper only reflects the authors' views, and funding agencies are not liable for any use that may be made of the information contained herein.

REFERENCES

[1] P. L. Nunez, *Neocortical Dynamics and Human EEG Rhythms*, Oxford University Press, New York, NY, USA, 1995.

[2] A. Gevins, P. Brickett, B. Costales, J. Le, and B. Reutter, "Beyond topographic mapping: towards functional-anatomical imaging with 124-channel EEGs and 3-D MRIs," *Brain Topography*, vol. 3, no. 1, pp. 53–64, 1990.

[3] A. M. Dale and M. I. Sereno, "Improved localization of cortical activity by combining EEG and MEG with MRI cortical surface reconstruction: a linear approach," *Journal of Cognitive Neuroscience*, vol. 5, no. 2, pp. 162–176, 1993.

[4] F. Babiloni, F. Cincotti, F. Carducci, P. M. Rossini, and C. Babiloni, "Spatial enhancement of EEG data by surface Laplacian estimation: the use of magnetic resonance imaging-based head models," *Clinical Neurophysiology*, vol. 112, no. 5, pp. 724–727, 2001.

[5] F. Cincotti, D. Mattia, C. Babiloni, et al., "Classification of EEG mental patterns by using two scalp electrodes and Mahalanobis distance-based classifiers," *Methods of Information in Medicine*, vol. 41, no. 4, pp. 337–341, 2002.

[6] R. Grave de Peralta, S. L Gonzalez Andino, J. Millan, T. Pun, and C. M. Michel, "Direct non invasive brain computer interface (BCIS)," in *Proceedings of the 9th International Conference on Functional Mapping of the Human Brain*, New York, NY, USA, June 2003, CD-Rom in *NeuroImage*, vol. 19, no. 2, poster 1027.

[7] G. Schalk, D. J. McFarland, T. Hinterberger, N. Birbaumer, and J. R. Wolpaw, "BCI2000: a general-purpose brain-computer interface (BCI) system," *IEEE Transactions on Biomedical Engineering*, vol. 51, no. 6, pp. 1034–1043, 2004.

[8] T. F. Oostendorp, J. Delbeke, and D. F. Stegeman, "The conductivity of the human skull: results of in vivo and in vitro measurements," *IEEE Transactions on Biomedical Engineering*, vol. 47, no. 11, pp. 1487–1492, 2000.

[9] F. Babiloni, C. Babiloni, L. Locche, F. Cincotti, P. M. Rossini, and F. Carducci, "High-resolution electro-encephalogram: source estimates of Laplacian-transformed somatosensory-evoked potentials using a realistic subject head model constructed from magnetic resonance images," *Medical and Biological Engineering and Computing*, vol. 38, no. 5, pp. 512–519, 2000.

[10] F. Babiloni, C. Babiloni, F. Carducci, et al., "Multimodal integration of high-resolution EEG and functional magnetic resonance imaging data: a simulation study," *NeuroImage*, vol. 19, no. 1, pp. 1–15, 2003.

[11] J. R. Wolpaw, N. Birbaumer, D. J. McFarland, G. Pfurtscheller, and T. M. Vaughan, "Brain-computer interfaces for communication and control," *Clinical Neurophysiology*, vol. 113, no. 6, pp. 767–791, 2002.

[12] P. R. Kennedy, R. A. E. Bakay, M. M. Moore, K. Adams, and J. Goldwaithe, "Direct control of a computer from the human central nervous system," *IEEE Transactions on Rehabilitation Engineering*, vol. 8, no. 2, pp. 198–202, 2000.

[13] D. M. Taylor, S. I. H. Tillery, and A. B. Schwartz, "Direct cortical control of 3D neuroprosthetic devices," *Science*, vol. 296, no. 5574, pp. 1829–1832, 2002.

[14] J. P. Donoghue, "Connecting cortex to machines: recent advances in brain interfaces," *Nature Neuroscience*, vol. 5, supplement, pp. 1085–1088, 2002.

Hindawi Publishing Corporation
Computational Intelligence and Neuroscience
Volume 2007, Article ID 39714, 9 pages
doi:10.1155/2007/39714

Research Article

An Algorithm for Idle-State Detection in Motor-Imagery-Based Brain-Computer Interface

Dan Zhang, Yijun Wang, Xiaorong Gao, Bo Hong, and Shangkai Gao

Department of Biomedical Engineering, School of Medicine, Tsinghua University, Beijing 100084, China

Correspondence should be addressed to Yijun Wang, wyj97@mails.tsinghua.edu.cn

Received 28 February 2007; Accepted 27 May 2007

Recommended by Andrzej Cichocki

For a robust brain-computer interface (BCI) system based on motor imagery (MI), it should be able to tell when the subject is not concentrating on MI tasks (the "idle state") so that real MI tasks could be extracted accurately. Moreover, because of the diversity of idle state, detecting idle state without training samples is as important as classifying MI tasks. In this paper, we propose an algorithm for solving this problem. A three-class classifier was constructed by combining two two-class classifiers, one specified for idle-state detection and the other for these two MI tasks. Common spatial subspace decomposition (CSSD) was used to extract the features of event-related desynchronization (ERD) in two motor imagery tasks. Then Fisher discriminant analysis (FDA) was employed in the design of two two-class classifiers for completion of detecting each task, respectively. The algorithm successfully provided a way to solve the problem of "idle-state detection without training samples." The algorithm was applied to the dataset IVc from BCI competition III. A final result with mean square error of 0.30 was obtained on the testing set. This is the winning algorithm in BCI competition III. In addition, the algorithm was also validated by applying to the EEG data of an MI experiment including "idle" task.

1. INTRODUCTION

People who suffer from severe motor disabilities but are still cognitively intact, need an alternative method to interact with the environment. Over the past decades, the development of the technology called brain-computer interface (BCI) has provided a novel and promising communication channel for these patients. A BCI is a communication system in which messages or commands that an individual wishes to convey to the external world do not pass through the brain's normal motor output pathways [1]. A BCI system can "read out" the intention of the patients and translates it into physical commands which control devices that serve the patients.

There are various BCI systems using different methods to extract the subjects' intentions from their EEG signals. One of the practical BCI systems is based on motor imagery (MI) [2, 3]. The advantage of this type of BCI systems is that no external stimulation is needed. Current development of MI-based BCI is focused on how to discriminate different MI tasks and many algorithms could be applied to get satisfied results. However, during practical use of BCI system, users may stay free of MI tasks (i.e., "idle state") at all. In order to make the system robust, the BCI system should be able to effectively detect the "idle state" and act properly. Moreover, because idle state may refer to various brain activities except the specific MI tasks, so it is not possible to acquire representative training samples for classifier designing. Therefore, to develop a new algorithm which cannot only discriminate different MI tasks but also effectively detect the idle state without any training samples is critical for improving present MI-based BCI system.

In this paper, an algorithm which integrates two two-class classifiers with different parameters into one three-class classifier is proposed to overcome the difficulties mentioned above. The algorithm was applied to dataset IVc of BCI competition III. A final result with mean square error of 0.30 was obtained. In addition, an EEG experiment was carried out with similar setting as the one for the dataset of BCI competition III; the results showed the effectiveness of the proposed algorithm.

2. METHODOLOGY

2.1. Data description

2.1.1. Dataset IVc of BCI competition III

BCI competitions are organized in order to foster the development of improved BCI technology by providing an unbiased validation of a variety of data-analysis techniques. The datasets of brain signals recorded during BCI experiments were from leading laboratories in BCI technology. Each data set is split into two parts: one part of labeled data ("training set") and another part of unlabeled data ("test set"). Researchers worldwide could tune their methods to the training data and submit the output of their translation algorithms for the test data.

Dataset IVc of BCI competition III was recorded from one healthy subject. The training dataset consisted of 3 sessions (70 trials for each session). Visual cues (letter presentation) indicated for 3.5 seconds which of the following 2 motor imageries the subject should perform: *left hand*, *right foot*. The presentations of target cues were intermitted by periods of random length, 1.75 to 2.25 seconds, in which the subject could relax. The testing data (6 sessions, 70 trials each) was recorded more than 3 hours after the training data. The experimental setup was similar to the training sessions, but the motor imagery had to be performed for 1 second only, compared to 3.5 seconds in the training sessions. The intermitting periods ranged from 1.75 to 2.25 seconds as before. The other difference was that a new task *relax* was added (also with visual cues as indications). The subject was required not to perform any MI tasks during *relax* task. 118-channel EEG signals were recorded during the experiment with sampling rate of 1000 Hz (see [4] for more details).

Competitors of this data set were required to classify a set of single-trial electroencephalograph (EEG) data recorded from three-class tasks in the testing set. The output of the classification must be a real number between -1 and 1 (ideally, -1 for *left hand*, 0 for *relax,* and 1 for *right foot*). The challenge was that the training set consists of only two-class data (*left hand* and *right foot*). One problem existed for the classification is that the testing set contains a new class *relax* with no training data. And there are two other problems: (1) the MI tasks in the testing set were performed for only 1 second instead of 3.5 seconds as in the training set; (2) the testing data was recorded more than 3 hours after the training data was acquired, so the distribution of some EEG features could be effected by long-term nonstationarities. All of these are practical problems in current MI-based BCI systems. The main difficulty is detecting an additional state *relax* without training samples, which is the same as "idle state" we mentioned in the previous section.

2.1.2. Datasets from our MI experiments

The data set provided by BCI competition III was acquired from only one subject and the details of the experiment were not so clear. In order to thoroughly investigate the effectiveness of our algorithm, an MI experiment was carried out with a similar paradigm.

Three right-handed volunteers (two females and one male, 22 to 24 years old) participated in this experiment. There were three kinds of tasks in the experiment: *left hand*, *right hand*, and *relax*. *Left hand* and *right hand* referred to two MI tasks; while the subject was required not to perform any MI tasks during *relax* period. The subject was informed about which task to be performed by a visual cue on a PC screen before each trial. The trials lasted for 4 seconds with intermitting period of 2 seconds. 32-channel EEG (ActiveTwo system, BioSemi Instrumentation, Netherland) was recorded at the scalp over the motor cortex areas with a sampling rate of 256 Hz. For every subject, 50 trials for each task were collected.

Compared to the data set of BCI competition III, "*relax* with no training data" was emphasized while the other issues were ignored: the tasks were performed for 4 seconds instead of 3.5 seconds/1 second and all trials were performed continuously. The purpose of increasing trial time was to improve the performance because it was difficult to get satisfied results for normal subjects in such a short time as 1 second. And long-term nonstationarities were not concerned here for the complexities and characteristics of MI tasks.

2.2. Feature selection

Motor imagery can be seen as mental rehearsal of a motor act without any obvious motor output [2]. It is broadly accepted that mental imagination of movements involves similar EEG patterns that are also found in real movements. The main difference between real movements and MI is that execution would be blocked at some corticospinal level in the latter case [3]. Recent studies show that when performing motor imagination, mu (8–12 Hz) and beta (18–26 Hz) rhythms are found to reveal event-related synchronization and desynchronization (ERS/ERD) over sensorimotor cortex just like when one actually does the motor tasks [5].

Event-related desynchronization (ERD) represents power decrease in given frequency bands of the ongoing EEG activity [5]. Preparation of movement is typically accompanied by ERD in mu and beta rhythms over somatosensory or motor cortex. Figure 1 displays the averaged ERD spatial mappings of the two MI tasks in the training set. We use the ratio of power decrease in the imagery state and the power in the rest state as the quantification of ERD [5]. The brain regions containing significant ERD over motor cortex are marked as A1 and A2 in Figure 1. The ERD of *right-foot* imagery exists in the central area (A2) while the ERD of *left hand* is localized in both hemispheres (A1) with contralateral dominance. This difference is the basis for classifying *left-hand* and *right-foot* imageries.

The mental state of *relax* differs substantially from those of *left hand* and *right foot* since no brain activity patterns similar with MI is evoked. It is reasonable to assume that during a *relax* task there is no obvious ERD over somatosensory or motor cortex. So *relax* status can be distinguished from *left hand* and *right foot*. *Left hand* can be recognized by existence

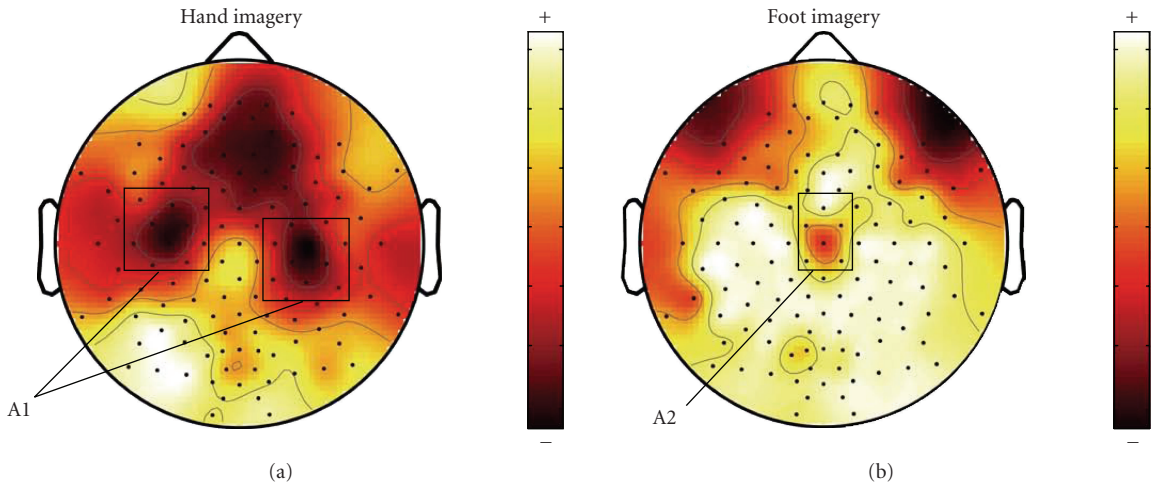

Figure 1: Averaged ERD spatial mappings of (a) *left hand* and (b) *right foot* in the training set.

of ERD in A1 area and *right-foot* is corresponding to the brain state with ERD in A2 area, while *relax* is just the brain state with no ERD in either A1 or A2 areas.

2.3. Feature extraction

The signals specific to the tasks are usually accompanied by interferences (such as noise, spontaneous EEG and other nontask activities). The common spatial subspace decomposition (CSSD) proposed by Wang et al. [6] was employed to extract the task-related source activities and to eliminate the background activities. The purpose of this method is to construct spatial filters which can distinguish two classes of signals based on simultaneous diagonalization of their covariance matrices [7].

In our method, we selected 37 EEG channels according to ERD distribution (see Figure 1), so only brain regions A1 and A2 are taken into consideration. Then we used the selected single-trial EEG data as the input matrix X with 37 (channels) by 280 (samples, 0.71–3.50 seconds) to construct spatial filters SF_H and SF_F for *left hand* and *right foot*, respectively. The spatial covariance of the EEG data can be obtained from

$$C = X \cdot X^T. \tag{1}$$

The spatial covariance of each class is calculated as C_H and C_F by averaging over the trials in the corresponding class. The sum covariance matrix C_{Sum} is factorized into the product of eigenvectors and eigenvalues

$$C_{\mathrm{Sum}} = C_F + C_H = U_0 \cdot \Sigma \cdot U_0^T. \tag{2}$$

The eigenvalues are assumed to be sorted in descending order. The whitening transformation matrix is then formed as

$$P = \Sigma^{-1/2} \cdot U_0^T. \tag{3}$$

If C_H and C_F are transformed as

$$SC_F = P \cdot C_F \cdot P^T, \qquad SC_H = P \cdot C_H \cdot P^T, \tag{4}$$

then C_H and C_F share common eigenvectors and the sum of the corresponding eigenvalues for the two matrices will always be 1, that is,

$$SC_F = U \cdot \Sigma_F \cdot U^T, \quad SC_H = U \cdot \Sigma_H \cdot U^T, \quad \Sigma_F + \Sigma_H = I. \tag{5}$$

As the sum of two corresponding eigenvalues is always one, the eigenvector with largest eigenvalue for S_F has the smallest eigenvalue for S_H. This transformation is an effective way for separating variances in the two matrices C_H and C_F. Taking out the first m_F eigenvectors from U as U_F and the last m_H eigenvectors from U as U_H, the spatial filters for class F and class H are

$$\mathrm{SF}_F = (U_F)^T \cdot P, \qquad \mathrm{SF}_H = (U_H)^T \cdot P. \tag{6}$$

The eigenvectors left in U correspond to the common spatial subspace of the two classes. The task-related components S_H and S_F are estimated by

$$S_F = \mathrm{SF}_F \cdot X, \qquad S_H = \mathrm{SF}_H \cdot X. \tag{7}$$

X is a recorded data matrix of multichannel single-trial EEG. The columns of $\mathrm{SF}_F^{-1}/\mathrm{SF}_H^{-1}$ are spatial patterns corresponding to *right-foot*/*left-hand* components as time-invariant EEG source distribution vectors [8].

The features used for classification are obtained by decomposing the EEG using SF_F and SF_H. The feature vectors of one single trial are defined as

$$\begin{aligned} f_{H,i} &= \log\left(\mathrm{var}\left(S_{H,i}\right)\right), \quad i = 1, \ldots, m_H, \\ f_{F,i} &= \log\left(\mathrm{var}\left(S_{F,i}\right)\right), \quad i = 1, \ldots, m_F. \end{aligned} \tag{8}$$

$S_{H,i}/S_{F,i}$ represents the ith row vector of S_H/S_F. The log-transformation serves to approximate normal distribution of the data. Our experiences on the training set indicated that setting $m_F = 3$ and $m_H = 3$ was enough to get a fairly good performance.

During *left-hand* imagery, ERD occurs in region A1, leading to a relatively decreased EEG variance in this area. Therefore, *right foot* has a higher EEG variance than *left hand* in region A1. This behavior is reflected by large coefficients for channels covering region A1 in the spatial pattern corresponding to *right-foot* imagery. Figure 2 displays the most important spatial pattern of the two tasks. As shown in Figure 2(b), the most important spatial pattern of *right foot* accords with the ERD distribution of *left hand*. The spatial filter SF_F serves as extracting the component with a source distribution like the corresponding spatial pattern. Therefore, the component extracted by SF_F can be considered as the source activity concerning *left-hand* ERD, which has a significant distribution over region A1. A weak source activity leads to a small variance of relative scalp EEG, which is corresponding to significant ERD. Due to no ERD in region A1, the component of *right foot* has a larger variance than that of *left hand* when filtered by SF_F, that is,

$$\mathrm{var}\left(\mathrm{SF}_F \cdot X_F\right) > \mathrm{var}\left(\mathrm{SF}_F \cdot X_H\right), \tag{9}$$

where X_H and X_F are single-trial EEG corresponding to *left hand* and *right foot*, respectively. We can also get another inequality as follows:

$$\mathrm{var}\left(\mathrm{SF}_H \cdot X_H\right) > \mathrm{var}\left(\mathrm{SF}_H \cdot X_F\right). \tag{10}$$

Note that according to the above definitions, *left-hand* MI causes a relatively increased EEG variance over area A2 (corresponding to *right-foot* task) because event-related desynchronization of EEG takes place on area A1. This behavior is reflected in large coefficients for electrodes on area A2 in the spatial filter of *left-hand* (SF_H) [8], and vice versa for *right foot*.

2.4. Classification method

The paper of Garrett et al. [9] showed that if features were properly extracted, the performance of linear classifiers can behave as well as that of complex nonlinear classifiers, so we simply used Fisher discriminant analysis (FDA) in our method.

After using CSSD to extract ERD feature out of the training set, FDA was applied for classification and an accuracy of $(99.1 \pm 1.2)\%$ was obtained on the training set using a 10×10-fold cross-validation. The result of FDA proves that there is no need to use other complicated methods.

2.5. Classification on the testing set

Denote X_R as a single-trial EEG of *relax*, as no ERD occurs in both regions A1 and A2 during *relax* tasks, the following inequalities come into existence:

$$\mathrm{var}\left(\mathrm{SF}_F \cdot X_R\right) > \mathrm{var}\left(\mathrm{SF}_F \cdot X_H\right), \tag{11}$$

$$\mathrm{var}\left(\mathrm{SF}_H \cdot X_R\right) > \mathrm{var}\left(\mathrm{SF}_H \cdot X_F\right). \tag{12}$$

Both components of *relax* and *right foot* are larger than that of *left hand* when filtered by SF_F, so *left-hand* motor imageries can be discriminated from *right-foot*/*relax*. Similarly, *right foot* can be discriminated from *left-hand*/*relax* when filtered by SF_H.

The required classification outputs of *left hand* and *right foot* are defined as -1 and $+1$. If we do a two-class classification based on the feature vectors f_H extracted by SF_H and set the classification outputs of *left hand* and *right foot* to -1 and $+1$ as required, then samples of *relax* are also classified to -1 as it is the same as *left hand* according to (9) and (11). Samples of *relax* are classified to $+1$ according to (10) and (12). Table 1 shows the different outputs of the three tasks in ideal conditions. Column "f_F" and "f_H" shows the two two-class classification results. Column "$(f_F + f_H)/2$" represents the mean value of two outputs corresponding to f_F and f_H in the same row. Ideally, the two classifiers corresponding to "f_F" and "f_H" will result in opposite outputs for *relax* $(+1/-1)$ and the final classification result of *relax* can be set to 0 easily by "$(f_F + f_H)/2$." Therefore, it is possible to separate the three classes.

Our strategy goes as following: at first, a two-class classifier was used to classify samples of *relax* to output 0 (see Table 1). Then the second two-class classifier was defined to classify the remaining samples into either *right foot* or *left hand*. The whole procedure of the classification algorithm is shown in Figure 3.

Step 1 (Discriminating the relax trials). The classification process of this step is showed in Figure 4. A subject-specific bandpass filter of 12–14 Hz (with most significant ERD feature for the subject of dataset IVc) and a time window of 0.71–3.50 seconds (eliminating the first 0.7 seconds as reaction time) were set for CSSD algorithm to calculate two spatial filters SF_{F1} and SF_{H1} from the training data. Because the duration of each trial in the testing set is much shorter than that of the training set, CSSD filter cannot get enough information with such a short time window to keep a high accuracy. Here we bring forward another assumption that the spatial pattern in the intermitted time (1.75–2.25 seconds) after a *relax* trial is similar to that of the *relax* trial (however, the intermitted time after an MI task cannot be simply considered as *relax* because the subject might keep on doing MI for a certain period even after he saw the cue for stop). With this assumption, a time window of 2.75 seconds (1 second for the task and at least 1.75 seconds for intermitted time) was selected as the input of the CSSD filters for the testing set. The effective duration of *relax* can thus be prolonged, making the classification results more reliable than those obtained by only using a short-time window.

Bagging strategy [10] was used here for reducing variance of classification accuracy. 160 trials were randomly selected

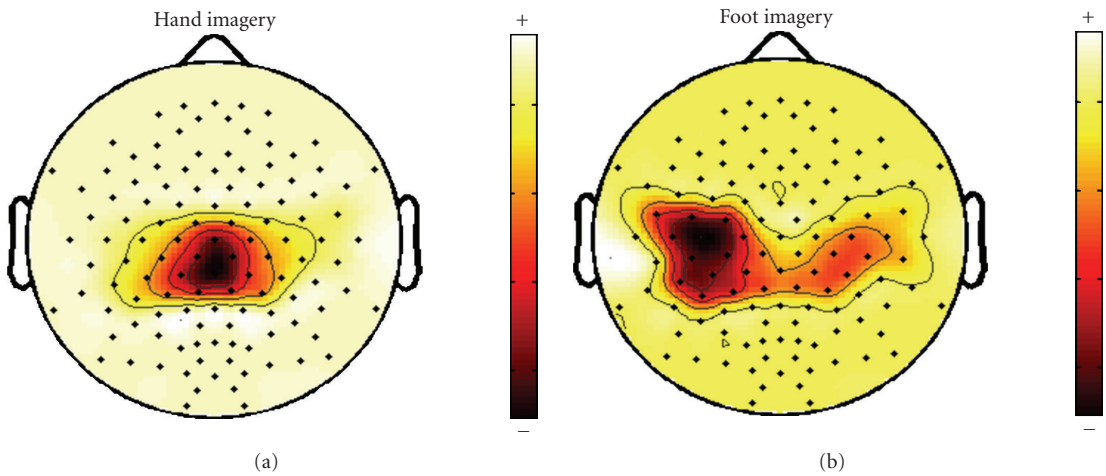

Figure 2: Most important spatial pattern of (a) *left hand* and (b) *right foot*.

Table 1: Ideal classification results of the three tasks.

Feature task	f_F	f_H	$(f_F + f_H)/2$
Left hand	−1 (ERD in A1)	−1 (no ERD in A2)	−1 (−1/ − 1)
Right foot	+1 (no ERD in A1)	+1 (ERD in A2)	+1 (+1/ + 1)
Relax	+1 (no ERD in A1)	−1 (no ERD in A2)	0 (+1/ − 1)

"$(f_F + f_H)/2$" represents the mean value of two outputs corresponding to f_F and f_H in the same row.

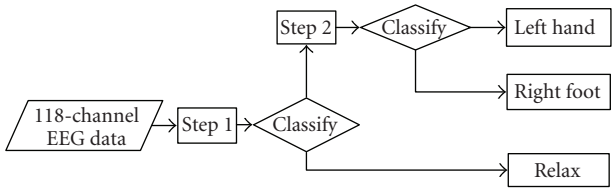

Figure 3: Flow chart of our algorithm.

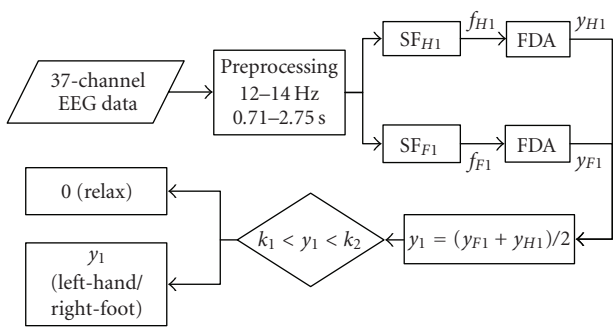

Figure 4: Classification process of Step 1.

out of all 210 trials in the training set to derive a classifier which was applied on each trial in the testing set. This process was repeated for 100 times, of which the classification outputs were averaged to get the final result. As shown in Figure 4 there are two FDA classifiers following two spatial filters SF$_{F1}$ and SF$_{H1}$. The outputs of these two classifiers (y_{F1} and y_{H1}) were normalized to real number between −1 and 1 and were averaged to get a higher classification accuracy [11]. In Step 1 the averaging also has an effect of setting *relax* to 0.

After classification, two thresholds (upper boundary above 0 and lower boundary below 0) were determined manually, according to the distribution of training samples. The samples with classification outputs near 0 were labeled as *relax*. The remaining samples are left unlabeled to be fed as the input of Step 2. The process is shown as following where k_1 and k_2 denote the two thresholds:

$$z = \begin{cases} 0, & \text{if } k_1 < y_1 < k_2, \\ y_1, & \text{if } y_1 < k_1 \text{ or } y_1 > k_2. \end{cases} \quad (13)$$

In our algorithm, we propose these two thresholds could be chosen to make P_1 (in percentage) of the trials of MI tasks with nonzero classification output. (P_1 was set to 70% for the results submitted to dataset IVc based on our former experiences)

Step 2 (Discriminating the remaining trials). Step 1 is good for picking out *relax* but not optimal for classifying *left hand* and *right foot* because the intermitted time has been taken into consideration. During the intermitted time after *left hand* and *right foot*, the subject is told to "*relax*." So a short time window (0.61–1.20 seconds) was defined as for this step. Besides, our investigation showed that a widepass band for

temporal filtering (11–27 Hz) was better for classifying *left hand* and *right foot*. This wider frequency band including both mu and beta band is also good for generalization. The same time window as in Step 1 (0.71–3.50 seconds) was applied to calculate SF_{F2} and SF_{H2} with the training set.

The classification process of this step is shown in Figure 5. After classification we also set two thresholds manually to label samples with outputs congregating near -1 and 1 to *right hand* and *left foot*, respectively, and the others to a real number between -1 and 1. The normalization process is as follows, where y is the original output and z is the normalized output, k_3 and k_4 denote the two thresholds:

$$z = \begin{cases} -1, & \text{if } y_2 < k_3, \\ -\dfrac{y_2}{k_3}, & \text{if } k_3 \le y_2 \le 0, \\ \dfrac{y_2}{k_4}, & \text{if } 0 \le y_2 \le k_4, \\ 1, & \text{if } y_2 > k_4. \end{cases} \tag{14}$$

In our algorithm, we propose these two thresholds could be selected to make P_2 (in percentage) of trials of MI tasks with classification outputs of ± 1. (P_2 was set to 70% for the results submitted to Data Set IVc).

For the data from our MI experiments, a time window of 0.5–4 seconds was applied to calculate spatial filters for both Steps 1 and 2. The frequency band used in Step 1 was subject-specific and 11–27 Hz were chosen in Step 2. Half samples of MI tasks (25 trials for *left hand*, 25 trials for *right hand*) were employed in the training set while the rest were used as the testing set. By randomly selecting trials for training, the classification process was repeated for 50 times to get average results. Features were extracted from both task and intermitting periods (6 seconds) in Step 1 while only task periods were considered in Step 2. Furthermore, we investigated how to choose threshold $k_1 - k_4$ to get a better performance (refer to Section 3 for details).

3. RESULTS

The result of dataset IVc was evaluated by mean square error criterion. Defining the true labels for 420 trials in the testing set as $y_1, y_2 \cdots y_{420}$, and the classification outputs as $z_1, z_2 \cdots z_{420}$, the mean square error (MSE) was calculated as

$$\text{MSE} = \frac{1}{420} \sum_{i=1}^{420} (y_i - z_i)^2. \tag{15}$$

As the winning algorithm in BCI competition III, a mean square error of 0.30 was achieved by our algorithm, which was much lower than the result of the second best competitor, who achieved 0.59 [12]. Figure 6 shows the distribution of the classification results of the three classes. Approximately 60% samples of true *left hand* and *right foot* are correctly classified to -1 and 1, and about 40% of *relax* samples are classified to 0. The particular strength of this method was that it managed to identify nearly half of the *relax* trials and none of the other submissions to this dataset handled the idle state well even if they discriminate the two MI tasks as well as our algorithm [12]. This could be the evidence that traditional algorithms are not so effective for classifying idle state. The results proved the effectiveness of this algorithm.

MSE is a specific performance measure used in BCI competition III. Two other measures with more direct meaning are defined as below.

(a) *Probability of detection (POD)*

For a certain task A, considering all trials of task A, let N_D denote the number of trials correctly detected as task A, N_M the number of trials missed, then POD is defined as

$$\text{POD} = \frac{N_D}{N_D + N_M}. \tag{16}$$

POD represents the true positive rate of certain brain states. Two values were calculated based on POD: POD of MI tasks and POD of idle states (*relax* task). For POD of MI tasks, we only care if MI tasks could be discriminated from idle states. Whether MI tasks were classified correctly is another issue. For a practical BCI system, the POD of idle states is critical because false alarms during idle states may lead to unexpected action of the BCI system when the subjects are resting or idling.

(b) *Classification accuracy (CA)*

For a certain MI task A, considering all trials of task A, let N_C denote the number of trials correctly classified as task A, N_W the number of trials classified as other MI tasks, then CA is defined as

$$\text{CA} = \frac{N_C}{N_C + N_W}. \tag{17}$$

According to this definition, the number of trials classified as idle states is not included in (17). It is easy to understand: failure of detection will not lead to execution of improper commands; only the average time for carrying out one command will be lengthened. From this point of view, the POD of MI tasks together with CA decides the speed of the synchronized BCI system. The mean CA value of both MI tasks was calculated as the average CA.

Referring to our proposed criterion for selecting thresholds, $k_1 - k_4$ were decided by P_1 and P_2. Varying these two probabilities leads to changes of the performance measures defined above. Ideally, a BCI system with good performance is associated with CA, POD of MI tasks and idle states close to 100%. Therefore, P_1 and P_2 should be chosen carefully to make the real BCI system with a good performance.

To simplify this problem, we make both P_1 and P_2 equal to a certain value P. Table 2 listed the results calculated by increasing P from 0.6 to 1 in step of .05 for subject FL. The values of CA and POD_{Idle} are negative correlated with P, while POD_{MI} is positive correlated with P. The basic principle for choosing P value is to reduce false alarm during idle states (i.e., increase POD_{Idle}) while keeping POD_{MI} and CA at an

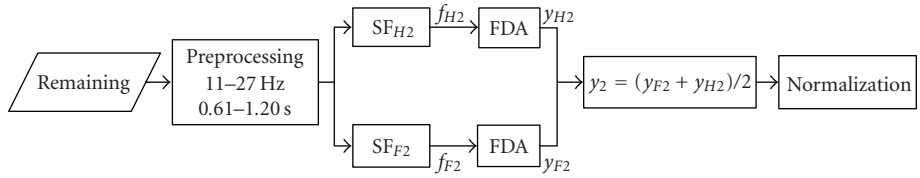

Figure 5: Classification process of Step 2.

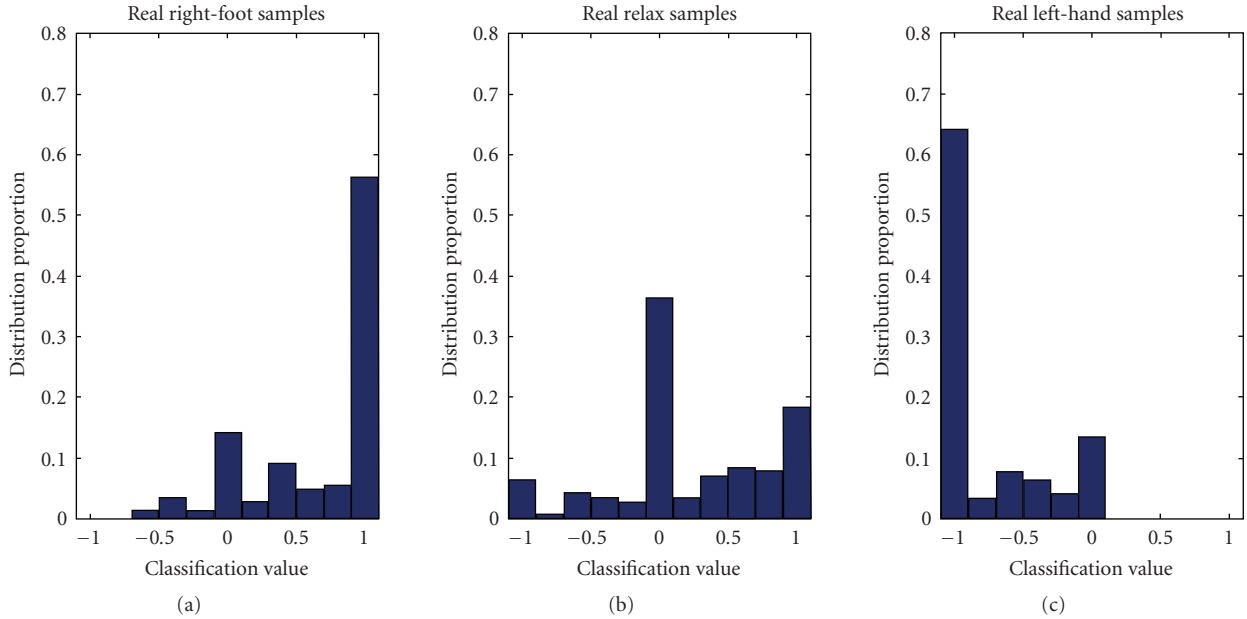

Figure 6: Distribution of classification results with respect to the three true labels.

acceptable level. The optimal P value for subject FL is manually selected as 70% with high CA and POD_{Idle} as well as a relatively high POD_{MI} (see Table 2). In the same way, the optimal P values for the other two subjects are chosen as 80% (ZD) and 90% (ZYJ); the corresponding results are shown in Table 3. The data of all three subjects achieved nearly 100% CA for discriminating the two MI tasks, with average POD_{MI} about 70% and average POD_{Idle} above 90%.

4. CONCLUSIONS AND DISCUSSION

The most important characteristic of our algorithm was combining two two-class classifiers to construct a three-class classifier. We broke down the problem into two steps and solved them consecutively with parameters separately optimized in each step for its own purpose. The analysis of the final result validated this strategy.

The basic assumption was that during *relax* task there is no obvious ERD over somatosensory or motor cortex. This assumption is shown to be reasonable according to the final results. Figure 7 displays the averaged spatial mapping of *relax* (calculated in a same way as in Figure 1) in the testing set. There is no obvious ERD in region A1 and A2. Figure 8 shows the classification results of the samples in the testing set by these two classifiers and the true labels are given by different legends. Most samples of *relax* are located in the second quadrant, while *right-foot* and *left-hand* samples are in the first and third quadrants. This distribution is in accordance with the analysis in Table 1.

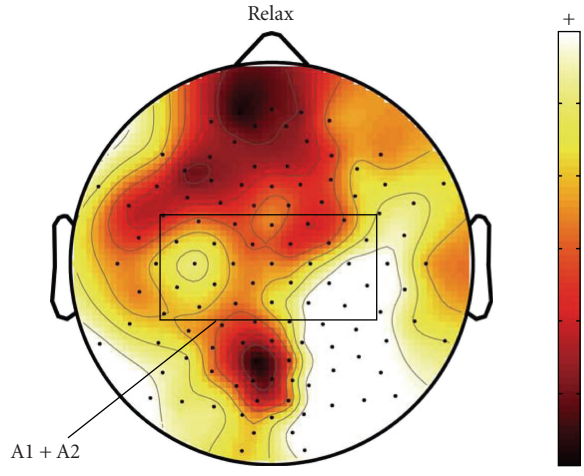

Figure 7: Averaged spatial mapping of *relax* (calculated in a same way as in Figure 1) in the testing set.

In Section 2.1 we listed three problems in dataset IVc, our algorithm addressed the problem of no training data for *re-*

Table 2: Performance measures of subject FL corresponding to different P values.

$P(P_1\&P_2)$	$\mathbf{POD_{MI}}$	$\mathbf{POD_{Idle}}$	CA
100%	100.0 ± 0.0%	0.0 ± 0.0%	89.0 ± 2.3%
95%	96.1 ± 1.8%	4.2 ± 1.2%	94.9 ± 1.8%
90%	90.0 ± 1.6%	61.2 ± 2.1%	96.8 ± 1.1%
85%	84.2 ± 2.3%	71.0 ± 3.2%	97.2 ± 2.5%
80%	74.1 ± 1.9%	81.4 ± 1.8%	96.6 ± 2.1%
75%	65.3 ± 2.2%	91.0 ± 1.6%	97.6 ± 1.4%
70%	62.7 ± 3.2%	95.5 ± 0.9%	98.9 ± 0.8%
65%	51.8 ± 2.0%	98.1 ± 2.2%	98.7 ± 1.0%
60%	45.1 ± 1.6%	99.6 ± 0.9%	99.3 ± 1.2%

Table 3: Performance measures of three subjects with the optimal P values.

Subject	Optimal P	$\mathbf{POD_{MI}}$	$\mathbf{POD_{Idle}}$	CA
ZYJ	90%	78.2 ± 1.7%	90.2 ± 1.3%	98.3 ± 1.2%
FL	70%	62.7 ± 3.2%	95.5 ± 0.9%	98.9 ± 0.8%
ZD	80%	61.2 ± 2.2%	96.1 ± 1.1%	99.4 ± 0.4%

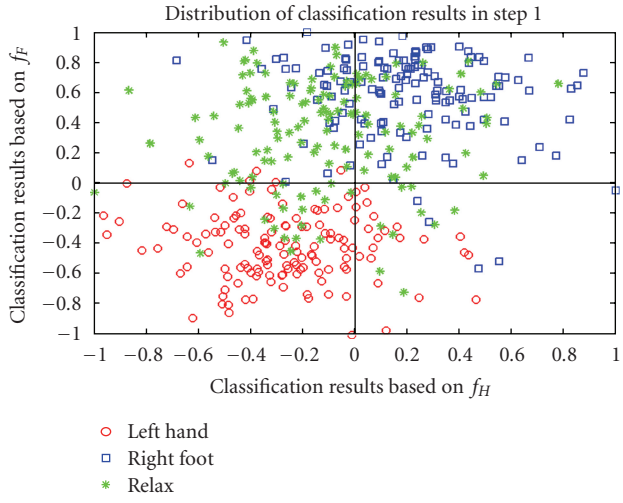

Figure 8: Distribution of classification results in Step 1.

lax. The other two problems may lead to nonsignificant interference with the application of CSSD algorithm, which is essentially determined by the spatial patterns of different MI tasks.

The problems of shortened trial time and long-term nonstationarities seem to be not so critical here because the two MI tasks still can be discriminated well (see Figure 6). One possible reason is because this data set is from a very good subject (classification accuracy on training set is around 99%). For subjects with ordinary performance, the results might be worse. However, most subjects could achieve better performances after a certain period of training.

Another issue worth mentioning is the difference between *relax* and idle states. *Relax* might be slightly different from idle states, which are always referred to a quite long period with no MI going on rather than 1-second trials in these testing sessions. The brain states during *relax* trials in the testing sessions could be better described as "noncontrol" or "non-MI" states. In our algorithm, *relax* trials are only considered as brain states quite different from MI trials and no information were retrieved from these trials for designing the algorithm. From this point of view, we consider them as equal terms in this paper.

The traditional ways of idle-state detection mainly focus on developing powerful and robust algorithm mathematically. Our strategy aims at building a practical BCI system. In our opinion, how to integrate these methods in an effective way is also very important. Because the nature of idle states is quite different from those MI states, it is worth to set up an additional step with optimal parameters for separating these *relax* trials from the rest trials.

The proposed algorithm achieved satisfied results on our MI datasets. It shows the effectiveness of our algorithm for practical BCI systems. This result is also much better than dataset IVc of BCI competition III. The main reason might be due to the lengthened trial time, which is important for the subjects' performance.

The probabilities (P_1 and P_2), which decide the thresholds $k_1 - k_4$, are crucial to the performance of our algorithm. For dataset IVc, we simply select 70% for both P_1 and P_2 based on our former experiences. These P values could be carefully chosen to make the performance better based on the three indexes ($\mathrm{POD_{MI}}$, $\mathrm{POD_{Idle}}$, CA) defined above. Decreasing P value will lead to higher $\mathrm{POD_{Idle}}$ but lower $\mathrm{POD_{MI}}$, which is the key factor for the speed of the synchronized BCI system. Also higher CA will be achieved because more ambiguous MI trials are labeled *relax*. Our current strategy is to insure a high $\mathrm{POD_{Idle}}$ (i.e., above 90%) first, and then make $\mathrm{POD_{MI}}$ and CA as high as possible. We have not established an automatic way to make a balance between $\mathrm{POD_{MI}}$ and $\mathrm{POD_{Idle}}$ yet. These results might be further improved by selecting optimal thresholds $k_1 - k_4$ based on advanced statistical theories.

A BCI system that can distinguish patterns not included in training data is very attractive. Solving the problem of dataset IVc is a good step towards this target. The proposed algorithm is especially useful to reduce the false alarms in current BCI system based on MI when the subjects are not performing MI tasks. Although we perform offline analysis here, this algorithm could be easily moved to online system.

ACKNOWLEDGMENTS

This project is supported by National Natural Science Foundation of China (no. 60318001, 30630022), and Tsinghua-Yuyuan Medicine Research fund. We are grateful to Klaus-Robert Müller, Benjamin Blankertz, and Gabriel Curio for providing the dataset. Also, we would like to extend our special thanks to Prof. Fusheng Yang for a very informative discussion and his valuable comments.

REFERENCES

[1] J. R. Wolpaw, N. Birbaumer, D. J. McFarland, G. Pfurtscheller, and T. M. Vaughan, "Brain-computer interfaces for communication and control," *Clinical Neurophysiology*, vol. 113, no. 6, pp. 767–791, 2002.

[2] G. Pfurtscheller and C. Neuper, "Motor imagery and direct brain-computer communication," *Proceedings of the IEEE*, vol. 89, no. 7, pp. 1123–1134, 2001.

[3] M. Jeannerod, "Mental imagery in the motor context," *Neuropsychologia*, vol. 33, no. 11, pp. 1419–1432, 1995.

[4] http://ida.first.fraunhofer.de/projects/bci/competition_iii/desc_IVc.html.

[5] G. Pfurtscheller and F. H. Lopes da Silva, "Event-related EEG/MEG synchronization and desynchronization: basic principles," *Clinical Neurophysiology*, vol. 110, no. 11, pp. 1842–1857, 1999.

[6] Y. Wang, P. Berg, and M. Scherg, "Common spatial subspace decomposition applied to analysis of brain responses under multiple task conditions: a simulation study," *Clinical Neurophysiology*, vol. 110, no. 4, pp. 604–614, 1999.

[7] Y. Wang, Z. Zhang, Y. Li, X. Gao, S. Gao, and F. Yang, "BCI competition 2003—data set IV: an algorithm based on CSSD and FDA for classifying single-trial EEG," *IEEE Transactions on Biomedical Engineering*, vol. 51, no. 6, pp. 1081–1086, 2004.

[8] H. Ramoser, J. Müller-Gerking, and G. Pfurtscheller, "Optimal spatial filtering of single trial EEG during imagined hand movement," *IEEE Transactions on Rehabilitation Engineering*, vol. 8, no. 4, pp. 441–446, 2000.

[9] D. Garrett, D. A. Peterson, C. W. Anderson, and M. H. Thaut, "Comparison of linear, nonlinear, and feature selection methods for EEG signal classification," *IEEE Transactions on Neural Systems and Rehabilitation Engineering*, vol. 11, no. 2, pp. 141–144, 2003.

[10] L. Breiman, "Bagging predictors," *Machine Learning*, vol. 24, no. 2, pp. 123–140, 1996.

[11] G. Dornhege, B. Blankertz, G. Curio, and K.-R. Müller, "Boosting bit rates in noninvasive EEG single-trial classifications by feature combination and multiclass paradigms," *IEEE Transactions on Biomedical Engineering*, vol. 51, no. 6, pp. 993–1002, 2004.

[12] B. Blankertz, K.-R. Müller, D. J. Krusienski, et al., "The BCI competition III: validating alternative approaches to actual BCI problems," *IEEE Transactions on Neural Systems and Rehabilitation Engineering*, vol. 14, no. 2, pp. 153–159, 2006.

Hindawi Publishing Corporation
Computational Intelligence and Neuroscience
Volume 2007, Article ID 48937, 12 pages
doi:10.1155/2007/48937

Research Article

Vibrotactile Feedback for Brain-Computer Interface Operation

Febo Cincotti,[1] Laura Kauhanen,[2] Fabio Aloise,[1] Tapio Palomäki,[2] Nicholas Caporusso,[1,3] Pasi Jylänki,[2] Donatella Mattia,[1] Fabio Babiloni,[1,4] Gerolf Vanacker,[5] Marnix Nuttin,[5] Maria Grazia Marciani,[1,6] and José del R. Millán[7,8]

[1] *Laboratory of Neuroelectrical Imaging and Brain Computer Interface, Fondazione Santa Lucia IRCCS, Via Ardeatina 306, 00179 Roma, Italy*
[2] *Laboratory of Computational Engineering, Helsinki University of Technology, P.O. Box 9203, 02015 TKK, Finland*
[3] *Department of Computer Science, University of Bari, Via Orabona 4, 70125 Bari, Italy*
[4] *Dipartimento di Fisiologia Umana e Farmacologia, Università degli Studi di Roma "La Sapienza", Piazzale Aldo Moro 5, 00185 Roma, Italy*
[5] *Department of Mechanical Engineering, Katholieke Universiteit Leuven, Celestijnenlaan 300 B, 3000 Leuven, Belgium*
[6] *Dipartimento di Neuroscienze, Università degli Studi di Roma "Tor Vergata", Via Montpellier 1, 00173 Roma, Italy*
[7] *IDIAP Research Institute, 1920 Martigny, Switzerland*
[8] *Ecole Polytechnique Fédérale de Lausanne (EPFL), 1015 Lausanne, Switzerland*

Correspondence should be addressed to Febo Cincotti, f.cincotti@hsantalucia.it

Received 18 February 2007; Accepted 26 June 2007

Recommended by Andrzej Cichocki

To be correctly mastered, brain-computer interfaces (BCIs) need an uninterrupted flow of feedback to the user. This feedback is usually delivered through the visual channel. Our aim was to explore the benefits of vibrotactile feedback during users' training and control of EEG-based BCI applications. A protocol for delivering vibrotactile feedback, including specific hardware and software arrangements, was specified. In three studies with 33 subjects (including 3 with spinal cord injury), we compared vibrotactile and visual feedback, addressing: (I) the feasibility of subjects' training to master their EEG rhythms using tactile feedback; (II) the compatibility of this form of feedback in presence of a visual distracter; (III) the performance in presence of a complex visual task on the same (visual) or different (tactile) sensory channel. The stimulation protocol we developed supports a general usage of the tactors; preliminary experimentations. All studies indicated that the vibrotactile channel can function as a valuable feedback modality with reliability comparable to the classical visual feedback. Advantages of using a vibrotactile feedback emerged when the visual channel was highly loaded by a complex task. In all experiments, vibrotactile feedback felt, after some training, more natural for both controls and SCI users.

1. INTRODUCTION

The human brain relies on inputs from different senses to form percepts of objects and events, during everyday life. These pieces of information usually complement and confirm each other, thereby enhancing the reliability of percept [1]. Somatosensory feedback is a vital component of motor planning, control, and adaptation, and there is a growing effort to include this feedback modality in neural prosthetic systems [2].

Visual presentation of stimuli is the most common feedback modality in neurofeedback paradigms for self-regulation of the brain's electrical activity. Thus, it is comprehensible that current brain-computer communication systems mainly operate with visual stimuli [3]. However, components of the visual system such as vision, visual attention, and focusing gaze are physiologically engaged during the dynamic contact between the body and environment. Furthermore, the visual sense may be compromised in some patients who are in need of BCI support. Thus, towards more efficient brain-computer communication, it seems important to also obtain evidence of how the extravision somatosensory modality performs during self-regulation of the brain's electrical activity.

Only few studies have tested other feedback modalities for brain-computer interfaces (BCIs). Hinterberger et al. [4] and Pham et al. [5, 6] tested auditory feedback, but, to our knowledge, no one has trained subjects with tactile feedback. Vibrotactile stimuli have been previously used [7, 8] for BCI operation in a different context, that is, as an external driving stimulus to elicit exogenous EEG rhythms.

In addition to freeing visual and auditory attention, tactile stimuli are more natural in a manipulation task than, for example, visual stimuli. Even though BCI training is strongly dependent on feedback, surprisingly, only two studies have explored how feedback affects the learning process. McFarland et al. [9] investigated what happens when feedback is removed from well-trained subjects and Neuper et al. [10] compared continuous and discrete feedback. No guidelines exist regarding somatosensory stimulation for BCIs.

This study aims to explore the benefits of vibrotactile feedback for user training and accurate control of an EEG-based brain-computer interface.

2. VIBROTACTILE STIMULATION

2.1. Physiological perception

Several receptors for the transduction of mechanical solicitation on the skin into neuronal signals are available in man: Merkel's receptors, which are slow adapting receptors with high spatial resolution; the Meissner's corpuscles, present in the glabrous skin (lips, finger), with characteristic of rapid adaptation and high spatial resolution; the Pacini's corpuscles which detect very rapid vibration and are quickly adapting. The somesthetic information travels from the receptors to the central nervous system using the fastest communication lines in the human body; the so-called dorsal-lateral column way, delivering information at a speed of over 100 m/s. This somesthetic system delivers very precise information of which two neighboring points on the human skin can be perceived as distinct. The spatial resolution of the skin has been tested since 1826 [11] using static pressure stimuli showing that it varies along the body, ranging from few millimeters (fingers) to more than four centimeters (trunk).

Vibrotactile devices delivering variable pressure on the skin have been employed as an alternative sensitive channel for blind or deaf individuals [12, 13]. The sensitivity for vibrotactile stimulation depends on body position and age of the subjects [14]. Frequency of vibration is a second parameter that influences the quality and intensity of perception, being modulated by factors like body position, skin temperature, and underlying tissue (bone, fat, muscle, or a combination). Values between 50 and 300 Hz should generally be chosen. The use of oscillating pressure also adds new degrees of freedom to the design of vibrotactile stimuli, such as waveform shape, for example, sinusoidal or square and amplitude modulations (at different modulation frequencies) of the carrier frequency.

In summary, several features of vibrotactile stimuli can be modulated to convey information over this sensory channel. The list can be divided into two subsets. The first includes features related to physical perception:

(1) *frequency*, the main spectral component of the periodic stimulus;
(2) *intensity*, the strength of stimulation (measured either as force applied or as displacement produced);
(3) *timbre*, the complexity of the stimulation waveform (i.e., the content of harmonics in the spectral representation);
(4) *duration*, the time length of the "on" time or an elementary stimulation;
(5) *spatial location*, the single body part or the pattern of parts that are stimulated.

Features in the second subset are clearly perceived by an individual, but do not rely on any property of the receptors (e.g., need to be interpreted on a cognitive level):

(1) *rhythm*, the sequences of stimulation and pauses, with specific durations, that compose the current message, that is, a triplet of stimuli, a Morse coded SOS, and so forth;
(2) *tempo*, the fastness, due to longer or shorter duration of the whole message, given at fixed rhythm;
(3) *flutter*, an amplitude modulation of the stimulation carrier frequency that can either be perceived as increase and decrease of the intensity (if modulation is slower than 5 Hz) or as "roughness" (if modulation is faster than 10 Hz).

Given the hardware at our disposal (described below), we designed an appropriate software framework to test the effectiveness of all the features mentioned above, as to maximize the capacity of the vibrotactile channel.

2.2. Generation and delivery of stimuli

We used C-2 tactors (Engineering Acoustics, Inc, Winter Park, FL, USA) (see Figure 1) that are magnetic actuators, similar in principle to audio speakers; the current flowing in their coil pushes a central structure named contactor against the skin and back. Different from acoustic transducers, the structure is tuned on a narrow band around 250 Hz, so only signals at these frequencies can be effectively transduced.

By driving a tactor with two mixed sine waves, complex waveforms can be obtained. Moreover, a third auxiliary input can be fed at the amplification stage. Even if efficiency issues suggest not to deviate from the resonance frequency of 250 Hz, the frequency of stimulation can be selected by the user. The output intensity can be set to four different values (amplification gains). A peripheral interface controller (PIC) included on the control board takes care of serial communication with the PC, and sets in the generation and amplification subsystems the appropriate values of frequency and gain. By using a battery as power supply and a serial port to a Bluetooth (BT) adapter, the host PC can send commands over the air to the vibrotactile device. Since both the control board and the BT adapter are battery powered, the users can wear a wireless system during the experiments.

The tactors are relatively lightweight and small ($\sim$4 cm diameter). The skin contactor is 7.5 mm diameter, raised to 0.6 mm from the surface of the case, so that it can be

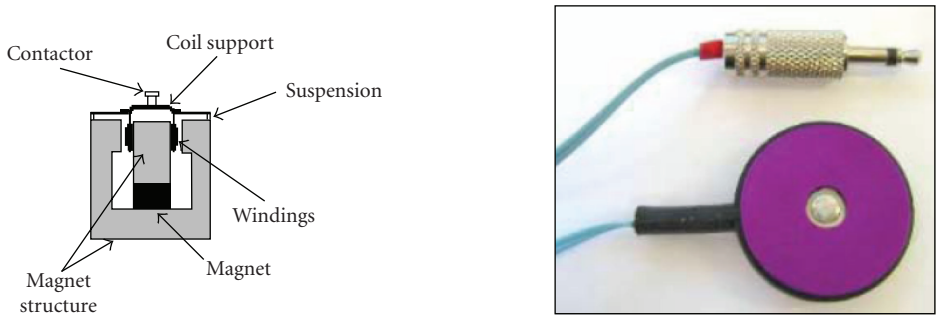

Figure 1: (a) Components of a C-2 tactor; (b) External aspect.

Figure 2: Dermatomes of the human body, that is, the levels innervated by each pair of spinal roots. A spinal cord injury may leave denervated all dermatomes, below the level of the lesion.

pre-loaded on skin. Since the nominal displacement is about 0.6 mm, the tactor-skin adhesion is never lost in any phase of the vibration. In principle, taping them to the body could be a solution for short term experimentations, but it is hardly satisfactory for longer sessions. The ideal placement technique should (i) be easy to wear, (ii) be comfortable to wear, (iii) guarantee good adhesion to skin, (iv) allow good skin sensitivity. Moreover, we need to take into account the possibility that some motor-disabled users could be spinal cord injured (SCI) suffering from sensory deficits in the lower part of their body. The position of tactors must be above the dermatome corresponding to the level of the lesion (see Figure 2).

We defined a common standard placement of the tactors where they are placed on the shoulders of the users, using an elastane T-shirt to keep them steadily in position and slightly pressed against the skin (see Figure 3(d)).

The software framework designed to drive the vibrotactile actuators was divided into several layers, aiming at implementing commands at different levels of abstraction. In particular, primitive stimulation modalities (tactons, [15, 16]) were used as a general library of stimuli.

3. PRELIMINARY EXPERIMENTATIONS

In the preliminary experiments, our aim was to address whether a subject is able to distinguish two separate stimuli delivered through the experimental setup described above, even when the stimulation characteristics are only slightly different. The vibrotactile features under investigation in this experiment were intensity and position.

3.1. Experimental setup

Five able bodied subjects (AB, one female) and three subjects with spinal cord injuries—leading to paraplegia (SCI, lesions from T3 to T8, all male)—, 29.5 ± 4.6 (SD) years old, were enrolled.

Eight tactors were positioned in a circle at even angles on the upper part of the trunk of the subjects (see Figure 3). The tactors were placed over a T-shirt, and kept in place by a second elastic T-shirt, which also provided the necessary preload. To avoid slipping and to help the preload even where the elastic force of the T-shirt is low, for example, between the scapulae, a circular sponge of appropriate size was stuck to the back side of each tactor.

Vibrotactile stimuli were given at 250 Hz, lasting for 500 milliseconds. During the tests, 256 separate stimuli were delivered to each subject, in four runs separated by short breaks. Each stimulus could be given to one of the eight tactors, and could have an intensity level of one to four. Positions and amplitudes were pseudorandomized, making sure that the total number of stimuli of each type would be the same.

In response to each stimulus, the subject had to respond with the perceived direction and intensity. A computer keyboard was used for this purpose. As shown in Figure 3, eight keys on the numeric keypad (pressed with fingers of the right hand) coded the perceived position, while four keys of the left part of the keyboard (pressed with fingers of the left hand) coded the perceived intensity. Two additional keys were provided for the subject to express his/her inability to recognize position or amplitude of the stimulus.

Before recording the response, the subjects practiced for a few minutes, until they declared to feel familiar with the stimuli and with the response procedure. During the practice period, the experimenter informed the subjects about the actual stimulus delivered, so that subjects could learn the association between stimulus and perception.

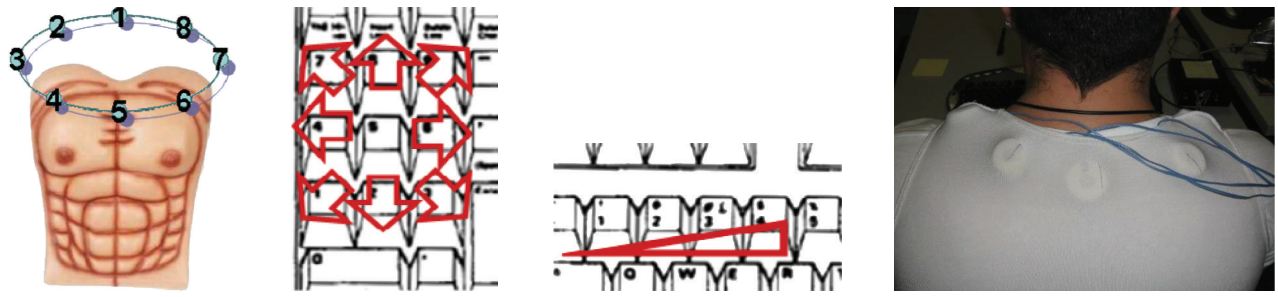

(a) (b) (c) (d)

Figure 3: (a) Tactors indexing, used in the results. (b) Mapping of perceived position of stimulation to keys of a computer's numeric keypad; correspondence does not rely on numbers, but on directions (e.g., leftmost key coded as a perceived stimulus to the left). (c) Mapping of perceived intensity of stimulation to keys of a computer's keyboard; 1 coded the weakest intensity, and 4 the strongest. (d) Montage of tactors on the subject's body.

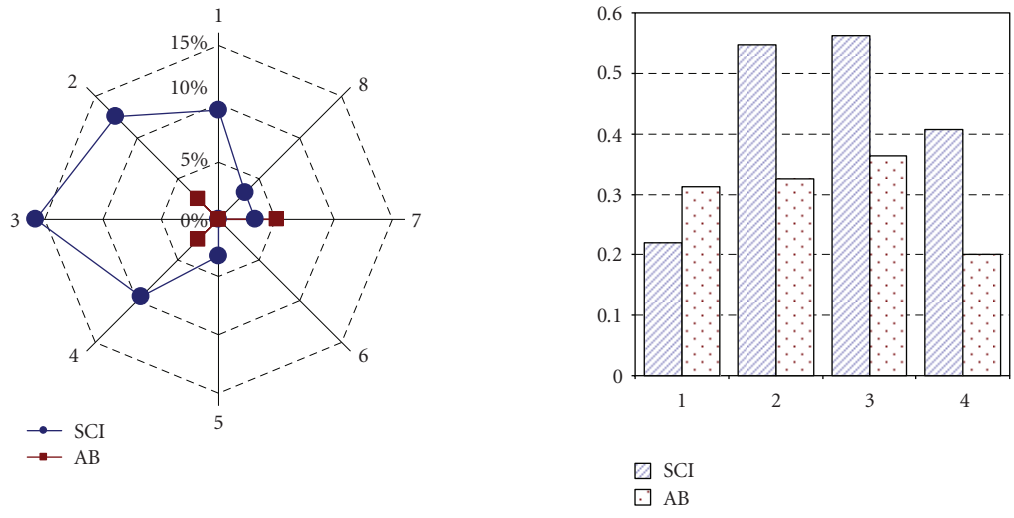

(a) (b)

Figure 4: Error occurrence, divided for position (a) and for intensity (b) of stimulation. SCI and AB groups are plotted separately.

3.2. Results

During the practice session, all subjects reported that they could perceive the stimulation, even at the lowest intensity. Some subjects reported discomfort with tactors number 1 and 5, since they stimulated a region of the body where a bone (sternum or spine) was immediately below the skin. The average response time of the two key presses, direction, and amplitude was 2.35 ± 0.52 seconds.

Overall errors in detecting the correct position were 3.8% and errors in detecting the intensity of stimulus were 35.9%. In both conditions, 0.2% of the responses were not classified. The distribution of errors as a function of positions and intensities is shown in Figure 4 for the SCI and the AB group separately. Most of the errors for the SCI group were made with stimuli delivered to the right part of the body; intermediate intensities were difficult to recognize for both groups.

Figure 5 shows the grand average confusion matrices of errors as a function of positions and intensities over all subjects; errors in detecting positions are almost exclusively confined to neighboring position. Errors in amplitude detection are more frequent, but mostly confined to adjacent (slightly higher or lower) intensities.

3.3. Discussion

Both subject groups could reliably distinguish stimuli delivered to the 8 tactors, with acceptable classification error. Errors were higher, but acceptable, on SCI subjects, possibly due to specific loss of sensitivity. A neurological examination and a preliminary experimentation to detect an individual optimal montage should be considered for further experimentations. All SCI subjects included in this study had lesions to toracic vertebrae. Lesions at higher level may prevent this solution to be effective. In such a case, an experiment in which analogous stimuli are delivered in different sites of the neck should be carried out, to assess an appropriate solution.

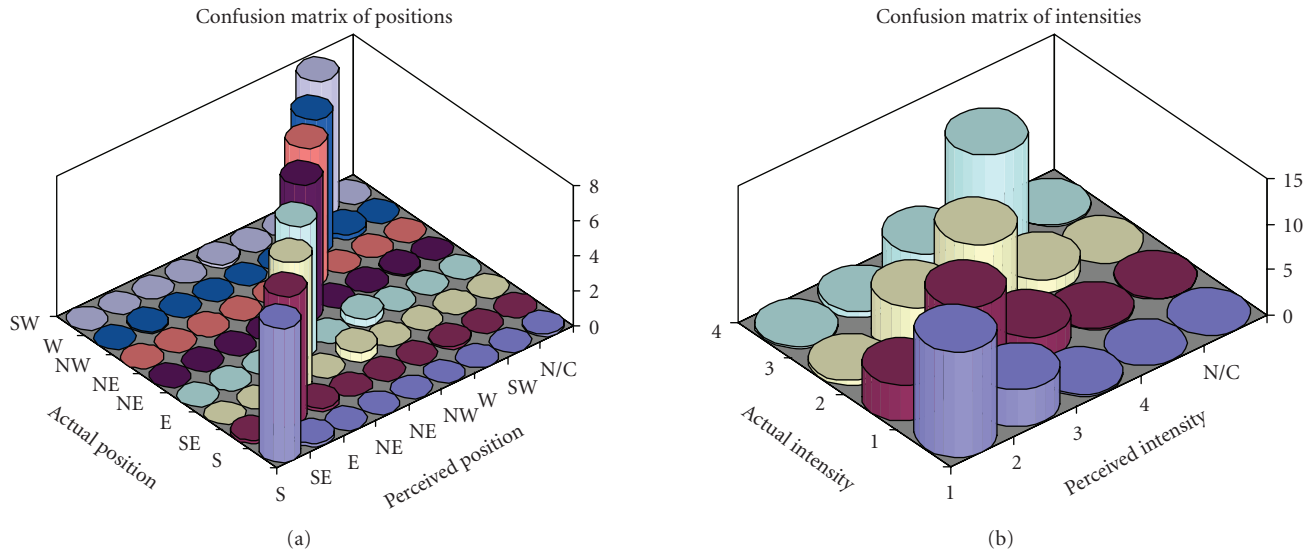

Figure 5: Graphical representation of confusion matrices of classification errors, that is, the number of stimli delivered to an "actual position" that were perceived as delivered to a "perceived position." Figures represent the grand average over all subjects participating in the experiment. Ideally, all nonzero values should lie on the main diagonal.

The pattern of direction errors shown in Figure 4 has no apparent physiological explanation. Since most of the errors are contributed by SCI subject, they should be discussed on an individual basis, using the result of the neurological examination. Possibly, a longer and more structured subject training period could help reduce misclassifications.

Intensity seems to be more difficult to classify, at least with the level of discrimination used in this experiment (4 levels). Errors mostly occur for the intermediate levels (2 and 3). Levels 1 and 4 seem to be less affected, possibly because they can be confused with only one neighboring intensity. Reducing the number of levels to two could bring misclassifications to an acceptable value.

Even though adaptation was not explicitely explored in this study, none of the subjects reported a reduction of the sensorial response with time. This was possibly prevented by the type of vibrotactile stimulation, which was not continuous, but intermittently on and off, as ruled by the temporal and spatial pattern of stimulation.

During this study, we did not experience artifacts on the EEG recordings produced by activation of the vibrotactile transducers.

Finally, due to discomfort of tactors placed in a bony region of the body (above the sternum and the spine) reported by some subjects, a slight rotation of the tactor configuration is suggested.

4. EXPERIMENTAL STUDIES

From the considerations of physiological and technical natures expressed so far, it is evident that somatosensory feedback is a vital component of motor planning, control, and adaptation, and there is a technical possibility to include this feedback in neural prosthetic system. To achieve this goal, it is first necessary to assess how the feedback channels would affect the training processes and compare them to the use of the dominant visual channel.

To this end, we aim to answer the following questions.

(1) Can the vibrotactile channel represent valuable feedback by conveying information of subject performance during BCI training, especially compared to the classical visual channel?

(2) Could vibrotactile feedback effectively integrate (or complement) visual feedback when the visual channel is engaged in monitoring the task, which is being controled using commands issued through a BCI?

In a *first experiment*, untrained subjects were trained to control a two-class BCI while receiving either visual or vibrotactile feedback. The subject performance achieved under both feedback modalities was compared (in terms of performance accuracy). Care was taken regarding the subject "adaptation" to the feedback modality by randomizing the delivery of visual and vibrotactile stimului.

In a *second experiment*, untrained subjects were exposed to both visual and/or vibrotactile feedbacks, which informed subjects about the classification outcome of a two-class BCI. We implemented an experiment in which a robot simulator program was included to mimic a distracting environment element (engaging the visual channel). This experiment addresses the question of using visual attention for monitoring the robot performance rather than the BCI performance.

Along with the previous experiments, where untrained subjects are gradually exposed to different feedback modalities with an element of "distraction," in a *last experiment* we mimic a "real-life" condition wherein subjects are engaged in a complex visual task (which requires focused visual attention) and simultaneously they receive the necessary continuous information about the status of the system they are

using.[1] BCI trained subjects were thus exposed either to a visuovisual or to a visuovibrotactile feedback of the outcome of BCI control and overall task, respectively, to assess whether the vibrotactile information may effectively complement the visual channel.

4.1. Study I

In the first study, we compared visual and vibrotactile feedbacks in a short experiment (six 7-minute sessions). When imagining left- and right-hand movements, six novice subjects received either visual (three sessions) or vibrotactile (three sessions) feedback of the classification performance of the BCI. Using correct class information, the classifier was updated after each prediction. Thus, up-to-date feedback could be given throughout the experiment. Model parameters were trained online and no separate offline training session was needed.

4.1.1. Material and methods

Subjects. Six right-handed subjects (20–30 years), who had no previous experience of BCIs, participated in the experiment.

Recordings. EEG was measured in a shielded room at 12 locations over the sensorimotor cortices. Signals from only two channels, C3 and C4, were used for BCI control. The sampling frequency was 500 Hz and the reference was situated between Cz and Fz.

Experimental setup. During the whole experiment, subjects were shown a visual target either on the right, left, or upper side of a small display in the middle of the screen. The subjects imagined either left- or right-hand movements, or did nothing (target up). The target was changed randomly every 10–15 seconds. The experiment was divided into six 7-minute sessions. Small breaks were kept between sessions. S1–S3 received vibrotactile feedback in the first three sessions and visual feedback in the following three sessions. The order was reversed for S4–S6.

Features. Movement-related activity (7–13 Hz) was used. FFT components were calculated from a 1 seconds time window, resulting in 2 channels $\times 7$ frequencies = 14 features. The window was moved and features were recalculated once the classifier function had finished with the previous sample ($\sim$every 100 microseconds).

Classification. A linear model with logistic output function was used to classify the features. The model was re-trained after each new feature sample ($\sim$every 100 microseconds) using a maximum of 300 previous labeled samples ($\sim$30 seconds) from both classes (less in the beginning of the experiment). The iterative least squares algorithm was used to update the model parameters. Classification and training was done only when the subject was performing either the left or right task.

Feedback. Vibrotactile feedback vibrating at 200 Hz and lasting for $\sim$100 microseconds was delivered either to the left or the right lower neck through the vibrotactile transducer. The amplitude was set to a value that the subjects reported being clearly perceivable. Visual feedback showed for $\sim$100 microseconds an arrow on the screen either to the left or right. Feedback was given once every second if the averaged posterior probabilities of 10 previous predictions exceeded 70% (S1 and S4) or 60% (others) for either of the two classes, that is, feedback was not given in uncertain cases. Feedback was given from the beginning of the experiment. No feedback was given during the target-up case.

Table 1: Mean classification accuracies for 3 sessions (%). HF, VF: vibrotactile and visual feedback, respectively.

	S1	S2	S3	S4	S5	S6	Mean±SD
HF	77	71	56	71	64	67	68 ± 7
VF	80	67	64	70	67	58	68 ± 7

4.1.2. Results

Table 1 shows the mean classification accuracy averaged over three sessions with different feedback modalities. Even during the short 42-minute experiment, high-classification accuracies (means 56–80%) were possible in some subjects.

Contralateral slow somatosensory evoked potential (SEP) could be detected in all subjects at $\sim$200 microseconds. The small visual feedback does not evoke any clear response. The vibrotactile feedback does not, however, show significant difference in the alpha-band frequencies that could interfere with the classification of motor imagination.

4.1.3. Discussion

No differences were found between training with vibrotactile or visual feedback during the 42-minute experiment. This indicates that, vibrotactile feedback could be used as an alternative to visual feedback if, for example, visual attention is needed for other tasks. These results should, however, be verified with more subjects. When asked, most subjects thought vibrotactile feedback felt more natural. However, one subject said that it sometimes, especially during misclassifications, interfered with the imagination of movements. Feedback was given discretely because continuous vibrotactile feedback was not possible due to technical difficulties. Even though SEPs can be detected in the averaged signals, the vibrotactile feedback did not interfere with the classified brain signals in the 7–13 Hz range.

[1] In this experiment, subjects were exposed to a situation similar to that experienced while driving a car along a given path and visually attending the route (task), while monitoring the speed of the vehicle (status) so that it does not exceed the limit. The working hypothesis is that when we compare driving performances when the speed information is given (a) by a visual gauge (same sensory modality challenged by the driving task) or (b) by an auditive beep (bimodal sensory input shared onto two sensory modalities), the second case will lead to better results.

Figure 6: Subject seated in front of screen. Both visual and vibrotactile feedbacks are given.

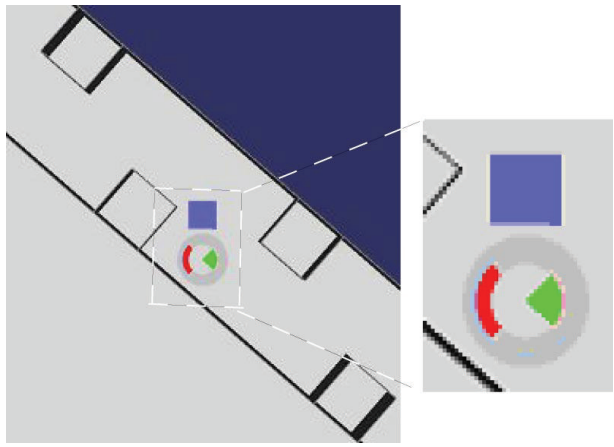

Figure 7: Top view of robot simulator program. The red task indicator showing left movement and visual feedback (green) showing feedback to the right side are displayed below the blue robot.

4.2. Study II

Study II continues the work of study I by comparing visual and vibrotactile feedback in a short experiment (nine 4.5-minute sessions). As in study I, six novice subjects received feedback of the classification performance of the BCI when imaging left- and right-hand movements. The experimental paradigm of study I was, however, slightly changed.

First, we used no threshold when giving feedback and thus feedback was always given once a second. Second, we used instant band power values and more several channels as features; these more sophisticated features require a feature selection, which we did during the first three breaks. To ensure that the reselection of features did not interfere with learning, we used the same features in the last six sessions. Third, in addition to feedback, a robot simulator program was also shown during the whole experiment on the screen to mimic a distracting environment of a BCI that generates a high visual workload.

4.2.1. Material and methods

Subjects. Six right-handed subjects (22–26 years, one female) with no previous experience of BCIs participated in the experiment.

Recordings. EEG was measured at 13 locations over the sensorimotor cortices (Fz, Cz, Pz, FC1, FC2, CP1, CP2, C3, C4, FC5, FC6, CP5, CP6) with a Brain Products 32-channel active electrodes system. The electrodes on the cap had built-in amplifiers, impedance level indicators, and active electromagnetic shielding. The sampling frequency was 500 Hz and the reference electrode was situated between Fz and Cz.

Experimental setup. Subjects were seated comfortably in a shielded room, in front of a monitor that displayed the top view of a simulated wheelchair (see Figure 6). The wheelchair was autonomously controlled by the computer; the purpose of the environment was to distract the subject by generating a high visual workload while making the change of target predictable. The target task indicator was situated below the wheelchair (see Figure 7). The wheelchair environment was an infinite circular corridor with obstacles requiring left and right turns.

The task indicator displayed a red target in either left, right, or up position. Subject's task was to imagine kinesthetic left- and right-hand movements or to do nothing (target up). The targets were predictably changed online by the experimenter from left target to right target (going through up target) and in reverse order. This suited the path of the robot best and made it easier for the subjects to prepare for the upcoming movement. Each left and right task lasted 5–10 seconds and each up-task lasted 1–2 seconds. The left and right tasks were alternated to approximately match the path taken in the environment by the wheelchair.

The experiment consisted of nine 4.5 minute sessions. In the first session, there was no feedback. In the next two sessions, both vibrotactile and visual feedbacks were presented simultaneously to familiarize the subject with them. Subjects S1–S3 received vibrotactile feedback in the next three sessions and visual feedback in the last three sessions. For subjects S4–S6, in the last six sessions, the order of the feedback modalities was changed.

Features. For each channel, one instant spectral/band power value was used as feature; the features were calculated once every second by convolving the EEG signals with Gabor filters. The length of each Gabor filter was two seconds corresponding to a bandwidth of approximately 0.5 Hz. The center frequency of each filter was determined in the feature selection from the 6–30 Hz frequency band.

Feature selection. Subject-specific center frequencies, as well as the classification relevance of each channel, were determined using Bayesian inference. Markov chain Monte Carlo (MCMC) methods were used to draw samples from the joint posterior distribution of the model parameters and input features. Reversible jump Markov Chain Monte Carlo (RJMCMC) was used to jump between models with different input feature combinations [17]. Joint probability of each channel and frequency component was determined based on the number of "visits" during the sampling process. As a criterion for selecting features, we required a given channel and the corresponding centre frequency to be included in the

Table 2: The average subject performance in the training sessions 2-3 (TS), vibrotactile feedback sessions (HF), and visual feedback sessions (VF). S1–S3 were given vibrotactile feedback in sessions 4–6; conversely S4–S6 were shown visual feedback in sessions 4–6.

	S1	S2	S3	S4	S5	S6	Mean±SD
TS	62	56	65	68	67	50	61 ± 7
HF	79	70	70	68	59	54	67 ± 9
VF	79	65	65	79	64	53	68 ± 10

model with sufficiently high posterior probability; we chose six or more of the most probable features for which the joint probability exceeded 0.25.

Feature selection was done during the breaks after sessions 1, 2, and 3. After sessions 1 and 2, the best Gabor frequency for each channel was determined using the data from the previous session. This Gabor frequency from all 13 channels was included in the model used in the following sessions, 2 and 3 correspondingly. After the third session, using data from sessions 2 and 3, RJMCMC sampling of input channels was combined with the sampling of the Gabor frequencies to determine the final channels and Gabor filters as features.

Classification. The classifier parameters were updated online once every second with the iterative least squares algorithm [18]. A prediction of the current class was made once every second for the newest sample before retraining of the model; a maximum of 300 most recent samples (5 minutes of data) with correct class labels was used as training data for each class.

In sessions 2–5 and 7-8, the model was trained online once every second. In the beginning of sessions 2 and 3, a model was used that was trained with the selected features using the data from the previous session. During the third break, the final features were used to initialize a model which was then used in sessions 4 and 7; the resulting models were then continued to be trained in sessions 5 and 8. The obtained models were tested, without training them, in sessions six and nine.

Feedback. The subject was given visual and/or vibrotactile feedback once every second. The visual feedback was displayed as a rose in the middle of the simulator screen with a green segment to each of the four directions. The left and the right segments were lit for 200 microseconds corresponding to the output of the classifier (see Figure 7). The vibrotactile feedback was given for 200 microseconds at 200 Hz with vibrating elements attached with tape to the subject's left- and right-side of the lower neck.

4.2.2. Results

Five subjects achieved high overall classification accuracies, on average as good as 59–79%, in the vibrotactile (HF), and visual feedback (VF) sessions (see Table 2). The subjects performed between 160 and 247 trials per session. S6 did not gain control over chance level (50–54%). S1 obtained an average accuracy of 79% for both feedback modalities and S4 reached 79% for the visual feedback modality. The average accuracies in the training sessions (TS) were 6-7% lower than the average accuracies in HF and VF sessions. We found no differences between average accuracies of the VF and HF sessions.

A response to the vibrotactile stimulation appears in the 0–8 Hz and 30–40 Hz bands in synchrony with the onset and end of the vibrotactile stimulation. In the event-related potentials (ERP) to the vibrotactile stimulation, low-pass filtered below 10 Hz, an N200 peak can be seen in both hemispheres during left- and right-side vibrotactile stimulation. However, both these responses have no role in real-time classification using time-frequency transformations in the 8–30 Hz frequency range.

4.2.3. Discussion

This study confirmed the results of study I; no differences were found between training with either vibrotactile or visual feedback, during the short 41-minute experiment. These results show that vibrotactile feedback could be used as an alternative to visual feedback when starting to learn to use a BCI. The choice of feedback modality is therefore largely dependent on subjects' preferences, indented environment of use, and the application. The use of the robot simulator program as a distracter did not disturb the subjects training. As in study I, when asked, most of the subjects felt that vibrotactile feedback was more natural. S1, S2, and S4 indicated that in the case of conflicting feedback, vibrotactile feedback was more disturbing than visual feedback. Even though vibrotactile responses could be detected in the averaged signals, the vibrotactile feedback did not interfere with the classification of the brain signals in the 6–30 Hz range.

S2–S5 performed better during the first feedback sessions compared to the second ones, independently of the type of feedback. This can partly be explained by the fact that the same model was used. Because the model was initialized after session 3 it was not as much up-to-date as during the second feedback modality. The model was not updated during the testing sessions explaning why the results of the training sessions are better.

From study I and II, we conclude that short-term learning is possible also with vibrotactile feedback. New experiments with more subjects are needed to evaluate the longer-term benefits of vibrotactile feedback. It should also be tested whether vibrotactile feedback is useful to patients with reduced sensing capabilities.

4.3. Study III

In study III, subjects were exposed to a joint visual and vibrotactile feedback, to assess whether the vibrotactile information could complement the visual channel for feedback, when the visual channel is intensively used as a carrier of task-related information. This experimental condition mimicked a "real-life" condition where the subject, engaged in a given task (spatial navigation), could simultaneously receive continuous information of his control strategy (feedback). Continuous state of the control signal, rather than a

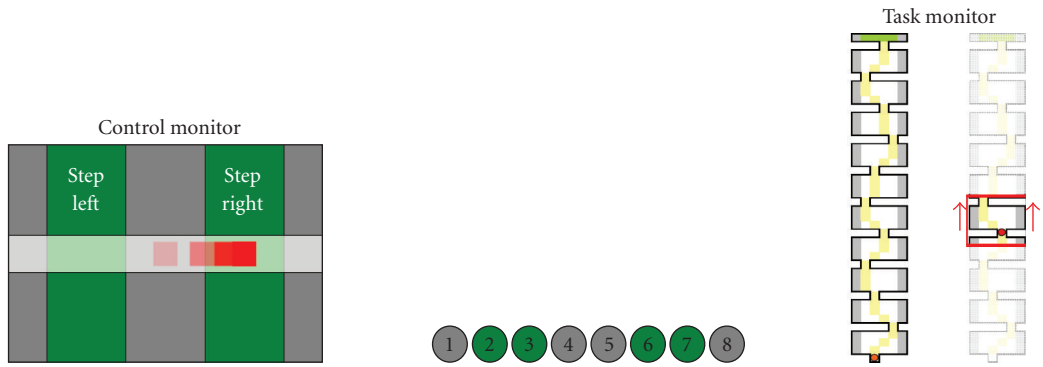

Figure 8: *Panel* (a): visual feedback of the pseudo-BCI controller; the subject had partial control on the red cursor, whose position was converted at discrete times (2 seconds) into navigation commands (step left, right, or no stepping). *Panel* (b): vibrotactile feedback of the pseudo-BCI controller; each tactor of the stripe encoded the tactile version of the visual cursor. *Panel* (c): scheme of the task; the drawing to the left represents the whole maze, with the ideal path marked in yellow. In the drawing to the right, the scrolling red frame shows the portion of the maze visible at once of the task display.

time-discrete classification was fed back to the user. To better focus on the properties of feedback and to reduce intersubject and intersession variabilities, due to different levels of training and fatigue, the "BCI" control signal was not derived by modulation of subject's brainwaves, but simulated by the movement of a PC mouse, to which a BCI-derived noise was added.

4.3.1. Material and methods

Thirteen subjects, two of which suffered from paraplegia due to lesions to their spinal cord, were involved in the experimentation. The experimental task consisted of moving a placeholder visible on a "task" monitor, with the goal of stepping through a sequence of 10 "rooms" (see Figure 8(c)), following a path constrained by narrow "gates" between adjacent rooms.

Control monitor

Subject's intention to move the placeholder was mediated by a BCI-like controller. In a first setting, the visual feedback of this controller was visible in a "control monitor" (see Figure 8(a)). The horizontal position of a cursor was partially regulated by the subject, moving a computer mouse. In fact, the cursor movement was affected by noise and delay, so that (inaccurate) motion was as similar as possible to a typical BCI-controlled cursor trajectory. To achieve this goal, the processing chain of the BCI2000 software [19] was set up like in a mu rhythm-based cursor control task, except that the amplitude of the spectral "EEG" component of interest was modulated by the mouse position. In addition, the time series of cursor drifted from an actual EEG-modulation recording was added sample by sample to the cursor control signal.

In a second setting, the feedback of this BCI-like controller was given through a stripe of eight tactors (see Figure 8(b)), positioned on the shoulders of the subject as

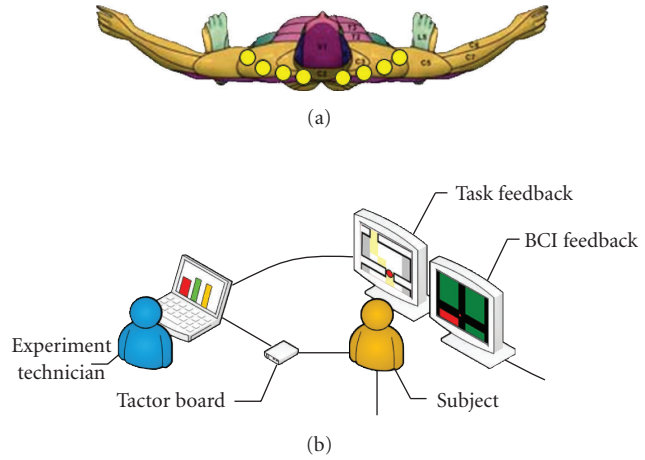

Figure 9: *Panel* (a): positions of the stripe of tactors on the subject's shoulders. *Panel* (b): experimental setup for visual feedback; the monitors in front of the subjects show the navigation task (task monitor, top) and the pseudo-BCI feedback (control monitor, bottom).

shown in Figure 9(a). Only one tactor at a time was active, encoding information about the horizontal position of a tactile cursor.

Once every 2 seconds, the (visual or tactile) cursor's horizontal position was sampled and compared to the limits of the five intervals defined on the screen; and the placeholder moved one step to the right, to the left, or stayed in its line, accordingly (see Figures 8(a) and 8(b)). If not impeded by a transverse "wall," the placeholder moved one step ahead at each time. Since the extreme left and right position of the control cursor did not produce a lateral movement of the placeholder, the subject could not simply grossly move the cursor in one direction, but had to attend the visual feedback on the control monitor, to make sure he did not under- or over-shoot cursor's position (which would be a too

Table 3: Performances of subjects included in study III. SAP: rate of steps in an acceptable path; SIP: rate of steps in the ideal path.

User	Average control (practice) (%)	Visual feedback				Vibrotactile feedback			
		Average control (task)		Time to destin. (mm:ss)	Correct keys (%)	Average control (task)		Time to destin. (mm:ss)	Correct keys (%)
		SAP (%)	SIP (%)			SAP (%)	SIP(%)		
S01	90	90	75	2:20	94%	86	79	2:06	100
S02	79	94	87	2:14	91	91	87	2:07	97
S03	80	89	78	2:37	86	85	78	2:08	100
S04	74	91	81	2:50	86	91	86	1:59	100
S05	81	92	84	3:04	73	90	86	2:17	91
S06	66	89	73	3:33	70	85	74	2:33	88
S07	78	92	82	2:31	91	91	87	2:00	100
S08	74	91	78	2:43	83	91	87	2:03	100
S09	84	95	85	2:10	94	91	86	2:03	100
S10	79	93	86	2:36	86	90	85	2:01	100
S11	64	93	79	2:23	94	92	87	2:02	100
S12	73	89	78	2:25	88	87	80	2:09	97
S13	84	92	80	2:46	81	89	85	2:14	94
Avg.	77.7%	92.1%	80.9%	3:02	86.0%	89.2%	83.7%	2:11	97.5%

easy control strategy). This designed produced (i) the need of attentive level, and (ii) a number of mistakes that were comparable to real BCI operation.

Subjects practiced for ∼30 minutes with the control monitor alone with both visual and tactile feedbacks to stabilize performance before challenging the task.

Task monitor

Each room of the navigation space measured 4×4 steps and access to the following room was allowed only through a narrow "gate." In the task monitor, movement was strongly discretized (one step every 2 seconds), so that the subject could not infer the status of the controller by looking at the placeholder's motion.

To force subjects to keep their visual attention on the task monitor, a colored green or yellow key appeared at random times once or twice for each "room." Before proceeding to the next "room," the subject had to report the color of the last key. If wrong, the subject had to navigate again the same room, thus making the path to the final goal longer and more time consuming.

Subjects had to perform six runs of the task. The visual or the vibrotactile feedback was provided in alternative runs. Type of feedback of the first run was randomized across subjects.

Control commands and navigation trajectories were recorded, and several indices of performance were computed offline: rate of steps in the ideal path (SIP), rate of steps in an acceptable path (SAP), time to complete the 10 room path, and rate of correct answers to the attentional task (key color).

T-test was performed on these indices to compare the effects of visual versus tactile feedback.

4.3.2. Results

Table 3 reports a summary of the performance indices.

The rate of steps within the ideal path was comparable in the two conditions (80.9% versus 83.7%, $p > 0.05$), in line with studies I and II. Considering slightly swinging trajectories around to the ideal path as acceptable, visual feedback allowed higher performance (92.1% versus 89.2%, $p = 0.004$). Nevertheless, the number of keys incorrectly reported is clearly higher during the runs with visual feedback (86.0% versus 97.5%, $p = 10^{-4}$). Given the payload set for wrong answer, this yielded a significantly longer time to destination in the same condition (182 seconds versus 131 seconds, $p = 2 \times 10^{-4}$).

Remarkably, two of the subjects reported appearance of blue and red keys (which were never delivered), only during runs with visual feedback.

4.3.3. Discussion

The tactile feedback modality was used and compared to the visual while subjects were required to perform a visually guided navigation task. We reduced the experimental variables, by setting up a pseudo-BCI control, which retains the typical inaccuracy, delay, and attention requirements of an EEG-based BCI.

If we only consider the ability of subjects to guide the placeholder towards the gates, the accuracy obtained with visual and tactile feedbacks looks comparable. A deeper analysis, showed that with tactile feedback, subjects tend to stay closer to the ideal path, thus pacing on a more straight line. The most notable difference was in the attentive resources that subjects were able to devote to the task. A significantly

higher rate of mistakes was made when visual attention was divided between the control and task monitors.

The subjects reported a good level of comfort in the experimental session lasting about 1 hour. Prolonged tests are needed to assess long-term compliance.

5. CONCLUSIONS

The importance of feedback in BCI experimentation is unquestionable, both during the training phase, and at a later stage. Visual feedback is most exploited in this field of research. In this experimental series, we tested how well we can convey an appropriate flow of information into vibrotactile stimulation. To this purpose, we developed a hardware system and a set of software programs that were interfaced to a BCI setup. Information from the BCI system was successfully translated into tactile stimuli, exploiting the features of the sensory channel that physiology are best detectable by users.

In the experiments we conducted the vibrotactile feedback was systematically compared to the usual visual feedback. In summary, we found that tactile feedback (i) permits an appropriate training of users to BCI operation; (ii) does not interfere with simultaneous visual stimuli; (iii) may improve performance when the subject's attention is highly loaded by a simultaneous visual task.

Although these observations have to be confirmed on a larger scale of experimentation with more subjects, it is conceivable to assume that the vibrotactile channel can be effective in relieving the visual channel whenever a dynamic environment overloads the visual channel. In fact, as in the last experimental setting, the user of a BCI system in a real-life context should be able to attend the continuous incoming information both from the BCI feedback itself and the task-relevant information, that is, navigation information, unexpected obstacles, and directions which would mostly be mediated by his/her visual sense. This information processing requires at this stage, a very high level of attentional effort and decrease of performance is likely to occur if this sensory load is not divided into different senses. In this regard, future experiments are needed to explore the natural integration between multimodal feedbacks (visual, auditory, and tactile) in oriented tasks executed under BCI control.

Vibrotactile feedback could be of practical use in applications of BCI technology. Not only would it allow a user to receive a private feedback message, that is, not perceivable by people close to him, but it could be packaged into a wearable device and hidden under clothes, thus improving portability of the system.

An intrinsically multisensorial BCI system can be envisaged, that could deliver BCI-specific information back to the user through the sensory channel (visual, auditory, or tactile) which is less engaged in the current BCI controlled task. This feedback could either be equally shared on different channels, or replicated on each of them. Alternatively, an intelligent system could even dynamically direct the stimuli to the least congested sensory channel.

In conclusion, our findings indicate that the vibrotactile channel can function as a valuable feedback modality in a BCI-controlled setting. Its reliability is comparable to the classical visual feedback, and it can improve performance during tasks that need a focused visual attention.

ACKNOWLEDGMENTS

This work is supported by the European IST Programme FET Project FP6-003758. This paper only reflects the authors' views and funding agencies are not liable for any use that may be made of the information contained herein. Cincotti and Kauhanen equally contributed to the paper.

REFERENCES

[1] B. E. Stein and M. A. Meredith, *The Merging of the Senses*, MIT Press, Cambridge, Mass, USA, 1993.

[2] A. B. Schwartz, X. T. Cui, D. J. Weber, and D. W. Moran, "Brain-controlled interfaces: movement restoration with neural prosthetics," *Neuron*, vol. 52, no. 1, pp. 205–220, 2006.

[3] J. R. Wolpaw, N. Birbaumer, D. J. McFarland, G. Pfurtscheller, and T. M. Vaughan, "Brain-computer interfaces for communication and control," *Clinical Neurophysiology*, vol. 113, no. 6, pp. 767–791, 2002.

[4] T. Hinterberger, N. Neumann, M. Pham, et al., "A multimodal brain-based feedback and communication system," *Experimental Brain Research*, vol. 154, no. 4, pp. 521–526, 2004.

[5] M. Pham, T. Hinterberger, N. Neumann, et al., "An auditory brain-computer interface based on the self-regulation of slow cortical potentials," *Neurorehabilitation and Neural Repair*, vol. 19, no. 3, pp. 206–218, 2005.

[6] F. Nijboer, A. Furdea, I. Gunst, et al., "An auditory brain-computer interface (BCI)," to appear in *Journal of Neuroscience Methods*.

[7] C. M. Giabbiconi, C. Dancer, R. Zopf, T. Gruber, and M. M. Müller, "Selective spatial attention to left or right hand flutter sensation modulates the steady-state somatosensory evoked potential," *Cognitive Brain Research*, vol. 20, no. 1, pp. 58–66, 2004.

[8] G. R. Müller-Putz, R. Scherer, C. Neuper, and G. Pfurtscheller, "Steady-state somatosensory evoked potentials: suitable brain signals for brain-computer interfaces?" *IEEE Transactions on Neural Systems and Rehabilitation Engineering*, vol. 14, no. 1, pp. 30–37, 2006.

[9] D. J. McFarland, L. M. McCane, and J. R. Wolpaw, "EEG-based communication and control: short-term role of feedback," *IEEE Transactions on Rehabilitation Engineering*, vol. 6, no. 1, pp. 7–11, 1998.

[10] C. Neuper, A. Schlogl, and G. Pfurtscheller, "Enhancement of left-right sensorimotor EEG differences during feedback-regulated motor imagery," *Journal of Clinical Neurophysiology*, vol. 16, no. 4, pp. 373–382, 1999.

[11] E. H. Weber, *The Sense of Touch*, Academic Press, New York, NY, USA, 1978.

[12] R. Kuc, "Binaural sonar electronic travel aid provides vibrotactile cues for landmark, reflector motion and surface texture classification," *IEEE Transactions on Biomedical Engineering*, vol. 49, no. 10, pp. 1173–1180, 2002.

[13] B. L. Richardson and M. A. Symmons, "Vibrotactile devices for the deaf: are they out of touch?" *The Annals of Otology, Rhinology & Laryngology. Supplement*, vol. 166, pp. 458–461, 1995.

[14] R. W. Cholewiak and A. A. Collins, "Vibrotactile localization on the arm: effects of place, space, and age," *Perception and Psychophysics*, vol. 65, no. 7, pp. 1058–1077, 2003.

[15] S. A. Brewster and L. M. Brown, "Non-visual information display using tactons," in *Proceedings of the Conference on Human Factors in Computing Systems (CHI '04)*, pp. 787–788, Vienna, Austria, April 2004.

[16] L. M. Brown, S. A. Brewster, and H. C. Purchase, "A first investigation into the effectiveness of tactons," in *Proceedings of the 1st Joint Eurohaptics Conference and Symposium on Haptic Interfaces for Virtual Environment and Teleoperator Systems (WHC '05)*, vol. 00, pp. 167–176, Pisa, Italy, March 2005.

[17] P. J. Green, "Reversible jump Markov chain Monte Carlo computation and Bayesian model determination," *Biometrika*, vol. 82, no. 4, pp. 711–732, 1995.

[18] P. McCullaghJ and A. Nelder, *Generalized Linear Models*, Chapman and Hall, London, UK, 1989.

[19] G. Schalk, D. J. McFarland, T. Hinterberger, N. Birbaumer, and J. R. Wolpaw, "BCI2000: a general-purpose brain-computer interface (BCI) system," *IEEE Transactions on Biomedical Engineering*, vol. 51, no. 6, pp. 1034–1043, 2004.

Hindawi Publishing Corporation
Computational Intelligence and Neuroscience
Volume 2007, Article ID 94397, 9 pages
doi:10.1155/2007/94397

Research Article

A Semisupervised Support Vector Machines Algorithm for BCI Systems

Jianzhao Qin,[1,2] Yuanqing Li,[1] and Wei Sun[3]

[1] *Institute of Automation Science and Engineering, South China University of Technology, Guangzhou 510640, China*
[2] *Shenzhen Institute of Advanced Integration Technology, Chinese Academy of Sciences, The Chinese University of Hong Kong, Hong Kong*
[3] *School of Maths, Central-South University, Changsha 410008, China*

Correspondence should be addressed to Jianzhao Qin, jz.qin@siat.ac.cn

Received 30 January 2007; Accepted 18 June 2007

Recommended by Andrzej Cichocki

As an emerging technology, brain-computer interfaces (BCIs) bring us new communication interfaces which translate brain activities into control signals for devices like computers, robots, and so forth. In this study, we propose a semisupervised support vector machine (SVM) algorithm for brain-computer interface (BCI) systems, aiming at reducing the time-consuming training process. In this algorithm, we apply a semisupervised SVM for translating the features extracted from the electrical recordings of brain into control signals. This SVM classifier is built from a small labeled data set and a large unlabeled data set. Meanwhile, to reduce the time for training semisupervised SVM, we propose a batch-mode incremental learning method, which can also be easily applied to the online BCI systems. Additionally, it is suggested in many studies that common spatial pattern (CSP) is very effective in discriminating two different brain states. However, CSP needs a sufficient labeled data set. In order to overcome the drawback of CSP, we suggest a two-stage feature extraction method for the semisupervised learning algorithm. We apply our algorithm to two BCI experimental data sets. The offline data analysis results demonstrate the effectiveness of our algorithm.

1. INTRODUCTION

A brain-computer interface is a communication system that does not depend on brain's normal output pathways of peripheral nerves and muscles. It provides a new augmentative communication technology to those who are paralyzed or have other severe movement deficits [1].

For many BCI systems, a tedious and time-consuming training process is needed to train the user and system parameters, for example, the parameters of the translation algorithm. In BCI competition III, reducing the training process has been explicitly proposed as a task by Schalk et al. [2].

In this paper, we resort to semisupervised learning to train an SVM classifier. Compared with the case of supervised learning, semisupervised learning can build better classifiers by using large amounts of unlabeled data, when the labeled data are expensive or time consuming to obtain [3, 4] (in BCI systems, the training process can be taken as the labeling process). Thus, the performance of semisupervised learning can still be satisfactory. The semisupervised learning algorithms that have been developed so far include EM algorithm [5], self-training algorithm [6], cotraining algorithm [7], graph-based methods [8, 9], and so forth. A survey of semisupervised learning can be found in [3, 4].

In [10], Bennett and Demiriz proposed a semisupervised SVM. Given a set of labeled data and a set of unlabeled data, a semisupervised SVM was trained using both the labeled data and unlabeled data. This algorithm can be implemented using mixed integer programming. However, since the computational burden of mixed integer programming will increase greatly with the number of integer variables (i.e., the number of unlabeled samples), it is unacceptable when the size of the unlabeled data set is large, especially when we apply this algorithm to the online BCI system. Thus, we propose a batch-mode incremental training method for the semisupervised SVM.

There are two basic ideas in this method: (1) we assume that the users' electroencephalography (EEG) change gradually during the use of BCI systems. Therefore we can decompose the unlabeled data set into several subsets; then we

use mixed integer programming to adjust the parameters of the semisupervised SVM incrementally with the entering of each subset, that is, we do mixed integer programming only based on a small-scale unlabeled data set each time. (2) For each unlabeled subset, we first select and label the most reliable data; then do the mixed integer programming based on the remaining unlabeled data set. This can further reduce the number of integer variables (i.e., the number of unlabeled data) for each running of the mixed integer programming.

Additionally, in BCI systems, the common spatial patterns (CSP) method is very effective for extracting features from the EEG recordings [11–13] (we refer to the feature extracted by CSP method as "CSP feature" in this paper). The extraction of the CSP feature is label dependent, that is, the CSP feature should be extracted from the labeled data set. If the number of labeled samples is too small, the transformation matrix for CSP feature extraction cannot be estimated accurately. This will result in an ineffective CSP feature. In order to overcome the drawback of CSP feature, we suggest a two-stage feature extraction method, that is, we first extract a dynamic power feature and perform an initial classification on a part of the unlabeled data at the first stage (the first several loops) of our semisupervised learning algorithm. Next, we extend the small labeled data set by including the most confidently classified unlabeled data with the predicted labels. Based on the extended labeled data set, somewhat reliable CSP features and better classification result can be obtained at the second stage (the remaining loops) of our semisupervised learning algorithm.

We evaluate the semisupervised SVM algorithm using a data set from an EEG-based cursor control experiment carried out in Wadsworth Center [14] and a data set from a movement imagination experiment provided by Department of Computer Engineering University of Tübingen, Germany, and Institute of Medical Psychology and Behavioral Neurobiology [15]. Data analysis results demonstrate the validity of our algorithm.

The organization of this paper is as follows. In Section 2, we introduce the proposed methods, including feature extraction, semisupervised SVM, and batch-mode incremental training. Section 3 presents the data analysis results. In Section 4, we discuss our algorithm in detail.

2. METHODS

In this section, we first present the dynamic CSP feature extraction and the dynamic power feature extraction method; then we combine them to form a two-stage feature extraction method. Next, we introduce the semisupervised SVM algorithm. Finally we present the batch-mode incremental learning method for training the semisupervised SVM.

2.1. Dynamic CSP feature extraction

The common spatial patterns (CSP) is a method that has been applied to EEG analysis to classify the normal versus abnormal EEGs [16] and find spatial structures of event-related (de-)synchronization [12]. We define two CSP feature in this paper: (1) nonnormalized CSP feature, (2) normalized CSP feature. The nonnormalized CSP feature is extracted directly from the covariance matrix of the raw or filtered EEG signal. The normalized CSP feature is extracted from the normalized covariance matrix of the raw or filtered EEG signal. The advantages of the nonnormalized CSP feature are: (1) it keeps the amplitude information of the EEG signal; (2) its dimension is usually half of the normalized CSP feature. The normalized CSP feature also has its advantages. It can reduce the influence of the scaling (due to the change of the electrode impedances or other causes) of the amplitude of the recorded EEG.

Now, we present the extraction of the dynamic nonnormalized CSP feature, which is similar to the method described in [11]. First, we filter the raw EEG in μ rhythm frequency band. The following CSP feature extraction is based on the filtered signals. In order to reflect the change of brain signals during a trial, we extract a dynamic CSP feature, that is, we separate the time interval of each trial into f overlapped time segments. For each time segment, we calculate a CSP feature vector as follows. The CSP analysis in the ith $(i = 1, \ldots, f)$ time segment involves calculating a matrix $\mathbf{W}_i$ and diagonal matrix $\mathbf{D}_i$ through a joint diagonalization method as (1):

$$\mathbf{W}_i \mathbf{Z}_i^n \mathbf{W}_i^T = \mathbf{D}_i, \qquad \mathbf{W}_i \mathbf{Z}_i^m \mathbf{W}_i^T = 1 - \mathbf{D}_i, \tag{1}$$

where $\mathbf{Z}_i^n$ and $\mathbf{Z}_i^m$ are covariance matrices of EEG data matrices $\mathbf{E}_i^n$ and $\mathbf{E}_i^m$ (one row of the EEG data matrices corresponds to one channel EEG signal). n and m denote two different classes (for the cursor control experiment, n and m represent two different targets; for the movement imagination experiment, n and m denote two different movement imaginations). Using all trials with class n, we construct the matrix $\mathbf{E}_i^n$ by trial-concatenating the filtered EEG data in the ith time segments of every trial. $\mathbf{E}_i^m$ is obtained similarly except that it corresponds to the trials with class m. The diagonal elements of $\mathbf{D}_i$ are sorted with a decreasing order.

After obtaining the transformation matrix $\mathbf{W}_i$, we now extract CSP feature in the ith time segment of a trial $(i = 1, \ldots, f)$. We first calculate a covariance matrix using the filtered EEG signals in the ith time segment; then we take the first p or the last p main diagonal elements of the transformed (by $\mathbf{W}_i$) covariance matrix. Note that the first p diagonal elements correspond to p largest eigenvalues in the diagonal matrix $\mathbf{D}_i$ above, the last p correspond to its p smallest eigenvalues. Thus we obtain a p-dimensional CSP feature for each time segment. We concatenate the CSP features of f time segments to construct the $p \cdot f$-dimensional dynamic CSP feature of each trial, which is denoted as $\mathbf{CF} = [\mathbf{CF}_1, \mathbf{CF}_2, \ldots, \mathbf{CF}_f]$.

The normalized CSP feature [12] is almost the same as the above CSP feature, except that: (1) the correlation matrix is normalized by dividing the trace of the correlation matrix; (2) the first p and the last p main diagonal elements of the transformed covariance matrix are taken, then normalized by dividing the sum of the $2p$ elements followed by a log-transformation. The log transformation serves to approximate normal distribution of the data [12]. Thus the

dynamic normalized CSP feature for f time segments is $2p \cdot f$-dimensional.

2.2. Dynamic power feature extraction and the two-stage feature extraction method

According to the above definition of CSP feature, it is obvious that the CSP feature extraction is dependent on the labels of the trials in the training set. If the number of labeled samples is too small, the transformation matrix of $\mathbf{W}_i$ cannot be estimated accurately, sometimes, even poorly. This will result in an ineffective CSP feature. In this subsection, we solve this problem by combining the power feature with the CSP feature to form a two-stage feature extraction method.

Our method is based on the following two facts: (1) the power feature extraction is not so dependent on sufficient labeled data set as CSP feature extraction; (2) the power feature is less powerful than CSP feature when the training data is sufficient. Thus, in the first several loops of our semisupervised algorithm (the first stage), we use power feature to obtain an initial classification on a part of the unlabeled data set. Based on the initial classification result, we perform CSP feature extraction and classification in the later loops of our semisupervised algorithm (the second stage).

The power feature extraction is as follows: we first calculate the power values of selected EEG channels in the μ frequency band for each time segment. Then, we scale the power values, that is, the power value of each selected channel is divided by the sum of the average power values of the two different classes of this channel (the average power values are calculated from the labeled data set).

For each time segment, we choose 2 channels which are the most discriminant for the power feature extraction. We denote the power feature for time segment i as $\mathbf{PF}_i = [\mathrm{PF}_{ij}, \mathrm{PF}_{ij}]$, $i = 1, \ldots, f$, $j = 1, 2$ (f is the number of time segments); then concatenate the power values of all the time segments of a trial to form the dynamic power feature of a trial, which is denoted as $\mathbf{PF} = [\mathbf{PF}_1, \mathbf{PF}_2, \ldots, \mathbf{PF}_f]$.

For each time segment, the selection of channels is dependent on the discriminant ability of the power feature of the channels. The discriminant ability of the power feature of each channel is calculated as follows:

$$\mathrm{FR}_{ij} = \left(\mathbf{mean}\left(\mathrm{PF}_{ij}^{n}\right) - \mathbf{mean}\left(\mathrm{PF}_{ij}^{m}\right)\right)^2 \quad \begin{matrix} i = 1, \ldots, f, \\ j = 1, \ldots, h, \end{matrix} \tag{2}$$

where i denotes the ith time segment, and j denotes the jth channel; f is the number of time segments; h is the number of channels; n and m represent two different classes. The bigger the value of FR_{ij} is, the stronger discriminant ability of the power feature for channel j and time segment i is.

At the first stage (first several loops of semisupervised learning), we only extract the above dynamic power feature from the trials. After these loops of semisupervised learning, a part of the unlabeled data set is classified. Then, at the second stage, using the most confidently classified data with predicted labels to extend the given small training data set, we extract somewhat reliable dynamical CSP feature and perform the later loops of semisupervised learning. The detailed procedure of our feature extraction method with the batch-mode incremental training method is presented in Section 2.4.

2.3. Semisupervised SVM

In this subsection, we review the semisupervised SVM introduced by Bennett and Demiriz [10].

Given a training set of labeled data

$$\{(\mathbf{x}_i, y_i) \mid (\mathbf{x}_i, y_i) \in R^n \times \{\pm 1\},\ i = 1, \ldots, \ell\}, \tag{3}$$

where $\mathbf{x}_1, \ldots, \mathbf{x}_\ell$ are the n dimensional features that have been labeled as $y_1, \ldots, y_\ell$; and a set of unlabeled data

$$\{\mathbf{x}_i \mid \mathbf{x}_i \in R^n,\ i = \ell + 1, \ldots, \ell + k\}, \tag{4}$$

in [10], a semisupervised SVM was defined as

$$\begin{aligned} &\min_{\mathbf{w},\mathrm{b},\eta,\xi,\delta} C\left[\sum_{i=1}^{\ell} \eta_i + \sum_{j=\ell+1}^{\ell+k} \min\left(\xi_j, \delta_j\right)\right] + \|\mathbf{w}\|_1, \\ &\text{s.t. } y_i(\mathbf{w} \cdot \mathbf{x}_i - b) + \eta_i \geq 1, \quad \eta_i \geq 0,\ i = 1, \ldots, \ell, \\ &\mathbf{w} \cdot \mathbf{x}_j - b + \xi_j \geq 1, \quad \xi_j \geq 0,\ j = \ell + 1, \ldots, \ell + k, \\ &-(\mathbf{w} \cdot \mathbf{x}_j - b) + \delta_j \geq 1, \quad \delta_j \geq 0, \end{aligned} \tag{5}$$

where $C > 0$ is a penalty parameter, and η_i, ξ_j, δ_j are the slack variables that present the classification error of $\mathbf{x}_i$ or $\mathbf{x}_j$.

The semisupervised SVM can be reformulated as follows:

$$\begin{aligned} &\min_{\mathbf{w},b,\eta,\xi,\delta,d} C\left[\sum_{i=1}^{\ell} \eta_i + \sum_{j=\ell+1}^{\ell+k} \left(\xi_j + \delta_j\right)\right] + \|\mathbf{w}\|_1, \\ &\text{s.t. } y_i(\mathbf{w} \cdot \mathbf{x}_i - b) + \eta_i \geq 1, \quad \eta_i \geq 0,\ i = 1, \ldots, \ell, \\ &\mathbf{w} \cdot \mathbf{x}_j - b + \xi_j + M(1 - d_j) \geq 1, \quad \xi_j \geq 0,\ j = \ell + 1, \ldots, \ell + k, \\ &-(\mathbf{w} \cdot \mathbf{x}_j - b) + \delta_j + M d_j \geq 1, \quad \delta_j \geq 0,\ d_j = \{0, 1\}, \end{aligned} \tag{6}$$

where d_j is a decision variable. For each point $\mathbf{x}_j$ in the unlabeled data set, $d_j = 1$ means that the point is in class 1, otherwise the point is in class -1. $M > 0$ is a sufficiently large constant. Mixed integer programming can be used to solve this problem. But, mixed integer programming problems are NP-hard to solve [17], even when restricted to 0-1 programs [18]. If the number of the integer variables is large, the computational burden will be very heavy. In practice, since we often encounter large amounts of unlabeled data, we should assign large amounts of integer variables for these unlabeled data. Thus, if we solve this problem using the mixed integer programming directly, the training time of semisupervised SVM is unacceptable.

2.4. Batch-mode incremental training method

In this section, we extend the semisupervised SVM in [10].

We divide the original unlabeled data set into several subsets, and mark them as $B_1, B_2, \ldots, B_n$. Each time, we do the

mixed integer programming based on a subset. It is reasonable to assume that the users' EEGs change gradually during the use of the BCI systems. Using the incremental training method, the parameters of the SVM can be adjusted gradually with the entering of these several subsets (the new entered subsets represent the changed status of the users' EEG). Additionally, in order to further reduce the number of integer variables for each running of mixed integer programming, when a new subset is added, we first temporarily label the unlabeled elements in this subset using the SVM which has been trained in the previous loop; then we choose the most confidently classified elements and add them, together with their predicted labels, to the training set; finally, we use the remaining unlabeled elements for mixed integer programming. The most confidently classified elements can be determined according to the distance between the element and the separating boundary. The criteria can be formulated as follows:

$$\left|\mathbf{x}\cdot\mathbf{w}-b\right| \geq L, \tag{7}$$

where constant $L > 0$ is the distance threshold. If the distance between the element and the separating boundary is larger than L, we take it as a confident element.

The outline of the batch-mode incremental training method is as follows.

Algorithm outline. Given two data sets: a labeled data set D_l, and an unlabeled data set D_u.

Step 1. Equally divide the unlabeled data set D_u into n subsets $B_1, B_2, \ldots, B_n$ (for the online condition, these subsets can be collected at several time intervals); then take D_l as the initial training set T and let $i = 1$ (i denotes the ith loop of the algorithm); next extract dynamic power feature from data set T and B_1 (see Section 2.2).

Step 2. Train an initial SVM classifier using the dynamic power features in T.

Step 3. Estimate the labels of B_i using the current classifier, then choose the most confidently classified elements using (7) and add them together with their predicted labels (we mark the most confidently classified elements with their predicted labels as set R), to the training set T, that is, $T = T \cup R$; next we denote the remaining elements of B_i as Q_i.

Step 4. Run the mixed integer programming based on T and Q_i to get the labels of Q_i and adjust the parameters of the SVM classifier; then add Q_i with predicted labels to T, that is, $T = T \cup Q_i$.

Step 5. $i = i + 1$, if i is smaller than or equals to M which denotes the number of steps for dynamic power feature extraction, extract dynamic power features from B_i; otherwise, extract dynamic CSP features from B_i. Note that, for each loop, the transformation matrix of the dynamic CSP feature should be estimated again from the most confidently labeled elements of T; then use the new transformation matrix to extract the dynamic CSP features from T again. Finally train a new SVM classifier based on the updated CSP features and their labels of T.

Step 6. If i equals n, terminate; otherwise, go back to Step 3.

Additionally, since the size of the training set is enlarged during the training procedure, the penalty parameter C of the semisupervised SVM should adapt to this change. Thus, we extend the empirical formula for C introduced in [10] as:

$$C_i = \frac{(1-\lambda)}{\lambda(\ell_i + k_i)}, \tag{8}$$

where i denotes the ith loop. ℓ_i is the size of training set of the ith loop. k_i is the size of unlabeled data set. We set $\lambda = 0.01$ in our following experimental data analysis.

Figure 1 shows a demo of the batch-mode incremental training method. The circles and the triangles denote the labeled training samples of two classes. The crosses denote the unlabeled samples. The solid line denotes the separating boundary of the SVM classifier. From Figures 1(a)–(d), the unlabeled samples were added gradually. The figure shows that the separating boundary of the SVM classifier was adjusted gradually according to the entering of the unlabeled samples.

3. EXPERIMENTAL DATA ANALYSIS

In this section, we evaluated the semisupervised SVM-based algorithm using the data set from an EEG-based cursor control experiment and an ECoG-based movement imagination experiment. The hardware and software environments of our data analysis are as follows.

Hardware: personal computer (CPU: Intel P4 1.7 Ghz; RAM: SDRAM 512 MB).

Software: operating system: Windows 2000 professional. The main program was coded by MATLAB 6.5. The mixed integer programming problem and 1-norm SVM were solved by a free software LP-solve 2.0 C library by Michel Berkelaar and Jeroen Dirks. We repacked this software and compiled it as the mex file which can be called by MATLAB. We used the commands "cputime" to calculate the CPU time needed for training the semisupervised SVM.

3.1. Data analysis of an EEG-based cursor control experiment

The EEG-based cursor control experiment was carried out in Wadsworth Center. In this experiment, the subjects sat in a reclining chair facing a video screen and was asked to remain motionless during performance. The subjects used μ or β rhythm amplitude to control vertical position of a target located at the right edge of the video screen. The data set was recorded from three subjects (AA, BB, CC). Each subject's data included 10 sessions. The data set and the details of this experiment are available at http://www.ida.first.fraunhofer.de/projects/bci/competition.

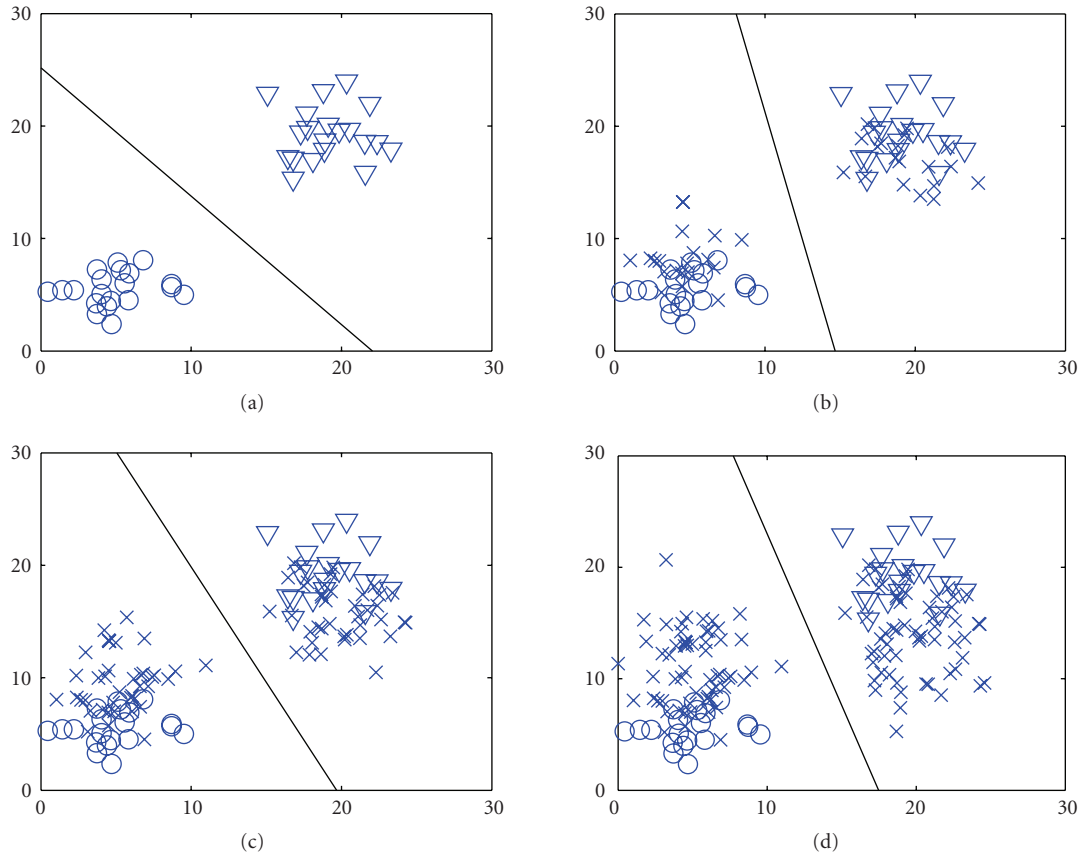

Figure 1: The demo of the batch-mode incremental training method (the circles and the triangles denote the labeled training samples of two classes. The crosses denote the unlabeled samples. The lines denote the separating boundary of the SVM classifier).

For convenience, only the trials with the targets who are at the highest and lowest position of the right edge of the screen were used in our offline analysis ($96 * 10$ trials for each subject).

To evaluate our proposed algorithm, we separated all the trials into three sets, that is, labeled data set, unlabeled data set, and independent test set. Labeled data set consists of 48 trials (about 10% of all labeled and unlabeled data) (24 trials for each target) from session 1. Unlabeled data set consists of 528 trials from the remaining trials of session 1 and all the trials of sessions 2–6; and the independent test set is composed of 384 trials of sessions 7–10. When implementing the batch-mode training method, we divided the unlabeled set into 9 subsets (each of the first 8 subset has 60 elements, and the 9th subset has 48 elements).[1]

In the data analysis, for the first two loops of our algorithm, we extracted five-time-segment dynamic power feature; then for the following loops, we extracted five-time-segments nonnormalized dynamic CSP feature from the 64-channel band pass filtered (11–14 Hz) raw EEG signal.[2] Based on the cross-validation results obtained from the training set, we find that the first 2 main diagonal elements were more significant for discriminating for subjects AA, CC and the last 2 main diagonal elements were more significant for subject BB. Therefore, in each time segment, the first 2 main diagonal elements for subject AA, CC and the last 2 main diagonal elements for subject BB were taken as the CSP feature. The dynamic CSP feature is of 10 dimensions.

We present our data analysis results as follows. We applied our algorithm to the independent test set. By comparing the predicted target position for each trial with the true target position, the accuracy rate is obtained. The accuracy rates for the three subjects are shown in the second row of Table 1.

To further demonstrate the validity of our algorithm (Case 1), we do the following comparison.

[1] The number of elements in a subset can be set according to the performance of the user's computer. If the number of elements in a subset is too small, the classifier will be updated too frequently. In contrast, if the number of elements is too large, the computer cannot solve the problem within an acceptable time period.

[2] Note that only the samples at the time when the user was controlling the cursor were used, that is, 368 samples each trial for subject AA and BB, 304 samples each trial for subject CC; the samples before and after cursor control were omitted.

Table 1: Accuracy rates (%) for the three subjects AA, BB, and CC.

Case	AA Accuracy rate	BB Accuracy rate	CC Accuracy rate	Average Accuracy rate
1	94.52	91.84	91.51	92.62
2	89.82	75.53	69.50	78.28
3	97.39	94.47	95.76	95.87
4	—	—	—	—
5	96.08	50.00	50.54	65.54
6	52.48	50.00	50.54	51.01

Table 2: CPU time (s) of the three subjects AA, BB, and CC for training the semisupervised SVM.

Case	AA Training time	BB Training time	CC Training time	Average Training time
1	1186.40	375.72	568.51	710.21
3	>86400	>86400	>86400	>86400

Case 1. The proposed semisupervised SVM trained from labeled and unlabeled data is used to classify the independent test set.

Case 2. A standard 1-norm SVM trained from the labeled data is used to classify the independent test set. Note that all the features extracted are the dynamic CSP features in this case.

Case 3. The true labels of the unlabeled data are assigned; then we use these data with the original labeled data to train a standard 1-norm SVM to classify the independent test set. Note that all the features extracted are the dynamic CSP features in this case.

Case 4. The original training method of semisupervised SVM introduced in [10] is used to replace the batch-mode incremental training method. Note that in this case, due to the heavy computational burden, we had run the mixed integer programming for more than 24 hours, but failed to get a result. So, the accuracy in Table 1 for Case 4 is empty.

Case 5. A full bayes classifier-based self-training algorithm is used to replace the semisupervised SVM-based algorithm. Note that in this case, all the features extracted are the dynamic CSP features.

Case 6. A full bayes classifier trained from the labeled data is used to classify the independent test set. Note that in this case, all the features extracted are the dynamic CSP features.

Table 1 shows the accuracy rates for the three subjects in Cases 1, 2, 3, 5, 6. It shows that our algorithm improves the accuracy rate significantly (by 14.34%), compared with the accuracy rates obtained in Case 2. Furthermore, compared with the accuracy rate of Case 3 in which all the data (including labeled and unlabeled data) were labeled, the accuracy rate (when only 10% data were labeled) obtained by using our algorithm is only lower than it by 3.25%. From the results of Cases 5, 6, we find that except for subject AA the full bayes classifier based self-training algorithm fails to improve the accuracy rate by using the unlabeled data. In most cases, when the number of labeled samples for training full bayes classifier is small, the estimation of the parameters of the full bayes classifier is often poor. Thus, when we use this classifier trained from the labeled data to predict the classes of the unlabeled data, only very small part of the unlabeled data can be classified correctly. When only very small part of correct classified unlabeled data is available, we cannot employ the information provided by the unlabeled data. This results in the poor performance in data sets BB and CC. In some rare cases, however, the distribution of the labeled small samples also can present partial distribution of the real data, that is, the labeled samples distribute on several representative places of the real data distribution. The bayes classifier trained from the labeled data can correctly classify part of the unlabeled data. The classification accuracy is better than the accuracy in the normal case. Therefore, for data set AA, the information embedded in the unlabeled data can be used to improve the performance of the classifier by the self-training algorithm.

Table 2 lists the CPU times of training the semisupervised SVM in Cases 1, 4 for 3 different subjects. Note that the values of the CPU time are the mean of five times running of the corresponding algorithm. In Case 4, we had run our program for more than 24 hours (86400 seconds) without getting a result. It shows that the batch-mode incremental training method is much faster than the method used in Case 4.

Figure 2 shows the change of the accuracy rate of the independent test set with the batch-mode incremental training process for the three subjects. It illustrates that the main trend of the accuracy rate of the independent test set increases along with the entering of the unlabeled data.

3.2. Data analysis of an ECoG-based movement imagination experiment

The data set of an ECoG-based movement imagination experiment was provided by Department of Computer Engineering University of Tübingen, Germany, (Prof. Rosenstiel) and Institute of Medical Psychology and Behavioral Neurobiology (Niels Birbaumer), and Max-Planck-Institute for Biological Cybernetics, Tübingen, Germany (Bernhard Schölkopf), Department of Epileptology and Universität

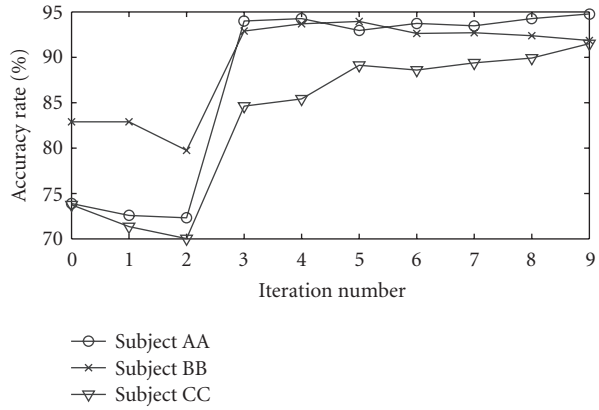

Figure 2: The change of the accuracy rate of the independent test set with the batch-mode incremental training process for the three subjects in the data analysis of an EEG-based cursor control experiment.

Bonn, Germany, (Prof. Elger) [15]; and is included by BCI competition III as data set I. This data set and its detailed description are available at http://www.ida.first.fraunhofer.de/projects/bci/competition_iii. During the BCI experiment, a subject had to perform imagined movements of either the remaining small finger or the tongue. The time series of the electrical brain activity was picked up during these trials using an 8×8 ECoG platinum electrode grid which was placed on the contralateral (right) motor cortex. The grid was assumed to cover the right motor cortex completely, but due to its size (approx. 8×8 cm) it partly covered also surrounding cortex areas. All recordings were performed with a sampling rate of 1000 Hz. After amplification, the recorded potentials were stored as microvolt values. Every trial consisted of either an imagined tongue or an imagined finger movement and was recorded for 3-second duration. To avoid visually evoked potentials being reflected by the data, the recording intervals started 0.5 seconds after the visual cue had ended. 278 trials were recorded in the same day which were taken as the training set in the competition. About 1 week later, 100 trials were recorded which were taken as the test set in the competition.

We took 28 trials (about 10% of all labeled and unlabeled data) from the 278 trials of training set as the labeled data set; and we took the remaining 250 trials of training set as the unlabeled data set; then took the 100 trials of test set as the independent test set. We first downsampled the original signals from 1000 Hz to 250 Hz for reducing the computational burden. In the first two loops of our algorithm, we extract five-time-segments dynamic power feature from the trials; in the remaining loops, we extract the 5-time-segments normalized dynamic CSP feature from the common average referenced (CAR) [19] and band-pass (8–12 Hz) filtered 32-channel (we chose 1 out of 2 original channels, that is, with channel numbers $2, 4, 8, \ldots, 64$) EEG data. In each time segment, the first 2 main diagonal elements and the last 2 main diagonal elements were taken as the CSP feature. The dimension of the dynamic CSP feature is 20. Note that the transformation matrix of the CSP feature of each time segment is calculated from the labeled data. We divided the unlabeled data into 4 batches. Each of the first 3 batches contains 63 elements. The fourth batch contains 61 elements.

Table 3: Accuracy rates (%) for the independent test set of movement imagination data analysis.

Case	1	2	3	4	5	6
Accuracy rate	89.00	72.00	90.00	—	69.00	69.00

Table 4: CPU time (s) for training the semisupervised SVM.

Case	1	4
Training time	233.66	>86400

We consider 6 cases as in EEG-based cursor control experiment data analysis.

Table 3 shows the accuracy rates in Cases 1, 2, 3, 5, 6. It shows that semisupervised learning improves the accuracy rate significantly (by 17%), compared with the accuracy rates obtained in Case 2. And, compared with the accuracy rate of Case 3 in which all the data (including labeled and unlabeled data) were labeled, the accuracy rate (when only 10% data was labeled) is only lower by 1%. From the results of Cases 5, 6, we see that bayes classifier-based self-training algorithm fails to improve the accuracy rate. In Case 4, we have run our algorithm for more than 24 hours without getting a result.

Table 4 lists the CPU time for training the SVM. Note that it is the average CPU time of five times running of the algorithm. The result also shows that the batch-mode incremental training method is much faster than the method used in Case 4.

Figure 3 shows the change of the accuracy rate of the independent test set with the batch-mode incremental training process. It illustrates that the main trend of the accuracy rate of the independent set increases along with the entering of the unlabeled data.

4. CONCLUDING REMARKS

In this paper, we present a semisupervised SVM algorithm for BCI systems, aiming at reducing the tedious and time-consuming training process.

The advantages of our algorithms are as follows.

(1) It achieves a satisfactory generalization performance by using the unlabeled data, even when only a small set of labeled data is available. The two experimental data analyses show that the accuracy rates have been improved significantly. Our algorithm can reduce the time needed for the initial training process of BCI systems.

(2) By dividing the whole unlabeled data set into several subsets and employing selective learning, the batch-mode incremental learning method significantly reduces the computational burden for training the semisupervised SVM. The data analysis shows that our

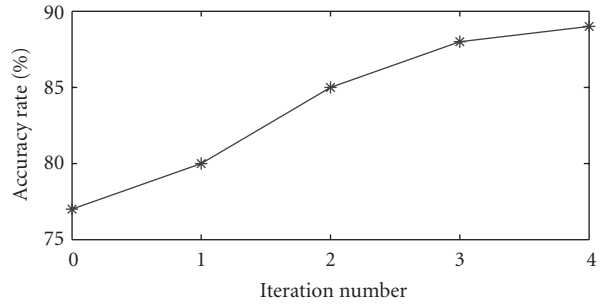

Figure 3: The change of the accuracy rate of the independent test set with the batch-mode incremental training process in the data analysis of an ECoG-based movement imagination experiment.

algorithm is much faster than the one using mixed integer programming directly.

(13) The incremental learning characteristic of our algorithm provides us with an online learning algorithm, which is useful for the real-world BCI systems since almost all the real-world BCI systems work online.

Our experimental data analysis shows that our semisupervised algorithm outperforms another commonly used semisupervised algorithm—the full bayes classifier-based self-training algorithm. In fact, in most cases of the data analysis, the full bayes classifier-based self-training algorithm fails to improve the accuracy rate. The reason may be that the dimensionality of the dynamic CSP feature is relatively too high compared with the size of the labeled data set, the generalization performance of the initial full bayes classifier is too poor to predict the labels of the unlabeled data. Consequently, it fails to utilize the information of the unlabeled data to improve its generalization performance. Contrarily, the initial classifier of the semisupervised SVM is SVM which obtains a good generalization performance even in the case of small-labeled data set. This enables the semisupervised SVM to predict the labels of unlabeled data accurately to some extent even when the size of labeled data set is small. Thus, it can successfully utilize the unlabeled data to adjust the parameters of the classifier and further improve its performance.

Although CSP feature is very powerful in discriminating two brain states, a sufficient training data set is needed to determine the transformation matrix. Otherwise, the obtained CSP features and subsequent classification result are not reliable. In this case, our semisupervised learning algorithm may not work. Thus, we suggest a two-stage feature extraction method, that is, we use a dynamic power feature to replace dynamic CSP feature in the first stage of our algorithm, then use the dynamic CSP feature in the second stage of our algorithm. Data analysis results also demonstrate the effectiveness of this method.

ACKNOWLEDGMENTS

The authors are grateful to Wadsworth Center, NYS Department of Health, (Jonathan R. Wolpaw) Department of Computer Engineering and University of Tübingen, Germany, (Prof. Rosenstiel), Institute of Medical Psychology and Behavioral Neurobiology (Niels Birbaumer), Max-Planck-Institute for Biological Cybernetics, Tübingen, Germany (Bernhard Schölkopf), and Department of Epileptology Universität Bonn, Germany, (Prof. Elger) for providing experimental data in BCI competitions II and III, respectively. The authors would like to thank Dr. Yu Pan, Dr. Huiyun Li, and the anonymous reviewers for their helpful comments. This work was supported by National Natural Science Foundation of China under Grant no. 60475004, the Program for New Century Excellent Talents in China University under Grant no. NCET-04-0816, Guangdong Province Science Foundation for Research Team program under Grant no. 04205783.

REFERENCES

[1] J. R. Wolpaw, N. Birbaumer, W. J. Heetderks, et al., "Brain-computer interface technology: a review of the first international meeting," *IEEE Transactions on Rehabilitation Engineering*, vol. 8, no. 2, pp. 164–173, 2000.

[2] G. Schalk, B. Blankertz, S. Chiappa, et al., "BCI competition III," 2004-2005, http://ida.first.fraunhofer.de/projects/bci/competition_iii/.

[3] M. Seeger, "Learning with labeled and unlabeled data," Tech. Rep., Institute for ANC, Edinburgh, UK, 2000.

[4] X. Zhu, "Semi-supervised learning with graphs," Ph.D. dissertation, Carnegie Mellon University, Pittsburgh, Pa, USA, 2005.

[5] A. P. Dempster, N. M. Laird, and D. B. Rubin, "Maximum likelihood from incomplete data via the em algorithm," *Journal of the Royal Statistical Society*, vol. 39, no. 1, pp. 1–38, 1977.

[6] C. Rosenberg, M. Hebert, and H. Schneiderman, "Semi-supervised self-training of object detection models," in *Proceedings of the 7th IEEE Workshops on Application of Computer Vision (WACV/MOTIONS '05)*, vol. 1, pp. 29–36, Brekenridge, Colo, USA, January 2005.

[7] A. Blum and T. Mitchell, "Combining labeled and unlabeled data with co-training," in *Proceedings of the 11th Annual Conference on Computational Learning Theory*, pp. 92–100, Morgan Kaufmann, Madison, Wis, USA, July 1998.

[8] A. Blum and S. Chawla, "Learning from labeled and unlabeled data using graph mincuts," in *Proceedings of the 18th International Conference on Machine Learning (ICML '01)*, pp. 19–26, Morgan Kaufmann, Williamstown, Mass, USA, June-July 2001.

[9] T. Joachims, "Transductive learning via spectral graph partitioning," in *Proceedings of the 20th International Conference on Machine Learning (ICML '03)*, vol. 1, pp. 290–297, Washington, DC, USA, August 2003.

[10] K. P. Bennett and A. Demiriz, "Semi-supervised support vector machines," in *Advances in Neural Information Processing Systems 11*, vol. 2, pp. 368–374, The MIT Press, Denver, Colo, USA, 1998.

[11] G. Blanchard and B. Blankertz, "BCI competition 2003-data set IIa: spatial patterns of self-controlled brain rhythm modulations," *IEEE Transactions on Biomedical Engineering*, vol. 51, no. 6, pp. 1062–1066, 2004.

[12] H. Ramoser, J. Müller-Gerking, and G. Pfurtscheller, "Optimal spatial filtering of single trial EEG during imagined hand movement," *IEEE Transactions on Rehabilitation Engineering*, vol. 8, no. 4, pp. 441–446, 2000.

[13] Y. Li, C. Guan, and J. Qin, "Enhancing feature extraction with sparse component analysis for brain-computer interface," in *Proceedings of the 27th IEEE Annual International Conference of Engineering in Medicine and Biology (EMBS '05)*, vol. 7, pp. 5335–5338, Shanghai, China, September 2005.

[14] J. R. Wolpaw, D. J. McFarland, G. W. Neat, and C. A. Forneris, "An EEG-based brain-computer interface for cursor control," *Electroencephalography and Clinical Neurophysiology*, vol. 78, no. 3, pp. 252–259, 1991.

[15] T. N. Lal, T. Hinterberger, G. Widman, et al., "Methods towards invasive human brain computer interfaces," in *Advances in Neural Information Processing Systems 17*, L. K. Saul, Y. Weiss, and L. Bottou, Eds., pp. 737–744, The MIT Press, Vancouver, Canada, 2004.

[16] Z. J. Koles, M. S. Lazar, and S. Z. Zhou, "Spatial patterns underlying population differences in the background EEG," *Brain Topography*, vol. 2, no. 4, pp. 275–284, 1990.

[17] R. M. Karp, "Reducibility among combinatorial problems," in *Complexity of Computer Computations*, R. E. Miller and J. W. Thatcher, Eds., pp. 85–103, Plenum Press, New York, NY, USA, 1972.

[18] S. Sahni, "Computationally related problems," *SIAM Journal on Computing*, vol. 3, no. 4, pp. 262–279, 1974.

[19] O. Bertrand, F. Perrin, and J. Pernier, "A theoretical justification of the average reference in topographic evoked potential studies," *Electroencephalography and Clinical Neurophysiology*, vol. 62, no. 6, pp. 462–464, 1985.

Hindawi Publishing Corporation
Computational Intelligence and Neuroscience
Volume 2007, Article ID 25130, 12 pages
doi:10.1155/2007/25130

Research Article

Context-Based Filtering for Assisted Brain-Actuated Wheelchair Driving

Gerolf Vanacker,[1] José del R. Millán,[2] Eileen Lew,[2] Pierre W. Ferrez,[2] Ferran Galán Moles,[2] Johan Philips,[1] Hendrik Van Brussel,[1] and Marnix Nuttin[1]

[1] *The Department of Mechanical Engineering, Katholieke Universiteit, 3001 Leuven, Belgium*
[2] *The IDIAP Research Institute, 1920 Martigny, Switzerland*

Correspondence should be addressed to Gerolf Vanacker, gerolf.vanacker@mech.kuleuven.be

Received 18 February 2007; Accepted 23 May 2007

Recommended by Fabio Babiloni

Controlling a robotic device by using human brain signals is an interesting and challenging task. The device may be complicated to control and the nonstationary nature of the brain signals provides for a rather unstable input. With the use of intelligent processing algorithms adapted to the task at hand, however, the performance can be increased. This paper introduces a shared control system that helps the subject in driving an intelligent wheelchair with a noninvasive brain interface. The subject's steering intentions are estimated from electroencephalogram (EEG) signals and passed through to the shared control system before being sent to the wheelchair motors. Experimental results show a possibility for significant improvement in the overall driving performance when using the shared control system compared to driving without it. These results have been obtained with 2 healthy subjects during their first day of training with the brain-actuated wheelchair.

1. INTRODUCTION

The continuing progress in the research for noninvasive BCI classification systems gives rise to a wealth of potential practical applications. The prospect of humans interfacing the mechanical world through brain-coupled devices and thereby controlling everyday machines through the process of mere thought is certainly an appealing one as discussed in [1–3]. A promising class of applications are those concerning assistive devices for people with serious impairments. The classical interfaces that disabled people commonly used to control or manipulate an assistive device typically require the patient to have adequate control over one or more physical components of his or her body. Typically, that would be one of the limbs: an arm, hand, or finger. Bioprosthetic systems that are controlled directly through brain signals on the other hand could provide for a more natural extention of human capabilities. Especially in the case where the patient is completely paralysed, this technology may provide for the only possible way for him/her to gain control over basic aspects of his/her daily life.

Amongst these, the ability to control the personal mobility is generally considered an important one. The reduction in mobility that many people experience, due to various impairments or simply due to the effects of ageing, often has a profound impact on the person's independence, social activity, and self-esteem. For many people suffering from a diverse range of impairments, the primary device that could provide for that mobility is the electrical wheelchair. It is worth noting, however, that in case of locked-in patients their highest priority is not mobility. Still, learning how to make it possible to drive complex devices such a wheelchair will also lead to better communication and domotic tools. Many patients, however, do not have the ability to exercise the demanding fine control that wheelchair steering requires, even with an input device capable of communicating a high level of detail, such as the classical joystick. Problems regarding not only the physical inability to accurately manipulate the joystick, but also a reduced kinematical and dynamical insight in the wheelchair motion regularly occur, as was seen in earlier work [4]. Therefore, the prospect of wheelchair control through a brain-coupled control interface, which is in general less reliable than a classical interface, may seem a

Figure 1: A subject controlling our robotic platform Sharioto in a natural indoor environment through noninvase EEG. Visible are the sensors of the platform: a laser range scanner in front and sonar sensors all around.

remote one. Nevertheless, recent results have shown the feasibility of such brain-actuated wheelchairs; see Figure 1 and [1].

Over the past years, important advances in research concerning *shared control* techniques have been made, as may be seen in [4–7]. Shared control systems typically feature one or more intelligent algorithms that aim at assisting the human to execute some task at hand. Both human(s) and intelligent controller(s) then *share* the control over a device whereby each of the actors may exercise influence through the manipulation of some control variables. Together, through cooperative behavior, they aim at completing the task in a way which is hoped to be superior to the situation where only a single actor is in control. In the specific case of assisted wheelchair driving, the actors are the patient and an intelligent controller. The variables to be shared are the translational and rotational velocity of the robot (v, ω). Also, in this class of applications, the human typically has *supervisory* control, meaning that it is him or her that defines the *global plan* that has to be executed. The other actors then need to adopt this plan and cooperate accordingly. Furthermore, an intelligent actor cooperating in a shared control system that is designed to operate with a brain computer interface (BCI) as the human input needs to accommodate for the specific properties that this particular input has.

This paper presents a shared control system for use with a brain computer interface (BCI). The intelligent controller is designed to *filter* out the possible erroneous mental commands inferred by the BCI from noninvasive electroencephalogram (EEG) signals. It estimates the environmental *context* and uses that to detect illogical steering signals, according to the intention—the global plan—the human has. In the proposed framework, the patient has *continuous* control over the wheelchair, parallel to classical joystick control. This allows for a more natural interaction with the robotic assistant, as well as *fine motion* control. The organization of this paper is as follows. In Section 2, we will briefly discuss related work in shared control techniques for wheelchair navigation. Section 3 introduces our new shared control system based on context estimation and signal filtering. In Section 4, we then present experimental results that validate this approach. Finally, Sections 5 and 6 present, respectively, a discussion of the results and the general conclusions of this work.

The brain-actuated wheelchair described in this paper is an extension of the brain-actuated mobile robot developed by Millán et al. [1]. In this paper, we focus on the main innovation of such first prototype, namely, novel features of the shared control framework specifically designed to work with a BCI. Details of the BCI can be found in [1].

2. RELATED WORK

In the past years, a fair number of research groups have ventured into the search for shared control techniques in order to provide assistance to patients as they experience problems when driving an electrical wheelchair. Because of the many different types of manoeuvres that may induce driving problems, for example, driving through a door, obstacle avoidance, driving in a small corridor, docking at a table and others, different algorithms have been developed to cope with these specific situations. This led to the fact that most of the existing approaches focus on the development and selection of such discrete *modes*. Roughly speaking, one may divide the approaches in those that require the user to *explicitly* choose the mode [8–12] on the one hand and those that provide automatic—*implicit*—mode changes based on an interpretation of the surroundings and the user input [6, 7, 13, 14].

Not only the latter group of approaches provide for a more natural interaction between patient and robot, but automatic mode changes are also necessary for a group of patients that are physically unable to communicate their choice on the provided interface. Consider, for example, an array of buttons, each of which activates another assistance mode. A patient suffering from, for instance, multiple sclerosis might experience large difficulties to accurately reach and press the wanted button. The central problem in these implicit approaches therefore is the question: "What is the user's intention?" [6, 7]. Research addressing that question is performed at the *Mobile Learning Robot* (MLR) research group of the Department of Mechanical Engineering at the K. U. Leuven.[1] Another approach centres on establishing a relation between the steering commands that a capable able-bodied user would give—the so-called *reference* signals—and the signals of the specific patient, given the same situation and the same global intention, introduced in [5]. Knowledge over both allows for a conversion of the less than optimal patient steering signals to the optimal reference signals, thereby *filtering* out the steering handicap.

A similar technique filtering may be used to improve the driving performance of a BCI-controlled wheelchair, keeping in mind the specifics of this particular interface. In

[1] http://www.mech.kuleuven.be/mlr.

comparison with the classical analog joystick, as used in [5], the BCI input generally has a limited resolution and higher uncertainty.

3. APPROACH

This paper presents an assistive algorithm specifically designed to help a BCI subject navigate an electrical wheelchair in an everyday environment. It uses an estimate of the environmental *context* to build a probability distribution over the possible steering commands and uses that information to "filter" out possible erroneous user signals. The hypothesis is that with this assistance, the overall driving performance will improve, especially for "novel" subjects, that is, subjects with little or no former experience in BCI control. Figure 2 illustrates the general architecture of the brain-actuated wheelchair.

3.1. BCI-generated commands and interpretation

The nature of BCI-classified mental commands, generated by the subject to indicate some desired movement is quite different from those generated by a continuous joystick. First and foremost, there is an important reduction in resolution due to the limited amount of different mental commands that a BCI classifier can reliably discern. As a consequence, a command-to-movement scheme must be adopted which ensures that smooth motion will result from these discrete input signals. The EEG classifier system used in this work (see [1]) is able to distinguish three discrete commands that may express the need for movement into a certain direction. The steering signals that the classifier outputs consist of a probability distribution over these three discrete steering commands: *Forward*, *Left*, and *Right*. In order to provide intuitive control, we would like to enable the patient to exercise *velocity control* over the platform, so the probability distribution expresses the BCI's belief about the intent of the user to alter the current *velocity* of the wheelchair. *Forward* means that the translational speed v should be increased or maintained—when the maximum speed is already reached. A *Left* or *Right* signal means that the user intends to rotate the wheelchair in the respective direction, thus increasing or decreasing the rotational velocity ω. Both velocities are superimposed, so that a command to turn when the wheelchair is already moving forward will result in a smoothly curved path.

To accommodate for smooth motion, the system maintains the translational speed for a number of seconds, so that the human does not have to constantly generate *Forward* commands when driving straight on. This also prevents the robot from coming to a halt when taking turns. When for a certain period no *Forward* command is issued, however, the robot does effectively stop. For similar reasons, a signal that triggers a rotational command is only executed for a small amount of time. This prevents that the platform keeps turning for too long and overshoots the direction in which the subject intended to continue his travel.

3.2. Context

In typical everyday life, a wheelchair user may come to face a large number of different situations. The nature of a situation is primarily dependent on the environmental settings. Together with the *intention* (the plan) of the user, this environmental situation is part of the *context* in which the controller needs to operate. The assistive system should be able to provide help in as many of these contexts as possible. Because of the different nature of each situation, the controller should be able to detect the specific type of context at hand automatically if it is to help the human in an appropriate manner.

3.2.1. Estimating the context

For this work, context estimation was done by defining a general, a priori-known user intention (smooth and efficient forward navigation through the environment) on the one hand and a constant automatic estimation of the environmental situation on the other hand. The situations were modelled as the number and location of *openings*: wide, open spaces to which the user might safely navigate. The principle is as follows: suppose the wheelchair is approaching a crossroad, as depicted in Figure 3. The laser scanner in front of the wheelchair scans 180 degrees and senses the distance to the environment for every degree. The algorithm then searches for regions with consecutive scans for which the distance is larger than a certain threshold T. This results in a number of regions that qualify as candidates for an opening. Next, for each of the resulting regions, the width of the opening O is calculated:

$$O = \sqrt{s_1^2 + s_2^2 - 2s_1 s_2 \cos(t_2 - t_1)}. \quad (1)$$

This length is then compared to the physical dimensions of the wheelchair (its width). If the length O exceeds the wheelchair width augmented with a safety margin, the corresponding region is accepted as an opening. Its orientation with respect to the current wheelchair position is then $\pi/2 - (t_2 - t_1)/2$.

3.2.2. Extracting a belief in user actions

Each opening then represents a general direction in which the user might opt to continue his travel. With this knowledge about the current situation, a probability distribution concerning the possible *local* user actions may be built. Note that inferring these probabilities requires the knowledge of the global intention of the human. In this case, it is supposed that the user wishes to navigate safely and efficiently through the environment without halting or going backwards. In other cases, a user might also wish to stop at certain locations, or dock at particular places.

When the directions in which the robot can travel are orthogonal, as in Figure 3, we can summarize the environmental belief in four quadrants, as depicted in Figure 4. The figure shows how the regions West and North are deemed probable navigation directions, as extracted from the environment (see Figure 3). The regions East and South, on the other

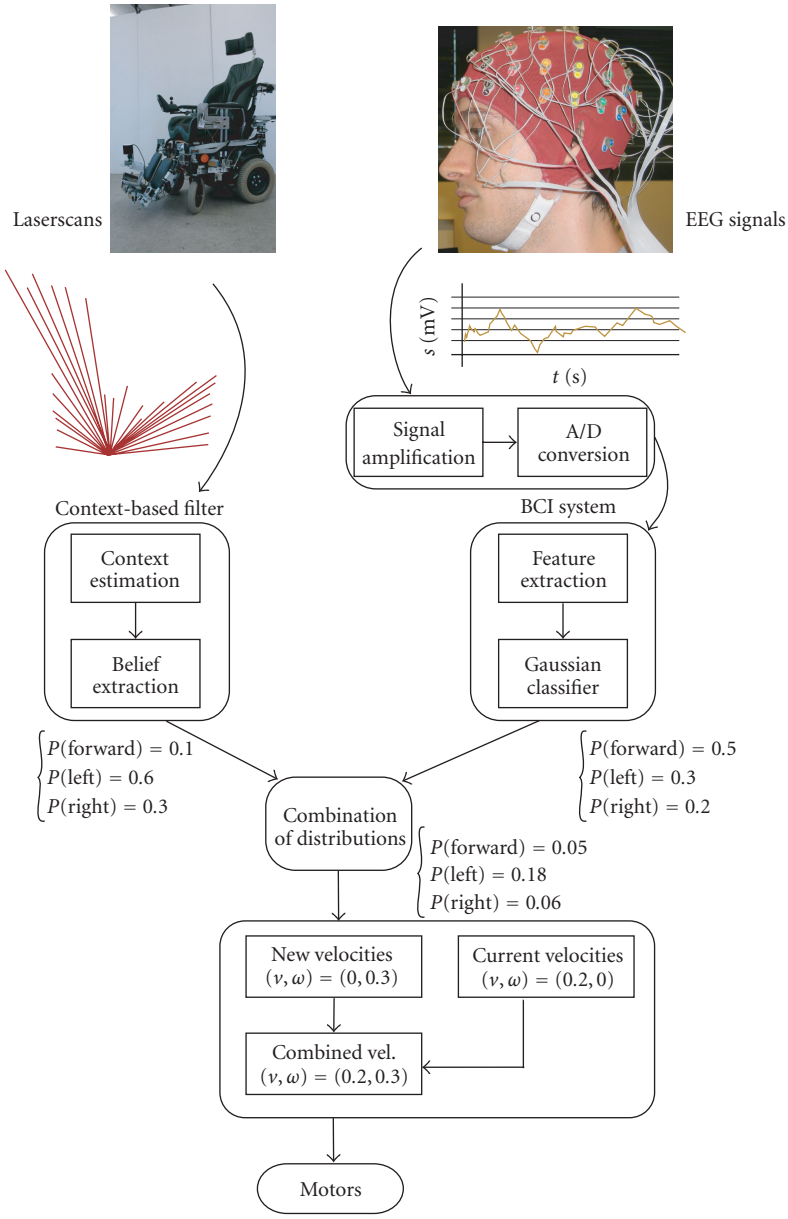

Figure 2: A schematic diagram showing the flow of information in the system. On the left-hand side, environmental information from the wheelchair's sensors (the laser range scanner) feeds the contextual filter that builds a probability distribution over the possible (local) user steering actions. On the right-hand side, the EEG data is fed into the BCI system that estimates the probability of the different mental commands. Both streams of information are combined to form a filtered estimate of the user's steering intent which is eventually sent to the wheelchair's motors as explained in Section 3.1.

hand, are improbable (as the scanner sees a wall on the right hand, and going backwards is also not probable given the intention of smooth forward navigation). If the wheelchair is oriented North, the controller attaches a probability of 0.5 to *Forward* and *Left*. $P_{\text{env}}(Right)$ is set to zero, because rotating to the right would make the robot turn towards an obstacle (the wall). The possibility of turning into the corridor to the left is reflected in $P_{\text{env}}(Left) = 0.5$. If the wheelchair is oriented 45 degrees North-West, $P_{\text{env}}(Forward)$ has become zero, while the possible commands now are *Left* and *Right*, with equal probability, reflecting the belief that one of the orthogonal directions North or West should be chosen. When the wheelchair is turning further towards West, *Forward* becomes possible again, and $P_{\text{env}}(Right)$ stays constant while $P_{\text{env}}(Left)$ diminishes completely. At the boundary between the probable directions and those that are improbable, the controller attaches a maximum belief to those commands that would keep the wheelchair in the half plane of high

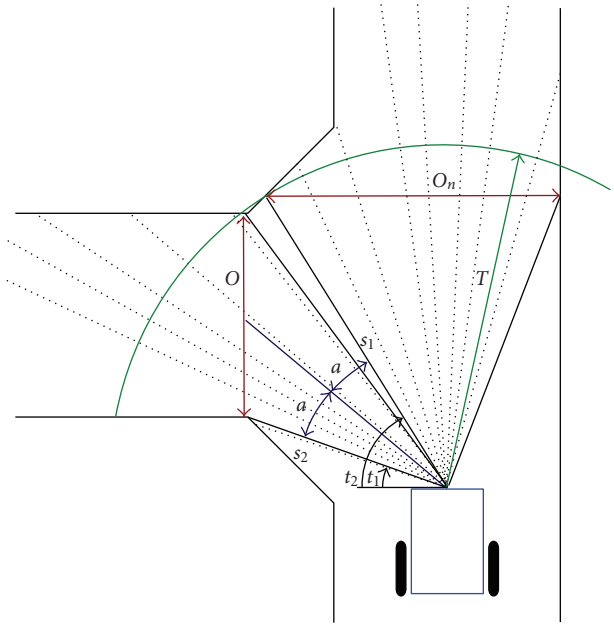

FIGURE 3: The principle of the context estimator. With a laser range scanner, a set of regions is detected that provide safe manoeuvrable openings in the environment. The number and location of these openings, together with the intention of the human, then provides the context. The figure shows how the region to the left and the one in front of the robot are detected as openings.

probability. Between the above-described orientations, the probabilities are interpolated linearly. This is depicted in Figure 4 as the linearly changing transparency of the respective circle.

3.2.3. *Combining the beliefs*

The intelligent controller now needs to combine the signals coming from the EEG classifier with the probability distribution generated from the environmental knowledge, so as to get a better estimation of the user's local steering intent. Different ways of combining the probabilities from EEG classifier and environment may be chosen [15]. In this work, the *product* operator was used, mainly because the classifier can occasionally attribute a high probability to the wrong class, and averaging the contributions of EEG classifier and environment may still lead to a fairly high probability for a command that is in fact very unlikely. Using the product in this case yields more likely combinations. The resulting probability for a certain class C thus becomes

$$P(C) = P_{\text{EEG}}(C) \cdot P_{\text{env}}(C). \tag{2}$$

From the resulting distribution, the command with the *highest* probability is selected and applied to the wheelchair motors.

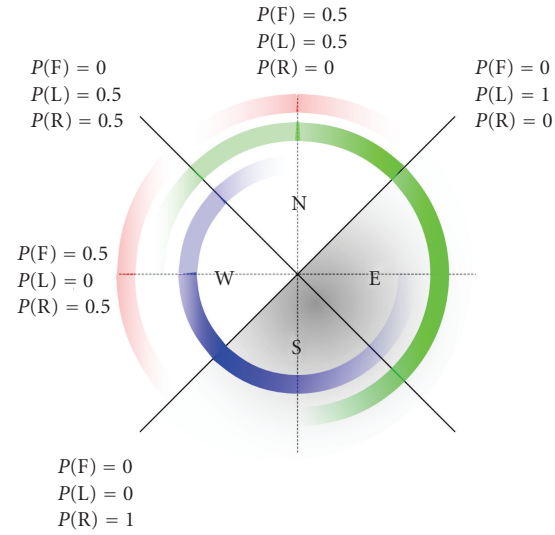

FIGURE 4: Extracting beliefs from the context in function of the wheelchair orientation. Four quadrants are shown, representing a situation in which possible directions are arranged orthogonal. The inner circle shows the probability of a *Right* command, the middle circle the probability of a *Left* command, and the outer circle the probability of a *Forward* command.

FIGURE 5: A subject controlling an intelligent wheelchair in a simulated environment. Visible is the EEG sensor cap with the cables that are connected to the BCI system and the computer that runs the shared control system.

4. EXPERIMENTS AND RESULTS

4.1. *Setup*

Experiments were conducted with a commercially available EEG system feeding the data to the BCI that estimates the user's mental commands. The classifier uses power spectrum information computed from the EEG as its input and outputs the estimated probability distribution over the classes *Left*, *Forward*, and *Right* at a rate of 2 Hz. A second computer running the shared control system is attached to the classifier system and uses its output to control the wheelchair. In this work, a simulated environment was used (mainly for safety reasons) in which a wheelchair was modelled featuring

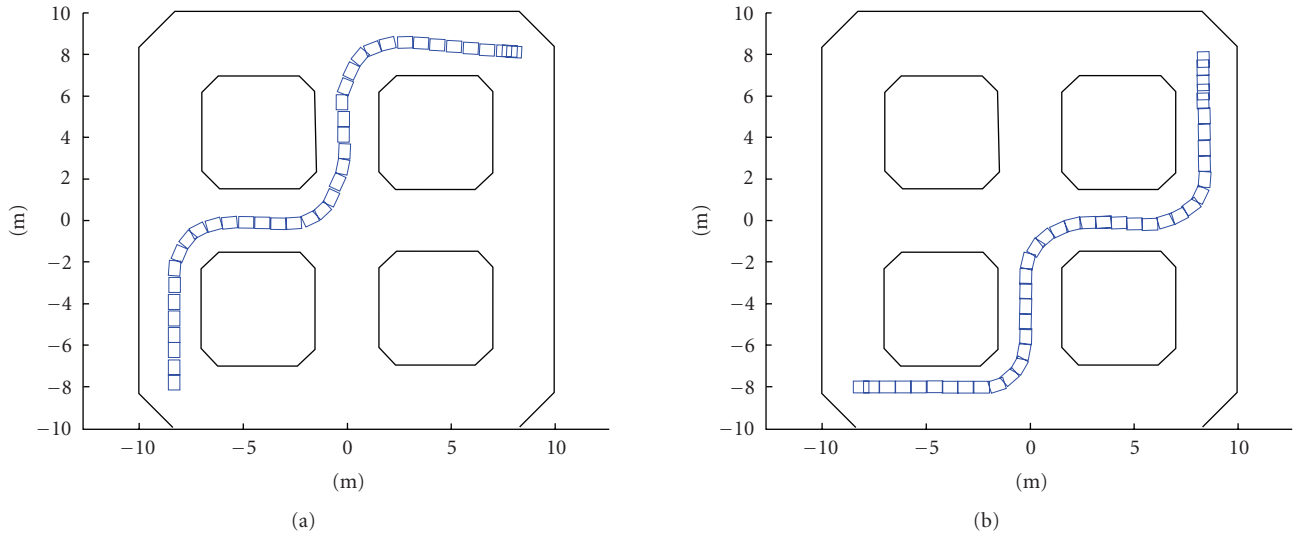

Figure 6: The environment in which the experiments were performed. The wheelchair's position is depicted as a small rectangle at consecutive time steps. Both the paths that the subjects were instructed to follow are shown. It is also worth noting that the initial orientation for each of the paths is different.

a laser range scanner in front capable of scanning 180 degrees (1 scan for each degree) at 5 Hz. The maximum range of this scanner was fixed to 4.5 m, in accordance with the real physical scanner on our platform Sharioto. The wheelchair was placed in the environment shown in Figure 6. The figure also shows the two paths the subjects were asked to follow. Figure 5 shows a subject during one of the sessions.

Furthermore, because of the inherent nonstationary nature of EEG data, a mild form of online learning was used in the EEG classifier system to continually track the subject's brain signals [16].

4.2. Experimental design

For the experiments, two able-bodied voluntary subjects were asked to control the wheelchair for a large number of sessions spanning over several days. This not only allowed to test the performance of the proposed shared control system, but also the *evolution* of the subject's control with and without filter. In between the sessions, the filter was occasionally (de-)activated without the subject's knowledge to investigate the effects of mental model switches and phenomena such as mode confusion [14]. Both subjects were novel with respect to BCI control as well as control of an electrical wheelchair. On the first day we asked the subjects to simply control the wheelchair regardless of any goals in the map, allowing them to get accustomed to using the system. On days 2 through 5, the subjects were instructed to follow a path to reach a certain goal position (see Figure 6). While driving, the subject continuously expressed his/her intended direction orally, allowing logging and comparison. When the wheelchair came too close to an obstacle (a wall), obstacle avoidance (OA, see [4] for details) was activated, to prevent the robot from getting stuck. Finally, the subject was allowed to take resting points while driving (simply because BCI control requires deep concentration which cannot be endured for long periods). When the user calls out "stop," the classifier is paused and no new steering commands are generated. The robot will continue the path it is currently following while the shared control system (obstacle avoidance in this case) would lead it safely away from obstacles, if necessary. For the interpretation of the BCI commands, the following scheme was used:

$$\begin{aligned} v_{\text{inc}} &= 0.5\,\text{m/s}, \\ \omega_{\text{inc}} &= 0.2\,\text{rad/s}, \\ v_{\max} &= 1\,\text{m/s}, \\ \omega_{\max} &= 0.6\,\text{rad/s}, \\ v_{\text{new}} &= \begin{cases} \max\{v_{\text{curr}} + v_{\text{inc}}, v_{\max}\} & \text{if } \delta t_v < 10\,\text{s}, \\ 0 & \text{if otherwise}, \end{cases} \\ \omega_{\text{new}} &= \begin{cases} \max\{\omega_{\text{curr}} \pm \omega_{\text{inc}}, \omega_{\max}\} & \text{if } \delta t_\omega < 1\,\text{s}, \\ 0 & \text{if otherwise}, \end{cases} \end{aligned} \tag{3}$$

where δt_v and δt_ω are the number of seconds since the last received command for, respectively, translational and rotational motion.

4.3. Results

Data was gathered on two distinct levels. First, every command sent by the classifier was logged, as well as the intent of the subject at that time. This allows to compare the output of the classifier with the actual intention of the human on the *individual command* level. Second, when driving towards the goal position, global measures such as the total time needed, the total distance travelled, and the percentage of the time that obstacle avoidance was active were logged to quantify *task performance*.

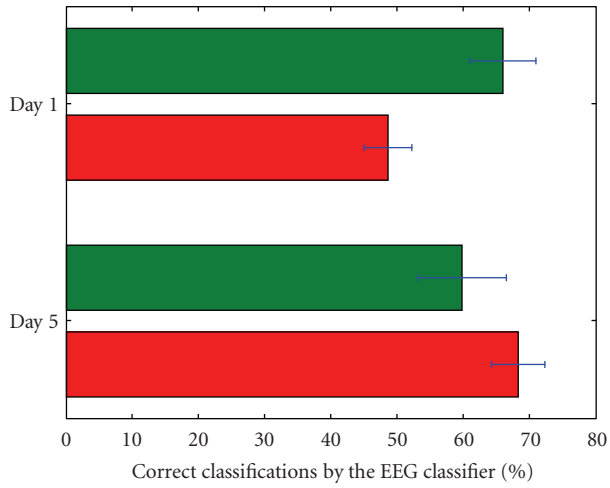

Figure 7: The EEG classifier performance for days 1 and 5 for subject 1. The lower bar in each day depicts the performance when driving without filter, the upper one shows the performance for sessions when filtering was active.

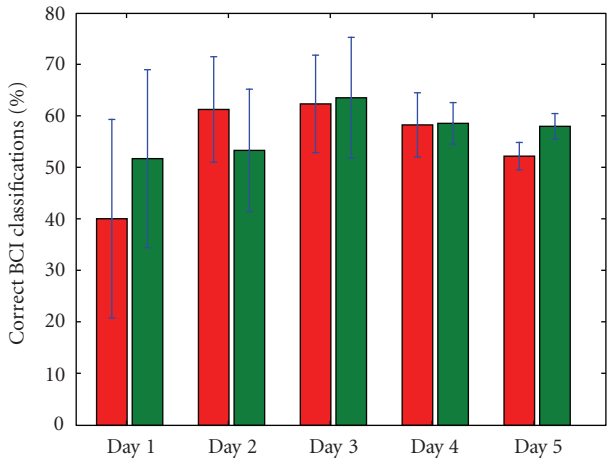

Figure 8: The EEG classifier performance for all days for subject 2. The left bar in each day depicts the performance when driving without filter, the right one shows the performance for sessions when filtering was active.

4.3.1. *Individual command level*

When comparing the number of times that the intended direction (*Forward*, *Left*, *Right*) was deemed the most likely one by the EEG classifier (attaching it the highest probability), subject 1 showed an overall increase in performance over the course of the five days (from 57.24% on day 1 to 63.98% on day 5). It has to be noted in this respect that this subject was completely new to BCI control as well as wheelchair control. The witnessed evolution may thus be attributed to the human gradually learning to control the system. Subject 2 shows a similar improvement over the first days, from 46.61% on day 1 to 63.14% on day 3 (although performance declines afterwards).

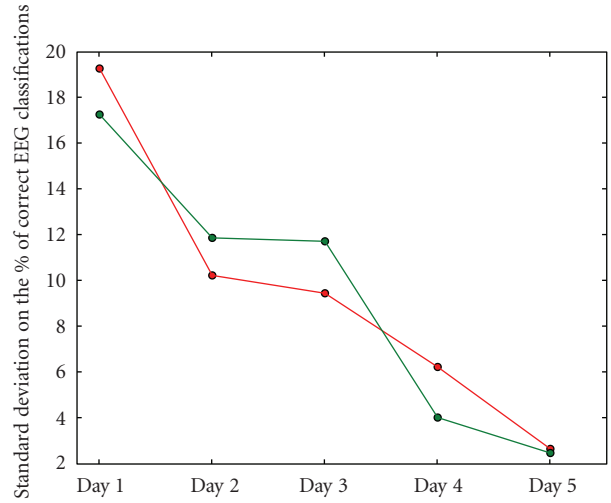

Figure 9: The standard deviations on the EEG classifier performance during the five days for subject 2; sessions with and without filter are shown in green and red, respectively. We can see that the subject shows a more constant performance over the sessions during one day as his experience with controlling the system develops.

For both subjects the classifier performance is different when controlling with or without the environmental filter as is visible in Figures 7 and 8. When the overall BCI performance is rather bad, it is much better to drive with the filter (e.g., subject 1, day 1). On the other hand, when the BCI performance is exceptionally good, driving with the shared control system may make it worse (e.g., subject 1, day 5). It is also worth mentioning that although subject 2 did not show the same increase in average classifier performance over all days (see Figure 8), he showed a steady improvement regarding the standard deviation on the performance (depicted in Figure 9). This reflects the gradually more constant driving behavior of the subject, as his mental driving models become more mature.

A similar picture is visible when we look at the actual resulting number of correct *decisions* that were sent to the wheelchair motors (the number of times that the speeds sent to the motors were in accordance with the subject's intent). Without filtering, this number equals that of the "raw" classifier performance. When environmental filtering is used, we get significantly more correct classifications if the EEG signal in itself is rather bad, but we can see that if the BCI performance gets very good (subject 1, day 5 and subject 2, day 2), the filter may actually deteriorate the percentage of correctly executed decisions (see Figures 10 and 11). We may conclude that if there is ample room for improvement (because of a bad EEG signal), the filter improves the situation. Whenever the human (and classifier) perform very well, however, the filter may actually hold back. However, the fact that the filter may impair the performance depends on the driving behavior of the subject, as can be seen in Figure 11, when we compare day 2 with day 3. Both days show almost the same performance without filter, but the performance *with* filtering is different. The difference may be attributed to a change

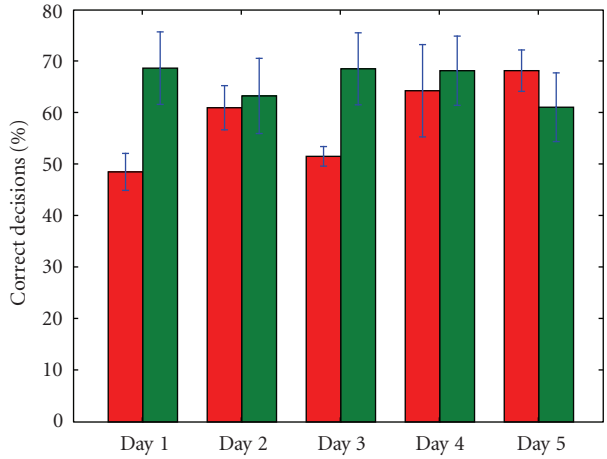

Figure 10: The percentage of control variables (v, ω) that is in accordance with the human's intention, for subject 1. On the left for each day, we see the performance without environmental filtering. On the right, the results when filtering is active. Also shown are the standard deviations.

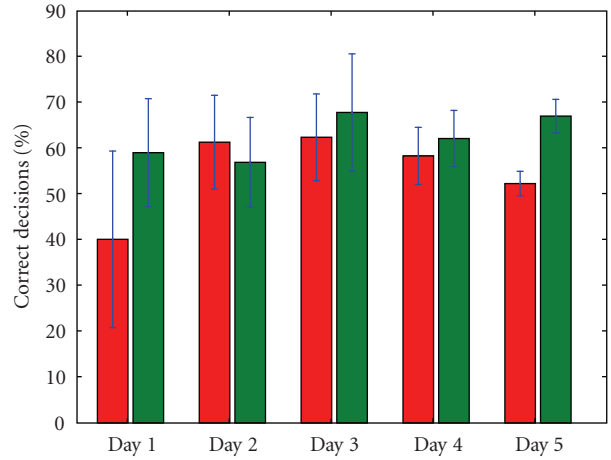

Figure 11: The percentage of control variables (v, ω) that is in accordance with the human's intention, for subject 2. On the left for each day, we see the performance without environmental filtering. On the right, the results when filtering is active. Also shown are the standard deviations.

in driving behavior. In the detail of Figure 12, for instance, we can see that the subject tries to turn 180 degrees in a corridor, behavior which is not deemed likely by the filter (remember that the filter assumes the intention of smooth and efficient *forward* motion). Because it is not deemed likely, many of the subject's steering commands during this manoeuvre are filtered out, which explains the decrease in classifier performance. During day 2 (from which Figure 12 was taken), subject 2 supposedly was still exploring the details of the driving model of the system *with* environmental filter and hence he tried some steering that is incompatible with the filtering assumptions. On day 3, manoeuvres as the one shown in Figure 12 were less in number, supposedly because the mental model that the subject had of the system was more mature by then. All in all, Figure 10 shows that the filter keeps the performance (on the individual command level) more or less constant over all days, roughly between 61% and 69%, in contrast with the more variable decision performance when no filtering is used. Over all sessions and days, the environmental filter improved the individual decision performance with 7.25% for subject 1 and 7.70% for subject 2.

4.3.2. The task level

Interesting in itself, the results obtained on the individual command level do not reflect the *driving behavior*. Even if the speeds that are sent to the motors are *on average* very much what the subject wants them to be, that does not necessarily result in good driving behavior. Much more is involved when controlling mobile robots such as the wheelchair. For one, *timing* is critical. When the corner arrives, the steering needs to be correct *at that very moment*, not just on average over the whole session. Also, the human needs to have good understanding of the kinematic and dynamical constraints of the robot, to predict its movement and hence correctly time the steering. To get a qualitative feeling of the typical driving

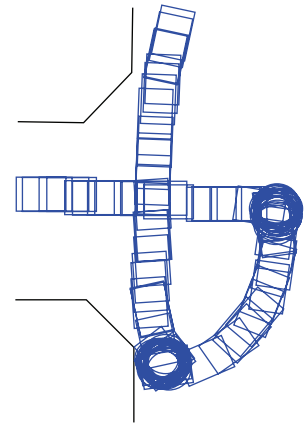

Figure 12: A detail of one trajectory followed by subject 2 on day 2. We can see that the subject tries to turn 180 degrees in a corridor, behavior which is deemed unlikely by the environmental filter.

problems that may occur, see Figure 13. It is clearly visible at Figure 13(a) that steering commands may arrive rather late, when the opportunity of turning into the corridor has already passed. Two main causes underlie this behavior. On the one hand, the subject's kinematic insight is impaired by the large mental workload that the fine steering requires. Therefore, the commands for turning may be generated too late or too soon. On the other hand, switching directions (i.e., from *Forward* to *Right*) always takes some time, because the user has to shift his/her thoughts to another mental task to generate another steering signal. While this switching is occurring, the wheelchair simply drives on and critical moments are passing by. Figure 16 schematically shows this process. Also visible is that a fair amount of "wall following" is occurring, that is, the subject gets too close to a wall and obstacle avoidance is activated, leading the wheelchair alongside the wall. When the subject does not take action to get away from

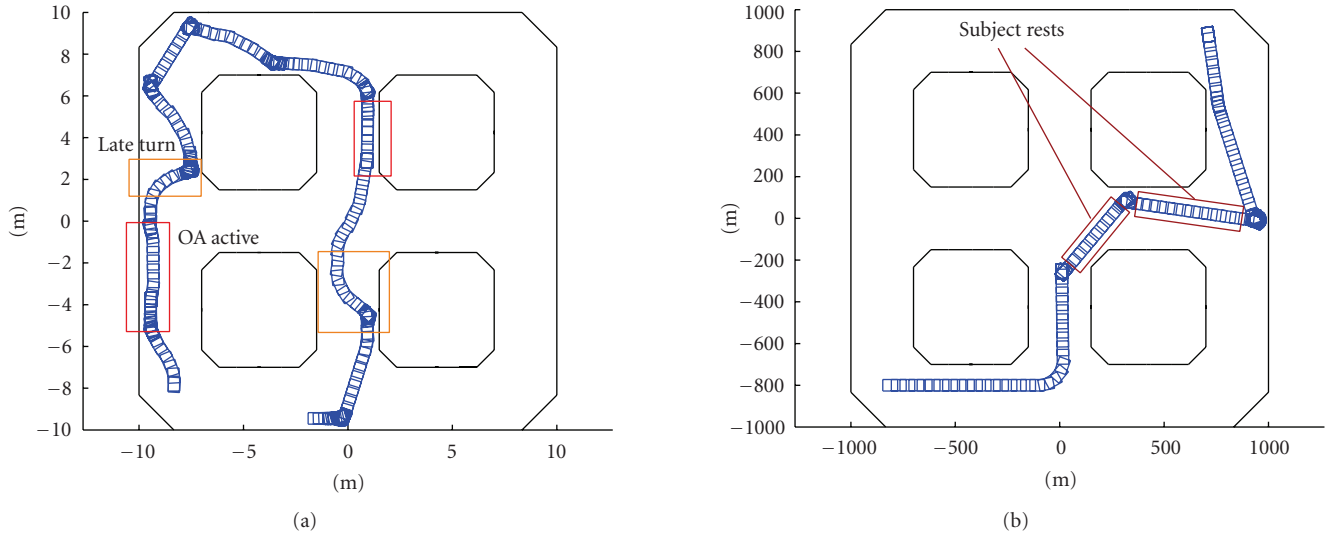

FIGURE 13: Typical problems that occur while driving. On the left, a path is shown that is driven without the environmental filter. We can see that there are many near collisions (obstacle avoidance gets active), resulting in a rather jagged path. On the right a session with filtering is shown. It is clear that the overall path is more smooth, although near collisions still occur (mainly due to inappropriate resting periods).

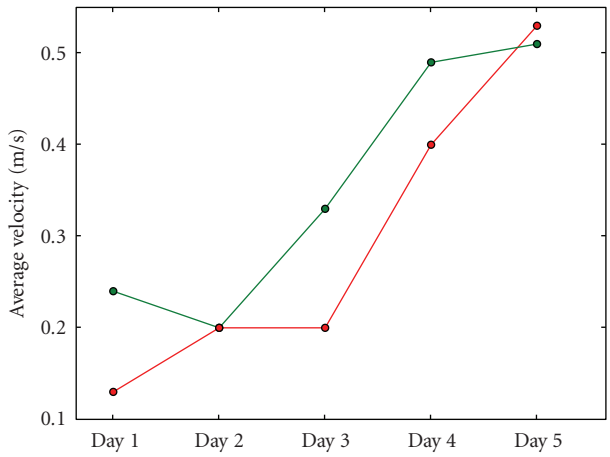

FIGURE 14: The evolution of the average velocity during sessions over all five days for subject 1. The lower line represents the performance when driving without filter, the upper one the average velocity when the filter is active. It is clear that the overall performance (with and without filter) improves significantly over the course of days.

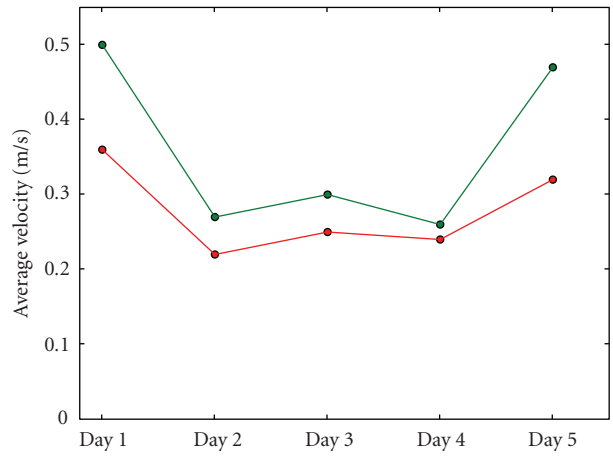

FIGURE 15: The evolution of the average velocity during sessions over all five days for subject 2. The lower line represents the performance when driving without filter, the upper one the average velocity when the filter is active. We can see that the average velocities are much higher when driving with filtering, especially during the first and last days.

the wall, a large percentage of the session time may be spent in OA mode. This is undesirable, as it results in a reduction of the average velocity and thus in a degraded overall task performance.

When driving with environmental filtering, the path is typically much smoother (see Figure 13(b)). Problems that may occur are that the subject chooses his/her resting periods at inappropriate moments. When driving the wheelchair, resting periods are most appropriate when driving straight on in a corridor. The robot will stay on course. Whenever a choice in the path (e.g., the possibility to turn left or right) arises, however, the subject needs to take control and convey his/her intention to the system. In other words, resting periods cannot be chosen arbitrarily but must be appropriately timed as well. For instance, as shown in Figure 13, the subject takes two long rests, right at the moment when he/she needs to decide over the general direction to take. This behavior has a negative impact on the smoothness of the path and the resulting average velocity.

It is also noteworthy to mention that the overall average velocity for subject 1 rises over the days as Figure 14 shows, indicating that the subject's driving skills improve gradually.

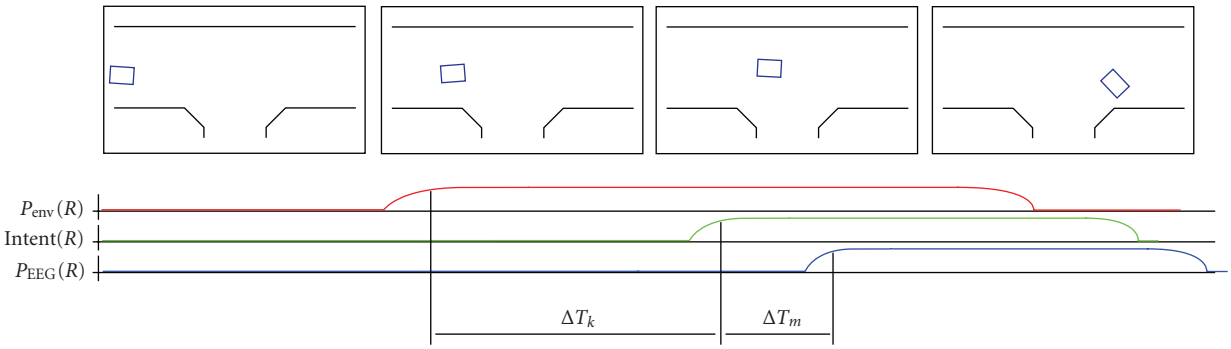

Figure 16: The timing problem. The upper row of figures shows a few frames in the path a subject may follow when the task is to turn south into the T-shaped corridor. We can see the evolution of the probabilities for *Right* commands as seen from the environmental filter and the BCI. Also visible is the moment at which the user decides to start turning, shown as intention(R). The timing issue has 2 components. First, there is a delay δT_k that denotes the suboptimal kinematic prediction by the subject; the turn should have started earlier for the current speed of the platform. Secondly, a mental task switching delay T_m occurs which increases the total time delay even more. Eventually, the opportunity has passed by and the wheelchair crashes into the wall.

Table 1: The percentage of sessions in which subject 1 reached the goal position within 4 minutes.

Day	Overall (all sessions)	Sessions without filtering	Sessions with filtering
Day 2	60%	40%	80%
Day 3	80%	66.67%	85.71%
Day 4	70%	60%	80%
Day 5	80%	100%	60%

Table 2: The time subject 2 needed to reach the goal position (in s).

Day	Overall (all sessions)	Sessions without filtering	Sessions with filtering
Day 2	151.32	164.25	138.4
Day 3	120.37	144.6	115.52
Day 4	138.7	145.6	127.2
Day 5	110.26	126.01	84.01

Subject 2 does not show a similar evolution (see Figure 15), but *in both cases* we can see that the average velocities are much higher when filtering is active. For subject 1, the average improvement the filter offers regarding the average velocity is 17.58%. For subject 2 the gain is even higher: 22.72%.

Another interesting factor is the time the user spent in obstacle avoidance mode, as this reflects an undesirable aspect: namely that the subject is controlling the robot to a lesser extent when in this mode. Furthermore, OA is designed as a safety measure, not to provide continuous navigational assistance. All in all, spending much time in OA does not constitute what we regard as "good driving behavior" and it slows the navigation down significantly. When we compare the average amount of time spent in OA mode when driving without filter to the amount when driving with environmental filtering, we see an overall 13.3% (subject 1) and 17.44% (subject 2) decrease for the latter case. This is reflected in the more efficient (centre of corridor) driving behavior.

Now, if we consider the task that the subjects had to perform (driving to a certain goal pose, if possible via a predetermined path, as shown in Figure 6) we get the results for subject 1 listed in Table 1. This table shows the figures for day 2 through 5 (there was no goal-directed task in day 1). It is clear that for the majority of days, the environmental filter significantly increases the probability of reaching the goal position within 4 minutes. Only during the last day, the subject had better control without the filter and could reach the goal 100% of the time. All sessions together, the filter proves to increase the task performance by about 10%. Considering only days 2 through 4, we see an increase of more than 26%. Subject 2 on the other hand, did not show a large difference in probability of reaching the goal with or without filtering (+7.5% when filtering is active). However, the *time* needed to reach the goal is significantly lower when using the environmental filter, as Table 2 shows. In total, subject 2 reached the goal 19.87% more rapidly when driving with filter compared to driving without.

5. DISCUSSION

The experiments were conducted with two subjects that had no previous experience in BCI control nor control of differentially driven robots such as the electrical wheelchair. From the data collected over all five days, we can clearly see how the subjects have gradually learned to improve this control. Yet, the problem of predicting the kinematic behavior of the wheelchair accurately remains a mentally demanding task. This may cause erroneous timing when initiating a turn into a corridor, leading to a worse overall driving behavior; refer to Figure 16 for a graphical overview of this problem.

During the course of the first days, when the subjects were still performing rather bad, the filter acts as a correctional tool that rectifies much of the misclassifications coming from the EEG classifier. This is visible in Figures 10,11, 14,15 and Table 1. As a result, filtering enables a novel subject

to achieve good levels of performance even on the *first* day of usage. It is clear from Figures 10 and 11 that the filter keeps the performance on the level of the individual commands more or less stable over all days. The environmental filter may thus be seen as a *learning tool* that keeps the subjects performance on a workable level even if that subject is just taking the first steps in learning to use BCI control for driving a wheelchair. Later on, when the subject shows an improved control, the filter corrects less, up to the point that the control is so good that the filter actually holds back. It is remarkable that on the first day, when the subjects still were completely new to the task, for some (filtered) sessions very good performance could be noted.

However, the collected data and the performance figures extracted from the experiments are to a large extent dependent on the *driving strategy* the subject employs. As the subjects gradually learned to control the system, different strategies were explored. One example is visible in Figure 13(a), where the subject exploited the behavior provided by the obstacle avoidance algorithm to lead the robot without much control effort alongside a wall. Similarly, the subject occasionally exploited the OA safety behavior to let the robot ride until it approaches a wall. At that point, OA slows the robot down and the subject has more time to choose the direction he/she wants to go into. This is, for instance, visible in Figure 13(b). Now, while exploring alternative strategies, the performance measures naturally change as well.

A further source of "noise" on the collected data is caused by inappropriate usage of the resting possibility, as already discussed before. Figure 13-right shows an example. Of course, this strategy also has a negative influence on the resulting performance.

Furthermore, the filter was regularly switched on and off in between sessions, without the subject's knowledge. Because of the fact that the driving system is different when the filtering is applied, the subject needs to use another mental model (or at least adapt his/her existing one) when the filter is switched on or off. Also, the subjects were not told how the environmental filter internally works, so that they needed to learn an appropriate mental model from scratch while driving. The result is that when the subject's acquired strategies built up using the one driving system (i.e., without filtering) were applied to the other situation, performance was seriously weakened. This effect is sometimes referred to as *mode confusion* [14] and it is a common problem in shared control systems. An illustrative example is that when driving without filtering, the subjects learned at a certain moment to turn 180 degrees in a corridor, whenever they got orientated in the wrong direction (see Figure 12). When the filter was switched on, he/she tried to use that same strategy. Because the filter assumes smooth and efficient forward motion, such behavior was deemed unlikely and the filter made it a difficult manoeuvre. This leads to a situation in which the environmental filter is actually working *against* the user's intention.

6. CONCLUSIONS AND FURTHER WORK

We have shown that the usage of an environmental filtering technique, which uses knowledge about the current context to filter out erroneous steering commands, can improve the overall driving behavior. Especially when the subject is not already trained for the task, the filter provides significant benefits. However, when the subject is performing really well and employs driving behavior that is not compatible with the logic of the filter, performance may be weakened. All in all, the subjects declared that driving with filtering was *more easy* to do, especially during the first days. As such, the system proves most useful as a learning tool, when the subject is in the learning phase of BCI control.

Probably the most notable weakness of the filter in its current form is the fixed user model. The system assumes a certain driving behavior that would lead to smooth and efficient forward motion. Whenever strategies are employed that contradict with this assumption, the performance gets worse (i.e., 180-degree turning in a corridor). Therefore, we need an *adaptive* model that constantly adapts to whatever strategies the user might employ. Besides that, we could also benefit from a detection mechanism that simply switches off the filter if user performance gets high, or more generally some mechanism to regulate the amount of influence the filter has. Also, a user model incorporating the specific BCI profile the particular subject has (how likely it is that he/she generates the correct steering commands) might lead to a better filtering of the individual commands.

ACKNOWLEDGMENTS

This research was funded by a Ph.D. grant of the Institute for the Promotion of Innovation through Science and Technology in Flanders (IWT-Vlaanderen). This work is supported by the Swiss National Science Foundation NCCR "IM2" and by the European IST Programme FET Project FP6-003758. This paper only reflects the authors' views and funding agencies are not liable for any use that may be made of the information contained herein.

REFERENCES

[1] J. d. R. Millán, F. Renkens, J. Mouriño, and W. Gerstner, "Noninvasive brain-actuated control of a mobile robot by human EEG," *IEEE Transactions on Biomedical Engineering*, vol. 51, no. 6, pp. 1026–1033, 2004.

[2] J. d. R. Millán, "Brain-computer interfaces," in *Handbook of Brain Theory and Neural Networks*, M. A. Arbib, Ed., pp. 178–181, MIT Press, Cambridge, Mass,USA, 2002.

[3] J. d. R. Millán, F. Renkens, J. Mouriño, and W. Gerstner, "Brain-actuated interaction," *Artificial Intelligence*, vol. 159, no. 1-2, pp. 241–259, 2004.

[4] M. Nuttin, D. Vanhooydonck, E. Demeester, and H. Van Brussel, "Selection of suitable human-robot interaction techniques for intelligent wheelchairs," in *Proceedings of the 11th IEEE International Workshop on Robot and Human Interactive Communication (ROMAN '02)*, pp. 146–151, Berlin, Germany, September 2002.

[5] G. Vanacker, D. Vanhooydonck, E. Demeester, et al., "Adaptive filtering approach to improve wheelchair driving performance," in *Proceedings of the 15th IEEE International Symposium on Robot and Human Interactive Communication (ROMAN '06)*, pp. 527–532, Hatfield, UK, September 2006.

[6] D. Vanhooydonck, E. Demeester, M. Nuttin, and H. Van Brussel, "Shared control for intelligent wheelchairs: an implicit estimation of the user intention," in *Proceedings of the 1st International Workshop on Advances in Service Robotics (ASER '03)*, pp. 176–182, Bardolino, Italy, March 2003.

[7] E. Demeester, M. Nuttin, D. Vanhooydonck, and H. Van Brussel, "A model-based, probabilistic framework for plan recognition in shared wheelchair control: experiments and evaluation," in *Proceedings of IEEE/RSJ International Conference on Intelligent Robots and Systems (IROS '03)*, vol. 2, pp. 1456–1461, Las Vegas, Nev, USA, October 2003.

[8] N. I. Katevas, N. M. Sgours, S. G. Tzafestas, et al., "The autonomous mobile robot SENARIO: a sensor-aided intelligent navigation system for powered wheelchairs," *IEEE Robotics & Automation Magazine*, vol. 4, no. 4, pp. 60–70, 1997.

[9] E. Prassler, J. Scholz, and M. Strobel, "MAid: mobility assistance for elderly and disabled people," in *Proceedings of the 24th Annual Conference of the IEEE Industrial Electronics Society (IECON '98)*, vol. 4, pp. 2493–2498, Aachen, Germany, August-September 1998.

[10] H. Yanco, *Shared user-computer control of a robotic wheelchair system*, Ph.D. thesis, Massachusetts Institute of Technology, Cambridge, Mass, USA, September 2000.

[11] G. Bourhis, O. Horn, O. Habert, and A. Pruski, "An autonomous vehicle for people with motor disabilities," *IEEE Robotics & Automation Magazine*, vol. 8, no. 1, pp. 20–28, 2001.

[12] R. S. Rao, K. Conn, S. H. Jung, et al., "Human robot interaction: application to smart wheelchairs," in *Proceedings of IEEE International Conference on Robotics and Automation (ICRA '02)*, vol. 4, pp. 3583–3588, Washington, DC, USA, May 2002.

[13] R. C. Simpson, S. P. Levine, D. A. Bell, L. A. Jaros, Y. Koren, and J. Borenstein, "NavChair: an assistive wheelchair navigation system with automatic adaptation," in *Proceedings of the Assistive Technology and Artificial Intelligence, Applications in Robotics, User Interfaces and Natural Language Processing*, vol. 1458 of *Lecture Notes in Computer Science*, pp. 235–255, 1998.

[14] T. Röfer and A. Lankenau, "Architecture and applications of the Bremen autonomous wheelchair," in *Proceedings of the 4th Joint Conference on Information Systems*, vol. 1, pp. 365–368, Association for Intelligent Machinery, October 1998.

[15] L. I. Kuncheva, *Combining Pattern Classifiers: Methods and Algorithms*, John Wiley & Sons, New York, NY, USA, 2004.

[16] A. Buttfield, P. W. Ferrez, and J. d. R. Millán, "Towards a robust BCI: error potentials and online learning," *IEEE Transactions on Neural Systems and Rehabilitation Engineering*, vol. 14, no. 2, pp. 164–168, 2006.

Hindawi Publishing Corporation
Computational Intelligence and Neuroscience
Volume 2007, Article ID 12725, 13 pages
doi:10.1155/2007/12725

Research Article

Connecting Neurons to a Mobile Robot: An In Vitro Bidirectional Neural Interface

A. Novellino,[1] P. D'Angelo,[2] L. Cozzi,[2] M. Chiappalone,[1] V. Sanguineti,[2,3] and S. Martinoia[1,3]

[1] *Neuroengineering and Bio-nanotechnology Group, Department of Biophysical and Electronic Engineering (DIBE), University of Genova, Via Opera Pia 11a, 16145 Genova, Italy*
[2] *NeuroLab, Department of Informatics Systems and Telematics (DIST), Via Opera Pia 13, 16145 Genova, Italy*
[3] *Center for Neuroscience and Neuroengineering "Massimo Grattarola", University of Genova, 16132 Genova, Viale Benedetto XV, 3, Italy*

Correspondence should be addressed to Antonio Novellino, antonio.novellino@ettsolutions.com

Received 27 December 2006; Revised 4 April 2007; Accepted 18 June 2007

Recommended by Fabio Babiloni

One of the key properties of intelligent behaviors is the capability to learn and adapt to changing environmental conditions. These features are the result of the continuous and intense interaction of the brain with the external world, mediated by the body. For this reason "embodiment" represents an innovative and very suitable experimental paradigm when studying the neural processes underlying learning new behaviors and adapting to unpredicted situations. To this purpose, we developed a novel bidirectional neural interface. We interconnected in vitro neurons, extracted from rat embryos and plated on a microelectrode array (MEA), to external devices, thus allowing real-time closed-loop interaction. The novelty of this experimental approach entails the necessity to explore different computational schemes and experimental hypotheses. In this paper, we present an open, scalable architecture, which allows fast prototyping of different modules and where coding and decoding schemes and different experimental configurations can be tested. This hybrid system can be used for studying the computational properties and information coding in biological neuronal networks with far-reaching implications for the future development of advanced neuroprostheses.

1. INTRODUCTION

Electrophysiological techniques, both in vivo and in vitro, are traditionally used to study spontaneous neural activity and its modifications in response to different kinds of external stimuli (e.g., chemical, electrical, electromagnetic). One of the main limitations of these studies is the total absence of a sensory and motor "context." This condition is particularly unnatural: complex mechanisms, like learning, are the result of a continuous interaction between the nervous system and the environment, mediated by the body. For this reason, during the last years, the growing interest in neuroscience for closed-loop experiments (cf. Society for Neuroscience Meeting 2004, San Diego (Calif, USA); http://apu.sfn.org) has led to the development of several innovative bidirectional platforms, under the hypothesis that the dynamical and adaptive properties of neural systems may be better understood in the context of the interaction between the brain and the external environment.

In the last few years, interaction has been studied at different levels of investigation: at the molecular level, by synthesizing the behavior of artificial ion channels—the dynamic-clamp technique (Sharp et al. [2]); at the single neuron level, by interfacing artificial and actual neurons (Le Masson et al. [3]); at the population level, by controlling the dynamic regime of neuronal populations (Wagenaar et al. [4]) and its adaptive properties (Shahaf and Marom [5]; Marom and Eytan [6]); and, finally, at the whole system level, by means of experiments in which portions of the ex vivo/in vivo brain of an animal are connected to artificial/virtual robots to form bioartificial/hybrid systems (Reger et al. [7]; Wessberg et al. [8]; Nicolelis [9]; Schwartz et al. [10]; Karniel et al. [11]).

An alternative and simplified paradigm to study the interaction between the brain and the external world is the "embodied electrophysiology," where dissociated neuronal networks are bidirectionally coupled to artificial systems (DeMarse et al. [12]; Bakkum et al. [13]; Martinoia et al.

[14]), which provide a physical body to the in vitro brain and allow it to interact with the environment (Potter [15]). This paradigm can be used to investigate the mechanisms that the nervous system uses to represent, store, and process sensorymotor information, understanding how living neurons lead to higher-level cognition and "intelligent behavior" (Bakkum et al. [13]).

The development of in vitro bidirectional neural interface offers the unique opportunity to explore the adaptive properties of a model of the neural system and it can be of valuable help for the future developments of in vivo neural interfaces (Mussa-Ivaldi and Miller [16]; Nicolelis [17]). Ideally, in vivo brain-machine interfaces should enable two-way communication, that is, both stimulation and recording at the same time. Two-way interaction would be particularly crucial in advanced neuroprostheses. Sensory systems cannot be fully restored by simply mapping input into the brain; instead, neuroprosthetic devices should be fused with the reciprocating neural interactivity that is responsible for ongoing conscious awareness.

The aim of this paper is to describe the architecture and the high potential of the developed neurorobotic system, that is, a neuronal network connected to a mobile robot. In the "methods" section, we discuss the issues underlying design and computational choices. The computational requirements for the closed-loop system are very demanding, mainly due to the necessity to simultaneously process high-frequency multichannel data, in real time. On the other hand, the novelty of this approach involves the necessity to explore different computational schemes (e.g., to change the coding/decoding strategy, the number of input/output electrodes, and the value of the parameters). In the "results" section, we describe the computational performances of the developed system and the strategies for selecting the input and output sites, an essential step when dealing with neuronal model with a no predefined architecture, such as dissociated cultures (see Figures 1(a), 1(b)). Finally, the preliminary experiments involving a network of cortical neurons and a robotic body are presented and the main improvements with respect to our previous results (Cozzi et al. [18]) are underlined, both in terms of computational architecture and experimental protocol. The use of a simple reactive behavior (i.e., obstacle avoidance) demonstrates the feasibility of the approach and the potential of this novel experimental paradigm.

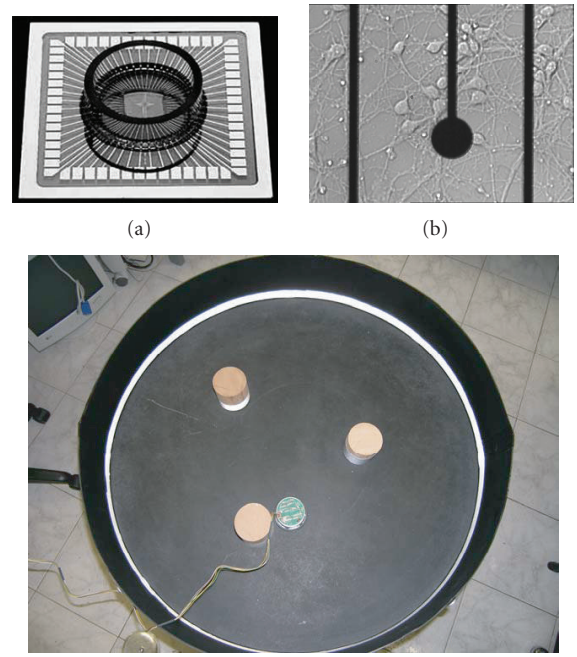

(a) (b)

(c)

Figure 1: The main actors of the neurorobotic set-up. (a) A commercial MEA by Multichannel Systems (Reutlingen, Germany) with 60 electrodes. (b) Cortical neurons grow and develop a 2D network over the MEA, in proximity of a recording microelectrode. (c) The Kephera robot wandering in its arena, filled with cylindrical wooden obstacles.

2. MATERIALS AND METHODS

2.1. Robot body, playground arena and obstacle avoidance task

Modeling of adaptive behavior by developing adaptive autonomous agents is an approach widely investigated in the fields of artificial intelligence and autonomous control (Maes [19]; Brooks [20]), and a particular model of adaptive behavior is represented by an agent who is motivated in trying to survive in a defined environment, without any external (i.e., human) help.

The agent may generate its actions exclusively from the available sensory information, or may use some kind of previous "experience." The former type of agent is generally referred as "reactive." One of the most studied implementations of this model is the "exploring" vehicle paradigm. In 1984, Braitenberg [21] proposed a simple architecture, that is, a vehicle with direct links between sensors and motors (the greater the sensors values are, the faster the motors run), that seems to mimic an intelligent behavior in a real context. The easiest example of the Braitenberg's vehicles is a two-wheeled robot with two light sensors that, according to the connection between sensors and motor-wheels, can produce different and interesting behaviors (fear, aggressiveness). Here we will show a neurorobotic Braitenberg "explorer" vehicle as an example of application of the closed-loop platform for embodied electrophysiology.

The artificial body consists of a small mobile robot (Khepera II, K-team, http://www.k-team.com), equipped with two wheels and eight infrared (IR) proximity sensors that provide information about the distance of the robot from obstacles. In our experiments, the robot (7 cm diameter) moves inside a circular arena (80 cm diameter), containing wooden cylindrical obstacles (7 cm diameter). The Khepera robot and its playground are shown in Figure 1(c). In order to partially compensate the high nonlinearity of the proximity sensors and the influence of the ambient light, the

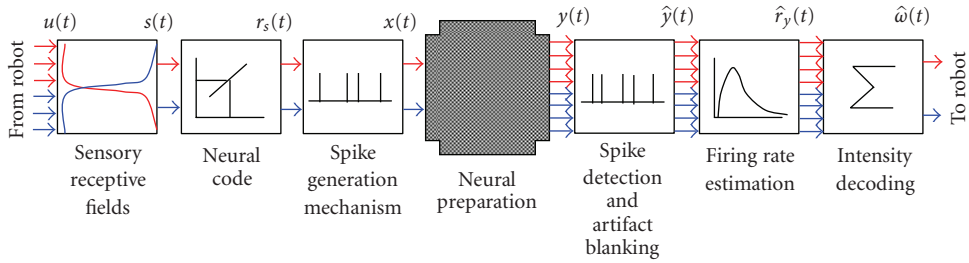

Figure 2: Computational architecture of the closed-loop system. The signals coming from the infrared sensors (IR) of the robot are translated into patterns of stimuli that are delivered to the neural preparation through a set of selected stimulating electrodes. Then the activity recorded by two groups of electrodes is evaluated in terms of firing rate (i.e., mean number of detected spikes/s) and used as driving speed for each of the robot's wheel.

internal perimeter of the playground and the border of the obstacles were covered with an IR reflective tape.

2.2. Computational architecture of the neural interface

To establish a bidirectional communication between the neuronal preparation and a mobile robot, the electrophysiological signals need to be translated into motor commands for the robot (decoding of neural activity), and at the same time the sensory signal from the robot need to be translated into a pattern of electrical stimulation (coding of sensory information). Figure 2 presents the general computational architecture of the proposed closed-loop system that can be summarized in the following three main parts (i.e., from left to right in Figure 2).

(1) Coding (from the robot to the neural preparation): while the robot freely moves into the playground, its IR sensors see whether or not an obstacle is in the proximity and where it is (left or right side). The IR signals $u(t)$ are weighted according to the sensory receptive field law and the two resulting stimulation signals $s(t)$, relative to the right and left "eye" of the robot, are then coded into a feedback stimulation $x(t)$.

(2) Processing of electrophysiological signals: the spontaneous or evoked electrophysiological activity $y(t)$ is sampled ($\hat{y}(t)$) and processed, in order to give an estimation of the instantaneous firing rate $\hat{r}_y(t)$.

(3) Decoding (from the neural preparation to the robot): the processed electrophysiological signal $\hat{r}_y(t)$ is translated into motor commands $\omega(t)$ for the robot, according to the specified decoding strategy.

To make our computational architecture as open as possible, we developed a library of coding/decoding schemes (Cozzi et al. [18]; Cozzi et al. [22]), and identified the most effective ones in achieving a desired behavioral task.

Library of coding schemes

Coding means the representation of external sensory input patterns in terms of electrical stimulation and hence of neuron's activity. In this perspective, the implemented *neural code* has been of two main typologies, both of them based on the rate coding concept.

(1) Proportional coding.
The rate of stimulation $r_s(t)$ is proportional to the sensory feedback $s(t)$. The maximum rate of stimulation, $r_s^{\max}$, is only attained when the robot hits an obstacle. It was suggested that this value has to be as large as possible for accurate coding of the temporal structure of sensory signal (Wagenaar et al. [1], DeMarse et al. [12]), but at the same time it has to be low in order not to damage the culture (Shahaf and Marom [5]), therefore, the maximum of the stimulation rate $r_s(t)$ was up to 2 Hz.

(2) Binary coding.
A binary coding scheme generates trigger signals for the electrical stimulator only when the sensory feedback $s(t)$ overcomes a threshold, approximately reflecting the presence of an obstacle at 5 cm distance. The stimulation rate $r_s(t)$ is therefore either 0 or 1 Hz. The maximum frequency of stimulation was chosen according to what reported in literature (Shahaf and Marom [5]).

Preprocessing of electrophysiological signal

Spike detection. The electrophysiological signals $\hat{y}(t)$ acquired from MEA electrodes must be preprocessed in order to remove the stimulus artifact and to isolate spikes from noise.

The spike detection algorithm uses a differential peak-to-peak threshold to follow the variability of the signal (Grattarola et al. [23]). A time window, sized to contain at most one single spike (4 ms), is shifted along the signal, sampled at the frequency of 10 kHz. Within the window when the difference between the maximum and the minimum exceeds the threshold, a spike is found and its time stamp is saved. In this way, the resulting spike train signal is sampled at 250 Hz. The threshold is proportional to the noise standard deviation (SD) and is calculated separately for each individual channel (typically as $7 \times$ SD) before the beginning of the actual experiment (i.e., the spontaneous activity recording, see Section 3.3).

Blanking of stimulus artifact. Stimulus artifacts are detected when the recorded signal exceeds a second, higher threshold. The artifact is then suppressed by cancelling the first sample in the spike train occurring immediately after it, corresponding to a signal blanking of 4 milliseconds after stimulus delivery. This quite conservative procedure could have been improved, but we found it effective for our applications.

Decoding schemes

Although several linear and nonlinear algorithms for translating neuronal activity into motor commands for external actuators have been proposed (Chapin et al. [24]; Wessberg et al. [8]; Carmena et al. [25]; Wessberg and Nicolelis [26]), here the decoding schemes are simply based on rate-coding (Fetz [27]), that has proven to be efficient in brain-machine-interfaces (Lebedev and Nicolelis [28]).

Firing rate estimation. The neural activity is represented by the instantaneous firing rate $\hat{r}_y(t)$ on each recording channel and it is estimated from the spike trains $y(t)$ through a low-pass filter. Two different filters have been implemented (a first-order and a second-order filter).

Decoding. The recording sites are divided into two groups, respectively used for controlling the left and right wheel, each of them formed by N electrodes. The motor commands $\omega(t)$, that is, the angular speeds of the wheels, are obtained by implementing the following winner-takes-all (WTA) mechanism:

$$\omega_L(t) = \begin{cases} \left(\omega_0 - \sum_{i=1}^{N} C_i \cdot \left[\hat{r}_i(t)\right]_R\right) & \text{if } \omega_L \geq \omega_R, \\ -\omega_b & \text{if } \omega_L < \omega_R, \end{cases}$$
$$\omega_R(t) = \begin{cases} \left(\omega_0 - \sum_{i=1}^{N} C_i \cdot \left[\hat{r}_i(t)\right]_L\right) & \text{if } \omega_R \geq \omega_L, \\ -\omega_b & \text{if } \omega_R < \omega_L, \end{cases} \quad (1)$$

where ω_b is a constant angular speed (up to 2 rad/s), ω_0 is the maximum angular speed (i.e., 5 rad/s); $\hat{r}_i(t)$ is the instantaneous firing rate of the recording site i, C_i is a normalization coefficient. L and R indicate signals pertaining respectively to the left and the right wheel. In absence of neuronal activity, the robot goes straight with a constant angular speed of 5 rad/s that corresponds to a linear velocity of 16 cm/s. The coefficients C_i can be computed according to different criteria: they represent an estimate of the strength of the connection between the corresponding input and output site (computed by means of a linear regression), as reported in (Cozzi et al. [18]), or they simply represent the inverse of the estimation of the maximum value that can be reached by the instantaneous firing rate on each group (left versus right) of electrodes. The first method is usually applied when decoding the activity of each unit in large population of neurons (Georgopoulos et al. [29]). For the experiments reported here, we adopted the second: the used algorithm already selects input-output pathways characterized by the maximal strength of the functional connection and we only need to equalize them, in other words, when the robot is far from obstacles the spontaneous activity should not cause the robot turning preferentially clockwise or counterclockwise. Assuming that neurons on the left and right sides are mostly excitatory, the minus sign in the control law allows us to implement inhibitory contralateral connections between inputs and outputs.

The WTA strategy has proven to be a more appropriate decoding scheme than those already presented in our previous work (Cozzi et al. [18]). In fact, even though the WTA mechanism may result in movements that are less smooth, the lowest values chosen for the angular speed (i.e., 2 or 5 rad/s instead of 10 rad/s) facilitate the robot rotation without affecting the general behavior and, as a consequence, the robot can reverse direction in much less space, actually realizing what the "brain" is ordering to its "body." This strategy is also suggested by the nonlinearity of the IR sensors (for further details see the "Khepera II-IR sensors report," http://ftp.k-team.com/khepera/documentation/Kh2IRAN.pdf) of the robot that are capable to reliably detect an obstacle only when the robot is closer than about 5 cm from an obstacle.

2.3. Neural preparation and control architecture

Neural preparation and electrophysiological set-up

Dissociated neurons in culture randomly rearrange in a bidimensional structure and, once they have established synaptic connections, they show spontaneous neural activity (starting from about 7 days in vitro DIVs) that can be modulated by means of electrical stimulation (Maeda et al. [30]; Jimbo et al. [31]; Marom and Shahaf [32]). We used dissociated cultures of cortical neurons, extracted from rat embryos (E18). Using standard methods previously described (Martinoia et al. [33]; Chiappalone et al. [34]), cells were plated on microelectrode arrays (MEAs) (Figures 1(a), 1(b)) with 60 TiN/SiN electrodes (diameter 30 μm, interdistance 200 μm) arranged on an 8×8 square grid. Experiments were performed in the range 18–42 DIVs, when the neuronal network reaches its "mature" state, consisting of synchronized clustered activity with minute-to-minute fluctuations in the probability of firing (Marom and Shahaf [32]).

The experimental set-up is based on the MEA60 system supplied by Multi Channel Systems (MCS, Reutlingen, Germany). The system is constituted by the following elements: a neuronal preparation cultured over an MEA, a mounting support with a 60-channel amplifier (gain 1200x), a home made 8-channel stimulus generator, to deliver both current and voltage desired stimulating signals, an inverted optical microscope, connected to a CCD camera (Hamamatsu, Japan), to visually monitor the cells during the experiment, an antivibration table and a Faraday cage.

Raw data are also monitored and recorded by using the commercial software MCRack (Multi ChannelSystems, Reutlingen, Germany) (sampling frequency was set to 10 kHz/channel). To confirm real-time behaviour, neural data were also processed offline by using ad-hoc developed software tools (Vato et al. [35]; Chiappalone et al. [34]).

Control architecture

The control architecture presented in our previous work (Cozzi et al. [18]) has partially changed and some feature has been added. In particular, we have moved from xPC-Target (http://www.mathworks.com/products/xpctarget) that was not able to handle and log the very large amount of data coming from neuronal network, to the QNX 6.1 (QNX software systems), a POSIX-compatible operating system specific for hard real-time applications.

The present architecture involves three PCs. PC1 (P4, 2.8 GHz, 512 MB RAM), that is, the one that runs QNX, is equipped with an A/D board PCI-6071E (National Instruments, Texas, USA) and it is responsible for (a) electrophysiological signals acquisition, (b) online spike detection and artifact blanking, (c) decoding of the spike trains, (d) handling the serial communication with the robot and PC3, (e) coding of robot's proximity sensors signals, (f) production of the pattern of stimuli that trigger the electrical stimulator, and (g) experimental data logging (spikes, sensors activity, wheel speeds, stimuli, robot trajectory). These tasks are processed by different threads at different sampling rates, in particular tasks (a)-(b) are at 10 Khz, tasks (c)–(e)-(f)-(g) are at 250 Hz, and task (d) is at 10 Hz.

A second computer, PC2 (P4, 2.8 GHz, 512 MB RAM, Win2000), connected to PC1 through an Ethernet link, is the experimental front-end. We used Simulink/Real-Time Workshop (the MathWorks) and the RT-Lab package (Opal-RT) as development environments. This package generates two processes that are executed in real-time on the target node, that is, PC1. This system allows simultaneous acquisition of neural signals from up to 32 recording sites.

PC3 (P4 2.8 GHz 512 MB RAM, QNX 6.1) is in charge of real-time tracking of the robot movement and it is connected through a serial cable to the main computational node of the architecture (PC1). A CCD camera (DSE TCC5 with 1/3 CCD SONY SuperHAD) is placed 1.5 m above the central position of the arena. This physical arrangement of the camera allows a good resolution while minimizing distortion at the boundaries of the arena. A frame-grabber (Arvoo Picasso PCI-2SQ) acquires samples at 5 Hz from the camera with a resolution of 640×480 pixels. One pixel on the CCD sensor corresponds to ~ 2 mm, so that the arena is contained in a 400×400 subwindow at the center of the image. The detection phase is performed in a small square portion (50×50 pixels) of the global field of the CCD camera (the detection in such small area is low demanding in computing performance and thus the process can be performed in real-time). This square area represents the predicted robot location. A red round marker placed onto the top of the robot and the detection of its position is based on a local evaluation of the intensity of the RGB values of every pixel belonging to the detection window.

2.4. Data analysis

Processing of electrophysiological signals

Poststimulus Time Histogram. To investigate the neural activity evoked by stimulation, we computed the poststimulus time histogram (i.e., PSTH), which represents the impulse response of each site of the neural preparation to electrical stimulation. The PSTHs were calculated by taking 400 ms time windows from the recordings that follow each stimulus. We then counted the number of spikes occurring in a 2–4 msec bin and divided this measure by the number of stimuli (Rieke et al. [36]). For our cultures, typical PSTHs show an "early" (less than 50 msec) and a "late" (50–250 milliseconds) component (Shahaf and Marom [5]; Marom and Shahaf [32]; Cozzi et al. [22]).

Stimulus-Triggered Speed. The stimulus-triggered speed (STS) is constructed by averaging the speed waveform due to each stimulus. The robot has two independent wheels, whose speeds are proportional to the neuronal activity of two "brain" regions (i.e., the two set of electrodes selected as motor areas within the network). These regions receive sensory feedback by two independent stimulating sites. It is possible to construct two STSs for each input-output, that is, sensory-motor pathways, for a total of 4 curves (i.e., the variations of the speed of the left and the right wheels in response to the left stimulus are the first two curves and constitute the first STS, and the variation of the speed of the left and the right wheels in response to the right stimulus constitute the second STS with the latter two curves), and it is also possible to study the performance of the robot behavior by studying the side-selectivity of the relationship between stimuli and speeds.

Indicators of robot performance

The behavior of the neurorobotic system can be evaluated by means of the *stimulus-triggered speed (STS)*, that is, the average motor commands elicited by a single electrical stimulus:

$$\mathrm{STS}(\tau) = \langle \omega(\tau - t_i) \rangle_i, \tag{2}$$

where t_i is the time instant of delivery of the ith stimulus and τ is the time coordinate.

In order to have a more general evaluation of the robot performance during each trail (5′), we also used the following three parameters:

(i) *number of hits*,

(ii) *trajectory length*,

(iii) *space covered*. The percentage of the arena area covered by the robot path:

$$\mathrm{SC} = \frac{\mathrm{NP} \cdot cf^2}{A_{\mathrm{arena}} - nA_{\mathrm{obstacle}}} \cdot 100\%, \tag{3}$$

where NP is the number of pixels covered by the robot, cf^2 is the area of one pixel, n is the number of obstacles in the playground, A_{arena} and A_{obstacle} are, respectively, the areas of the playground and of each obstacle.

The software tools for of-line signal processing aimed at the analysis of the behavior of the neurorobotic system were developed using Matlab 6.5 (the MathWorks).

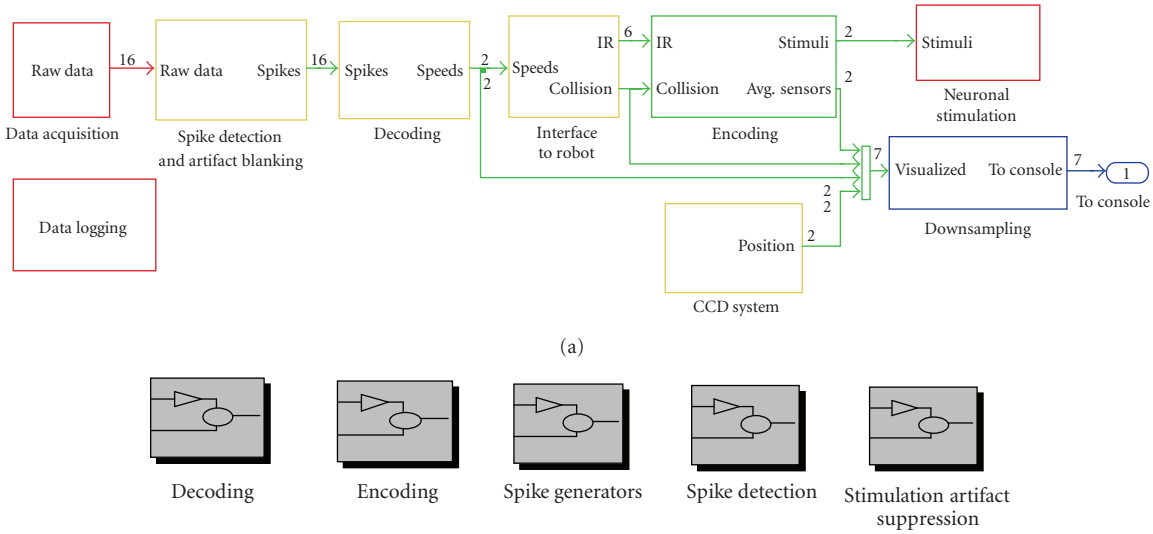

Figure 3: Computing performances in the Simulink implementation of the neurorobotic interface. Different colors correspond to different sampling rates (red = 10 kHz, green = 250 Hz, blue = 5 Hz, yellow = mixed values), whereas the numbers indicate signal dimensions (i.e., in this case, we had 2 inputs and 16 outputs). The percentages in each block indicate the relative simulation time for each of the modules of the neurorobotic interface (2 inputs and 16 outputs). (b) Library of the modules that can be used in the neurorobotic interface. Each subset encloses Simulink blocks implementing different algorithms for that purpose.

3. RESULTS

3.1. Computing performance

The feedback loop computation time reached by our final neurorobotic architecture is under 1 millisecond; therefore, the real-time performance in the closed-loop system is compatible with the response time (4 ms) of our neuronal model. This value includes the time needed for (I) the electrophysiological signals acquisition, (II) the spike detection and the artifact suppression, (III) decoding of neural activity, (IV) computing of the speeds of the robot's wheels, and (V) coding of sensory feedback. The relative computational loads for each block are displayed in Figure 3(a): the most time-consuming parts are those running at 10 kHz, for technical reasons, and the blocks including sampling rate transitions, such as the interface with the robot, with the CCD camera system and with the stimulator. In these experiments, we used a robot with a standard RS232 interface that supports a baud rate of 9600 bit/s. We expect that by including a more recent protocol (e.g., USB2 or Firewire), the block would be less time consuming and would assure better performance. Spike detection and artifact blanking are also time-consuming due to the high dimension of the signals being processed. The performances were evaluated by means of Simulink Profiler, reported schematically in Figure 3(b).

3.2. Identification of input-output sites

In order to obtain a reactive behavior, we need the network to respond soon after the feedback stimulation, that is, we need input-output pathways characterized by a relatively early (up to 50 ms) and sustained response meaning a "high strength" in the functional connectivity (Shahaf and Marom [5]). If the network reacts to the sensory feedback and the evoked electrophysiological response is characterized by a relatively long activation phase (up to 200–300 ms), the robot would not be able to react to the presence of an obstacle in 100 ms (i.e., the delay among successive serial communications between the system and the robot). This is one of the reasons why we need to accurately select the input-output pathways, beside the fact that only low-frequency stimulation can be delivered for not fatiguing the culture (Shahaf and Marom [5]; Eytan et al. [37]). We need the stimulus-evoked response to be fast, prolonged, reliable, and therefore effective for the entire duration of the experiments (i.e., all day long).

As already said, the general aim is to have a robot that follows a specific task on the basis of the spontaneous/stimulated electrophysiological activity shown by the neuronal culture. To this end, it is a fundamental prerequisite to characterize the collective activity of the network that will be connected to the robot (i.e., analysis of both spontaneous and stimulus evoked neuronal activity). This characterization phase is necessary since the unstructured nature of the culture does not allow us to a priori define the sensory and motor areas that will be connected with the sensory and motor areas of the robot, as it happens with portion of tissue with a well-defined sensorimotor architecture (Reger et al. [7]; Karniel et al. [11]).

Thus, the goal of the characterization phase is to select those channels of the MEA to be used as sensory inputs (i.e.,

connected to the robot's sensors) and motor outputs (i.e., connected to the robot's wheels) of the biological network.

To test the response to stimulation from different sites in different areas of the neuronal network, trains of 50 electrical stimuli are delivered (1.5 V peak to peak-extracellular stimulation, 500 μs, and duty cycle 50%). This procedure is repeated from at least 5 arbitrarily chosen electrodes (Wagenaar et al. [38]).

The poststimulus time histogram-(PSTH) (i.e., the average number of spikes obtained in response to a stimulus, at different latencies) is then used for quantifying the strength of connections between a specific stimulating sites and all the other recording sites. It is the impulse response (in terms of instantaneous firing rate) to a single test stimulus.

The algorithm for the selection of the output (motor) and input (sensory) sites supplies the I/O pairs corresponding to maximum selectivity and it is based on network effective functional interconnectivity. The ideal case is described in the following: given two (or more) stimulating channels (e.g., S1 and S2) and two groups of recording sites (e.g., R1 and R2), the strength of the connectivity S1-R1 and S2-R2 is "high" and simultaneously, the strength of the connectivity S1-R2, and S2-R1 is "low" (i.e., good selectivity in input-output pairs). The described scheme guarantees, somehow, that the responses in the two (groups of) recording sites are different on the basis of the stimulating electrodes. Of course the above is an ideal situation and, since the mean connectivity of the network is high, also due to the high density of plated cells, it is hard to get highly specific responses in the input-output pathways.

The methodology that we developed to make a selection of the pathways is the "selectivity map" (see Section 3.3 for a typical map). Each dot represents the PSTH area at a specific recording site given that there was a stimulation from a couple of stimulating sites. All the possible input-output combinations are explored and only the pathways producing responses lying more distant from the diagonal (i.e., closer to the axis) are selected.

Those specific pathways (of sensory-motor activations) can be then conveniently utilized for driving the robot and for implementing simple reactive behaviors (e.g., obstacle avoidance), as presented in Section 3.1.

3.3. *Example behaviors of the neurorobotic system*

Once the role of the microelectrodes (i.e., selection of input-output sites) has been decided, the experiment can start. A desired result is achieved when an improvement of the robot behavior is confirmed by possible modification of the neuronal network dynamics (i.e., adaptation).

Each experiment with the neurorobotic system is usually divided into the following phases:

(i) spontaneous activity recording (5 minutes);

(ii) preprocessing: test stimulus from 8 channels (serial stimulation);

(iii) input-output channel selection: at least 2 channels for input (sensors) and 2 channels for output (motors).

(iv) closed–loop experiment: Robot running (5 + 5 + 5 minutes):

  (a) free running;

  (b) obstacle avoidance with the application of a learning protocol (when the robot hits an obstacle, a conditioning stimulus at 20 Hz frequency is delivered from the collision side). The learning protocol is based on what reported in literature: only a few examples of learning (i.e., potentiation and depression) have been demonstrated for dissociated neurons cultured over MEAs and all of them are based on the application of trains of stimuli at "high" frequency (Jimbo et al. [39]; Jimbo et al. [40]; Tateno and Jimbo [41]; Bonifazi et al. [42]; Ruaro et al. [43]). We have evidence that similar protocols have the effects to mainly potentiate the network electrophysiological response in terms of number of evoked spikes (Chiappalone et al. [44]);

  (c) free running.

(v) post-processing:

  (a) spontaneous activity recording (5′);

  (b) test stimulus from the two chosen stimulating channels.

To avoid manual removal of the robot and possible damage due to wheels' motors heating in case of a collision against an obstacle, a step-back mechanism (2 seconds backward movement with an angular speed of 5 rad/s) was implemented.

A user-friendly GUI allows (i) to select input and output channels (i.e., recording and stimulation sites), (ii) to choose among different coding and decoding strategies, and (iii) to change all the experimental parameters (e.g., spike-detection threshold, maximum robot speed, cut-off frequency of the filter for the estimation of neural activity, maximum stimulation rate).

The signals obtained at different levels in the bidirectional interface are represented in Figure 4. The spike trains are then low-pass filtered to obtain instantaneous firing rates that are considered as indicators of the level of neural activity. The cutoff frequency of the filter is set, in this case, at 1 Hz. The values corresponding to reasonable response times range from 0.5 to 1 Hz: in fact they represent a good compromise between fast response and time integration requirements. The previously adopted cutoff frequency of 0.1 Hz (Cozzi et al. [18]) was not suitable for bursting networks because the long-term effect of time integration lets the past events (previous bursts) to weight more than instantaneous activity.

The motor commands (i.e., the speeds) are then obtained according to the control law which implements inhibitory contro-lateral connections between inputs and outputs (see decoding schemes section for details), thus we expect that a feedback stimulus coming from left sensors would result in a decrease of the speed of the right wheel of the robot, and a stimulus coming from right sensors would determine a deceleration of the speed of the robot's left wheel. The

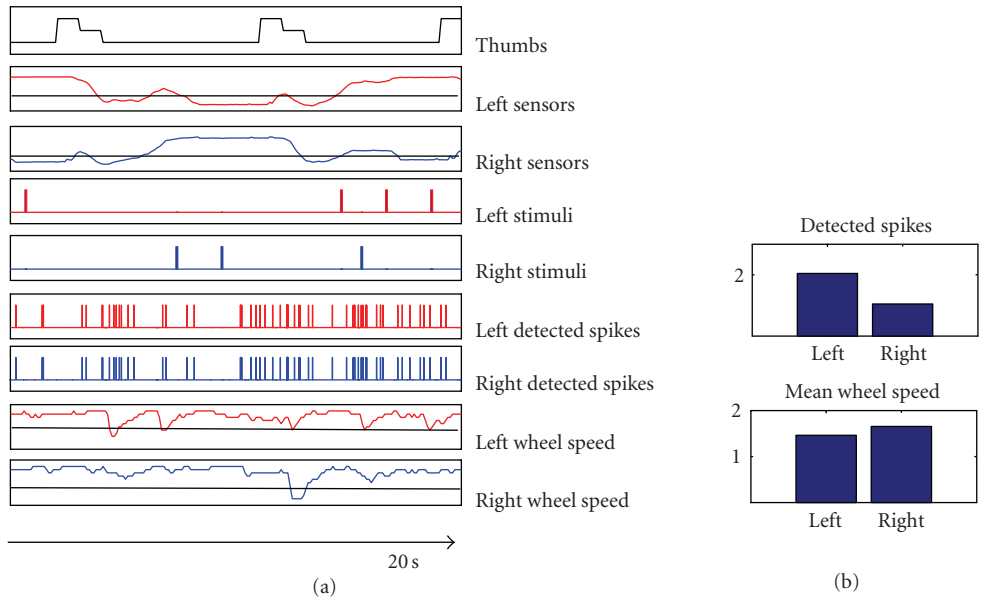

FIGURE 4: Signals obtained at different levels of the neurorobotic interface during 20 seconds of a free running session (c.f. Results, for a detailed description of the experimental protocol). In this particular experiment we used 2 stimulation sites and 2 recording sites. When the robot is approaching an obstacle, the value of sensors increases and when it overcomes a threshold (i.e., 500 levels) a feedback stimulus is delivered (max frequency 1 Hz). The left and right detected spike trains are then processed into motor commands, that is, left and right wheel speeds (the line corresponds to 0 rad/s). The network was spontaneously active and during this phase we recorded 2046 spikes from left and 1057 from the right one, resulting in a mean wheel speed of 1.4 rad/s (left) and 1.6 rad/s (right).

proximity signals coming from the sensors placed on the two sides of the robot are averaged in order to obtain two feedback signals, each of them related to one side of the robot. Figure 4 shows the patterns of stimuli obtained from the feedback signals, according to the binary coding scheme.

A number of preliminary experiments were performed using, respectively, 2 stimulation and 2 recording sites. In the following, the results of two example experiments are reported to let the reader better understand the experimental procedure and appreciate the performances of the developed closed-loop system.

Figure 5 shows the PSTHs obtained during the characterization phase of one example experiment. The responses evoked from different stimulation sites are similar (i.e., Figures 5(a) and 5(b)), thus revealing a low degree of selectivity and a high degree of connectivity. In a case like the one presented in Figure 5, the preparation can hardly be used to control the robot and it is discarded.

Figure 6 presents an example of good connectivity maps obtained during the characterization phase (Figure 6(a)) and after the robotic experiment (Figure 6(b)): the electrodes 15 and 45, that will be further chosen as recording electrodes, are positioned close to the axis, indicating that their responses to the stimulating channel are selective (see Section 3.2 for further details).

Figures 7(a) and 7(b) show the PSTHs corresponding to the inputs/outputs chosen after the characterization phase; during an experimental session with the robot (i.e., experiment is different from the previous one). In this example, the recording electrode 15 is very sensitive to the stimulation delivered from electrode 16 (top left) while it is quite unaffected by stimuli delivered form electrode 48 (top right). At the same time, the recording site 45 is not sensitive to stimuli coming from electrode 16 (bottom left) while it is very affected by stimulation from electrode 48. In this case, different stimulation sites evoke very different response, thus revealing a high degree of selectivity that is also confirmed by the connectivity maps presented in Figure 6.

The shapes of the PSTHs must be similar to those of the PSTHs obtained during the characterization phase in order to ensure the stability of the response of the neuronal culture. If the area of the PSTHs drastically decreases at the end of the closed loop phases it means that the neuronal network has been fatigued by excessive repeated stimulations (Shahaf and Marom [5]). The wellness and stability of the culture are "sine qua non" conditions to be verified before describing the neurorobotic behavior by means of the robot's performance indicators. Under these conditions, the performance of the neural preparation in controlling the robot can be represented by the STSs, depicted in Figures 7(c) and 7(d).

Examples of the robot trajectories are presented in Figures 8(a) and 8(b). Figure 8(c) shows the indicators generally used for quantifying the robot performance. The first indicator alone, that is, the number of hits, is not sufficient for describing the performances of an obstacle avoidance task. In fact, a low number of hits could result from limited robot movements or from the repetition of the same trajectory. For this reason, it is necessary to consider also the fraction of space covered by the robot and the length of its trajectory. Together, these simple indicators evaluate the robot performances inside the arena, even if they are not related

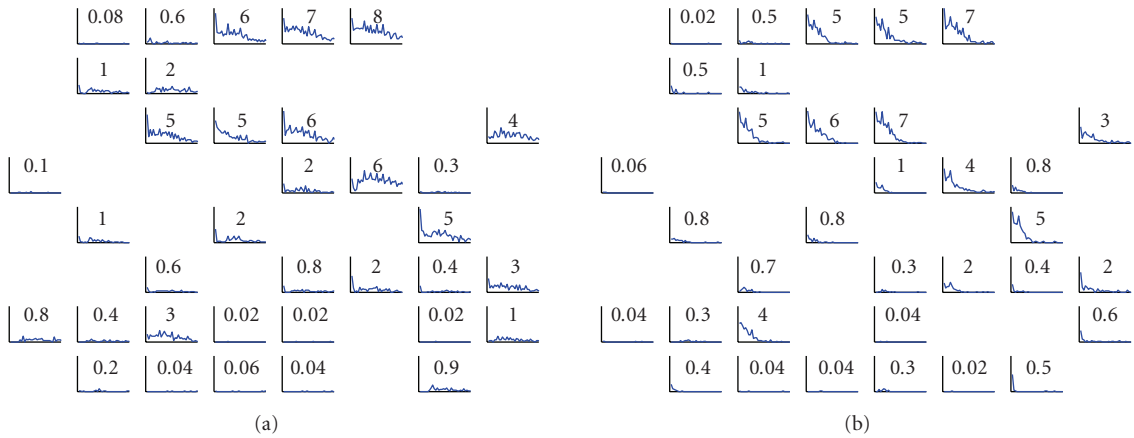

FIGURE 5: PSTHs of the evoked responses in a cortical neuronal network. (a) The post stimulus time histograms obtained in all the responding channels are reported over an 8×8 grid (i.e., reproducing the layout of the MEA) after the stimulation from site 46—fourth column, sixth row. The small number reported in each box represents the area of the histogram. Not responding channels are excluded. (b) Responses evoked in the network by stimulation from site 62. As it can be clearly notices the channels responding to site 46 respond also to channel 62, denoting an absence of strong selection with respect to the stimulating electrode. X-scale $[0, 1]$; Y-scale $[0, 400]$ milliseconds.

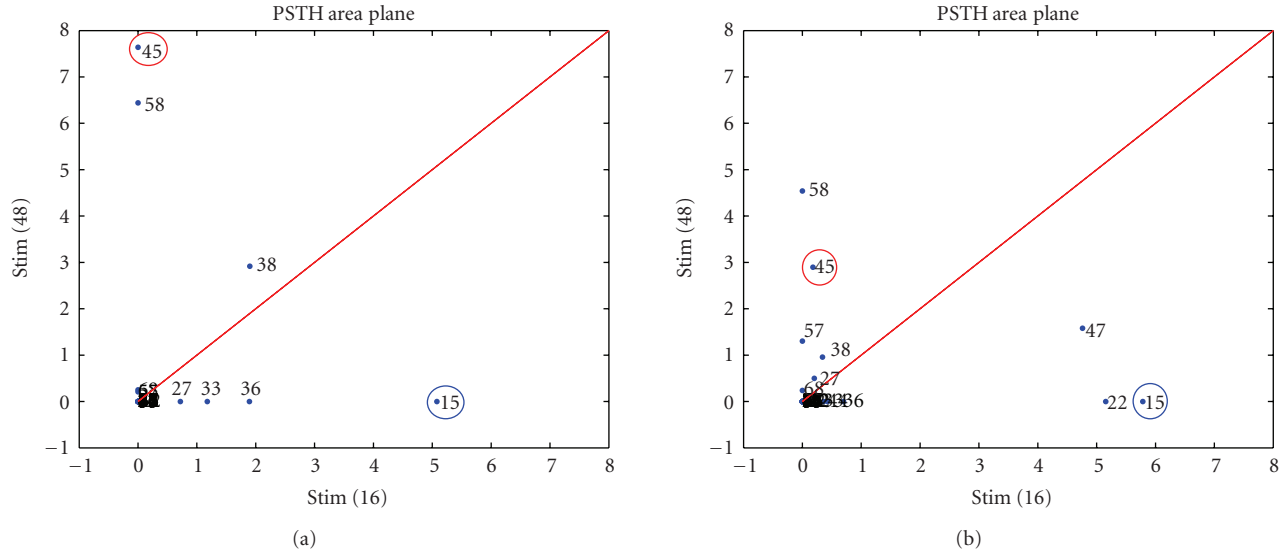

FIGURE 6: Connectivity maps (same data reported in Figure 4). The connectivity map represents a plot of the PSTH areas evoked by a couple of stimulating electrodes on a specific electrode. In this way we are able to represent the network response to a specific choice of stimulating sites. The ideal case should be to have two recording electrodes placed on the axis, far from the origin (i.e., maximum response to one stimulating electrode and zero to the other). (a) Before the robotic experiment. (b) After the robotic experiment.

to the sensory feedback coming from the external environment. These parameters do not allow quantifying any relationship between the motor response and the sensory information, but, considering different phases, if the robot covered the same area and the trajectories are in the same order, then the two phases are comparable, and a reduction of the number of hits should indicate an improvement of the robot's behavior. An improvement in the robot's behavior must correspond to an improvement in the relationship between the motor response and the feedback sensory information (i.e., the STSs). The STS is the only parameter that permits to understand and demonstrate whether a different behavior of the robot actually corresponds to a different dynamics of the neuronal activity, and for this reason it can be considered the best indicator of the performance of the overall neurorobotic system.

The comparison of the STSs and connectivity maps obtained during each phase illustrates that a modification in the robot's behavior has occurred. Therefore, one couldspeculate that the origin of such a modification relies on specific synaptic changes, (i.e., Hebbian potentiation in terms of number of evokes spikes) of the neurons placed at the recording electrodes (Jimbo et al. [39]; Jimbo et al. [40]; Tateno and Jimbo [41]; Bonifazi et al. [42]; Ruaro et al. [43]). We cannot infer or demonstrate that synaptic changes are pathways specific but considering

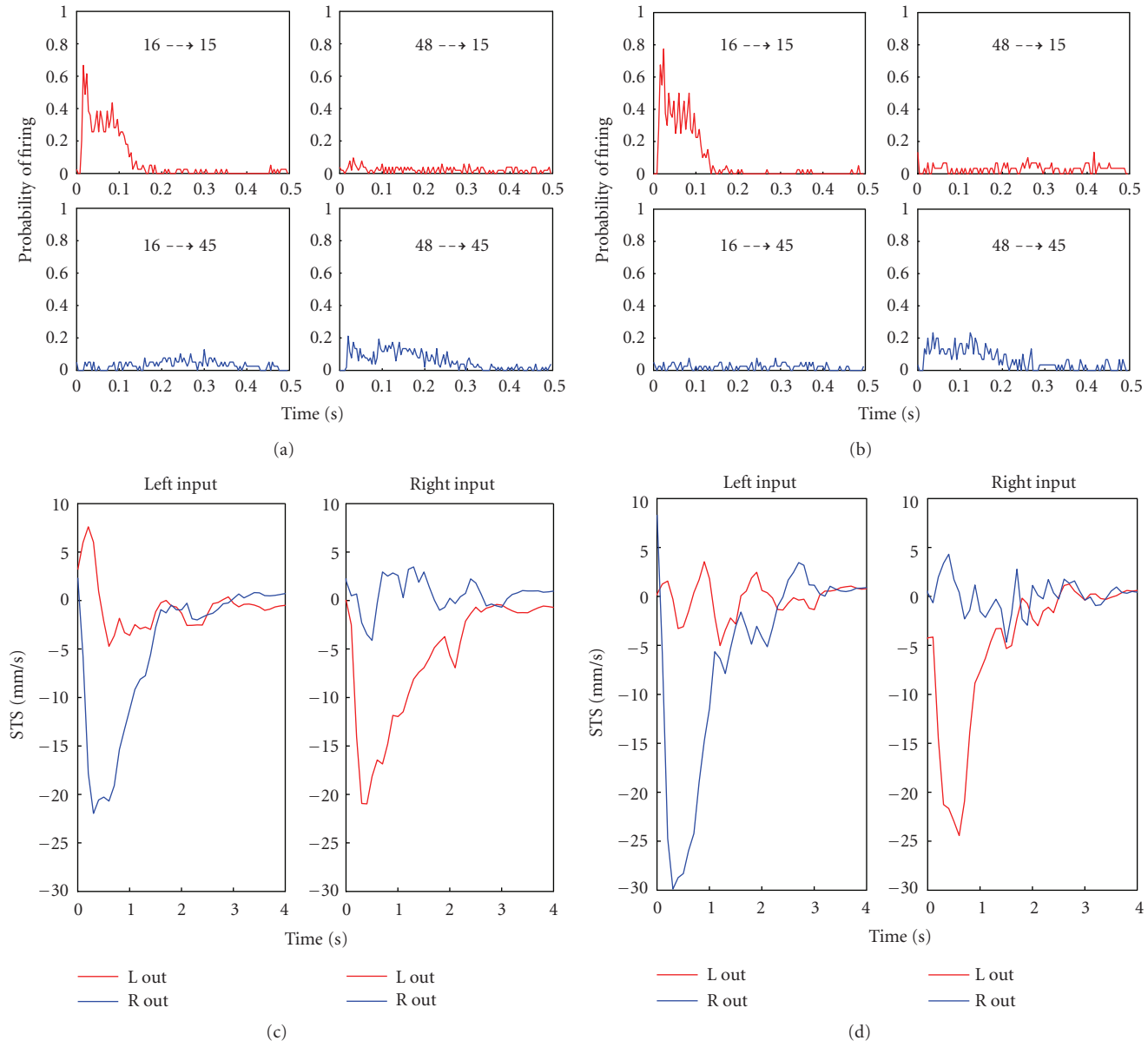

Figure 7: PSTH and STS in a neurorobotic experiment. (a) PSTHs for two electrodes (chosen as recording—motor electrodes) with respect to two stimulating sites. Electrode 15 responds well to stimulation from electrode 16 and bad to stimulation from electrode 48; on the contrary electrode 45 responds well to 48 and bad to 16. This tendency is maintained and even improved after the robotic experiment (b). The STS graphs before (c) and after (d) the robotic experiment prove again the selectivity of the chosen electrodes and the improvement in the performances (increased STS area).

the global behavior of the recording sites after a neurorobotic experiments a possible effect at (sub)population level (i.e., a kind of network plasticity) has occurred induced by the external correlated stimulation (Chiappalone et al. [44]).

4. DISCUSSION AND CONCLUSION

"We have this common internal neural language that we are born with and so if you can exploit that with the right stimuli then you are going to help the brain develop to do the things like reason." (Shaw [45].)

We have developed a general real-time, bidirectional neural interface platform. The system is capable of acquiring multisite electrophysiological activity at 10 kHz per channel, to perform spike detection and artifact suppression, from up to 32 channels. That is a step forward with respect to simpler systems (Reger et al. [7]; Karniel et al. [11]) or to bidirectional systems implemented by others (DeMarse et al. [12]; Bakkum et al. [13]) or by ourselves (Martinoia et al. [14]; Cozzi et al. [18]).

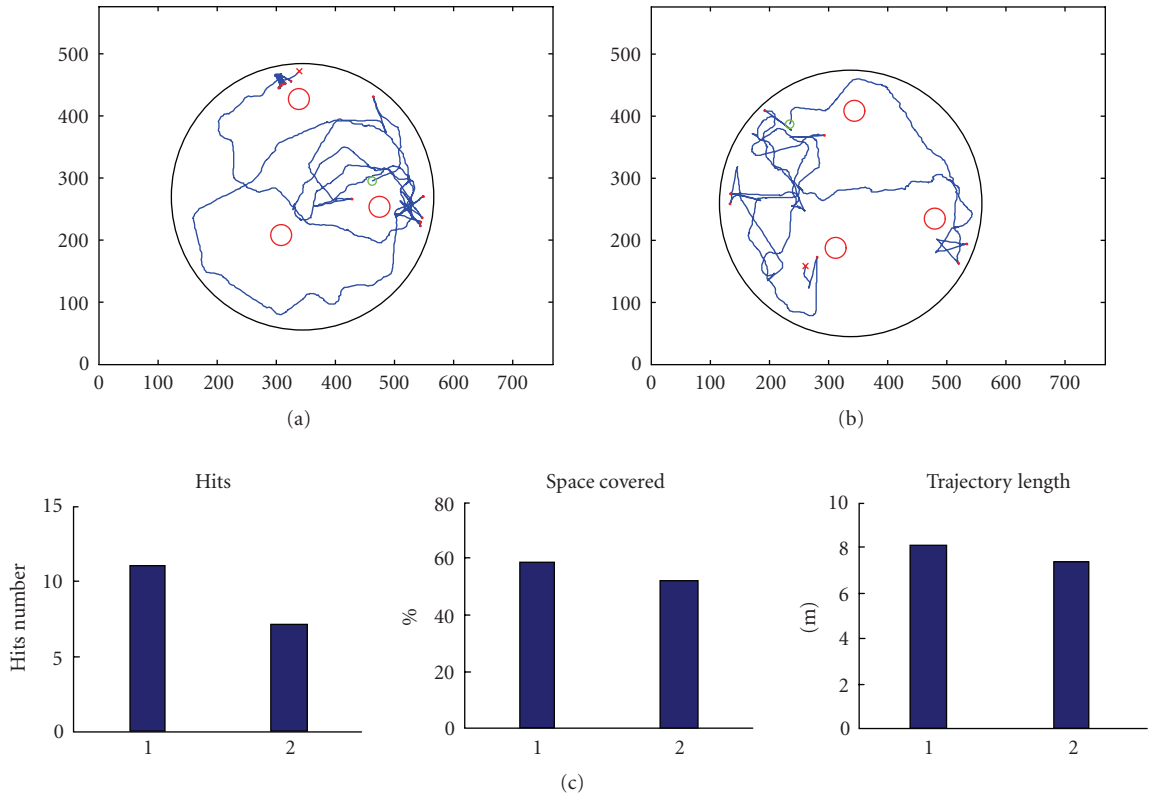

FIGURE 8: Robot trajectories and performances in a neurorobotic experiment. (a) Robot trajectory during the first free running phase. (b) Robot trajectory during the last free running phase (i.e., after the learning phase). (c) Indicators of the robot's performance. The last two parameters only show that the two phases are comparable in terms of covered space and trajectory length during the robot's movement inside the arena. For this reason, the reduction of hits in the second phase (i.e., first parameter) suggests an improvement of performances during the obstacle-avoidance task. The conclusion is that an improvement in the robot's behavior in terms of a decreased number of hits must depend from the modulation of the neuronal activity, as also confirmed by the graphs of the STS presented in the previous figure.

The use of portions of brain, such as the brainstem of a sea lamprey, connected to an artificial device represents the very first application of the "embodied electrophysiology" paradigm. The main difference between the lamprey-based neurorobotic system and the bidirectional interface we developed is the fact that in the lamprey preparation the circuitry governing the stabilization and orientation during swimming (Deliagina [46]; Deliagina et al. [47]) maintains the original citoarchitecture and the natural input-output system is used as a controller to drive the robotic body (Reger et al. [7]; Karniel et al. [11]).

Potter and colleagues (DeMarse et al. [12]; Bakkum et al. [13]) overcame the simplification of an already structured portion of brain presenting an innovative embodied electrophysiology paradigm in which a randomly grown neuronal networks controlled a simulated body. As they reported, it was simply a "neuroethology experiment" to merely observe the effect of feedback stimulation on the general behavior and where their "animat" has not to perform any particular task. Our neurorobotic interface, on the contrary, has to work in a reactive manner expressing a kind of "stimulus-driven behavior." Here we reported, in details, the methodology of the system (including hardware and software features), an optimized way to identify the "functional I/O pathways" and we presented a method to analyze the robot behavior and correlate it to the network electrophysiology.

As described in the previous sections, in our system, the spike trains can be decoded into motor commands (at 250 Hz) through a variety of decoding strategies. Such motor commands are then used to control a mobile robot, to which a specific task is assigned. Conversely, sensory signals can be coded into patterns of stimulation (again, according to a variety of coding schemes) and sent to a custom electrical stimulator with up to 8 stimulation channels. Although the algorithms used for spike detection and artifact blanking are simple, compared to those adopted in other experimental frameworks (Wagenaar and Potter [48]; Obeid and Wolf [49]), they allow a good level of reliability with the advantage of an extremely light computational load. It should be underlined that the presented experimental paradigm can be extended to other computational schemes and one of the key features of the system is to allow testing different coding and decoding strategies in relationship with optimal coding and performances and with the capability of the neuronal system to adapt for a new task in an actual closed loop environment.

The software architecture is flexible and modular, and allows fast prototyping of new modules according to the experimental requirements. Real-time performance was very

good and it is comparable to other simpler systems (in terms of recording/stimulating channels), previously described in the literature (Reger et al. [7]; Martinoia et al. [14]; Wagenaar and Potter [38]; Cozzi et al. [18]; Karniel et al. [11]; Wagenaar et al. [50]). We developed a library of coding and decoding modules, which, as mentioned, could be easily extended. This is a key point with respect to possible implication for the development of novel brain-machine interface with enhanced capabilities and bidirectional interactivity.

Concerning our particular application, we also developed the tools for studying the ability of a culture of cortical neurons to process information in order to drive a robot according to a defined motor task (with a particular emphasis on the method for input-output pathways selection), and at the same time it allows to supervise the population activity changes in response to external feedbacks. It should be stressed that this is the first time that a closed-loop neurorobotic system (with in vitro neuronal populations) is utilized for performing specific behavioral oriented tasks.

The proposed experimental framework creates new possibility for investigating basic mechanisms of learning and adaptation (e.g., distributed synaptic plasticity, long term potentiation (LTP) and long term depression (LTD)) by directly studying how behavior arises from the emerging collective dynamics of a neuronal ensemble. Additionally, the experimental system could be also conveniently utilized and adapted to other in vitro models such as acute, organotypic slices, and patterned neurons, where the network architecture is partly preserved or can be designed.

Finally, on a long term perspective, this approach could have a relevant impact in the field of bio-inspired computational systems and for the development of novel brain-computer interfaces and of advanced neuroprosthetic devices.

ACKNOWLEDGMENTS

The authors wish to thank Dr. M. Tedesco (Brunella) for cell culture preparation. This work is partly supported by the EU Grant IST-2001-33564 (Neurobit), and by a grant from the Italian Ministry of University, Education and Research. Novellino's Ph.D. fellowship was supported by ett s.r.l. (http://www.ettsolutions.com).

REFERENCES

[1] D. A. Wagenaar, J. Pine, and S. M. Potter, "Effective parameters for stimulation of dissociated cultures using multi-electrode arrays," *Journal of Neuroscience Methods*, vol. 138, no. 1-2, pp. 27–37, 2004.

[2] A. A. Sharp, M. B. O'Neil, L. F. Abbott, and E. Marder, "The dynamic clamp: artificial conductances in biological neurons," *Trends in Neurosciences*, vol. 16, no. 10, pp. 389–394, 1993.

[3] G. Le Masson, S. Renaud-Le Masson, D. Debay, and T. Bal, "Feedback inhibition controls spike transfer in hybrid thalamic circuits," *Nature*, vol. 417, no. 6891, pp. 854–858, 2002.

[4] D. A. Wagenaar, R. Madhavan, J. Pine, and S. M. Potter, "Controlling bursting in cortical cultures with closed-loop multi-electrode stimulation," *Journal of Neuroscience*, vol. 25, no. 3, pp. 680–688, 2005.

[5] G. Shahaf and S. Marom, "Learning in networks of cortical neurons," *Journal of Neuroscience*, vol. 21, no. 22, pp. 8782–8788, 2001.

[6] S. Marom and D. Eytan, "Learning in ex-vivo developing networks of cortical neurons," *Progress in Brain Research*, vol. 147, pp. 189–199, 2005.

[7] B. D. Reger, K. M. Fleming, V. Sanguineti, S. Alford, and F. A. Mussa-Ivaldi, "Connecting brains to robots: an artificial body for studying the computational properties of neural tissues," *Artificial Life*, vol. 6, no. 4, pp. 307–324, 2000.

[8] J. Wessberg, C. R. Stambaugh, J. D. Kralik, et al., "Real-time prediction of hand trajectory by ensembles of cortical neurons in primates," *Nature*, vol. 408, no. 6810, pp. 361–365, 2000.

[9] M. A. L. Nicolelis, "Actions from thoughts," *Nature*, vol. 409, no. 6818, pp. 403–407, 2001.

[10] A. B. Schwartz, D. M. Taylor, and S. I. H. Tillery, "Extraction algorithms for cortical control of arm prosthetics," *Current Opinion in Neurobiology*, vol. 11, no. 6, pp. 701–708, 2001.

[11] A. Karniel, M. Kositsky, K. M. Fleming, et al., "Computational analysis in vitro: dynamics and plasticity of a neuro-robotic system," *Journal of Neural Engineering*, vol. 2, no. 3, pp. S250–S265, 2005.

[12] T. B. DeMarse, D. A. Wagenaar, A. W. Blau, and S. M. Potter, "The neurally controlled animat: biological brains acting with simulated bodies," *Autonomous Robots*, vol. 11, no. 3, pp. 305–310, 2001.

[13] D. J. Bakkum, A. C. Shkolnik, G. Ben-Ary, P. Gamblen, T. B. DeMarse, and S. M. Potter, "Removing some 'A' from AI: embodied cultured networks," in *International Seminar on Embodied Artificial Intelligence*, vol. 3139 of *Lecture Notes in Artificial Intelligence*, pp. 130–145, Dagstuhl Castle, Germany, July 2004.

[14] S. Martinoia, V. Sanguineti, L. Cozzi, et al., "Towards an embodied in vitro electrophysiology:the NeuroBIT project," *Neurocomputing*, vol. 58–60, pp. 1065–1072, 2004.

[15] S. M. Potter, "Chapter 4 distributed processing in cultured neuronal networks," *Progress in Brain Research*, vol. 130, pp. 49–62, 2001.

[16] F. A. Mussa-Ivaldi and L. E. Miller, "Brain-machine interfaces: computational demands and clinical needs meet basic neuroscience," *Trends in Neurosciences*, vol. 26, no. 6, pp. 329–334, 2003.

[17] M. A. L. Nicolelis, "Brain-machine interfaces to restore motor function and probe neural circuits," *Nature Reviews Neuroscience*, vol. 4, no. 5, pp. 417–422, 2003.

[18] L. Cozzi, P. D'Angelo, M. Chiappalone, et al., "Coding and decoding of information in a bi-directional neural interface," *Neurocomputing*, vol. 65-66, pp. 783–792, 2005.

[19] P. Maes, "Modeling adaptive autonomous agents," *Artificial Life*, vol. 1, no. 1-2, pp. 135–162, 1994.

[20] R. A. Brooks, *Robot: The Future of Flesh and Machines*, Allen Lane, The Penguin Press, London, UK, 2002.

[21] V. Braitenberg, *Vehicles: Experiments in Synthetic Psychology*, The MIT Press, Cambridge, Mass, USA, 1984.

[22] L. Cozzi, P. D'Angelo, and V. Sanguineti, "Encoding of time-varying stimuli in populations of cultured neurons," *Biological Cybernetics*, vol. 94, no. 5, pp. 335–349, 2006.

[23] M. Grattarola, M. Chiappalone, F. Davide, et al., "Burst analysis of chemically stimulated spinal cord neuronal networks cultured on microelectrode arrays," in *Proceedings of the 23rd Annual International Conference of the IEEE Engineering in Medicine and Biology Society*, vol. 1, pp. 729–732, Istanbul, Turkey, October 2001.

[24] J. K. Chapin, K. A. Moxon, R. S. Markowitz, and M. A. L. Nicolelis, "Real-time control of a robot arm using simultaneously recorded neurons in the motor cortex," *Nature Neuroscience*, vol. 2, no. 7, pp. 664–670, 1999.

[25] J. M. Carmena, M. A. Lebedev, R. E. Crist, et al., "Learning to control a brain-machine interface for reaching and grasping by primates," *PLoS Biology*, vol. 1, no. 2, pp. 193–208, 2003.

[26] J. Wessberg and M. A. L. Nicolelis, "Optimizing a linear algorithm for real-time robotic control using chronic cortical ensemble recordings in monkeys," *Journal of Cognitive Neuroscience*, vol. 16, no. 6, pp. 1022–1035, 2004.

[27] E. E. Fetz, "Real-time control of a robotic arm by neuronal ensembles," *Nature Neuroscience*, vol. 2, no. 7, pp. 583–584, 1999.

[28] M. A. Lebedev and M. A. L. Nicolelis, "Brain-machine interfaces: past, present and future," *Trends in Neurosciences*, vol. 29, no. 9, pp. 536–546, 2006.

[29] A. P. Georgopoulos, A. B. Schwartz, and R. E. Kettner, "Neuronal population coding on movement direction," *Science*, vol. 233, no. 4771, pp. 1416–1419, 1986.

[30] E. Maeda, Y. Kuroda, H. P. C. Robinson, and A. Kawana, "Modification of parallel activity elicited by propagating bursts in developing networks of rat cortical neurones," *European Journal of Neuroscience*, vol. 10, no. 2, pp. 488–496, 1998.

[31] Y. Jimbo, A. Kawana, P. Parodi, and V. Torre, "The dynamics of a neuronal culture of dissociated cortical neurons of neonatal rats," *Biological Cybernetics*, vol. 83, no. 1, pp. 1–20, 2000.

[32] S. Marom and G. Shahaf, "Development, learning and memory in large random networks of cortical neurons: lessons beyond anatomy," *Quarterly Reviews of Biophysics*, vol. 35, no. 1, pp. 63–87, 2002.

[33] S. Martinoia, L. Bonzano, M. Chiappalone, M. Tedesco, M. Marcoli, and G. Maura, "In vitro cortical neuronal networks as a new high-sensitive system for biosensing applications," *Biosensors and Bioelectronics*, vol. 20, no. 10, pp. 2071–2078, 2005.

[34] M. Chiappalone, M. Bove, A. Vato, M. Tedesco, and S. Martinoia, "Dissociated cortical networks show spontaneously correlated activity patterns during in vitro development," *Brain Research*, vol. 1093, no. 1, pp. 41–53, 2006.

[35] A. Vato, L. Bonzano, M. Chiappalone, et al., "Spike manager: a new tool for spontaneous and evoked neuronal networks activity characterization," *Neurocomputing*, vol. 58–60, pp. 1153–1161, 2004.

[36] F. Rieke, D. Warland, R. de Ruyter van Steveninck, and W. Bialek, *Spikes: Exploring the Neural Code*, The MIT Press, Cambridge, Mass, USA, 1997.

[37] D. Eytan, N. Brenner, and S. Marom, "Selective adaptation in networks of cortical neurons," *Journal of Neuroscience*, vol. 23, no. 28, pp. 9349–9356, 2003.

[38] D. A. Wagenaar and S. M. Potter, "A versatile all-channel stimulator for electrode arrays, with real-time control," *Journal of Neural Engineering*, vol. 1, no. 1, pp. 39–45, 2004.

[39] Y. Jimbo, H. P. C. Robinson, and A. Kawana, "Strengthening of synchronized activity by tetanic stimulation in cortical cultures: application of planar electrode arrays," *IEEE Transactions on Biomedical Engineering*, vol. 45, no. 11, pp. 1297–1304, 1998.

[40] Y. Jimbo, T. Tateno, and H. P. C. Robinson, "Simultaneous induction of pathway-specific potentiation and depression in networks of cortical neurons," *Biophysical Journal*, vol. 76, no. 2, pp. 670–678, 1999.

[41] T. Tateno and Y. Jimbo, "Activity-dependent enhancement in the reliability of correlated spike timings in cultured cortical neurons," *Biological Cybernetics*, vol. 80, no. 1, pp. 45–55, 1999.

[42] P. Bonifazi, M. E. Ruaro, and V. Torre, "Statistical properties of information processing in neuronal networks," *European Journal of Neuroscience*, vol. 22, no. 11, pp. 2953–2964, 2005.

[43] M. E. Ruaro, P. Bonifazi, and V. Torre, "Toward the neurocomputer: image processing and pattern recognition with neuronal cultures," *IEEE Transactions on Biomedical Engineering*, vol. 52, no. 3, pp. 371–383, 2005.

[44] M. Chiappalone, P. Massobrio, M. Tedesco, and S. Martinoia, "Stimulus-induced synaptic changes in networks of cortical neurons," in *Proceedings of the 5th International Meeting on Substrate-Integrated Micro Electrode Arrays (SIMEA '06)*, pp. 32–33, BIOPRO Baden-Wurttemberg GmbH, Reutlingen, Germany, 2006.

[45] G. L. Shaw, *Keeping Mozart in Mind*, Academic Press, San Diego, Calif, USA, 2nd edition, 2003.

[46] T. G. Deliagina, "Vestibular compensation in lampreys: impairment and recovery of equilibrium control during locomotion," *The Journal of Experimental Biology*, vol. 200, no. 10, pp. 1459–1471, 1997.

[47] T. G. Deliagina, P. V. Zelenin, P. Fagerstedt, S. Grillner, and G. N. Orlovsky, "Activity of reticulospinal neurons during locomotion in the freely behaving lamprey," *Journal of Neurophysiology*, vol. 83, no. 2, pp. 853–863, 2000.

[48] D. A. Wagenaar and S. M. Potter, "Real-time multi-channel stimulus artifact suppression by local curve fitting," *Journal of Neuroscience Methods*, vol. 120, no. 2, pp. 113–120, 2002.

[49] I. Obeid and P. D. Wolf, "Evaluation of spike-detection algorithms for a brain-machine interface application," *IEEE Transactions on Biomedical Engineering*, vol. 51, no. 6, pp. 905–911, 2004.

[50] D. Wagenaar, T. B. DeMarse, and S. M. Potter, "MeaBench: a toolset for multi-electrode data acquisition and on-line analysis," in *Proceedings of the 2nd International IEEE EMBS Conference on Neural Engineering*, pp. 518–521, Arlington, Va, USA, March 2005.

Hindawi Publishing Corporation
Computational Intelligence and Neuroscience
Volume 2007, Article ID 82827, 7 pages
doi:10.1155/2007/82827

Research Article

Novel Features for Brain-Computer Interfaces

W. L. Woon[1,2] and A. Cichocki[1]

[1] *Laboratory for Advanced Brain Signal Processing, RIKEN Brain Science Institute, 2-1 Hirosawa, Wako, Saitama 351-0198, Japan*
[2] *Malaysia University of Science and Technology, Unit GL33, Block C, Kelana Square, 17 Jalan SS7/26, Petaling Jaya Selangor 47301, Malaysia*

Correspondence should be addressed to W. L. Woon, wlwoon@must.edu.my

Received 29 December 2006; Revised 2 May 2007; Accepted 21 June 2007

Recommended by Fabio Babiloni

While conventional approaches of BCI feature extraction are based on the power spectrum, we have tried using nonlinear features for classifying BCI data. In this paper, we report our test results and findings, which indicate that the proposed method is a potentially useful addition to current feature extraction techniques.

1. INTRODUCTION AND MOTIVATIONS

It is widely believed that both the underlying generators of EEG as well as the recorded signals have at least some nonlinear components [1–3]. Indeed, nonlinear tools and techniques have already been usefully deployed on problems such as the diagnosis of Alzheimer's disease [4], Schizophrenia [5], and the early prediction of epileptic seizures [6–8]. However, there appears to be a lack of interest in such methods for BCI feature extraction, which remains largely dependent on frequency-based methods. This is especially conspicuous when viewed in contrast with the enthusiastic uptake of advanced signal processing techniques for noise and artifact rejection (see, e.g., [9–11]).

To address this apparent shortcoming, we have experimented with a number of nonlinear and complexity-based feature extraction techniques. While our investigations are still preliminary, we have already obtained promising results which will hopefully encourage further progress and development in this research direction.

The rest of the paper is structured as follows. Section 2 describes the nonlinear features investigated while Section 3 explains the simulation procedures, including the data set used and preprocessing methods. The test results are presented in Section 4. Finally, Section 5 summarizes the findings and suggests possible avenues for further investigation.

2. EEG FEATURE EXTRACTION FOR BCI

While a variety of BCI modalities are in common use, this paper will focus on systems exploiting the modulation of μ (often referred to as the "sensory motor rhythm" (SMR)) and β rhythms [12]. Often described as attenuation of the spectral power in these bands, the associated EEG phenomena are in fact believed to be due to the desynchronization of cortical circuits related to motor function [13, 14]. From this perspective, an appropriate framework for studying these event-related EEG phenomena might be in terms of signal *complexity*.

Towards this end, some work has already been done in exploiting spatial complexity for BCI [15, 16]. However, we believe that additional information may be extracted by extending this approach to the temporal domain. As an initial review, the following measures were chosen:

(1) singular spectral entropy (SSE),
(2) spectral profile (SP),
(3) temporal asymmetry (TA).

The above selection represents a pragmatic balance of computational simplicity and a desire to approach the nonlinear characterization problem from the complexity (SSE and SP) and statistics-based (TA) perspectives. For comparison, we also compute the averaged signal power in the μ (10–15 Hz)

and β_2 (23–28 Hz) bands, which will be referred to as the "power feature" or PF. Note that at present we only consider the high beta range (β_2), as is done in a number of other studies on this data set, for example [10, 17, 18]. The exact frequency ranges mentioned above are based on the work described in [17].

These features will now be briefly described.

2.1. Singular spectral entropy (SSE)

If we define complexity as the number of independent though possibly interacting components which are active in a signal or system at a particular time, then one way by which complexity may be characterized is through the notion of *entropy*. While a variety of power distributions might be suitable candidates for this purpose, the shape of the singular spectrum provides an efficient representation of the constituent components of a time series. The approach chosen here is to obtain the singular spectrum of the *delay embedding* of a time series (described in further detail below), then to model this spectrum as a probability distribution before calculating the entropy of the singular values; the resulting measure will henceforth be termed the singular spectral entropy (SSE). An initial study was conducted in [19], where it was noted that imagined movements correlated with fluctuations of the SSE. Unfortunately, there was no attempt to further characterize these fluctuations or to build a classifier based on this approach. Since then, however, SSE has been applied to other aspects of EEG such as sleep [20] and ictal (seizure) EEG [6]. Hence, while its use is not widespread, SSE is a promising candidate for BCI feature extraction, motivating its use in this study.

For a time series $\mathbf{x}(t)$, SSE is calculated by first constructing a delay embedding matrix, $\mathbf{X}$, of dimension m:

$$\mathbf{X} = \left[\mathbf{x}(t), \mathbf{x}(t+1), \ldots, \mathbf{x}(t+n)\right] \in \mathcal{R}^{m\times(n+1)}, \tag{1}$$

where $\mathbf{x}(t) = [x(t), x(t-1), \ldots, x(t-m)]^T$. Next, $\mathbf{X}$ is decomposed using singular value decomposition (SVD) to obtain

$$\mathbf{X} = \mathbf{U}\mathbf{S}\mathbf{V}^T, \tag{2}$$

where $\mathbf{U}$ and $\mathbf{V}$ are orthogonal matrices, and $\mathbf{S}$ is a diagonal matrix containing the singular values of the embedding matrix, s_i. These are then normalized to one and used to calculate SSE as follows:

$$\mathrm{SSE}_m = -\sum_{i=1}^{m} s_i \log s_i. \tag{3}$$

2.2. Spectral profile (SP)

The intuition behind the SSE feature can equally be applied to the frequency spectrum (in fact, an additional complexity measure proposed in [21] used the entropy of the power spectral density). However, experimentally we have found this measure to be extremely noisy and unsuitable for use with BCI.

However, as an alternative to SSE, we wish to define a further feature based on the shape of the power spectra; it was decided to evaluate the effectiveness of directly using the ordinates of the frequency spectra as a feature vector. To prevent the power of the signal from dominating or even affecting the classification process in any way, the extracted spectral components were first normalized to one before incorporation into the feature set. For convenience, we will refer to this feature as the *spectral profile* (SP) of the trial.

To obtain the SP vector, the elements of the spectra corresponding to the μ and β bands were extracted then normalized as follows:

$$\begin{aligned}\boldsymbol{\mu} &= \left\{\frac{\theta_i}{\sum_{j\in\Sigma_\mu}\theta_j} : i \in \Sigma_\mu\right\},\\ \boldsymbol{\beta} &= \left\{\frac{\theta_i}{\sum_{i\in\Sigma_\beta}\theta_j} : j \in \Sigma_\beta\right\},\end{aligned} \tag{4}$$

where θ_i is the ith ordinate of the power spectrum, and Σ_μ and Σ_β are the sets of frequency ordinates falling within the two bands, respectively. $\boldsymbol{\mu}$ and $\boldsymbol{\beta}$ are the sets containing the normalized spectral ordinates and if we define μ_i and β_j as the enumerated elements of these sets, the SP feature vector is then written as follows:

$$\mathrm{SP}_{\Sigma_\mu,\Sigma_\beta} = [\mu_i, \ldots, \mu_{N_\mu}, \beta_j, \ldots, \beta_{N_\beta}], \tag{5}$$

where N_μ and N_β are the sizes of sets $\boldsymbol{\mu}$ and $\boldsymbol{\beta}$.

2.3. Temporal asymmetry (TA)

If we assume that the desynchronization process accompanying motor visualization reflects the activation of previously dormant neuronal circuits, then this might also be accompanied by a detectable increase in signatures of nonlinear dynamics.

One property of linear time series is that the associated statistics remain constant under time reversal, since a linear process is essentially a combination of sinusoids which are symmetric in time. This fact can be exploited to provide a particularly powerful indicator of nonlinearity, temporal asymmetry (TA); this is frequently defined as [22]

$$\mathrm{TA}_\tau = \frac{\sum_{n=\tau+1}^{N}\left(x(n)-x(n-\tau)\right)^3}{\left[\sum_{n=\tau+1}^{N}\left(x(n)-x(n-\tau)\right)^2\right]^{3/2}}, \tag{6}$$

where τ is the time delay. To restrict the analysis to components of the signal which exhibit the highest variability with respect to the classes of interest, a pair of bandpass filters was used to extract signal components in the μ and β bands (details provided later in Section 4), from which the TA was calculated and used to create a feature vector based on temporal asymmetry.

2.4. Power feature (PF)

In addition to the features mentioned above, the power feature (PF) was included for comparison. This represents the

conventional approach to BCI feature extraction (variations of which are used in [10, 17, 18], e.g.) and is defined as the spectral power contained in the μ and β bands. PF is calculated, thus

$$\mathrm{PF} = \left[\sum_{f\in[10,15]} \theta_f, \sum_{f\in[23,28]} \theta_f \right], \tag{7}$$

where θ_f is the power spectrum at frequency f.

Finally, for the calculation of the SSE and TA features, we use bandpass filters to restrict the analysis to the μ and β bands of the signal, as these are known a priori to be active during motor imagery. As the actual magnitudes of the signals in these two bands are removed via normalization, we hope to focus on the overall shape of the spectrum rather than on particular peaks, as nonlinear phenomena are likely to have broader spectra compared to oscillatory generators.

3. PROCEDURES

3.1. Data

To test the proposed approach, we used dataset IIA from BCI competition 2003 [23, 24], which was provided by the Wadsworth Center, New York State Department of Health . The data consists of 64-channel recordings from three subjects (AA, BB, and CC) for ten 30-minute sessions. Each session consists of 192 trials in which the subject is required to use motor imagery to guide a cursor to one of four possible target positions. As was done during the competition, we use data from the first six sessions as the training set, while recordings of the last four sessions were used to test the trained classifiers.

3.2. Preprocessing and channel selections

As an initial preprocessing step, we evaluated two methods commonly used for EEG analysis: the common average reference (CAR) and the Laplacian spatial filtering methods. The CAR filter was found to significantly improve classification performance and was subsequently retained as a basic first stage in the classification process, (e.g., of its use in BCI, see [10, 18]). The CAR filter is applied as follows:

$$\mathbf{v}_i^{\mathrm{CAR}} = \mathbf{v}_i^{\mathrm{Raw}} - \frac{1}{N}\sum_{j=1}^{N} \mathbf{v}_j^{\mathrm{Raw}}, \tag{8}$$

where N is the number of channels in the data set, $\mathbf{v}_i^{\mathrm{Raw}}$ is the unprocessed signal from channel number i, and $\mathbf{v}_i^{\mathrm{CAR}}$ is the same channel after CAR filtering.

As CAR filtering is primarily for noise rejection, projection onto CSP (common spatial patterns) features is used to further emphasize information relevant to the BCI classification task. CSP is widely used in EEG analysis [17, 25] to find spatial filters that maximize the variance of trials corresponding to one particular class at the expense of another.

Briefly, the CSP filters are found as follows.

(1) Partition the full data matrix $\mathbf{X}$ into the two class-specific matrices $\mathbf{X}_A$ and $\mathbf{X}_b$ corresponding to the two classes to be discriminated.

(2) Calculate the corresponding covariance matrices $\mathbf{C}_A$ and $\mathbf{C}_B$ as well as the sum $\mathbf{C} = \mathbf{C}_A + \mathbf{C}_B$.

(3) Find the whitening matrix $\mathbf{W}$ such that $\mathbf{W}^T\mathbf{C}\mathbf{W} = \mathbf{I}$, where $\mathbf{W}$ may be found via the eigenvector decomposition

$$\mathbf{C} = \tilde{\mathbf{U}}^T\Sigma\tilde{\mathbf{U}}, \tag{9}$$

then $\mathbf{W} = \tilde{\mathbf{U}}\Sigma^{-1/2}$. Hence,

$$\mathbf{W}^T\mathbf{C}\mathbf{W} = \mathbf{I} \Longrightarrow \mathbf{W}^T\mathbf{C}_A\mathbf{W} + \mathbf{W}^T\mathbf{C}_B\mathbf{W} = \mathbf{I}. \tag{10}$$

(4) Apply a rotation matrix $\mathbf{Y}$ to both sides of (10),

$$\mathbf{Y}^T(\mathbf{W}^T\mathbf{C}_A\mathbf{W} + \mathbf{W}^T\mathbf{C}_B\mathbf{W})\mathbf{Y} = \mathbf{I}. \tag{11}$$

(5) Choose $\mathbf{Y}$ such that it diagonalizes $\mathbf{W}^T\mathbf{C}_A\mathbf{W}$, that is,

$$\mathbf{Y}^T[\mathbf{W}^T\mathbf{C}_A\mathbf{W}]\mathbf{Y} = \begin{bmatrix} \sigma_A^1 & 0 & \cdots & 0 \\ 0 & \sigma_A^2 & \cdots & 0 \\ & & \ddots & \\ 0 & 0 & & 0 \\ 0 & \cdots & 0 & \sigma_A^n \end{bmatrix}. \tag{12}$$

(6) From (10)–(12), it follows that $\mathbf{Y}^T[\mathbf{W}^T\mathbf{C}_B\mathbf{W}]\mathbf{Y}$ will also be diagonal, and the sum of corresponding diagonal elements will be 1.

(7) Hence, to create a spatial filter that maximizes the variance of class A trials while minimizing the variance of class B trials, set $\mathbf{Y}$ to be the eigenvectors of $\mathbf{W}^T\mathbf{C}_A\mathbf{W}$. Then, the columns of the matrix $\mathbf{WY}$ provide the CSP spatial filters and may be sorted based on the eigenvalues.

For both of the data sets presented above, a bandpass filter with the following passbands: 10–15 Hz (μ) and 23–26 Hz (β) was applied. This creates two filtered signals which are then added together. As was done in [17, 18], only classes 1 and 4 are considered at this stage. Trials belonging to these two classes are extracted and combined to form $\mathbf{X}_A$ and $\mathbf{X}_B$, respectively. These are then used to obtain the CSP filters as described above.

For operations requiring the power spectra, the Welch method was used to estimate the power spectral density. This method has been used in a number of other BCI related studies (e.g., [9], in which it was noted for producing superior performance). A 128-point window with 50% overlap was used. For bandpass filtering operations, we used third order Butterworth filters as they provided frequency responses with maximal flatness, (and hence minimal distortion of the amplitude spectra). The use of FIR filters was also considered for their linear phase property. However, subsequent inspections of the frequency responses revealed that a similar amplitude response would have required an FIR with around 50 taps; in comparison, the trials for subject CC are 304 samples long.

In the actual experimental setting, two CSP channels were used at any time (the actual choice of channels used varied with the subject, as will be described later). In addition, it was discovered that submitting the entire set of 64 channels to CSP processing resulted in problems with matrix singularity, as many channels are highly correlated. As such, only a subset consisting of 18 channels situated over the motor cortex was used. These were 8–10, 12–17, 19–21, 48–50, and 52–54 [18].

3.3. Feature translation

For feature classification, we adopt a probabilistic approach similar to that used in [26]. However, because the present data set is a lot larger, Gaussian mixture models (GMM) were used in place of the single Gaussians used in [26]. Preliminary experimentations were conducted with the case of 1 and 2 Gaussians.

To train the models, the selected features were first extracted from the training data and grouped according to target classes. For each class $c \in \{1, 2, 3, 4\}$, we train a two-Gaussian GMM using the expectation-maximization (EM) algorithm.

To classify a test vector $\mathbf{f}$ into one of the four classes, the maximum a posteriori (MAP) decision rule is used:

$$c_{\text{MAP}}(\mathbf{f}) = \text{argmax}_c\, P(c \mid \mathbf{f}). \tag{13}$$

$P(c|\mathbf{f})$ can be found via Bayes' theorem. Also, in this case, we have uniform prior and constant evidence terms, hence

$$\begin{aligned} P(c \mid \mathbf{f}) &= \frac{P(\mathbf{f} \mid c)p(c)}{P(\mathbf{f})} = kP(\mathbf{f} \mid c) \\ &\propto \sum_{i \in \{1,2\}} \pi_{i,c} \exp\Big[-(\mathbf{f} - \mu_{i,c})^T \mathbf{C}_{i,c}^{-1} (\mathbf{f} - \mu_{i,c}) \Big], \end{aligned} \tag{14}$$

where $\mu_{i,c}$ and $\mathbf{C}_{i,c}$ are the mean and covariance of Gaussians i in class mixture c, and $\pi_{i,c}$ are the mixing coefficients determined during training.

The effectiveness of the features can now be evaluated in terms of the classification rates, which are calculated as follows:

$$\text{Accuracy (\%)} = 100 \times \frac{\Big[\sum_{i=1}^{n} \delta(c_{\text{MAP}}(\mathbf{f}_i) - c(i)) \Big]}{n}, \tag{15}$$

where i is the trial index and n is the number of trials. $\mathbf{f}_i$ and $c(i)$ denote the feature vector and class labels for trial i, respectively, and $\delta(\cdot)$ is Dirac's delta function.

4. RESULTS AND OBSERVATIONS

The procedures and features described in the preceding sections were applied to the BCI data and classification accuracy evaluated according to (15). For SSE, an embedding dimension of $m = 15$ was used, while for the delay parameter in TA, $\tau = 2$ was used. These values were selected based on an evaluation of a range of potential combinations. The performances of all four features are compared in Tables 1 and 2 for the 1 and 2 Gaussian cases, respectively.

As can be seen, the classification performance obtained using both SSE and SP is encouraging when compared to the performance of PF. SSE in particular is more accurate than both SP and PF. SP also produced higher classification rates compared to PF though the disparity was a lot narrower. However, PF has better classification rates in the case of subject CC when compared with SP.

On the negative side, the TA feature performed very poorly. However, while disappointing, this result is not surprising considering that measures based on high-order statistics are notoriously sensitive to noise. In most cases, TA is used only in combination with surrogate data and then only to establish the presence of nonlinearity, not to characterize it.

Table 1: Feature-wise classification accuracy using 1 Gaussian (%).

Features	Subjects			
	AA	BB	CC	Mean
SSE	68.5	52.3	68.6	63.2
SP	61.3	54.7	62.5	59.5
TA	36.8	27.9	35.0	33.2
PF	57.7	49.9	64.6	57.4

Table 2: Feature-wise mean classification accuracy using 2 Gaussians (%).

Features	Subjects			
	AA	BB	CC	Mean
SSE	68.4	52.3	68.7	63.1
SP	62.5	54.7	62.1	59.8
TA	36.3	29.9	35.5	33.9
PF	55.2	52.1	67.4	58.2

Finally, in terms of the classification algorithm, the performance of the 1 and 2 gaussian models did not appear to differ very much. Henceforth, for brevity, we only present results produced by the two Gaussian models, which performed slightly better. However, it must be noted that the choice of either of these two models does not appear to be critical.

4.1. Detailed comparisons of SSE, SP, and PF

Given the disappointing classification rates obtained using TA, we exclude it from further discussions and focus now on the relative performances of SSE, SP, and PF. To better understand the performance characteristics of these three features, the per-session classification accuracies for each of the three features are presented in Table 3. For comparison, the average online accuracies (this is the success rate of the subject in hitting the target) obtained during the actual recording at the Wadsworth centre have also been included.

Some observations were as follows.

(1) As mentioned before, SSE was the best all-round performer, producing the best classification rates in 7 out of 12 sessions. SP was superior to PF in 9 sessions.
(2) However, SP emerged as the best feature in only 2 sessions, compared to 3 sessions in the case of PF. PF performed particularly well with subject CC, especially in session 7 where it had by far the best results. For subject BB, PF had the best classification rate for session 7 while its accuracy for session 8 was clearly better than SSE and comparable to SP.
(3) Similarly, though the overall results obtained using SSE were the best, SP produced the highest average classification rate for subject BB.
(4) This variability in the results implies that SSE, SP, and PF are monitoring independent aspects of the signal

Table 3: {SSE, SP, PF}: Classification accuracy (%). Scores in bold are top scores for the respective sessions.

Features		Sessions					
	Subjects	7	8	9	10	Mean	Online
SSE	AA	**67.4**	**67.9**	**71.2**	**67.0**	68.4	73.4
	BB	52.6	52.1	**54.2**	50.5	52.3	77.2
	CC	55.4	**78.6**	**67.2**	73.6	68.7	69.0
SP	AA	65.6	62.4	68.4	53.5	62.5	73.4
	BB	58.9	**54.2**	53.1	**52.6**	54.7	77.2
	CC	53.9	67.6	60.7	66.4	62.1	69.0
PF	AA	55.2	58.9	55.7	51.0	55.2	73.4
	BB	**60.9**	52.6	43.2	51.6	52.1	77.2
	CC	**68.8**	70.8	51.6	**78.6**	67.4	69.0

and that a classifier which combines the information extracted using these different features might be of value. To test this idea, we have conducted some preliminary tests, the results of which are described in Section 4.2.

(5) One curious result was that the offline classification rates almost seemed to be inversely related with the online classification rates. For example, EEG recordings from subject BB, who was the highest scorer during online tests, proved to be the most difficult to analyze and resulted in the lowest offline scores. It is unclear what the cause of this inconsistency was, but we note that the same trend is observed in other studies which use this data set [10, 17, 18].

(6) The choice of CSP-based spatial filter was highly dependent on the subject being tested. For EEG recordings of subjects AA and CC, CSPs specific to class 1 provided the best discrimination performance, while for subject BB, the CSPs specific to class 4 were a lot more suitable.

4.2. Combination classifier

Based on the variability in the results, we decided to test a combination classifier incorporating all three features {SSE, SP, PF}.

As creating a combination feature vector would greatly increase the number of parameters to be optimized, we adopted the approach used in [10], which was to train classifiers on each of the feature sets, then combine these using a committee machine. As in [10], the combined output was generated by averaging the predictions of the individual classifiers. While relatively simple, this method is acceptable as the performances of the experts do not differ too significantly.

The results of this approach are shown in Table 4. The overall impression is that the results seem to have benefited from using the combination approach. Some more detailed observations are as follows.

(1) In general, the results of the combination classifier are a lot more robust compared to the results of the individual classifiers. Even though the relative performances of the three component classifiers vary quite a bit, the performance of the combination classifier either exceeds or is very close to the best of the three. This helps to confirm that the proposed features are more robust in respect to noise or variability in the data and moreover enables us to extract information which is simply not present in the power features.

Table 4: Combination: classification accuracy (%).

Subjects	Sessions					
	7	8	9	10	Mean	Online
AA	69.3	69.9	69.5	61.7	67.6	73.4
BB	59.9	59.4	53.1	53.6	56.5	77.2
CC	63.4	80.0	65.5	76.5	71.3	69.0

(2) Similarly, on a session-by-session basis, the results of the combination classifier frequently exceeds that of any of the three component classifiers. By comparing the results in Table 3 with the results in Table 4, it can be seen that in five out of twelve sessions, the combination classifier is better than all three component classifiers.

(3) The classification performance of the combination classifier was comparable to results published in [10, 18]. In both cases, the combination classifier produced the best classification rate in the case of subject CC but did not fare as well in the cases of subjects AA and BB. However, the winning entry to the competition still had better performance [17], though this was obtained using a higher resolution feature extraction procedure based on dividing the trials into smaller time segments. As will be explained in Section 5, increasing the time resolution of the proposed method is certainly one of our current objectives.

(4) Similarly, the second placed entry in the competition [18] included an "energy accumulation function" to improve performance, while in [10] independent component analysis (ICA) is used to help remove noise from the signal. As a future work, we might certainly incorporate some of these enhancements but this is beyond the scope of the present paper.

5. DISCUSSIONS

While preliminary, the results presented here suggest that features which allow for nonlinear dynamics are promising and potentially useful in the development of BCI systems.

As the tests were conducted using offline recordings, our initial objective was not to directly compare the proposed features with existing frequency-based techniques. Because these were used as the online control signals, subjects might have been conditioned to directly modulate the power spectrum, thus biasing the results in favour of traditional approaches. As such, we did not perform extensive optimization of the feature extraction parameters; in any case, though this might have produced slight improvements to the results, it could also have resulted in overfitting or overcustomization to a particular subject and was thus avoided.

Rather than obsessing with the final classification figures, our main aim was to demonstrate the general feasibility of complexity-based feature extraction. On this count, it appears that the proposed method is potentially useful for BCI. As far as we know, this is the first publication which seriously studies the performance of a temporal complexity measure on a BCI problem. If the results presented in this paper can be supported by further studies, it will provide an efficient new set of features for use with motor-imagery-based BCI systems. However, many issues need to be investigated before the practical utility of the method can be established. In particular, it should be noted that the experiments decribed in this paper process entire trials at a time to produce the classifications. While this is consistent with the approach taken in [18], a shorter-time window needs to be considered before the method can be tested for online (real-time) scenarios.

At present, we are either actively investigating or seriously considering a number of avenues for further investigation. In particular, we are interested in extracting SSE features from shorter-time windows (e.g., in the BCI experiments for this data, time windows of 200 ms were used to control the cursor motion). A separate but important issue is to find and test other practical measures of system complexity, for example, approximate entropy. If found to be promising, findings and results of these ongoing investigations will be described in a further publication in the hope of stimulating broader interest and development in this area.

REFERENCES

[1] G. Nolte, T. Sander, A. Lueschow, and B. A. Pearlmutter, "Nonlinear time series analysis of human alpha rhythm," in *The International Conference on Biomagnetism (BIOMAG '03)*, Jena, Germany, August 2003.

[2] C. J. Stam, "Nonlinear dynamical analysis of EEG and MEG: review of an emerging field," *Clinical Neurophysiology*, vol. 116, no. 10, pp. 2266–2301, 2005.

[3] M. Breakspear and J. R. Terry, "Nonlinear interdependence in neural systems: motivation, theory, and relevance," *International Journal of Neuroscience*, vol. 112, no. 10, pp. 1263–1284, 2002.

[4] B. Jelles, J. H. van Birgelen, J. P. J. Slaets, R. E. M. Hekster, E. J. Jonkman, and C. J. Stam, "Decrease of non-linear structure in the EEG of Alzheimer patients compared to healthy controls," *Clinical Neurophysiology*, vol. 110, no. 7, pp. 1159–1167, 1999.

[5] M. S. Keshavan, J. D. Cashmere, J. Miewald, and V. K. Yeragani, "Decreased nonlinear complexity and chaos during sleep in first episode schizophrenia: a preliminary report," *Schizophrenia Research*, vol. 71, no. 2–3, pp. 263–272, 2004.

[6] C. J. James and D. Lowe, "Extracting multisource brain activity from a single electromagnetic channel," *Artificial Intelligence in Medicine*, vol. 28, no. 1, pp. 89–104, 2003.

[7] M. Palus, V. Komarek, Z. Hrncir, and T. Prochazka, "Is nonlinearity relevant for detecting changes in EEG?" *Theory in Biosciences*, vol. 118, no. 3–4, pp. 179–188, 1999.

[8] K. Lehnertz and C. E. Elger, "Can epileptic seizures be predicted? evidence from nonlinear time series analysis of brain electrical activity," *Physical Review Letters*, vol. 80, no. 22, pp. 5019–5022, 1998.

[9] S. Chiappa and D. Barber, "EEG classification using generative independent component analysis," *Neurocomputing*, vol. 69, no. 7–9, pp. 769–777, 2006.

[10] J. Qin, Y. Li, and A. Cichocki, "ICA and committee machine-based algorithm for cursor control in a BCI system," in *Proceedings of the 2nd International Symposium on Neural Networks (ISNN '05)*, vol. 3496 of *Lecture Notes in Computer Science*, pp. 973–978, Chongqing, China, May-June 2005.

[11] H. Lee, A. Cichocki, and S. Choi, "Nonnegative matrix factorization for motor imagery EEG classification," in *Proceedings of the International Conference on Artificial Neural Networks (ICANN '06)*, vol. 4132 of *Lecture Notes in Computer Science*, pp. 250–259, Athens, Greece, September 2006.

[12] J. R. Wolpaw, N. Birbaumer, D. J. McFarland, G. Pfurtscheller, and T. M. Vaughan, "Brain-computer interfaces for communication and control," *Clinical Neurophysiology*, vol. 113, no. 6, pp. 767–791, 2002.

[13] G. Pfurtscheller and F. H. Lopes da Silva, "Event-related EEG/MEG synchronization and desynchronization: basic principles," *Clinical Neurophysiology*, vol. 110, no. 11, pp. 1842–1857, 1999.

[14] G. Pfurtscheller, C. Brunner, A. Schlögl, and F. H. Lopes da Silva, "Mu rhythm (de)synchronization and EEG single-trial classification of different motor imagery tasks," *NeuroImage*, vol. 31, no. 1, pp. 153–159, 2006.

[15] L. Song and J. Epps, "Classifying EEG for brain-computer interfaces: learning optimal filters for dynamical system features," in *Proceedings of the 23rd International Conference on Machine Learning (ICML '06)*, pp. 857–864, Pittsburgh, Pa, USA, June 2006.

[16] X.-M. Pei, C.-X. Zheng, J. Xu, G.-Y. Bin, and H.-W. Wang, "Multi-channel linear descriptors for event-related EEG collected in brain computer interface," *Journal of Neural Engineering*, vol. 3, no. 1, pp. 52–58, 2006.

[17] G. Blanchard and B. Blankertz, "BCI competition 2003: data set IIa: spatial patterns of self-controlled brain rhythm modulations," *IEEE Transactions on Biomedical Engineering*, vol. 51, no. 6, pp. 1062–1066, 2004.

[18] M. Cheng, W. Jia, X. Gao, S. Gao, and F. Yang, "Mu rhythm-based cursor control: an offline analysis," *Clinical Neurophysiology*, vol. 115, no. 4, pp. 745–751, 2004.

[19] S. J. Roberts, W. Penny, and I. Rezek, "Temporal and spatial complexity measures for electroencephalogram based brain-computer interfacing," *Medical and Biological Engineering and Computing*, vol. 37, no. 1, pp. 93–98, 1999.

[20] I. Rezek, S. Roberts, and P. Sykacek, "Complexity features for sleep stage analysis," in *Proceedings of the European Medical*

and Biological Engineering Conference (EMBEC '99), pp. 1650–1651, Vienna, Austria, November 1999.

[21] I. A. Rezek and S. J. Roberts, "Stochastic complexity measures for physiological signal analysis," *IEEE Transactions on Biomedical Engineering*, vol. 45, no. 9, pp. 1186–1191, 1998.

[22] T. Schreiber, "Interdisciplinary application of nonlinear time series methods," *Physics Reports*, vol. 308, no. 1, pp. 1–64, 1999.

[23] D. J. McFarland, A. T. Lefkowicz, and J. R. Wolpaw, "Design and operation of an EEG-based brain-computer interface with digital signal processing technology," *Behavior Research Methods, Instruments, and Computers*, vol. 29, no. 3, pp. 337–345, 1997.

[24] B. Blankertz, K.-R. Müller, G. Curio, et al., "The BCI competition 2003: progress and perspectives in detection and discrimination of EEG single trials," *IEEE Transactions on Biomedical Engineering*, vol. 51, no. 6, pp. 1044–1051, 2004.

[25] P. Shenoy, M. Krauledat, B. Blankertz, R. P. N. Rao, and K.-R. Müller, "Towards adaptive classification for BCI," *Journal of Neural Engineering*, vol. 3, no. 1, pp. R13–R23, 2006.

[26] S. Lemm, C. Schäfer, and G. Curio, "BCI competition 2003-data set III: probabilistic modeling of sensorimotor μ rhythms for classification of imaginary hand movements," *IEEE Transactions on Biomedical Engineering*, vol. 51, no. 6, pp. 1077–1080, 2004.

Hindawi Publishing Corporation
Computational Intelligence and Neuroscience
Volume 2007, Article ID 74895, 12 pages
doi:10.1155/2007/74895

Research Article

Channel Selection and Feature Projection for Cognitive Load Estimation Using Ambulatory EEG

Tian Lan,[1] Deniz Erdogmus,[1] Andre Adami,[2] Santosh Mathan,[3] and Misha Pavel[1]

[1] *Department of Biomedical Engineering, Oregon Health and Science University, Portland, OR 97239, USA*
[2] *Department of Computer Science, University of Caxias do Sul, 95070-560 Caxias do Sul, RS, Brazil*
[3] *Human Centered Systems, Honeywell Laboratories, Minneapolis, MN 55401, USA*

Correspondence should be addressed to Deniz Erdogmus, derdogmus@ieee.org

Received 14 February 2007; Accepted 18 June 2007

Recommended by Andrzej Cichocki

We present an ambulatory cognitive state classification system to assess the subject's mental load based on EEG measurements. The ambulatory cognitive state estimator is utilized in the context of a real-time augmented cognition (AugCog) system that aims to enhance the cognitive performance of a human user through computer-mediated assistance based on assessments of cognitive states using physiological signals including, but not limited to, EEG. This paper focuses particularly on the offline channel selection and feature projection phases of the design and aims to present mutual-information-based techniques that use a simple sample estimator for this quantity. Analyses conducted on data collected from 3 subjects performing 2 tasks (n-back/Larson) at 2 difficulty levels (low/high) demonstrate that the proposed mutual-information-based dimensionality reduction scheme can achieve up to 94% cognitive load estimation accuracy.

1. INTRODUCTION

Following the successful demonstration of a P300 oddball detector [1], many brain computer interfaces (BCIs) are designed on similar concepts [2]—evoked response potential (ERP) detection or sliding window classification. Artifact removal using adaptive filtering source separation techniques have been proposed [3, 4], wavelet coefficients [5], short-term power spectrum [6–8], and chaos/fractal structure [9, 10] have been investigated as potential features. Various standard classifiers including linear discriminants, neural networks, and support vector machines are employed [11–16], parametric and nonparametric approximate Bayes classifiers and boosting techniques have been evaluated [17–22]. Some benchmark datasets for BCI design evaluations have been proposed [23] and have met reasonable acceptance.

Accurate assessment of cognitive load from ambulatory electroencephalogram (EEG) could lead to a wide variety of applications for brain interface systems [24]. Of specific interest to us is the concept of augmented cognition (AugCog), which is applicable where the cognitive load of human operators needs to be monitored to design optimal information flow protocols from the computer to the human in order to maximize task performance [25]. These applications include, but are not limited to, vehicle drivers, machinery operators, air traffic controllers, and robotic surgery operators. Optimizing the information flow for seamless human-computer interaction requires the real-time assessments of cognitive states during the execution of certain tasks leading to a prescribed goal. An accurate cognitive load estimator is essential for the successful implementation of assistive systems that are aware of the user's status and environment. Instantaneous estimates of mental state and workload can be used to control the rate and the modality of the information presented to the operator, which in turn helps the operator allocate mental resources to maximize performance [26]. As the envisioned applications require ambulatory EEG recordings, special care must be given to proper signal conditioning, noise and artifact reduction.

The use of EEG, as the basis of assessment in brain-computer interface (BCI) and AugCog systems, is predicated on characteristics such as good temporal resolution, non-invasiveness, low cost, and portability [27]. However, the following factors make it particularly difficult to deal with

ambulatory EEG signals: (1) noise resulting from motion artifacts; (2) contamination with muscular activities, including the usual eye movements and blinks; (3) influence of concurrent but irrelevant neural activities; (4) environmental noise; (5) nonstationarity. Under these circumstances, both robustness and precision of the designed system are particularly critical. Furthermore, the system must be portable and able to work in real-time. *The focus of this paper is on feature and channel selection for real-time cognitive state classification based on EEG* in order to address items (1) to (4) in this list. Note that nonstationarity could also be partially addressed to the extent that training session provided sufficiently rich data to represent various sources of nonstationarity.

From a machine learning point-of-view, an EEG characterization system (such as a BCI) requires a robust pattern recognition system to assess the cognitive states or the intent of the operator. A typical classification system contains five parts: preprocessing, feature extraction, dimensionality reduction, classification, and postprocessing. Although any improvement in one of these parts can boost the performance of the system, *in this paper, our focus will be on dimensionality reduction*, because criteria such as accuracy, real-time performance, and wireless networking require all rely on a set of compact features. Furthermore, choosing the most informative and stable feature subset can also partly solve the subject-to-subject transfer, session to session transfer, and nonstationarity problem. The other modules of the classification system were designed following well-established techniques. For example, we employed a standard adaptive filtering technique for the removal of eye artifacts. We used FFT based power spectrum density (PSD) estimation procedures to estimate the power at various frequency bands broadly accepted to be associated with cognitive activity—these estimates served as the primary features for classification. Additionally, we used Gaussian mixtures model (GMM), K nearest neighbor (KNN), and Parzen window density estimate (Parzen) methods for classification. The PSD features constitute a high-dimensional vector that contains information pertinent to the classification of cognitive states, as well as irrelevant components and noise. Direct classification using such input features is undesirable since the unwanted components have an adverse effect on the overall classification performance and the generalization ability of the system. Consequently, a practical technique for extracting the relevant information from these features is necessary.

We present the following: (1) a nonparametric sample estimator for mutual information that combines fast linear ICA solutions with sample-spacing entropy estimators to achieve computational simplicity; (2) EEG channel selection and linear feature projection techniques based on mutual information to achieve dimensionality reduction for computational and generalization benefits.

2. METHODS

Hardware platform

A mobile wireless sensor suite was assembled using a variety of off-the-shelf components. EEG was collected from 32 channels using a BioSemi Active Two system [28]. Vertical and horizontal eye movements and blinks are recorded with electrodes below and lateral to the left eye. This system integrates an amplifier with an Ag−AgCl electrode—this affords extremely low noise measurements without any skin preparation. Information from the sensors is transmitted (via a combination of Bluetooth, serial port, and USB) to and recorded on a body-worn laptop (Pentium 4.3 GHz with 1 GB RAM). A base station computer controls the experiment and communicates with the laptop via an 802.11 wireless network.[1]

Signal processing and classification

All channels reference the right mastoid. EEG is recorded at 256 Hz sampling frequency while the subject is performing tasks with various cognitive loads. EEG signals are preprocessed to remove eye blinks using an adaptive linear filter based on the Widrow-Hoff training rule [18]. Information from the VEOGLB ocular reference channel was used as the noise reference source for the adaptive ocular filter. DC drifts were removed using high-pass filters (0.5 Hz cutoff). A bandpass filter (between 2 Hz and 50 Hz) was also employed, as this interval is generally associated with cognitive activity. The PSD of the EEG signals, estimated using the Welch method [29] with 1-second windows, is integrated over 5 frequency bands: 4–8 Hz (theta), 8–12 Hz (alpha), 12–16 Hz (low beta), 16–30 Hz (high beta), 30–44 Hz (gamma). The energy levels in these bands sampled every 0.2 seconds (i.e., sliding windows with 80% overlap) are used as the basic input features for cognitive classification. The particular selection of the frequency bands is based on well-established interpretations of EEG signals in prior experimental and clinical contexts [24]. The overall schematic diagram of the signal processing system is shown in Figure 1.

In the design phase, the PSD features are used to rank and select EEG channels to reduce dimensionality. For this purpose, we assume that training patterns are representative of the spectral patterns one would expect in the performance environment. The final feature vector, with a much lower dimensionality than the original input, is then fed to a committee of three classifiers. Since the distribution of the feature vectors is unknown, we used both parametric and nonparametric classifiers in the committee: GMM, KNN, and Parzen. The classification component signal flow is illustrated in Figure 1. The GMM is a parametric approach where the class probability distributions are approximated

[1] A real-time AugCog system based on the selected channels is implemented successfully in a communication-routing system that prioritizes information and messages for timely delivery to the subjects in a high-communication task, resulting in increased accuracy of situation awareness (measured by correct responses to questions in postsession interview). Besides EEG, the system incorporates a wearable arousal meter. This unit senses a subject's electrocardiogram (ECG) signals and outputs interbeat interval data in conjunction with a derived measure of a subect's cognitive arousal. The details of this implementation and results are not the subject of this paper.

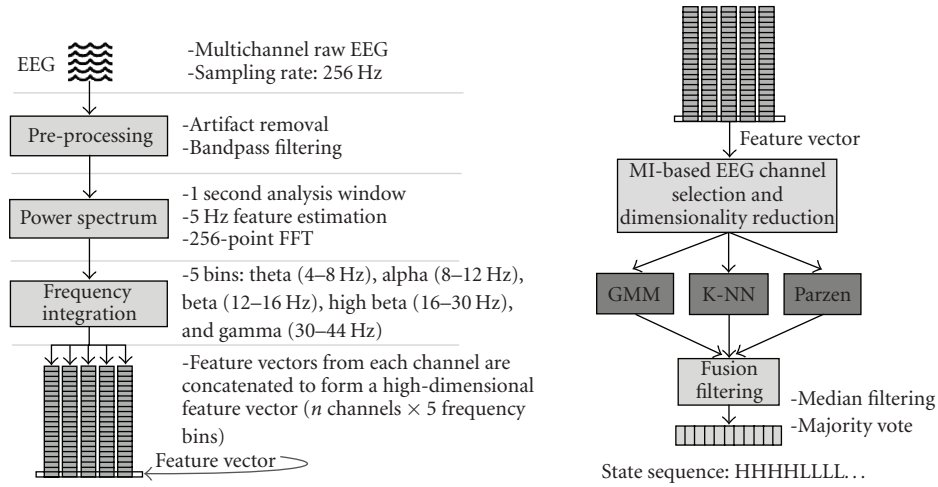

Figure 1: PSD-based feature extraction (left) and dimensionality reduction, classification, and postprocessing flow diagrams (right).

by a small number of Gaussians. KNN is a nonparametric approach where the classification is based on the count of nearest neighbors from each class (can be understood as a variable-size rectangular Parzen estimate of the class distributions). The *Parzen classifier* is a nonparametric approach to estimate the posterior probability of a feature vector belonging to a given class, using Gaussian kernels in this case. The estimate is a mixture-of-Gaussians with smooth contributions from all samples and this represents a compromise between discrete votes from nearest neighbors and the small number of Gaussian components of the parametric model. The details of the classifiers are discussed in the appendix. We now describe the EEG channel selection and feature projection procedures in more detail, as this is the main focus of this paper.

3. DIMENSIONALITY REDUCTION

Feature extraction is the process of discovering a statistical pattern that can differentiate various classes that lead to distinct observations. In contrast, dimensionality reduction is a process of finding optimal feature vectors with reduced dimensionality from a large pool of candidates to keep the useful information and eliminate irrelevant information. This reduces the computational load and increases the robustness of the classification system. Both feature extraction and dimensionality reduction are important steps in classifying EEG signals. Note that some researchers use the term *feature extraction* to mean dimensionality reduction via linear or nonlinear projections. In our terminology, feature extraction is the process of determining candidate features from raw measurements (in this particular case, the act of calculating energies in five frequency bands from the PSD estimates of all EEG electrodes).

The PSD features of EEG signals constitute a high-dimensional vector (5 frequency bands for 32 EEG channels yield 160 features) that contains information pertinent to the classification of cognitive states, as well as irrelevant components and noise. Direct classification using these raw input features yields poor generalization performance. We therefore propose a mutual information based technique to preserve channels and feature subspaces with maximal generalizable. We, therefore, propose a mutual information based learning technique for finite size training sets to preserve channels and feature subspaces that maximize the generalization of discriminative power. Dimensionality reduction can be achieved by feature transformations. The transformation generates either a new feature space, which is called feature projection; or generates a subset of the original feature space, which is called feature selection. Feature selection is a special case of linear projections where the projection matrix is sparse with only one unit per row. Linear transformations are widely used due to their simplicity and robustness. Therefore, they are often preferred to computationally complex and more fragile nonlinear counterparts, especially with small training sets.

Optimal feature selection coupled with a specific classifier topology, namely the *wrapper* approach, is computationally very complex (combinatorial complexity—overall $2^n - 1$ feature subsets to evaluate in selection for n candidate features); thus, is in feasible for large number of features. In contrast, a filter-based approach, which selects features by optimizing a given criterion, is independent of the classifier and is more flexible, but might not yield classifier-tuned optimal results. Since we use a committee of classifiers, the filter approach is found more suitable.

Principal component analysis (PCA) is a widely used dimensionality reduction technique [30, 31]; however, the projections it finds are not necessarily related to the class labels, hence are not particularly useful in pattern recognition. Linear discriminant analysis (LDA) attempts to eliminate this shortcoming of PCA by finding linear projections that maximize class separability as measured by Fisher's criterion that is based on a unimodal class conditional distribution (e.g., Gaussian) assumption [32]. The LDA projections are optimized based on the means and the covariance matrices of classes, which are not descriptive of an arbitrary multimodal probability density function (pdf). Independent component

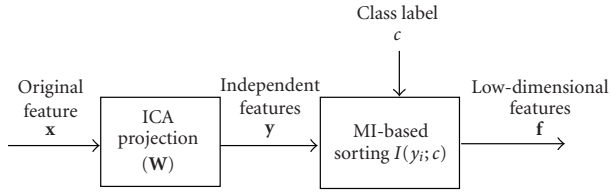

Figure 2: Feature projections using ICA preprocessing and mutual information sorting.

analysis (ICA) has also been used as a tool to find linear transformations that maximize the statistical independence of random variables [33, 34]. However, like PCA, the projection that ICA finds has no necessary relationship with class labels in itself, hence, are not able to enhance class separability [35].

In the filter approach, it is important to optimize a criterion that is relevant to Bayes risk, which is typically measured by the probability of error (for equal class-error risks). Therefore, a suitable criterion for assessing the *quality* of a low-dimensional feature vector $\mathbf{f}$ (either in selection or projection) is the mutual information (MI) between $\mathbf{f}$ and the class label c as defined by

$$I_S(\mathbf{f}; c) = H_S(\mathbf{f}) - \sum_c p_c H_S(\mathbf{f} \mid c), \tag{1}$$

where p_c is the class prior, H_S and I_S denote Shannon's definitions of entropy and mutual information [36]. The justification for (1) is intuitively found in argument that $\mathbf{f}$ should exhibit maximal class label (i.e., cognitive load) relevant information. More formally, lower and upper bounds in information theory that relate mutual information to the Bayes probability of error p_e [37, 38], such as $p_e(\mathbf{f}) \leq (H_S(c) - I_S(\mathbf{f}; c))/2$ [38], as well as Fano's bound, motivate the use of MI in discriminative dimensionality reduction. Several MI-based methods have been proposed for feature selection [39–43]. However, since features are typically not independent, these approaches cannot guarantee optimal feature selection that would maximize mutual information, and joint information among multiple features (redundancy) is usually ignored or approximated with pairwise mutual information estimates. In this paper, we propose a greedy framework for feature selection and dimensionality reduction based on maximal mutual information as (1) suggests (Figure 2).

3.1. Estimating mutual information

A computationally efficient sample estimator for MI that exploits fast linear ICA algorithms to separate mixed features into approximately independent features is proposed. The estimator then employs a one-dimension entropy estimator. In a square invertible ICA transformation $\mathbf{y} = \mathbf{W}^T\mathbf{f}$, the relationship between the entropy of the low-dimensional features $\mathbf{f} \in \Re^d$ and the entropy of the transformed features $\mathbf{y}$ satisfies [36]

$$\begin{aligned} H_S(\mathbf{f}) &= H_S(\mathbf{y}) - \log|\mathbf{W}|, \\ H_S(\mathbf{f} \mid c) &= H_S(\mathbf{y} \mid c) - \log|\mathbf{W}^c|, \end{aligned} \tag{2}$$

where $\mathbf{W}$ is the ICA separation matrix for all data, and $\mathbf{W}^c$ is the ICA separation matrix for the data from class c (in case classes are oriented differently).[2] If the components of the random vector $\mathbf{y}$ in (2) are approximately independent, the joint entropy becomes the sum of marginal entropies. Similarly, if $\mathbf{y}$ conditioned on c has approximately independent components, the conditional joint entropy becomes the sum of marginal-conditional entropies:

$$\begin{aligned} H_S(\mathbf{f}) &= \sum_{l=1}^{d} H_S(y_l) - \log|\mathbf{W}| - I_S(\mathbf{y}), \\ H_S(\mathbf{f} \mid c) &= \sum_{l=1}^{d} H_S(y_l) - \log|\mathbf{W}^c| - I_S(\mathbf{y} \mid c). \end{aligned} \tag{3}$$

Above, $I_S(\mathbf{y})$ and $I_S(\mathbf{y} \mid c)$ denote any residual mutual information after the linear ICA procedure. Overall, assuming that these residual dependencies are negligible, we have

$$\begin{aligned} I_S(\mathbf{f}; c) &= H_S(\mathbf{f}) - \sum_c p_c H_S(\mathbf{f} \mid c) \\ &\approx \sum_{l=1}^{d} \left(H_S(y_l) - \sum_c p_c H_S(y_l \mid c) \right) \\ &\quad - \left(\log|\mathbf{W}| - \sum_c p_c \log|\mathbf{W}^c| \right). \end{aligned} \tag{4}$$

For simplicity, in the following, we further assume that the linear transformations satisfy $\mathbf{W} = \mathbf{W}^c$ for all c. Thus,

$$I_S(\mathbf{f}; c) = I_S(\mathbf{y}; c) \approx \sum_{l=1}^{d} I_S(y_l; c). \tag{5}$$

Consequently, the MI between the classes and d-dimensional feature vector can then be computed by evaluating d one-dimensional MI estimates as in (5).

Fast linear ICA solution

There are several efficient algorithms for solving the linear ICA problem based on a variety of assumptions including maximization of non-Gaussianity, minimization of mutual information, nonstationarity of the sources, and so forth [46–48]. The fourth-order statistical methods can be compactly formulated in the form of a generalized eigendecomposition problem that gives the ICA solution in an analytical form [49]. This formulation will be employed in this work for its simplicity. Under the assumption of iid samples, the separation matrix $\mathbf{W}$ is the solution to the following generalized eigendecomposition problem:

$$\mathbf{R}_\mathbf{f}\mathbf{W} = \mathbf{Q}_\mathbf{f}\mathbf{W}\Lambda, \tag{6}$$

[2] Given an arbitrary random vector $\mathbf{f}$, one can always find a nonlinear transformation $\mathbf{y} = \mathbf{g}(\mathbf{f})$ that is invertible and results in independent components $\mathbf{y} = \{y_1, \ldots, y_n\}$ [44]. However, in small datasets, finding a robust nonlinear ICA solution is difficult. An approximate linear ICA solution can be sufficient [45].

where $\mathbf{R_f}$ is the covariance matrix of $\mathbf{f}$ and $\mathbf{Q_f}$ is the cumulant matrix estimated using sample averages: $\mathbf{Q_f} = E[\mathbf{f}^T\mathbf{fff}^T]$, $\mathbf{R_f}\,\mathrm{tr}(\mathbf{R_f})$, $E[\mathbf{ff}^T]E[\mathbf{ff}^T]$, $\mathbf{R_f}\mathbf{R_f}$. Given these matrices, the ICA solution can be easily determined using efficient generalized eigendecomposition algorithms.[3]

Once the ICA transform is determined and employed to obtain $\mathbf{y}$ such that (5) holds (approximately), the marginal mutual information of each independent feature y_i with the class label c can be computed using (1) and a simple one-dimensional entropy estimator. One needs to estimate the overall feature entropy $H_S(y_i)$ using all samples regardless of class labels, and the conditional entropy of each class using only the samples from the corresponding class.

Marginal entropy estimator

There exist many entropy estimators in the literature for single-dimensional variables [50]. Here, we use sample-spacings estimator, which is based on order statistics. This estimator is selected because of its consistency, rapid asymptotic convergence, and its computational efficiency. Given a set of iid samples $\{y_1, \ldots, y_N\}$ of a random variable y, the estimator first sorts the samples in increasing order such that $y_{(1)} \leq \cdots \leq y_{(N)}$. The m-spacing entropy estimator is given in terms of the sorted samples by [46]:

$$\hat{H}(y) = \frac{1}{N-m}\sum_{i=1}^{N-m}\log\frac{(N+1)\left(y_{(i+m)} - y_{(i)}\right)}{m}, \tag{7}$$

where N is a sample number. This estimator is based on two assumptions: the true density $p(y)$ is approximated by a piecewise uniform density determined by m-neighbors and outside of the sample range; the contribution of the true density is negligible and/or does not change the expected entropy computed by (7). The selection of the parameter m is determined by a bias-variance tradeoff and typically $m = N^{1/2}$. In general, for asymptotic consistency, the sequence $m(N)$ should satisfy

$$\lim_{N\to\infty} m(N) = \infty \qquad \lim_{N\to\infty}\frac{m(N)}{N} = 0. \tag{8}$$

3.2. EEG channel selection using mutual information

In real-time brain interface applications such as the ambulatory cognitive load estimation problem considered in this work, the reduction in the number of input features is further motivated by the limited data acquisition and processing capabilities of the hardware. While collecting measurements from all EEG channels and then projecting their combined feature vector to a lower-dimensional linear or nonlinear manifold would be desirable, the hardware limitations and the prohibitive cost of collecting and processing each additional EEG channel signal beyond the capacity of the hardware imposes us to focus on identifying the salient EEG channels that contain the most useful information for accurate estimation of the cognitive state in the design phase. Each channel yields several (five in our case) features and our goal is to find a quasi-optimal subset of EEG channels such that the MI between features obtained from the selected channels and class labels is maximized for the given number of channels (our hardware can handle up to 7 channels):

$$\max_{\{i_1,\ldots,i_m\}} I_S(\mathbf{f}^{i_1},\ldots,\mathbf{f}^{i_m};c), \tag{9}$$

where $\mathbf{f}^i$ is the feature vector that contains all features from channel i, c is the class label, and m is the number of EEG channels being considered in $\mathbf{f}^T = [\mathbf{f}^{i_1 T},\ldots,\mathbf{f}^{i_m T}]$. $I_S(\mathbf{f};c)$ can be estimated using the method described in Section 3.1.

In order to determine an effective subset of the available features or channels (which encompass multiple features), we rank the channels using a forward incremental strategy. We first select the channel whose features have maximum mutual information with class labels and assign it rank 1. Rank 2 is assigned to the channel that has maximum MI when used in conjunction with the previously selected rank-1 channel. The procedure then ranks iteratively all features or channels taking into account the joint mutual information with previously ranked channels.[4] Algorithm 1 summarizes the proposed method.

The procedure results in an ordering of EEG channels such that the rank-d channel is the optimum choice given the previous d-1 channels. While the top d channels do not necessarily have to be the best d-subset, determining the latter requires a combinatorial search, and is infeasible for very

Initialize *ChannelSet* to include all channel indices and *RankedChannelSet* to empty set. Iterate the following until *ChannelSet* is left empty.

(A) Select channel i from *ChannelSet*. Let *CandidateChannelSet_i* be the union of *RankedChannelSet* and $\{i\}$. Estimate the joint MI between all features obtained from the channels in *CandidateChannelSet_i* and let this estimate be I_i. Evaluate I_i for all channels in *ChannelSet*.

(B) Include the channel index that has maximum I_i in step (A) in *RankedChannelSet* and remove it from *ChannelSet*.

Algorithm 1

[3] Note that fourth-order cumulant-based ICA algorithms typically require a much larger sample size than information theoretic methods such as Infomax [49] and Mermaid [50], thus has much larger estimation variance for a given sample size. Also, joint diagonalization of more than two higher-order cumulants is usually preferred.

[4] Note that when ranking channels, since all features associated with the signals of an EEG channel must be included or excluded simultaneously, the algorithm considers concatenating feature vectors of channels to form candidate feature subsets. In contrast, if all channels could be measured, one could also do feature subset selection using the same algorithm, this time concatenating features individually to form candidate subset feature vectors.

large dimensional situations (such as with 32 EEG channels or 160 features). Using the incremental ranking strategy, the computational complexity is $(n+1)n/2$ (n is the total number of EEG channels) instead of the $(2^n - 1)$ of exhaustive search. The search procedure could be modified easily to include a channel subtraction phase where a previously ranked channel is removed to the unranked set if it does not contribute to the joint information of the current ranked subset. Another advantage of this method is that, using MI for ranking results in classifier-independent EEG channel ranking, thus it is computationally efficient compared to wrapper techniques (it uses a simple MI estimator and does not require repeated classifier training).

3.3. Maximally informative linear feature projections

Even after channel selection, further dimensionality reduction might be desirable to improve classifier generalization performance. This can also be achieved using the maximum MI framework because an invertible transformation does not change the mutual information. In particular, the linear invertible ICA mapping guarantees that $I_S(\mathbf{f}; c) = I_S(\mathbf{y}; c)$ for $\mathbf{y} = \mathbf{W}^T\mathbf{f}$. Furthermore, since (5) holds for the independent features and since MI is a nonnegative quantity, the best d-dimensional linear projection consists of the d components of $\mathbf{y}$, that have maximum individual mutual information with c. After the ICA mapping, one needs to evaluate the mutual information $I_S(y_i; c)$ for $i = 1, \ldots, n$, n is the dimension of the transformed features $\mathbf{y}$. The projection matrix then consists of the d columns of the ICA matrix $\mathbf{W}$ that corresponds to the top d components of $\mathbf{y}$. This projection scheme is illustrated in Figure 2. Typically, the channel selection procedure described in Section 3.2 is employed for selecting the useful sensors motivated by physical constraints; and the feature projection procedure described here is employed to the selected channels to improve classifier robustness and generalization capability in the availability of only a relatively small training data set.

3.4. Bias analysis

The approximations in Section 2 introduce an estimation bias to each MI evaluation step. From the derivation, we can see that the bias, defined as the expected difference between the estimation and the true MI, is

$$E[\hat{I}_S(\mathbf{f}; c) - I_S(\mathbf{f}; c)] = \left(\log|\mathbf{W}| - \sum_c p_c \log|\mathbf{W}^c|\right) + \left(I_S(\mathbf{y}) - \sum_c p_c I_S(\mathbf{y} \mid c)\right), \tag{10}$$

where $\mathbf{y} = \mathbf{W}^T\mathbf{f}$ is the ICA transformation.

4. EXPERIMENTS AND RESULTS

In this section, we present analyses carried out on data collected from three subjects performing two tasks in multiple sessions (used for training and testing). Note that in many BCI experiments, reports are provided in terms of leave-one-out performance on the complete data set due to scarcity. However, in our experience, this overestimates actual generalization performance (due to nonstationarity being nulled by the leave-one-out procedure).

4.1. EEG channel selection

In this experiment, we demonstrate the performance of the channel selection procedure outlined to examine the effectiveness of the selection procedure outlined in Section 3.2. Based on hardware limitations for real-time processing of EEG, the goal of identifying up to 7 channels out of the 30 available ones (we omitted 2 extremely noisy channels in this dataset) is set. Three subjects S_1–S_3 executed two mental tasks called *Larson* and *n-back* [24, 51, 52]. In the Larson task, the subjects are required to maintain a mental count according to the presented configuration of images on the monitor. The combination of mental activities during this task includes *attention*, *encoding*, *rehearsal*, *retrieval*, and *match*. The complexity of this task was manipulated by varying the interstimulus interval (low and high). In the n-back task, subjects are required to match the letter in either spatial location or verbal identity in the previous trials. The easy task only requires comparing the current stimuli with the first one, involving the combination of mental activities include attention and match. The difficult task requires comparing the current stimuli with stimuli presented two trials previously, and involves a complex combination of mental activities that includes attention, encoding, rehearsal, retrieval, and match. All three subjects performed both tasks at the two designated difficulty levels. Each case consists of about 3000 data samples in a 150-dimensional feature space (30 EEG channels $\times$ 5 frequency bands) with two classes: low and high workloads. We applied the EEG channel-ranking algorithm to the data to study the subject and task dependency of the selected channels. Prior work suggested that the optimal EEG channels may vary for different mental tasks and different subjects.

We first applied the approach on individual subject-task combinations, and obtained specialized EEG channel rankings, designated as *Local n* (n is the number of the selected EEG channels). To examine the ability to select optimal channels for all tasks and all subjects, we also used data from all subjects and tasks to get another ranking called *Global n*. An instance of Local 10 (optimal for subject-task pairs) and Global 10 (optimal across subject-task pairs) EEG channels are shown in Table 1. The 7 channels selected based on literature suggestions for these tasks (see Section 4.2) are also listed for reference as *Phy 7*. Note that the individual best channels vary for each subject and task combination as expected. Nevertheless, the global ranking strongly coincides with these individual rankings as observed from Table 1.

To validate the proposed method, we employed a committee of 3 classifiers: GMM, KNN, and Parzen, with majority vote and decision fusion on the selected EEG channels. For jackknife evaluation of performance, the data for each case is partitioned to five sets and each set is saved for testing using the other four for training. The confusion matrices

Table 1: Optimal EEG channels illustration. Phy 7: 7 EEG channels from physiological literature; Local 10: 10 best EEG channels evaluated from individual subject-task pair; Global 10: 10 best EEG channels evaluated from pairs (boldface highlighted).

Phy 7			Cz, P3, P4, Pz, **O2**, PO4, **F7**
Local 10	S_1	Larson	CP5, **Fp2**, **FC5**, Fp1, C4, P4, **F7**, **AF3**, P7, **FC6**
		n-back	**AF3**, **FC5**, Fp1, **Fp2**, **F8**, **F7**, **FC6**, **O1**, **CP6**, P4
	S_2	Larson	**Fp2**, **O1**, AF4, **F7**, C3, PO3, **FC6**, CP2, C4, Pz
		n-back	C4, **O1**, **F8**, Fz, **F3**, **FC5**, FC1, C3, Cz, CP1
	S_3	Larson	**Fp2**, **F8**, **F7**, **FC5**, **FC6**, **AF3**, C3, F4, P4, AF4
		n-back	CP5, **F8**, C4, **FC6**, **Fp2**, **FC5**, P3, AF4, C3, P7
Global 10			Fp2, FC5, O1, F3, FC6, F8, F7, AF3, O2, CP6

Table 2: Correct classification rate for three subjects: S_1, S_2, and S_3, in two mental tasks: Larson and *n*-back, for different subsets of EEG channels. Average is arithmetic average of the 6 correct classification rates for a particular EEG channel subset.

		Phy 7	7 Local	10 Local	7 Global	10 Global
S_1	Larson	0.78	0.92	0.90	0.92	0.85
	n-back	0.86	0.92	0.94	0.93	0.92
S_2	Larson	0.76	0.83	0.88	0.83	0.87
	n-back	0.56	0.75	0.74	0.79	0.73
S_3	Larson	0.53	0.67	0.65	0.59	0.65
	n-back	0.54	0.64	0.68	0.74	0.72
Average		0.67	0.79	0.80	0.80	0.79

are estimated and the correct classification rates are calculated. The classification accuracies averaged over the five test sets are shown in Table 2. Note that the MI-selected channels significantly outperform the literature-motivated channels. On average, keeping 7 or 10 channels does not make significant difference in accuracy. The MI-selected features perform around 80% accuracy on average for all subjects; the specific subject-task optimal selections (local) are observed to be similar to the global selections. This indicates that the proposed channel selection method can partly solve the subject-to-subject transfer and the session-to-session transfer problems.

To provide a wrapper-benchmark for the proposed ICA-MI channel selection method, we also apply error-based ranking to the ICA projections on the same EEG datasets. The error based ranking method uses the same forward search strategy described in the algorithm of Section 3.2. The difference is, this method uses the classification error of the committee-classifier as its ranking criterion instead of mutual information. The classification results using different channel ranking methods for different subjects and mental tasks are shown in Figure 3 (we only show the classification results for top 10 EEG channels). Horizontal axis denotes the number of selected features used for classification; vertical axis denotes the classification accuracy in percentage. The error based ranking yields more accurate ranking than ICA-MI method. However, it is not practical because it is very slow and inflexible (classifier specific).

4.2. Feature projections

In this section, we demonstrate how an optimal ICA-feature subspace selected according to the mutual information criterion performs in reducing feature dimensionality without adversely affecting classification performance. Data was collected from one subject as four predetermined ambulatory tasks were executed: *slow walking*, *navigating and counting*, *communicating with radio*, and *studying written information while standing*. Tasks are assigned class labels from 1 to 4, corresponding to the assigned task. After preprocessing and feature extraction, approximately 6000 data samples were obtained, each with 35-dimensional feature vectors (7 EEG channels with 5 frequency bands each) and a desired class label. In this experiment, the channels corresponded to sites CZ, P3, P4, PZ, O2, P04, F7. These were selected based on a saliency analysis of EEG collected from various subjects performing cognitive test battery tasks [53]. A randomly selected one third of these samples were used as the training set for feature projection and classification, and the remaining two-thirds were used as the test set. The feature projections were obtained as described in Section 3.3. Correct classification rates for different dimensionality of optimally selected features were evaluated using the classifier committee over 50 Monte Carlo runs (random partitions of training and testing data). To provide benchmarks for the proposed ICA-MI linear projections, we also present results using other linear feature projection methods. These are ICA transformation followed by classification error based selection (instead of MI), as a wrapper benchmark, and LDA (major generalized eigenvectors of between and within class scatter matrices), as a filter-type common contender. To compare these methods fairly, we normalize the data before we apply the KNN classifier to the projected features (see Appendix B).

The classification results for different feature ranking methods are shown in Figure 4. The horizontal axis denotes the number of selected features used for classification;

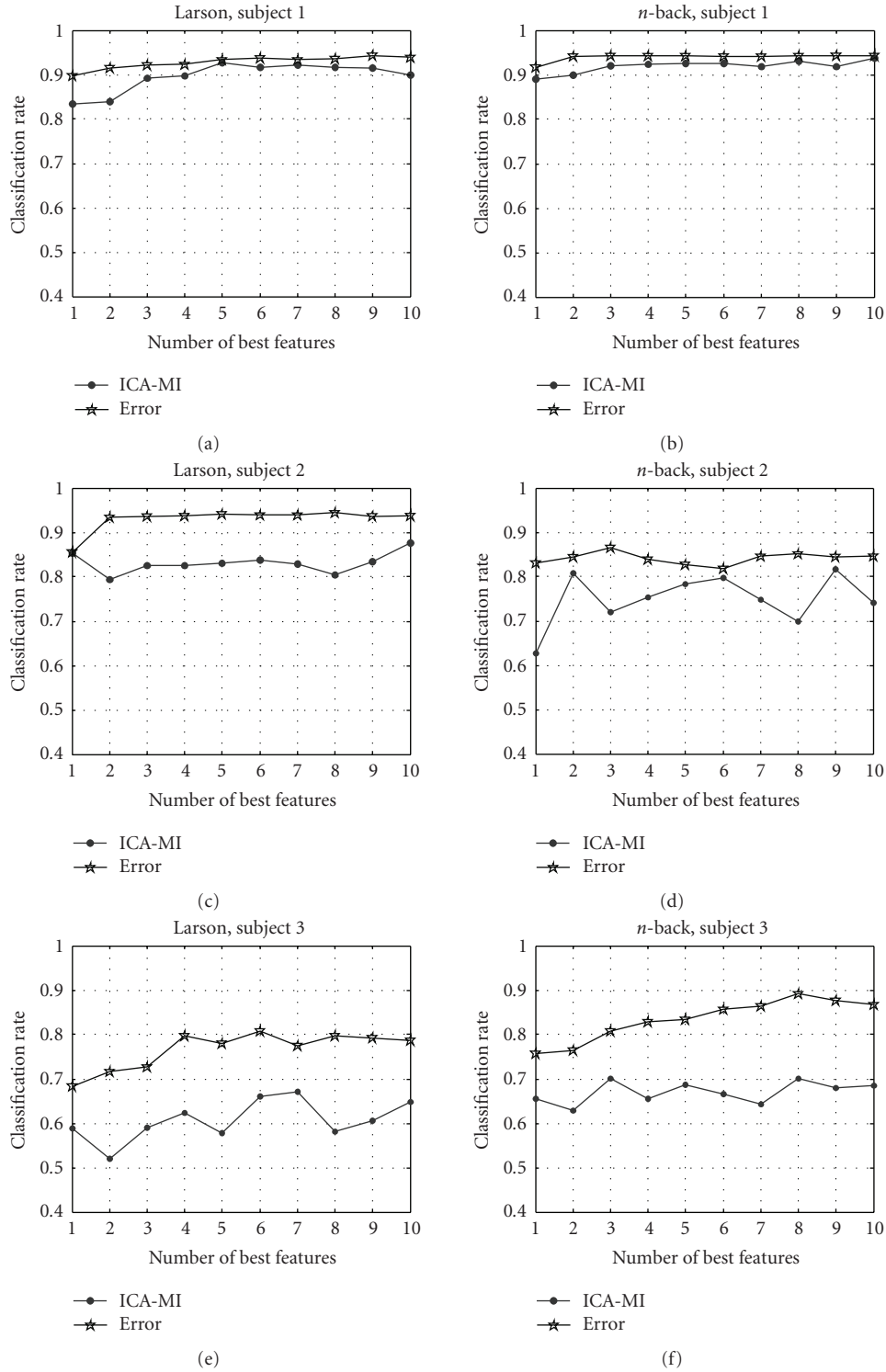

Figure 3: Correct classification rate versus number of optimally selected channels (up to 10, using ICA-MI and error based methods) for three subjects performing two mental tasks.

the vertical axis denotes the classification accuracy. From Figure 4 we see that ICA-MI can yield an accuracy of 80% with 14-dimensional projections, while the remaining 21 dimensions do not significantly contribute to the classification accuracy. The classification results based on 10, 14, and 35-dimensional optimally selected features using ICA-MI algorithm are compared in Table 3 via the confusion matrix of the classification results (The ijth entry of confusion matrix $\mathbf{P}$ shows P (decide class i | true class is j)). Although in this particular experiment keeping all 35 features yielded the

Table 3: Confusion matrix for classifiers on 4 cognitive states using 10, 14, and 35-dimensional input feature vectors.

Dimensions	10-dimensional input	14-dimensional input	35-dimensional input
Confusion matrix	$\begin{bmatrix} 0.38 & 0.33 & 0.25 & 0.04 \\ 0.03 & 0.82 & 0.15 & 0 \\ 0 & 0 & 1 & 0 \\ 0 & 0.01 & 0.24 & 0.75 \end{bmatrix}$	$\begin{bmatrix} 0.6 & 0.22 & 0.17 & 0.01 \\ 0.01 & 0.91 & 0.08 & 0 \\ 0 & 0 & 1 & 0 \\ 0 & 0 & 0.18 & 0.82 \end{bmatrix}$	$\begin{bmatrix} 0.6 & 0.29 & 0.1 & 0.01 \\ 0.02 & 0.83 & 0.15 & 0 \\ 0 & 0 & 1 & 0 \\ 0 & 0 & 0.02 & 0.98 \end{bmatrix}$

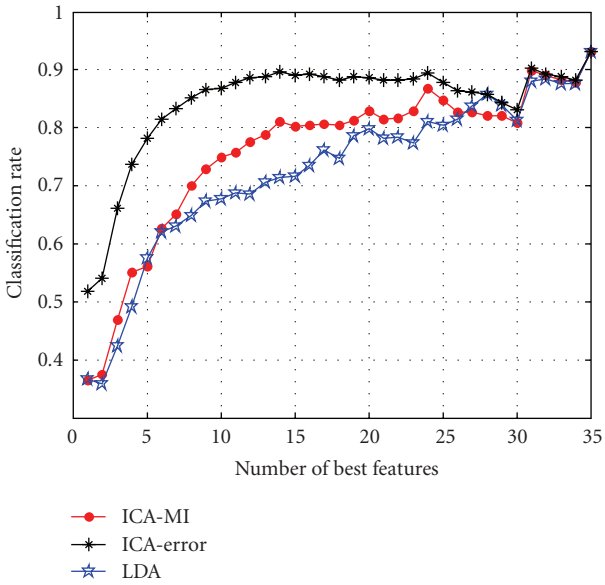

Figure 4: Correct classification rate versus dimensionality of optimally selected features for different methods.

best performance, the classification results illustrated here shows that this feature selection method is able to capture the low-dimensional relevant components in the original feature space. This suggests that the additional features may introduce irrelevant and confusing information that might impair the classification accuracy. In conclusion, mutual information based feature projections are expected to eliminate unnecessary dimensions from the feature vector if not improve performance.

The classification result for ICA-error ranking expectedly exhibits better performance than that of ICA-MI, however, it takes much longer time.[5] The result of LDA ranking is similar to that of ICA-MI for the first 5 features, but the classification performance decreases dramatically when the number of features increases due to the unimodality assumption. In experiments not shown here, we also compare the proposed feature projection method to the Mermaid-SIG algorithm [54]. The results show that the classification performances are similar. However, the ICA transformation followed by MI sorting algorithm is much faster.

5. DISCUSSION

We described a framework based on mutual information maximization to solve the EEG feature/channel selection and dimensionality reduction problems in order to perform cognitive state classification. The initial real-time and offline experiments suggest that the developed practical and fast algorithm that combines ICA transformations and sample-spacing entropy estimators can classify a small set of discrete cognitive states with a reasonable accuracy when combined with 3 parametric and nonparametric classifiers

The experiments demonstrated that the important EEG sites are consistent with prior physiological knowledge—frontal sites associated with working memory tasks are rated high [24]. Some classification performance when using the EEG channels, which were selected from ICA-MI method are even better than the performance of using pre-defined EEG channels. The actual ranking of the most salient sites are highly dependent on subjects and particular tasks they are performing. Nevertheless, a global ranking of EEG sites using the MI principle resulted in virtually no performance loss in classification accuracy on average (across subjects and tasks). This is an important observation that needs to be validated by other BCI researchers, since it indicates that subject-to-subject and task-to-task transfer might indeed be possible, thus making predesigned BCI systems practical.

As a comparison, we also implemented the wrapper approach for feature/channel selection: use classification error as the criterion. As expected, the wrapper approach exhibited better performance than filter approach because it is optimal to specific classifiers; however, it is much more slower, which makes it infeasible in practice with dense array EEG systems that are becoming increasingly popular in BCI research.[6] The proposed system is feasible; however, the nonstationarity of the EEG data still poses a great challenge making session-to-session transfer a difficult problem to solve. This means we have to retrain the system for different subjects and different

[5] As an indication of the order-of-magnitudes of difference in speed, in this experiment, it takes a few seconds for the ICA-MI projection, but it takes tens of hours for ICA-error ranking.

[6] We applied both classification error-based wrapper approach and our MI-based filter approach on the same data set with the same computer platform. The wrapper approach used more than one day. In contrast, the proposed filter approach used only 20 minutes on the same computer using Matlab.

sessions, unless a very large training set encompassing a variety of operating conditions, numerous subjects, and tasks is available. We have utilized PSD-based features, and perhaps higher-order statistics or wavelet-based time-frequency features are more stationary and could lead to more robust designs. Future work will focus on determining *better* features.

APPENDICES

A. CLASSIFIERS

Gaussian mixture model (GMM) classifier

Gaussian mixture models are widely used to model the probability density functions. In this paper, they are employed to approximate class-conditional distributions. It is assumed that each class distribution consists of four Gaussian models and the parameters of the mixture is optimized using the expectation-maximization (EM) algorithm [55]. The estimated distributions are then utilized to form an approximate Bayes classifier.

K nearest neighbor (KNN) classifier

The KNN classification approach is a nonparametric technique that makes no assumptions about the form of the probability densities underlying a particular set of data. Given a particular test sample, the K nearest training samples (usually in an Euclidean sense) are determined and the test sample is assigned to the class which lends the most neighbors to this set. It can be shown that if K is large, this classifier will approach the best possible classification performance given by the true Bayes classifier [56].

Parzen window classifier

Parzen windowing [57] is a nonparametric density estimation technique. It is employed to estimate the class distributions and to form a nonparametric approximation to the Bayes classifier. In this context, it serves as a bridge between the KNN where each sample contributes discretely to the decision (depending on whether they are in the neighborhood or not) and the GMM classifier where each sample indirectly contributes to the Gaussian models. In our implementation, we used Gaussian window functions, thus the Parzen classifiers is essentially a KNN classifier with decreasing influence by distance, and at the same time it is a GMM itself, where a Gaussian is placed on each sample.

Fusion

The classifiers output a decision at 10 Hz and the majority vote determines the final cognitive state estimate. The Parzen classifier decision was accepted when there was no agreement. It is also assumed that this state will not change over a period of 2 seconds, thus a median filter applied to the most recent 10 decisions is utilized to smoothen the classification output. This postprocessing step significantly improves performance and reduces flickering.

B. SCALE NORMALIZATION ACROSS LINEAR PROJECTIONS

When comparing different linear projection propositions using a classifier whose training and performance depends on Euclidean sample distances and angles for the purpose of having a controlled environment, it is important to guarantee that the classifier performances are not affected by Euclidean transformations of data across projection methodologies. Data normalization to satisfy this desirable property is essential to conclude with certainty that differences in performances of classifiers due to various linear projections are invariant to affine transformations.

Suppose that a linear projection matrix $\mathbf{W} \in \Re^{m\times n}$, where $m < n$, is proposed as the *optimal projection* according to the criterion of that particular technique (e.g., PCA, LDA, ICA, MI would yield different propositions). Let $\mathbf{W} = \mathbf{UDV}^T$ be the singular value decomposition of this matrix, where $\mathbf{D}$ is the diagonal matrix of eigenvalues, and $\mathbf{U}$ and $\mathbf{V}$ are orthonormal left and right eigenvector matrices. Define the multiplicative group inverse $\mathbf{W}^+ = \mathbf{VD}^+\mathbf{U}^T$, where $\mathbf{D}^+_{ii} = \mathbf{D}^{-1}_{ii}$ if $\mathbf{D}_{ii} \neq 0$ and $\mathbf{D}^+_{ii} = 0$ if $\mathbf{D}_{ii} = 0$ (i.e., $\mathbf{D}^+$ is the group inverse for diagonal matrices under multiplication).

In the comparison of linear projections using a particular classifier (e.g., KNN, SVM, etc.), instead of utilizing the samples obtained by $\mathbf{y} = \mathbf{Wx}$, where $\mathbf{y} \in \Re^m$, utilize the samples generated with $\mathbf{z} = \mathbf{W}^+\mathbf{Wx}$. Note that, although $\mathbf{z} \in \Re^n$, since $\text{rank}(\mathbf{W}^+\mathbf{W}) = \text{rank}(\mathbf{VI}_m\mathbf{V}^T) = m$—where $\mathbf{I}_m = \text{diag}(1,\ldots,1,0,\ldots,0)$ is $n \times n$ diagonal with m ones on its diagonal—the samples of the random vector $\mathbf{z}$ lie on an m-dimensional hyperplane determined by the rows of $\mathbf{W}$. The variable $\mathbf{z}$ is a scale-normalized version of the desired projection $\mathbf{y}$, and its use eliminates the problems that might arise from the scale dependency of particular classifier topologies and improper training procedures that might not take these into account.

ACKNOWLEDGMENTS

This research was supported by DARPA under Contract DAAD-16-03-C-0054 and NSF under Grants ECS-0524835 and ECS-0622239.

REFERENCES

[1] L. A. Farwell and E. Donchin, "Talking off the top of your head: toward a mental prosthesis utilizing event-related brain potentials," *Electroencephalography and Clinical Neurophysiology*, vol. 70, no. 6, pp. 510–523, 1988.

[2] S. G. Mason and G. E. Birch, "A general framework for brain-computer interface design," *IEEE Transactions on Neural Systems and Rehabilitation Engineering*, vol. 11, no. 1, pp. 70–85, 2003.

[3] P. He, M. Kahle, G. Wilson, and C. Russell, "Removal of ocular artifacts from EEG: a comparison of adaptive filtering method and regression method using simulated data," in *Proceedings of the 27th IEEE Annual International Conference of the Engineering in Medicine and Biology (EMBS '05)*, vol. 7, pp. 1110–1113, Shanghai, China, September 2005.

[4] Y. Li, Z. Ma, W. Lu, and Y. Li, "Automatic removal of the eye blink artifact from EEG using an ICA-based template matching approach," *Physiological Measurement*, vol. 27, no. 4, pp. 425–436, 2006.

[5] R. Fazel-Rezai and J. F. Peters, "P300 wave feature extraction: preliminary results," in *Proceedings of the 18th Annual Canadian Conference on Electrical and Computer Engineering (CCECE '05)*, pp. 390–393, Saskatoon, Saskatchewan, Canada, May 2005.

[6] A. Subasi, "Application of classical and model-based spectral methods to describe the state of alertness in EEG," *Journal of Medical Systems*, vol. 29, no. 5, pp. 473–486, 2005.

[7] D. J. McFarland, L. A. Miner, T. M. Vaughan, and J. R. Wolpaw, "Mu and beta rhythm topographies during motor imagery and actual movements," *Brain Topography*, vol. 12, no. 3, pp. 177–186, 2000.

[8] T. Wang, J. Deng, and B. He, "Classifying EEG-based motor imagery tasks by means of time-frequency synthesized spatial patterns," *Clinical Neurophysiology*, vol. 115, no. 12, pp. 2744–2753, 2004.

[9] G. Perea, S. Màrquez-Gamiño, S. Rodríguez, and G. Moreno, "EEG-like signals generated by a simple chaotic model based on the logistic equation," *Journal of Neural Engineering*, vol. 3, no. 3, pp. 245–249, 2006.

[10] X. Li, J. Polygiannakis, P. Kapiris, A. Peratzakis, K. Eftaxias, and X. Yao, "Fractal spectral analysis of pre-epileptic seizures in the terms of criticality," *Journal of Neural Engineering*, vol. 2, no. 2, pp. 11–16, 2005.

[11] V. Bostanov, "BCI competition 2003-data sets Ib and IIb: feature extraction from event-related brain potentials with the continuous wavelet transform and the t-value scalogram," *IEEE Transactions on Biomedical Engineering*, vol. 51, no. 6, pp. 1057–1061, 2004.

[12] D. Garrett, D. A. Peterson, C. W. Anderson, and M. H. Thaut, "Comparison of linear, nonlinear, and feature selection methods for EEG signal classification," *IEEE Transactions on Neural Systems and Rehabilitation Engineering*, vol. 11, no. 2, pp. 141–144, 2003.

[13] R. Scherer, G. R. Müller, C. Neuper, B. Graimann, and G. Pfurtscheller, "An asynchronously controlled EEG-based virtual keyboard: improvement of the spelling rate," *IEEE Transactions on Biomedical Engineering*, vol. 51, no. 6, pp. 979–984, 2004.

[14] A. Rakotomamonjy, V. Guigue, G. Mallet, and V. Alvarado, "Ensemble of SVMs for improving brain computer interface P300 speller performances," in *Proceedings of the 15th International Conference on Artificial Neural Networks (ICANN '05)*, vol. 3696, pp. 45–50, Warsaw, Poland, September 2005.

[15] C. W. Anderson and Z. Sijercic, "Classification of EEG signals from four subjects during five mental tasks," in *International Conference on Engineering Applications of Neural Networks (EANN '96)*, pp. 407–414, London, UK, June 1996.

[16] R. Palaniappan, "Brain computer interface design using band powers extracted during mental tasks," in *Proceedings of the 2nd International IEEE EMBS Conference on Neural Engineering*, pp. 321–324, Arlington, Va, USA, March 2005.

[17] X. Zhu, J. Wu, Y. Cheng, and Y. Wang, "GMM-based classification method for continuous prediction in brain-computer interface," in *Proceedings of the 18th International Conference on Pattern Recognition (ICPR '06)*, vol. 1, pp. 1171–1174, Hong Kong, August 2006.

[18] B. Widrow and M. Hoff, "Adaptive switching circuits," in *IRE Western Electronic Show and Convention (WESCON '60)*, vol. 4, pp. 96–104, Los Angeles, Calif, USA, August 1960.

[19] J. F. Borisoff, S. G. Mason, A. Bashashati, and G. E. Birch, "Brain-computer interface design for asynchronous control applications: improvements to the LF-ASD asynchronous brain switch," *IEEE Transactions on Biomedical Engineering*, vol. 51, no. 6, pp. 985–992, 2004.

[20] R. Boostani and M. H. Moradi, "A new approach in the BCI research based on fractal dimension as feature and Adaboost as classifier," *Journal of Neural Engineering*, vol. 1, no. 4, pp. 212–217, 2004.

[21] U. Hoffmann, G. Garcia, J.-M. Vesin, K. Diserenst, and T. Ebrahimi, "A boosting approach to P300 detection with application to brain-computer interfaces," in *Proceedings of the 2nd International IEEE EMBS Conference on Neural Engineering*, pp. 97–100, Arlington, Va, USA, March 2005.

[22] J. Qin, Y. Li, and A. Cichocki, "ICA and committee machine-based algorithm for cursor control in a BCI system," in *Proceedings of the 2nd International Symposium on Neural Networks (ISNN '05)*, vol. 3496, pp. 973–978, Chongqing, China, May 2005.

[23] M. M. Jackson, S. G. Mason, and G. E. Birch, "Analyzing trends in brain interface technology: a method to compare studies," *Annals of Biomedical Engineering*, vol. 34, no. 5, pp. 859–878, 2006.

[24] A. Gevins, M. E. Smith, L. McEvoy, and D. Yu, "High-resolution EEG mapping of cortical activation related to working memory: effects of task difficulty, type of processing, and practice," *Cerebral Cortex*, vol. 7, no. 4, pp. 374–385, 1997.

[25] A. Kruse and D. Schmorrow, "Foundations of augmented cognition," in *Proceedings of the 1st International Conference on Human-Computer Interaction (HCI '05)*, Las Vegas, Nev, USA, July 2005.

[26] M. Pavel, G. Wang, and K. Li, "Augmented cognition: allocation of attention," in *Proceedings of the 36th Annual Hawaii International Conference on System Sciences (HICSS '03)*, p. 6, Big Island, Hawaii, USA, January 2003.

[27] J. R. Wolpaw, N. Birbaumer, D. J. McFarland, G. Pfurtscheller, and T. M. Vaughan, "Brain-computer interfaces for communication and control," *Clinical Neurophysiology*, vol. 113, no. 6, pp. 767–791, 2002.

[28] http://www.biosemi.com/.

[29] P. Welch, "The use of fast Fourier transform for the estimation of power spectra: a method based on time averaging over short, modified periodograms," *IEEE Transactions on Audio and Electroacoustics*, vol. 15, no. 2, pp. 70–73, 1967.

[30] E Oja, *Subspace Methods of Pattern Recognition*, Wiley, New York, NY, USA, 1983.

[31] P. A. Devijver and J. Kittler, *Pattern Recognition: A Satistical Approach*, Prentice Hall, London, UK, 1982.

[32] K. Fukunaga, *Introduction to Statistical Pattern Recognition*, Academic Press, New York, NY, USA, 2nd edition, 1990.

[33] R. Everson and S. Roberts, "Independent component analysis: a flexible nonlinearity and decorrelating manifold approach," *Neural Computation*, vol. 11, no. 8, pp. 1957–1983, 1999.

[34] A. Hyvärinen, E. Oja, P. Hoyer, and J. Hurri, "Image feature extraction by sparse coding and independent component analysis," in *Proceedings of the 14th International Conference on Pattern Recognition (ICPR '98)*, vol. 2, pp. 1268–1273, Brisbane, Australia, August 1998.

[35] K. Torkkola, "Feature extraction by non parametric mutual information maximization," *Journal of Machine Learning Research*, vol. 3, pp. 1415–1438, 2003.

[36] T. M. Cover and J. A. Thomas, *Elements of Information Theory*, Wiley-Interscience, New York, NY, USA, 1991.

[37] R. M. Fano, *Transmission of Information: A Statistical Theory of Communications*, Wiley, New York, NY, USA, 1961.

[38] M. Hellman and J. Raviv, "Probability of error, equivocation, and the Chernoff bound," *IEEE Transactions on Information Theory*, vol. 16, no. 4, pp. 368–372, 1970.

[39] R. Battiti, "Using mutual information for selecting features in supervised neural net learning," *IEEE Transactions on Neural Networks*, vol. 5, no. 4, pp. 537–550, 1994.

[40] A. Ai-Ani and M. Deriche, "An optimal feature selection technique using the concept of mutual information," in *Proceedings of the 6th International Symposium on Signal Processing and Its Applications (ISSPA '01)*, vol. 2, pp. 477–480, Kuala Lumpur, Malaysia, August 2001.

[41] N. Kwak and C.-H. Choi, "Input feature selection for classification problems," *IEEE Transactions on Neural Networks*, vol. 13, no. 1, pp. 143–159, 2002.

[42] H. H. Yang and J. E. Moody, "Feature selection based on joint mutual information," in *Advances in Intelligent Data Analysis (AIDA), Computational Intelligence Methods and Applications (CIMA)*, International Computer Science Conventions, Rochester, NY, USA, June 1999.

[43] H. H. Yang and J. E. Moody, "Data visualization and feature selection: new algorithms for nongaussian data," in *Advances in Neural Information Processing Systems 12 (NIPS '99)*, pp. 687–702, Denver, Colo, USA, November-December 2000.

[44] A. Hyvärinen and P. Pajunen, "Nonlinear independent component analysis: existence and uniqueness results," *Neural Networks*, vol. 12, no. 3, pp. 429–439, 1999.

[45] T. Lan and D. Erdogmus, "Maximally informative feature and sensor selection in pattern recognition using local and global independent component analysis," *Journal of VLSI Signal Processing Systems*, vol. 48, no. 1-2, pp. 39–52, 2007.

[46] E. G. Learned-Miller and J. W. Fisher III, "ICA using spacings estimates of entropy," *Journal of Machine Learning Research*, vol. 4, no. 7-8, pp. 1271–1295, 2004.

[47] K. E. Hild II, D. Erdogmus, and J. Príncipe, "Blind source separation using Renyi's mutual information," *IEEE Signal Processing Letters*, vol. 8, no. 6, pp. 174–176, 2001.

[48] A. Hyvärinen and E. Oja, "A fast fixed-point algorithm for independent component analysis," *Neural Computation*, vol. 9, no. 7, pp. 1483–1492, 1997.

[49] L. Parra and P. Sajda, "Blind source separation via generalized eigenvalue decomposition," *Journal of Machine Learning Research*, vol. 4, no. 7-8, pp. 1261–1269, 2004.

[50] J. Beirlant, E. J. Dudewicz, L. Györfi, and E. C. van der Meulen, "Nonparametric entropy estimation: an overview," *International Journal of Mathematical and Statistical Sciences*, vol. 6, no. 1, pp. 17–39, 1997.

[51] E. Halgren, C. Boujon, J. Clarke, C. Wang, and P. Chauvel, "Rapid distributed fronto-parieto-occipital processing stages during working memory in humans," *Cerebral Cortex*, vol. 12, no. 7, pp. 710–728, 2002.

[52] A. Gevins and M. E. Smith, "Neurophysiological measures of working memory and individual differences in cognitive ability and cognitive style," *Cerebral Cortex*, vol. 10, no. 9, pp. 829–839, 2000.

[53] C. A. Russell and S. G. Gustafson, "Selecting salient features of psychophysiological measures," Tech. Rep. AFRL-HE-WP-TR-2001-0136, Air Force Research Laboratory, Rome, NY, USA, 2001.

[54] K. E. Hild II, *Blind source separation of convolutive mixtures using Renyi's divergence*, Ph.D. thesis, University of Florida, Gainesville, Fla, USA, 2003.

[55] A. P. Dempster, N. M. Laird, and D. B. Rubin, "Maximum likelihood from incomplete data via the EM algorithm," *Journal of the Royal Statistical Society*, vol. 39, no. 1, pp. 1–38, 1977.

[56] R. O. Duda, P. E. Hart, and D. G. Stork, *Pattern Classification*, Wiley, New York, NY, USA, 2nd edition, 2000.

[57] E. Parzen, "On estimation of a probability density function and mode," in *Time Series Analysis Papers*, Holden-Day, San Diego, Calif, USA, 1967.

Hindawi Publishing Corporation
Computational Intelligence and Neuroscience
Volume 2007, Article ID 41468, 9 pages
doi:10.1155/2007/41468

Research Article

Extracting Rhythmic Brain Activity for Brain-Computer Interfacing through Constrained Independent Component Analysis

Suogang Wang and Christopher J. James

Signal Processing and Control Group, ISVR, University of Southampton, Southampton SO17 1BJ, UK

Correspondence should be addressed to Suogang Wang, sgw@soton.ac.uk

Received 31 December 2006; Accepted 18 June 2007

Recommended by Andrzej Cichocki

We propose a technique based on independent component analysis (ICA) with constraints, applied to the rhythmic electroencephalographic (EEG) data recorded from a brain-computer interfacing (BCI) system. ICA is a technique that can decompose the recorded EEG into its underlying independent components and in BCI involving motor imagery, the aim is to isolate rhythmic activity over the sensorimotor cortex. We demonstrate that, through the technique of spectrally constrained ICA, we can learn a spatial filter suited to each individual EEG recording. This can effectively extract discriminatory information from two types of single-trial EEG data. Through the use of the ICA algorithm, the classification accuracy is improved by about 25%, on average, compared to the performance on the unpreprocessed data. This implies that this ICA technique can be reliably used to identify and extract BCI-related rhythmic activity underlying the recordings where a particular filter is learned for each subject. The high classification rate and low computational cost make it a promising algorithm for application to an online BCI system.

1. INTRODUCTION

The electroencephalogram (EEG) is a recording of the brain's electrical activity and is one of the most important measurements used to evaluate neurological disorders in the clinic and to investigate brain function in the laboratory. The recording is obtained by placing electrodes on the scalp, generally according to the 10/20 electrode placement system [1].

A brain-computer interface (BCI) is a communication system in which messages or commands that an individual sends to the external world do not pass through the brain's normal output pathways of peripheral nerves and muscles [2]. In an EEG-based BCI, the messages are carried through EEG activity. The primary aim is to provide people with a new channel for communication with the outside environment. Many different disorders, such as amyotrophic lateral sclerosis (ALS), brainstem stroke, brain or spinal cord injury, and numerous other diseases can disrupt the neuromuscular channels through which the brain communicates with its environment and exerts control. These kinds of severe diseases may cause people to lose voluntary muscle control and to be unable to communicate in any way (this is known as being "locked in"). As current knowledge about these disorders is rather limited, there are no effective treatments which can provide a cure or even a significant recovery. In the absence of methods for repairing the damage caused by these diseases, a BCI system provides an option that conveys messages and commands to use some devices such as assistive applications and computers. This type of direct brain interface would increase an individual's independence and improve quality of life and also reduce the costs on society.

Historically, EEG activity is divided into four types of continuous rhythmic sinusoidal waves known as δ, θ, α, and β frequency bands. In this study, it is the function that allows users to control the amplitude of their μ (8–12 Hz) or β (18–22 Hz) brain rhythmic activity over the sensorimotor cortices caused by motor imagery (MI) [3, 4] (i.e., hand or foot movement imagination), that is of interest. For MI, the users are instructed to imagine a specific motor action without any related motor output. The imagination of the movement is accompanied by an effect known as event-related (desynchronization/synchronization) (ERD/ERS) [5]. When

ERD is present, it is relatively detectable and can be used as a feedback signal to control specially designed electrical devices, for instance, to control the movement of a cursor on a computer screen or to drive/steer a wheelchair. However, imagery is dependent on the individual's ability to generate a good ERD, and hence such a BCI will have variable performance. Moreover, artifacts (such as movement artifacts, eyeblinks, and electrical interference) where they appear change the raw EEG and render the recording virtually unusable.

Many signal processing techniques have been developed and used in BCI studies, such as autoregressive modelling [6], and common spatial patterns [7]. These methods tend to find a spatial filter to maximally improve the signal noise ratio (SNR). In order to reach an optimal performance, some additional processing methods are required as preprocessing steps before the application of, for example, bandpass filtering, common average reference, or manual artifact rejection. A combination of preprocessing methods could improve the performance, but also results in a less flexible and robust BCI system. Moreover, the application of more additional processing methods brings with it the problem of increased computation time.

Blind source separation (BSS) techniques such as Independent component analysis (ICA) have the ability to extract the relevant information buried within noisy signals and allow the separation of measured signals into their fundamental underlying independent components (ICs). Generally, the signal is assumed to be a linear mixture of statistically independent, possibly nonstationary sources which may be decomposed using either statistical and information theoretic signal properties (such as the popular method of fast ICA [8] and infomax ICA [9]), or signal time structure (time-structure-based ICA) [10]. ICA has already been quite broadly applied to the analysis of biomedical signals, such as analysis of EEG [11], ECG [12], MEG [13], and fMRI [14].

Recent studies have applied ICA in BCI applications [15–17]. The results indicate that ICA performed well in extracting *time-locked* features, such as event-related potentials (ERPs). However, since MI-based BCI does not use time-locked activity but rather relies on rhythmic activities as features, traditional applications of ICA are unable to track the changes in power spectra among the different sources. Using time-structure-based source decomposition methods, we can capture the sources with stationary waveforms and unique power spectra. Furthermore, when the power spectrum of the particular source activity is known, the spatial extent of the sources can be extracted by introducing *a priori* constraint(s) through constrained ICA (cICA). Our previous studies where we extracted rhythmic EEG signal components (such as epileptic seizures) have been shown in [18, 19].

In this work, we examine the use of existing cICA algorithms that we have previously developed to extract reliable spectral features in the BCI paradigm of MI. The ultimate aim of applying cICA is to extract rhythmic scalp EEG activity automatically and repeatedly from the recorded signals, so that the MI-based BCI system is more reliable and robust—especially for use outside of the clinical laboratory (i.e., in the presence of artifacts and across different subjects). In the following sections, we describe the cICA algorithm, the selection of power features from the datasets, and the overall classification system used. We then present the results obtained and discuss the performance enhancements to be achieved from the use of this algorithm.

2. METHODS

2.1. Independent component analysis

In the standard, noise-free formulation of the ICA problem, the observed signals $\mathbf{x}(t)$ are assumed to be a linear mixture of an equal number of unknown but statistically independent source signals $\mathbf{s}(t)$:

$$\mathbf{x}(t) = \mathbf{A}\mathbf{s}(t), \tag{1}$$

where the square mixing matrix $\mathbf{A}$ is also unknown but invertible. The columns of $\mathbf{A}$ each depicts a spatial topography for each of the ICs in $\mathbf{s}(t)$. The problem is solvable up to a permutation, and sign and power indeterminacy of the sources, by finding an appropriate de-mixing matrix $\mathbf{W} = \mathbf{A}^{-1}$ which allows estimation of the source waveforms by

$$\mathbf{s}(t) = \mathbf{W}\mathbf{x}(t). \tag{2}$$

Source decomposition on the basis of signal time structure may be achieved through temporal decorrelation (TD). For sources with stationary waveforms and unique power spectra, the time structure is adequately captured by temporal cross-covariances [20, 21]. The decorrelation operation in time structure ICA methods involves the joint diagonalization of a set of symmetric matrices which reflect the spatio-temporal covariance structure of the source mixture. Furthermore, algorithms have recently been developed for nonorthogonal joint diagonalization that processes signal covariances directly with no need for prewhitening, one such algorithm is used here and is called $\text{LSDIAG}_{\text{TD}}$ [22].

Assume that there is a set $\{\mathbf{C}_1, \ldots, \mathbf{C}_k\}$ of real-valued symmetric matrices, the TD approaches find a transformation $\mathbf{W}$ that in some sense diagonalizes all the given matrices based such that

$$\mathbf{C}_\tau^s = \mathbf{W}\mathbf{C}_\tau^x\mathbf{W}^T \tag{3}$$

for time lags $\tau = 1, 2, 3, \ldots$, where $\mathbf{C}_\tau^x$ is the signal covariance matrix and $\mathbf{C}_\tau^s$ is source covariance matrix. Estimation of $\mathbf{W}$ reduces to the well-researched problem of joint (approximate) diagonalization of the stack of matrices given by $\mathbf{W}\mathbf{C}_\tau^x\mathbf{W}^T$, for which a fast and efficient new algorithm $\text{LSDIAG}_{\text{TD}}$ is used.

2.2. Constrained ICA

Once a set of sources is determined through ICA, the ICs of interest must be identified. This is made difficult as the nature of the square mixing matrix means that a great many more sources will be identified over the expected (smaller) number of sources underlying the measurement set. A practical way to extract only the sources of interest automatically is to use prior knowledge or additional constraints on the

source model—cICA—through the use of a constraint or reference vector. The reference vector can be any vector which incorporates appropriate prior knowledge into the system. In this work, as we are interested in rhythmic EEG signals within our EEG recordings (specifically μ-rhythm activity), we propose to use a predefined spectral reference as the constraint. This spectral constraint then allows only those source activities with the same power spectrum to be extracted via the cICA algorithm. In [23], our innovation was to include a reference channel added as an extra row to the measurement matrix $\mathbf{x}(t)$, such that a new matrix $\hat{\mathbf{x}}(t)$ is created with

$$\hat{\mathbf{x}}(t) = \begin{bmatrix} \mathbf{x}(t) \\ \mathbf{c}_1(t) \end{bmatrix}, \tag{4}$$

where $\mathbf{c}_1(t)$ is a suitable reference vector. In order to observe changes in rhythmic activity in specific frequency bands, we use band-pass- (BP-) filtered white noise to derive a reference signal. Particularly, we use an 8th order Butterworth BP filter with lower and upper corner frequencies set appropriate to the desired constraint. The ICA problem is now such that the extra row in the measurement space due to the reference vector results in an extra row in the IC space after the ICA step (as well as a corresponding extra column in the mixing matrix). For an n-channel system, the first n elements of the extra mixing matrix column $[\mathbf{a}_1^{n+1}, \mathbf{a}_2^{n+1}, \ldots, \mathbf{a}_n^{n+1}]$ depict the spatial distribution (topography) of the new IC given by the row vector $\mathbf{s}_{n+1}(t)$. Furthermore, each of the elements of the $(n+1)$th row of the mixing matrix reflects a weighting of each corresponding IC. This row vector, $\mathbf{a}_{n+1}$, can in fact be used to depict the contribution of each topography described by the columns of the mixing matrix, due to the reference channel $\mathbf{c}_1(t)$. In this way, ICA now provides the desired convenient spanning basis, and can also be used to obtain the topography of interest (extracted by summing the weighted contribution of each column of the mixing matrix). Furthermore, the weighting value of each IC provides us with a spectrum of values that can be interpreted to gain some insight into the complexity for a given reference. The above technique can be readily extended to more than one reference. However, in this work we apply the method using just a single (μ-rhythm) reference. Some techniques, such as this, have already been included in the popular free ICA toolbox—ICALab [24].

2.3. The reference channel

Since the phase information of this added reference channel is meaningless (i.e., we cannot expect the phase of the reference signal to be connected in any way to that of the desired brain response), we overcome the problem of matching the phase of the reference channel with that of the desired activity in the recordings, through calculating the lagged covariance matrices that $\text{LSDIAG}_{\text{TD}}$ requires via the fast Fourier transform (FFT) and then removing the phase information of the signal in the frequency domain. Recall that the cross-correlation of two functions $f(t)$ and $g(t)$ can be obtained through convolution of f and g, such that

$$f * g = F^{-1}\left[\overline{F}(\nu)G(\nu)\right], \tag{5}$$

where $*$ denotes convolution, F^{-1} denotes the inverse Fourier Transform, $F(\nu)$ and $G(\nu)$ denotes the Fourier transform of f and g, respectively, and $\overline{F}(\nu)$ denotes the complex conjugate.

2.4. The dataset

In this work, we used two datasets: the 2003 BCI competition dataset IIa (self-regulation of μ- and/or central β-rhythm) and the BCI competition III dataset IVa (motor imagery, small training sets) which are obtainable from ida.first.fraunhofer.de/projects/bci/competition_ii and competition_iii. In dataset IIa, the subjects either increase or decrease their μ- or β-rhythm amplitude power to control a cursor's vertical position aiming to the height of the correct target through visual feedback. In dataset IVa, the subjects imagine either right-hand or right-foot movements indicated by a visual cue on-screen without feedback. Although these two experiments were designed in different ways, they both used the property of ERD power spectrum adjusted by different specific activation.

Dataset 1

The 2003 BCI competition dataset IIa (self-regulation of μ- and/or central β-rhythm) was used, which was provided by the Wadsworth Center [25]. This dataset contains a whole record of an actual BCI system from 3 trained subjects in 10 sessions (about 30 minutes per session) each. EEG was recorded from 64 scalp electrodes (10/20 system) sampled at 160 Hz. For this BCI to work, after a one-second resting period during which the screen stays blank, a target appears at one of four possible positions on the right-hand side of the screen. One second later, a cursor appears at the middle of the left of the screen and starts moving at constant speed across the screen from left to right. When the cursor reaches the right-hand side, the screen is cleared and the next trial begins. The experiment includes visual feedback whereby the vertical position of the cursor on the screen is determined through brain activity. Three data subsets marked as AA, BB, and CC are supplied. Each session consisted of 192 trials (48 trials for each target can be "top," "upper middle," "lower middle," or "bottom"). The first six sessions are labelled as *training* sets. The remaining four sessions are *test* sets and not labelled initially for the purposes of the competition. After the competition, the labels for testing sets were released and the datasets become available for developing new methods towards improving BCI studies. In this work, we only select trials with the target position code: "top" (Target 1) and "bottom" (Target 2) to examine our proposed method.

Dataset 2

The BCI competition III dataset IVa from the Berlin BCI group [26] was used. This dataset contains 118 multichannel (extended 10/20 system) EEG signals recorded from five healthy subjects (labelled "aa," "al," "av," "aw," and "ay," resp.) at a sampling rate of 100 Hz. During the experiments, subjects were prompted by a displayed letter (R/right hand,

or F/right foot) to imagine for 3.5 seconds either right-hand (Target A) or right-foot movements (Target B) without feedback. Each type of MI was recorded 140 times, thus in total there are 280 trials for each subject. Between the trials, there was a random period of time (1.75 to 2.25 seconds) in which the subject could relax. This dataset also brings with it a challenge in that only a little amount of training data are available, this allows us to examine the influence of using small training sets in order to reduce the training time. The task is to classify the type of the imagined movement for each trial in an offline fashion.

2.5. The proposed algorithm

The algorithm we propose includes three parts: (a) spatial filter generation, (b) power feature extraction, and (c) classification. This is depicted in diagrammatic form in Figure 1.

2.5.1. Spatial filter generation

For the analysis, a number of epochs of the training dataset were used to estimate the lagged covariance matrix stack $\mathbf{C}_\tau^x$. We treat the stack of matrices as arising from two-part averaged lagged covariance matrix stacks $\mathbf{C}_\tau^{XT_1}$, $\mathbf{C}_\tau^{XT_2}$ in which each part is obtained from trial data corresponding to one of two targets, such that

$$\begin{aligned}\mathbf{C}_\tau^x &= [\mathbf{C}_\tau^{XT_1}; \mathbf{C}_\tau^{XT_2}],\\ \mathbf{C}_\tau^{XT_1} &= \left[\frac{1}{m}\sum_{x_k \in XT_1}\mathbf{C}_0^{x_k}, \ldots, \frac{1}{m}\sum_{x_k \in XT_1}\mathbf{C}_l^{x_k}\right],\\ \mathbf{C}_\tau^{XT_2} &= \left[\frac{1}{n}\sum_{x_k \in XT_2}\mathbf{C}_0^{x_k}, \ldots, \frac{1}{n}\sum_{x_k \in XT_2}\mathbf{C}_l^{x_k}\right],\end{aligned} \tag{6}$$

where $\tau = [0, \ldots, l]$ depicts the range of lags (here $l = 5$ as determined in previous work [27]). $x \in [XT_1, XT_2]$ denotes that trial data are from training set corresponding to the labels: Target 1/A and Target 2/B. The number of trials in each dataset, XT_1 and XT_2, is m and n, respectively. Here we set the value of m equal to n to balance the proportion of trials for both targets.

The spectrum, $\mathbf{P}(i)$, is defined as a trial spectrum in ith channel by the sum of the ordinates of the frequency bins ($\mathbf{h}_d$) within the proposed frequency band, that is,

$$\mathbf{P}(i) = \sum_{d \in D}\mathbf{h}_d, \tag{7}$$

where D denotes the number of frequency bins. After cICA decomposition, the EEG data are extracted into the ICs. Thus, the power spectrum after cICA is defined as the sum of the weighted spectra of sources (ICs) within the μ band. So, for given source epochs, the power feature reflected in an individual channel is defined as

$$\mathbf{f}_p(i) = \sum_{j=1}^{k}\mathbf{a}_{k+1,j}\mathbf{P}_{ic}(j)\mathbf{a}_{i,j}, \tag{8}$$

where k denotes the number of sources. As this implementation of cICA assumes a square mixing matrix, then the number of sources is the same as the number of measurement channels, and $\mathbf{a}_{i,j}$ is an element in the mixing matrix $\mathbf{A}$. $\mathbf{a}_{k+1,j}$ is a particular element in the last row of $\mathbf{A}$. $\mathbf{P}_{ic}(j)$ denotes a trial spectrum in the jth IC source.

2.5.2. Feature selection

In order to find discriminative power bands for each subject, we calculated the power spectra of two targets in these two datasets, and then combined the variables on each individual channel into r^2 values which represent the proportion of the variance of spectral power values from the labelled training sets. By comparing to the averaged power spectra corresponding to two targets, this describes the relationship between power intensity and target labels. These parameters were slightly different due to differences in each individual recording. For example, in dataset IIa, two discriminative power bands roughly around 10–15 Hz and 23–28 Hz (Figure 2) are used. In this work we chose 10–15 Hz as the working band. Increased power is taken to correspond to Target 1 which raises the cursor in Subject AA and Subject CC while it makes the cursor go down in Subject BB (Figure 3). In dataset IVa, we selected the subband approximately around 8–15 Hz to calculate power (Figure 4). Increased power is related to Target 2 which is the right-foot imagination (Figure 5) in all subjects.

As described in the above section, the data were originally recorded from 64 scalp electrodes for dataset IIa and 118 electrodes for dataset IVa. We are only interested in the activity in the motor cortex, so the electrodes around the sensorimotor cortex were chosen manually, these included C5, C3, C1, C2, C4, C6, CP5, CP3, Cp1, Cp2, Cp4, Cp6, P5, P3, P1, P2, P4, and P6. We only used a small segment of EEG data for training in the proposed algorithm: for dataset IIa, the data between 0.5–2 seconds of each trial are used after the cursor is displayed on the screen; for dataset IVa, the data between 0.5–2.5 seconds are considered after the instruction is displayed on the screen.

2.5.3. Classification

In order to evaluate the performance of the proposed algorithm, we only consider a simple one-dimensional linear classifier based on thresholding the power feature(s) in the chosen frequency band for the final classification. The threshold value is selected by minimizing the number of trials misclassified in both classes from the training set for individual subjects. In addition, as a comparison for the classification performance, we also applied a more complex classifier, a support vector machine (SVM) [28] which constructs a nonlinear separation hyperplane based on a machine-learning algorithm.

The next procedure is to decide which power feature will be suitable to use for the classification. Based on the distribution of r^2 values across the topography maps in the previous section, a number of channels (between 1 and 3) around the left sensorimotor cortex were selected. The power on C3 was used in the threshold classifier and the power on C3, CP1,

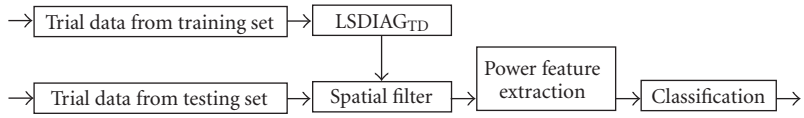

FIGURE 1: A diagram depicting the proposed algorithm. It includes three parts: spatial filter generation, power feature extraction, and classification.

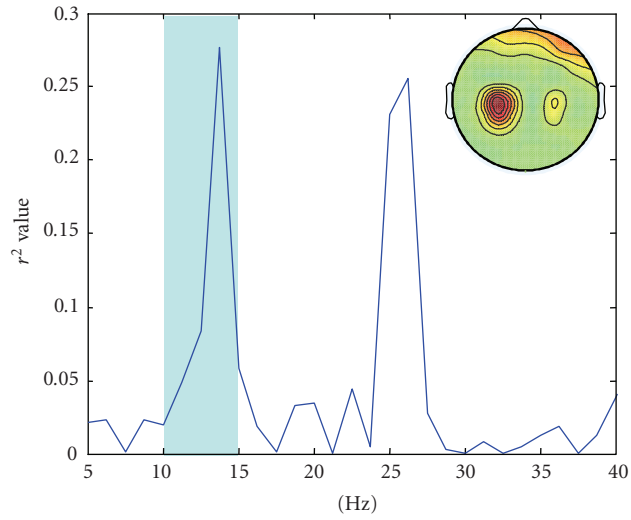

FIGURE 2: r^2 values across the spectrum on C3 channel for Target 1 and Target 2 (Subject CC). The shadowed frequency band was chosen in this work. Inset is the topography of the r^2 values at 13.75 Hz across channels.

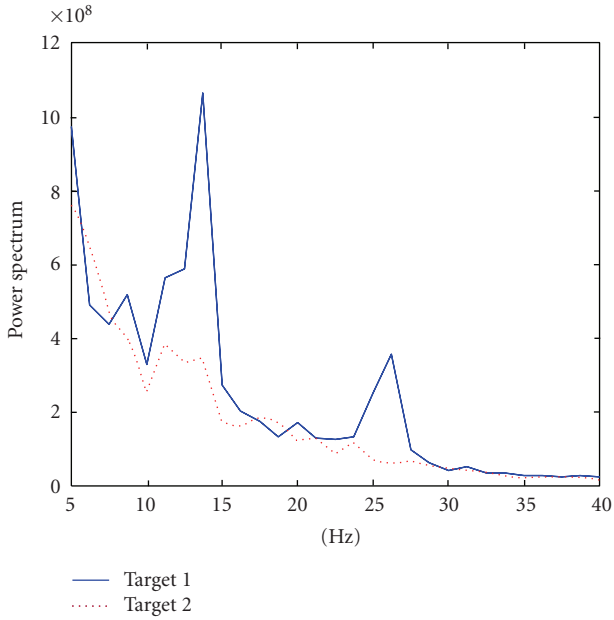

FIGURE 3: Averaged power spectra of trials corresponding to Target 1 and Target 2 (Subject CC). In this experiment, greater power (Target 1) implies the cursor going up and vice versa.

and CP5 for the SVM classifier as the use of these power features was found to be able to achieve better classification accuracy in our study.

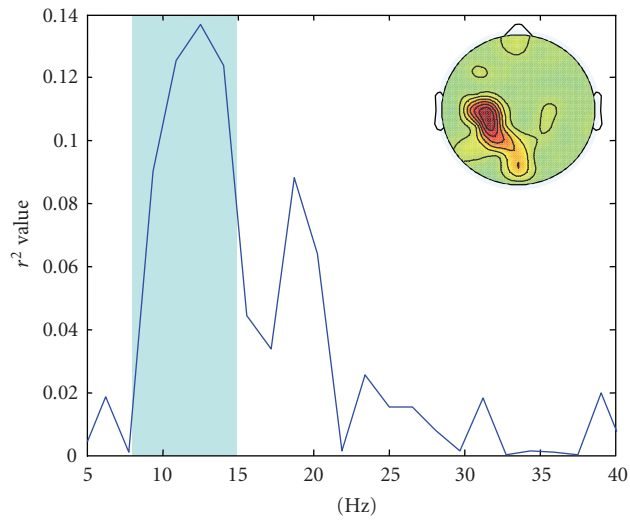

FIGURE 4: r^2 values across the spectrum on C3 channel for Target A and Target B (Subject "ay"). The shadowed frequency band was chosen in this work. Inset is the topography of the r^2 values at 12.25 Hz across channels.

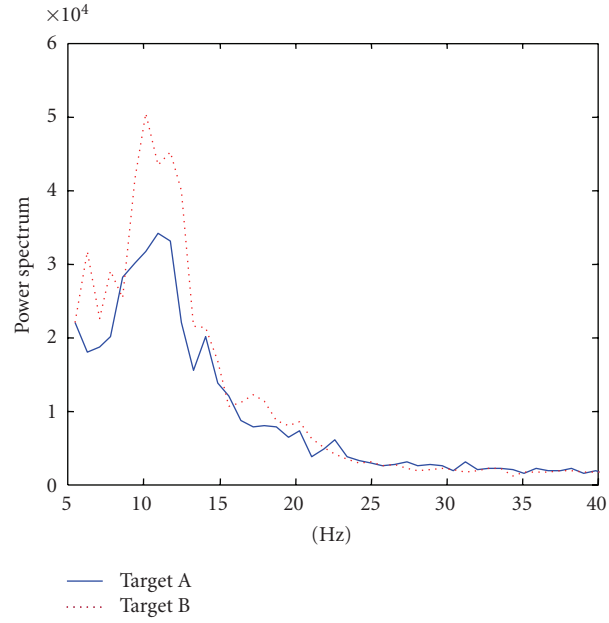

FIGURE 5: Averaged power spectra of trials corresponding to Target A and Target B (Subject "ay"). The averaged power for imagined foot movement (Target A) is greater than the power for hand movement imagination (Target B).

3. RESULTS

Using the proposed method, the designed spatial filters will be able to capture the relevant dynamics of the subject's brain

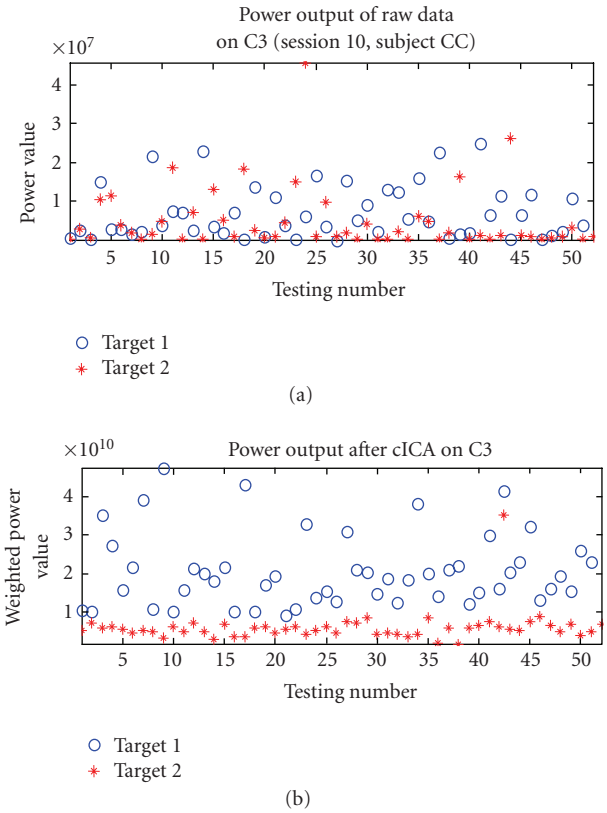

Figure 6: The power feature outputs of Subject CC for Testing session 10. (a) shows the power features on C3 using unprocessed data; (b) shows the power features on C3 after cICA processing. A circle denotes Target 1 (drive cursor up); a star indicates Target 2 (cursor down).

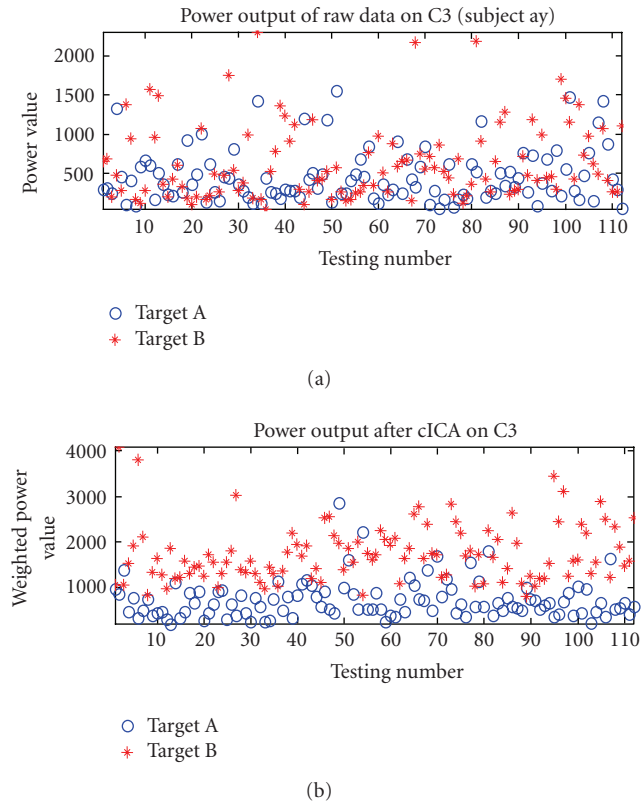

Figure 7: The power feature outputs for Subject "ay" on testing set. (a) shows the power features on C3 using unprocessed data; (b) shows the power features on C3 after cICA processing. A circle denotes the power feature for Target A (right hand imagination); a star indicates the power feature for Target B (right foot imagination).

state more robustly. Furthermore, the resulting time series would have optimized the spectra which could result in better discrimination between two different brain states. The results show that following this pre-processing, even a simple linear classifier can achieve superior classification accuracy.

Figures 6 and 7 depict the power features related to different targets before and after the processing for channel C3. In Figure 6, we plot the power features of testing session 10 for Subject CC in dataset IIa. Ideally, the higher power feature is for Target 1 and lower power for Target 2 (Figure 3). However, without spatial filtering, the power features between two targets from the original data appear overlapped, and a classifier based on either a simple linear method or a potentially complicated advanced method is hardly able to separate these patterns efficiently. After the cICA processing, the weighted power values for two different targets are more widely separated than the power features from the unprocessed data. Figure 7 shows the power features of Subject "ay" from dataset IVa. The power related to the right-hand movement imagination is marked as Target A and the power for right-foot movement imagination is marked as Target B. As shown in Figure 5, the averaged power for imagined foot movement is larger than the power for hand movement imagination, but powers correlated to two different targets do not show much different in the raw data. After processing, the power features are maximally separated into the different levels, which further demonstrate the improved separation achieved by using this spatial filter. The above examples suggest that the use of this spatial filter can help to extract different brain activities within a particular μ rhythmic band.

Table 1 lists the classification results on the test sets (most sessions have 52 trials for each target, several have 51 trials) in dataset IIa. For each subject, we use 80 randomly chosen trials in total (40 for each target) to calculate the spatial filter. The results are shown as three columns for each individual subject. The first column shows the results using the unprocessed data. The results of using a threshold-based classifier with one power feature on C3 are shown in the second column. The third column is for the results from an advanced SVM-based classifier using three power features on C3, CP1, and CP5. Table 2 shows the classification performance on the testing data in dataset IVa. There are five subjects contributing to individual subsets with different sizes of training and testing sessions. The numbers of available trial data for training/testing sessions are shown in the first column. To construct the spatial filter, the total number of training trials is selected between 28 and 80 (average of 65 trials was used) due to the different size of training sets. As before, one power

Table 1: Classification accuracy of the test set based on power feature(s) in dataset IIa. The three columns for each individual subject show the performance of linear classification on unprocessed data, linear classification and SVM classification on the processed data.

Testing dataset	Data AA			Data BB			Data CC		
	Linear classifier on raw data	Linear classifier on extracted data	SVM on extracted data	Linear classifier on raw data	Linear classifier on extracted data	SVM on extracted data	Linear classifier on raw data	Linear classifier on extracted data	SVM on extracted data
Set 7	64.6%	80.2%	85.4%	65.6%	72.0%	73.0%	58.3%	85.4%	87.4%
Set 8	59.4%	88.5%	89.6%	71.9%	72.9%	72.9%	62.1%	92.2%	90.3%
Set 9	61.5%	80.2%	79.2%	66.8%	63.5%	67.7%	60.1%	86.1%	88.1%
Set 10	65.6%	80.2%	80.2%	59.4%	68.8%	72.9%	61.2%	96.1%	98.1%

Table 2: Classification accuracy of the testing set based on power feature(s) in dataset IVb. The columns depict the results using the three proposed classification schemes, and the last column lists published [29] for comparison.

dataset	Training/test trials	Linear classifier on raw data	Linear classifier on extracted data	SVM on extracted data	SVM on DS features
al	224/56	48.2%	85.7%	89.3%	96.3%
aa	168/112	46.0%	83.0%	85.7%	83.3%
av	84/196	49.5%	75.0%	75.0%	72.7%
aw	56/224	55.4%	80.3%	85.3%	86.9%
ay	28/252	54.3%	85.0%	85.0%	89.0%

feature on C3 is used for the final classification based on a threshold and a linear classifier. Moreover, three features on channel C3, CP1, and CP5 were also applied to examine the performance of an SVM classifier. In addition, as a comparison, the last column lists the classification results from previous published work [29] which proposes a method based on dynamical system (DS) features together with an SVM classifier. The overall classification accuracy is about 85% by this DS+SVM method. From the two tables, we can see that cICA implementation extracts the related rhythmic information very effectively. After processing, the classification accuracy was of 82% for Subject AA, 69% for Subject BB, and 90% for Subject CC in comparison with the average 62% accuracy before processing in dataset IIa. In dataset IVa, the classification accuracy was of an average of 82% through five testing sets, which is 30% higher than the accuracy using the unprocessed data. It is worth noting that the more advanced SVM-based classifier did not show a significant improvement in performance on the same data, although an increase of about 2% compared to the simple linear classifier was observed.

4. DISCUSSION AND CONCLUSIONS

Two datasets have been used to examine the performance of the proposed algorithm. Dataset IVa concerns MI data, and dataset IIa regards the self-regulation of μ/β-rhythm data. Both of these datasets use the characteristic that changes in the amplitude of sensorimotor rhythms over the right/left hemisphere act as the major control pattern. The difficulty here is to maximally and reliably identify two classes from single-trial data. The proposed ICA technique using constraints has been developed and applied to isolate and extract the power spectrum in the rhythmic band of interest. In order to demonstrate the performance of the proposed cICA, we only applied the power feature in the μ-rhythm frequency band as the major classification pattern. The results, using a simple linear classifier and an advanced SVM to classify the ICA processed data, show that the classification accuracy has considerably increased over processing the raw data. After the basic analysis, the overall classification accuracy is improved about 20% in dataset IIa and 30% in dataset IVa. As an additional comparison of classification performance to cICA in dataset IVa, we cited the results of a method using DS features as well as an SVM in a publication. This method also includes two steps for data pre-processing (an identical temporal filter and a spatial filter). The accuracy was about 3% more than the results of cICA with a linear classifier and 1% more than cICA with an SVM. If we use a set of well-tuned parameters to the proposed method, then the classification would be expected to reach a slightly better performance. Furthermore, the use of a linear classifier following a simple spatial filter as in our system is desirable from a computational complexity perspective.

As this work is an application to single trial classification, the sensitivity to artifacts in the EEG becomes a major problem. The $\text{LSDIAG}_{\text{TD}}$ ICA algorithm uses the covariance of the trail data to estimate the covariance stack matrices which are the essentials to calculate the unmixing matrix and hence the spatial filter. The random selection of training trials with artifacts can cause serious changes to the final filter. Therefore, most methods require that the data should be artifact-free, which can be achieved by several preprocessing steps such as filtering or manual artifact rejection. Here, instead of applying any preprocessing methods before hand,

we estimate the stack matrices by using the averaged lagged covariance matrices from the data. The idea behind the process is that the influence of artifacts is reduced since the procedure of averaging the covariance matrices acts as a filter which could balance and minimize the random noise level. Moreover, the system includes a training phase used to tune the proper unmixing matrix (spatial filter) using the proposed ICA. Once the unmixing matrix has been computed, it works as a spatial filter to remove the additional artifacts by weighted spatial averaging the testing data trials and returns the processed time series patterns. After filtering, the different brain activities in the form of power can be clearly extracted. It indicates that through the use of cICA, it is possible to track the rhythmic changes of different brain states in the EEG. These results show a clear improvement for use in this kind of BCI system.

In order to bring a BCI system to work outside of laboratory conditions, several items need to be taken into account in future work. The number of electrodes used in the system usually decides the cost of hardware and the related difficulty of processing the ensuing data. The application of ICA using fewer channels or even a single channel may be the solution of the problem and is one area we are actively pursuing [30]. Similarly, classification pattern selection may be improved as the use of similar patterns (even if the features are from different channels) might limit the capability of the classifier so that even this advanced method cannot work most effectively. Therefore, careful selection of diverse features may alleviate the problem, that is, features in time or in different frequency bands, and so forth. This may further improve classification accuracy.

ACKNOWLEDGMENTS

This work forms part of the Southampton Brain-Computer Interfacing Research Programme (www.bci.soton.ac.uk). Funding in the form of an ISVR Rayleigh Scholarship for SW is greatfully acknowledged.

REFERENCES

[1] S. Rush and D. A. Driscoll, "EEG electrode sensitivity—an application of reciprocity," *IEEE Transactions on Biomedical Engineering*, vol. 16, no. 1, pp. 15–22, 1969.

[2] J. R. Wolpaw, N. Birbaumer, D. J. McFarland, G. Pfurtscheller, and T. M. Vaughan, "Brain-computer interfaces for communication and control," *Clinical Neurophysiology*, vol. 113, no. 6, pp. 767–791, 2002.

[3] J. W. Kozelka and T. A. Pedley, "Beta and mu rhythms," *Journal of Clinical Neurophysiology*, vol. 7, no. 2, pp. 191–207, 1990.

[4] J. R. Wolpaw, D. J. McFarland, G. W. Neat, and C. A. Forneris, "An EEG-based brain-computer interface for cursor control," *Electroencephalography and Clinical Neurophysiology*, vol. 78, no. 3, pp. 252–259, 1991.

[5] G. Pfurtscheller, "Graphical display and statistical evaluation of event-related desynchronization (ERD)," *Electroencephalography and Clinical Neurophysiology*, vol. 43, no. 5, pp. 757–760, 1977.

[6] N.-J. Huan and R. Palaniappan, "Classification of mental tasks using fixed and adaptive autoregressive models of EEG signals," in *Proceedings of the 26th Annual International Conference of the IEEE Engineering in Medicine and Biology Society (EMBC '04)*, pp. 507–510, San Francisco, Calif, USA, September 2004.

[7] H. Ramoser, J. Müller-Gerking, and G. Pfurtscheller, "Optimal spatial filtering of single trial EEG during imagined hand movement," *IEEE Transactions on Rehabilitation Engineering*, vol. 8, no. 4, pp. 441–446, 2000.

[8] A. Hyvärinen and E. Oja, "A fast fixed-point algorithm for independent component analysis," *Neural Computation*, vol. 9, no. 7, pp. 1483–1492, 1997.

[9] A. J. Bell and T. J. Sejnowski, "An information-maximization approach to blind separation and blind deconvolution," *Neural Computation*, vol. 7, no. 6, pp. 1129–1159, 1995.

[10] C. J. James and C. W. Hesse, "A comparison of time structure and statistically based BSS methods in the context of long-term epileptiform EEG recordings," in *Proceedings of the 5th International Conference on Independent Component Analysis and Blind Signal Separation (ICA '04)*, pp. 1025–1032, Granada, Spain, September 2004.

[11] O. Gibson and C. J. James, "On the analysis of seizure onset in the EEG: the application of constrained ICA," in *Proceedings of the 2nd European Medical and Biological Engineering Conference (EMBEC '02)*, pp. 424–426, Vienna, Austria, December 2002.

[12] A. K. Barros, A. Mansour, and N. Ohnishi, "Removing artifacts from electrocardiographic signals using independent components analysis," *Neurocomputing*, vol. 22, no. 1–3, pp. 173–186, 1998.

[13] R. Vigário, J. Särelä, V. Jousmäki, M. Hämäläinen, and E. Oja, "Independent component approach to the analysis of EEG and MEG recordings," *IEEE Transactions on Biomedical Engineering*, vol. 47, no. 5, pp. 589–593, 2000.

[14] M. J. McKeown, T.-P. Jung, S. Makeig, et al., "Spatially independent activity patterns in functional MRI data during the Stroop color-naming task," *Proceedings of the National Academy of Sciences of the United States of America*, vol. 95, no. 3, pp. 803–810, 1998.

[15] N. Xu, X. Gao, B. Hong, X. Miao, S. Gao, and F. Yang, "BCI competition 2003—data set IIb: enhancing P300 wave detection using ICA-based subspace projections for BCI applications," *IEEE Transactions on Biomedical Engineering*, vol. 51, no. 6, pp. 1067–1072, 2004.

[16] S. Wang and C. J. James, "Enhancing evoked responses for BCI through advanced ICA techniques," in *Proceeding of IET 3rd International Conference on Advances in Medical, Signal and Information Processing (MEDSIP '06)*, p. 38, Glasgow, UK, July 2006.

[17] A. Erfani and A. Erfanian, "The effects of mental practice and concentration skills on EEG brain dynamics during motor imagery using independent component analysis," in *Proceedings of the 26th Annual International Conference of the Engineering in Medicine and Biology Society (EMBC '04)*, vol. 1, pp. 239–242, San Francisco, Calif, USA, September 2004.

[18] C. J. James and C. W. Hesse, "Independent component analysis for biomedical signals," *Physiological Measurement*, vol. 26, no. 1, pp. R15–R39, 2005.

[19] C. J. James and O. J. Gibson, "Temporally constrained ICA: an application to artifact rejection in electromagnetic brain signal analysis," *IEEE Transactions on Biomedical Engineering*, vol. 50, no. 9, pp. 1108–1116, 2003.

[20] A. Ziehe and K.-R. Müller, "TDSEP—an efficient algorithm for blind separation using time structure," in *Proceedings of the 8th International Conference on Artificial Neural Networks (ICANN '98)*, pp. 675–680, Skovde, Sweden, September 1998.

[21] A. Belouchrani and M. G. Amin, "Blind source separation based on time-frequency signal representations," *IEEE Transactions on Signal Processing*, vol. 46, no. 11, pp. 2888–2897, 1998.

[22] A. Ziehe, P. Laskov, K.-R. Müeller, and G. Nolte, "A linear least-squares algorithm for joint diagonalization," in *Proceedings of the 4th International Symposium on Independent Component Analysis and Blind Signal Separation*, pp. 469–474, Nara, Japan, April 2003.

[23] C. J. James and C. W. Hesse, "Mapping scalp topographies of rhythmic EEG activity using temporal decorrelation based constrained ICA," in *Proceedings of the 26th Annual International Conference of the IEEE Engineering in Medicine and Biology Society (EMBC '04)*, vol. 2, pp. 994–997, San Francisco, Calif, USA, September 2004.

[24] A. Cichocki, S. Amari, and K. Siwek, "ICALAB toolbox for signal processing," http://www.bsp.brain.riken.jp/ICALAB/.

[25] B. Blankertz, K.-R. Müller, G. Curio, et al., "The BCI competition 2003: progress and perspectives in detection and discrimination of EEG single trials," *IEEE Transactions on Biomedical Engineering*, vol. 51, no. 6, pp. 1044–1051, 2004.

[26] G. Dornhege, B. Blankertz, G. Curio, and K.-R. Müller, "Boosting bit rates in noninvasive EEG single-trial classifications by feature combination and multiclass paradigms," *IEEE Transactions on Biomedical Engineering*, vol. 51, no. 6, pp. 993–1002, 2004.

[27] C. J. James and C. W. Hesse, "Observing and tracking brain dynamics in electromagnetic brain signals through blind source separation," in *Proceedings of the IEE Medical Signal and Information Processing Conference (MEDSIP '04)*, pp. 145–152, Malta, September 2004.

[28] S. R. Gunn and J. S. Kandola, "Structural modelling with sparse kernels," *Machine Learning*, vol. 48, no. 1–3, pp. 137–163, 2002.

[29] L. Song and J. Epps, "Classifying EEG for brain-computer interfaces: learning optimal filters for dynamical system features," in *Proceedings of the 23rd International Conference on Machine Learning (ICML '06)*, pp. 857–864, Pittsburgh, Pa, USA, June 2006.

[30] C. J. James and S. Wang, "Blind source separation in single-channel EEG analysis: an application to BCI," in *Proceedings of the 28th Annual International Conference of the IEEE Engineering in Medicine and Biology Society (EMBS '06)*, pp. 6544–6547, New York, NY, USA, August-September 2006.

Hindawi Publishing Corporation
Computational Intelligence and Neuroscience
Volume 2007, Article ID 79826, 9 pages
doi:10.1155/2007/79826

Research Article

The Self-Paced Graz Brain-Computer Interface: Methods and Applications

Reinhold Scherer,[1,2] Alois Schloegl,[3] Felix Lee,[4] Horst Bischof,[4] Janez Janša,[5] and Gert Pfurtscheller[1,2]

[1] *Laboratory of Brain-Computer Interfaces, Institute for Knowledge Discovery, Graz University of Technology, Krenngasse 37, 8010 Graz, Austria*
[2] *NeuroCenter Styria, Krenngasse 37/I, 8010 Graz, Austria*
[3] *Intelligent Data Analysis Group, Fraunhofer-Institut für Rechnerarchitektur und Softwaretechnik, FIRST, Kekulestrasse 7, 12489 Berlin, Germany*
[4] *Institute for Computer Graphics and Vision, Graz University of Technology, Inffeldgasse 16, 8010 Graz, Austria*
[5] *Aksioma - Institute for Contemporary Art, Neubergerjeva 25, 1000 Ljubljana, Slovenia*

Correspondence should be addressed to Reinhold Scherer, reinhold.scherer@tugraz.at

Received 25 February 2007; Revised 13 June 2007; Accepted 19 July 2007

Recommended by Fabio Babiloni

We present the self-paced 3-class Graz brain-computer interface (BCI) which is based on the detection of sensorimotor electroencephalogram (EEG) rhythms induced by motor imagery. Self-paced operation means that the BCI is able to determine whether the ongoing brain activity is intended as control signal (intentional control) or not (non-control state). The presented system is able to automatically reduce electrooculogram (EOG) artifacts, to detect electromyographic (EMG) activity, and uses only three bipolar EEG channels. Two applications are presented: the freeSpace virtual environment (VE) and the Brainloop interface. The freeSpace is a computer-game-like application where subjects have to navigate through the environment and collect coins by autonomously selecting navigation commands. Three subjects participated in these feedback experiments and each learned to navigate through the VE and collect coins. Two out of the three succeeded in collecting all three coins. The Brainloop interface provides an interface between the Graz-BCI and Google Earth.

1. INTRODUCTION

A brain-computer interface (BCI) transforms electrophysiological or metabolic brain activity into control signals for applications and devices (e.g., spelling system or neuroprosthesis). Instead of muscle activity, a specific type of mental activity is used to operate such a system. For a review on BCI technologies see [1–4].

After years of basic research, modern BCIs have been moving out of the laboratory and are under evaluation in hospitals and at patients' homes (e.g., [5–11]). However, BCIs have to meet several technical requirements before they are practical alternatives to motor controlled communication devices. The most important requirements are high information transfer rates, ease-of-use, robustness, on-demand operability, and safety [12]. In summary, for the end-user, BCI systems have to carry information as quickly and accurately as needed for individual applications, have to work in most environments, and should be available without the assistance of other people (self-initiation). To fulfill these issues, the Graz group focused on the development of small and robust systems which are operated by using one or two bipolar electroencephalogram (EEG) channels only [13]. Motor imagery (MI), that is, the imagination of movements, is used as the experimental strategy.

In this work, we aim at two important issues for practical BCI systems. The first is detection of electromyographic (EMG) and reduction of electrooculographic (EOG) artifacts and the second is the self-paced operation mode. Artifacts are undesirable signals that can interfere and may change the characteristics of the brain signal used to control the BCI [14]. Especially in early training sessions, EMG artifacts are present in BCI training [15]. It is therefore crucial to ensure that (i) brain activity and not muscle activity is used as source of control and that (ii) artifacts are not producing undesired BCI output. Self-paced BCIs are able

to discriminate between intentionally generated (intentional control, IC) and ongoing (non-control, NC) brain activity [16]. This means that the system is able to determine whether the ongoing brain pattern is intended as control signals (IC) or not (NC). In this mode the user has control over timing and speed of communication.

In addition to the above stated methods, two applications, designed for self-paced operation, are presented. The first is a computer game like virtual environment (VE) that users navigate through and collect points, and the second is a user-interface which allows operating the Google-Earth (Google, Mountain View, CA, USA) application.

2. METHODS

2.1. Electromyography (EMG) artifact detection

The results of [17] showed that muscle and movement artifacts can be well detected by using the principle of inverse filtering. The inverse filtering method aims to estimate an autoregressive (AR) filter model (see (1)) of the EEG activity. The output y_t of the AR model is the weighted sum of the number of model order p last sample values y_{t-i} and the model parameters a_i with $i = 1 \dots p$. ν_t is a zero-mean-Gaussian-noise with variance σ_ν^2. Applying the filter model inversely (using the inverted transfer functions) to the measured EEG yields a residual (i.e., prediction error) which is, usually, much smaller than the measured EEG. In effect, all EEG frequencies are suppressed. If some transient or other high-frequency artifacts (like EMG artifacts) are recorded at the EEG channels, the average prediction error will increase. This increase can be detected by computing the time-varying root-mean-square (RMS) of the residual and comparing it with a predefined threshold value. Once the AR parameters a_i are identified from an artifact free EEG segment, these parameters can be applied inversely to estimate the prediction error x_t from the observed EEG y_t,

$$y_t = \sum_{i=1}^{p} a_i \cdot y_{t-i} + \nu_t \quad \text{with } \nu_t = N(0,\sigma_\nu^2). \tag{1}$$

For on-line experiments, the detection threshold of five times RMS from artifact-free EEG was used. Each time the inversely filtered process exceeded this threshold, the occurrence of an EMG artifact in form of a yellow warning marker, positioned in the lower-left part of the screen, was reported back to the user. After any occurrence, users were instructed to relax until the warning disappeared. The warning was disabled once the threshold was not exceeded for a 1-second period.

At the beginning of each BCI session, a 2-minute segment of artifact free EEG was recorded in order to estimate the AR-parameters a_i (model order $p = 10$) by using the Burg method. See Figure 1(a) for details on the protocol used to collect the artifact free EEG. Subjects were instructed to sit relaxed and not move.

2.2. Automatic reduction of electrooculography (EOG) artifacts

Electrooculogram (EOG) artifacts are potential shifts on the body surface resulting from retinal dipole movements or blinking of the eyes. Since generally both eyes are in the same line of sight, one single dipole consisting of three spatial components (horizontal, vertical, and radial) should be sufficient to model the bioelectrical eye activity [18]. Assuming that (i) for each channel the recorded EEG Y_t is a linear superposition of the real EEG signal S_t and the three spatial EOG components ($N_{t,\text{horizontal}}$, $N_{t,\text{vertical}}$, and $N_{t,\text{radial}}$) weighted by some coefficient b (2) and that (ii) EEG S and EOG N are independent, the weighting coefficient $\mathbf{b}$ can be estimated according to (3) (matrix notation) by computing the autocorrelation matrix $\mathbf{C}_{N,N}$ of the EOG and the cross-correlation $\mathbf{C}_{N,Y}$ between EEG $\mathbf{Y}$ and EOG $\mathbf{N}$. Equation (4) describes how the "EOG-corrected" EEG is computed.

$$Y_{\text{channel},t} = S_{\text{channel},t} + \left[N_{\text{horizontal},t}, N_{\text{vertical},t}, N_{\text{radial},t}\right] \cdot \begin{bmatrix} b_{\text{horizontal,channel}} \\ b_{\text{vertical,channel}} \\ b_{\text{radial,channel}}, \end{bmatrix} \tag{2}$$

$$\mathbf{Y} = \mathbf{S} + \mathbf{N} \cdot \mathbf{b} \Longrightarrow \mathbf{b} = \left(\mathbf{N}^T\mathbf{N}\right)^{-1}\mathbf{N}^T\mathbf{Y} = \mathbf{C}_{N,N}^{-1}\mathbf{C}_{N,Y}, \tag{3}$$

$$\mathbf{S} = \mathbf{Y} - \mathbf{N} \cdot \mathbf{b}. \tag{4}$$

To limit the total number of channels, the EOG was measured by using three monopolar electrodes, from which two bipolar EOG channels, covering the horizontal and the vertical EOG activity, were derived (Figure 1(b)).

In order to compute the weighting coefficient $\mathbf{b}$, at the beginning of each BCI session, a 1-minute segment of EEG and EOG with eye movement artifacts was recorded. Subjects were instructed to repetitively perform eye blinks, clockwise and counter-clockwise rolling of the eyes and perform horizontal and vertical eye movements. The eyes should circumscribe the whole field of view without moving the head. Figure 1(a) summarizes the recording protocol used. A more detailed description as well as the evaluation of the EOG correction method can be found in [18].

2.3. Self-paced BCI operation

Essential for the development of self-paced motor imagery (MI)-based BCIs is to train (i) the user to reliably induce distinctive brain patterns and to train (ii) the BCI to detect those patterns in the ongoing EEG. In this work, prior to participate in self-paced experiments, subjects learned to generate three different MI patterns by performing cue-based feedback training. The resulting classifier is named CFR_{MI}. Once a reliable classification performance was achieved, a second classifier (CFR_{IC}) was trained to discriminate between characteristic EEG changes induced by MI and the ongoing EEG. Self-paced control was obtained by combining both classifiers. Each time MI-related brain activity was detected by CFR_{IC} the type of motor imagery task was determined by CFR_{MI}. If no MI-related activity was detected from CFR_{IC}, the output was "0" or "NC."

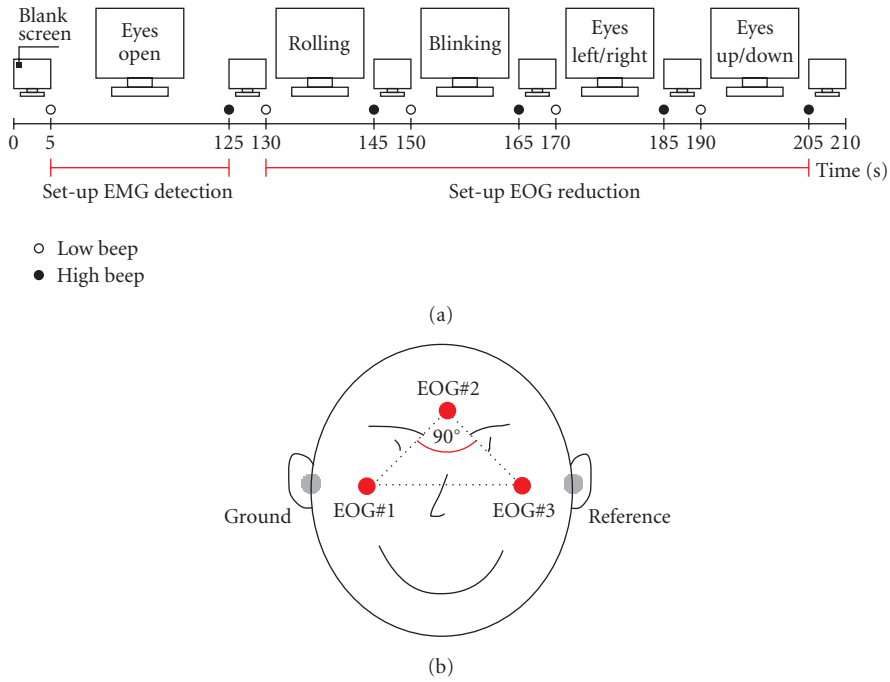

FIGURE 1: (a) Protocol used for the collection of EEG and EOG samples to set up the EMG detection and EOG reduction. The recording was divided into several segments, each separated by a 5-s resting period. Instructions were presented on a computer screen. At the beginning and end of each task low -and high-warning tones were presented, respectively. (b) Positions of EOG electrodes (reference left mastoid, ground right mastoid). The three EOG electrodes are placed above the nasion, and below the outer canthi of the eyes, generating in a right-angled triangle. The legs of the triangle form two spatially orthogonal components (modified from [18]).

Three healthy subjects (2 males, 1 female, right handed) participated in self-paced experiments. Subject specific electrode positions (according to the international 10–20 system), motor imagery tasks and the on-line classification accuracies of CFR_{MI} after about 4 hours of cue-based 3-class feedback training are summarized in Figure 2(a). Three bipolar EEG channels (named C3, C*z*, and C4) and three monopolar EOG channels (Figure 1(a)) were recorded from Ag/AgCl electrodes, analog filtered between 0.5 and 100 Hz and sampled at a rate of 250 Hz. Figure 2(b) shows the timing of the cue-based paradigm. Classifier CFR_{MI} was realized by combining 3 pairwise trained Fisher's linear discriminant analysis (LDA) functions with a majority vote. A maximum of six band power (BP) features were extracted from the EEG by band pass filtering the signal (5th-order Butterworth), squaring and applying a 1-second moving average filter. From the averaged value the logarithm was computed (BP_{log}).

CFR_{IC} consisted of one single LDA. To identify the most discriminative BP_{log} the distinction sensitive learning vector quantization (DSLVQ [19, 20]) method was used. DSLVQ is an extended learning vector quantizer (LVQ) which employs a weighted distance function for dynamical scaling and feature selection [20]. The major advantage of DSLVQ is that it does not require expertise, nor any a priori knowledge or assumption about the distribution of the data. To obtain reliable values for the discriminative power of each BP_{log} the DSLVQ method was repeated 100 times. For each run of the DSLVQ classification, 50% of the features were randomly selected and used for the training and the remaining 50% were kept to test the classifier. The classifier was fine-tuned with DSLVQ type C training (10000 iterations). The learning rate α_t decreased during this training from an initial value of $\alpha_t = 0.05$ to $\alpha_t = 0$. The DSLVQ relevance values were updated with the learning rate $\lambda_t = \alpha_t/10$.

DSLVQ was applied to the last session of the cue-based feedback training data (4 runs with 30 trials each; 10 per class). From each trial at two time points t_1 and $t_2 = t_1 +$ 1.0 second around the best on-line classification accuracy during motor imagery, ninety-three BP_{log} features were extracted; thirty-one for each bipolar EEG channel between 6–36 Hz with a bandwidth of 2 Hz (1 Hz overlap). Motor imagery tasks were pooled together and labeled as class IC (intentional-control). For class NC (noncontrol), in contrast, BP_{log} were extracted at time of cue onset ($t = 3.0$ seconds, see Figure 2(b)). This time was selected to prevent the classifier to detect "unspecific" MI preactivations, resulting from the "beep" presented 1 second before the cue. Additionally from the 2-minute segment of artifact free EEG, used to set up EMG detection (Figure 1(b)), in step sizes of 1-second BP_{log} features were extracted. The 6 most discriminative BP_{log} were selected and used to set up CFR_{IC}. To increase the robustness of CFR_{IC}, an additional threshold TH_{IC} was introduced which had to be exceeded (dropping below) for a subject-specific transition time t_T before a switch between NC and IC (IC and NC) occurred. Increasing or decreasing the value

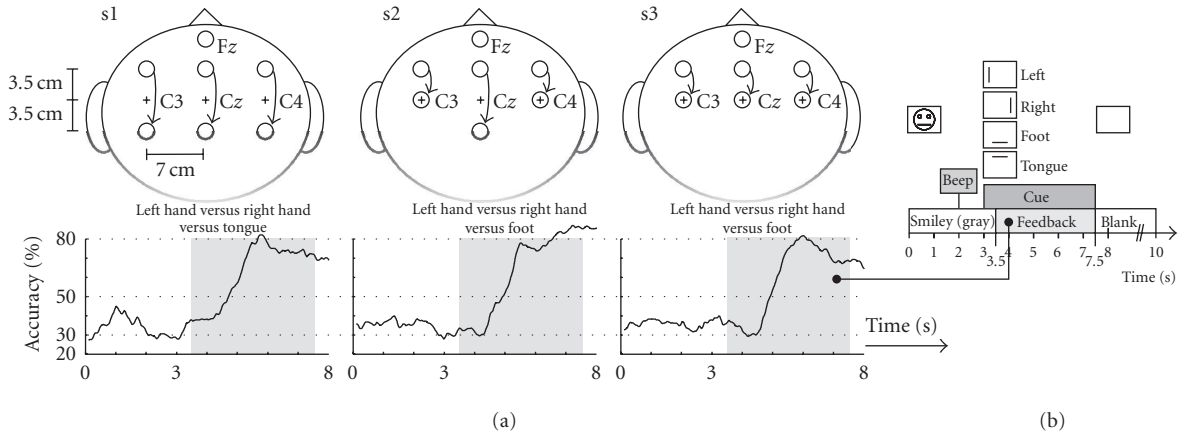

Figure 2: (a) Electrode positions used for self-paced feedback experiments. Fz served as ground. The curves show the average classification accuracy (40 trials/class) of the specified motor imagery tasks. (b) Timing of the cue-based training paradigm. The task was to move a smiley-shaped cursor into the direction indicated by the cue.

of the threshold was synonymous with shifting the optimal LDA decision border. In doing so, at least to some extent, nonstationary changes of the EEG (from session to session) could be adapted.

2.4. Navigating the freespace virtual environment

The "freeSpace" virtual environment (VE) was developed as a platform-independent application based on the Qt application framework (Trolltech, Oslo, Norway) and intended as a test platform for self-paced BCIs. The virtual park consists of a flat meadow, several hedges, and a tree positioned in the middle (Figure 3(a)). Like in computer games, coins were positioned on fixed locations inside the park and users had the task of navigating through the virtual world and collecting them. The coins were automatically picked by contact; hedges or the tree had to be bypassed (collision detection). Four commands were implemented. These are "turn left," "turn right," "move forward," and "no operation." The user datagram protocol (UDP) was used to realize the communication between BCI and VE. For easier orientation, a map showing the current position was presented (Figure 3(a)). The VE was presented in first-person-view perspective on a conventional computer screen (Figure 3(b)). However, given that proper hardware is available, also a stereoscopic 3D representation is possible (Figure 3(c)). In order to provide feedback on received navigation commands and upcoming state switches as fast as possible, during the transition time t_T the command arrows were steadily growing (NC to IC) or shrinking (IC to NC), before performing the requested action.

By autonomously selecting the navigation commands, subjects had the task of picking up the three coins within a three-minute time limit. For each run the starting position inside the VE was altered. No instructions on how to reach the coins were given to the subjects. Two sessions with 3 feedback training runs were recorded. Each session started with free-training lasting about 20 minutes. At the beginning of this period the subject-specific threshold TH_{IC} and transition time t_T (maximum value 1 second) were identified empirically according to the statements of the subjects and fixed for the rest of the session. At the end of each session subjects were interviewed on the subjective-experienced classification performance. The BCI and the VE were running on different computers.

For more details on user training, self-paced BCI sytem set-up and evaluation of the freeSpace VE see [21].

2.5. Operating Google Earth-Brainloop

The Brainloop interface for Google Earth was implemented in Java (Sun Microsystems Inc., Santa Clara, CA, USA). The communication with the BCI was realized by means of the UDP protocol; the communication with Google Earth by using the TCP/IP protocol. A multilevel selection procedure was created to access the whole functional range of Google Earth. Figure 4(a) shows a screen shot of the interface. The user was represented by an icon positioned in the center of the display. The commands at the user's disposal were placed around this icon and could be selected by moving the feedback cursor into the desired direction. The three main commands "scroll," "select" and "back" were selected by moving the cursor to the left, right, or down, respectively. After each command Google Earth's virtual camera moved to the corresponding position. By combining the cursor movement down with left or right, the commands "show borders" and "show cities" were activated (Figure 4(b)). During the transition time t_T the feedback cursor was moving towards the desired control command (NC to IC) or back to the user icon presented in the middle of the screen (IC to NC). Once the feedback cursor was close to the command, this was highlighted and accepted. Figure 4(c) summarizes the four hierarchically arranged selection levels. Levels 1 to 3 were needed to select the continent, the continental area and the country. The scroll bar at level 4 contained commands for the virtual camera ("scan," "move," "pan," "tilt," and "zoom"). For this level also the assignment of the commands was changed (see Figure 4(b)). Every selection was

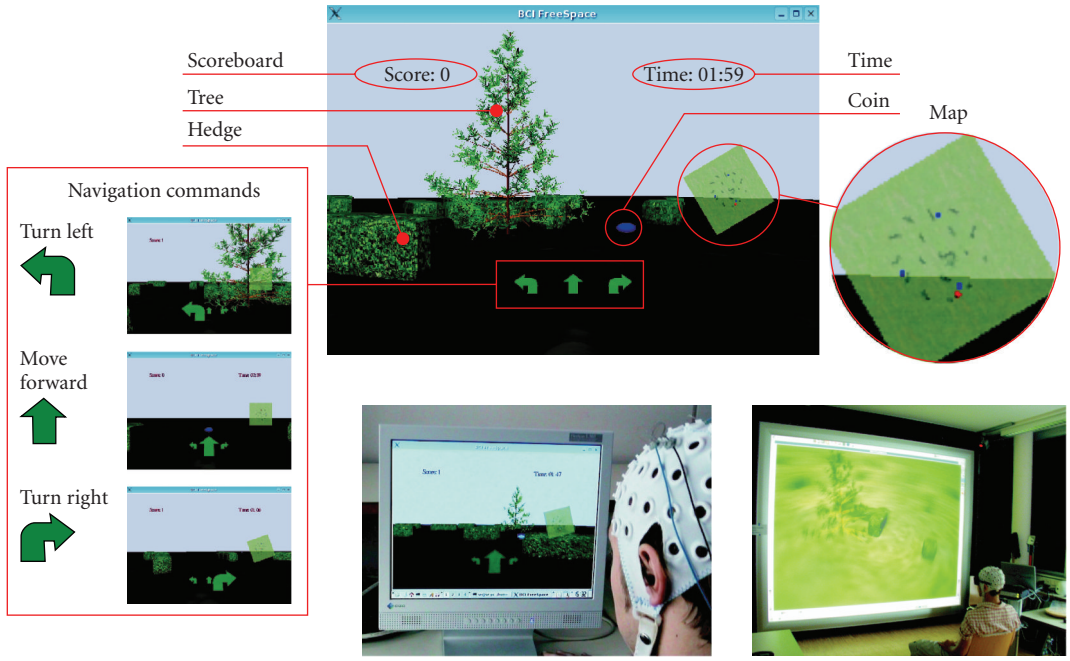

FIGURE 3: (a) The freeSpace virtual environment. The screenshot shows the tree, some hedges, and a coin to collect. In the lower mid part of the screen, the navigation commands are shown. The number of collected coins and the elapsed time are presented in the upper left and right sides, respectively. For orientation, a map showing the current position (red dot) was presented. (b) Presentation of the VE on a conventional computer screen. (c) Stereoscopic visualization of the VE on a projection wall (perspective point of view).

made by scrolling through the available options and picking the highlighted one. While the "scroll" command was selected, the options were scrolling at a speed of approximately 2 items/s from the right to the left. For more details on the interface please see [22].

Subject s2 took part in self-paced on-line experiments. Figure 4(b) summarizes the MI tasks used to operate the feedback cursor. After three consecutive days of training (about 2.5 hours/day) on December 14, 2006, a media performance lasting about 40 minutes was presented to the audience. Figure 4(d) shows pictures taken during the Brainloop media performance. Because it is very difficult to compute self-paced BCI performance measures, after the media performance the subject self-reported on the BCI classification accuracy.

3. RESULTS

The percentage of EEG samples classified as EMG artifact during the training procedure was less than 0.9% for each subject. Figure 5(a) shows example EMG detections. The method works well for minor (upper plot) as well as for massive muscle activity (lower plot). The power density spectrum for each channel and motor imagery task is summarized in Figure 6. The power density spectrum was computed by averaging the power spectrum of the forty motor imagery trials for each class recorded during the last cue-based feedback session. Before computing the discrete Fourier transform of the 4-second motor imagery segment (see Figure 2(b)) a hamming window was applied. The spectra show clear peaks in the upper-alpha (10–12 Hz) and upper-beta bands (20–25 Hz).

The EOG reduction method is able to reduce about 80% of EOG artifacts [18]. The example in Figure 5(b) shows clearly that eye blinks were removed from the EEG.

The relevant frequency components for the discrimination between IC and NC identified for each subject by DSLVQ are summarized in Table 1. The therewith trained LDA classifiers achieved classification accuracies (10×10 cross-validation) of 77%, 84%, and 78% for subjects s1, s2, and s3, respectively [21].

Each subject successfully navigated through the freeSpace VE and collected coins. Subjects s2 and s3 succeeded in collecting all three items within the 3-minute time limit. Subject s1 was able to collect only 2 of the 3 coins. While s1 and s2 were able to improve their performance (reflected in the covered distance and number of collected items), the results of session two for s3 were poor compared to the first. The best performance for each subject out of the 6 runs recorded on 2 different days is shown in Figure 6. The covered distances (Figure 6(a)), however, show that subjects (depending also on the ability to control the BCI) choose different ways to collect the coins. The corresponding distribution of the BCI classification in Figure 6(b) show that each class occurred during the experiment. Interviews with the subjects confirmed that all 3 motor imagery mental states as well as NC were deliberately used for navigation. The "no operation" command (non-control state) was necessary during

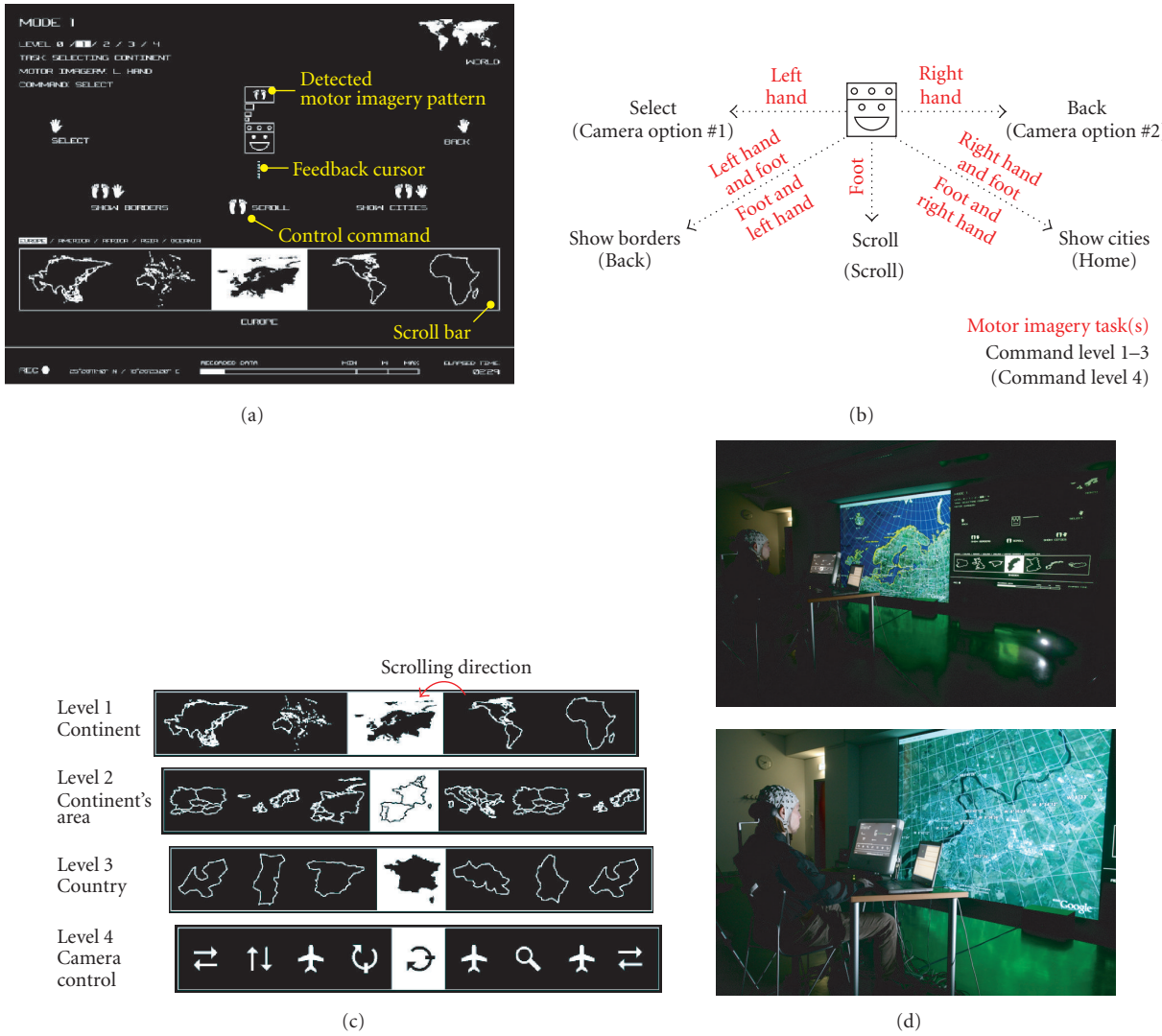

FIGURE 4: (a) Screenshot of the "Brainloop" interface. The upper part of the screen was used to select the command. The available options were presented in a scroll bar in the lower part of the screen. (b) Available commands for operating Google Earth and used motor imagery tasks. (c) The four levels of selections. (d). Photographs of the "Brainloop" performance.

non-MI related mental activity, like, for example, orientation or routing, or whenever subjects needed a break.

The Brainloop interface is a very intuitive graphical user interface for Google Earth. The developed selection procedure enables users to quickly pick a country and to manipulate the virtual camera. Although audience was present during the performance, subject s2 succeeded in operating Google Earth. After the performance, the subject stated that most of the time the BCI was correctly detecting the intended motor imagery patterns as well as the non-control state.

4. DISCUSSION

The presented BCI is able to automatically reduce EOG artifacts, detect EMG activity, and support the self-paced operation mode. Each of these issues is important for the realization of practical BCI systems. Additionally only three bipolar channels were used which makes the system easy to use and inexpensive compared to a system with more channels.

The proposed EOG reduction and EMG detection methods are simple to implement, computationally not demanding, and can easily be adapted at the beginning of each feedback session. One still open issue, however, is the long-term stability of the methods. Both methods are part of the BioSig open source toolbox [23] and freely available under the GNU General Public License.

Since the proposed EOG reduction method modifies the recorded EEG, an analysis of the influence on the classification accuracy was performed. DSLVQ was applied to the EEG (cue-based training) before and after EOG reduction. The computed DSLVQ feature relevance showed that the same frequency components are relevant before and after applying the EOG reduction method. A statistical analysis of

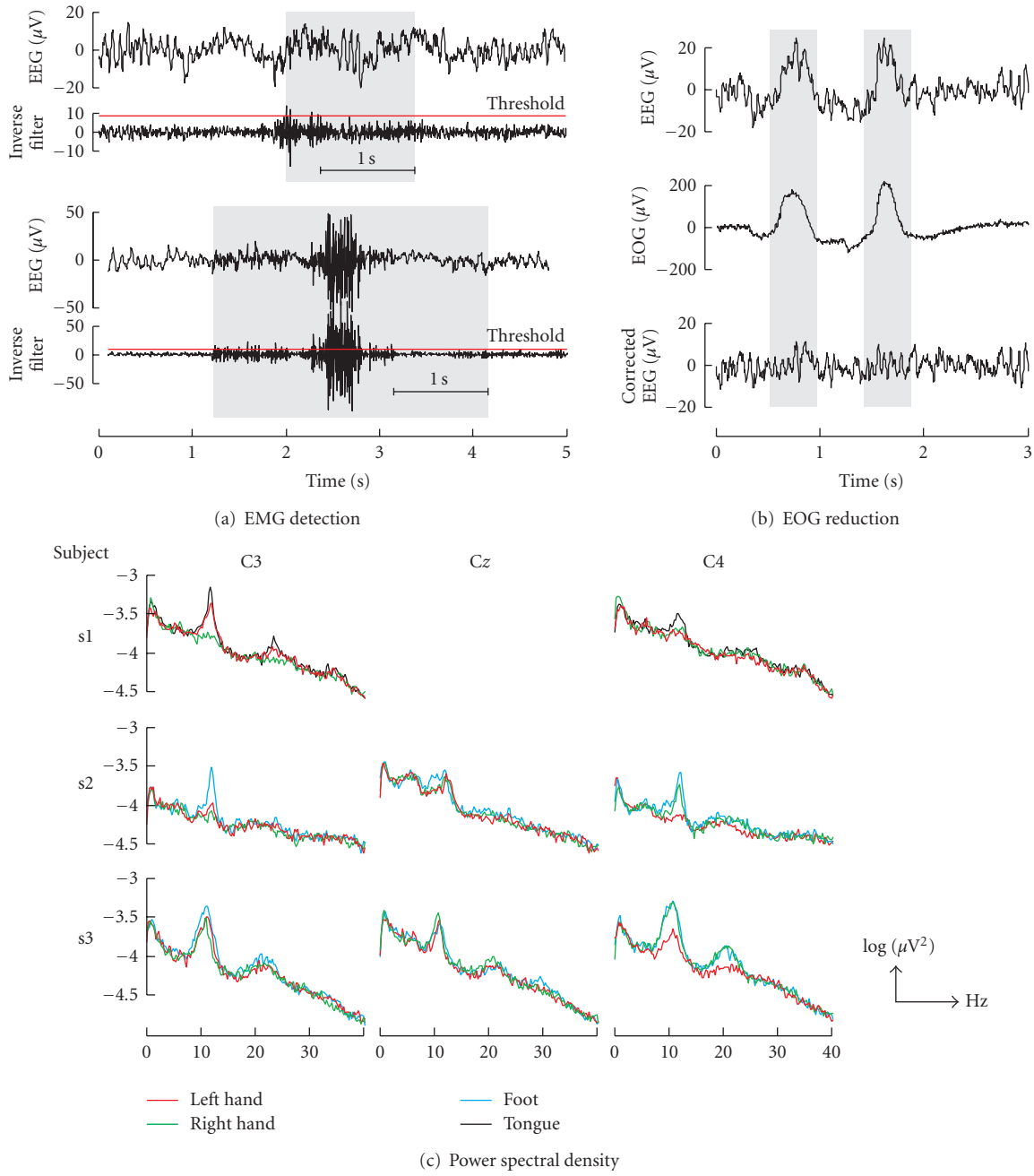

Figure 5: (a) EMG detection example. The EEG and the inverse filter output are shown for minor (upper part) and massive (lower part) EMG artifacts. (b) Example of EOG reduction. The recorded EEG, EOG channel #2, and the corrected EEG are presented in the upper, middle, and lower parts, respectively. (c) Logarithmic power density spectra of cue-based motor imagery trials (40 each) after 4 hours of feedback training.

the DSLVQ classification results revealed no significant difference ($P < 0.05$). Since the frequency range of EOG artifacts is maximal at frequencies below 4 Hz (we were looking in the range 8–30 Hz) and prominent over anterior head regions [14], this result was not surprising.

Although both methods have no direct impact on the system classification performance, the robustness of the BCI could be increased. Artifacts did not cause wrong system responses, but were either reduced or detected and reported back. After artifact detection different options are possible. These include a "pause-mode" (or "freeze-mode") or to "reset" the system to the initial status. In both cases the BCI suspends execution. While in the former case, after a predefined period of artifact-free EEG, the BCI resumes working, in the latter case, the system resets itself. The choice, however,

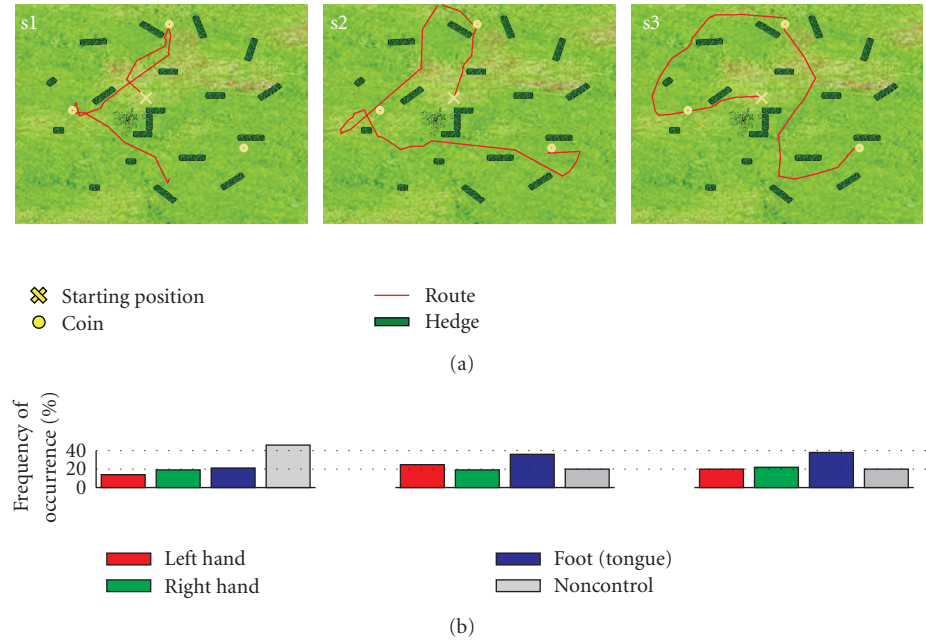

Figure 6: (a) Map of the freeSpace virtual environment showing the best performance (covered distance) for each subject. (b) Frequencies of occurrence of the detected motor-imagery tasks (selected navigation commands).

Table 1: Relevant frequency components in Hz identified by DSLVQ for the discrimination of intentional control (IC) and the non-control state (NC).

Subject	C3	Cz	C4
s1	12–14, 15–17, 20–22, 25–27	9–11, 21–23	—
s2	12–14, 19–21, 27–29	9–11, 11–13	21–23
s3	8–10, 16–18	8–10	15–17, 24–26

primarily depends on the robustness of the selected signal processing method in the presence of artifacts.

Even though very simple feature extraction and classification methods were used to create a self-paced system, subjects reported they were quite satisfied with the BCI classification performance. An open question is determining the optimum detection threshold TH_{IC} and the transition time t_T. We used an empirical approach and changed the parameters according to the statements of the subjects, which is only a suboptimum solution.

For cue-based systems a variety of different performance measures exist. Since only a few groups investigate asynchronous or self-paced systems [24–26], appropriate benchmark tests and performance measures are not available yet [27].

The "freeSpace" paradigm was introduced because no instructions, except the overall aim to collect coins, had to be given to the subjects. The paradigm is motivating, entertaining and most important there is an endless number of ways to collect the coins.

The Brainloop interface provides a new way to interact with complex applications like Google Earth. By remapping commands and options the interface can be customized also for other applications. Self-report was selected to characterize BCI performance, since performance can be difficult to measure objectively with asynchronous BCIs. Interesting is that there was no need to adapt the detection threshold TH_{IC} and the transition time t_T. The values fixed during the last freeSpace session were used.

The results of the experiments show that subjects learned to successfully use applications by autonomously switching between different mental states and thereby operating the self-paced Graz-BCI.

ACKNOWLEDGMENTS

This work is supported by the "Fonds zur Förderung der Wissenschaftlichen Forschung" in Austria, project P16326-BO2 and funded in part by the EU research Project no. PRESENCCIA IST 2006-27731. The authors would also like to thank Suncica Hermansson, Brane Zorman, Seppo Gründler, and Markus Rapp for helping to realize the Brainloop interface, and Brendan Allison for proofreading the manuscript.

REFERENCES

[1] J. Wolpaw, N. Birbaumer, D. McFarland, G. Pfurtscheller, and T. Vaughan, "Brain-computer interfaces for communication and control," *Clinical Neurophysiology*, vol. 113, no. 6, pp. 767–791, 2002.

[2] G. Pfurtscheller, C. Neuper, and N. Birbaumer, "Human brain-computer interface (BCI)," in *Motor Cortex in Voluntary Movements: A Distributed System for Distributed Functions*, A. Riehle and E. Vaadia, Eds., pp. 367–401, CRC Press, Boca Raton, Fla, USA, 2005.

[3] N. Birbaumer, "Brain-computer-interface research: coming of age," *Clinical Neurophysiology*, vol. 117, no. 3, pp. 479–483,

2006.

[4] B. Z. Allison, E. W. Wolpaw, and J. R. Wolpaw, "Brain-computer interface systems: progress and prospects," *Expert Review of Medical Devices*, vol. 4, no. 4, pp. 463–474, 2007.

[5] E. W. Sellers and E. Donchin, "A P300-based brain-computer interface: initial tests by ALS patients," *Clinical Neurophysiology*, vol. 117, no. 3, pp. 538–548, 2006.

[6] F. Piccione, F. Giorgi, P. Tonin, et al., "P300-based brain computer interface: reliability and performance in healthy and paralysed participants," *Clinical Neurophysiology*, vol. 117, no. 3, pp. 531–537, 2006.

[7] N. Birbaumer, A. Kübler, N. Ghanayim, et al., "The thought translation device (TTD) for completely paralyzed patients," *IEEE Transactions on Rehabilitation Engineering*, vol. 8, no. 2, pp. 190–193, 2000.

[8] G. Pfurtscheller, G. R. Müller-Putz, J. Pfurtscheller, H. J. Gerner, and R. Rupp, "'Thought'—control of functional electrical stimulation to restore hand grasp in a patient with tetraplegia," *Neuroscience Letters*, vol. 351, no. 1, pp. 33–36, 2003.

[9] G. R. Müller-Putz, R. Scherer, G. Pfurtscheller, and R. Rupp, "EEG-based neuroprosthesis control: a step towards clinical practice," *Neuroscience Letters*, vol. 382, no. 1-2, pp. 169–174, 2005.

[10] C. Neuper, G. R. Müller-Putz, A. Kübler, N. Birbaumer, and G. Pfurtscheller, "Clinical application of an EEG-based brain-computer interface: a case study in a patient with severe motor impairment," *Clinical Neurophysiology*, vol. 114, no. 3, pp. 399–409, 2003.

[11] C. Neuper, G. R. Müller-Putz, R. Scherer, and G. Pfurtscheller, "Motor imagery and EEG-based control of spelling devices and neuroprostheses," *Progress in Brain Research*, vol. 159, pp. 393–409, 2006.

[12] F. Cincotti, L. Bianchi, G. Birch, et al., "BCI Meeting 2005-Workshop on technology: hardware and software," *IEEE Transactions on Neural Systems and Rehabilitation Engineering*, vol. 14, no. 2, pp. 128–131, 2006.

[13] G. Pfurtscheller, G. R. Müller-Putz, A. Schlögl, et al., "15 years of BCI research at Graz university of technology: current projects," *IEEE Transactions on Neural Systems and Rehabilitation Engineering*, vol. 14, no. 2, pp. 205–210, 2006.

[14] M. Fatourechi, A. Bashashati, R. K. Ward, and G. E. Birch, "EMG and EOG artifacts in brain computer interface systems: a survey," *Clinical Neurophysiology*, vol. 118, no. 3, pp. 480–494, 2007.

[15] D. J. McFarland, W. A. Sarnacki, T. M. Vaughan, and J. R. Wolpaw, "Brain-computer interface (BCI) operation: signal and noise during early training sessions," *Clinical Neurophysiology*, vol. 116, no. 1, pp. 56–62, 2005.

[16] S. G. Mason, A. Bashashati, M. Fatourechi, K. F. Navarro, and G. E. Birch, "A comprehensive survey of brain interface technology designs," *Annals of Biomedical Engineering*, vol. 35, no. 2, pp. 137–169, 2007.

[17] A. Schlögl, *The Electroencephalogram and the Adaptive Autoregressive Model: Theory and Applications*, Shaker, Aachen, Germany, 2000.

[18] A. Schlögl, C. Keinrath, D. Zimmermann, R. Scherer, R. Leeb, and G. Pfurtscheller, "A fully automated correction method of EOG artifacts in EEG recordings," *Clinical Neurophysiology*, vol. 118, no. 1, pp. 98–104, 2007.

[19] M. Pregenzer and G. Pfurtscheller, "Frequency component selection for an EEG-based brain to computer interface," *IEEE Transactions on Rehabilitation Engineering*, vol. 7, no. 4, pp. 413–419, 1999.

[20] M. Pregenzer, *DSLVQ*, Ph.D. thesis, Graz University of Technology, Graz, Austria, 1998.

[21] R. Scherer, F. Lee, A. Schlögl, R. Leeb, H. Bischof, and G. Pfurtscheller, "Towards self-paced brain computer communication: navigation through virtual worlds," to appear in *IEEE Transactions on Biomedical Engineering*.

[22] D. Grassi, "Brainloop media performance," June 2007, http://www.aksioma.org/brainloop/index.html.

[23] A. Schlögl, "BioSig—an open source software package for biomedical signal processing," http://biosig.sourceforge.net/.

[24] R. Scherer, G. R. Müller-Putz, C. Neuper, B. Graimann, and G. Pfurtscheller, "An asynchronously controlled EEG-based virtual keyboard: improvement of the spelling rate," *IEEE Transactions on Biomedical Engineering*, vol. 51, no. 6, pp. 979–984, 2004.

[25] J. D. R. Millán and J. Mouriño, "Asynchronous BCI and local neural classifiers: an overview of the adaptive brain interface project," *IEEE Transactions on Neural Systems and Rehabilitation Engineering*, vol. 11, no. 2, pp. 159–161, 2003.

[26] J. Borisoff, S. Mason, A. Bashashati, and G. Birch, "Brain-computer interface design for asynchronous control applications: improvements to the LF-ASD asynchronous brain switch," *IEEE Transactions on Biomedical Engineering*, vol. 51, no. 6, pp. 985–992, 2004.

[27] S. Mason, J. Kronegg, J. Huggins, M. Fatourechi, and A. Schlögl, "Evaluating the performance of self-paced brain computer interface technology," Tech. Rep., Neil Squire Society, Vancouver, Canada, 2006. http://www.bci-info.tugraz.at/Research_Info/documents/articles/.

Hindawi Publishing Corporation
Computational Intelligence and Neuroscience
Volume 2007, Article ID 37695, 14 pages
doi:10.1155/2007/37695

Research Article

Temporal and Spatial Features of Single-Trial EEG for Brain-Computer Interface

Qibin Zhao and Liqing Zhang

Department of Computer Science and Engineering, Shanghai Jiao Tong University, Shanghai 200240, China

Correspondence should be addressed to Qibin Zhao, qbzhao@sjtu.edu.cn

Received 31 December 2006; Revised 23 February 2007; Accepted 18 June 2007

Recommended by Fabio Babiloni

Brain-computer interface (BCI) systems create a novel communication channel from the brain to an output device bypassing conventional motor output pathways of nerves and muscles. Modern BCI technology is essentially based on techniques for the classification of single-trial brain signals. With respect to the topographic patterns of brain rhythm modulations, the common spatial patterns (CSPs) algorithm has been proven to be very useful to produce subject-specific and discriminative spatial filters; but it didn't consider temporal structures of event-related potentials which may be very important for single-trial EEG classification. In this paper, we propose a new framework of feature extraction for classification of hand movement imagery EEG. Computer simulations on real experimental data indicate that independent residual analysis (IRA) method can provide efficient temporal features. Combining IRA features with the CSP method, we obtain the optimal spatial and temporal features with which we achieve the best classification rate. The high classification rate indicates that the proposed method is promising for an EEG-based brain-computer interface.

1. INTRODUCTION

Brain-computer interfaces (BCIs) provide new communication and control channels that do not depend on the brain's normal output channels of peripheral nerves and muscles [1]. The BCI research aims at the development of a system that allows direct control of a computer application or a neuroprosthesis, solely by human intentions reflected by certain brain signals [2]. We mainly focus on noninvasive, electroencephalogram- (EEG-) based BCI systems which can be used as tools of communication for the disabled or for healthy subjects who might be interested in exploring a new path of human-machine interfacing.

EEG-based BCI has received increasing attention recently [3–5]. The EEG allows the observation of gross electrical fields of the brain and reflects changes in neural mass activity associated with various mental processes. A physically disabled person with controlling his thoughts has potential to use the mental processes for communication. The feasibility of this communication depends on the extent to which the EEGs associated with these mental processes can be reliably recognized automatically. The electrophysiological phenomena investigated most in the quest for an automatic discrimination of mental states are event-related potential (EP) [3], and localized changes in spectral power of spontaneous EEG related to sensorimotor processes [4, 5]. For noninvasive BCI systems that based on discrimination of voluntarily induced brain states, some approaches have been proposed. The Tübingen thought translation device (TTD) [6] enables subjects to learn self-regulation of slow cortical potentials (SCP), that is, electro cortical positivity and negativity. After training in experiments with vertical cursor movement as feedback navigated by the SCP from central scalp position, patients are able to generate binary decisions in a 4–6 seconds pace with an accuracy of up to 85%. Users of the Albany BCI system [7] are able to control a cursor movement by their oscillatory brain activity into one of two or four possible targets on the computer screen and achieve over 90% hit rates after adapting to the system during many feedback sessions with a selection rate of 4-5 seconds in the binary decision problem. Based on event-related modulations of the pericentral μ- or β-rhythms of sensorimotor cortices (with a focus on motor

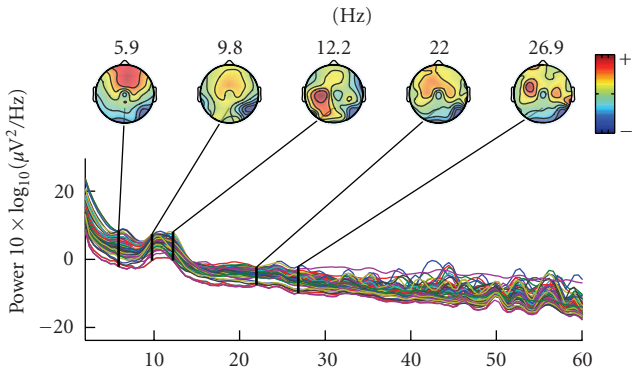

FIGURE 1: Channel spectra and associated topographical maps during hand movement imagery.

preparation and imagination), the Graz BCI system achieved accuracies of over 96% in a ternary classification task with a trial duration of 8 seconds by evaluation of adaptive autoregressive (AAR) models. Note that there are other BCI systems which rely on stimulus/response paradigms, for example, P300, see [2] for an overview. In [8, 9], the common spatial subspace decomposition (CSSD) method was proposed for classification of finger movement and BCI competition 2003-data set IV. The common spatial patterns (CSPs) approach [10, 11] was suggested to be used in the BCI context. This algorithm extracts event-related desynchronization (ERD), that is, event-related attenuations in some frequency bands, for example, μ/β-rhythm. Further in [12], a first multiclass extension of CSP was presented based on pairwise classification and voting. In this paper, we further extend this approach for extracting both temporal and spatial features of EEG recordings of imaginary left- and right-hand movements. In order to find better features for classification, we use temporal independent component analysis (i.e., IRA) [13] and CSP together for feature extraction. The rest of the paper is organized as follow. In Section 2, we introduce the neurophysiological background about BCI. In Section 3, temporal independent component analysis method is derived in detail. In Section 4, we elaborate the whole procedure of EEG processing including data acquisition, preprocessing, feature extraction, and classification. Finally, classification results are presented and compared with other algorithms.

2. NEUROPHYSIOLOGICAL BACKGROUND

Macroscopic brain activity during resting wakefulness contains distinct "idle" rhythms located over various brain areas, for example, the μ-rhythm can be measured over the pericentral sensorimotor cortices in the scalp EEG, usually with a frequency of about 10 Hz. Furthermore, there also exists β-rhythm around 20 Hz over the human motor cortex. Therefore, 10 Hz μ-rhythm and 20 Hz β-rhythm usually coexist in noninvasive scalp EEG recordings (see Figure 1).

As described in [14], each part of the human body exists a corresponding region in the primary motor and primary somatosensory area of the neocortex. The "mapping" from the body part to the respective brain areas approximately preserves topography, that is, neighboring parts of the body are represented in neighboring parts of the cortex. For example, the left hand is represented lateralized on the right hemisphere and the right hand almost symmetrically on the left hemisphere. The temporal amplitude fluctuations of these local rhythms reflect variable functional states of the underlying neuronal cortical networks and can be used for brain-computer interfacing. In particular, the pericentral μ- and β-rhythms are diminished, or even almost completely blocked by movements of the corresponding body part. Blocking effects are visible bilateral but with a clear predominance contralateral to the moved limb. This attenuation of brain rhythms is termed event-related desynchronization [15].

Since a focal ERD can be observed over the motor and/or sensory cortex even when a subject is only imagining a movement or sensation in the specific limb, this feature can be used well for BCI control: the discrimination of the imagination of movements of left hand versus right hand can be based on the somatotopic arrangement of the attenuation of the μ- and/or β-rhythms. Figure 2 shows the average scalp spectra distribution of left hand versus right hand in one trial. The μ- and/or β-rhythms appeared in both left- and right-hand trials, it is difficult to distinguish them only from frequency spectra of single trial; but they have different characteristics of temporal amplitude fluctuations and spatial distribution (see Figure 3). Therefore, more advanced feature extraction methods should be developed to extract the low diversification of ERD. The CSP algorithm is an effective way to improve the classification performance. There still exists another type of features different from the ERD reflecting imagined or intended movements, the movement-related potentials (MRP), denoting a negative DC shift of the EEG signals in the respective cortical regions. This combination strategy utilizes both temporal and spatial characteristics of EEG data and is able to greatly enhance classification performance in offline studies. In this paper, we focus only on improving the ERD-based classification.

3. TEMPORAL INDEPENDENT COMPONENT ANALYSIS

Independent component analysis (ICA) has been accepted as a standard data analysis tool in the neural network and signal processing societies. However, there still exist a number of problems in dealing with real world data using ICA. In many applications, the problem usually does not satisfy the basic assumptions of ICA model. One typical application of ICA is electroencephalographic (EEG) data analysis. EEG usually is very noisy and its mixing model is time-variable. One challenging problem is to extract potential source from single-trial EEG measurements in a very short time window. Still another problem is that ICA generally extract spatial mutual independent source, it did not consider the temporal structures of source signals and then lost the temporal information. Based on that, we suggest to explore both the high-order statistics and temporal structures of source signals. The main idea is to analyze the mutual independence of the residual signals.

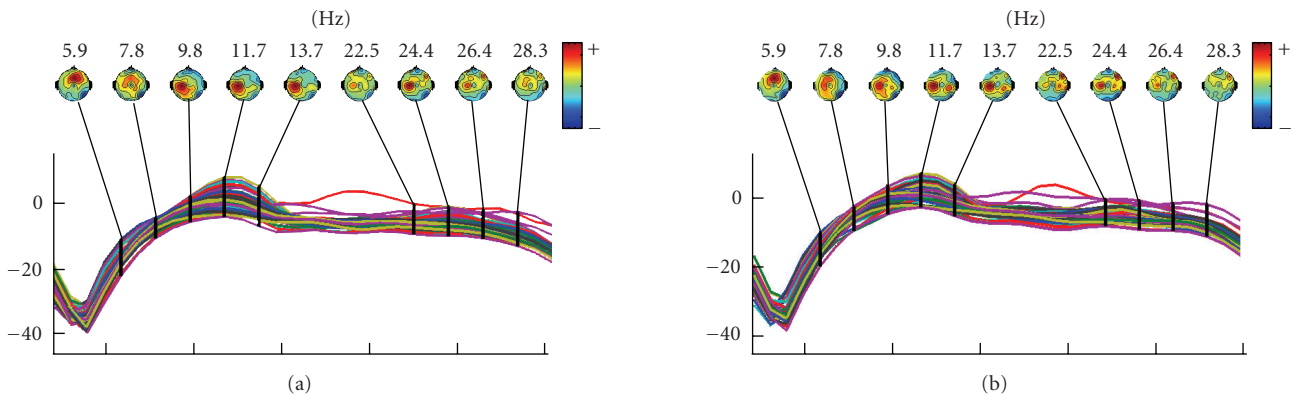

Figure 2: (a) Channels spectra and associated topographical during left-hand movement imagery. (b) Channels spectra and associated topographical during right-hand movement imagery.

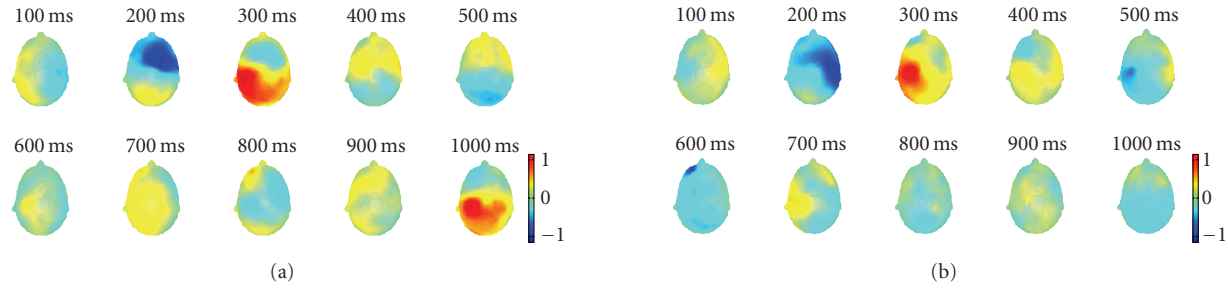

Figure 3: Different temporal amplitude fluctuations and spatial distribution during left- and right-hand movement imagery. (a) A series of 3D scalp maps representing potential distributions at a selected series of time points during left-hand movement imagery. (b) A series of 3D scalp maps representing potential distributions at a selected series of time points during right-hand movement imagery.

3.1. Formulation

Assume that $\mathbf{s}(k) = [s_1(k), s_2(k), \ldots, s_N(k)]$ are mutually spatially independent source signals, of which each temporally correlated with zero mean. Suppose that source $s_i(k)$ is modelled by a stationary AR model,

$$s_i(k) = \sum_{p=1}^{N} a_p^i s_i(k-p) + \varepsilon_i(k), \tag{1}$$

where N is the degree of the AR model and $\varepsilon_i(k)$ is zero-mean, independently and identically distributed (i.e., white) time series called the residual. For the sake of simplicity, we use the notation $A_i(z) = 1 - \sum_{p=1}^{N} a_p^i z^{-p}$, z is the z-transform variable. Since in the blind separation setting the source signals are unknown, we need to impose some constraints on the linear filters. We assume that the linear filters $A_i(z)$ are minimum phase throughout this paper. Suppose that sensor signals are instantaneous mixtures of the source signals. Let $\mathbf{x}(k) = [x_1(k), \ldots, x_n(k)]^T$ be the set of linearly mixed signals,

$$\mathbf{x}(k) = \mathbf{H}\mathbf{s}(k). \tag{2}$$

Here, $\mathbf{H} = (H_{ij})$ is an $n \times n$ unknown nonsingular mixing matrix. Blind source separation problem is to find a linear transform which transforms the sensor signals into maximally mutually independent components, which are considered as the estimates of source signals. Let $\mathbf{W}$ be an $n \times n$ nonsingular matrix which transforms the observed signals $\mathbf{x}(k)$ to

$$\mathbf{y}(k) = \mathbf{W}\mathbf{x}(k). \tag{3}$$

The general solution to the blind separation problem is to find a matrix $\mathbf{W}$ such that $\mathbf{WA} = \mathbf{\Lambda P}$, where $\mathbf{\Lambda} \in \mathbf{R}^{n\times n}$ is a nonsingular diagonal matrix and $\mathbf{P} \in \mathbf{R}^{n\times n}$ is a permutation matrix.

3.2. Cost function

In this section, we introduce the mutual information of residual signals as a criterion for training the demixing matrix and temporal structure parameters. The residual independent analysis provides us a new way to explore both the temporal structures and high-order statistics of source signals. From the source model, we have $\varepsilon(k) = \mathbf{A}(z)\mathbf{s}(k)$, where $\mathbf{A}(z)$ can be estimated via the linear prediction method if the source signals $\mathbf{s}(k)$ are known. When the temporal structure $\mathbf{A}(z)$ and the demixing matrix $\mathbf{W}$ are not well estimated, the residual signals

$$\mathbf{r}(k) = (r_1(k), \ldots, r_n(k))^T = \mathbf{A}(z)\mathbf{W}\mathbf{x}(k) \tag{4}$$

are not mutually independent. Therefore, it provides us a new criterion for training the demixing model and temporal structures to make the residuals $\mathbf{r}(k)$ spatially mutually independent and temporally identically independently distributed.

Assume $q(\mathbf{r})$ is the probability density function of $\mathbf{r}$ and $q_i(r_i)$ is the marginal probability density function of r_i, $i = 1, \ldots, n$. Now we introduce the mutual information rate $I(\mathbf{r})$ between a set of stochastic processes $r_1, \ldots, r_n$ as

$$I(\mathbf{r}) = -H(\mathbf{r}) + \sum_{i=1}^{n} H(r_i), \tag{5}$$

where $H(r_i)$ and $H(\mathbf{r})$ are the entropies of random variables r_i and $\mathbf{r}$, respectively. For blind deconvolution problem, Amari et al. [16] and Pham [17] simplify the first term of cost function (5) and derive a cost function as follows:

$$\begin{aligned} l(\mathbf{W}, \mathbf{A}(z)) = &-\frac{1}{2\pi j} \oint_r \log \mid \det\left(\mathbf{A}(z)\mathbf{W}\right) \mid z^{-1} dz \\ &- \frac{1}{L} \sum_{k=1}^{L} \sum_{i=1}^{n} \log q_i(r_i(k)), \end{aligned} \tag{6}$$

where j is the imaginary unit of complex numbers, and the path integral is over the unit circle γ of the complex plane. The first term of right side of (6) is introduced to prevent the filter $\mathbf{W}$ from being singular. To simplify the cost function, we calculate the first term of the right side of (6) as follows:

$$\log \mid \det\left(\mathbf{A}(z)\mathbf{W}\right) \mid = \log \mid \det(\mathbf{W}) \mid + \log \mid \det\left(\mathbf{A}(z)\right) \mid. \tag{7}$$

Because the temporal filters $A(z)$ is causal and minimum phase, we can easily verify

$$\frac{1}{2\pi j} \oint_\gamma \log \mid \det\left(\mathbf{A}(z)\right) \mid z^{-1} dz = 0. \tag{8}$$

Now combining equations (7), (8) with (6), we obtain a simplified cost function for independent residual analysis

$$l(\mathbf{W}, \mathbf{A}(z)) = -\log\left(\mid \det(\mathbf{W}) \mid\right) - \frac{1}{L} \sum_{k=1}^{L} \sum_{i=1}^{n} \log q_i(r_i(k)). \tag{9}$$

Independent residual analysis can be formulated into the semiparametric model [18]. The probability density function q and the temporal filter $\mathbf{A}(z)$ are seen as the nuisance parameters in the semiparametric model. The demixing matrix $\mathbf{W}$ is called as the parameters of interest. The semiparametric approach suggests using an estimating function to estimate the parameter of interest, regardless of the nuisance parameters. We suggest to estimate the nuisance parameters in order to have better separating performance of the algorithm.

3.3. Conjugate gradient algorithm

In this section, we derive a learning algorithm based on the conjugate gradient descent approach for the demixing matrix. We assume that the probability density functions and the temporal filters are known for a moment during the derivation of a learning algorithm for the demixing matrix. To describe the conjugate gradient method for minimizing cost function, we need first to calculate the natural gradient

$$\nabla l(\mathbf{W}, \mathbf{A}(z)) = \left(-\mathbf{I} + \frac{1}{L} \sum_{k=1}^{L} \sum_{p=0}^{N} \mathbf{A}_p[\varphi(\mathbf{r}(k))\mathbf{y}^T(k-p)] \right)\mathbf{W}, \tag{10}$$

where $\varphi(\mathbf{r}) = (\varphi_1(r_1), \ldots, \varphi_n(r_n))^T$ is the vector of activation functions, defined by $\varphi_i(r_i) = -q_i'(r_i)/q_i(r_i)$.

Given an initial value $\mathbf{W}_0$ and $k = 1$, the conjugate gradient algorithm starts out by searching in the steepest descent direction (negative of the gradient) on the first iteration.

$$\mathbf{H}_0 = -\nabla l(\mathbf{W}_0, \mathbf{A}(z)). \tag{11}$$

Now we perform one-dimensional search algorithm to find the minimum point of the cost function $l(\mathbf{W}, \mathbf{A}(z))$

$$\mathbf{W}_k = \exp\left(t_* \mathbf{H}_{k-1} \mathbf{W}_{k-1}^{-1}\right)\mathbf{W}_{k-1}, \quad t_* = \arg\min_t l(\mathbf{W}_{k-1}(t)), \tag{12}$$

along the geodesic: $\mathbf{W}_{k-1}(t) = \exp(t_* \mathbf{H}_{k-1} \mathbf{W}_{k-1}^{-1})\mathbf{W}_{k-1}$. The new search direction $\mathbf{H}_k$ is defined by the following equation:

$$\mathbf{H}_k = -\nabla l(\mathbf{W}_k) + \gamma_k \tau \mathbf{H}_{k-1}, \tag{13}$$

where $\tau\mathbf{H}_{k-1}$ is the parallel translation from $\mathbf{W}_{k-1}$ to $\mathbf{W}_k$, that is,

$$\tau \mathbf{H}_{k-1} = \mathbf{H}_{k-1} \mathbf{W}_{k-1}^{-1} \mathbf{W}_k. \tag{14}$$

The value γ_k in (13) is evaluated by

$$\tau_k = \frac{\langle \mathbf{G}_k - \tau\mathbf{G}_{k-1}, \tau\mathbf{G}_k \rangle}{\langle \tau\mathbf{G}_{k-1}, \tau\mathbf{G}_{k-1} \rangle}. \tag{15}$$

For the geometrical structures, such as the geodesic and Riemannian metric of nonsingular matrices, refer to [19]. The conjugate gradient algorithm search the minimum point along the geodesic which produces generally faster convergence than steepest descent directions. Both theoretical analysis and computer stimulations show that the conjugate gradient algorithm has much better learning performance than the natural gradient does. Here we briefly introduce learning algorithms for adapting the nuisance parameters in the semiparametric ICA model. By using the gradient descent approach, we obtain the learning algorithm for the filter coefficients a_k^i

$$\Delta a_p^i(k) = -\eta_k' \frac{1}{L} \sum_{k=1}^{L} \varphi_i\{r_i(k)\} y_i(k-p), \tag{16}$$

where η_k' is the learning rate. For the detailed information about activation function adaptation, refer to [20].

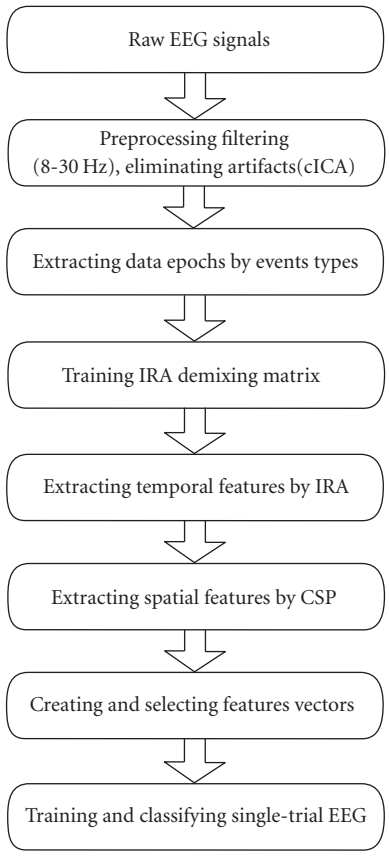

Figure 4: Flowchart of single-trial classification process.

(a) (b)

Figure 5: Visual stimulation signals in the experiment paradigm (a) At 3 second, an arrow appeared at the center of the monitor, pointing either to the right or to the left (b) After 4 seconds of imagination, cursor was moved to the next letter.

4. METHODS

Our procedure to classify the single-trial EEG evoked by left- and right-hand movement imagery is summarized in Figure 4. First, the multichannel EEG signals are preprocessed by cICA method to remove artifacts and/or noise (e.g., EOG). Next, frequency bands (8–30 Hz) are then extracted using band filters, because it mainly contains μ- and β-rhythm in somatosensory area of the neocortex (see Figure 1). In order to extract both temporal and spatial features of event-related potential, we used combination of IRA and CSP methods followed by a feature selection procedure according to mutual information of each feature and events labels. Finally, two pattern recognition methods of Support Vector Machine (SVM) and linear discrimination analysis (LDA) were carried out, respectively, to give classification results.

4.1. Data acquisition

Our purpose is to develop an online speller paradigm using hand movement imagery EEG to select the letter according to the user's intention. In this paper, we only deal with the offline analysis and test the classification performances of our proposed method. In the experimental sessions used for the present study, labeled trials of brain signals were recorded in the following way: The subjects were seated in an armchair and looked at a computer monitor placed approximately 1.5 m in front at eye level. They were asked to keep their arms and hands relaxed, and to avoid eye movements during the recordings. Each trial started with the presentation of a row of letters at the center of the monitor with cursor on one letter, followed by a short warning tone ("beep") at 2 second . At 3 second, an arrow appeared at the center of the monitor, pointing either to the right or to the left ("cue") (Figure 5(a)). Depending on the direction of the arrow, the subject was requested to imagine a movement of the right or the left hand. After 4 seconds, the subject was asked to relax by the "cue" of moving cursor to the next letter towards the direction which the subject imagined (Figure 5(a)). Then next trial began after relaxing for 2 seconds. The experiment comprised six experimental runs of 60 trials in each (30 left and 30 right trials). In the analysis, none of trials was removed for noise.

EEG was recorded referentially from 64 electrodes placed over central and related areas using NeuroScan ESI 128 system at the center for Brain-like Computing and Machine Intelligence, Shanghai Jiao Tong University. The reference electrode was mounted on the left and right mastoids and the grounding electrode on the forehead. The EEG was filtered in a 0.5–200 Hz frequency band. Horizontal and vertical Electrooculogram (HEOG,VEOG) were derived bipolarly using four electrodes. All signals, including 64 channels EEG, EOG, were sampled at 500 Hz. In this study, we use four subjects' experiment data for analysis.

4.2. Artifact detection

EEG is often contaminated with ocular and other artifacts. Many methods have been developed in the literature to remove (or attenuate) artifacts in the recordings. Temporally constrained ICA (cICA) [21] can extract signals that are statistically independent, which are constrained to maximizing the correlation with some reference signals. This constraining signal do not need to be a perfect match but it should be enough to point the algorithm in the direction of a particular IC spanning the measurement space.

We assume a set of k measured time series $\mathbf{x}(t) = [x_1(t), x_2(t), \ldots, x_k(t)]^T$ to be a linear combination of l unknown and statistically independent sources $\mathbf{s}(t) = [s_1, s_2, \ldots, s_l]^T$

(assuming $l \leq k$). A common preprocessing step is to apply a linear "whitening" transformation to the time series so that they have unit variance and are uncorrelated. The cICA is desired to extract a single source of interest and is known as one-unit ICA methods. The natural information-theoretic one-unit contrast function is the negentropy $J(\mathbf{y})$:

$$J(\mathbf{y}) = H(\mathbf{y}_{\text{gaus}}) - H(\mathbf{y}), \tag{17}$$

where $H(\cdot)$ is the differential entropy and $\mathbf{y}_{\text{gaus}}$ is a Gaussian random variable with the same variance as the output signal $\mathbf{y}$. A more flexible and reliable approximation of negentropy was introduced such that

$$J(\mathbf{y}) \approx \rho[E\{G(\mathbf{y})\} - E\{G(v)\}]^2, \tag{18}$$

where ρ is a positive constant, v is a zero mean, unit variance Gaussian random variable, and $G(\cdot)$ can be any nonquadratic function. The cICA algorithm brings in the use of a constraint which is used to obtain an output which is statistically independent from other sources and is closest to some reference signal $\mathbf{r}(t)$. The closeness constraint can be written as

$$g(\mathbf{w}) = \varepsilon(\mathbf{w}) - \xi \leq 0, \tag{19}$$

where $\mathbf{w}$ denotes a single demixing weight vector, such that $\mathbf{y} = \mathbf{w}^T\mathbf{x}$; $\varepsilon(\mathbf{w})$ represents the closeness between the estimated output and the reference $\mathbf{r}$, and ξ represents some closeness threshold. The measure of closeness can take any form, such as mean squared-error (MSE) or correlation, or any other suitable closeness measure. In our implementation of the algorithm, we use correlation as a measure of closeness such that $g(\mathbf{w})$ becomes

$$g(\mathbf{w}) = \xi - E\{\mathbf{r}(\mathbf{w}^T\mathbf{x})\} \leq 0, \tag{20}$$

where ξ now becomes the threshold that defines the lower bound of the optimum correlation. With the constraint in place, the cICA problem is formulated as follows:

$$\begin{aligned} &\text{maximize } f(\mathbf{w}) = \rho[E\{\mathbf{w}^T\mathbf{x}\} - E\{G(v)\}]^2 \\ &\text{Subject to } g(\mathbf{w}) \leq 0; \\ &\qquad h(\mathbf{w}) = E\{\mathbf{y}^2\} - 1 = 0; \\ &\qquad E\{\mathbf{r}^2\} - 1 = 0; \end{aligned} \tag{21}$$

where $f(\mathbf{w})$ denotes the one-unit ICA contrast function, $g(\mathbf{w})$ is the closeness constraint, $h(\mathbf{w})$ constrains the output $\mathbf{y}$ to have unit variance, and the reference signal $\mathbf{r}$ is also constrained to have unit variance. In [22], the problem of cICA is expressed as a constrained optimization problem which is solved through the use of an augmented Lagrangian function, where learning of the weights and Lagrange parameters is achieved through a Newton-like learning process.

In the field of EEG analysis, it is feasible to assume that some prior information on reference signals is available. In the case of artifact rejection in EEG, the morphologies and relative timings of contaminating eye-blinks or eye-movements can easily be derived in an automated fashion. The relative morphology of the reference is relatively unimportant as long as the temporal features of interest are captured; for example, the use of square "pulses" over the region of interest with a zero reference elsewhere should be reasonable as a temporal constraint when looking for transients such as eye blinks or other similar waveforms. We directly use the channel EOG as a reference function $\mathbf{r}(t)$ to serve as a temporal constraint in the cICA algorithm.

The one-unit cICA method employed for this paper extracts only the single component which is closest to the reference signal in certain sense. However, it is not necessary to assume in advance the number of actual underlying sources, and no manual selection of components is required. These are two very important points for practical implementations of ICA. Generally, the algorithm converges to the desired solution within a small number of iterations and the exact morphology of the reference signal is not too critical in obtaining a plausible solution. This makes it possible for the algorithm to be implemented as an online automatic artifact rejection system. After extracting single component which was regraded as an artifact, we can get the reconstructed noise-free EEG signals by the deflation procedure.

Before feature extraction, the EEG signals are filtered in an 8–30 Hz band. The filter used is a zero-phase forward/backward FIR filter with a width of 20 points. The frequency band was chosen because it encompasses the alpha and beta frequency bands, which have been shown to be most important for movement classification [4]. Furthermore, in a recent movement study, it was shown that a broad frequency band (e.g., 8–30 Hz) gives better classification results compared with narrow bands.

4.3. Feature extraction

The IRA is to find the independent source components which also retain temporal structures. These source components can be regarded as different source of neuron electricity and some of them may be related to the motor imagery task. The CSP method is to find a spatial filter according to class labels which maximaize the distance of different class samples. Therefore, theoretically using CSP on IRA components will get better performance than using CSP on mixing signals of EEG. First, we use IRA method to extract some components which mainly contain noise-free EEG components of interest that are of temporal structures. Then CSP will be performed on the components of IRA.

4.3.1. Temporal feature extraction by IRA

Because the temporal structures of event-related potentials may be more obvious after averaging all trials, the IRA was chosen to analyze the averaged source signal obtained from all EEG trials. After the IRA procedure, we obtained separating matrix and source signal sets (see Figure 6). The average-imagined potentials were used for training the IRA demixing matrix which would be used to project the single-trial EEG to IRA bases. The averaged trial can be seen as combination of trials and source components. The common demixing weight matrix will be found by decomposition of averaged

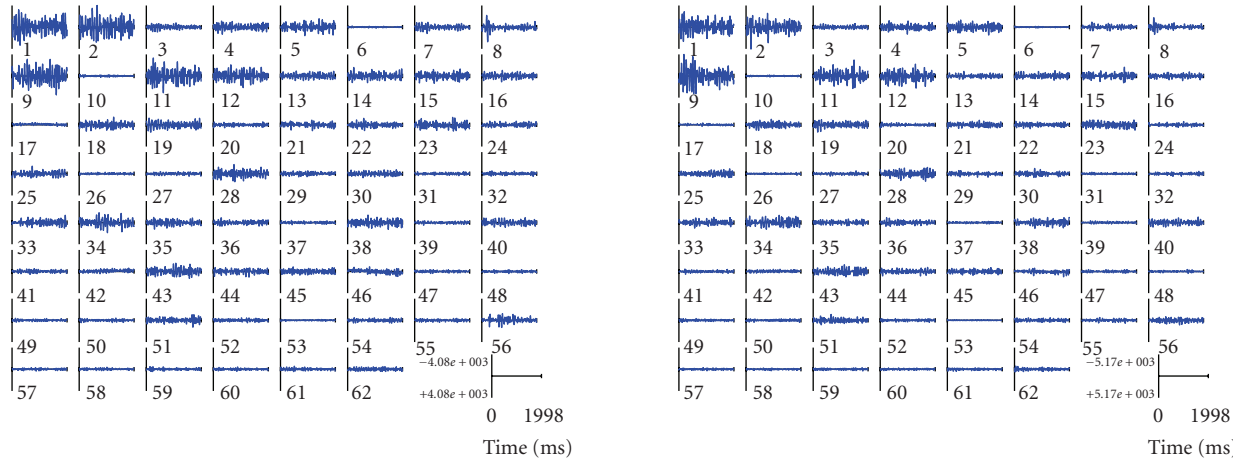

Figure 6: (a) Average 62 components during left-hand movement imagery. (b) Average 62 components during right-hand movement imagery.

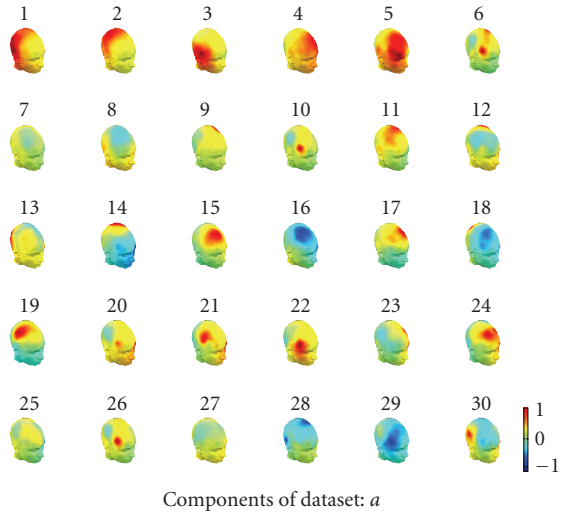

Figure 7: The scalp map projection of the IRA components in 3D head model. Components 9 and 19 were highly related to the motor imagery task, while components 1 and 2 were associated with the occipital alpha rhythm.

trial. After finding the demixing matrix W, we will use it for single-trial EEG. In this way, for each movement imagery task, the set of sources signals $\mathbf{s}(k)$ became the features themselves.

According to IRA algorithm, the components are mutually independent, each column in the mixing matrix, represents a spatial map describing the relative projection weights of the corresponding temporal components at each EEG channel. These spatial maps will hereinafter be referred to as IC spatial map. Figure 7 shows 30 IC spatial maps for 30 temporal independent components. In IRA maps, IC9 and IC19 mainly cover left and right motor field of brain which are highly related to the motor imagery task. Therefore, these components can be regarded as source signals that are most effective for classification, which are testified further by mutual information in the Section 4.4.

4.3.2. *Spatial feature extraction by common spatial patterns (CSP)*

The common spatial pattern (CSP) algorithm is very useful when calculating spatial filters for detecting ERD effects [23] and for ERD-based BCIs. Given two distributions in a high-dimensional space, the (supervised) CSP algorithm finds directions (i.e., spatial filters) that maximize variance for one class and at the same time minimize variance for the other class. After having band-pass filtered the EEG signals to the rhythms of interest, high variance reflects a strong rhythm and low variance reflects a weak (or attenuated) rhythm.

This criterion is exactly what the CSP algorithm optimizes: maximizing variance for the class of right-hand trials and at the same time minimizing variance for left-hand trials. Moreover, a series of orthogonal filters of both types can be determined. For the analysis, the raw EEG data of a single trial is represented as an $N \times T$ matrix $\mathbf{E}$, where N is the number of channels (i.e., recording electrodes) and T is the number of samples per channel. The normalized spatial covariance of the EEG can be obtained from

$$\mathbf{C} = \frac{\mathbf{E}\mathbf{E}'}{\text{trace}(\mathbf{E}\mathbf{E}')}, \tag{22}$$

where $\mathbf{E}'$ denotes the transpose of E and trace($\mathbf{x}$) is the sum of the diagonal elements of $\mathbf{x}$. For each of the two distributions to be separated (i.e., left- and right-movement imagery), the spatial covariance $\overline{\mathbf{C}}_{d\in[l,r]}$ is calculated by averaging over the trials of each group. The composite spatial covariance is given as

$$\mathbf{C}_c = \overline{\mathbf{C}}_l + \overline{\mathbf{C}}_r \tag{23}$$

$\mathbf{C}_c$ can be factored as $\mathbf{C}_c = \mathbf{U}_c \boldsymbol{\lambda}_c \mathbf{U}_c'$, where $\mathbf{U}_c$ is the matrix of eigenvectors and $\boldsymbol{\lambda}_c$ is the diagonal matrix of eigenvalues. Note that throughout this section, the eigenvalues are assumed to be sorted in descending order.

The whitening transformation

$$\mathbf{P} = \sqrt{\boldsymbol{\lambda}_c^{-1}}\mathbf{U}_c' \tag{24}$$

equalizes the variances in the space spanned by $\mathbf{U}_c$, that is, all eigenvalues of $\mathbf{P}\mathbf{C}_c\mathbf{P}'$ are equal to one. If $\overline{\mathbf{C}}_l$ and $\overline{\mathbf{C}}_r$ are transformed as

$$\mathbf{S}_l = \mathbf{P}\overline{\mathbf{C}}_l\mathbf{P}', \qquad \mathbf{S}_r = \mathbf{P}\overline{\mathbf{C}}_r\mathbf{P}' \tag{25}$$

then $\mathbf{S}_l$ and $\mathbf{S}_r$ share common eigenvectors, that is, if $\mathbf{S}_l = \mathbf{B}\boldsymbol{\lambda}_l\mathbf{B}'$, then $\mathbf{S}_r = \mathbf{B}\boldsymbol{\lambda}_r\mathbf{B}'$ and $\boldsymbol{\lambda}_l + \boldsymbol{\lambda}_r = \mathbf{I}$, where $\mathbf{I}$ is the identity matrix. Since the sum of two corresponding eigenvalues is always one, the eigenvector with largest eigenvalue for $\mathbf{S}_l$ has the smallest eigenvalue for $\mathbf{S}_r$ and vice versa. This property makes the eigenvectors $\mathbf{B}$ useful for classification of the two distributions.

With the projection matrix $\mathbf{W} = \mathbf{B}'\mathbf{P}$, the decomposition (mapping) of a trial is given as

$$\mathbf{Z} = \mathbf{W}\mathbf{E}. \tag{26}$$

The columns of $\mathbf{W}^{-1}$ are the common spatial patterns and can be seen as time-invariant EEG source distribution vectors. The signals $\mathbf{Z}_p (p = 1 \cdots 2m)$ that maximize the difference of variance of left versus right-movement imagery EEG are the ones that are associated with the largest eigenvalues λ_l and λ_r. These signals are the m first and last rows of $\mathbf{Z}$ due to the calculation of $\mathbf{W}$.

4.3.3. Visualization

We examine the changes in performance of all trials using a variety of measures and new ideas for visualization that help us to characterize the type and degree of changes seen in EEG features used for BCI classification. We used EEGLAB software package which was an open source toolbox for data visualization. Figure 8 shows components activity along trials and power spectrum. Event-related spectral perturbations (ERSPs) [24] gave each single-trial component activity time series which was transformed to a baseline-normalized spectrographic image using a moving-window average of FFT spectra computed. Intertrial coherence (ITC) is a frequency domain measure of the partial or exact synchronization of activity at a particular latency and frequency to a set of experimental events to which EEG data trials are time locked. The term "inter-trial coherence" refers to its interpretation as the event-related phase coherence (ITPC) or event-related linear coherence (ITLC) between recorded EEG activity and an event-phase indicator function. (See Figure 9.) From ERSP and ITC of components 9 and 19, we found that component 9 of left-hand events and right-hand events has different time-frequency spectral. In left-hand events, featured brief (20–25 Hz) appeared near the middle of the trial, by contrast, right-hand events appeared only near the beginning of the trial. Furthermore, the components 19 of right-hand trials has a little similar time-frequency changes as component 9 of left-hand trials.

4.4. Classification

The features used for classification are obtained by IRA and CSP. For each direction-imagined movement, the variances of feature signals suitable for discrimination are used for the construction of the classifier. The feature should maximize the difference of variance of left versus right movement imagery EEG.

$$f_p = \log\left(\frac{\operatorname{var}(Z_p)}{\sum_{i=1}^{n}\operatorname{var}(Z_i)}\right), \tag{27}$$

where $Z_p (p = 1 \cdots n)$ are the CSP components. The feature vectors f_p are used for classification. The log-transformation serves to approximate normal distribution of the data. In order to view the performance of feature extraction methods, we used PCA to reduce feature vectors' dimensions and then viewed ability of separating different classes in 2-D or 3-D space (see Figure 10).

Because some of these features are not sensitive to discriminate different types of single-trial EEG. In fact, there are even irrelevant and redundant features in the feature set. By selecting the relevant features before the classification, we could not only simplify the classifier but also improve the classification performance. The definition of relevant feature is proposed by Blum and Langley [25]. The improved mutual information feature selector (MIFS) algorithm [26] that is chosen in our system for feature selection tries to maximize $I(C; f_i \mid f_s)$, and this can be rewritten as

$$I(C; f_i, f_s) = I(C; f_s) + I(C; f_i \mid f_s). \tag{28}$$

Here $I(C; f_i \mid f_s)$ represents the remaining mutual information between class C and feature f_i for given f_s. For all the candidate features to be selected in the ideal feature selection algorithm, $I(C; f_s)$ is common and not necessary to evaluate it. So the ideal greedy algorithm now tries to find the feature that maximizes $I(C; f_i \mid f_s)$ (area 3) in (28); but, in general, to calculate $I(C; f_i \mid f_s)$, we need to divide the input feature space into lots of partitions and this is practically impossible. So we will approximate $I(C; f_i \mid f_s)$ with $I(f_s; f_i)$ and $I(C; f_i)$, which are relatively easy to calculate. The conditional mutual information $I(C; f_i \mid f_s)$ can be represented as

$$I(C; f_i \mid f_s) = I(C; f_i) - \{I(f_s; f_i) - I(f_s; f_i \mid C)\}. \tag{29}$$

The term $I(f_s; f_i \mid C)$ means the mutual information between already selected feature f_s and the candidate feature f_i for given class C. If conditioning by the class C does not change the ratio of the entropy of f_s and the mutual information between f_s and f_i, then the following relation holds:

$$I(f_s; f_i \mid C) = \frac{H(f_s \mid C)}{H(f_s)} I(f_s; f_i). \tag{30}$$

Using the equation above and (29) together, we obtain

$$I(f_i; C \mid f_s) = I(f_i; C) - \frac{I(f_s; C)}{H(f_s)} I(f_s; f_i). \tag{31}$$

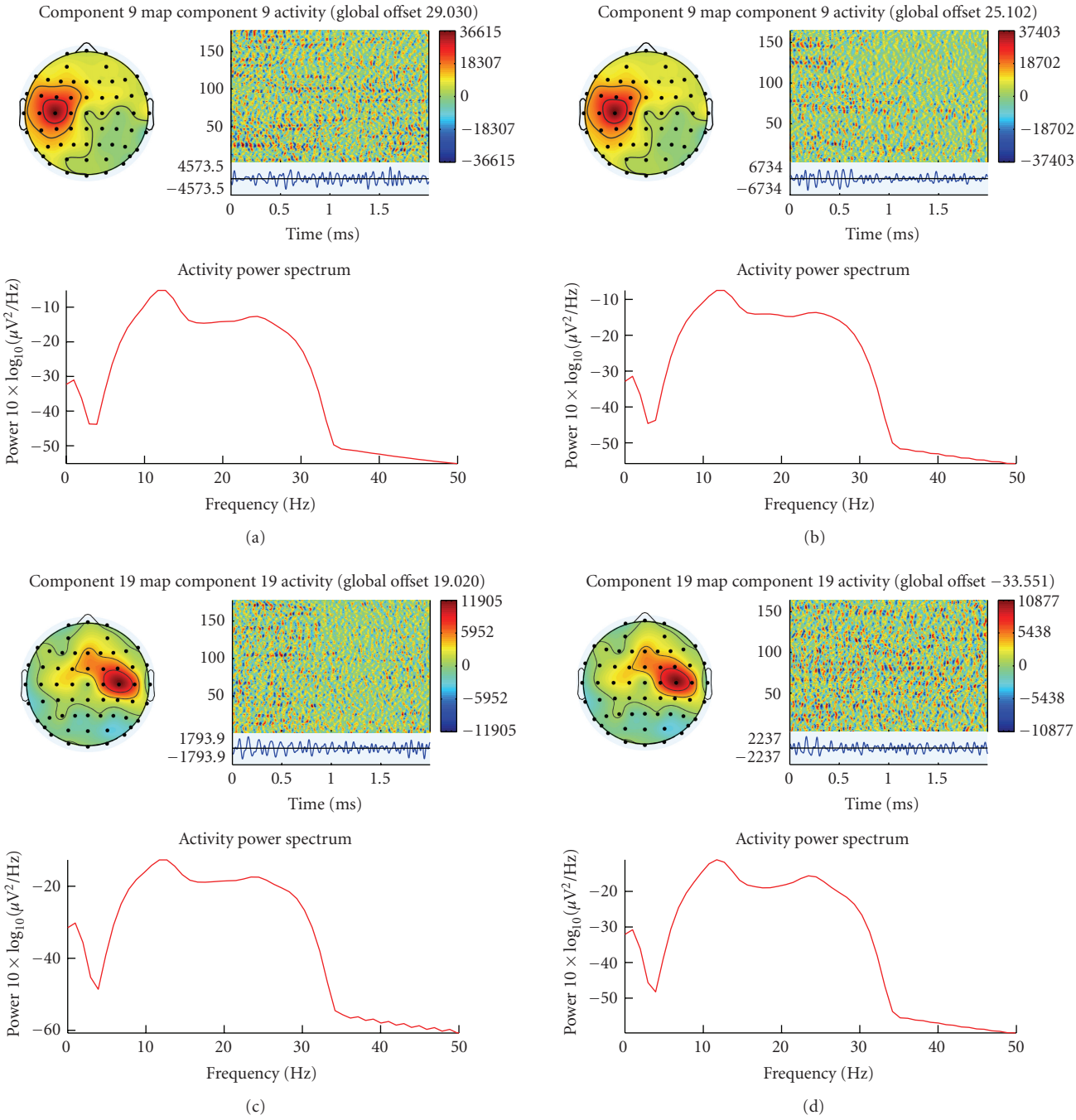

Figure 8: The properties of component which including scalp component map, component activity along trials and power spectrum. (a) Component 9 during left-hand movement imagery. (b) Component 9 during right-hand movement imagery. (c) Component 19 during left-hand movement imagery. (d) Component 19 during right-hand movement imagery. Though the similarity of power spectrum, the temporal amplitude fluctuations of component 9 are obviously different during left- and right-hand movement imagery. In (b), the amplitude has obviously attenuation for all trials while it did not appear in (a).

With this formula, the revised greedy selection algorithm is depicted as follows.

(Greedy selection) repeat until desired number of features are selected.

(a) (Computation of entropy) for all $s \in S$, compute $H(s)$ if it is not already available.

(b) (Computation of the MI between variables) for all couples of variables (f, s) with $f \in F$, $s \in S$ compute $I(f; s)$ if it is not already available.

(c) (Selection of the next feature) choose feature $f \in F$ as the one that maximizes $I(C; f) - \beta \sum_{s \in S} (I(C; s)/H(s)) I(f; s)$; set $F \leftarrow F\{f\}$, $S \leftarrow \{f\}$.

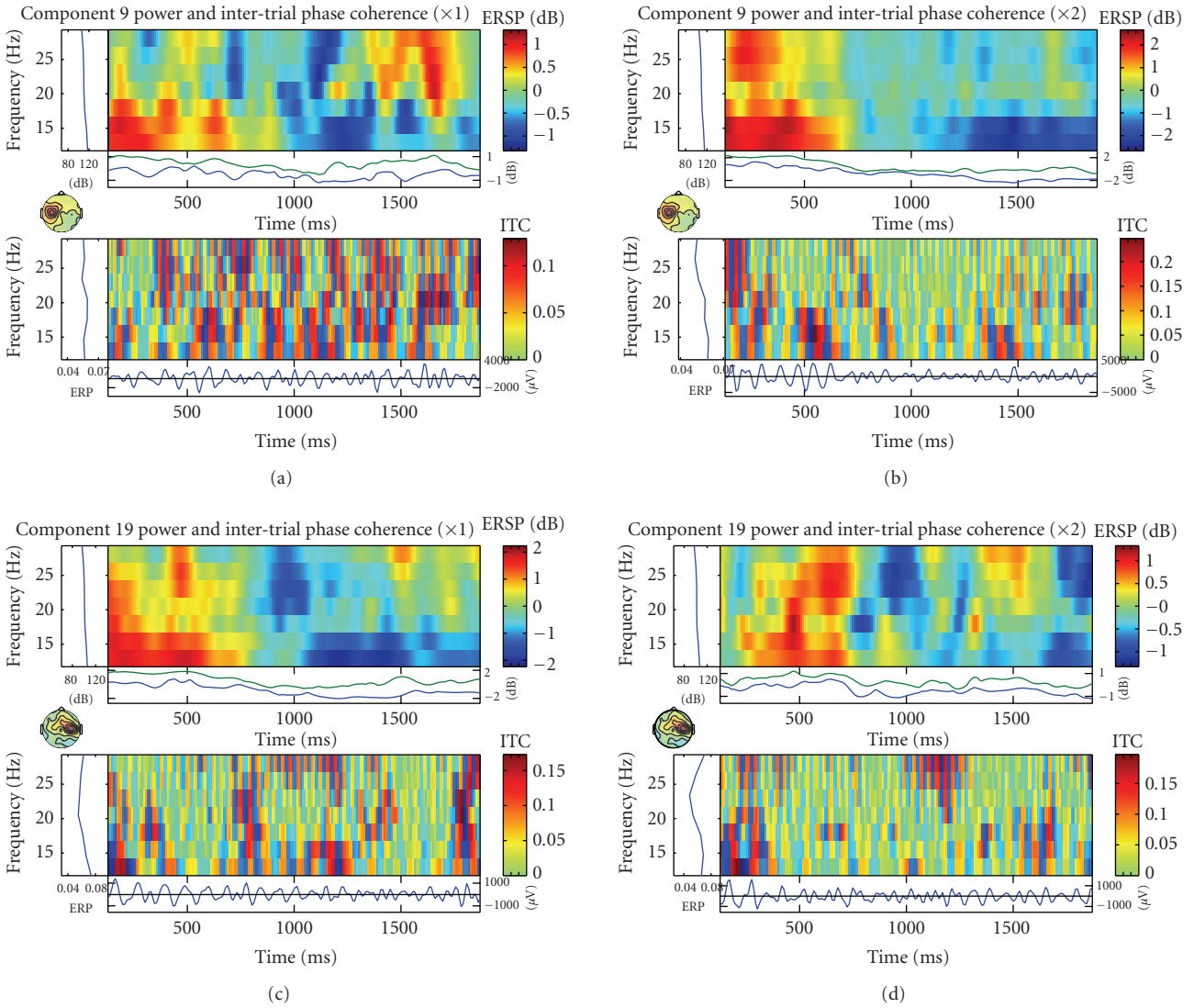

FIGURE 9: The event-related spectral perturbation (ERSP) shows mean event-related changes in spectral power at each time during the epoch and at each frequency. Intertrial coherence (ITC) indicates degree of that the EEG activity at a given time and frequency in single trials are phase-locked (not phase-random with respect to the time-locking experimental event). (a) ERSP and ITC of component 9 during left-hand movement imagery. (b) ERSP and ITC of component 9 during right-hand movement imagery. (c) ERSP and ITC of component 19 during left-hand movement imagery. (d) ERSP and ITC of component 19 during right-hand movement imagery.

Here the entropy $H(s)$ can be computed in the process of computing the mutual information with output class C, so there is little change in computational load with respect to MIFS. The variable β gives flexibility to the algorithm as in MIFS. If we set β zero, the proposed algorithm chooses features in the order of the mutual information with the output. As β grows, it deselects the redundant features more efficiently. In general, we can set $\beta = 1$ in compliance with (31). For all the experiments to be discussed later, we set it to 1. The estimation of mutual information (MI) between each feature and event labels are showed in Figure 11. Based on the algorithm, we obtain a subset of relevant features, which possess the larger MI of all the features, for the classification procedure. Figure 12 shows joint distribution of four features with maximal mutual information.

Two classification methods of Support Vector Machine (SVM) and linear discrimination analysis (LDA) were used to validate the result. To evaluate the classification performance, the generalization classification accuracy was estimated by 10-fold cross-validation.

5. RESULTS AND DISCUSSIONS

Table 1 summarizes the results of single-trial EEG classification for left- versus right-hand movement imagery. The first row denotes the different classification method with different number of features, the first column denotes different feature extraction methods for the subjects. In the feature extraction methods, temporal spatial pattern (TSP) represents the method of combining IRA and CSP which we have

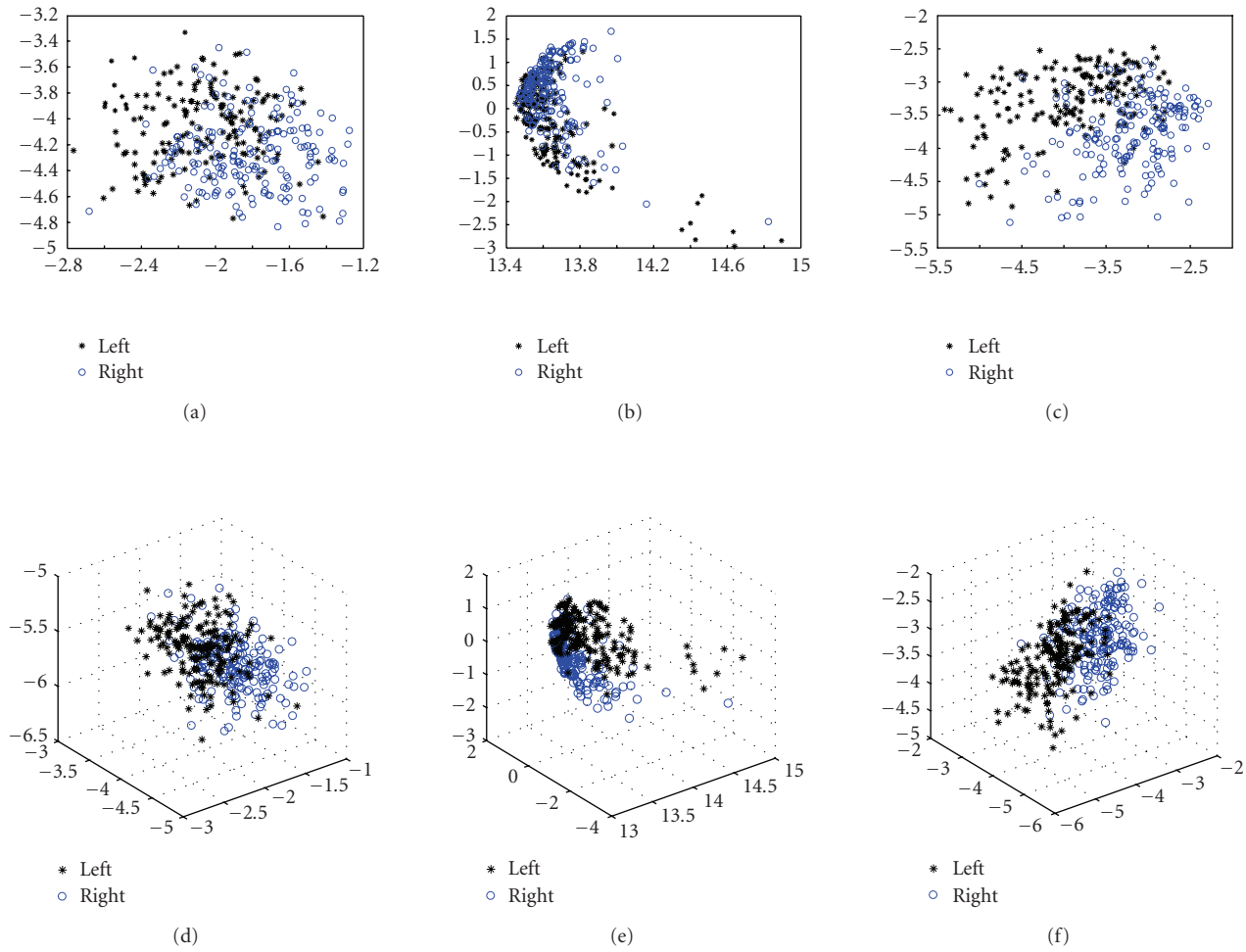

FIGURE 10: Data distribution of feature vectors in 2-D or 3-D views by using PCA method to reduce dimensions. (a)(d) Feature distribution of two type events which extracted by IRA method. (b)(e) Feature distribution of two type events which extracted by CSP method. (c)(f) Feature distribution of two type events which extracted by our method.

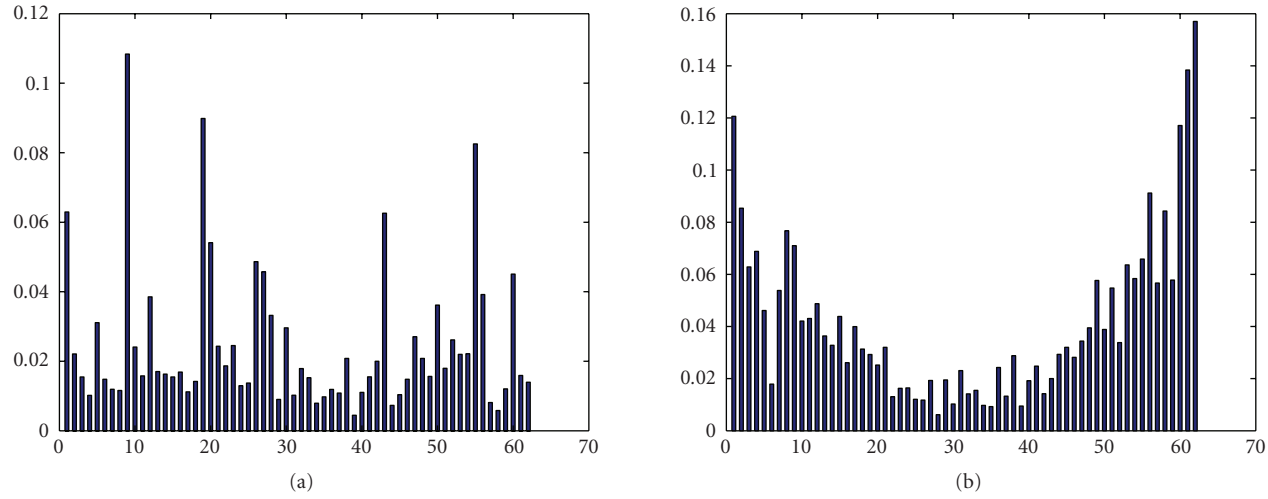

FIGURE 11: (a) The mutual information of IRA components and events labels. (b) The mutual information of CSP components and events labels.

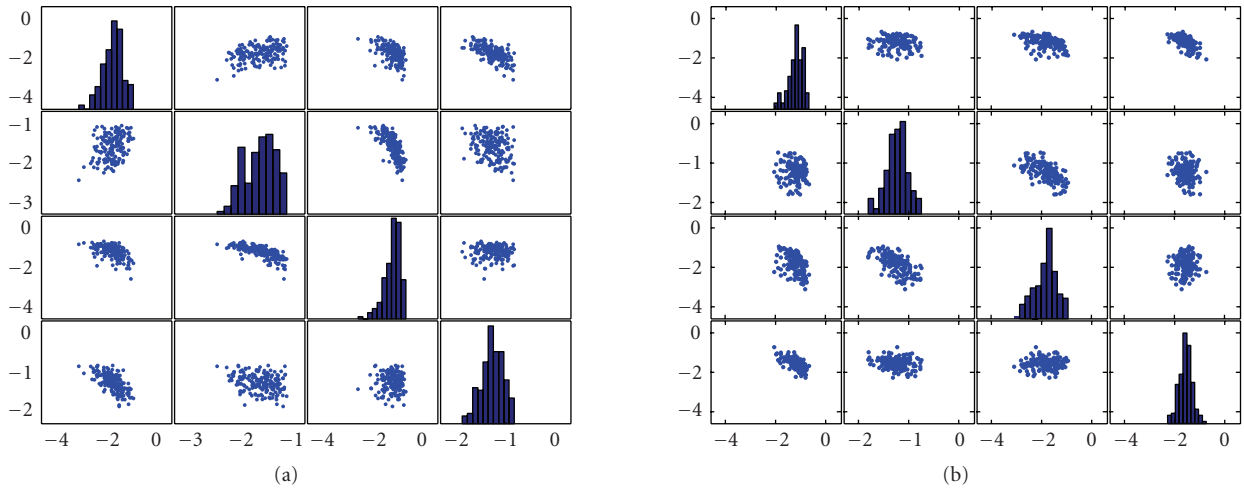

Figure 12: (a) The joint distribution of four features with maximal mutual information between features and events types during left-hand movement imagery. (b) The joint distribution of four features with maximal mutual information between features and events types during right-hand movement imagery.

Table 1: Classification rates (%) for four subjects with different methods. Denoting temporal spatial pattern (TSP) as method which using both temporal and spatial structure information implemented by IRA and CSP algorithms. The first row denotes different classification method with different number of features and the first column denotes different feature extraction methods for the subjects.

	LDA(4)	SVM(4)	LDA(10)	SVM(10)	LDA(16)	SVM(16)	LDA(24)	SVM(24)	LDA(30)	SVM(30)
Subject A										
CSP (no filtering)	71.23	72.78	81.50	82.06	87.14	87.86	87.14	87.86	88.90	89.88
ICA (no filtering)	77.43	77.10	76.69	76.81	76.17	75.94	74.91	74.49	74.17	74.49
TSP (no filtering)	76.55	77.13	87.94	89.01	91.83	92.49	90.02	91.04	90.02	91.04
CSP ([8–30 Hz])	85.48	86.67	87.82	88.69	88.26	88.41	90.96	90.72	91.86	91.88
ICA ([8–30 Hz])	86.85	87.53	86.05	87.53	85.51	86.95	84.06	86.37	83.37	86.95
TSP ([8–30 Hz])	85.56	86.09	85.90	87.24	89.49	89.56	91.96	92.46	93.56	93.90
Subject B										
CSP ([8–30 Hz])	65.37	65.66	84.15	85.66	85.86	87.66	90.91	90.33	91.58	92.00
ICA ([8–30 Hz])	85.41	85.33	87.44	87.00	85.97	86.33	86.51	85.66	86.21	86.67
TSP ([8–30 Hz])	76.66	77.33	86.00	86.00	89.00	89.00	92.33	92.33	92.67	94.00
Subject C										
CSP ([8–30 Hz])	71.03	72.67	74.70	76.00	79.77	80.67	84.32	86.33	85.25	86.33
ICA ([8–30 Hz])	79.92	80.00	81.42	80.33	79.93	79.67	78.29	78.33	78.04	79.00
TSP ([8–30 Hz])	79.03	80.66	80.90	80.33	86.37	85.00	88.63	88.00	88.14	88.00
Subject D										
CSP ([8–30 Hz])	71.89	72.33	82.68	84.00	83.55	83.66	87.82	87.66	86.31	88.00
ICA ([8–30 Hz])	72.63	73.33	74.47	76.00	73.65	76.00	75.31	75.66	75.70	76.00
TSP ([8–30 Hz])	78.01	77.00	84.52	85.00	84.51	84.33	88.27	88.33	88.72	88.66

proposed in this paper. In the table, ICA results are computed by infomax ICA technique through decomposing the data into 62 components and then selecting different number of features based on mutual information method. From the table, we can see that CSP algorithm is sensitive for the frequency (i.e., frequency-specific). ICA results have no obvious improvement with increasing number of features. We also see clearly that the TSP method improves the accuracy of classification. Without applying filtering on EEG signals, TSP method always get better results than the CSP algorithm. Furthermore, Figure 13 shows the curves of classification rate according to number of features. The most optimal result can be obtained by the TSP method and the accuracy is about 93.9% for subject A, 95% for subject B, 92.33% for subject C, and 91.3% for subject D. In the Graz BCI system, subjects were asked to perform the actual finger movement at 8 second and the system also has the feedback to subjects at 1 second after the movement according to the estimate of DSLVQ

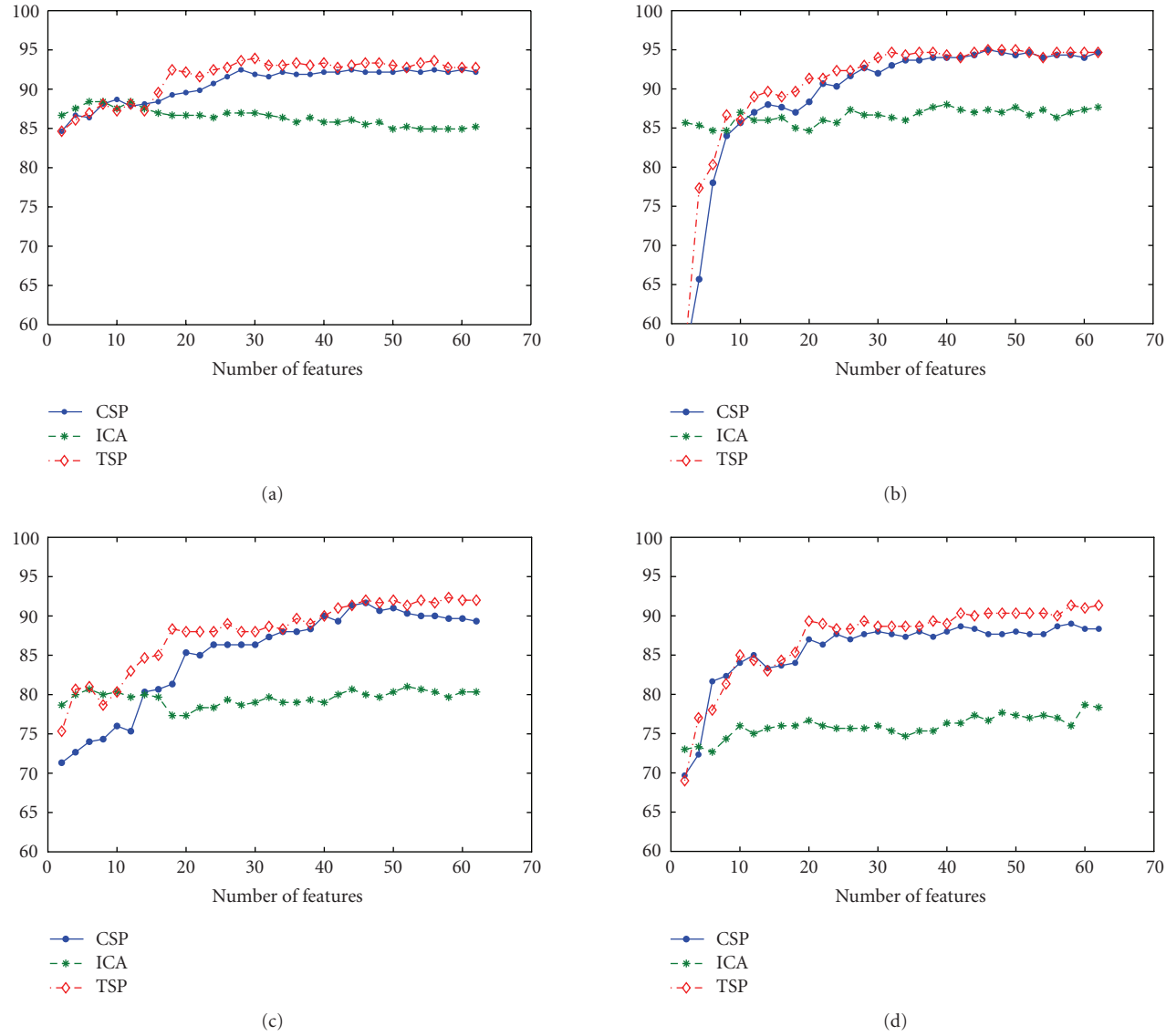

FIGURE 13: The classification accuracy versus the number of features for CSP, ICA and TSP (combination of IRA and CSP) methods. (a) Subject A. (b) Subject B. (c) Subject C. (d) Subject D.

classifier. However, in our system, the subject only was asked to imagine hand movement but none of actual movement and feedback were performed. In fact, the actual movement will improve the classification rate greatly. Moreover, there is no preselection for artifact trials in our system. Therefore, TSP can provide better features for EEG classification during hand movement imagery and is more suitable for the online BCI system.

The results can be summarized as follows.

(1) TSP method (combination of IRA and CSP) can generally increase the classification accuracy of the EEG patterns.

(2) CSP is very sensitive to frequency of filtering and is severely subject-specific, while TSP will get better classification rate when dealing with original EEG signals.

(3) Temporal features of single-trial EEG which reflects event-related potentials can be used to classify movement imagery tasks.

(4) Interrelated feature analysis based on mutual information may improve the EEG classification rate.

6. CONCLUSIONS

Single-trial EEG classification is a very difficult and challenging problem in BCI. How to extract effective information or features from original EEG signals becomes a central problem of the EEG-based BCI. In the past BCI research, CSP algorithm has been proven to be very successful in determining spatial filters which extract discriminative brain rhythms. However, the performance can suffer from nondiscriminative brain rhythms with an overlapping frequency range.

Meanwhile, IRA algorithm successfully overcomes this problem by finding the latency source related to events. Through IRA decomposition, we will separate useful source components with temporal structures from noise. Therefore, it will overcome the problem of losing temporal information that is very useful for classification of event-related potential. Furthermore, through feature selection based on mutual information, most interrelated or effective features have been selected for classification. It allows to clearly reveal discriminating parts in features set, thus contributes to a better understanding of mechanism for an imagination task. Finally, it would be useful to explore configurations with more than two classes which are more natural and also more friendly from the psychological perspective.

ACKNOWLEDGMENTS

This work was supported by the National Basic Research Program of China (Grant no. 2005CB724301) and National Natural Science Foundation of China (Grant no. 60375015).

REFERENCES

[1] J. R. Wolpaw, N. Birbaumer, W. J. Heetderks, et al., "Brain-computer interface technology: a review of the first international meeting," *IEEE Transactions on Rehabilitation Engineering*, vol. 8, no. 2, pp. 164–173, 2000.

[2] J. R. Wolpaw, N. Birbaumer, D. J. McFarland, G. Pfurtscheller, and T. M. Vaughan, "Brain-computer interfaces for communication and control," *Clinical Neurophysiology*, vol. 113, no. 6, pp. 767–791, 2002.

[3] L. A. Farwell and E. Donchin, "Talking off the top of your head: toward a mental prosthesis utilizing event-related brain potentials," *Electroencephalography and Clinical Neurophysiology*, vol. 70, no. 6, pp. 510–523, 1988.

[4] G. Pfurtscheller, C. Neuper, D. Flotzinger, and M. Pregenzer, "EEG-based discrimination between imagination of right and left hand movement," *Electroencephalography and Clinical Neurophysiology*, vol. 103, no. 6, pp. 642–651, 1997.

[5] J. R. Wolpaw and D. J. McFarland, "Multichannel EEG-based brain-computer communication," *Electroencephalography and Clinical Neurophysiology*, vol. 90, no. 6, pp. 444–449, 1994.

[6] N. Birbaumer, N. Ghanayim, T. Hinterberger, et al., "A spelling device for the paralysed," *Nature*, vol. 398, no. 6725, pp. 297–298, 1999.

[7] J. R. Wolpaw, D. J. McFarland, and T. M. Vaughan, "Brain-computer interface research at the Wadsworth Center," *IEEE Transactions on Rehabilitation Engineering*, vol. 8, no. 2, pp. 222–226, 2000.

[8] Y. Li, X. Gao, H. Liu, and S. Gao, "Classification of single-trial electroencephalogram during finger movement," *IEEE Transactions on Biomedical Engineering*, vol. 51, no. 6, pp. 1019–1025, 2004.

[9] Y. Wang, Z. Zhang, Y. Li, X. Gao, S. Gao, and F. Yang, "BCI competition 2003-data set IV: an algorithm based on CSSD and FDA for classifying single-trial EEG," *IEEE Transactions on Biomedical Engineering*, vol. 51, no. 6, pp. 1081–1086, 2004.

[10] H. Ramoser, J. Müller-Gerking, and G. Pfurtscheller, "Optimal spatial filtering of single trial EEG during imagined hand movement," *IEEE Transactions on Rehabilitation Engineering*, vol. 8, no. 4, pp. 441–446, 2000.

[11] J. Müller-Gerking, G. Pfurtscheller, and H. Flyvbjerg, "Designing optimal spatial filters for single-trial EEG classification in a movement task," *Clinical Neurophysiology*, vol. 110, no. 5, pp. 787–798, 1999.

[12] G. Dornhege, B. Blankertz, G. Curio, and K.-R. Müller, "Increase information transfer rates in BCI by CSP extension to multi-class," in *Advances in Neural Information Processing Systems 16 (NIPS '03)*, vol. 3, Vancouver, BC, Canada, December 2004.

[13] L. Zhang, "Temporal independent component analysis for separating noisy signals," in *Proceedings of the 11th International Conference of Neural Information Processing (ICONIP '04)*, vol. 3316 of *Lecture Notes in Computer Science*, pp. 1064–1069, Calcutta, India, November 2004.

[14] H. Jasper and W. Penfield, "Electrocorticograms in man: effect of voluntary movement upon the electrical activity of the precentral gyrus," *European Archives of Psychiatry and Clinical Neuroscience*, vol. 183, no. 1–2, pp. 163–174, 1949.

[15] G. Dornhege, B. Blankertz, M. Krauledat, F. Losch, G. Curio, and K.-R. Müller, "Combined optimization of spatial and temporal filters for improving brain-computer interfacing," *IEEE Transactions on Biomedical Engineering*, vol. 53, no. 11, pp. 2274–2281, 2006.

[16] S. Amari and A. Cichocki, "Adaptive blind signal processing-neural network approaches," *Proceedings of the IEEE*, vol. 86, no. 10, pp. 2026–2048, 1998.

[17] D. T. Pham, "Mutual information approach to blind separation of stationary sources," *IEEE Transactions on Information Theory*, vol. 48, no. 7, pp. 1935–1946, 2002.

[18] S.-I. Amari and J.-F. Cardoso, "Blind source separation-semiparametric statistical approach," *IEEE Transactions on Signal Processing*, vol. 45, no. 11, pp. 2692–2700, 1997.

[19] L.-Q. Zhang, A. Cichocki, and S. Amari, "Geometrical structures of FIR manifold and multichannel blind deconvolution," *Journal of VLSI Signal Processing Systems*, vol. 31, no. 1, pp. 31–44, 2002.

[20] L. Zhang, A. Cichocki, and S. Amari, "Self-adaptive blind source separation based on activation functions adaptation," *IEEE Transactions on Neural Networks*, vol. 15, no. 2, pp. 233–244, 2004.

[21] C. J. James and O. J. Gibson, "Temporally constrained ICA: an application to artifact rejection in electromagnetic brain signal analysis," *IEEE Transactions on Biomedical Engineering*, vol. 50, no. 9, pp. 1108–1116, 2003.

[22] W. Lu and J. C. Rajapakse, "ICA with reference," in *Proceedings of the 3rd International Conference on Independent Component Analysis and Blind Source Separation (ICA '01)*, pp. 120–125, San Diego, Calif, USA, December 2001.

[23] Z. J. Koles and A. C. K. Soong, "EEG source localization: implementing the spatio-temporal decomposition approach," *Electroencephalography and Clinical Neurophysiology*, vol. 107, no. 5, pp. 343–352, 1998.

[24] A. Delorme and S. Makeig, "EEGLAB: an open source toolbox for analysis of single-trial EEG dynamics including independent component analysis," *Journal of Neuroscience Methods*, vol. 134, no. 1, pp. 9–21, 2004.

[25] A. L. Blum and P. Langley, "Selection of relevant features and examples in machine learning," *Artificial Intelligence*, vol. 97, no. 1–2, pp. 245–271, 1997.

[26] N. Kwak and C.-H. Choi, "Improved mutual information feature selector for neural networks in supervised learning," in *International Joint Conference on Neural Networks (IJCNN '99)*, vol. 2, pp. 1313–1318, Washington, DC, USA, July 1999.

Hindawi Publishing Corporation
Computational Intelligence and Neuroscience
Volume 2007, Article ID 71863, 5 pages
doi:10.1155/2007/71863

Research Article

Nessi: An EEG-Controlled Web Browser for Severely Paralyzed Patients

Michael Bensch,[1] Ahmed A. Karim,[2,3] Jürgen Mellinger,[2] Thilo Hinterberger,[2] Michael Tangermann,[4] Martin Bogdan,[1,5] Wolfgang Rosenstiel,[1] and Niels Birbaumer[2,6]

[1] *Department of Computer Engineering, University of Tübingen, 72076 Tübingen, Germany*
[2] *Institute of Medical Psychology and Behavioral Neurobiology, University of Tübingen, Gartenstrasse 29, 72074 Tübingen, Germany*
[3] *Graduate School of Neural and Behavioral Sciences, International Max Planck Research School, University of Tübingen, 72076 Tübingen, Germany*
[4] *Fraunhofer FIRST, Intelligent Data Analysis Group, 12489 Berlin, Germany*
[5] *Department of Computer Engineering, University of Leipzig, 04103 Leipzig, Germany*
[6] *Human Cortical Physiology Unit, National Institute of Neurological Disorders and Stroke (NINDS), National Institutes of Health (NIH), Bethesda, MD 20892, USA*

Correspondence should be addressed to Ahmed A. Karim, ahmed.karim@uni-tuebingen.de

Received 28 February 2007; Accepted 26 June 2007

Recommended by Shangkai Gao

We have previously demonstrated that an EEG-controlled web browser based on self-regulation of slow cortical potentials (SCPs) enables severely paralyzed patients to browse the internet independently of any voluntary muscle control. However, this system had several shortcomings, among them that patients could only browse within a limited number of web pages and had to select links from an alphabetical list, causing problems if the link names were identical or if they were unknown to the user (as in graphical links). Here we describe a new EEG-controlled web browser, called Nessi, which overcomes these shortcomings. In Nessi, the open source browser, Mozilla, was extended by graphical in-place markers, whereby different brain responses correspond to different frame colors placed around selectable items, enabling the user to select any link on a web page. Besides links, other interactive elements are accessible to the user, such as e-mail and virtual keyboards, opening up a wide range of hypertext-based applications.

1. INTRODUCTION

Neurological diseases such as amyotrophic lateral sclerosis (ALS), Guillain-Barré syndrome, or brainstem stroke can lead to severe or total motor paralysis often referred to as locked-in syndrome, where the intact intellect is locked into a paralyzed body. One of the most terrifying aspects of this "locked-in syndrome" is that the loss of muscle control prevents the expression of even the most basic needs. Conventional augmentative communication devices, which depend on some rudimental muscle control, may not be feasible for patients in the end stage of ALS if they have no remaining reliable muscle control. Thus, the final option for restoring communication to those patients is to provide the brain with a nonmuscular communication and control channel, a direct brain-computer interface (BCI) for conveying messages and commands to the external world. In the late 1990s, Birbaumer et al. [1, 2] were the first to provide ALS patients with a BCI system, the so-called thought translation device (TTD). The TTD is a noninvasive, EEG-controlled BCI based on regulation of slow cortical potentials (SCPs) which humans can learn to control in an operant conditioning procedure [3]. Further studies have successfully applied sensorymotor EEG rhythms (SMR) [4, 5], P300 evoked potentials [6], and neuronal action potentials [7–9] for different BCI systems. While letter spelling is a state-of-the-art application for BCI systems today, interactive access to the world wide web (WWW) is one of the most promising BCI applications, as it enables severely paralyzed patients to participate in the broad portion of life reflected by the WWW. Karim et al. [10] have recently shown that an EEG-controlled web browser based on self-regulation of SCP can be reliably

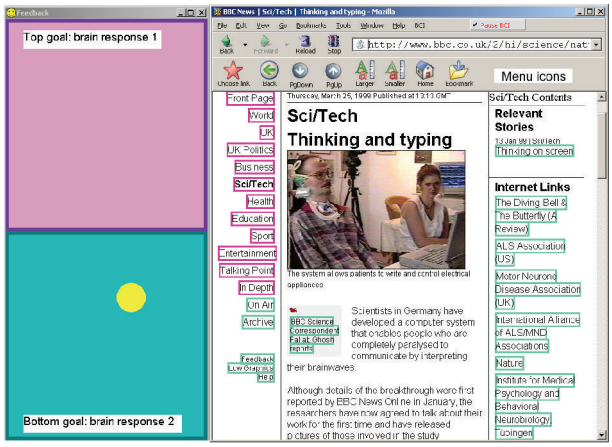

Figure 1: Web surfing with Nessi. Colored in-place link markers correspond to brain responses of the user, which are shown as goals in the BCI feedback window (left). After a page has loaded, the link markers are applied to a set of menu icons (top), allowing the user to choose a link, go back, scroll down the page, and use other configurable options. The number of goals and accordingly link marker colors can be increased for multiclass BCIs.

operated by a locked-in patient suffering from end stage ALS. Moreover, it was shown that this BCI web browser, called Descartes, can help severely paralyzed patients to regain a certain level of autonomy in the interaction with the outside world, and thereby enhance their quality of life [10–12]. However, Descartes had several shortcomings, among them that patients could only browse within a limited number of web pages and were not able to choose a link, if they did not know its link text (as, e.g., in graphical links). Here we introduce a new EEG controlled web browser, called Nessi (neural signal surfing interface), which overcomes these shortcomings. In Nessi, the web browser, Mozilla, was extended by graphical in-place markers, whereby different brain responses correspond to frame colors placed around selectable items, enabling the user to choose any link on a web page (see Figure 1).

2. IMPLEMENTATION OF NESSI

The implementation of Nessi within the Mozilla framework allows customization on various levels. The supervisor is able to adjust parameters concerning the user interface, such as the number of frame colors to use (each color representing one class) or the length of the reading pause. Some HTML knowledge is required to create custom virtual keyboards or start pages. With programming experience, dynamic pages (games) or new decision structures can be created. We have included a game (an image consisting of 6 parts has to be "uncovered" by selecting each part separately) to accustom users to the new interface and increase motivation. Nessi is available open source at http://nessi.mozdev.org and contributions are welcome. The following subsections describe three integral aspects of Nessi: (1) graphical display of in-place link markers; (2) construction of finite-state transducers (FSTs) (cf. [13]), which represent internally the brain responses required to select a link; (3) communication with the BCI software that records and processes the EEG signals.

2.1. *In-place link markers*

Colored frames are placed around selectable items on a web page, circumventing any need to maintain a separate presentation of choices (see Figure 1). By default, red frames are selected by producing negative SCP shifts and green frames are selected by the production of positive SCP shifts. As an aid, feedback is displayed at the left rim of the screen by depicting the vertical movement of a cursor that can be moved upwards into a red goal or downwards into a green goal. The user only has to watch the current color of the desired link's frame that indicates the brain response which has to be produced for its selection. By presenting a series of brain responses as indicated by changing the color of the frame around that link, it can be chosen with binary decision neglecting any knowledge about its position in a selection tree.

The advantages of graphical display of in-place link markers on web pages instead of presenting links in an alphabetical list were discussed previously by Mellinger et al. [14] and Karim et al. [12]. In the following, we give a more technical description of the finite state transducers (decision graphs) used to determine the color of the link markers at each selection step.

Nessi's task mode makes it possible for the supervisor to ask the patient which link he/she wishes to choose and to mark that link as a task. This way, the patient's accuracy can be recorded, enabling a comparison of patients' performance between standard spelling tasks and web surfing.

2.2. *Construction of finite-state transducers*

We represent each step in the selection process as a state transition of an FST [13]. Depending on the FST's input, which is represented by the user's brain response, a transition from one state to the next occurs together with an output. The final states represent the colored marked elements (links on a web page or letters on a virtual keyboard). The input alphabet of the FST is the set of brain responses recognized by the BCI, that is, (1, 2) for a typical two-class BCI. However, transducer construction is not limited to two classes and can be adjusted to multiclass BCIs, whereby the number of outgoing transitions of a state matches the number of classes used. The output of the FST represents the depth of the transducer, that is, how close the user is to choosing a final state. This output string can be evaluated by supervisors to see where a patient is having trouble in the selection process. All links pointing to the same URL are merged into one node of the FST. This dramatically reduces the number of choices for many web pages. Link marker colors are determined by finding the input symbol of the first transition representing the shortest path from the current state to the desired link (cf. Figure 2). If the user desires to write the letter "N" on a virtual keyboard, beginning at state s0, the shortest path is 2, 1, 1 (visiting the states i1 and i5). The first transition thus requires the input symbol "2." Assigning red markers to brain response 1 and green

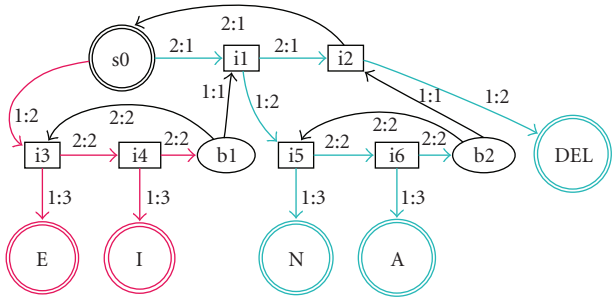

FIGURE 2: LSP transducer with scanning structure depicting a virtual keyboard with four output letters. The initial state is s0. Transitions are labeled with the classification answer and the logical "depth." Internal states are marked with an "i" and states allowing for correction of errors by moving back to higher levels (*back* nodes) are marked with a "b." From the current state, s0, the red states are reached with brain response 1 and the green states are reached with brain response 2.

markers to brain response 2, the "N" is marked green while the current state is s0.

We examined various techniques to construct FSTs for decision making with the objective of quick link or letter selection. In previous studies with ALS patients, the language support program (LSP) [15] and the internet browser Descartes [10] used a "scanning" interface, whereby the brain responses represented *select* or *reject* and the classifier had a strong bias towards *reject*. An example of an LSP transducer is shown in Figure 2.

If the user has reached high accuracy and his/her interaction with the classifier generates two brain responses with equal probability, a Huffman-coded FST [16] might be more efficient. An example is shown in Figure 3. The user is able to correct mistakes by choosing the *back* nodes that are inserted at every second level of the FST.

2.3. Communication with BCI software

A communication protocol was defined to interface Nessi with existing BCI systems such as the TTD [2] and BCI2000 [17]. Once a connection is established, the user's favorite bookmark is shown and the links are marked red or green. Feedback of brain responses (e.g., SCP or SMR) can be displayed on the left of the screen in the form of a ball that the user moves into a red or green goal. Each brain response is sent from the BCI to Nessi and used as an input to the FST, which causes a state transition. Once a new web page is selected, Nessi sends a signal to the BCI software to stop feedback and the user has a predefined time (adjusted to the user's reading speed by the supervisor) to read the page. Thereafter, feedback continues and link selection restarts. Other external programs, such as switch interfaces, could also be used to control Nessi. Communication between Nessi and external programs is illustrated in Figure 4.

3. E-MAIL

Nessi includes an e-mail interface that allows the user to read and compose e-mails. A screenshot is shown in Figure 5.

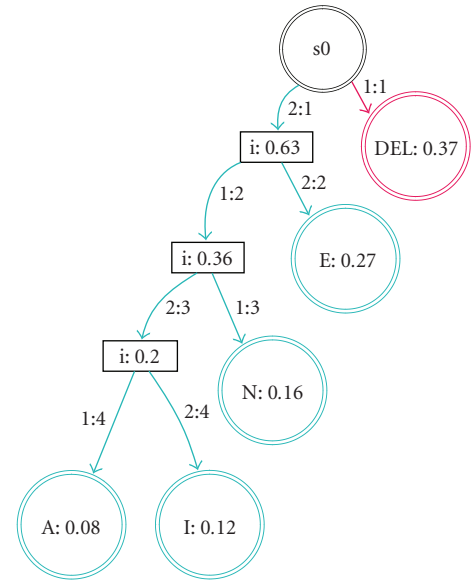

FIGURE 3: Huffman-coded transducer. The probability that a node will be chosen, based on a language model (or web revisitation patterns for links), is shown inside the node. The *back* nodes have been omitted for clarity. Beginning at state s0, the red state is reached with brain response 1 and the green states are reached with brain response 2.

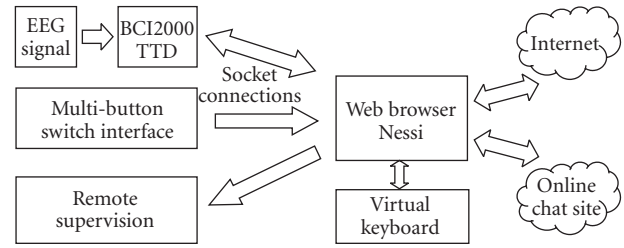

FIGURE 4: BCI software communicates with Nessi via a socket protocol. Text is entered into web forms or chat sites with a virtual keyboard. Switch interfaces for non-BCI users could be added. Remote supervision can be realized by starting a remote instance of Nessi, which synchronizes with the patient's display.

To allow quick selection and prevent confusion, the user chooses either the reply, compose, or next e-mail icon. The selection process is the same as for links on a web page. Addresses can be chosen from an address book created by the supervisor. Considering the fact that BCI users will generally read and write short messages, these two windows were placed next to each other, preventing the need to open new windows. E-mails are composed with a virtual keyboard.

4. USER INTERFACE SIMULATIONS

Simulations were carried out to determine the interface's efficiency, given the user's accuracy of correct *selection* p and correct *rejection* q. As an example, the average number of brain responses needed to select a link on the page shown in Figure 1 is 16, if $p = q = 0.75$. For spelling, the standard LSP

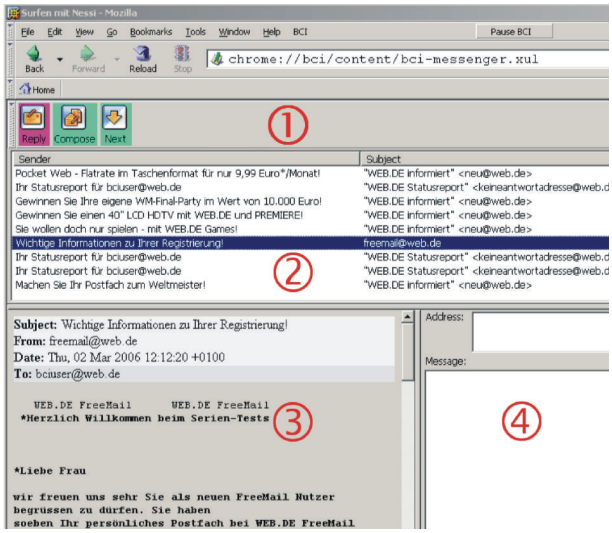

FIGURE 5: E-mail interface. (1) presents the current menu choices to the user. (2) displays incoming messages. There is an area for reading (3) and writing (4) e-mails.

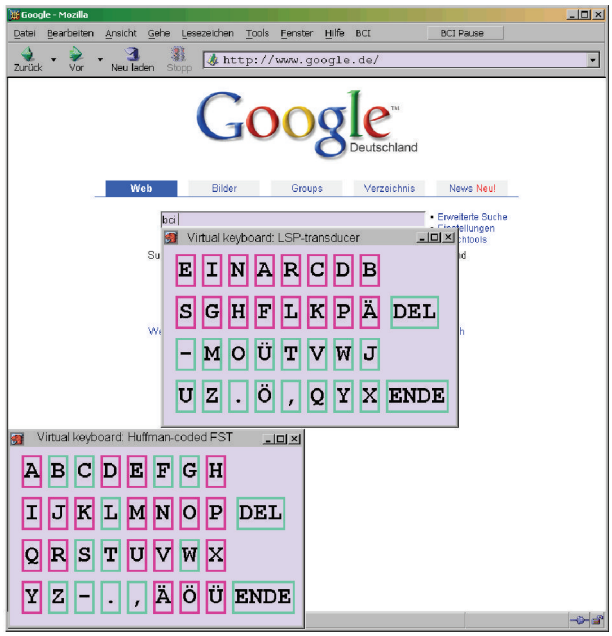

FIGURE 6: Virtual keyboards for entering text into web forms, displaying the LSP transducer (center) and the Huffman-coded transducer (bottom), which are used in the simulations.

transducer and a Huffman-coded transducer with *back* nodes on every second level were compared using Nessi's simulation mode. The average number of brain responses required to select a letter with the virtual keyboard (German language model), as shown in Figure 6, was simulated. The number of additional brain responses required for the Huffman-coded FST is displayed in Figure 7. A typical SCP or SMR brain response takes about 5 seconds.

Especially for low values of p, the LSP transducer is more efficient than the Huffman-coded FST with *back* nodes. The

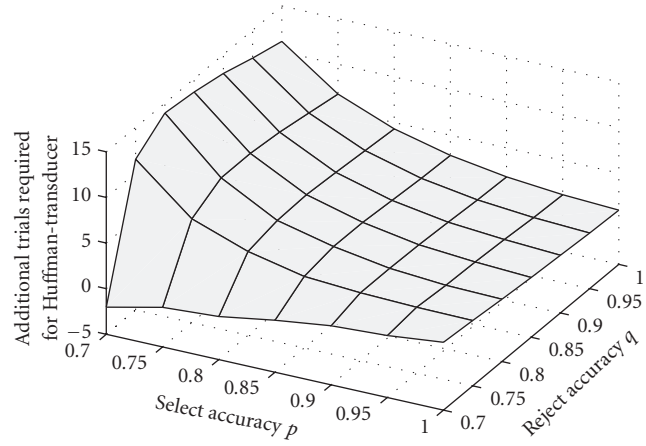

FIGURE 7: Number of additional brain responses to write a letter, required by the Huffman-transducer compared to the scanning transducer, as a function of the select and reject accuracies p and q (based on German letter frequencies).

difference is negligible for very low values of p and q. A further simulation showed that the placement of letters commonly found in LSP transducers, which is optimal for users with an accuracy of 100%, is suboptimal once p and q are below 1. If p and q are known for a particular user, an improved LSP transducer can be generated by the simulation module.

5. CONCLUSION AND DISCUSSION

Karim et al. [10] have previously shown that an EEG-controlled web browser can help locked-in patients to regain a certain level of autonomy in the interaction with the outside world and thereby enhance their quality of life. However, this web browser required the user to select links from an alphabetical list, causing problems if the link names were identical or if they were unknown to the user (as in graphical links). These shortcomings have been resolved with the web browser Nessi. Graphical in-place markers are used instead of link text, whereby different brain responses correspond to frame colors placed around selectable items, enabling the user to select any link on a web page. Other interactive elements, such as e-mail and virtual keyboards, are also accessible and open up a wide range of hypertext-based applications to the user.

Moreover, the user interface has been optimized for low-bandwidth input. Even though classifier optimization is crucial to brain-computer interfaces, patients can benefit additionally from intelligent user interfaces. A language model was used to construct FSTs with options for error correction for entering URLs or text in web forms. We incorporated knowledge of the user's web page revisitation patterns to allow quick selection of pages that are visited often. Intelligent decisions are taken wherever possible, for example, links pointing to a common URL are subsumed in a single transducer state, and web pages without links result in Nessi returning to the previous page after the reading pause. A game was implemented to accustom users to the new interface and to increase motivation to use the interface.

Different types of transducers were compared by simulating the user input. The LSP transducer should be used for the virtual keyboards as well as link selection. However, it can be improved for known values of p and q. Note that the simulations do not consider factors such as user preferences or difficulties when generating the same brain response often in succession.

Future work will involve testing Nessi with patients communicating via the SCP or SMR paradigm, and testing a link selection interface for patients who prefer the P300 paradigm. In this case, each link is assigned to a letter, which is selected from a standard P300 speller matrix. Finally, we would like to evaluate the benefits of Nessi's user interface for other low-bandwidth users such as cerebral palsy patients or binary switch users.

ACKNOWLEDGMENTS

This study was supported by the Deutsche Forschungsgemeinschaft (DFG), the Volkswagen Foundation, and the US National Institutes of Health (NIH). M. Bensch and M. Tangermann were supported by DFG Grant Ro1030/12-1.

REFERENCES

[1] N. Birbaumer, N. Ghanayim, T. Hinterberger, et al., "A spelling device for the paralysed," *Nature*, vol. 398, no. 6725, pp. 297–298, 1999.

[2] N. Birbaumer, A. Kübler, N. Ghanayim, et al., "The thought translation device (TTD) for completely paralyzed patients," *IEEE Transactions on Rehabilitation Engineering*, vol. 8, no. 2, pp. 190–193, 2000.

[3] A. Kübler, B. Kotchoubey, H.-P. Salzmann, et al., "Self-regulation of slow cortical potentials in completely paralyzed human patients," *Neuroscience Letters*, vol. 252, no. 3, pp. 171–174, 1998.

[4] J. R. Wolpaw and D. J. McFarland, "Control of a two-dimensional movement signal by a noninvasive brain-computer interface in humans," *Proceedings of the National Academy of Sciences of the United States of America*, vol. 101, no. 51, pp. 17849–17854, 2004.

[5] B. O. Peters, G. Pfurtscheller, and H. Flyvbjerg, "Automatic differentiation of multichannel EEG signals," *IEEE Transactions on Biomedical Engineering*, vol. 48, no. 1, pp. 111–116, 2001.

[6] E. Donchin, K. M. Spencer, and R. Wijesinghe, "The mental prosthesis: assessing the speed of a P300-based brain-computer interface," *IEEE Transactions on Rehabilitation Engineering*, vol. 8, no. 2, pp. 174–179, 2000.

[7] M. D. Serruya, N. G. Hatsopoulos, L. Paninski, M. R. Fellows, and J. P. Donoghue, "Instant neural control of a movement signal," *Nature*, vol. 416, no. 6877, pp. 141–142, 2002.

[8] J. M. Carmena, M. A. Lebedev, R. E. Crist, et al., "Learning to control a brain-machine interface for reaching and grasping by primates," *PLoS Biology*, vol. 1, no. 2, p. E42, 2003.

[9] D. M. Taylor, S. I. H. Tillery, and A. B. Schwartz, "Direct cortical control of 3D neuroprosthetic devices," *Science*, vol. 296, no. 5574, pp. 1829–1832, 2002.

[10] A. A. Karim, T. Hinterberger, J. Richter, et al., "Neural Internet: web surfing with brain potentials for the completely paralyzed," *Neurorehabilitation and Neural Repair*, vol. 20, no. 4, pp. 508–515, 2006.

[11] A. A. Karim, "Neural Internet: future BCI applications," in *The 2nd International Brain-Computer Interface Meeting*, Rensselaerville, NY, USA, June 2002.

[12] A. A. Karim, M. Bensch, J. Mellinger, et al., "Neural Internet for ALS patients," in *Proceedings of the 3rd International Brain-Computer Interface Workshop*, G. R. Müller-Putz, C. Brunner, and R. Leeb, Eds., pp. 114–115, Verlag der Technischen Universität Graz, Graz, Austria, September 2006.

[13] M. Mohri, "Finite-state transducers in language and speech processing," *Computational Linguistics*, vol. 23, no. 2, pp. 269–311, 1997.

[14] J. Mellinger, T. Hinterberger, M. Bensch, M. Schröder, and N. Birbaumer, "Surfing the web with electrical brain signals: the brain web surfer (BWS) for the completely paralysed," in *Proceedings of the 2nd World Congress of the International Society of Physical and Rehabilitation Medicine (ISPRM '03)*, Prague, Czech Republic, May 2003.

[15] J. Perelmouter, B. Kotchoubey, A. Kübler, E. Taub, and N. Birbaumer, "Language support program for thought-translation-devices," *Automedica*, vol. 18, no. 1, pp. 67–84, 1999.

[16] J. Perelmouter and N. Birbaumer, "A binary spelling interface with random errors," *IEEE Transactions on Rehabilitation Engineering*, vol. 8, no. 2, pp. 227–232, 2000.

[17] G. Schalk, D. J. McFarland, T. Hinterberger, N. Birbaumer, and J. R. Wolpaw, "BCI2000: a general-purpose brain-computer interface (BCI) system," *IEEE Transactions on Biomedical Engineering*, vol. 51, no. 6, pp. 1034–1043, 2004.

Hindawi Publishing Corporation
Computational Intelligence and Neuroscience
Volume 2007, Article ID 79642, 8 pages
doi:10.1155/2007/79642

Research Article

Self-Paced (Asynchronous) BCI Control of a Wheelchair in Virtual Environments: A Case Study with a Tetraplegic

Robert Leeb,[1] Doron Friedman,[2,3] Gernot R. Müller-Putz,[1] Reinhold Scherer,[1] Mel Slater,[2,4] and Gert Pfurtscheller[1]

[1] *Laboratory of Brain-Computer Interfaces, Institute for Knowledge Discovery, Graz University of Technology, Krenngasse 37, 8010 Graz, Austria*
[2] *Department of Computer Science, University College London, Gower Street, London WC1E 6BT, UK*
[3] *Sammy Ofer School of Communications, The Interdisciplinary Center, P.O. Box 167, Herzliya 08010, Israel*
[4] *Catalan Institute of Research and Advanced Studies (ICREA), Polytechnic University of Catalunya, 08010 Barcelona, Spain*

Correspondence should be addressed to Robert Leeb, robert.leeb@tugraz.at

Received 18 February 2007; Accepted 17 July 2007

Recommended by Andrzej Cichocki

The aim of the present study was to demonstrate for the first time that brain waves can be used by a tetraplegic to control movements of his wheelchair in virtual reality (VR). In this case study, the spinal cord injured (SCI) subject was able to generate bursts of beta oscillations in the electroencephalogram (EEG) by imagination of movements of his paralyzed feet. These beta oscillations were used for a self-paced (asynchronous) brain-computer interface (BCI) control based on a single bipolar EEG recording. The subject was placed inside a virtual street populated with avatars. The task was to "go" from avatar to avatar towards the end of the street, but to stop at each avatar and talk to them. In average, the participant was able to successfully perform this asynchronous experiment with a performance of 90%, single runs up to 100%.

1. INTRODUCTION

Virtual reality (VR) provides an excellent training and testing environment for rehearsal of scenarios or events that are otherwise too dangerous or costly—or even currently impossible in physical reality. The technological progress in the last decade has made VR systems attractive for various research fields and applications ranging from aviation and military applications, simulation and training programs (where real-life training is too expensive or difficult to monitor and control), psychotherapy, and medical surgery. In particular, the area of medical rehabilitation exploits the possibilities and advances made available by VR systems, specifically the rehabilitation of motor functions [1, 2] including stroke rehabilitation (upper and lower extremity training) [3], spatial and perceptual motor training, Parkinson's disease, orthopedic rehabilitation [4], balance training, and wheelchair mobility [5]. A major finding in this field is that people with disabilities can perform motor learning in VR, which can then be transferred to reality [6, 7]. In some cases it is even possible to generalize to other untrained tasks including improved efficiency of virtual training and learning [1, 2, 8]. It is important to note that VR is not a treatment by itself, and therefore it is impossible to study whether it is effective or not for rehabilitation. Although VR rehabilitation was undertaken in patients with acquired brain injury or damage with some success [9, 10], it is rather a new technological tool, which may be exploited to enhance motor retraining.

Virtual environments (VE) have already been used as a feedback media for brain-computer interface (BCI) experiments. BCI technology deals with the development of a direct communication channel between the human brain and machines which does not require any motor activity [11, 12]. This is possible through the real-time analysis of electrophysiological brain signals recorded by electroencephalogram (EEG) or electrocorticogram (ECoG). Other than the EEG and ECoG, brain signals can also be recorded invasively by implanted electrodes in the brain. Voluntary mental activity (e.g., a sequence of thoughts) modifies bioelectrical brain activity and consequently the EEG and ECoG. A BCI is able to detect such changes and generate operative control signals. Particularly for people suffering from severe

physical disabilities or are in a "locked-in" state, a BCI offers a possible communication channel. Recently, the BCI has been used to control events within a VE, but most of the previously conducted VR-BCI research is based on two types of visually evoked responses; either the steady-state visual evoked potential (SSVEP) [13] or the event-related P300 potential [14]. These methods typically force the subjects to perform a visual task which might be unnatural (e.g., to gaze at a blinking object). In contrast, no visual stimuli are necessary if oscillatory EEG components, modulated by specific mental strategies (e.g., motor imagery), are used for the BCI [11]. With such a system participants are able to navigate through VEs by imagination of hand or foot movements [15, 16]. Thereby, the EEG is analyzed in predefined time intervals (cue-based or synchronous BCI) and the participants can decide between two states (either go right/left or forward/stop), but only whenever they are triggered by the system. The disadvantage of such a synchronous BCI and of a BCI based on evoked potentials is that an external stimulus from the system is always necessary and that the system always makes a decision (out of a predefined set of choices, e.g., movement imaginations). Up to now, most of the existing BCI systems are operated in this synchronized (or cue-based) paradigm, but this is not the natural way of human-machine interaction.

Transferring the BCI from laboratory conditions towards real-world applications needs the identification of brain patterns asynchronously without any timing constraints: the computer is no longer in control of timing and speed but the user. An asynchronous (self-paced) BCI is continuously analyzing the ongoing brain activity, however, not only the intentional-control (IC) states have to be detected (e.g., motor imagery) but also the in-between periods, whereas the user is in a non-control state (NC, formerly called idling state). In the later, the user may be idle, daydreaming, thinking about something else, or performing some other action, but is not trying to control the BCI. Asynchronous BCIs are much more complicate than synchronous ones, nevertheless, the community is more and more addressing these problems [17–21]. A big challenge in case of asynchronous BCIs is the validation. The performance is mostly measured in percentage of successful switching (true positive rate, TP) between IC and NC (or between the different IC states) and percentage of false or not intended switching (false positive rate, FP). For computing the correct TP/FP rates, it is necessary to access the subjects "real" intend and to compare it with the BCI output. Unfortunately, this information is not directly accessible. So either the system is telling the user to perform a switch or the user is reporting immediately if a switch occurred correctly or not. In the first scenario, analogical to a cue-based (synchronous) application, the system and not the user is in control of the timing [22]. In the second scenario, verbal comments or keystrokes could be used to verify the correctness of the BCI output, nevertheless the execution of such response tasks is modifying the EEG and thereby influencing the BCI output as well. A different approach is to give the user a task, which is only accomplishable by having control over NC and IC states and measuring only the task performance. Thereby, no concrete values for the TP and FP rates are computable, but the definition of the task involves that a high number of TP and a low number of FP is necessary. This procedure has been applied in this paper.

In this case study we want to demonstrate that it is possible for a tetraplegic subject to intentionally control his wheelchair within virtual reality by self-paced motor imagery using an EEG-based BCI. The participant is placed inside a virtual street populated with avatars and the task is to "move" from avatar to avatar towards the end of a street by imagination of movements of his paralyzed feet. The reason for the VR-setup is that the visual-rich virtual street with the avatars ensured that the experiment is diversified and engaging but contains enough distraction as it would be in a real street. The defined experiment has a simple goal with clear tasks, nevertheless, no instructions or cues from the BCI are necessary. A minimized setup of one bipolar EEG recording should be enough for this asynchronous control under real-world-like VR conditions.

2. METHODS

2.1. The tetraplegic subject

Here, we report on a 33-year-old male tetraplegic subject. After a traumatic injury of the spinal cord in 1998, he has a complete motor and sensory lesion below C5 and an incomplete lesion below C4. During an intensive training period of approximately 4 months, he has learned to control the cue-based Graz-BCI. The training was carried out with different types of motor imagery (MI; left- and right-hand motor imageries, idling, and foot movement imaginations) because of the insufficient accuracy in the beginning. The MI had to be performed within 4 seconds following the cue-stimulus. Finally, his cue-based performance during right-hand versus foot motor imagery was between 90% and 100% (details about this training are reported elsewhere [23]). Specifically, the midcentral-focused beta oscillations with a dominant frequency of approximately 17 Hz allowed a brain-switch like application of a neuro-prosthesis [24, 25]. Thereby, he had to focus on a foot movement imagination over a period of 1 second (dwell time) to activate a trigger and initiate a grasp sequence. After each trigger, a refractory period of 5 seconds guaranteed that no further grasp sequence could be initiated. The same brain rhythms have been used in this work for the self-paced control of the VE.

2.2. Data acquisition and signal processing

One single EEG channel was recorded bipolarly 2.5 cm anterior and posterior to the electrode position Cz (foot representation area) of the international 10/20 system [26]. The ground electrode was positioned on the forehead (position Fz). The EEG was amplified (sensitivity was set to 50 μV and the power-line notch filter was activated), bandpass filtered between 0.5 and 30 Hz with a bipolar EEG amplifier (g.tec, Guger Technologies, Graz, Austria) recorded and online processed with a sampling frequency of 250 Hz [27]. The recording and processing was handled by rtsBCI [28], based on MATLAB 7.0.4 (MathWorks, Inc., Natick, USA) in

Figure 1: Picture of the virtual street populated with 15 avatars and the tetraplegic subject in his wheelchair in the middle of the multiprojection wall VR system. The subject was wearing the electrode cap with one bipolar channel connected to the BCI system (amplifier and laptop on the right side).

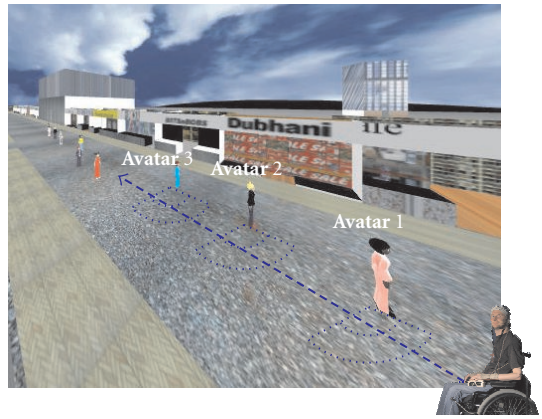

Figure 2: The task of the participant was to go from avatar to avatar towards the end of the street (outlined with a dashed line). The avatars were lined up and each avatar had its invisible communication sphere (drawn as dotted lines here). The subject had to stop within this sphere, not too close and not too far away from the avatar.

combination with Simulink 6.2, Real-Time Workshop 6.2, and the open source package BIOSIG [29].

A single logarithmic band power (BP) feature was estimated from the ongoing EEG by digital band-pass filtering the recording (Butterworth IIR filter of order 5, between 15 and 19 Hz), squaring, averaging (moving average) the samples over the past second, and computing the logarithm from this time series. A simple threshold (TH) was used to distinguish between foot movement imagination (intentional control, (IC)) and rest (non-control state (NC)). Whenever the band power exceeded the threshold, a foot MI was detected (see Figures 3(a)–3(e)).

An "idling" recording (approximately 120 seconds) without any foot movement imagination was recorded before the experiment for the calculation of the TH. The BP was calculated and the mean $\bar{x}$ and the standard deviation SD were extracted. The TH was set to

$$\mathrm{TH} = \bar{x} + 3 \cdot \mathrm{SD}. \quad (1)$$

Unlike previous asynchronous studies no, dwell time (minimum time over threshold before the action is triggered) or refractory period (minimum time between two successful actions) was used [22, 24].

2.3. The virtual environment

The participant was placed with his wheelchair in the middle of a multiprojection-based stereo and head-tracked VR system that commonly known as a "Cave" [30]. The particular VR system used was a ReaCTor (SEOS Ltd. West Sussex, UK) which surrounds the user with three back-projected active stereo screens (3 walls) and a front-projected screen on the floor (see Figure 1). Left- and right-eye images are alternately displayed at 45 Hz each, and synchronized with CrystalEye stereo glasses. A special feature of any multiwall VR system is that the images on the adjacent walls are seamlessly joined together, so that participants do not see the physical corners but the continuous virtual world that is projected with active stereo [31]. The application was implemented in DIVE [32] and the communication between the BCI and the VR occurred every 40 milliseconds via the Virtual Reality Peripheral Network (VRPN, [33]) communication protocol. The used VE was a virtual street with shops on both sides and populated with 15 virtual characters (avatars), which were lined up along the street (see Figure 2, [15]).

2.4. Experimental setup

The task of the participant was to "move" from avatar to avatar towards the end of the virtual street (65 length units) by movement imagination of his paralyzed feet. Only during the time when the TH was exceeded (IC, foot MI detected), the subject moved forward (moving speed 1.25 units/second, see Figures 3(e)-3(f)). Every time he was short before passing an avatar, he had to stop very close to it. Each avatar was surrounded by an invisible communication sphere (0.5–2.5 units) and the subject had to stop within this sphere (see Figures 2 and 3(g)). The size of the sphere was adequate to the distance for a conversation in the real world and corresponded to a stopping time slot of approximately 1.6 seconds. The avatar started talking to the subject, if he was standing still for one second within this sphere (see Figure 3(i)). After finishing a randomly chosen short statement (like "Hi," "My name is Maggie," "It was good to meet you," etc.), the avatar walked away. Communication was only possible within the sphere; if the subject stopped too early or stopped too close to the avatar nothing happened. After a while, on his own free will, the subject could imagine another foot movement and started moving again towards the next avatar, till the end of the street was reached. The distance traversed depended only on the duration of the foot motor imagery, longer foot MI resulted in a larger distance than short bursts of MI. The 15 avatars were placed on the

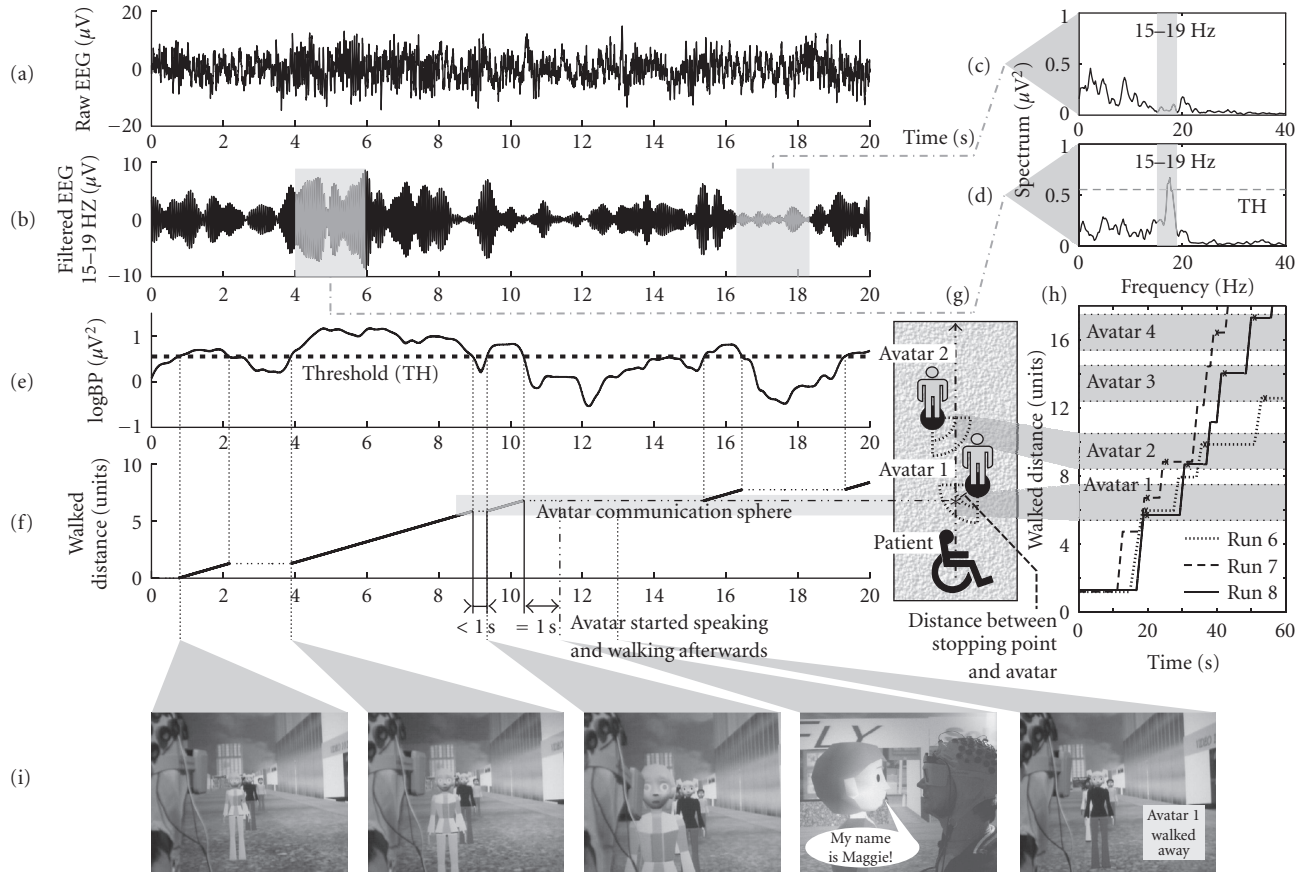

Figure 3: (a) Raw EEG during periods of foot MI and rest. (b) Bandpass-filtered (15–19 Hz) EEG. (c), (d) Power spectra of 2-second periods during rest (c) and foot MI (d). The frequency band and the threshold are indicated. (e) Logarithmic band power time course with threshold (TH). (f) Periods of moving and covered distance. The contact with avatar 1 occurred at second 11.4 after a 1 second pause within the communication sphere (because at second 8.9 the subject stopped shorter than 1-second). (g) Spatial placement of the avatars with corresponding communication sphere and direction of walking. The communication sphere of avatar 1—stopping range for the subject—is also marked with a gray rectangle (f). (h) Spatial-temporal tracking data of the first four avatars of three runs. The communication spheres of avatars are again indicated with a gray rectangle. The time and position of the contact with the avatar are marked with an "∗". In run 7, the third avatar was missed. (i) Picture sequence before, during, and after the contact with avatar 1.

same positions in all ten experiments and the participant always started from the same point. The subject was encouraged to look around in the street during the experiment and to answer the statements of the avatars, like it would be in reality.

3. RESULTS

In two days, the tetraplegic subject performed ten runs and he was able to stop at 90% of the 150 avatars and talked to them. In four runs, he achieved a performance of 100% (see Table 1). In general, the distance between the avatar and the subject during talking was 1.81 ± 0.49 units, whereby, the communication range (allowed gap between avatar and subject) was 0.5 to 2.5 units. In the example given in Figure 3(f), the subject entered the communication sphere of avatar 1 (5.5–7.5 units) at second 8.3 and stopped at second 8.9 (6.1 units). Unfortunately, he started moving again at second 9.3, so the pause was below 1 second and, therefore, the stop did not activate the avatar. Nevertheless, he managed to stop again at second 10.4 (7.1 units), which was still in the communication sphere and at this time, he was standing still for longer than 1 second, so he correctly stopped at the avatar, which replied: "My name is Maggie" at second 11.4. At second 15.4, he started moving towards avatar 2. In general, it took him 6.66 seconds ± 4.85 seconds to restart moving after the contact with the avatar.

In Figure 3(h), spatial-temporal tracking data of the first four avatars of three runs are presented. In some runs, the subject started earlier with foot MI and walked straight to the avatar, whereby in other runs stops between the avatars occurred. Detailed information of all runs is given in Table 1. The duration of one run (each run lasted approximately 355 ± 60 seconds) depended only on the performance of the subject. In the Graz-BCI, the EEG is classified sample-by-sample and the EEG data revealed that foot motor imagery could be detected in 18.2% ± 6.4% of the run time. The averaged duration of MI periods was 1.58 seconds ± 1.07 seconds,

Table 1: Positions and times of the contacts between the subject and the avatars of all runs. The position is given in units and the time (in seconds) of the speaking avatar is given in brackets behind the position. In the first two columns, the number of the avatar (No.) and the spatial placement of the avatar (AvPos) are shown. In case of missed avatars, the number of occurred stops within the communication sphere is given in square brackets. In the last row, the performance (perf., in %) of each run is specified.

No.	AvPos	Run 1	Run 2	Run 3	Run 4	Run 5	Run 6	Run 7	Run 8	Run 9	Run 10
1	8	6.7 (48.2)	6.3 (56.7)	6.8 (33.0)	5.9 (12.0)	5.9 (14.8)	5.6 (19.5)	6.6 (20.0)	5.6 (19.8)	6.6 (53.4)	5.9 (18.8)
2	11	9.3 (65.3)	9.2 (76.0)	9.1 (43.7)	9.0 (20.8)	9.0 (22.1)	9.7 (36.6)	9.0 (25.4)	8.7 (31.7)	10.0 (60.7)	9.8 (52.0)
3	15	13.7 (84.6)	12.7 (98.5)	13.2 (55.9)	12.4 (31.6)	— [1]	12.7 (54.0)	— [1]	14.1 (42.4)	— [1]	13.1 (56.4)
4	18	15.7 (92.1)	16.6 (111.7)	17.2 (67.8)	16.6 (43.3)	15.4 (37.0)	16.4 (66.7)	16.4 (40.1)	17.2 (51.0)	15.6 (75.9)	16.1 (61.4)
5	22	20.5 (117.4)	20.3 (127.2)	20.0 (82.0)	20.6 (55.5)	19.5 (48.2)	— [1]	20.2 (45.4)	20.9 (61.2)	20.9 (99.0)	— [0]
6	32	30.2 (131.3)	30.6 (149.8)	29.7 (100.4)	29.9 (74.6)	— [1]	30.4 (96.6)	30.3 (59.3)	29.4 (83.0)	30.1 (113.3)	30.9 (78.6)
7	35	33.2 (150.3)	— [1]	33.6 (109.6)	33.5 (92.2)	— [1]	34.1 (113.0)	33.5 (72.2)	33.1 (101.9)	33.6 (122.5)	33.3 (84.4)
8	39	37.8 (175.0)	36.5 (180.6)	37.7 (120.8)	36.4 (97.7)	36.4 (85.9)	36.6 (119.5)	36.4 (80.3)	37.8 (117.2)	37.3 (135.0)	36.4 (90.6)
9	44	41.5 (182.0)	42.0 (199.6)	42.3 (136.6)	42.8 (113.3)	41.5 (96.3)	42.6 (150.5)	41.9 (92.8)	42.1 (126.8)	42.8 (142.6)	41.9 (98.2)
10	47	44.5 (198.9)	44.8 (215.7)	45.3 (146.6)	44.7 (122.8)	45.6 (112.3)	46.2 (175.8)	45.1 (101.4)	45.3 (139.3)	45.3 (150.6)	45.0 (108.3)
11	51	48.7 (223.5)	50.0 (244.5)	48.6 (159.6)	49.7 (134.8)	— [1]	— [0]	49.1 (110.3)	49.3 (153.1)	49.0 (162.7)	49.8 (131.5)
12	56	54.1 (251.7)	55.0 (272.4)	53.9 (172.7)	53.7 (143.7)	53.6 (147.9)	54.0 (206.7)	54.5 (127.4)	54.1 (167.8)	55.1 (182.4)	— [1]
13	60	57.9 (277.6)	58.0 (283.5)	58.4 (187.1)	58.0 (156.7)	57.5 (165.3)	— [2]	58.4 (135.7)	58.1 (181.1)	— [0]	58.2 (157.4)
14	63	62.2 (305.5)	61.8 (300.0)	61.1 (198.0)	60.5 (164.3)	61.3 (177.7)	61.6 (239.8)	60.5 (150.2)	61.0 (191.5)	— [0]	60.9 (163.8)
15	67	65.3 (355.8)	66.4 (322.2)	65.2 (213.7)	65.2 (175.8)	65.8 (198.7)	— [1]	64.9 (160.7)	65.1 (204.9)	64.9 (212.7)	64.6 (172.2)
Perf.		100%	93.3%	100%	100%	73.3%	73.3%	93.3%	100%	80%	86.6%

with a maximum of 5.24 seconds and a median of 1.44 seconds.

In 11 of the 15 missed avatars (of all runs), the subject stopped within the communication range, but the stopping time was too short (between 0.08 and 0.88 seconds, mean $\pm$SD = 0.47 second $\pm$ 0.27 second). In Table 1, the number of these occurred stops is given in square brackets for each missed avatar. The stops occurred at 1.43 $\pm$ 0.47 units before the avatar. At one avatar he stopped twice but both stops where too short (0.76 and 0.56 seconds).

3.1. Simulation with surrogate data: random walk simulation

For evaluation purposes, a "random walk" simulation was performed. The aim of this simulation was to demonstrate that only the intentional thought-based control of the subject allowed a successful completion of the task. No coincindentally created sequence should result in any correct accessed avatar. As surrogate data a random sequence has been used instead of the EEG for simulating IC (go) and NC (stop). The ratio of IC to NC was varied and always 10 000 repetitions were simulated. In the case with the same ratio as in the performed experiments (IC : NC = 0.182 : 0.818), no avatars were correctly accessed. It is clear that, if the surrogate data would contain only one go (IC) sample followed by, for example, thousands of stop (NC) samples and then the next go sample and so on, a completely perfect performance (contact with every avatar) would be produced, but the duration of the run would increase towards infinity. Therefore, several ratios were examined $(0.5, 0.1, 0.05, \ldots : 1)$ and almost all of them returned zero hits (correctly accessed avatars). The first avatar contact occurred at a ratio of 0.001 : 1 (IC to NC samples). For this test, the duration of the run had to be extended by 200 times (about 20 hours) and the number of correctly stopped avatars was 0.002 $\pm$ 0.015, compared to 13.5 $\pm$ 1.6 avatars within 355 seconds (about 6 minutes) in the performed experiment with the tetraplegic subject.

4. DISCUSSION

The implementation of a self-paced (asynchronous) EEG-based BCI for the control of applications in virtual environment was successfully demonstrated with a

tetraplegic subject. The patient was able to move forward in the virtual street and to stop at each avatar with a single bipolar EEG recording. The prominent induced centrally localized beta oscillations, allowed a very simple signal processing approach (compare Figure 3(c) with Figure 3(d)). In an interview, the subject confirmed that moving occurred only during periods of foot motor imagery, but he reported that it was hard to stop precisely. Specifically, when the avatars were placed more to the left or right, it was difficult to find the "correct distance" to the avatar. The instructions given to the participant before the experiment did not imply the restriction to perform the experiment as fast as possible, but to take his time to look around, talk to the avatars or enjoy the VR world. Therefore, no statement about the duration of the runs can be given.

In four runs, the subject was able to reach a performance of 100%, in all other runs, in minimum one avatar was missed. In most of the missed avatars (except two), the subject stopped either too shortly within the communication sphere or stopped close before (too early) or shortly after the sphere (too late). The reason for these missed avatars was the invisible communication sphere around the avatars, which was reported by the subject as the biggest disadvantage of this VE. So it was not clear for the subject where the sphere started or ended, especially when the avatars were placed further away from the middle of the street and the sphere was, therefore, very small. Sometimes he thought to be close enough, but maybe missed it by a hairbreadth, so an additional very small "step" (very short foot MI) was necessary to come inside the sphere. Unfortunately, it could happen that this step was too large (too long) and the sphere already passed by. Oscillatory EEG components need some time to appear and stop, so very short bursts (necessary for such small steps) are very unlikely to be produced. Maybe it would have been better to visualize the communication sphere or to change the appearance of the avatar (e.g., the color, the expression on the face, etc.) whenever the subject has entered the sphere. Nevertheless, the design of the experiment with necessary periods of IC (moving) and defined positions of NC (stopping close to the avatars) guaranteed that the performance during the asynchronous control could be verified. A drawback of the experimental design is that it forced the subject to be able in minimum to stop for 1 second (NC), but did not force the participant for shorter or longer periods of IC (no impact on the performance, just influencing the duration of a run). So good NC control was more crucial than IC control. Unfortunately, no values for TP and FP can be given for the experiment. Successful stops (90%) could be reported as TP and missed avatars (10%) as FN (false negative), but FP and TN (true negative) cannot be evaluated. The experiment itself required only periods of NC for stopping at the avatars and talking to them. Therefore, after reaching the last avatar, the BCI was not stopped and the subject was instructed to stand still and wait till the VE was shut down. In this period of NC no movement happened (duration between 8 and 93 seconds, mean = 44 seconds). The outcome of the simulation with surrogate data showed that only the intentional control of the subject allowed a successful accomplishment of the given task, almost all simulated data resulted in zero hits (no correct avatar contact).

The usage of a visually-rich VE with avatars, which were talking to the subject, ensured that the experiment was diverse and even distracting for the subject, somewhat like in the real world. Nevertheless, the subject was able to succeed with 90%. It is known that the development of skills or knowledge that are obtained while someone is in a VE can be transferred to real-world behavior and performance [6, 7]. Indeed, VEs have also been shown to reinforce the building of new neural pathways through imaginations or intention to move a paralyzed limb [1, 2]. For a person who is wheelchair-bound, VEs are especially attractive. First, simply using a VE that includes, for example, immersion in an almost all-surrounding stereo world [31] with the freedom to move at will can give such persons access to experiences that may be long forgotten (or which they have never had). Another advantage here is that the simulation power of VEs can be used to create virtual prototypes of new navigation or control methods, and give potential users experience of them in a safe environment, before they are ever built physically.

The next step would be to extend the BCI to more than one IC state, and thereby increase the degree of freedom and allow the subject to choose the direction of moving, for example, by imagining a left- or right-hand movement [34]. In the future, the final goal will be to control a real wheelchair in a real street. This could be supported by applying a similar procedure as Millán [35] reported during the control of a miniaturized robot through an 80×60 cm representation of an empty flat. Thereby, the BCI was sending only high-level commands (forward, right, follow left wall, etc.) every 0.5 second to a finite state automation. The robot was executing the high-level command (e.g., turn right at next occasion) autonomously using its on-board sensors (infrared proximity sensors for obstacles detection) and was continuing the command till the next high-level command was sent. Although the difficulties and challenges are more on the side of the robot/wheelchair as on the side of the BCI, the feasibility of a successful completion of such real-world navigation task is increased.

5. CONCLUSION

For the first time, it was demonstrated that a tetraplegic subject, sitting in a wheelchair, could control his movements in a VE by the usage of a self-paced (asynchronous) BCI based on one single EEG recording. The usage of a visual-rich VE with talking avatars ensured that the experiment is diversified and engaging but contains enough distraction as it would be in a real street. Controlling a VE (e.g., the virtual wheelchair) is the closest possible scenario for controlling the real wheelchair in a real street, so virtual reality allows patients to perform movements in a safe environment. So a further step of transferring the BCI from laboratory conditions towards real-world applications could be performed.

ACKNOWLEDGMENTS

This work was carried out as part of the PRESENCCIA project, an EU funded Integrated Project under the IST

program (Project no. 27731) and supported by October Films, Hewlett-Packard and the EU COST B27 program. The authors would like to thank the subject for his participation.

REFERENCES

[1] M. K. Holden, "Virtual environments for motor rehabilitation: review," *Cyberpsychology & Behavior*, vol. 8, no. 3, pp. 187–211, 2005.

[2] J. Broeren and O. Scott, "Commentary on Holden, M. K., virtual environments for motor rehabilitation: review," *CyberPsychology & Behavior*, vol. 8, no. 3, pp. 212–219, 2005.

[3] D. Jack, R. Boian, A. S. Merians, et al., "Virtual reality-enhanced stroke rehabilitation," *IEEE Transactions on Neural Systems and Rehabilitation Engineering*, vol. 9, no. 3, pp. 308–318, 2001.

[4] M. Girone, G. Burdea, M. Bouzit, V. Popescu, and J. E. Deutsch, "Orthopedic rehabilitation using the "rutgers ankle" interface," *Studies in Health Technology and Informatics*, vol. 70, pp. 89–95, 2000.

[5] J. S. Webster, P. T. McFarland, L. J. Rapport, B. Morrill, L. A. Roades, and P. S. Abadee, "Computer-assisted training for improving wheelchair mobility in unilateral neglect patients," *Archives of Physical Medicine and Rehabilitation*, vol. 82, no. 6, pp. 769–775, 2001.

[6] R. V. Kenyon and M. B. Afenya, "Training in virtual and real environments," *Annals of Biomedical Engineering*, vol. 23, no. 4, pp. 445–455, 1995.

[7] F. D. Rose, E. A. Attree, B. M. Brooks, et al., "Training in virtual environments: transfer to real world tasks and equivalence to real task training," *Ergonomics*, vol. 43, no. 4, pp. 494–511, 2000.

[8] E. Todorov, R. Shadmehr, and E. Bizzi, "Augmented feedback presented in a virtual environment accelerates learning of a difficult motor task," *Journal of Motor Behavior*, vol. 29, no. 2, pp. 147–158, 1997.

[9] F. D. Rose, B. M. Brooks, and A. A. Rizzo, "Virtual reality in brain damage rehabilitation: review," *Cyberpsychology & Behavior*, vol. 8, no. 3, pp. 241–262, 2005.

[10] N. Foreman and J. Stirk, "Commentary on Rose, F. D., Brooks, B. M. & Rizzo, A. A., virtual reality in brain damage rehabilitation: review," *CyberPsychology & Behavior*, vol. 8, no. 3, pp. 263–271, 2005.

[11] G. Pfurtscheller and C. Neuper, "Motor imagery and direct brain-computer communication," *Proceedings of the IEEE*, vol. 89, no. 7, pp. 1123–1134, 2001.

[12] J. R. Wolpaw, N. Birbaumer, D. J. McFarland, G. Pfurtscheller, and T. M. Vaughan, "Brain-computer interfaces for communication and control," *Clinical Neurophysiology*, vol. 113, no. 6, pp. 767–791, 2002.

[13] E. C. Lalor, S. P. Kelly, C. Finucane, et al., "Steady-state VEP-based brain-computer interface control in an immersive 3D gaming environment," *EURASIP Journal on Applied Signal Processing*, vol. 2005, no. 19, pp. 3156–3164, 2005.

[14] J. D. Bayliss, "Use of the evoked potential P3 component for control in a virtual apartment," *IEEE Transactions on Neural Systems and Rehabilitation Engineering*, vol. 11, no. 2, pp. 113–116, 2003.

[15] R. Leeb, C. Keinrath, D. Friedman, et al., "Walking by thinking: the brainwaves are crucial, not the muscles!," *Presence: Teleoperators and Virtual Environments*, vol. 15, no. 5, pp. 500–514, 2006.

[16] G. Pfurtscheller, R. Leeb, C. Keinrath, et al., "Walking from thought," *Brain Research*, vol. 1071, no. 1, pp. 145–152, 2006.

[17] J. F. Borisoff, S. G. Mason, A. Bashashati, and G. E. Birch, "Brain-computer interface design for asynchronous control applications: improvements to the LF-ASD asynchronous brain switch," *IEEE Transactions on Biomedical Engineering*, vol. 51, no. 6, pp. 985–992, 2004.

[18] S. G. Mason, J. Kronegg, J. E. Huggins, M. Fatourechi, and A. Schlögl, "Evaluating the performance of self-paced brain-computer interface technology," Tech. Rep., Brain-Interface Laboratory, Neil Squire Society, Vancouver, Canada, 2006. http://www.bci-info.org/.

[19] J. R. Millán and J. Mouriño, "Asynchronous BCI and local neural classifiers: an overview of the adaptive brain interface project," *IEEE Transactions on Neural Systems and Rehabilitation Engineering*, vol. 11, no. 2, pp. 159–161, 2003.

[20] G. R. Müller-Putz, R. Scherer, G. Pfurtscheller, and R. Rupp, "EEG-based neuroprosthesis control: a step towards clinical practice," *Neuroscience Letters*, vol. 382, no. 1-2, pp. 169–174, 2005.

[21] R. Scherer, G. R. Müller-Putz, C. Neuper, B. Graimann, and G. Pfurtscheller, "An asynchronously controlled EEG-based virtual keyboard: improvement of the spelling rate," *IEEE Transactions on Biomedical Engineering*, vol. 51, no. 6, pp. 979–984, 2004.

[22] G. Townsend, B. Graimann, and G. Pfurtscheller, "Continuous EEG classification during motor imagery-simulation of an asynchronous BCI," *IEEE Transactions on Neural Systems and Rehabilitation Engineering*, vol. 12, no. 2, pp. 258–265, 2004.

[23] G. Pfurtscheller, C. Guger, G. R. Müller-Putz, G. Krausz, and C. Neuper, "Brain oscillations control hand orthosis in a tetraplegic," *Neuroscience Letters*, vol. 292, no. 3, pp. 211–214, 2000.

[24] G. R. Müller-Putz, R. Scherer, G. Pfurtscheller, and R. Rupp, "Brain-computer interfaces for control of neuroprostheses: from synchronous to asynchronous mode of operation," *Biomedizinische Technik*, vol. 51, no. 2, pp. 57–63, 2006.

[25] G. Pfurtscheller, G. R. Müller-Putz, J. Pfurtscheller, H. J. Gerner, and R. Rupp, "'Thought'—control of functional electrical stimulation to restore hand grasp in a patient with tetraplegia," *Neuroscience Letters*, vol. 351, no. 1, pp. 33–36, 2003.

[26] H. H. Jasper, "The ten-twenty electrode system of the international federation," *Electroencephalography and Clinical Neurophysiology*, vol. 10, no. 2, pp. 370–375, 1958.

[27] G. Pfurtscheller, G. R. Müller-Putz, A. Schlögl, et al., "15 years of BCI research at Graz university of technology: current projects," *IEEE Transactions on Neural Systems and Rehabilitation Engineering*, vol. 14, no. 2, pp. 205–210, 2006.

[28] rtsBCI, "Graz brain-computer interface real-time open source package," http://sourceforge.net/projects/biosig/, 2004-2007.

[29] BioSig, "An open source software package for biomedical signal processing under matlab," http://biosig.sf.net/, 2003-2007.

[30] C. Cruz-Neira, D. J. Sandin, and T. A. DeFanti, "Surround-screen projection-based virtual reality: the design and implementation of the CAVE," in *Proceedings of the 20th Annual Conference on Computer Graphics and Interactive Techniques*, pp. 135–142, Anaheim, Calif, USA, August 1993.

[31] M. Slater, A. Steed, and Y. Chrysanthou, *Computer Graphics and Virtual Environments: From Realism to Real-Time*, Addison-Wesley, Boston, Mass, USA, 2001.

[32] E. Frécon, G. Smith, A. Steed, M. Stenius, and O. Ståhl, "An overview of the COVEN platform," *Presence: Teleoperators and Virtual Environments*, vol. 10, no. 1, pp. 109–127, 2001.

[33] VRPN, "Virtual reality peripheral network," http://www.cs.unc.edu/Research/vrpn/.

[34] R. Scherer, A. Schlögl, F. Lee, H. Bischof, D. Grassi, and G. Pfurtscheller, "The self-paced Graz brain-computer interface: methods and applications," to appear in *Computational Intelligence and Neuroscience*, 2007.

[35] J. R. Millán, F. Renkens, J. Mouriño, and W. Gerstner, "Non-invasive brain-actuated control of a mobile robot by human EEG," *IEEE Transactions on Biomedical Engineering*, vol. 51, no. 6, pp. 1026–1033, 2004.

Hindawi Publishing Corporation
Computational Intelligence and Neuroscience
Volume 2007, Article ID 28692, 12 pages
doi:10.1155/2007/28692

Research Article

Enhanced Detection of Visual-Evoked Potentials in Brain-Computer Interface Using Genetic Algorithm and Cyclostationary Analysis

Cota Navin Gupta and Ramaswamy Palaniappan

Department of Computing and Electronic Systems, University of Essex, Wivenhoe Park, Colchester CO4 3SQ, UK

Correspondence should be addressed to Ramaswamy Palaniappan, rpalan@essex.ac.uk

Received 18 February 2007; Accepted 4 July 2007

Recommended by Andrzej Cichocki

We propose a novel framework to reduce background electroencephalogram (EEG) artifacts from multitrial visual-evoked potentials (VEPs) signals for use in brain-computer interface (BCI) design. An algorithm based on cyclostationary (CS) analysis is introduced to locate the suitable frequency ranges that contain the stimulus-related VEP components. CS technique does not require VEP recordings to be phase locked and exploits the intertrial similarities of the VEP components in the frequency domain. The obtained cyclic frequency spectrum enables detection of VEP frequency band. Next, bandpass or lowpass filtering is performed to reduce the EEG artifacts using these identified frequency ranges. This is followed by overlapping band EEG artifact reduction using genetic algorithm and independent component analysis (G-ICA) which uses mutual information (MI) criterion to separate EEG artifacts from VEP. The CS and GA methods need to be applied only to the training data; for the test data, the knowledge of the cyclic frequency bands and unmixing matrix would be sufficient for enhanced VEP detection. Hence, the framework could be used for online VEP detection. This framework was tested with various datasets and it showed satisfactory results with very few trials. Since the framework is general, it could be applied to the enhancement of evoked potential signals for any application.

1. INTRODUCTION AND MOTIVATION

Oscillating potentials derived from the scalp surface using electrodes and believed to originate from outer layer of brain (neurons in the cortex) are called visual-evoked potential (VEP) signals [1]. These signals are derived from the brain's response to visual stimulation and have applications in numerous neuropsychological studies [1]. However, a major hurdle in analysing VEP, which is considered as a subset of event-related potential (ERP), is the extremely poor signal-to-noise ratio (SNR) of the VEP signals embedded within the ongoing background electroencephalogram (EEG). Averaging is commonly used to reduce the effects of EEG because VEP signals are assumed to be loosely time-locked to the stimulus, thereby adding up with averaging while EEG will be reduced due to its random property [2]. It is known that ERP is not a homogeneous signal, but instead a combination of different components due to which variations in amplitude and latency between trials are caused. Also, identical stimuli do not necessarily evoke identical responses [3, 4]; trial-to-trial variability can be appreciable, and ERP waveform, amplitude, and latency can change appreciably with time [3, 4]. Therefore, average ERP does not elicit the valid estimate of the VEP components amplitude and shape and hence is usually considered biased [4]. Next, the assumption that background EEG noise is random and uncorrelated seems untrue. Research has shown that EEG is not entirely uncorrelated with event-related activity [5]. Hence, the basic assumptions underlying signal averaging is generally violated with the above discussion.

ERPs consist of exogenous and endogenous components [6]. Exogenous components are obligatory responses which result on the presentation of physical stimuli. The endogenous components (say P300 component of the ERP signal) manifest the processing activities which depend on the stimuli's role within the task being performed by the subject [7]. P300-based brain-computer interface (BCI) systems [8–10] usually control the variance of the endogenous

components. However, latency jitters are likely to affect endogenous VEP components more than exogenous components because variations due to cognitive process will affect the latencies of endogenous components that are less time locked to the event onset and are more dependent on the task [5]. It can, therefore, be problematic to compare the amplitudes of ERPs computed over trials with varying latency jitter [10]. These facts seem to question the validity of using the average ERP for clinical analysis; but however these issues are the main motivations for this work.

Techniques to improve conventional averaging like the Woody's method [11] have been proposed. In Woody's method individuals, trials are time shifted to compensate for latency shifts which are assumed to occur uniformly over the entire trial. However, this time-consuming technique's validity decreases when numerous iterations are used and it might not be the optimal solution under conditions of very low SNR [12]. A simple lowpass filter with a predetermined passband may improve SNR but may not necessarily provide an optimal separation of signal from noise in overlapping spectral ranges for all subjects under different experimental conditions. Weiner filter may be considered but the approach was devised for uncorrelated stationary signals with known spectra [4]. Also, the procedure for estimating filter weights, when the entire ERP epoch is used, has to strike a balance between short duration latency (i.e., sensory evoked) and large long duration (i.e., P300) components [4]. The differing power spectra do not make the resulting filter optimal for either type of components. Since these requirements are not met in ERP analysis, the optimality of Wiener filter is questionable.

Independent component analysis (ICA) has been extensively used for removal of artifacts from EEG data [13] as well as for analysis and detection of VEP signals [9, 14, 15]. However, [14, 15] also highlight the inherent limitations of ICA: first, VEP is assumed to be completely independent of the ongoing EEG. Temporal independence is not satisfied when training dataset is too small. In [9], ICA was used to separate P300 source from background EEG and it required a matched filter to be constructed uniquely for each subject. It uses a scheme similar to averaging for the identification of letters. ERP classification procedures proposed recently [16–18] are unsuitable for online implementation because none of them actually identify embedded variable ERP waveforms. In this paper, we present an alternative framework to enhance VEP detection by first identifying the embedded variable VEP frequency bands (which are highly masked by the background EEG activity) using cyclostationary analysis (CS). This allows us to remove the nonoverlapping frequency bands between VEP and EEG which increases the independence between background EEG artifacts and VEP signals for the genetic algorithm and independent component analysis module (G-ICA). Cyclostationary algorithm which is used in this paper has applications in many areas, for example, blind channel identification and equalisation [19], rotating machine monitoring [20], filter bank optimisation [21], and system identification [22]. This property has been used in the past for many communication applications [23, 24] and is the result of the implicit periodicity of these signals related to the baud rate, carrier frequency, or any other periodic component.

We then use a variation of our previous genetic algorithm (GA) work [25] to remove in-band EEG artifacts. Basic principles of ICA were used in the work. The G-ICA idea with kurtosis maximisation proposed in [26] was applied to denoise heart (ECG) signals in our recent study [25]. GA is a computational model inspired by evolution which may be used to solve search and optimisation problems and is a form of artificial intelligence. The basic approach creates a population of chromosomes, which are a string of values representing potential solutions to a problem. Through the theory of natural selection and genetic recombination, these solutions evolve into future populations where only the important combinations of chromosomes survive. The ability to investigate many possible solutions simultaneously is the main advantage of GA [27]. GA minimises the mutual information (MI) criterion [28], the fitness function used in this work to separate EEG artifacts from VEP signals. MI measures general statistical dependence between variables and is invariant to monotonic transformations performed on the variables. The G-ICA method is simpler when compared to the ICA because it does not require complex neural learning algorithms [25]. We apply the proposed framework to enhance the detection of P300 components for BCI design.

2. METHODOLOGY

The novel framework to reduce background EEG artifacts from multitrial VEP signals for use in BCI design is shown diagrammatically in Figure 1. This scheme exploits the intertrial similarities of the VEP components in the frequency domain using CS analysis and removes the in-band EEG artifacts using G-ICA. This scheme overcomes the latency distortions of the many techniques proposed so far to detect the endogenous VEP components.

2.1. Cyclostationary analysis for VEP band detection

2.1.1. Theory

We briefly discuss the theory of cyclostationary signals. A discrete-time signal which has periodic mean and correlation is said to be cyclostationary [29]. In particular, a signal $x(t)$ is called first-order cyclostationary [30] if its time-varying mean $m_x(t) = E[x(t)]$ is periodic:

$$m_x(t + lp_1) = m_x(t) \quad \forall t, l \in Z. \tag{1}$$

Similarly, x is second-order cyclo-stationary [30] if its time-varying correlation

$$R_{xx}(t;\tau) = E[x(t)x(t+\tau)] \tag{2}$$

is periodic in t for any fixed τ:

$$R_{xx}(t + lp_2;\tau) = R_{xx}(t;\tau) \quad \forall t, l \in Z. \tag{3}$$

Here, p_1 and p_2 are the smallest positive integers such that (1) and (3) hold, respectively. If p_1 and $p_2 = 1$, we observe from

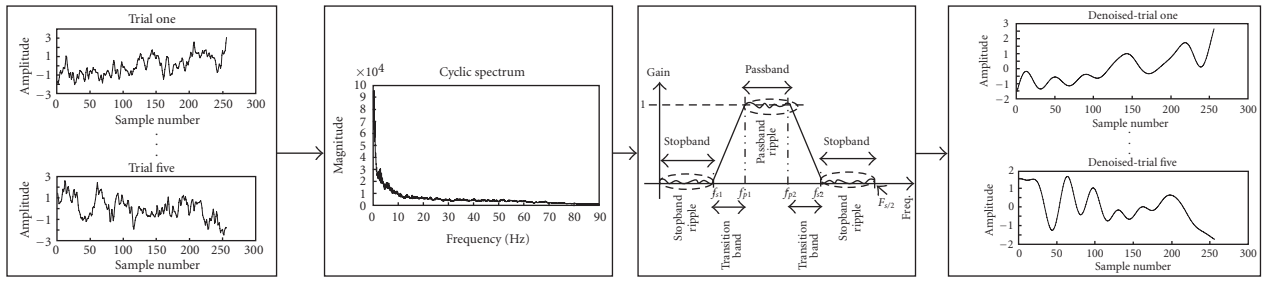

Figure 1: Block diagram of the proposed approach for use in VEP-based BCI design.

(1) and (3) that mean is time invariant and the correlation depends on the time difference only. Then, $x(t)$ is considered as a stationary signal or in the given discussion context a cyclostationary signal with period of one.

In the frequency domain cyclostationary (CS) analysis, if $x(t)$ considered in the above discussion is cyclostationary and has a time period T_o or fundamental frequency $f_o(= 1/T_o)$. We can define cyclic autocorrelation function of the same signal as follows [23]:

$$R_{xx}(\tau, f) = E\{x(t)x(t+\tau)\exp(-j2\pi f t)\}. \tag{4}$$

On averaging the various lags of the cyclic autocorrelation in frequency domain (4), we obtain a cyclic spectrum. The cyclic autocorrelation function (4) also satisfies the following property:

$$R_{xx}(\tau, f) = \begin{cases} \text{finite} & \text{if } f = nf_o, \\ 0, & \text{otherwise,} \end{cases} \tag{5}$$

where n is a nonzero integer. In the frequency domain, cyclostationary processes are characterized by the cyclic spectrum, which represents the density of correlation between the spectral components of a process which are separated by an amount equal to the cycle frequency. The frequency components in a stationary signal are not correlated with each other so the cyclic autocorrelation of a stationary signal which is not cyclostationary is zero for all values of f, except $f = 0$ [31].

2.1.2. Cyclo model for signal analysis

Based on the cyclostationary literature [23, 31], we discuss the cyclo model for signal analysis. Consider any recorded signal $x(t)$ obtained by corrupting the clean signal $s(t)$ with an additive noise signal $n(t)$ as below [31]:

$$x(t) = s(t) + n(t). \tag{6}$$

The noise $n(t)$ is assumed to be nonperiodic with any statistical distribution.

Let $R_x(\tau, f)$, $R_s(\tau, f)$, $R_n(\tau, f)$ be the cyclic autocorrelation functions of $x(t)$, $s(t)$ and $n(t)$, respectively. We can then write (6) in cyclic autocorrelation domain as [31]:

$$R_x(\tau, f) = R_s(\tau, f) + R_n(\tau, f). \tag{7}$$

Since $n(t)$ is not cyclostationary, it means that $R_n(\tau, f) = 0$, for $f \neq 0$ and (7) becomes

$$R_x(\tau, f) = R_s(\tau, f) \quad \text{for } f \neq 0. \tag{8}$$

This model suggests that, independent of noise statistics, the cyclic autocorrelation function is insensitive to noise as long as the noise is not periodic.

2.1.3. VEP signal band detection using cyclostationary analysis

We present a scheme based on the above model for enhanced detection of VEP band by exploiting the cyclostationarity property. The salient feature of this technique is the fact that trials are not required to be phase locked when recorded. To exploit the intertrial similarities of the VEP signal components in the frequency domain, cyclostationary is introduced by concatenating the recorded trials. The periodic repetition of the P300 components in the VEP trials for all trials (i.e., 300–600 ms after the occurrence of stimuli) enables cyclic analysis of the VEP signals.

To help study the cyclostationary property, we emulated the VEP and EEG signals that were similar to real-signal recordings. Gaussian waveforms were chosen to emulate the real-VEP-signal components as in a previous study [32] due to their suitability. The Gaussian waveform equation is given below [32]:

$$G(n) = \left[\frac{A}{\sqrt{2\pi\sigma^2}}\right] \exp\left(-\frac{(n-\mu)^2}{2\sigma^2}\right), \tag{9}$$

where μ is the mean, σ is the standard deviation, and A is the amplitude of the signal. Variability between trials of the VEP signals was achieved by varying μ, σ, and A for the Gaussian waveforms. The simulated VEP signal and its cyclic spectrum are shown in Figure 2. The cyclic spectrum which exploits the inter trial similarities in the frequency domain depicts the cyclic VEP components at 0–10 Hz as Figure 2. In the experimental study section, similar fact is ascertained with other datasets.

The stationarity of the background EEG noise has been reported in the literature [33] for periods of several hundred milliseconds. The EEG was constructed using whitening method and the AR model [34], which is as follows. Several real-EEG-signals, extracted while the subjects are at rest,

were first whitened to remove correlation between their components to achieve unit variance and zero mean. Common whitening method based on the eigenvalue decomposition of the covariance matrix was used [32]. AR coefficients are then obtained from the whitened EEG signal. These AR coefficients are used for the generation of simulated background EEG noise. The simulated EEG signal and its cyclic spectrum are shown in Figure 3.

Since the background EEG noise is not cyclostationary, the cyclic spectrum is approximately flat for $f \neq 0$ as discussed in the above cyclo model signal analysis section, which seems to justify the earlier assumed fact about the stationarity of the background EEG. Also, an important fact that the magnitude of cyclic VEP components is much more appreciable in the 0–10 Hz range than that of the background EEG is inferred from the cyclic spectrums of emulated VEP and stimulated EEG signals.

Additive noise assumption is usually made by all VEP estimation algorithms since there is no clear evidence in literature to suggest the nonlinear interaction of the noise and signal components. The cyclic spectrum of VEP signal with EEG noise in Figure 4 clearly highlights the cyclic VEP components. The similar magnitude spectra in the 0–10 Hz range in Figures 2 and 4 along with the discussed model seems to verify that cyclostationary model is suitable for VEP analysis.

To affirm the simulations and the discussed model, we further tested the cyclostationary algorithm with the BCI competition III (dataset IIb) provided by Wadsworth Centre, NYS Department of Health. Channel (Cz) of the training data from subject A was used to test the proposed algorithm. Figure 5 depicts the obtained cyclic spectrum of the VEP characterized by the P300 component for a character. It clearly depicts the delta (0–4 Hz) and theta (4–10 Hz) ranges as the main components of power in frequency domain for P300 waves [35, 36]. Thus, it is possible to identify the embedded endogenous components of the ERP signal with varying latency jitters in P300-based BCI systems.

A lowpass or bandpass filter can be designed based on the observed cyclic spectrum to filter the nonoverlapping EEG background noise from VEP signals for different experimental conditions and various subjects.

2.2. *In-band denoising using genetic algorithm and mutual information*

This section explores an information-theory-based approach using MI to remove the in-band EEG artifacts for VEP signal applications. It involves a variation of our previous work which makes use of G-ICA [25]. Techniques to reduce noise like adaptive filtering, ICA, and wavelets have been proposed in literature [14, 15]. ICA is a statistical method which transforms an observed multicomponent dataset into independent components that are statistically as independent as possible. For better removal of artifacts, the estimated components should be least dependent on each other. We can use measures like kurtosis, negentropy, and MI to evaluate the independence among the estimated sources [37]. In terms of robustness, cumulant-based estimators (like kurtosis) are not optimal. The main reasons are: higher-order cumulant measure the tails of the distributions, and are not influenced by structure in the middle of the distribution; the estimators of the higher order cumulants are very sensitive to outliers [37]. Their value can depend on the outliers alone. Among these various measures, MI seems to be the best choice to measure the independence of the estimated sources. MI is a

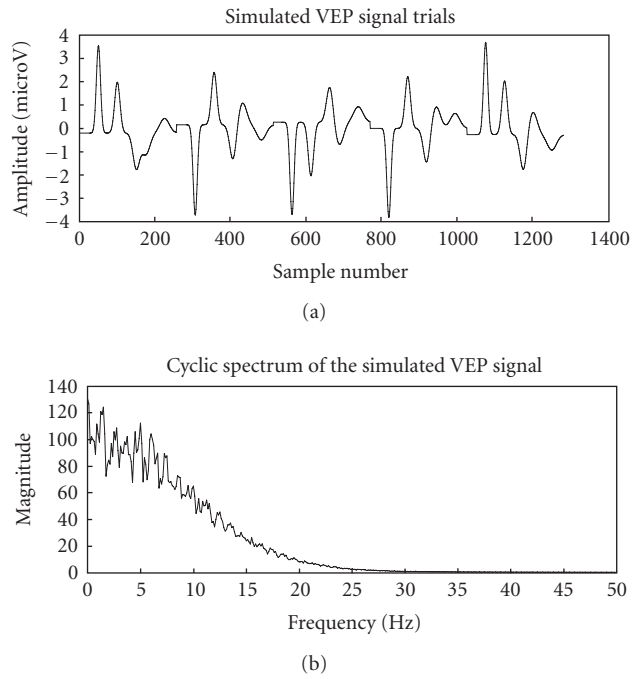

Figure 2: Simulated VEP signal and its cyclic spectrum.

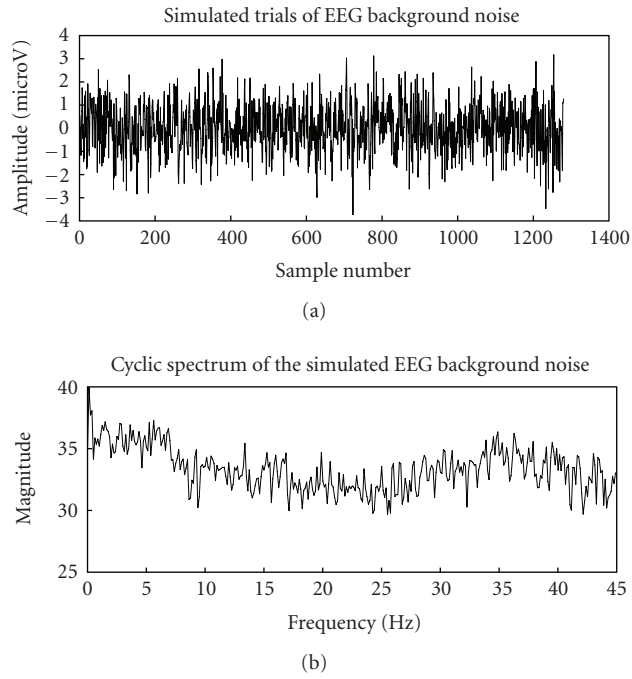

Figure 3: Simulated background EEG noise and its cyclic spectrum.

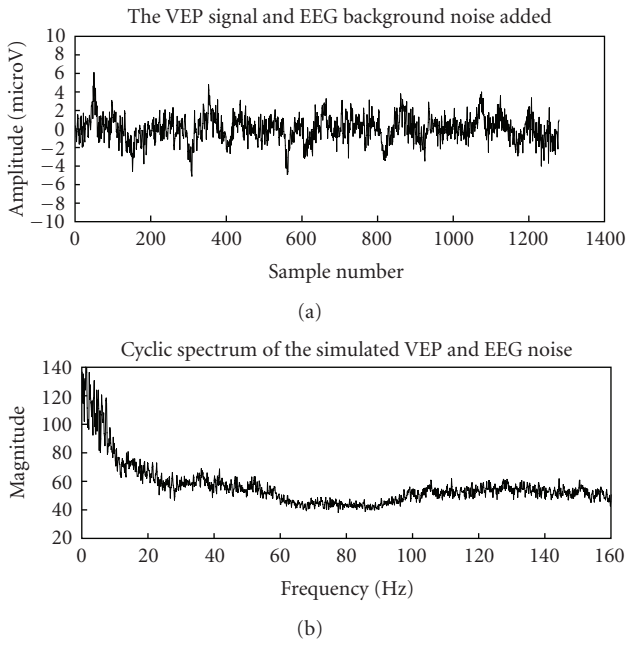

Figure 4: VEP with background EEG noise and its cyclic spectrum.

measure of general dependence between two random variables [38]. Given two random variables X and Y, the mutual information $I(X;Y)$ is defined as follows:

$$I(X;Y) = H(X) + H(Y) - H(X,Y), \tag{10}$$

where $H(\cdot)$ denotes the entropy of random variable and measures the uncertainty associated with it. Since the EEG data is discrete we can define $H(X)$ as follows:

$$H(X) = -\sum p(X)\log_2 p(X), \tag{11}$$

where $p(X)$ represents the marginal probability distribution of the data. Mutual information has a maximum value when two time series are exactly same. The MI between random variables (here the components of the VEP signal with EEG artifacts after ICA decomposition) was estimated.

ICA seems to be the most successful of all methods to obtain independent components. Here, we present a variation from our recent work [25] using GA that minimises the MI of the extracted components to reduce the overlapping EEG noise. The mixing matrix is iteratively improved for EEG artifact separation where MI is used as the fitness function to be minimised by the GA. ICA aims at finding linear projections of the data that maximise their mutual independence [39]. It is a technique which exploits higher-order statistics and optimisation techniques for obtaining independent sources, S from their linear mixtures, X, when neither the original sources nor the actual mixing matrix A are known as shown below in (12) [39]. The illustration of the mathematical model is given as:

$$X = AS \longrightarrow \hat{S} = WX. \tag{12}$$

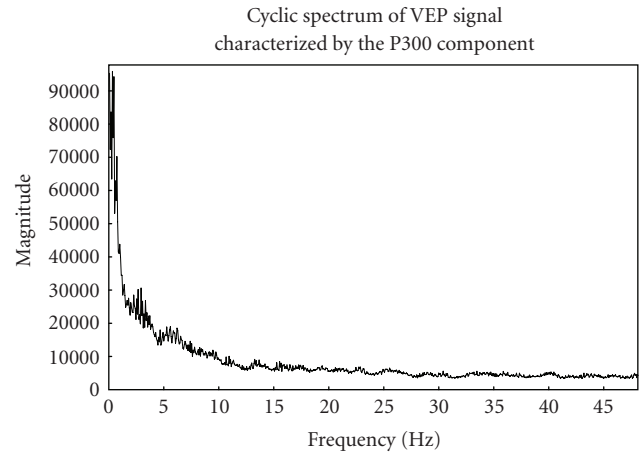

Figure 5: Cyclic spectrum of dataset IIb (BCI competition III).

To delve deep into the method, let us consider an example. Assuming 5 trials of recordings as shown below:

$$\begin{bmatrix} X_1 \\ X_2 \\ X_3 \\ X_4 \\ X_5 \end{bmatrix} = \begin{bmatrix} a_{11} & a_{12} & a_{13} & a_{14} & a_{15} \\ a_{21} & a_{22} & a_{23} & a_{24} & a_{25} \\ a_{31} & a_{32} & a_{33} & a_{34} & a_{35} \\ a_{41} & a_{42} & a_{43} & a_{44} & a_{45} \\ a_{51} & a_{52} & a_{53} & a_{54} & a_{55} \end{bmatrix} \begin{bmatrix} \text{VEP}_{\text{signal}} \\ \text{EEG}_{\text{signal}} \\ \text{EEG}_{\text{signal}} \\ \text{EEG}_{\text{signal}} \\ \text{EEG}_{\text{signal}} \end{bmatrix}. \tag{13}$$

It is known that in ICA methods, the task is to obtain the matrix $[W]$ as in (12) to reconstruct the source matrix $\hat{S}$ as below:

$$\begin{bmatrix} \text{VEP} + \text{EEG}_1 \\ \text{VEP} + \text{EEG}_2 \\ \text{VEP} + \text{EEG}_3 \\ \text{VEP} + \text{EEG}_4 \\ \text{VEP} + \text{EEG}_5 \end{bmatrix} = \begin{bmatrix} w_{11} & w_{12} & w_{13} & w_{14} & w_{15} \\ w_{21} & w_{22} & w_{23} & w_{24} & w_{25} \\ w_{31} & w_{32} & w_{33} & w_{34} & w_{35} \\ w_{41} & w_{42} & w_{43} & w_{44} & w_{45} \\ w_{51} & w_{52} & w_{53} & w_{54} & w_{55} \end{bmatrix} \begin{bmatrix} X_1 \\ X_2 \\ X_3 \\ X_4 \\ X_5 \end{bmatrix}. \tag{14}$$

We then have: $\hat{S}$ = Components of (VEP + EEG)

$$\begin{aligned} &\text{Component of } (\text{VEP} + \text{EEG}_1) \text{ signal} \\ &\quad = W_{11}X_1 + W_{12}X_2 + W_{13}X_3 + W_{14}X_4 + W_{15}X_5 \\ &\qquad \vdots \\ &\text{Component of } (\text{VEP} + \text{EEG}_5) \text{ signal} \\ &\quad = W_{51}X_1 + W_{52}X_2 + W_{53}X_3 + W_{54}X_4 + W_{55}X_5. \end{aligned} \tag{15}$$

G-ICA is an attractive alternative to current ICA techniques and in this proposed method, the entire matrix $[W]$, will be reconstructed as GA iterates minimising the MI between the VEP signals and EEG artifacts. MI was calculated based on entropy estimates from k-nearest neighbour distances since they are data efficient, adaptive, and have minimal bias [40]. The mixing matrix is iteratively improved for source separation using decrements in MI which is used as the fitness function to be minimised by the GA. GA is explained using (14) and (15). GA operates on the coding of parameters

Table 1: Parameters for genetic algorithm.

Coding of genes	Binary coding converted to real value [1, 0] for fitness computation
Fitness function	Mutual information (MI)
Population size	20
no of genes	6 bits for each gene
Reproduction	Elitist selection (30% of population), tournament selection (35% of population), and roulette selection (35% of population)
Crossover type and rate	Uniform crossover, 0.5
Mutation type and rate	Randomly mutate selected bits, 0.01
Inversion type and rate	Inversion between 2 randomly selected points, 0.01
Convergence	100
Repetition	3

rather than the parameter itself. These parameters are called chromosomes and are a string of values which represent potential solutions to the given problem. Binary chromosomes converted to realvalues represent the mixing matrix that iterates through the GA operators: selection, crossover, mutation, and inversion minimising the fitness function given by the MI between the components. Genes (bits) is used to represent each of the coefficients in $[W]$as in (15). Since 5 signals are assumedly observed as in (13) and 6 bits are used for each coefficient, then each chromosome will have 150 bits. A population will consist of a certain number of chromosomes; say 20, as used for this study. The gene values in the chromosomes of the initial population are randomly set for each component. These bit-valued genes are converted to realvalued in the range of $[0, 1]$. Next, these 150 realvalued gene values are used in (15) to generate five components and then MI between the components is computed which is minimised over 100 generations to separate the in-band EEG artifacts and VEP signals.

Next selection (reproduction) is performed based on these fitness values, here, the MI between the components. During this phase of GA, chromosomes are selected from the population and recombined, producing offspring chromosomes that form the population for next generation. GA starts with an initial population and applies selection randomly from the initial population using a scheme that favours the more fit individuals (usually evaluated using the fitness function) to create the intermediate population. Good and fit chromosomes will probably be selected several times in a generation while the poor ones may not be selected at all. The common methods for performing the parent selection process are roulette wheel selection, elitist selection, and rank-based methods such as tournament selection. All three selection operators are used in this work. In tournament selection, certain numbers of chromosomes are picked randomly (in this case, 5) and the best chromosome (i.e., with the highest fitness) is stored. Since 35% of the new population will be selected using this method, this procedure is repeated to obtain 7 chromosomes, where there maybe more than one similar chromosome. Tournament selection is naturally inspired and has advantages like: absence of premature convergence and it also does not require explicit fitness function. Another 35% of the new population is selected using the roulette-wheel method. In this method, the fitness values of each chromosome are cumulatively added into a roulette wheel and when the wheel spins, there are more chances for chromosomes with higher fitness to get selected. A random number is generated to represent the wheel spin and the particular chromosome with the cumulative fitness range denoted by the number will be selected. Like in tournament selection, this is repeated 7 times to add to the existing 7 chromosomes. Rest of the population (30%) is selected using the elitist selection. In elitist selection, a number of best individuals in the population are always passed onto the next generation and this type of selection has the advantage of guaranteed convergence. Even though reproduction increases the percentage of better fitness chromosomes, the procedure is considerably sterile; it cannot create new and better chromosomes. This function is left over to crossover, mutation, and inversion operators. These operations are performed in a similar way as in our previous work [25]. Table 1 summarises the used GA parameters for this study.

3. EXPERIMENTAL STUDY AND RESULTS

The proposed framework to reduce background EEG noise from VEP signals was tested with BCI competition III (dataset IIb) and the P300 datasets of a subject recorded at BCI lab, University of Essex. Only a single channel (Cz) was used with 5 trials to detect the target.

3.1. BCI competition III (dataset IIb)

This dataset allowed a subject to communicate one of the 36 symbols presented on a 6×6 matrix. The dataset had specifications of 36 classes, 64 EEG channels (0.1–60 Hz), 240 Hz sampling rate, 85 training, and 100 test trials, recorded with the BCI2000 system. It followed the standard procedure developed by Farwell and Donchin for P300-based BCIs. The method assumes that the EEG epoch associated with the relevant column and the relevant row will contain a detectable P300 for a single intensification, while the other epochs will not. The data presented to our framework were obtained by averaging together each combination of row and column single-trial epochs. Thus, there were 6 rows by 6 columns = 36 row-column intersection average (RCIA).

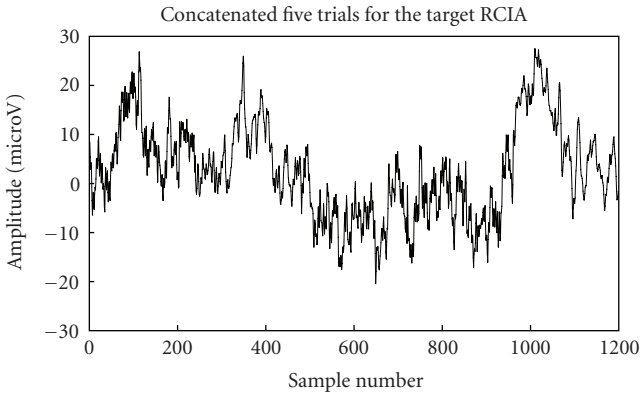

Figure 6: Signal trials for target RCIA from BCI competition III (dataset IIb).

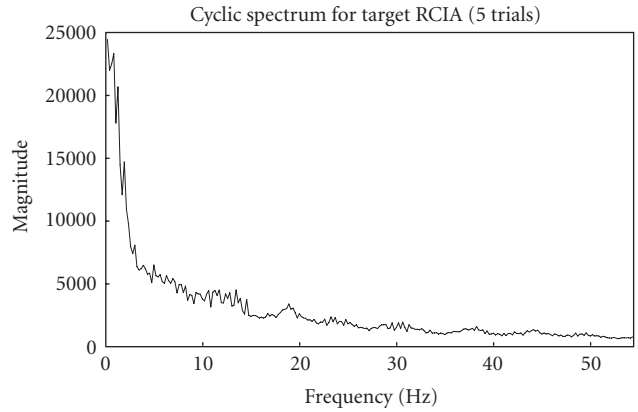

Figure 8: Five-trials cyclic spectrum for target RCIA.

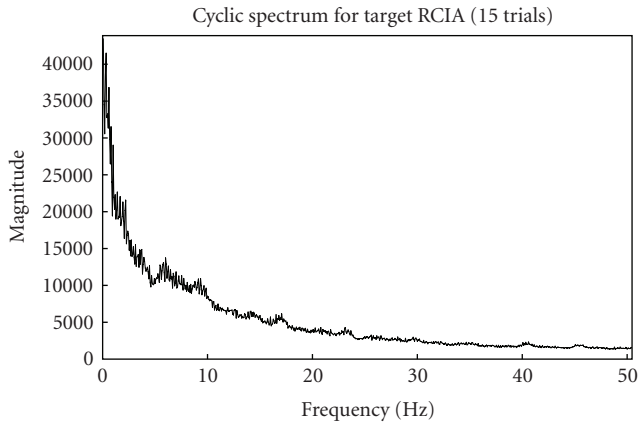

Figure 7: Fifteen-trials cyclic spectrum for target RCIA (just to illustrate similarity with five-trials).

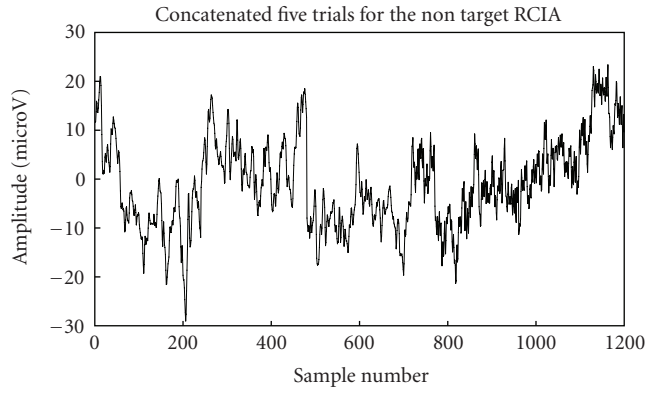

Figure 9: Signal trials for nontarget RCIA from BCI competition III (dataset IIb).

The relationship between the number of trials required and the speed of communication is direct. If detection could be achieved using just less trials, the system would allow communication at a better rate. We tested the framework using only 5 trials from channel Cz to detect "I" which is the chosen target character in the above chosen dataset. With respect to the target character "I" detection, we discuss the proposed framework's performance diagrammatically below. Figures 6 and 9 show the concatenated trials (target and nontarget RCIA) used for cyclostationary analysis while Figures 7-8 and 10-11 show their corresponding cyclic spectrums for varying number of trials.

The cyclic spectrum which exploits the inter trial similarities in the frequency domain depicts the cyclic VEP components at 0–10 Hz as in Figure 2. It can also be inferred that enhanced and better spectrum is obtained for more number of trials. The lag parameter for cyclostationary analysis was set to length of data to obtain a better spectrum. After some preliminary experimentation, five-trial cyclic spectrum was selected as optimum for analysis as it seemed to highlight the VEP signal band appreciably. A threshold for the magnitude of the cyclic spectra was used to obtain the VEP signal frequency band of (0–10 Hz) for lowpass filtering. Based on this obtained band from cyclostationary analysis, the five-trials are lowpassed-filtered using an 11th-order Chebyshev digital filter with a 3-dB cut-off frequency at 10 Hz because P300 responses are limited to this frequency range. Order 11 was used since it was sufficient to give a minimum attenuation of 60 dB in the stop band. To avoid phase distortion forward, and reverse filtering were performed since Chebyshev is a nonlinear filter. The out of band EEG artifacts is thus removed using cyclostationary analysis.

The lowpass filtered five-trials (target and nontarget RCIA) are then passed to the G-ICA fusion module to separate the in-band EEG artifacts. As discussed before, the G-ICA module works by minimising the MI of the extracted components (for 100 generations) to reduce overlapping EEG artifacts. The obtained denoised P300 response for target and nontarget cases is shown in Figures 12-13. The P300 amplitudes for target RCIA trials were found to have a higher-peak amplitude value than that for the nontarget RCIA trials. The single trial with maximum P300 amplitude (in the range 300–600 ms) is highlighted with an increased line width in both figures.

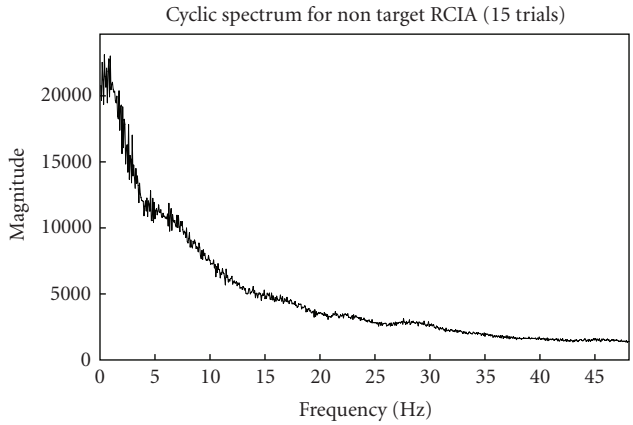

Figure 10: Fifteen-trial cyclic spectrum for nontarget RCIA.

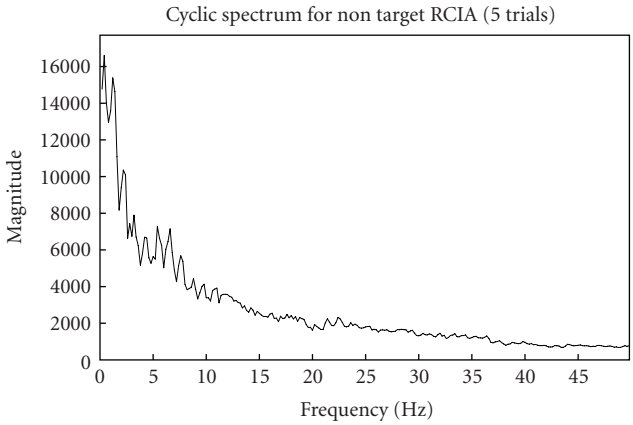

Figure 11: Five-trials cyclic spectrum for nontarget RCIA.

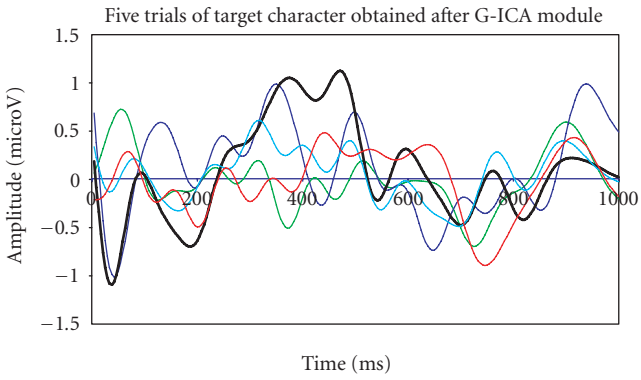

Figure 12: Detected P300 component for target RCIA showing higher peak amplitude.

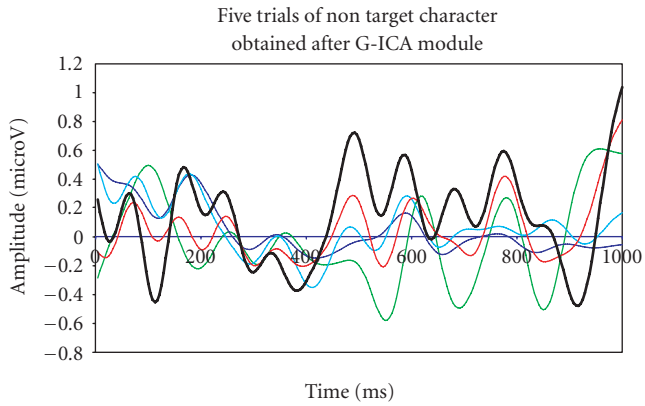

Figure 13: Detected P300 component for nontarget RCIA showing lower peak amplitude.

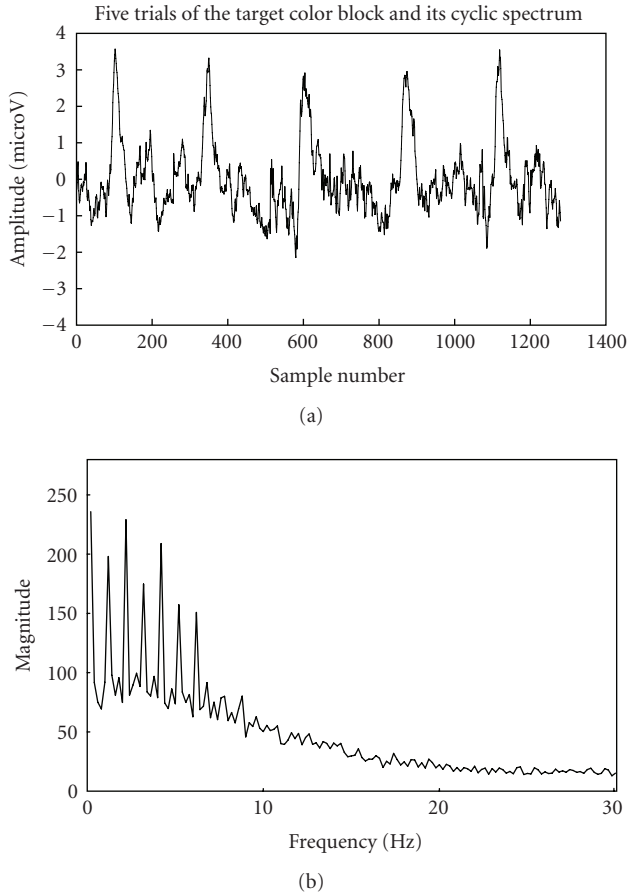

Figure 14: Trials for target colour block and its cyclic spectrum.

3.2. *BCI labs, Essex dataset*

The presented framework was also tested offline from a dataset for a biometric application. Similar to the Donchin paradigm, the application had seven blocks of colours which were flashed to evoke P300 components. Sequences were block randomised, which means, after seven flashes each colour was flashed once, after fourteen flashes each colour was flashed twice. Forty trials were recorded (each trial had 7 flashes of the colour block). The subject was asked to focus on a single-colour block (say red) and also keep a count of the number of times it flashed, which enabled monitoring the performance of the subject. The colour blocks were flashed for 100 millisecond with an interstimulus interval

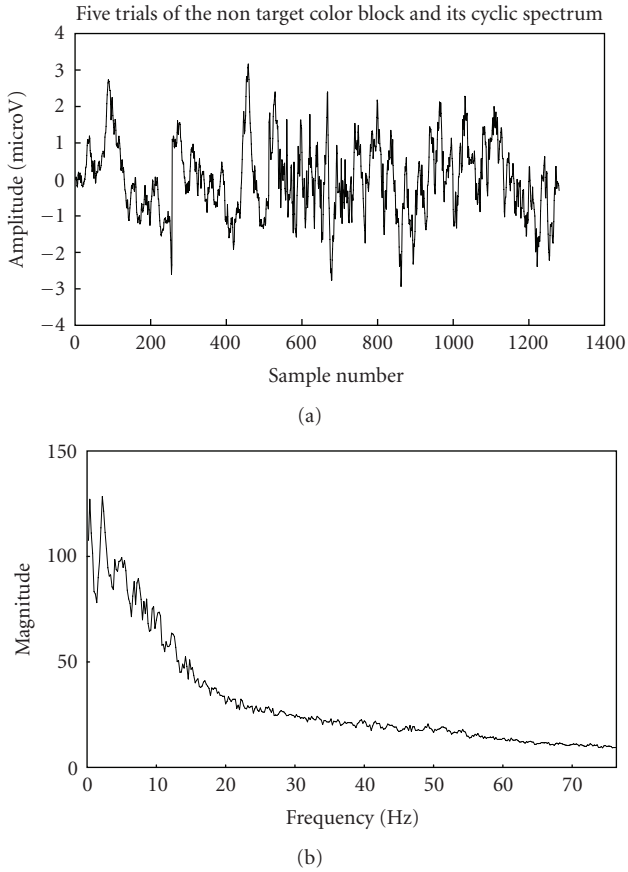

FIGURE 15: Trials for nontarget colour block and its cyclic spectrum.

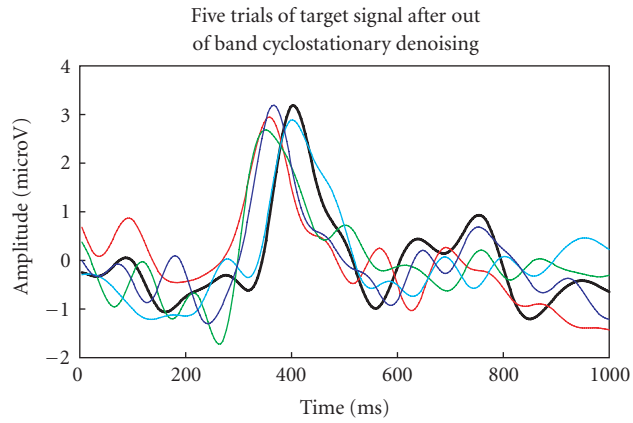

FIGURE 16: Lowpassed-filtered trials for target colour block.

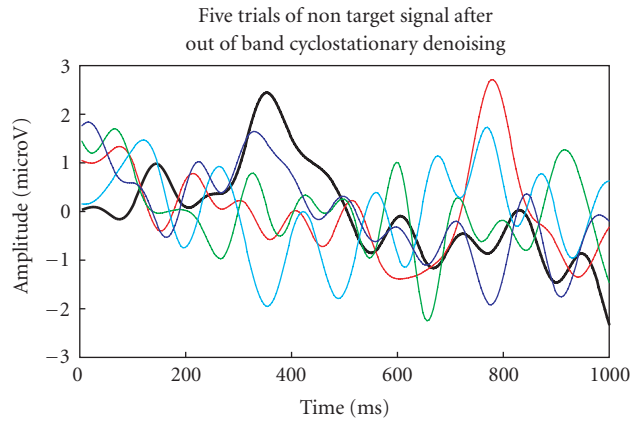

FIGURE 17: Lowpassed-filtered trials for nontarget colour block.

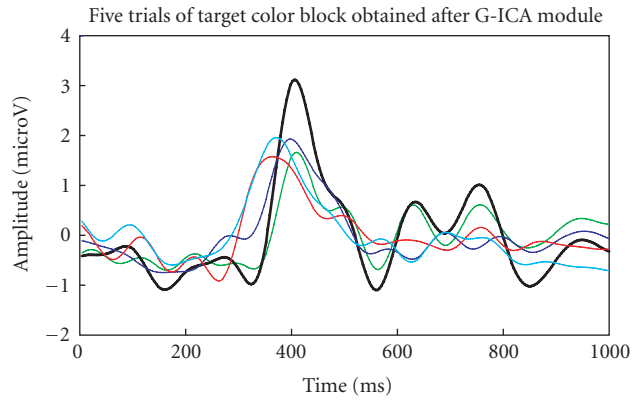

FIGURE 18: P300 components of the five-trials for target colour block using G-ICA.

of 300 millisecond. EEG recordings were carried out on a Biosemi Active Two system using 34 channels (32 on a scalp and 2 on either mastoids); however, only channel Cz was used. Data was sampled at 256 Hz with no filtering. The subject was a male aged 27 who had experience of using the BCIs before, with no known neurological disorders. The performance of the framework for target and nontarget color blocks is discussed below diagrammatically. It can be seen from Figure 14 that the target-trial data is cyclic in time domain and also that the magnitude of the cyclic spectrum is much higher than that of the nontarget data as in Figure 15. The lag parameter for cyclostationary analysis was set to length of data. After some preliminary experimentation, five-trial cyclic spectrums were again found to be optimum for analysis as it seemed to highlight the VEP signal band appreciably. A threshold for the magnitude of the cyclic spectra was used to obtain the VEP signal frequency band of (0–10 Hz) for lowpass filtering. Based on this obtained band from cyclostationary analysis, a lowpass filter for (target colour block and nontarget colour block) was used as in Section 3.1 to remove nonoverlapping EEG artifacts and the output is shown in Figures 16-17.

The five-trials (target colour block and nontarget colour block) are then passed to G-ICA fusion module. Investigating Figures 18-19 clearly shows that the P300 component amplitude in the 300–600 millisecond range is higher for target-colour block than the nontarget colour block. The single trial with maximum P300 amplitude is highlighted with an increased line width in both the figures. It was also observed that the frequency band (CS analysis) and the unmixing matrix (G-ICA) do not change over trials.

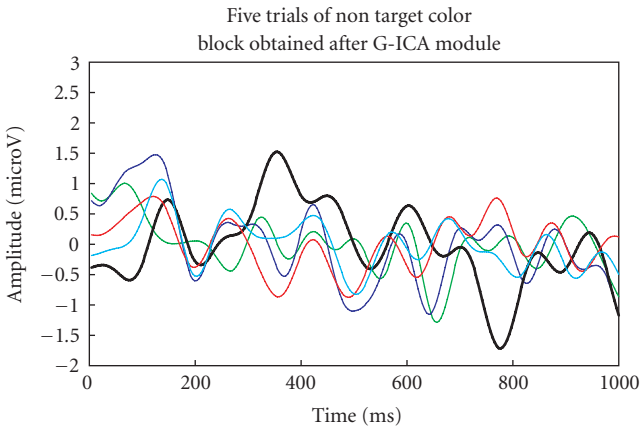

Figure 19: P300 components of the five-trials for nontarget colour block using G-ICA.

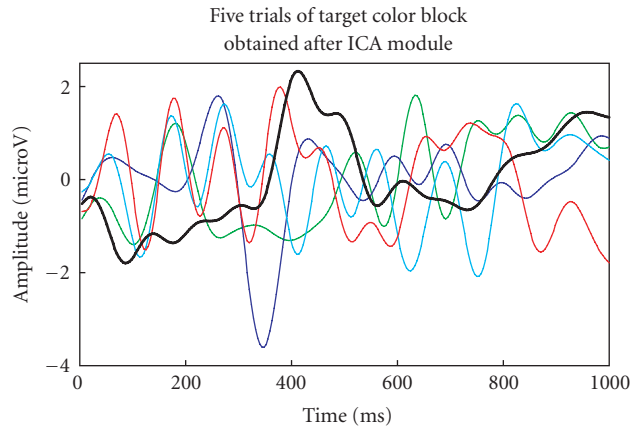

Figure 20: P300 components of the five-trials for target colour block using ICA.

Table 2: Runtime comparison between G-ICA and ICA.

	G-ICA	ICA
Target color block	97.23 s	96.16 s
Nontarget color block	98.03 s	97.05 s

We also compared the performance of G-ICA with ICA (fixed point-ICA). The five-trials (target colour block and nontarget colour block) after lowpass filtering, when passed through ICA module gave the outputs as depicted in Figures 20-21. Again, the single trial with maximum P300 amplitude (300–600 ms) is highlighted with an increased line width in both the figures. It can be observed from Figures 18–21 that the threshold of difference between target and nontarget for G-ICA is higher than that obtained using ICA. Comparison in terms of runtime in seconds is indicated in Table 2 and it was found to be comparable.

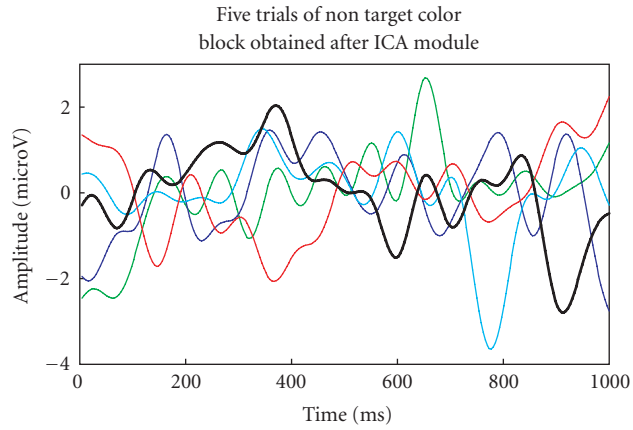

Figure 21: P300 components of the five-trials for nontarget colour block using ICA.

4. DISCUSSION AND CONCLUSION

A new framework for enhanced VEP signal detection is presented. The two-stage framework makes use of cyclostationary and G-ICA techniques to separate VEP signals from EEG artifacts. Brain signals were emulated using VEP contaminated with EEG in the simulation study to analyse the cyclo model for brain signal analysis. Studies from this work seem to suggest that cyclostationary model might be suitable for VEP signal analysis. To validate the method, further the algorithms were tested to identify an arbitrarily chosen character "I" from the BCI competition III challenge (dataset IIb) and also with datasets recorded at BCI lab, University of Essex which gave satisfactory results with very few trials (5 trials). The G-ICA fusion module does not assume any property of noise hence it can be used to separate any type of linear additive noise. The runtime performance of G-ICA and ICA was similar and comparable. It was also observed that the frequency bands and unmixing matrix do not change over trials for a given subject; hence the CS and G-ICA methods need to be applied only to training data. It is known that in a P300-based BCI system the communication speed of characters is dependent on the number of trials. Hence, this proposed signal preprocessing framework may be used to reduce the number of trials and thereby increase the rate of communication.

ACKNOWLEDGMENTS

The first author gratefully acknowledges the support from Overseas Research Students Award Scheme (ORSAS), United Kingdom, and the University of Essex research studentship for funding the Phd programme. A part of the work was funded by University of Essex Research Promotion Fund (DDQP40). We thank Wadsworth Center, NYS Department of Health for providing the datasets to test our methodologies on the BCI competition III challenge website. We also thank and acknowledge the use of MILCA software provided by Koch lab, California Institute of Technology and ICALAB software provided by Brain Science Institute, Riken to calculate MI and ICA, respectively, in this work.

REFERENCES

[1] K. E. Misulis, *Sphelmann's Evoked Potential Primer: Visual, Auditory, and Somatosensory Evoked Potentials in Clinical Diagnosis*, Butterworth-Heinemann, Oxford, UK, 1994.

[2] J. I. Aunon, C. D. McGillem, and D. G. Childers, "Signal processing in event potential research: averaging and modelling," *CRC Critical Reviews in Bioengineering*, vol. 5, pp. 323–367, 1981.

[3] D. H. Lange, H. T. Siegelmann, H. Pratt, and G. F. Inbar, "Overcoming selective ensemble averaging: unsupervised identification of event-related brain potentials," *IEEE Transactions on Biomedical Engineering*, vol. 47, no. 6, pp. 822–826, 2000.

[4] C. T. Handy, *Event-Related Potentials: A Methods Handbook*, MIT Press, Cambridge, Mass, USA, 2005.

[5] M. Kutas, G. McCarthy, and E. Donchin, "Augmenting mental chronometry: the P300 as a measure of stimulus evaluation time," *Science*, vol. 197, no. 4305, pp. 792–795, 1977.

[6] E. Donchin, W. Ritter, and C. McCallum, "Cognitive psychophysiology: the endogenous components of the ERP," in *Brain Event-Related Potentials in Man*, E. Callaway, P. Tueting, and S. H. Koslow, Eds., pp. 349–411, Academic Press, New York, NY, USA, 1978.

[7] M. G. H. Coles and M. D. Rugg, "Event-related brain potentials: an introduction," in *Electrophysiology of Mind: Event-Related Brain Potentials and Cognition*, M. D. Rugg and M. G. H. Coles, Eds., pp. 1–26, Oxford University Press, New York, NY, USA, 1995.

[8] E. Donchin, K. M. Spencer, and R. Wijesinghe, "The mental prosthesis: assessing the speed of a P300-based brain-computer interface," *IEEE Transactions on Rehabilitation Engineering*, vol. 8, no. 2, pp. 174–179, 2000.

[9] H. Serby, E. Yom-Tov, and G. F. Inbar, "An improved P300-based brain-computer interface," *IEEE Transactions on Neural Systems and Rehabilitation Engineering*, vol. 13, no. 1, pp. 89–98, 2005.

[10] L. A. Farwell and E. Donchin, "Talking off the top of your head: toward a mental prosthesis utilizing event-related brain potentials," *Electroencephalography and Clinical Neurophysiology*, vol. 70, no. 6, pp. 510–523, 1988.

[11] C. D. Woody, "Characterization of an adaptive filter for the characterization of variable latency neuroelectric signals," *Medical and Biological Engineering and Computing*, vol. 5, no. 6, pp. 539–553, 1967.

[12] D. G. Wastell, "Statistical detection of individual evoked responses: an evaluation of Woody's adaptive filter," *Electroencephalography and Clinical Neurophysiology*, vol. 42, no. 6, pp. 835–839, 1977.

[13] T.-P. Jung, S. Makeig, M. Westerfield, J. Townsend, E. Courchesne, and T. J. Sejnowski, "Analysis and visualization of single-trial event-related potentials," *Human Brain Mapping*, vol. 14, no. 3, pp. 166–185, 2001.

[14] S. Makeig, M. Westerfield, T.-P. Jung, et al., "Functionally independent components of the late positive event-related potential during visual spatial attention," *Journal of Neuroscience*, vol. 19, no. 7, pp. 2665–2680, 1999.

[15] M. Drozd, P. Husar, A. Nowakowski, and G. Henning, "Detecting evoked potentials with SVD- and ICA-based statistical models," *IEEE Engineering in Medicine and Biology Magazine*, vol. 24, no. 1, pp. 51–58, 2005.

[16] J. M. Moser and J. I. Aunon, "Classification and detection of single evoked brain potentials using time-frequency amplitude features," *IEEE Transactions on Biomedical Engineering*, vol. 33, no. 12, pp. 1096–1106, 1986.

[17] A. S. Gevins, N. H. Morgan, S. L. Bressler, J. C. Doyle, and B. A. Cutillo, "Improved event-related potentials estimation using statistical pattern classification," *Electroencephalography and Clinical Neurophysiology*, vol. 64, no. 2, pp. 177–186, 1986.

[18] G. Zouridakis, B. H. Jansen, and N. N. Boutros, "A fuzzy clustering approach to EP estimation," *IEEE Transactions on Biomedical Engineering*, vol. 44, no. 8, pp. 673–680, 1997.

[19] L. Tong, G. Xu, and T. Kailath, "Blind identification and equalization based on second-order statistics: a time domain approach," *IEEE Transactions on Information Theory*, vol. 40, no. 2, pp. 340–349, 1994.

[20] D. Koenig and J. Boehme, "Application of cyclostationary and time-frequency signal analysisto car engine diagnosis," in *Proceedings of IEEE International Conference on Acoustics, Speech, and Signal Processing (ICASSP '94)*, vol. 4, pp. 149–152, Adelaide, Australia, April 1994.

[21] S. Ohno and H. Sakai, "Optimization of filter banks using cyclostationary spectral analysis," *IEEE Transactions on Signal Processing*, vol. 44, no. 11, pp. 2718–2725, 1996.

[22] W. A. Gardner, "Identification of systems with cyclostationary input and correlated input/output measurement noise," *IEEE Transactions on Automatic Control*, vol. 35, no. 4, pp. 449–452, 1990.

[23] W. A. Gardner, "Exploitation of spectral redundancy in cyclostationary signals," *IEEE Signal Processing Magazine*, vol. 8, no. 2, pp. 14–36, 1991.

[24] W. A. Gardner, "Signal interception: a unifying theoretical framework for feature detection," *IEEE Transactions on Communications*, vol. 36, no. 8, pp. 897–906, 1988.

[25] R. Palaniappan and C. N. Gupta, "Genetic algorithm based independent component analysis to separate noise from Electrocardiogram signals," in *Proceedings of IEEE International Conference on Engineering of Intelligent Systems (ICEIS '06)*, pp. 1–5, Islamabad, Pakistan, April 2006.

[26] X.-Y. Zeng, Y.-W. Chen, Z. Nakao, and K. Yamashita, "Signal separation by independent component analysis based on agenetic algorithm," in *Proceedings of the 5th International Conference on Signal Processing (ICSP '00)*, vol. 3, pp. 1688–1694, Beijing, China, August 2000.

[27] D. E. Goldberg, *Genetic Algorithms in Search, Optimization and Machine Learning*, Addison-Wesley, Reading, Mass, USA, 1989.

[28] F. Rojas, C. G. Puntonet, M. Rodríguez-Álvarez, I. Rojas, and R. Martín-Clemente, "Blind source separation in post-nonlinear mixtures using competitive learning, simulated annealing, and a genetic algorithm," *IEEE Transactions on Systems, Man and Cybernetics*, vol. 34, no. 4, pp. 407–416, 2004.

[29] J. Wang, T. Chen, and B. Huang, "Cyclo-period estimation for discrete-time cyclo-stationary signals," *IEEE Transactions on Signal Procesing*, vol. 54, no. 1, pp. 83–94, 2006.

[30] G. B. Giannakis, "Cyclo-stationary signal analysis," in *Digital Signal Processing Handbook*, CRC Press, Boca Raton, Fla, USA, 1999.

[31] K. K. Paliwal and Y. Sagisaka, "Cyclic autocorrelation-based linear prediction analysis of speech," in *Proceedings of the 5th European Conference on Speech Communication and Technology (EUROSPEECH '97)*, pp. 279–282, Rhodes, Greece, September 1997.

[32] P. Sharmilakanna and R. Palaniappan, "EEG artifact reduction in VEP using 2-stage PCA and N4 analysis of alcoholics," in

Proceedings of the 3rd International Conference on Intelligent Sensing and Information Processing (ICISIP '05), pp. 1–7, Bangalore, India, December 2005.

[33] J. A. McEwen and G. B. Anderson, "Modeling the stationarity and gaussianity of spontaneous electroencephalographic activity," *IEEE Transactions on Biomedical Engineering*, vol. 22, no. 5, pp. 361–369, 1975.

[34] P. A. Karjalainen, J. P. Kaipio, A. S. Koistinen, and M. Vauhkonen, "Subspace regularization method for the single-trial estimation of evoked potentials," *IEEE Transactions on Biomedical Engineering*, vol. 46, no. 7, pp. 849–860, 1999.

[35] W. Klimesch, "The P300 wave and band power in the alpha and theta range," *Psycoloquy*, vol. 6, no. 44, 1995, memory-brain.5.klimesch.

[36] R. Verleger, "Memory-related EEG potentials: slow negativities, priming positivity, recognition positivity, and Dm," *Psycoloquy*, vol. 6, no. 27, 1995, memory-brain.3.verleger.

[37] A. Hyvarinen and E. Oja, "A survey on independent component analysis," *Neural Computing Surveys*, vol. 2, pp. 94–128, 1999.

[38] D. W. Scott, *Multivariate Density Estimation: Theory, Practice, and Visualization*, John Wiley & Sons, New York, NY, USA, 1992.

[39] P. Comon, "Independent component analysis, a new concept?" *Signal Processing*, vol. 36, no. 3, pp. 287–314, 1994.

[40] A. Kraskov, H. Stögbauer, and P. Grassberger, "Estimating mutual information," *Physical Review E*, vol. 69, no. 6, Article ID 066138, 16 pages, 2004.

Hindawi Publishing Corporation
Computational Intelligence and Neuroscience
Volume 2007, Article ID 23864, 11 pages
doi:10.1155/2007/23864

Research Article

EEG-Based Brain-Computer Interface for Tetraplegics

Laura Kauhanen,[1,2] Pasi Jylänki,[1] Janne Lehtonen,[1] Pekka Rantanen,[3] Hannu Alaranta,[4] and Mikko Sams[1]

[1] *Laboratory of Computational Engineering, Helsinki University of Technology, 00280 Helsinki, Finland*
[2] *Robotics Research Group, Department of Engineering Science, Oxford University, Oxford OX1 3PJ, UK*
[3] *ORTON Orthopaedic Hospital, Invalid Foundation, 00280 Helsinki, Finland*
[4] *Käpylä Rehabilitation Centre, Finnish Association of People with Mobility Disabilities, 00251 Helsinki, Finland*

Correspondence should be addressed to Laura Kauhanen, laura.kauhanen@tkk.fi

Received 16 February 2007; Revised 8 June 2007; Accepted 2 August 2007

Recommended by Shangkai Gao

Movement-disabled persons typically require a long practice time to learn how to use a brain-computer interface (BCI). Our aim was to develop a BCI which tetraplegic subjects could control only in 30 minutes. Six such subjects (level of injury C4-C5) operated a 6-channel EEG BCI. The task was to move a circle from the centre of the computer screen to its right or left side by attempting visually triggered right- or left-hand movements. During the training periods, the classifier was adapted to the user's EEG activity after each movement attempt in a supervised manner. Feedback of the performance was given immediately after starting the BCI use. Within the time limit, three subjects learned to control the BCI. We believe that fast initial learning is an important factor that increases motivation and willingness to use BCIs. We have previously tested a similar single-trial classification approach in healthy subjects. Our new results show that methods developed and tested with healthy subjects do not necessarily work as well as with motor-disabled patients. Therefore, it is important to use motor-disabled persons as subjects in BCI development.

1. INTRODUCTION

A brain-computer interface (BCI) enables the control of applications based on brain signals, measured invasively or noninvasively. BCIs can help severely motor-disabled persons to communicate and control their environment. Single-EEG epochs measured during a few different mental or real tasks can be classified accurately enough to be translated into simple computer commands (for reviews see [1, 2]). Unfortunately, for successful performance, subjects often need several weeks or even months of training [3–5]. If learning takes place very slowly, it can decrease the motivation and willingness to use BCIs.

When advanced machine learning techniques are used, a BCI can learn to recognize signals generated by a novice user after less than one hour training period (see, e.g., [6–10]). Many of these analysis techniques have only been tested with offline data, or data are first collected in a 5–20 minutes calibration session without feedback and the classifier is then trained with this data and used in the next session where feedback is presented. Therefore, subjects receive either no feedback, or feedback is not up to date. Vidaurre et al. [11] used an alternative approach, in which they trained the classifier online with correct class labels during the feedback sessions. Their model was, however, never tested without supervised learning. Therefore, its performance in a BCI application could not be evaluated.

BCIs utilizing machine learning use various features of EEG signals as a basis for classification, such as P300 event-related potentials to visual or auditory stimuli [12], and EEG frequency patterns [13–16]. The most commonly used frequency pattern is the Rolandic mu-rhythm consisting of 10 Hz and 20 Hz frequency components recorded over the sensorimotor cortex [17]. These components are suppressed contralaterally during the movement execution [18, 19]. Another commonly used feature in healthy subjects is the slow premovement EEG potential called lateralized readiness potential (LRP/Bereitschaftspotential) [7, 20].

Paralyzed patients cannot move their extremities, but their sensorimotor cortices are activated during attempted movements. An fMRI study on five tetraplegic patients, paralyzed for 1–5 years due to spinal cord injuries, showed that these patients' sensory and motor cortices are activated during attempted hand and foot movements [21]. Very

similar activations were found in healthy control subjects during real movements. In another fMRI study of nine paraplegic patients having complete spinal cord injury between T6 and L1 (1 month–33 years), activation patterns during motor attempts resembled those of a control group performing the corresponding movements, but were weaker in the patients [22]. The activation patterns, however, differed more between motor imagery of the control group and the patients' motor attempts.

The aim of the present study was to develop and evaluate a two-command BCI that tetraplegic patients could learn to control after a short training period. Six patients participated in a 30-minute online BCI experiment. The task was to move a circle on a computer screen by attempting either right- or left-hand movements every two seconds after a cue stimulus. Feature extraction and classification methods were first tested on healthy subjects performing real finger movements [23]. The classifier was trained after each movement attempt using the correct class labels. This enabled online feedback to the subjects already after the first ten trials (~20 seconds from the beginning of the experiment). In applications, subject's intent cannot be directly known and thus supervised learning is impossible. Therefore, the classifier was not trained when testing the BCI performance.

2. MATERIAL AND METHODS

2.1. Subjects

Six male tetraplegic subjects participated in the study (Table 1). Neurological level C5 corresponds to the elbow flexors, level C6 to the wrist extensors, and level C7 to the elbow extensors. Subject S4 reported being left handed and the rest right handed. The tetraplegia in S3 was caused by Guillain-Barre syndrome, and in the rest of the subjects by trauma-induced spinal-cord injury (SCI). All the subjects, interviewed one week before they participated in the study, were volunteers and were not paid for their participation. They were all highly motivated and interested in the experiment.

The study was approved by the ethical Committee of the Hospital district of Helsinki and Uusimaa. The subjects were assisted to sign their informed consent to participate in the study.

2.2. Experimental setup

The experiment was performed with the BCI system developed at the Helsinki University of Technology (TKK-BCI) [24].

Subject's task was to move a circle from the centre of the computer screen to the target located on the left or right side of the screen by means of EEG signals related to attempted right- or left-hand movements (Figure 1). The subjects were instructed to attempt fast movements. They were shown movement examples which included finger lifting and pinching, and fist closing. The subjects were instructed to chose one of the movements and use it during the whole experiment. Subjects S1, S2, S4 attempted to close their fists, subject S5 attempted to lift his index fingers, and subjects S3 and S6 attempted to pinch their index finger and thumb together. The subjects were unable to move the body parts they attempted to move.

Figure 1: A tetraplegic subject using the BCI in his patient room at the rehabilitation centre. The BCI controller is on the subject's right side. The subject's task was to move the red circle to the yellow target on the side of the screen.

The experiment consisted of 6–20 seconds long games. A game started with an arrow indicating which target the subjects should try to reach with the circle, that is, which hand they were to attempt to move during the game. After the disappearance of the arrow, the circle appeared in the middle of the screen and two targets on both of its sides (Figure 1). A visual trigger was displayed below the circle. This trigger was a rectangle that decreased in size until it disappeared 0.8 second after its appearance. The subjects were instructed to attempt the movement when this trigger disappeared; this timing is later referred to as the cue. The gradually diminishing trigger enabled the subjects to prepare for the movements. Each attempted movement is called a trial. The rectangle re-appeared every 2 seconds (trial ISI = 2 seconds). A game consisted of 3–10 trials and lasted 6–20 seconds; there were short 2-second breaks between the games. If the trial was classified correctly, the circle moved to the direction of the correct target, otherwise it moved to the opposite direction. The game ended when the subject reached one of the targets, or a maximum of 10 trials was exceeded. It was also possible to reach the wrong target if enough trials were classified incorrectly. The subjects were instructed to fixate on the middle of the trigger during the games. Thus, the visual view was identical between the left and right tasks.

Based on a suggestion of subject S1, the game was modified for S2–S6. In the new version, the circle moved proportionally to the class probability given by the classifier: $(P - .5)\cdot k$, where P is the output of the classifier, that is, the posterior probability of the most probable class given the model and the training data, and k is a distance measure in pixels adjusted according to the size of the screen. In other words, the higher the probability predicted by the classifier the longer the step the circle moved.

Table 1: The subjects' age, time since injury, and cite of injury, as well as the lowest site where some (albeit less than normal) movement could be detected are displayed.

Subject	Age	Time since injury	Cite of injury (movement detected)		ASIA [25]	Cause of tetraplegia
			Left	Right		
S1	46	4 yr.	C4(C4)	C4(C4)	A	SCI
S2	59	1.5 yr.	C4(C7)	C4(C7)	—	Syndroma Guillain Barre
S3	26	4 mo.	C4(C5)	C4(C5)	A	SCI
S4	47	4 mo.	C5(C4)	C5(C5)	B	SCI
S5	50	3 mo.	C5(C7)	C5(C7)	A	SCI
S6	63	35 yr.	C5(C6)	C5(C6)	B	SCI

Figure 2 displays the overall structure of the experiment. Data was collected in 3.5–4 minutes sessions. There were approximately one-minute breaks between the sessions to avoid subjects getting tired. Each session consisted of 10–27 games, depending on how quickly the subjects hit the targets. The whole experiment contained three parts each consisting of one to four sessions depending on how the subjects felt and how well they performed. Longer breaks were kept between the three parts, during which individual EEG features were defined for each subject.

2.3. Recording

The experiments were conducted in patient rooms at the Käpylä Rehabilitation Centre in Helsinki (Figure 1). The patient was sitting in a wheelchair in front of the computer screen. During the measurements, one to three additional people were in the room. To decrease electrical interferences, lights, TV, and electrical beds were turned off. The data acquisition and BCI software were run on a 3 GHz, Pentium 4 PC.

Recordings were made with a 32-channel EEG electrode cap and amplifier. EEG was measured from 14 locations of the international 10–20 system: Fp1, Fp2, F3, F4, C3, C4, Cz, Fc1, Fc2, Cp1, Cp2, Fc5, Fc6, Fz. Horizontal and vertical eye movements were measured with three additional electrodes. Two of them were located at the outer canthi of the left and the right eye and the third one below the left eye. All electrodes were referenced to an electrode located in the middle of electrodes Cz and Fz. Electrode impedances, checked in the beginning of the experiment and during the longer breaks, were below 10 kOhm. The sampling frequency was 500 Hz and passband 0.1–225 Hz.

2.4. Features and classification

The selection and computation of features as well as classification were done using the same methods as described in [24]; here we give a short overview of the methods. Figure 3 shows an example of the feature extraction process (S6, channel C4) for two different frequency bands. The disappearance of the visual trigger is marked with a vertical line. One-second long EEG trials (starting 0.6 seconds before and ending 0.4 seconds after the cue) were extracted from each channel. First, linear trends were removed from the raw signals. Fast Fourier transform (FFT) was computed for each channel [26]. Different frequency bands were filtered by adjusting the Fourier components outside the passband to zero. For the 1–3 Hz band, temporal features were extracted by computing the inverse FFT. For all bands above 3 Hz, for example, the 19–21 Hz band (bottom row), the instantaneous amplitude of the signal was computed with the Hilbert transform [26]. The lower half of the two-sided spectrum was multiplied by two and the upper half was set to zero after which the magnitude of the inverse FFT was computed. The bottom left graph illustrates how the instantaneous amplitude follows the envelope of the fast varying filtered signal. The right second and bottom rows show how the actual features were computed from the signals by averaging amplitude values over short time windows.

In the first part of the experiment identical features were used for all subjects. Based on earlier studies with tetraplegics [27], the features were computed from the 1–3 Hz frequency band from seven adjacent 100 milliseconds time windows starting 400 milliseconds before and ending 300 milliseconds after the cue. Six electrodes over the sensorimotor cortex (C3, C4, Cp1, Cp2, Fc1, Fc2) were used. This gave a total of 42 features (six channels $\times$ seven time windows).

Due to good performance, the same set of features was used throughout the experiment with S1. During the first longer break, individual features were determined for S2–S6 from the data recorded in the first four sessions. For subjects S2 and S4–S6 new features were also determined during the second break based on the data from the previous three sessions.

For the feature selection process, a large set of features was computed from the training data using the same six channels. The features were computed from 2 Hz wide frequency bands starting from 1,2,...,38 Hz. Both 100 milliseconds and 50 milliseconds long, over lapping time windows starting from 400 milliseconds before and ending 300 milliseconds after the cue were investigated. Kolmogorov-Smirnov (KS) test statistic (see, e.g., [28]) was used as a difference measure between the class-conditional distributions for each feature independently. The KS test statistic is the maximum absolute difference between the cumulative distributions of two random variables (in this case the amplitude values related to the two tasks) describing how different the distributions are. All features were ranked according to the KS test statistic. When a particular frequency band and time window were chosen from one channel, the corresponding feature (the same band and time window)

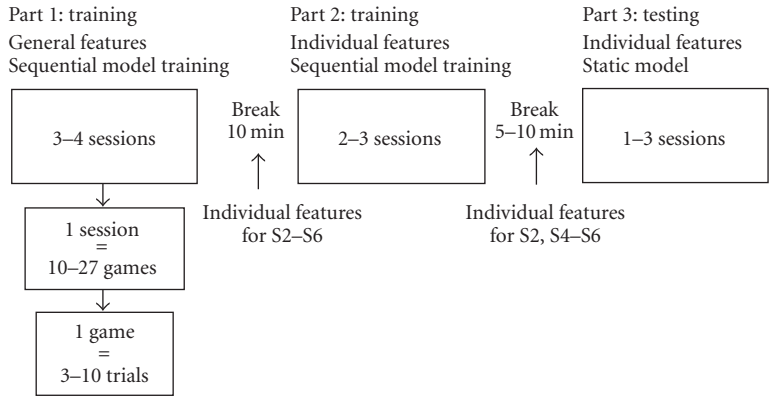

Figure 2: The structure of the experiment. The experiment consisted of three parts. Each part consisted of 1–4 sessions, each session of 10–27 games, and each game of 3–10 trials.

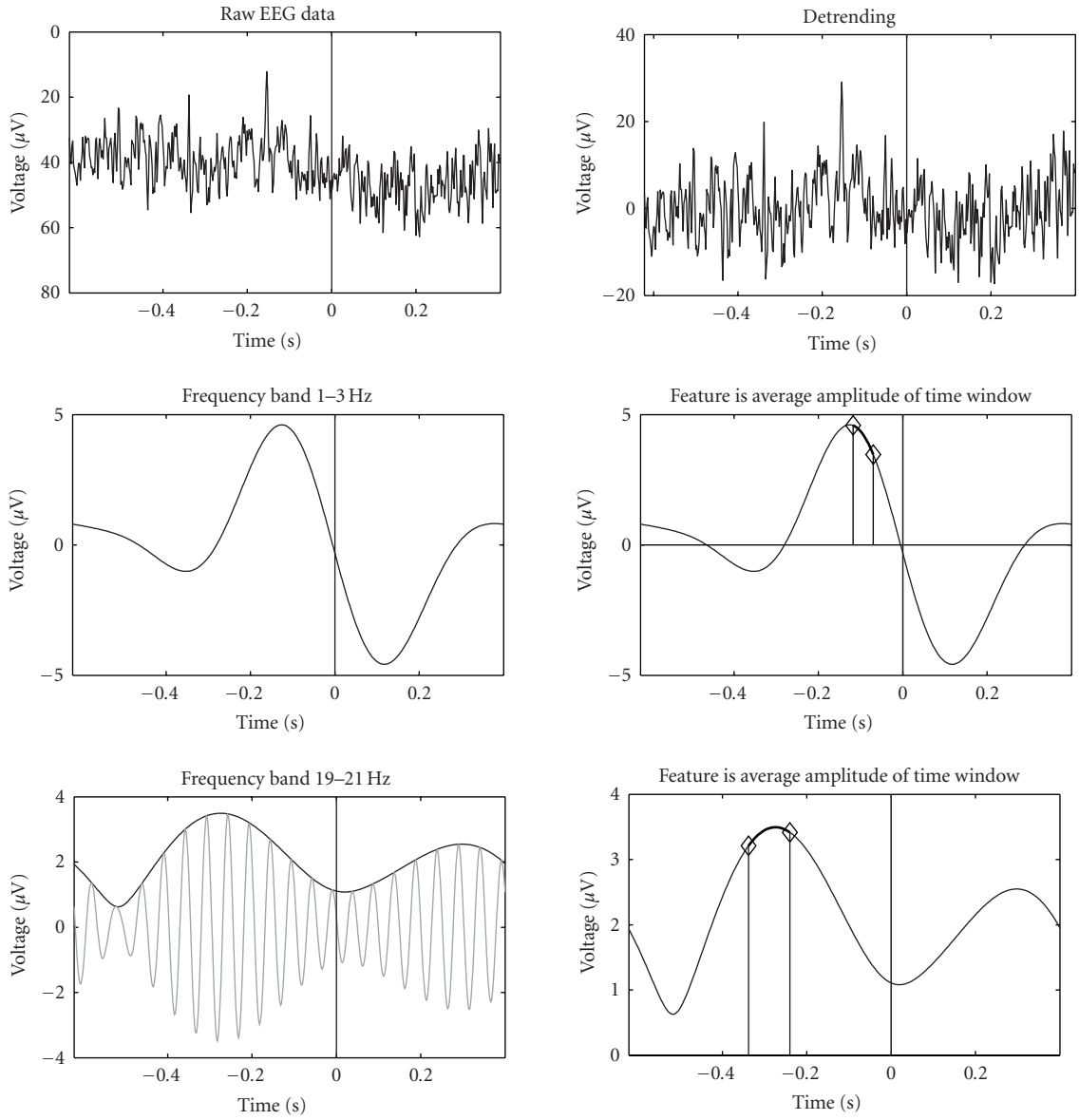

Figure 3: Computation of the features. The raw EEG signals were first preprocessed and detrended. The frequency components were extracted using fast Fourier transform. For frequencies over 3 Hz, the instant amplitude of the signal is taken using Hilbert transform. The feature is the average amplitude of some time window (second and third rows, right).

was also chosen from the rest of the channels. To decrease redundancies among the features, no overlapping frequency bands or time windows from the same channel were allowed. Seven different frequency-band and time-window combinations were included resulting in a total of 42 features.

Classification was based on several linear transformations of the feature space and a nonlinear logistic decision function. First, linear whitening transformation was used to reduce the dimensionality of the feature space and to produce uncorrelated features. This was applied to the whole data set, that is, data from both classes were combined. Second, three linear combinations of the whitened features to separate the classes were determined; Fisher's linear discriminant and the principal components corresponding to the largest variance for the both classes separately. Finally, a linear classifier with a logistic output function was used to transform the activation of the Fisher's discriminant and the magnitude of the feature vector in the directions of the principal components to class probabilities.

After feature extraction, each new feature vector was classified with the existing model. Based on the result, feedback was given to the subject. After each prediction, the oldest sample in the memory from the corresponding class was replaced with the new one and the classifier was updated with a maximum of 200 of these correctly labeled samples from both classes.

Online training of the model was started immediately after five samples (features) were acquired from each class. During the first ten trials of the experiment the circle was made to move in the correct direction. After that, the circle moved according to the prediction of the classifier and the user received visual feedback from his performance. Because supervised training of the classifier is not possible in real applications, the classifier was not updated in the testing part, in which the performance of the BCI was evaluated based on the classification accuracy.

3. RESULTS

3.1. Event-related potentials and features

The upper part of Figure 4 displays averaged signals (± standard deviations, passband 1–3 Hz) of all subjects in the training sessions at electrodes C3 and C4 during the attempted right- and left-hand movements (attempt onset indicated by the blue line). This activity was used as a feature in the first part of the experiment. The lower part of the figure shows how much the class-conditional distributions differ in the consecutive 100 milliseconds time windows according to the KS-statistic. Notice that the KS-statistic was calculated for the features, that is, amplitude values averaged over a 100 milliseconds time window (see Figure 3). The value of the test statistic is plotted for each feature in the middle of the corresponding time window. Channel C3 for S1, S2, and S6 and channel C4 for S1–S3 show a difference between the left- and right-attempted movements at several time points. Figure 5 shows the corresponding signals during the testing sessions. S1–S3 show rather similar patterns as during the training sessions but especially for S1 the class difference in C4 is more prominent.

The initial feature selection was not modified for S1 and thus seven adjacent time windows from the 1–3 Hz band were used as features throughout the experiment. Also, for S2 the first four and for S3 the first three selected features were from various precue time windows in the 1–3 Hz band. Each selected feature was taken from all eight channels leading to 24 and 18 features correspondingly. For S2, one feature was chosen from the 9–11 Hz band, the rest were close to the 20 Hz band. For S4–S6, the chosen features were widely distributed from 6 to 38 Hz; no features were chosen from the low frequency band.

3.2. BCI performance

BCI performance can be measured in two ways. We can measure how well subjects perform in the application. In the present experiment, this means how many times and how quickly the subjects were able to reach the target. We can also determine the classification accuracy of the single trials and the bit rate based on it.

Table 2 shows how well the subjects performed in the application. It shows the number of correct and incorrect hits in the last session in the test part of the experiment as well as the number of games in which the maximum number of trials was exceeded (maxes). Having perfect performance, the subjects could have hit the correct target in one session ∼27 times. S1–S3 reached the correct target 8–15 times. S1 made no mistakes, and S2 and S3 each made one mistake. S4 had only 3 hits, but did not make any mistakes. Thus, these four subjects could make binary choices very accurately. However, the performance speed of S4 was slow because most games were not finished. The last column in the table displays how often, on average, subjects could hit the target per minute. This is calculated as a number of hits divided by the overall duration of the session. Thus, it includes time needed to display the arrow and time between the games. For S1–S4, these numbers are comparable to bit rates (bits/min) as they made very few mistakes. For example, S1 could make on average 3.8 binary choices per minute.

The two columns in the middle of Table 2 show the percentage of correct hits both with all games included (correct/games), and nonfinished games excluded (correct/hits), that is, including only games in which one of the targets was reached. The percentage of correct/games can be compared with classification accuracy, that is, how often the game was classified correctly, but note that it includes games that were not classified at all (maxes). The percentage of correct/hits reveals how many mistakes the subjects made. S5 had more misses than hits, and could not control the BCI. S4 had 100% accuracy, but he made only three hits, meaning that he performed accurately but very slowly.

3.3. Classification accuracy and bit rate of single trials

The BCI performance was based on classification of EEG epochs related to single movement attempts. Assuming that these trials are independent, that is, EEG activation related

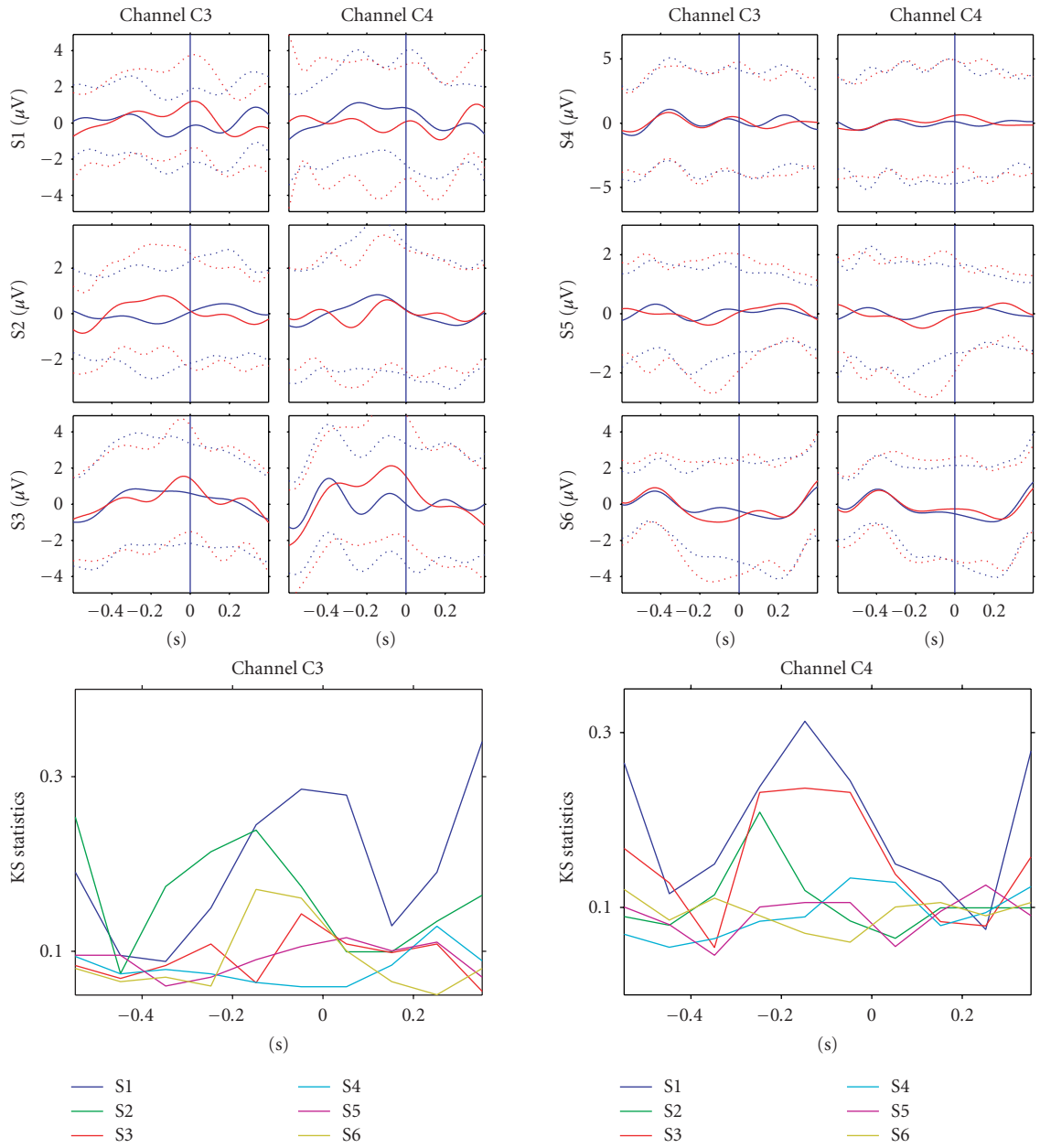

Figure 4: The upper part displays averaged signals ((± standard deviations, N∼150, filtered 1–3 Hz) for all subjects from electrodes C3 and C4 during both the right- (red) and left- (blue) attempted hand movement during the first part of the experiment. The blue vertical line indicates when the subjects were asked to perform the movement. The lower part of the figure shows the Kolmonogorov-Smirnov statistic between the classes of corresponding single trials.

Table 2: The number of games in which the subjects hit the correct/incorrect target (or exceeded maximum of ten trials) in the last session in the third part of the experiment (static model). The subjects did different amount of sessions depending on how tired they got. The percentage of games where the target was hit as well as the correct hits of all hits is displayed in the middle. The right-most column shows the correct hits/min calculated as the number of correct hits divided by the overall duration of the experiment.

Subject	Correct/incorrect (max) games	Correct games (%)	Correct hits (%)	Correct hits/min
S1	15/0 (1)	94	100	3.8
S2	10/1 (4)	67	91	2.7
S3	8/1 (5)	57	89	2.2
S4	3/0 (7)	30	100	0.9
S5	1/2 (8)	9	33	0.3
S6	9/5 (4)	50	64	2.4

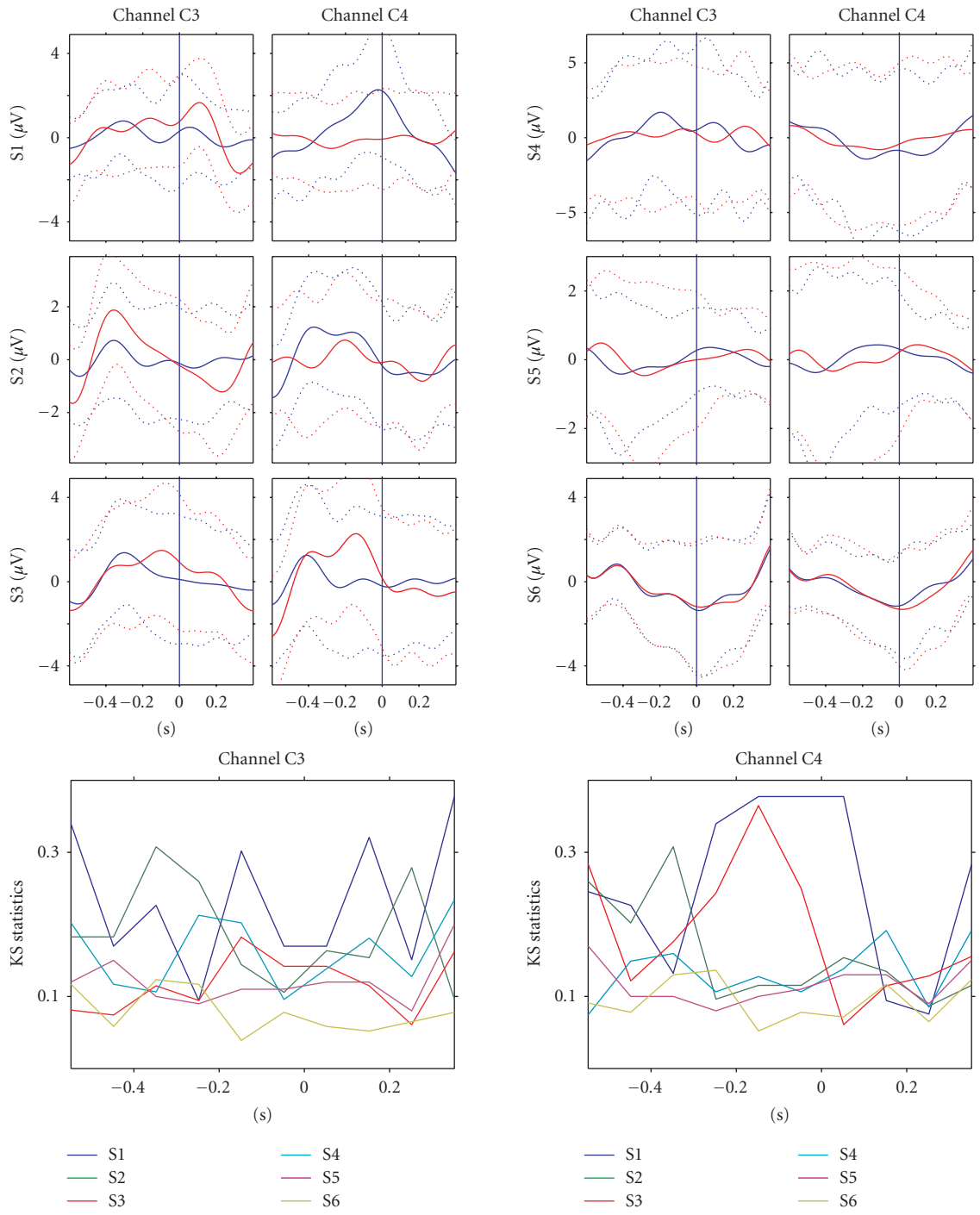

FIGURE 5: Displays averaged signals ((± standard deviations, N~150, filtered 1–3 Hz) for all subjects from electrodes C3 and C4 during both the right- (red) and left- (blue) attempted hand movement during the first part of the experiment. The blue vertical line indicates when the subjects were asked to perform the movement.

to one movement attempt was unaffected by the previous movement attempts in the same game, we can calculate single trial classification accuracy and bit rate (Table 3). The number of single trials in the testing part, that is, that used to calculate the accuracy and bit rate is displayed in the column on the right; we rejected no trials due to artefacts. S1 achieved 79% mean accuracy. Although S2 and S3 were able to control the application with almost no mistakes, their mean classification accuracies were only 69% and 61%. Perelmouter and Birbaumer [29] suggest that a classification accuracy of ≈70% is the requirement to control a binary language support program. S1 and S2 reached this criterion. The single trials of S4–S6 could not be classified above chance level. The bit rates, calculated as Wolpaw et al. [1], are shown per trial as

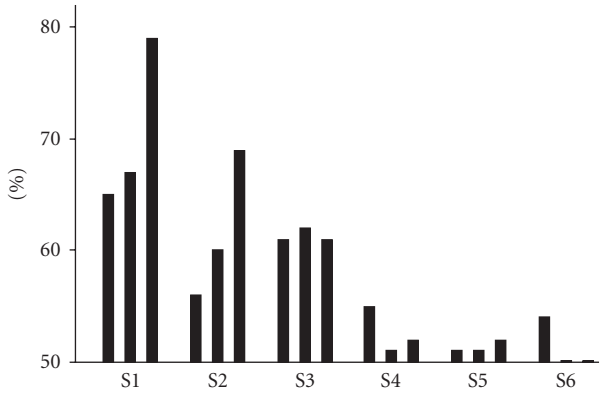

Figure 6: Part 1–3 average classification accuracy for subjects S1–S6.

well as per minute. The maximum bit rate per trial with two classes is 1 bit/trial. Predictions every two seconds result in a maximum of 30 bits per minute. The breaks between games were ignored because they depend on application. Subject S1 obtained a very high bit rate of 8 bits/min. The 3.1 per minute bit rate of S2 is still practical for control purposes, but one binary decision per minute of S3 is impractically slow. Subjects S1 and S2 had higher classification accuracies in the test part than in the beginning of the experiment (Figure 6). S3 and S4 did not improve their performance during the experiment.

To be able to exclude the possibility of BCI control based on eye movements, we simulated the experiment using only the EOG channels. Given the recorded data, this analysis is deterministic, that is, the single trial accuracies reported in the results section could be recovered by simulating the experiment with the given EEG channels. As in the online experiment, features were selected based on the data from the first training part, the classifier was optimized with the data from the second training part, and finally the single EOG trials of the test part were predicted with the obtained classifier. In the individual subjects, the offline single-trial classification accuracies were from 46% to 61% (mean 52%) for all subjects. S2 showed the highest classification accuracies of 61% in the last two testing sessions. These numbers are lower than the classification accuracies of the EEG channels.

4. DISCUSSION

Three out of six subjects (S1–S3) with complete tetraplegia learned to control a BCI after five to seven 4-minute training sessions. They moved a circle several times from the centre of the computer screen to the correct target on one of its sides. S1–S3 hit the target with an accuracy of 94%, 67%, and 57% (every game included), respectively. Despite the relatively low hit accuracy due to high number of games ending nonfinished, that is, ten trials were exceeded, these subjects made very few or no mistakes. The average correct hit rates were 2.2–3.8 hits/min. Assuming the single EEG trials independent, their attempted left- versus right-hand movements could be classified with mean accuracies of 79%, 69%, and 61% in a testing period when the classifier was no more trained. Transmitted information rate of the best subject (S1) was 8 bits/min.

S1 and S2 improved their performance during the experiment. Improvement was probably due both to the classifier adapting to subjects' signals and the subjects learning to control the BCI better. It is difficult to say to what extent the subjects learned control of their EEG signals in such a short training time. They might have learned to time their movement attempts better towards the end of the experiment. In addition, up-to-date feedback probably helped subjects to sustain concentration and try harder.

Real or attempted hand movements are appropriate for BCI use, because many tasks occur in body coordinates (moving a cursor or prosthesis). Only a few earlier EEG studies have examined how the sensorimotor cortex of tetraplegics reacts to movement imagery or attempts. Our recent magnetoencephalographic (MEG) and EEG studies showed that the sensorimotor rhythms of three tetraplegics (level of injury C4-C5; ASIA A classification) respond to attempted cued left- and right-hand finger movements [27]. In contrast to healthy subjects, the 10 and 20 Hz activity in these patients was not contralateral. Surprisingly, the best feature in the present experiment was the amplitude of the slow cortical brain activity (passband 0.5–3 Hz). It could be argued that these slow frequency features are related to eye movements or visual evoked potentials and not sensorimotor cortical activity. However, in the current experimental design we tried to ascertain that the subject's view was identical during both movement (left versus right) tasks; the cue was displayed in the center of the screen and the subjects were instructed to focus on it, not on the circle. The arrow indicating the correct target was presented before a game began and during the game, similar targets were displayed on both sides of the screen (Figure 1). To exclude the possibility that the trial classification was based on eye movements, we performed an offline analysis in which the trial classification was based on signals recorded by the EOG channels. Classification was on chance level in S1 and S3–S6. The classification accuracy of S2 was 61%, lower than 67% obtained on the basis of EEG channels. For S2, it is quite possible that the same features which were used in EEG trial classification were also picked up by the EOG channels. However, we cannot exclude the possibility that eye movements influenced the classification of his data.

Green et al. [30] measured 120 channel EEG while 24 tetraplegic patients attempted cued (ISI 7–10 seconds) finger and toe movements. Movement attempts evoked contralateral potentials in the motor cortex. We used the amplitude of the slow cortical brain activity (1–3 Hz) as initial features. These features were also chosen by the feature extraction algorithm for two good performing subjects (S2 and S3). We did not select features for S1 because he performed well with low-band signals as did subjects S2 and S3 who had several low frequency band features after the selection. In our previous studies, the best features for healthy subjects were nearly always in the 10 and 20 Hz range [24, 31] which was not the case for the present patients.

The methods for feature extraction, selection, and classification worked well in our previous study with ten healthy

Table 3: Theoretical classification accuracy, bitrate and bitrate/min in the third part of the experiment. The number of right/left single trials are displayed on the right.

Subject	R(%)	L(%)	Mean	Bitrate/trial	Bitrate/min	# trials right/left
S1	81	78	79	0.27	8.00	53/54
S2	71	66	69	0.1	3.12	104/104
S3	63	58	61	0.03	1.00	157/151
S4	55	49	52	0	0.04	94/105
S5	50	53	52	0	0.02	115/100
S6	45	53	50	0	0.00	154/163

subjects [24]. Seven out of the ten healthy subjects could choose the correct target in 84–100% cases, 3.5–7.7 times a minute; their mean single trial classification rate was 79.6% and bit rate 10 bits/min. These results are much better than with the present tetraplegic subjects. The selected features also differed. In five healthy subjects the best features were around 10 Hz, in one around 20 Hz, and in four around 2 Hz. Especially, the contralaterality of the sensorimotor-cortex signals during attempted movements was not as clear as that with the healthy subjects performing real movements. The differences may be explained by two factors. First, the features were extracted around the visual trigger. Timing of single trials could jitter a lot and affect the low frequency features. Second, performing real movements is more natural than attempting movements. It is possible that tetraplegic subjects could improve their performance after more training; they could learn to produce more distinctive brain activations during the attempted movements and learn to time their movement attempts more accurately. As an example, Pfurtscheller et al. [32] showed that when one tetraplegic patient learned to control a hand orthosis by controlling his sensorimotor EEG by imagining a foot movement, the amplitude of mu-rhythm in his EEG increased over the five months of training.

In the present experiment, we used a supervised approach to classifier training during the training sessions [24]. Our approach has several advantages. First, a separate training session to determine the model parameters is unnecessary and feedback can be given almost from the beginning of the experiment. Second, subjects receive up-to-date feedback and can change their strategy in response to the feedback. Third, to give more informative feedback to subjects, the circle moved according to the posterior probability of the classifier for subjects S2–S6. The larger the class probability, the longer step the circle took. This informed the subjects about the EEG activity related to the current attempted movement compared to the previous ones that the model was trained with. It also made possible the low number of mistakes in the application, as consecutive wrong classifications with low probabilities did not result to miss. These features probably facilitated the learning of the BCI control.

It is difficult to compare our application performance with other studies because the game ended if the subject did not reach the target in ten trials. In addition, our single-trial bit rates are difficult to compare with those obtained by others, because we assume that the consecutive movement attempts are independent, which is not necessarily true. Most studies do not even show single trial accuracies. The use of BCIs by motor-disabled persons has been examined only in a few studies (see, e.g., [3, 33, 34]). Neuper et al. [35] trained a patient with infantile cerebral paresis over a period of 22 weeks, to use the *"Graz-BCI"*. The subject's task was to move an arrow or choose letters from either side of the screen during an eight-second long trial. The subject was trained to control the 20 Hz activity, using two mental tasks performed continuously for 4 seconds: imagination of right-hand movement and mental relaxation. After this 22-week extensive training period, the subject could choose one out of two letters with 70% accuracy. In another study, Pfurtscheller et al. [32] showed that one subject with a high-level spinal cord injury (C4/C5) could produce cue-stimulus dependent changes to the sensorimotor rhythms after five months of training; the patient could open a hand orthosis by imagining right hand movement.

The user group gaining the most from BCI technology are probably locked-in patients—not tetraplegics. The latter can use various switches such as head and eye mice, puff controls, and so forth. However, use of these methods can become tiresome after a long use. BCIs could offer an additional or alternative control method in producing text, and controlling environment and internet or email applications. In future, tetraplegics could use BCIs to control a hand prosthesis. Working with tetraplegics also provides us insight into how BCIs would work also with other motor-disabled groups.

In conclusion, we studied whether tetraplegic subjects could gain control of a BCI after a short training period. Our approach was based on recognition of features in single EEG trials without knowing the exact timing of the movement. Data from six electrodes is used. Model parameters could be trained quickly and no separate offline calibration session was needed. The results show that some tetraplegic subjects could learn to control a two-command BCI after only a short training period. Compared with a similar study performed with healthy subjects [24], our results show that methods developed and tested with healthy subjects do not necessarily work as well with motor-disabled patients. Therefore, it is important to use motor-disabled persons as subjects in BCI development.

ACKNOWLEDGMENTS

This work was supported by the Academy of Finland (102508, 213938) and by the European IST Programme FET Project FP6-003758. We thank Riitta Passi for help with the

EEG measurements and Harri Valpola and Stephen Roberts for useful comments.

REFERENCES

[1] J. R. Wolpaw, N. Birbaumer, D. J. McFarland, G. Pfurtscheller, and T. M. Vaughan, "Brain-computer interfaces for communication and control," *Clinical Neurophysiology*, vol. 113, no. 6, pp. 767–791, 2002.

[2] A. Kübler, B. Kotchoubey, J. Kaiser, J. R. Wolpaw, and N. Birbaumer, "Brain-computer communication: unlocking the locked in," *Psychological Bulletin*, vol. 127, no. 3, pp. 358–375, 2001.

[3] J. R. Wolpaw and D. J. McFarland, "Control of a two-dimensional movement signal by a noninvasive brain-computer interface in humans," *Proceedings of the National Academy of Sciences of the United States of America*, vol. 101, no. 51, pp. 17849–17854, 2004.

[4] G. Pfurtscheller, C. Neuper, G. R. Müller, et al., "Graz-BCI: state of the art and clinical applications," *IEEE Transactions on Neural Systems and Rehabilitation Engineering*, vol. 11, no. 2, pp. 177–180, 2003.

[5] N. Birbaumer, T. Hinterberger, A. Kübler, and N. Neumann, "The thought-translation device (TTD): neurobehavioral mechanisms and clinical outcome," *IEEE Transactions on Neural Systems and Rehabilitation Engineering*, vol. 11, no. 2, pp. 120–123, 2003.

[6] S. Lemm, B. Blankertz, G. Curio, and K.-R. Müller, "Spatio-spectral filters for improving the classification of single trial EEG," *IEEE Transactions on Biomedical Engineering*, vol. 52, no. 9, pp. 1541–1548, 2005.

[7] G. Dornhege, B. Blankertz, G. Curio, and K.-R. Müller, "Boosting bit rates in noninvasive EEG single-trial classifications by feature combination and multiclass paradigms," *IEEE Transactions on Biomedical Engineering*, vol. 51, no. 6, pp. 993–1002, 2004.

[8] Y. Li, X. Gao, H. Liu, and S. Gao, "Classification of single-trial electroencephalogram during finger movement," *IEEE Transactions on Biomedical Engineering*, vol. 51, no. 6, pp. 1019–1025, 2004.

[9] P. Sykacek, S. J. Roberts, and M. Stokes, "Adaptive BCI based on variational Bayesian Kalman filtering: an empirical evaluation," *IEEE Transactions on Biomedical Engineering*, vol. 51, no. 5, pp. 719–727, 2004.

[10] J. D. R. Millán and J. Mouriño, "Asynchronous BCI and local neural classifiers: an overview of the adaptive brain interface project," *IEEE Transactions on Neural Systems and Rehabilitation Engineering*, vol. 11, no. 2, pp. 159–161, 2003.

[11] C. Vidaurre, A. Schlögl, R. Cabeza, R. Scherer, and G. Pfurtscheller, "Adaptive on-line classification for EEG-based brain computer interfaces with ARR parameters and band power estimates," *Biomedizinische Technik*, vol. 50, no. 11, pp. 350–354, 2005.

[12] E. W. Sellers, A. Kübler, and E. Donchin, "Brain-computer interface research at the University of South Florida Cognitive Psychophysiology Laboratory: the P300 speller," *IEEE Transactions on Neural Systems and Rehabilitation Engineering*, vol. 14, no. 2, pp. 221–224, 2006.

[13] J. Müller-Gerking, G. Pfurtscheller, and H. Flyvbjerg, "Designing optimal spatial filters for single-trial EEG classification in a movement task," *Clinical Neurophysiology*, vol. 110, no. 5, pp. 787–798, 1999.

[14] E. Curran, P. Sykacek, M. Stokes, et al., "Cognitive tasks for driving a brain-computer interfacing system: a pilot study," *IEEE Transactions on Neural Systems and Rehabilitation Engineering*, vol. 12, no. 1, pp. 48–54, 2004.

[15] J. D. R. Millán, F. Renkens, J. Mouriño, and W. Gerstner, "Noninvasive brain-actuated control of a mobile robot by human EEG," *IEEE Transactions on Biomedical Engineering*, vol. 51, no. 6, pp. 1026–1033, 2004.

[16] B. Obermaier, C. Neuper, C. Guger, and G. Pfurtscheller, "Information transfer rate in a five-classes brain-computer interface," *IEEE Transactions on Neural Systems and Rehabilitation Engineering*, vol. 9, no. 3, pp. 283–288, 2001.

[17] H. Gaustaut, "Étude électrocorticographique de la réactivité des rhythmes rolandiques," *Revue Neurologique*, vol. 87, no. 2, pp. 176–182, 1952.

[18] R. Salmelin and R. Hari, "Spatiotemporal characteristics of sensorimotor neuromagnetic rhythms related to thumb movement," *Neuroscience*, vol. 60, no. 2, pp. 537–550, 1994.

[19] G. Pfurtscheller, "Central beta rhythm during sensorimotor activities in man," *Electroencephalography and Clinical Neurophysiology*, vol. 51, no. 3, pp. 253–264, 1981.

[20] B. Blankertz, K.-R. Müller, G. Curio, et al., "The BCI competition 2003: progress and perspectives in detection and discrimination of EEG single trials," *IEEE Transactions on Biomedical Engineering*, vol. 51, no. 6, pp. 1044–1051, 2004.

[21] S. Shoham, E. Halgren, E. M. Maynard, and R. A. Normann, "Motor-cortical activity in tetraplegics," *Nature*, vol. 413, no. 6858, p. 793, 2001.

[22] P. Sabbah, S. de Schonen, C. Leveque, et al., "Sensorimotor cortical activity in patients with complete spinal cord injury: a functional magnetic resonance imaging study," *Journal of Neurotrauma*, vol. 19, no. 1, pp. 53–60, 2002.

[23] P. Jylänki, L. Kauhanen, J. Lehtonen, J. Heikkonen, and M. Sams, "Use of feedback in classification of single EEG trials during finger movements," in *Proceedings of the 12th Annual Meeting of the Organization for Human Brain Mapping*, Florence, Italy, June 2006.

[24] J. Lehtonen, P. Jylänki, L. Kauhanen, and M. Sams, "Online classification of single EEG trials during finger movements," in press.

[25] F. M. Maynard Jr., M. B. Bracken, G. Creasey, et al., "International standards for neurological and functional classification of spinal cord injury," *Spinal Cord*, vol. 35, no. 5, pp. 266–274, 1997.

[26] A. V. Oppenheim and R. V. Schafer, *Discrete-Time Signal Processing*, Prentice-Hall, Upper Saddle River, NJ, USA, 1989.

[27] L. Kauhanen, T. Nykopp, J. Lehtonen, et al., "EEG and MEG brain-computer interface for tetraplegic patients," *IEEE Transactions on Neural Systems and Rehabilitation Engineering*, vol. 14, no. 2, pp. 190–193, 2006.

[28] W. J. Conover, *Practical Nonparametric Statistics*, John Wiley ' Sons, New York, NY, USA, 3rd edition, 1999.

[29] J. Perelmouter and N. Birbaumer, "A binary spelling interface with random errors," *IEEE Transactions on Rehabilitation Engineering*, vol. 8, no. 2, pp. 227–232, 2000.

[30] J. B. Green, E. Sora, Y. Bialy, A. Ricamato, and R. W. Thatcher, "Cortical sensorimotor reorganization after spinal cord injury: an electroencephalographic study," *Neurology*, vol. 50, no. 4, pp. 1115–1121, 1998.

[31] L. Kauhanen, T. Nykopp, and M. Sams, "Classification of single MEG trials related to left and right index finger movements," *Clinical Neurophysiology*, vol. 117, no. 2, pp. 430–439, 2006.

[32] G. Pfurtscheller, C. Guger, G. Müller, G. Krausz, and C. Neuper, "Brain oscillations control hand orthosis in a tetraplegic," *Neuroscience Letters*, vol. 292, no. 3, pp. 211–214, 2000.

[33] A. Kübler, F. Nijboer, J. Mellinger, et al., "Patients with ALS can use sensorimotor rhythms to operate a brain-computer interface," *Neurology*, vol. 64, no. 10, pp. 1775–1777, 2005.

[34] N. Birbaumer, N. Ghanayim, T. Hinterberger, et al., "A spelling device for the paralysed," *Nature*, vol. 398, no. 6725, pp. 297–298, 1999.

[35] C. Neuper, G. R. Müller, A. Kübler, N. Birbaumer, and G. Pfurtscheller, "Clinical application of an EEG-based brain-computer interface: a case study in a patient with severe motor impairment," *Clinical Neurophysiology*, vol. 114, no. 3, pp. 399–409, 2003.

Hindawi Publishing Corporation
Computational Intelligence and Neuroscience
Volume 2007, Article ID 51363, 9 pages
doi:10.1155/2007/51363

Research Article

A Concept for Extending the Applicability of Constraint-Induced Movement Therapy through Motor Cortex Activity Feedback Using a Neural Prosthesis

Tomas E. Ward,[1] Christopher J. Soraghan,[2] Fiachra Matthews,[3] and Charles Markham[4]

[1] *Department of Electronic Engineering, National University of Ireland, Maynooth, County Kildare, Ireland*
[2] *Department of Computer Science and Department of Experimental Physics, National University of Ireland, Maynooth, County Kildare, Ireland*
[3] *Hamilton Institute, National University of Ireland, Maynooth, County Kildare, Ireland*
[4] *Department of Computer Science, National University of Ireland, Maynooth, County Kildare, Ireland*

Correspondence should be addressed to Tomas E. Ward, tomas.ward@eeng.nuim.ie

Received 17 February 2007; Revised 11 May 2007; Accepted 14 July 2007

Recommended by Fabio Babiloni

This paper describes a concept for the extension of constraint-induced movement therapy (CIMT) through the use of feedback of primary motor cortex activity. CIMT requires residual movement to act as a source of feedback to the patient, thus preventing its application to those with no perceptible movement. It is proposed in this paper that it is possible to provide feedback of the motor cortex effort to the patient by measurement with near infrared spectroscopy (NIRS). Significant changes in such effort may be used to drive rehabilitative robotic actuators, for example. This may provide a possible avenue for extending CIMT to patients hitherto excluded as a result of severity of condition. In support of such a paradigm, this paper details the current status of CIMT and related attempts to extend rehabilitation therapy through the application of technology. An introduction to the relevant haemodynamics is given including a description of the basic technology behind a suitable NIRS system. An illustration of the proposed therapy is described using a simple NIRS system driving a robotic arm during simple upper-limb unilateral isometric contraction exercises with healthy subjects.

1. INTRODUCTION

Strokes are characterised by an acute, nonconvulsive loss of neurological function as a result of an ischemic or hemorrhagic intracranial vascular event [1]. Worldwide, there are over 20 million cases of stroke each year [2] and of these approximately 75% are nonfatal with survivors left with a spectrum of poststroke disabilities ranging from mild numbness to severe motor and cognitive impairments. The dysfunction introduced depends on the site and extent of the infarction. Immediately following stroke, there is generally some degree of spontaneous recovery where some lost function is restored as a result of collateral circulation, reduction in inflammation, and haematoma compression among other factors. However, there are in nearly all cases significant residual neurological impairment, which if left untreated will result in severe degradation in life quality for the survivor. It is not surprising then that stroke is the leading cause of physical disability in Europe and the United States [3], and with 75% of stroke survivors suffering syndromes severe enough to affect their employability, the economic cost of the cerbrovascular disease stretches far beyond the immediate medical one. Poststroke rehabilitation is therefore critical to restore as much function as possible for the patient. This takes the form of neuro-rehabilitation, an interdisciplinary branch of clinical and medical science; the purpose of which is to restore neurological function and quality of life to people following disease or injury of the nervous system. Neurorehabilitation science draws on many techniques and therapies but the cornerstone of most treatments lies in physical therapy as most strokes seem to result in some form of hemiparesis or hemiplegia usually contralateral to the site of the stroke. The basic tenet of physical therapy or motor rehabilitation as it is often termed is that repetitive practise of proscribed movement can have a highly significant effect on rehabilitation outcome [4].

Currently, a particular type of motor rehabilitation termed constraint-induced movement therapy (CIMT) [5, 6] has been shown to be highly effective for use in hemiplegic stroke rehabilitation [7]. CIMT requires the subject have the unaffected limb constrained while they are encouraged actively to use the affected limb over long periods. With large periods of practise, the weakened side is strengthened significantly—possibly as a result of cortical reorganisation and changes in motor cortex excitability [8]. It appears that this method has statistically significant outcome improvements over equal intensity approaches [9, 10] and is currently the focus of concerted refinement and development to expand its theoretical basis and extend the application scope [11].

The flurry of research around this technique has had an impact on rehabilitation engineering where over the past few years the therapy has been augmented by robot-assisted training [12]. Such techniques extend CIMT to patients who have such severe disability that they are unable to engage in unassisted movement. This concept is underpinned by studies which have shown that the benefits of CIMT could be extended to such patients through the application of external forces applied to the limb [13] or functional electrical stimulation [14, 15]. The philosophy behind the approach envisaged in this paper is that perhaps the CIMT process can be enhanced further for this group if some measure of attempted activity in the motor regions could be presented either as a direct form of biofeedback or harnessed as a trigger to induce robotic-assisted movement or FES. Functional magnetic resonance imaging (fMRI) studies have shown that increases in bilateral cortical activation [16] are exhibited during CIMT; therefore appropriate feedback could be established using a brain-machine interface driven by signals derived directly from the motor cortical areas—a neural or more specifically, neurocortical prosthesis. It has been widely reported that NIRS systems are capable of detecting haemodynamic changes associated with motor movement both imagined and executed [17–19]; therefore an ideal neural prosthesis for this application is a NIRS-based brain computer interface (NIRS-BCI). The successful evoking of cortical NIRS responses could serve as the triggering event for biofeedback. NIRS has the additional benefit of showing oxyhaemoglobin (HbO) level changes as well as blood volume and deoxyhaemoglobin (Hb) changes which are the reported etiology of the MRI signal. The idea of extending the biofeedback loop directly to the motor areas responsible for movement is novel in this case of CIMT and the technique sits well with current opinions in neurorehabilitation which advocate enhanced motor learning techniques [18, 20]. The remainder of this paper is as follows. Section 2 begins with a description of the rehabilitation context for stroke survivors including a short presentation of the CIMT model. In addition, some background to BCI and robotics in a neurorehabilitation context is given including the relevant physiological measurement modality of NIRS. Section 3 comprises a technical illustration of the proposed concept to facilitate an appreciation for obstacles and issues facing practical embodiments of the idea. Section 4 discusses implications and prospects before a short summary is given.

2. BACKGROUND AND RELATED WORK

Stroke rehabilitation therapies have until recently been characterised by empirically derived approaches rather than on the basis of scientifically derived theories. Traditional practises have a compensatory philosophy where targeted muscular and action accommodation techniques serve to circumnavigate impaired function. Lack of standards, poor validation, poor evaluation, and above all the lack of a neuroscientific basis has meant that neurorehabilitation clinical practises have languished outside the realm of evidence-based medicine. The advent of CIMT changed this perception and revolutionised rehabilitation medicine. CIMT is derived from a rigorously constructed conceptual framework which has its origins in the theory of learned non-use—an explanation for certain neurocortical and behavioural phenomena evident in monkey models of neurological dysfunction. [21]. In such models, the consequence of the paretic limb, for example, is the onset of a neuroplastic process in which the motor circuits undergo alteration which has degenerative impacts for the affected limb. CIMT aims to undo the learned nonuse through constraining the unaffected limb and forced repetitive training—a practise somewhat analogous to the use of the eye patch in amblyopia or lazy eye. With its efficacy confirmed during the largest ever controlled trial in neurological rehabilitation [10], the continued clinical practise of this therapy and its further refinement and extension are assured.

The rigorous psychological and neurological basis underlying CIMT makes it very amenable to integration with assistive technologies which yield quantitative measures and assessment criteria. The development of robotic actuators in tandem with neural prosthetic devices for such rehabilitation procedures is a natural development for future CIMT variants. The recent literature exhibits a growing and versatile range of potential systems that may be effective in application with CIMT.

2.1. Robot-assisted neurorehabilitation

The use of robotic systems as aids in neurorehabilitation is not new with systems such as MIT-MANUS [22] demonstrating the efficacy of the technique almost ten years ago. Their application to neurorehabilitation is quite natural as it is well known that intensive goal-directed movement repetition facilitates improved recovery outcome following stroke [23, 24] and as robots can engage in repetitive tasks consistently and unobtrusively, they are excellent deliverers of rehabilitation therapy. Clinical effectiveness has been reported in several studies [25–27] and it seems that these rehabilitative devices will be incorporated into standard clinical practise in the near future. Comprehensive reviews of such devices and their efficacy can be found in the literature [28, 29]. Such systems also have the benefit that they may be altered to incorporate automatic kinematic and kinetic data collection allowing the possibility of quantitative measures of subject performance and recovery of function. While there are many devices reported at present, the common feature is their facilitation of repetitious exercise. The most notable recent

developments which provide context for this work are electromyogram feature-triggered systems reported by Dipietro et al. [30]. One of the advantages highlighted by Dipietro and her colleagues is that "*It may allow highly-impaired subjects to activate robot assistance; such patients might be able to generate EMG signals even though they were unable to produce sufficient movement to trigger the robot*." Previous systems rely on exceeding kinematic/kinetic thresholds based on limb velocity, for example, to trigger movement. Therefore, Dipietro's system can be regarded as harnessing peripheral nervous system activity as recorded through electrical muscular activity to trigger feedback. It is proposed in the present paper that central nervous system activity measures may serve as an alternative trigger—a concept that suggests a new application area for brain-computer interfaces.

2.2. Brain-computer interfaces in neurorehabilitation

Brain-computer interfaces (BCIs) are devices that act as neural prostheses. They facilitate communication or information transfer between the brain and the outside world independent of the peripheral nervous system. While the primary focus of BCI research within neurorehabilitation has been to provide assistive technology to enable communication for the severely disabled, there have been suggestions that the technology may have something to offer in terms of physical recovery for certain conditions through reinforcement of damaged neural pathways [31], plasticity-induced cortical reorganization [32], and triggering of functional electrical stimulation [33]. While there has been movement of BCI research towards this area, most rehabilitation efforts have been directed towards harnessing neural prostheses for controlling robotic limbs for reaching and manipulating tasks or control of wheelchairs. To these particular ends, great progress has been made in terms of practicality [34, 35], speed [36, 37], and ease of use [38]. Such advances are continuing, however the more subtle application of the technology as a biofeedback mechanism for physical rehabilitation has hitherto been underdeveloped. One of the most impressive attempts in this direction is the Brain-Orthosis-Interface reported as a solution for chronic stroke sufferers [39]. The technology based on magnetoencephalography methods monitors sensorimotor rhythm to derive control signals to open and close an orthotic hand coupled to the patient's own. In this way, the patient receives enhanced feedback through both watching and feeling their own hand moving. Such operant conditioning enhances the biofeedback process and improves neural prosthesis performance. Such a case represents a more extreme rehabilitative application of a BCI in that the neural prosthesis is a permanent one. The paradigm presented in this paper casts the BCI in the role of a temporary neural prosthetic splint that provides feedback in lieu of feedback from actual movement. The contribution of this paper is in this context. When, if ever, movement, however minimal, is restored, more conventional forms of CIMT may be applied probably removing the necessity for the BCI. A related concept is the provision of an afferent neural prosthetic for rehabilitation. In a recent work, transcranial direct current stimulation of the motor cortex is used to improve rehabilitation outcome [40]. This can be interpreted as a neural prosthetic encouraging cortical activation associated with movement.

2.3. Near infrared spectroscopy-based brain-computer interface

A near infrared spectroscopy-based brain-computer interface utilises an optical modality for inferring changes in brain state. It is possible to measure changes in cerebral blood volume and oxygenation associated with cortical activity through the use of light in the 600–1000 nm wavelength range yielding a cerebral haemodynamic monitor. The optical absorption and scattering properties of scalp, hair, skull, and the meninges surrounding the brain allow photons of these wavelengths to penetrate in to the surface of the cortex where they undergo scattering and absorption events with a wide range of chromophores in the tissue. The significant scattering component means that a small proportion of the injected light will exit at some distance from the source carrying information about chromophore concentration dynamics at the upper surface of the brain. A suitably sensitive well-positioned detector can detect this photon flux and allow noninvasive monitoring of these changes. There are a number of chromophores in brain tissue in this band whose optical properties are correlated with mental activation. Of these, the most germane is haemoglobin—the oxygen carrying molecule of the body. Haemoglobin exists principally in two forms in the body: an oxidised state and a reduced state. These two states generally referred to as oxyhaemoglobin (HbO) and deoxyhaemoglobin (Hb) have distinctly different absorption spectra allowing their relative concentrations to be determined through multiple wavelength interrogation. During concerted cortical activity, a neurovascular process occurs whereby changes occur in cerebral blood flow, volume, and metabolic rate of consumption. This manifests itself principally as an increased demand for oxygen with the local vasculature responding through flooding the cortical area and surrounding tissue with oxygenated haemoglobin. Usually this is accompanied by a corresponding drop in deoxyhaemoglobin concentration—a component thought to be responsible for the signal recorded during fMRI. The relative changes in haemoglobin can be distinguished through interrogation at a number of wavelengths in the near infrared band described above and therefore changes in cortical activation associated with mental activity can be monitored. This is the basis of NIRS-BCI. A detailed review of near infrared spectroscopy techniques for biomedical application can be found in [41].

The measurement principle in more quantitative terms can be expressed using a modified version of the Beer-Lambert Law. The attenuation due to absorption and scattering effects may be described therefore as

$$A = \log_{10} \frac{I_o}{I} = \alpha c L B + G. \tag{1}$$

Here A is attenuation, I_0 is incident light intensity, I is transmitted light intensity. On the right-hand side, α is the specific extinction coefficient for the absorber which is wavelength

dependent in this case, c is the concentration of the absorber, L is the distance between the source and detector, B is the differential path length factor, and G is a term to account for scattering losses.

Changes in haemoglobin levels are calculated then as a superposition of the changes for each absorber species—in this case oxy- and deoxyhaemoglobin:

$$\Delta A = \left(\alpha_{\mathrm{HbO}}\Delta c_{\mathrm{HbO}} + \alpha_{\mathrm{Hb}}\Delta c_{\mathrm{Hb}}\right)BL. \quad (2)$$

Equation (2) is evaluated at two wavelengths, either side of the isobestic point to enable separation of the two haemoglobin states.

Previous functional NIRS studies have documented haemodynamic changes as a result of motor, cognitive, visual, and auditory activities [41]. The device used here has been used previously to record evoked responses arising from motor imagery in the sensorimotor cortex [19]. The general form is an increase in HbO coupled with a decrease in Hb 3–5 seconds after the onset of movement execution or imagery. While the idea of monitoring cerebral oxygenation using NIRS has been around for some time, it has as yet found only limited application in brain-computer interfacing mostly due to the slow baud rate of the device. Currently, two working devices have been reported [17, 18], however the area is nascent and undoubtedly more in-depth investigations of the efficacy of such devices will appear.

As an illustration of how CIMT might be augmented through the provision of biofeedback of motor cortical effort, the next section describes a simple practical embodiment in which a NIRS-BCI is used to trigger movement of a robotic actuator as a result of elevated motor cortical activity.

3. AN ILLUSTRATIVE EMBODIMENT

An example of how an embodiment of the concept described in this paper might work is now given based on a synchronous BCI paradigm in which the activation signal is derived from bilateral cortical activity over the sensorimotor region (SMR). Unlike most BCI experiments, however, overt motor activity is employed by the subjects as imagined activity is not required or indeed germane for the rehabilitative therapy envisaged. Actual movement allows the experimenter to determine that the motor areas must indeed be active and hence eliminates the effect of poor engagement on the part of the subjects in the results. A computer is used to present movement instructions to the subjects (audio and visual cues). Appropriate activation of the SMR during movement triggers feedback in the form of movement of a robotic arm.

The signals, collected simultaneously, are cerebral changes in HbO and Hb, the respiration pneumogram and the digital photoplethysmograph (PPG).

3.1. Hardware

A continuous wave dual channel NIRS system is used to interrogate the cerebral cortex on each hemisphere. The light source comprises light emitting diodes (LEDs) at wavelengths of 760 nm and 880 nm (Opto Diode corp., Inc., APT-0010/OD-880F, Calif, USA) having a narrow beam angle of 8° and a spectral bandwidth at 50% of 30 nm and 80 nm, respectively. The light output of each LED is modulated in the low kilohertz range to facilitate lock-in detection at the output. The LEDs are placed in direct contact with the scalp. Avalanche photodiodes (APD), Hamamatsu C5460-01, were used as the detector; the output of which was fed via a 3 mm diameter, 1 m long, fibre optic bundle to lock-in amplifiers (Signal Recovery, model 7265). A more detailed account of the optical setup and other design considerations can be found in [42].

Figure 1: The Armdroid-1 robotic arm used in the feedback protocol.

For data acquisition (offline analysis), the *Biopac UIM100C interface module* in tandem with a *Biopac MP100* was used to collect the four analogue channels of NIRS data (two wavelengths, two sites) from the lock-in amplifiers at 16-bit resolution. In addition, two other analogue channels of data were collected by the *MP100* for respiration and PPG (*Biopac* amplifiers models *PPG100C* and *RSP100C*) with gains of 100 and 10, respectively. *PPG100C* settings comprised a low-pass filter of 10 Hz and high-pass filter of 0.05 Hz. *RSP100C* settings implemented a low-pass filter of 10 Hz.

Feedback was provided through movement of a robotic arm (Figure 1) in sympathy with sustained elevation in HbO levels during the motor execution tasks. The outputs of the lock-in amplifiers was tapped to provide drive signals via a simple *12-bit National Instruments USB-6008* DAQ at 10 samples per second. Online and real-time processings for Hb and HbO using standard algorithms [43] based on (2) provided control of the robotic arm and feedback. The robotic arm was driven using control signals from the DAQ system allowing predetermined movement patterns to be invoked when haemodynamic activity exceeded rest period levels.

3.2. A simple experimental protocol

In this work, we enlisted 5 healthy subjects (4 males, 1 female), 2 left handed and 3 right handed (determined, using Edinburgh Handedness Inventory [44]). The subjects age

Table 1: Optode locations referenced to EEG 10–20 system.

Optode descriptions	Light source location	Detector location
Channel 1 (left-hand side)	$C3 : 1.5(3\pi/2)$	$C3 : 1.5(\pi/2)$
Channel 1 (right-hand side)	$C4 : 1.5(3\pi/2)$	$C4 : 1.5(\pi/2)$

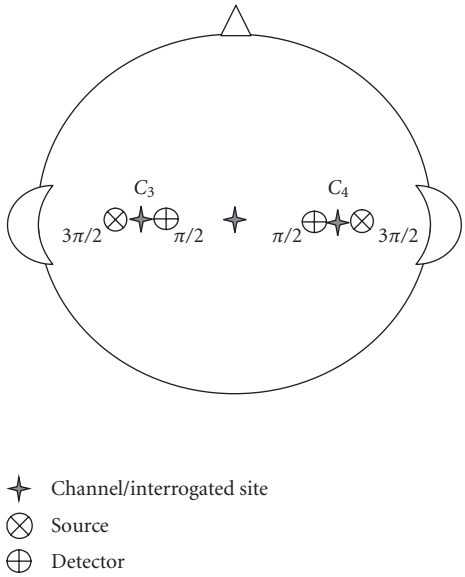

Figure 2: Illustration of relative positioning of optode sources and detectors.

range was 23-25 years old (mean age 24years). One subject (female) was removed from analysis due to poor SNR and optode placement problems. The remaining four subjects underwent online feedback experiments. All remaining subjects were included in the full analysis. Two of the subjects had no previous experience with NIRS experiments.

Each subject was seated in a near supine position to reduce the effects of low-frequency blood oscillations (Mayer wave) in a dimly lit room. The respiration monitoring device (*Biopac-TSD201*) was strapped around the chest of each subject to monitor the respiratory signal during trials. The PPG probe (*Biopac-TSD200*) was attached to the index finger on the inactive limb to monitor the cardiac pulse during trials. Subjects' head measurements were taken to locate positions *C*3 and *C*4. These 10–20 system positions are approximately over primary motor cortex centres in the brain responsible for right- and left-hand movements. The distance between the source and detector was 30 mm. A more precise positioning descriptor is available using the optode placement system proposed in [45]. Using this system, the optode location is described in terms of distance and angle with respect to a defined EEG 10–20 system landmark position which serves as an origin. In this study, angles are referenced to C_z. This yields optode descriptors as in Table 1, illustrated in Figure 2.

Hair was parted under the optode for both the source and detector to leave ample hair-free scalp. The optodes and fibre optic bundles were inserted into cushioned pads in contact with the subject's scalp. The subject's hands were placed under restraining straps in order to facilitate isometric exercise during the stimulus trials. Once positioned and instrumented, the subject was given instructions to follow, before commencing the experiment. Prior to experiment each subject was informed about the nature and purpose of the experimental study and given precise instruction as to the task required of them. To reduce artefact ,subjects were asked to minimise head and body movements as well as given instructions to breathe gently and regularly.

The paradigm for performing the overt motor task is shown in Figure 3. An initial 30 seconds rest was followed by alternating periods of 25 seconds of motor effort (isometric maximal voluntary contractions—MVCs of the indicated forearm, pivoting at the elbow on a rigid support surface) and 15-second rest. For each "experimental session," there were 10 stimulus periods. Each of the four subjects carried out two sessions on each arm, thus a total of 20 stimulus periods per arm per subject. Thus, a total of 80 online trials for each left and right arm are used in the final analysis.

Audio-visual cues indicating the task and rest periods were presented via an LCD monitor to the subjects. Feedback was provided in two forms: a symbolic form which on the LCD monitor presented itself as a change from a black rectangle to an upwards pointing arrow when HbO levels in excess of the previous rest period's level were present, and a physical action cue where movement of the robotic arm took place under the same conditions. When the HbO levels dipped below the threshold during the motor task period, the icon reverted to the black rectangle form and motion of the robotic arm ceased.

3.3. A basic signal classification scheme

Raw signals from the lock-in amplifiers were sampled at 10 Hz, and the Hb and HbO concentrations were calculated in real-time, on a sample-by-sample basis. Simple moving average filters were used in all experiments. A 10-point moving average filter was used to low-pass filter data in real time. Once Hb and HbO concentrations were calculated, a further moving average filter was used for classification. For the detection of significant activity during the activation period, a simple thresholding scheme was employed whereby a datum was taken during the preceding rest period. This datum consisted of the average HbO level during the 15 seconds of the rest period. Neither Hb nor total haemoglobin levels were used as an information signal in the online experiments. The 10 point running average of the HbO signal calculated during the motor task period was thresholded against this reference signal. When the level was exceeded during this period, significant motor cortical activity was inferred and

Table 2: Success rate in moving robot arm. Figures indicate the percentage of time subjects were able to keep the robot moving during each trial. That is, subject 4 successfully moved the robot 96.7% of the time during all 10 stimulus trials for the first session of left-arm maximum voluntary contraction (left 1).

Subject	Left 1 (%)	Left 2 (%)	Right 1 (%)	Right 2 (%)	Subject average (%)
1	87.2 ± 23.9	90.4 ± 11.0	91.8 ± 15.9	95.4 ± 5.1	91.2 ± 13.9
2	82.4 ± 20.2	88.2 ± 13.4	73.5 ± 25.9	82 ± 25.2	81.5 ± 21.2
3*	74.7 ± 25.8	64.3 ± 21.7	63.7 ± 33.6	46.8 ± 38.7	62.4 ± 29.9
4	96.7 ± 3.2	98.4 ± 2.9	90.2 ± 19.1	86.5 ± 23.6	93 ± 12.2

* Subject 3 experiments had low-light levels, thus a lower SNR. A previous X-ray has also shown that he has a relatively thick skull.

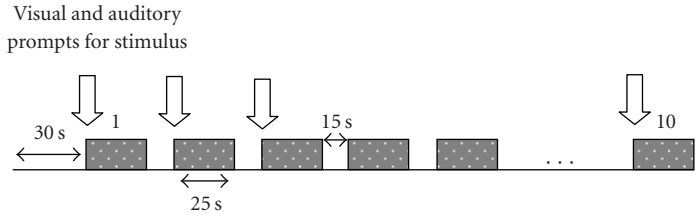

Figure 3: Illustration of the experimental sequencing. Shaded boxes are motor task periods.

appropriate feedback was presented. In summary, activation occurs where $s[i] - \bar{r} > 0$,

$$s[i] = \frac{1}{W} \sum_{j=1}^{W-1} \mathrm{HbO}[i + j] \quad \text{for } i = 1, \ldots, N, \tag{3}$$

where $s[i]$ is the derived control signal at the ith sample, $W = 10$, N is the number of samples acquired during the motor task and $\bar{r}$ is the average HbO signal during the rest period.

So long as the stimulus moving average was greater than the rest average, activity was sensed and the robotic arm was activated.

3.4. Results

Table 2 presents the results of the experiment as described. This table shows the percentage of time that subjects were able to move the robot during the motor activation task. All the subjects were successful in achieving some control of the robotic arm. For example, subject 1 was able to activate the robot almost all the time when engaged in right forearm movement (>95%). Subject 3 unfortunately was not as successful as the others, only realising movement of the robot arm just over 60% of the time (a footnote to the table may suggest why). However, the measures presented here are rather conservative as they indicate the percentage of time by which the threshold was exceeded during the motor task. If the results were reworked to indicate the percentage of motor task periods where the robotic arm was activated, then the results would be almost perfect. This of course would be a disingenuous summary of the experiment for many reasons. A more insightful observation of the experiments can be obtained from Figure 4 which shows the averaged responses (including standard deviations) for two paradigmatic subject tests during both the motor task and rest periods.

Figure 4 was produced using the Matlab-based NIRS analysis tool HomER [46] and illustrates mean and standard deviation levels that indicate consistent differences between rest and activation. The smoothness of the plot is attributable both to averaging over all trials from both channels and-a 3rd to order low-pass Butterworth filter with cutoff frequency of 0.7 Hz implemented before calculating averages and standard deviations.

4. POTENTIALS AND PROSPECTS

The key contribution of this paper is the presentation of the idea that a neurocortical prosthesis may serve as a means to extend CIMT to severe stroke sufferers as part of an therapeutic regime. The very simple illustration of this idea in Section 3 highlights well the basic operation of a NIRS-BCI in a CIMT-like scenario. It is reasonable to suggest that even the toy system above may provide a basic platform on which to develop more sophisticated systems for comprehensive studies with the intended population of stroke sufferers. The results, which in themselves are nonsurprising in nature, are useful for facilitating assessment of potential design issues for more developed systems with the caveat that acquiring good quality signals may be difficult with damaged cortex and that even with robust signals, there is perhaps the possibility of habituation effects which may limit applicability. Notwithstanding these concerns, the responses and activation levels evident in Figure 4 show all the characteristics expected [18, 42] of NIRS-BCI signals. While the results show high variability, they have been calculated for real-time biofeedback. This presents a significantly more difficult scenario than offline analysis which would allow for removal of artefact and screening of signals and would undoubtedly show improved figures. However, real-time control is important for the application envisaged and the results do

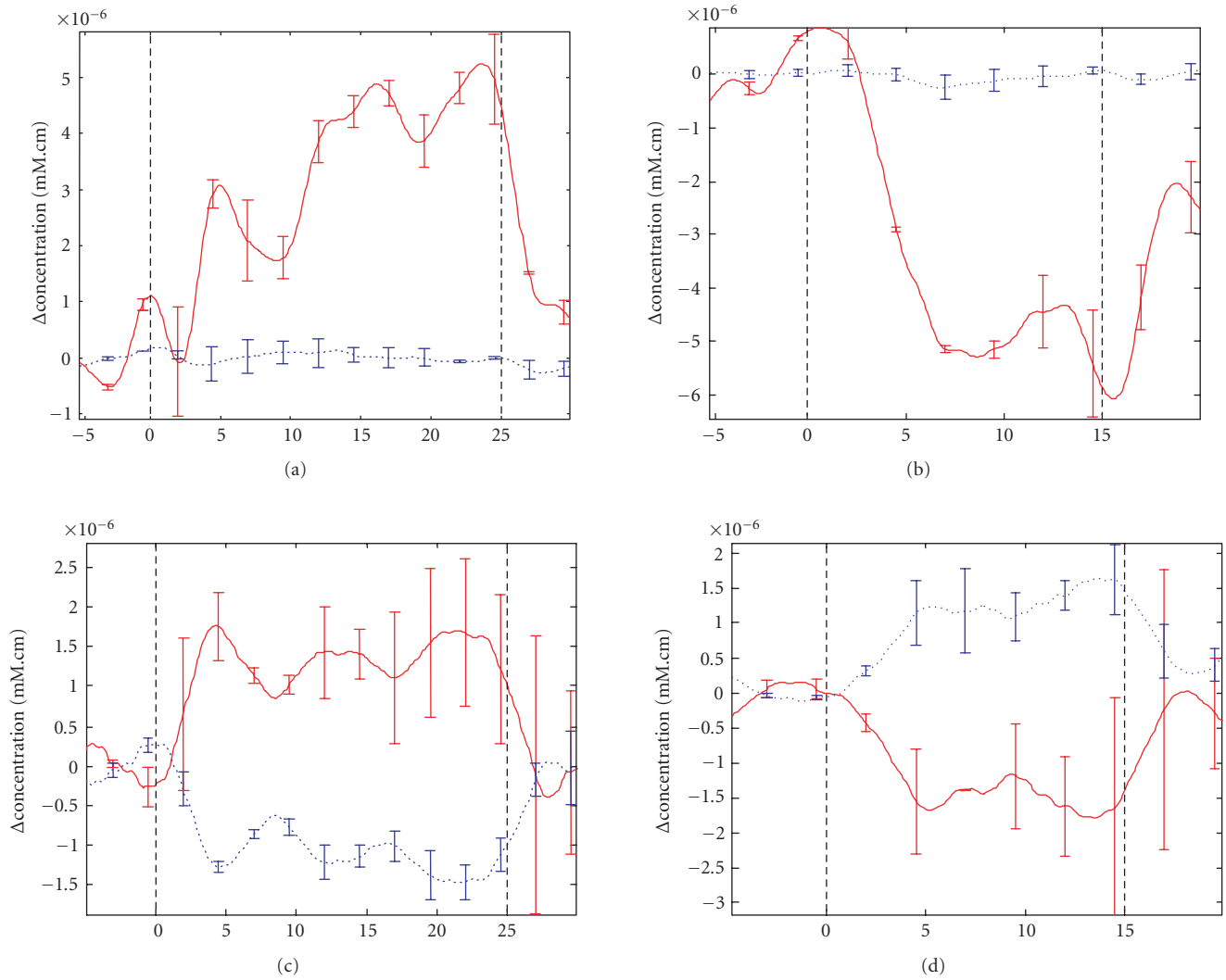

FIGURE 4: Top row shows average Hb (dashed trace) and HbO (solid trace) levels ± SD for subject 2. The bottom row shows average readings for subject 1. The left-hand column shows activity during motor task (between vertical dashed lines) while the right-hand column shows corresponding activity during rest. The abscissa for all plots is in seconds.

indicate that such biofeedback is possible. The signal processing necessary crude, given the real-time requirements, is certainly worth more sustained development to compensate for motion-contaminated trials and other extrageneous forms of artefact. Online adaptive filtering is a necessary component for a more robust system. Clearly, a better understanding of the underlying responses may allow better integration of other signals such as the Hb signal. The variability of the Hb response meant that it was difficult to reliably use it as a trigger signal and although discarded here, it is a useful signal to collect for future work in improving performance. The idea of integrating other signals can be taken further, for example, the provision of a multimodal neurocortical prothesis harnessing motor rhythm EEG would clearly enhance the system further as it is probable that the compound signal would offer greater sensitivity to weaker cortical activation and better insight into neurological function [47]. In addition, such a system could provide some measures of neurovascular coupling; the parameterisation of which may lead to greater insight in the rehabilitative process. It is also worth considering if perhaps a motor-rhythm EEG BCI may work better as a neurocortical prosthesis for these applications independent of any vascular response-oriented method. Only further research will answer this.

The work reported in this paper clearly represents only first steps towards extending CIMT to more severe motor stroke patients and the authors would be first to admit that there are very many questions unanswered which all merit further exploration. One obvious question from the technological point of view taken here is whether or not the haemodynamic signal required is as pronounced for sufferers of stroke. In the case of cortical haemorrhagic stroke, for example, the presence of scar tissue and haemotoma may absorb a significant portion of the introduced near infrared light attenuating the signal. Similarly constructed arguments may be made for ischemic stroke; however in all cases, the

severity of such effects if they occur at al,l clearly depends on the site and extent of the injury. One might envisage that initial fMRI scans during attempted movement would facilitate the deployment of the optode configurations required in such cases. To answer these concerns, clinical trials are required with appropriately selected stroke patients. An intriguing possibility for controlled studies is the monitoring of changes in the haemodynamic signals themselves along with motor movement efficacy. Additional quantitative measures such as those which might be provided through this method would surely prove useful in measuring rehabilitative outcome. The pioneers in this area have noted in a recent paper that NIRS monitoring may provide a technological breakthrough in terms of developing and understanding CIMT [9]. Techniques such as the one espoused here may make some contribution to the realisation of this suggestion. There are other concerns too. As mentioned during the background section, the neural prosthesis advocated here is not intended as a permanent replacement for the patient's own nervous system. It is envisaged that the device serve as a temporary channel to convey some feedback for stroke sufferers who have none. As soon as any other more conventional feedback is available, then the prosthesis may be discarded. This philosophy is suggested in response to suggestions that repetitive use of stereotyped brain signals metabolic in origin or otherwise could within this disease context produce unwanted plasticity phenomena such as tics, obsessive thoughts, and other aberrant neurological functioning [32].

5. SUMMARY

This paper has highlighted the possibility of enhancing the application of CIMT for stroke sufferers through the addition of a neuro-cortical prosthesis. Generally it is proposed that a fruitful avenue for new research in the application of brain computer interfaces is in their measurement of volitional motor effort for biofeedback purposes in CIMT. The intended target treatment group is severe stroke patients with little or no perceptible movement although the idea may have utility in the broader stroke population. More specifically NIRS-based BCI are proposed as suitable candidates for such purposes. A simplified illustration of such a system is presented which demonstrates the basic feasibility of the approach. Testing with actual stroke sufferers is clearly the next step and will in itself undoubtedly introduce a number of significant challenges. Nevertheless we believe the concept described in this paper has merit as a specific extension of brain computer interfaces into the neurorehabilitation domain.

ACKNOWLEDGMENTS

This work is supported by Science Foundation Ireland Grant no. SFI/05/RFP/ENG0089. The authors would like to acknowledge the contributions of Professor Barak P. Pearlmutter and Dr. Ray O'Neill in discussions concerning this work. Dr. Ward would also like to thank the reviewers and editors for their comments, advice, and suggestions during the reviewing process.

REFERENCES

[1] R. Adams, M. Victor, and A. Ropper, *Adam's & Victor's Principles of Neurology*, McGraw-Hill, New York, NY, USA, 6th edition, 1997.

[2] World Health Organization Global Report 2002, "World Health Organization," http://www.who.int/whr/2002/en/index.html, January 2007.

[3] The Internet Stroke Centre, http://www.strokecenter.org/pat/stats.htm, January 2007.

[4] R. W. Bohannon, "Muscle strength and muscle training after stroke," *Journal of Rehabilitation Medicine*, vol. 39, no. 1, pp. 14–20, 2007.

[5] E. Taub, N. E. Miller, T. A. Novack, et al., "Technique to improve chronic motor deficit after stroke," *Archives of Physical Medicine and Rehabilitation*, vol. 74, no. 4, pp. 347–354, 1993.

[6] E. Taub, G. Uswatte, and R. Pidikiti, "Constraint-induced movement therapy: a new family of techniques with broad application to physical rehabilitation—a clinical review," *Journal of Rehabilitation Research and Development*, vol. 36, no. 3, pp. 237–251, 1999.

[7] W. H. Miltner, H. Bauder, M. Sommer, C. Dettmers, and E. Taub, "Effects of constraint-induced movement therapy on patients with chronic motor deficits after stroke: a replication," *Stroke*, vol. 30, no. 3, pp. 586–592, 1999.

[8] J. Liepert, "Motor cortex excitability in stroke before and after constraint-induced movement therapy," *Cognitive and Behavioral Neurology*, vol. 19, no. 1, pp. 41–47, 2006.

[9] V. W. Mark, E. Taub, and D. M. Morris, "Neuroplasticity and constraint-induced movement therapy," *Europa Medicophysica*, vol. 42, no. 3, pp. 269–284, 2006.

[10] S. L. Wolf, C. J. Winstein, J. P. Miller, et al., "Effect of constraint-induced movement therapy on upper extremity function 3 to 9 months after stroke: the EXCITE randomized clinical trial," *Journal of the American Medical Association*, vol. 296, no. 17, pp. 2095–2104, 2006.

[11] V. W. Mark and E. Taub, "Constraint-induced movement therapy for chronic stroke hemiparesis and other disabilities," *Restorative Neurology and Neuroscience*, vol. 22, no. 3-4, pp. 317–336, 2004.

[12] P. S. Lum, C. G. Burgar, D. E. Kenney, and H. F. M. Van der Loos, "Quantification of force abnormalities during passive and active-assisted upper-limb reaching movements in post-stroke hemiparesis," *IEEE Transactions on Biomedical Engineering*, vol. 46, no. 6, pp. 652–662, 1999.

[13] J. H. van der Lee, R. C. Wagenaar, G. J. Lankhorst, T. W. Vogelaar, W. L. Devillé, and L. M. Bouter, "Forced use of the upper extremity in chronic stroke patients: results from a single-blind randomized clinical trial," *Stroke*, vol. 30, no. 11, pp. 2369–2375, 1999.

[14] J. Chae, F. Bethoux, T. Bohinc, L. Dobos, T. Davis, and A. Friedl, "Neuromuscular stimulation for upper extremity motor and functional recovery in acute hemiplegia," *Stroke*, vol. 29, no. 5, pp. 975–979, 1998.

[15] J. Powell, A. D. Pandyan, M. Granat, M. Cameron, and D. J. Stott, "Electrical stimulation of wrist extensors in poststroke hemiplegia," *Stroke*, vol. 30, no. 7, pp. 1384–1389, 1999.

[16] A. J. Butler and S. J. Page, "Mental practice with motor imagery: evidence for motor recovery and cortical reorganization after stroke," *Archives of Physical Medicine and Rehabilitation*, vol. 87, no. 12, supplement, pp. 2–11, 2006.

[17] S. Coyle, T. E. Ward, C. Markham, and G. McDarby, "On the suitability of near-infrared (NIR) systems for next-generation brain-computer interfaces," *Physiological Measurement*, vol. 25, no. 4, pp. 815–822, 2004.

[18] R. Sitaram, H. Zhang, C. Guan, et al., "Temporal classification of multichannel near-infrared spectroscopy signals of motor imagery for developing a brain-computer interface," *NeuroImage*, vol. 34, no. 4, pp. 1416–1427, 2007.

[19] S. Coyle, T. E. Ward, and C. Markham, "An optical brain computer interface," in *Proceedings of the 2nd International Brain-Computer Interface Workshop and Training Course*, vol. 49 of *Biomedizinische Technik*, pp. 45–46, Graz, Austria, 2004.

[20] J. W. Krakauer, "Motor learning: its relevance to stroke recovery and neurorehabilitation," *Current Opinion in Neurology*, vol. 19, no. 1, pp. 84–90, 2006.

[21] E. Taub and G. Uswatte, "Constraint-induced movement therapy: answers and questions after two decades of research," *NeuroRehabilitation*, vol. 21, no. 2, pp. 93–95, 2006.

[22] H. I. Krebs, N. Hogan, M. L. Aisen, and B. T. Volpe, "Robot-aided neuro-rehabilitation," *IEEE Transactions on Rehabilitation Engineering*, vol. 6, no. 1, pp. 75–87, 1998.

[23] E. J. Plautz, G. W. Milliken, and R. J. Nudo, "Effects of repetitive motor training on movement representations in adult squirrel monkeys: role of use versus learning," *Neurobiology of Learning and Memory*, vol. 74, no. 1, pp. 27–55, 2000.

[24] J. H. van der Lee, R. C. Wagenaar, G. J. Lankhorst, T. W. Vogelaar, W. L. Devillé, and L. M. Bouter, "Forced use of the upper extremity in chronic stroke patients: results from a single-blind randomized clinical trial," *Stroke*, vol. 30, no. 11, pp. 2369–2375, 1999.

[25] B. T. Volpe, H. I. Krebs, N. Hogan, L. Edelsteinn, C. M. Diels, and M. L. Aisen, "Robot training enhanced motor outcome in patients with stroke maintained over 3 years," *Neurology*, vol. 53, no. 8, pp. 1874–1876, 1999.

[26] M. Ferraro, J. J. Palazzolo, J. Krol, H. I. Krebs, N. Hogan, and B. T. Volpe, "Robot-aided sensorimotor arm training improves outcome in patients with chronic stroke," *Neurology*, vol. 61, no. 11, pp. 1604–1607, 2003.

[27] R. Colombo, F. Pisano, S. Micera, et al., "Robotic techniques for upper limb evaluation and rehabilitation of stroke patients," *IEEE Transactions on Neural Systems and Rehabilitation Engineering*, vol. 13, no. 3, pp. 311–324, 2005.

[28] B. T. Volpe, M. Ferraro, D. Lynch, et al., "Robotics and other devices in the treatment of patients recovering from stroke," *Current Neurology and Neuroscience Reports*, vol. 5, no. 6, pp. 465–470, 2005.

[29] M. J. Johnson, "Recent trends in robot-assisted therapy environments to improve real-life functional performance after stroke," *Journal of NeuroEngineering and Rehabilitation*, vol. 3, no. 1, p. 29, 2006.

[30] L. Dipietro, M. Ferraro, J. J. Palazzolo, H. I. Krebs, B. T. Volpe, and N. Hogan, "Customized interactive robotic treatment for stroke: EMG-triggered therapy," *IEEE Transactions on Neural Systems and Rehabilitation Engineering*, vol. 13, no. 3, pp. 325–334, 2005.

[31] A. Kübler, V. K. Mushahwar, L. R. Hochberg, and J. P. Donoghue, "BCI meeting 2005-workshop on clinical issues and applications," *IEEE Transactions on Neural Systems and Rehabilitation Engineering*, vol. 14, no. 2, pp. 131–134, 2006.

[32] B. H. Dobkin, "Brain-computer interface technology as a tool to augment plasticity and outcomes for neurological rehabilitation," *The Journal of Physiology*, vol. 579, no. 3, pp. 637–642, 2007.

[33] G. Pfurtscheller, G. R. Müller, J. Pfurtscheller, H. J. Gerner, and R. Rupp, "'Thought'—control of functional electrical stimulation to restore hand grasp in a patient with tetraplegia," *Neuroscience Letters*, vol. 351, no. 1, pp. 33–36, 2003.

[34] A. Buttfield, P. W. Ferrez, and J. D. R. Millán, "Towards a robust BCI: error potentials and online learning," *IEEE Transactions on Neural Systems and Rehabilitation Engineering*, vol. 14, no. 2, pp. 164–168, 2006.

[35] Y. Wang, R. Wang, X. Gao, B. Hong, and S. Gao, "A practical VEP-based brain-computer interface," *IEEE Transactions on Neural Systems and Rehabilitation Engineering*, vol. 14, no. 2, pp. 234–240, 2006.

[36] D. J. McFarland, D. J. Krusienski, and J. R. Wolpaw, "Brain-computer interface signal processing at the Wadsworth Center: mu and sensorimotor beta rhythms," *Progress in Brain Research*, vol. 159, pp. 411–419, 2006.

[37] E. W. Sellers, D. J. Krusienski, D. J. McFarland, T. M. Vaughan, and J. R. Wolpaw, "A P300 event-related potential brain-computer interface (BCI): the effects of matrix size and inter stimulus interval on performance," *Biological Psychology*, vol. 73, no. 3, pp. 242–252, 2006.

[38] C. Vidaurre, A. Schlögl, R. Cabeza, R. Scherer, and G. Pfurtscheller, "A fully on-line adaptive BCI," *IEEE Transactions on Biomedical Engineering*, vol. 53, no. 6, pp. 1214–1219, 2006.

[39] N. Birbaumer and L. G. Cohen, "Brain-computer interfaces: communication and restoration of movement in paralysis," *The Journal of Physiology*, vol. 579, no. 3, pp. 621–636, 2007.

[40] F. Hummel, P. Celnik, P. Giraux, et al., "Effects of non-invasive cortical stimulation on skilled motor function in chronic stroke," *Brain*, vol. 128, no. 3, pp. 490–499, 2005.

[41] P. Rolfe, "In vivo near-infrared spectroscopy," *Annual Review of Biomedical Engineering*, vol. 2, pp. 715–754, 2000.

[42] S. Coyle, *Near-infrared spectroscopy for brain computer interfacing*, Ph.D. thesis, National University of Ireland, Maynooth, Ireland, 2005.

[43] M. Cope and D. T. Delpy, "System for long-term measurement of cerebral blood and tissue oxygenation on newborn infants by near infra-red transillumination," *Medical and Biological Engineering and Computing*, vol. 26, no. 3, pp. 289–294, 1988.

[44] R. C. Oldfield, "The assessment and analysis of handedness: the Edinburgh inventory," *Neuropsychologia*, vol. 9, no. 1, pp. 97–113, 1971.

[45] S. Coyle, C. Markham, W. Lanigan, and T. Ward, "A mechanical mounting system for functional near-infrared spectroscopy brain imaging studies," in *Opto-Ireland 2005: Optical Sensing and Spectroscopy*, vol. 5826 of *Proceedings of SPIE*, pp. 618–627, Dublin, Ireland, April 2005.

[46] HomER, http://www.nmr.mgh.harvard.edu/PMI/resources/homer/home.htm.

[47] F. Babiloni, D. Mattia, C. Babiloni, et al., "Multimodal integration of EEG, MEG and fMRI data for the solution of the neuroimage puzzle," *Magnetic Resonance Imaging*, vol. 22, no. 10, pp. 1471–1476, 2004.

Hindawi Publishing Corporation
Computational Intelligence and Neuroscience
Volume 2007, Article ID 84386, 8 pages
doi:10.1155/2007/84386

Research Article

Towards Development of a 3-State Self-Paced Brain-Computer Interface

Ali Bashashati,[1,2,3] Rabab K. Ward,[1,4] and Gary E. Birch[1,3,4]

[1] *Electrical and Computer Engineering Department, University of British Columbia, Vancouver, BC, Canada V6T 1Z4*
[2] *Terry Fox Laboratory, British Columbia Cancer Research Center, Vancouver, BC, Canada V5Z 1L3*
[3] *Brain Interface Laboratory, Neil Squire Society, Suite 220, 2250 Boundary Road, Burnaby, BC, Canada V5M 3Z3*
[4] *Institute for Computing, Information & Cognitive Systems, Vancouver, BC, Canada V6T 1Z4*

Correspondence should be addressed to Ali Bashashati, alibs@ece.ubc.ca

Received 15 February 2007; Accepted 22 August 2007

Recommended by Andrzej Cichocki

Most existing brain-computer interfaces (BCIs) detect specific mental activity in a so-called synchronous paradigm. Unlike synchronous systems which are operational at specific system-defined periods, self-paced (asynchronous) interfaces have the advantage of being operational at all times. The low-frequency asynchronous switch design (LF-ASD) is a 2-state self-paced BCI that detects the presence of a specific finger movement in the ongoing EEG. Recent evaluations of the 2-state LF-ASD show an average true positive rate of 41% at the fixed false positive rate of 1%. This paper proposes two designs for a 3-state self-paced BCI that is capable of handling idle brain state. The two proposed designs aim at detecting right- and left-hand extensions from the ongoing EEG. They are formed of two consecutive detectors. The first detects the presence of a right- or a left-hand movement and the second classifies the detected movement as a right or a left one. In an offline analysis of the EEG data collected from four able-bodied individuals, the 3-state brain-computer interface shows a comparable performance with a 2-state system and significant performance improvement if used as a 2-state BCI, that is, in detecting the presence of a right- or a left-hand movement (regardless of the type of movement). It has an average true positive rate of 37.5% and 42.8% (at false positives rate of 1%) in detecting right- and left-hand extensions, respectively, in the context of a 3-state self-paced BCI and average detection rate of 58.1% (at false positive rate of 1%) in the context of a 2-state self-paced BCI.

1. INTRODUCTION

Brain-computer interface (BCI) systems form a possible alternative communication and control solutions for individuals with severe disabilities. For a review of the field, see [1–3]. In BCI systems, the user's cortical activity associated with an intentional control of a device (such as attempted finger movements) is directly mapped to an application-specific control signal. This allows the user to control various devices such as a neural prosthetic by cognitive processes only, that is, by bypassing traditional interface pathways (which cannot be used by individuals with severe disabilities).

In developing noninvasive BCI systems, the majority of research has concentrated on developing synchronous systems. These systems are only operational at specific periods. Asynchronous (self-paced) systems, on the other hand, have the advantage of being operational at all times. The 2-state low frequency-asynchronous switch design (LF-ASD) was the first BCI introduced for self-paced or asynchronous control applications [4]. LF-ASD seeks to recognize the movement related potentials (MRPs) of a *finger-flexion movement* in the EEG signal. In a self-paced brain-computer interface the users affect the BCI transducer output whenever they want by intentionally changing their brain states. Between periods of intentional control (IC), users are said to be in a no-control (NC) state; they may be idle, daydreaming, thinking about a problem or lunch, or performing any other action other than trying to control the BCI transducer. These BCI transducers are thus designed to respond only when there is an intentional user control. The appropriate BCI response to no-control (NC) would be a neutral or inactive output. We refer to this ability as NC support. NC support is necessary for most types of machine or device interactions where

frequent intentional controls (IC) are spaced by periods of inaction.

Like LF-ASD, the 2-state BCI systems tested in [5–7] attempt to detect an intentional control state from the ongoing brain signal in a self-paced manner. The 3-state self-paced BCI implemented in [8] attempts to differentiate between right-hand, left-hand, and foot movements to operate a virtual keyboard. However, this BCI requires the subject to constantly engage in control without the option of going to the no control (NC) state. In a recent work, Scherer et al. [9] has proposed a 4-state self-paced BCI that has mean true positive and false positive rates of 28.4% and 16.9%. In the study of [10] the subjects were asked to perform one of the following three actions: (1) imagine right-hand movement, (2) imagine left-hand movement, and (3) relax. A 3-state self-paced BCI was designed to navigate a mobile robot in an 80 cm∗60 cm house-like environment by differentiating amongst these three states. The system generates "unknown state output" when there is not enough confidence in choosing one of the three above-mentioned mental tasks. The classifier of this system was not explicitly trained to recognize idle (NC) state [10]. According to the authors, it could process them adequately by responding "unknown". It was also reported that the task of steering the robot between rooms was so engaging that the two tested subjects preferred to emit continuously mental commands rather than to go through idle state. Therefore, the response of this system on NC (idle) state was evaluated on a dataset with limited amount of idle-state. Moreover, having the choice of "unknown state output" may represent some neutral output but it is not clear whether the unknown state output was caused by the actual idle (NC) state or by lack of confidence in detecting one of the three commands. Additionally, there is no evidence that the NC state will fall into the unknown state in these designs.

In this paper, a noninvasive 3-state self-paced BCI system is proposed. This system is a 3-state self-paced BCI that is (a) designed specifically to support the NC state EEG signal, and (b) has a higher true positive rate at a considerably lower false positive rate (FP=1%) compared to existing 3-state and 4-state self-paced BCIs that support the NC state [9]. It should, however, be mentioned that it is difficult to directly compare the results of our study with other BCI studies because (a) the recording equipment, recording and classification protocols, and mental tasks considered are different, (b) the amount of data involved and the degree of training the subjects received before and during participation in the BCI experiments varies for different studies, and (c) there is not a unified framework of reporting performance of BCI systems, that is, the performance metrics are different across different studies.

Unlike the 2-state self-paced system which detects the presence of a single movement from the ongoing EEG signal, the 3-state self-paced BCI design aims at detecting two different movements. Figure 1 shows examples of outputs of the 2-state and 3-state self-paced BCIs. Overall, a 2-state self-paced BCI is in an inactive state (NC state) for most of the time and is in an IC state when a specific brain state (e.g., finger-flexion movement) is detected in the brain signal. Unlike a 2-state self-paced BCI which has only one active (IC) state, a 3-state self-paced BCI has two active state outputs, IC1 and IC2, which are activated by two different brain states (e.g., right- and left-hand extensions). While a 2-state self-paced BCI can provide the user with the option of executing only one command (e.g., turn right), a 3-state system gives the user two command options (e.g., turn right or turn left). This has the advantage of giving the user more control options.

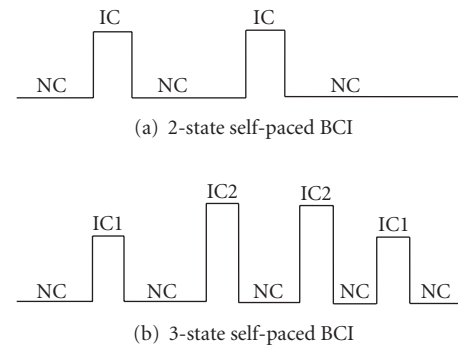

(a) 2-state self-paced BCI

(b) 3-state self-paced BCI

Figure 1: Samples of outputs of 2-state and 3-state self-paced BCIs, where NC = no-control state, IC = intended control state.

The 2-state self-paced BCI (LF-ASD) in [4] aimed at detecting attempted right finger flexions. Recent studies with the 2-state LF-ASD have demonstrated that this system correctly detects the presence of a movement (true positive (TP) rate) in 41% and 42% of the cases for able-bodied and spinal-cord-injured subjects, respectively [11]. This is when the parameters were set so that the false positive rate is fixed at 1%. The TP rate of the system improves at higher FP rates, for example, at an FP rate of 5%, the TP rate is almost 100%. Despite these encouraging results, our experience indicates that even a 1% false positive rate is too high for most practical self-paced control applications.

This paper reports on the preliminary results of a pilot study that investigates the feasibility of a 3-state "self-paced" brain-computer interface system whose aim is the detection of right- and left-hand extension movements in a self-paced manner. This system has the ability to handle the no-control (NC) state as well as two additional control options for the user.

Two consecutive detectors were designed to detect the presence of the left- or the right-hand extensions from the ongoing EEG. The first detector, DET1, determines whether or not a movement is present. If such a movement is detected then the second detector, DET2, classifies the movement as a right- or a left-hand extension.

Two designs of a 3-state self-paced BCI are proposed and implemented. Power spectral density and a specific template matching method [4] are used in the feature extraction stages, and the k-nearest neighbour and linear discriminant analysis (LDA) classifiers are used in the classification stages.

The performances of the designs are evaluated using EEG recordings of right- and left-hand extension movements of four able-bodied individuals. The goals of this paper are twofold.

(1) To perform an initial investigation of the performance of the system as a 2-state self-paced BCI, that is, detecting whether a left- or a right-hand movement (regardless of the type of movement) has occurred. If the performance of the system in detecting any such movement is better than detecting the previously used movement (i.e., the right-finger flexion), then such these movements can be used in other 2-state self-paced brain-computer interface designs.

(2) To introduce and carry out an initial evaluation of two possible designs of a 3-state self-paced BCI and to investigate whether a 3-state self-paced brain-computer interface that supports the no-control (NC) state has promise.

In Sections 2–4 of this paper, details of experiments, the structure of the proposed designs and the evaluation method are explained. The results, discussions, and conclusions are presented in Sections 5–7, respectively.

2. EXPERIMENTS

2.1. Selection of movement tasks

A 3-state self-paced BCI has two active state outputs, IC1 and IC2, which should be activated by two different movements (as neurophysiologic sources of control). However, selection of these movements is not a trivial task and one needs to find the movements that generate more differentiable patterns in the EEG. More differentiable patterns would make it easier for a BCI system to detect IC states and may yield improvements in the performance of the system.

Many studies by the neurophysiologic research community have explored the effects of different movements on the EEG signal. These studies show that movements that involve more parts of the body (e.g., hand movement) or movements that need more effort (e.g., finger extension) generate more differentiable patterns in the ongoing EEG signal than for example natural finger flexions [12–14]. It has also been reported that right and left movements (regardless of the type of movement) generate patterns in different locations of the brain [15]. As our aim is to use movements that generate more differentiable patterns, based on the evidence in [12–15], we choose the right-hand and the left-hand extensions in this study since (a) hand movements involve more parts of the body than, for example, finger movements, (b) extension movements need more effort to execute compared to flexion movements, and (c) right and left movements generate movement-specific patterns in different locations of the brain. We speculate that these two movements generate more discriminative patterns than a finger flexion does. If that is the case, then using these movements would improve our BCI's performance in detecting the presence of a movement. To our best knowledge, the right- and the left-hand extension movements have not yet been studied in the context of BCI systems.

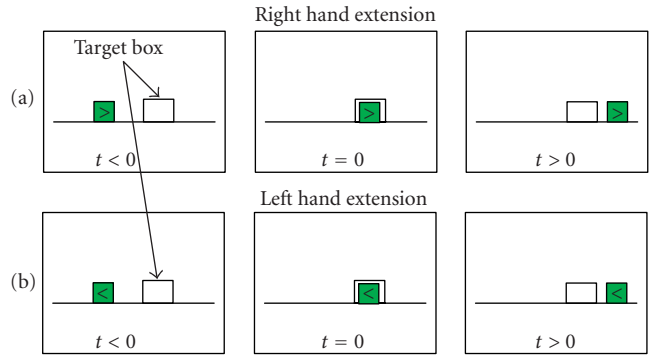

Figure 2: Screen contents for each of the right-hand (a) and left-hand (b) extension movement trials, $t = 0$ is the time of movement execution.

2.2. Experimental paradigm

The EEG data used in this study were recorded from 15 monopolar electrodes positioned over the supplementary motor area and the primary motor cortex (defined with reference to the International 10–20 System at F1, F2, F3, F4, Fz, FC1, FC2, FC3, FC4, FCz, C1, C2, C3, C4, and Cz). Electrooculographic (EOG) activity was measured as the potential difference between two electrodes, placed at the corner and below the right eye. The ocular artifact was considered present when the difference between the EOG electrodes exceeded $+/-25\,\mu$v, a threshold level similar to the one used in previous studies [3, 15]. All signals were sampled at 128 Hz. This study has been approved by the Behavioural Research Ethics Board (BREB) of the University of British Columbia.

Four able-bodied subjects participated in this study. All subjects were male (except subject 4), right-handed (except subject 4), 25–30 years old, and only subject 2 had prior BCI experience. Subjects were seated 150 cm in front of a computer monitor. The data were collected while the subjects were performing a cue-based (synchronized) task. At random intervals of 5.6–7 seconds (mean of 6.7 seconds), a target window was displayed on the subject's monitor. As shown in Figure 2, a box moved from the left side to the right side of the screen. When the box reached the target window, the subject attempted to activate the custom-made switch by extending his/her right- or left-hand. An arrow in the moving box, pointing to the left or the right showed the subject whether to move the right- or the left-hand. For each subject, an average of 150 trials for each movement was collected in two sessions carried in the same day.

3. PROPOSED 3-STATE SELF-PACED BRAIN COMPUTER INTERFACE

Figure 3 shows the overall structure of the proposed designs. These designs include two major blocks:

(a) *"Detector 1"* which determines whether or not a movement is performed, and

(b) *"Detector 2"* which determines whether the detected movement is a right-hand or a left-hand extension.

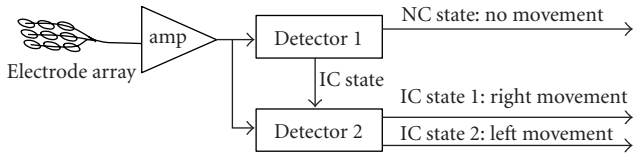

Figure 3: Structure of the 3-state self-paced brain-computer interface design.

In this study, two different designs for Detector 1 and one design for Detector 2 have been proposed and evaluated. The details of both detectors are explained below. Detectors 1 and 2 are referred to as DET1 and DET2.

3.1. Detector 1

Two different designs for DET1 are proposed and compared. These are referred to as DET1-LF-1NN and DET1-PSD-LDA.

DET1-LF-NN uses one of the latest designs of the LF-ASD [14] as shown in Figure 4(a). It employs features extracted from the 0–4 Hz band in six bipolar EEG channels (defined with reference to the International 10–20 System at F1-FC1, Fz-FCz, F2-FC2, FC1-C1, FCz-Cz, and FC2-C2). After amplification, a lowpass FIR filter (0–4 Hz) is used to decrease the interference with the features in the high-frequency band.

Previous studies show that when a movement is performed, a bipolar pattern similar to the one shown in Figure 5 is generated in the ongoing EEG [4]. A specific template matching algorithm based on the one employed in [4] is implemented. This algorithm generates large feature values when there is such a pattern in the spontaneous EEG. The delay parameters α_i and α_j, shown in Figure 5, determine the locations of the peaks of the pattern that need to be detected. Thus, these delay parameters need to be properly determined in order to detect the presence of a specific movement. For each subject, the ensemble averages of the EEG around the movements of the training data are generated and then used to determine the values of α_i and α_j according to the method presented in [16]. Table 1 shows the mean values of α_i and α_j across all five runs (refer to Section 4) that are estimated from the ensemble averages of the training data of each run. This feature extraction procedure is repeated for each of the six bipolar channels. The resulting feature vector is a six-dimensional vector, with each dimension reflecting the value of the feature in each channel. While we used the same α_i and α_j parameter values for all the six channels because the evidence in [16] suggests that they are not significantly different, we have also checked the ensemble averages of all the six channels to make sure that this assumption is valid in this study.

The Karhunen-Loève transform (KLT) component is used to reduce the 6-dimensional feature vector to a 2-dimensional feature vector. A 1-NN (1-nearest neighbour) classifier is used as the feature classifier. Finally, a moving average (with length of 39 milliseconds) and a debounce block (with length of 125 milliseconds) are employed to further improve the classification accuracy of DET1 by reducing the number of false activations (for details, see [4, 17]). DET1 classifies the input patterns, at every 1/16th of a second, to one of the two classes, no-control (NC) or intentional-control (IC) states.

Table 1: Estimated mean values of α_i and α_j parameters for each subject. Note all values are in milliseconds.

	Subject 1	Subject 2	Subject 3	Subject 4
α_i	125	195	398	195
α_j	578	141	297	313

The second design of DET1 (referred to as DET1-PSD-LDA) is shown in Figure 4(b). It extracts the power spectral density features of the EEG from a group of bipolar EEG channels and then selects the most informative channels for classification. Specifically, thirty bipolar combinations of EEG channels that may contribute to the detection of movements were generated. These bipolar EEG channels were Cz-C1, Cz-C2, Cz-C3, Cz-C4, C1-C2, C1-C4, C1-C3, C2-C3, C2-C4, C3-C4, FCz-Cz, FC1-C1, FC2-C2, FC3-C3, FC4-C4, Fz-FCz, F1-FC1, F2-FC2, F3-FC3, F4-FC4, FCz-FC1, FCz-FC2, FCz-FC3, FCz-FC4, FC1-FC2, FC1-FC4, FC1-FC3, FC2-FC3, FC2-FC4, FC3-FC4. These bipolar channels were chosen to capture possible discriminatory information between left and right and also between frontal and central areas of the head. In the feature extraction block, the power spectral density (PSD) components of each of the 30 bipolar EEG channels are calculated in each frequency bin from 1 Hz to 25 Hz using Welch's Periodogram method [18] with window length of one second (equivalent to 128 samples). This results in 25 frequency components for each of the 30 bipolar channels and a total of $25*30$ features at each time instant. We then use stepwise linear discriminant analysis (stepwise LDA) [19] to find the most informative features that better discriminant between IC and NC classes. Stepwise LDA is a method that results in a linear combination of selected features that contribute to the classification and omits the features that have redundant information for discrimination. Once the features are extracted and selected, a linear discriminant classifier (LDA) [19] is used for classification. Other details about the other components of the feature translator (moving average and debounce blocks) are the same as in DET1-LF-1NN above.

3.2. Detector 2

Existing studies show that the cortical activation, related to movement preparation and execution, desynchronizes the alpha (8–12 Hz) rhythm and increases the beta (13–25 Hz) rhythm of the EEG. These phenomena are known as event-related desynchronization (ERD) and event-related synchronization (ERS), respectively [15, 20]. The ERD of a hand movement is more prominent over contralateral sensorimotor areas during motor preparation and extends bilaterally after movement initiation [15, 21]. Some studies, however, show that the frequency bands of the ERD and ERS patterns are variable from subject to subject [22].

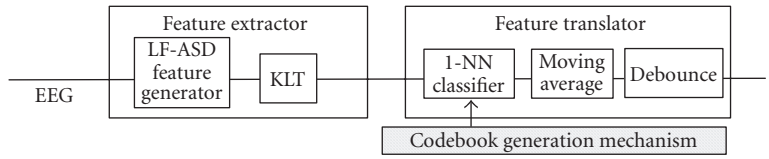

(a) DET1-LF-1NN

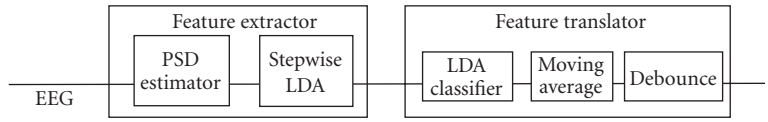

(b) DET1-PSD-LDA

Figure 4: Structure of the two designs of DET1, where KLT = Karhunen-Loève transform, and 1-NN = 1-nearest neighbour, PSD = power spectral density, and LDA: linear discriminant analysis.

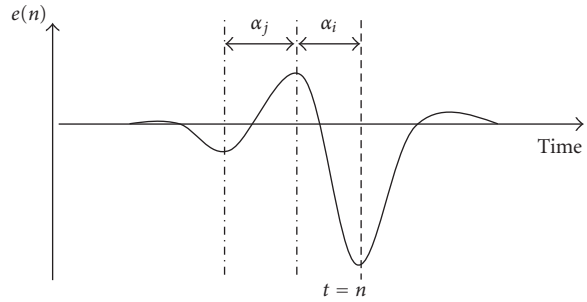

Figure 5: Description of delay terms (α_i, α_j), where $e(n)$ is the amplitude of the bipolar signal.

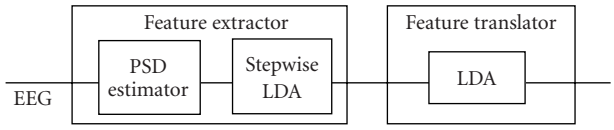

Figure 6: Structure of DET2-PSD-LDA, where PSD = power spectral density, and LDA = linear discriminant analysis.

As shown in Figure 6, DET2 which aims at differentiating between right- and left-hand movements is similar to the second design of DET1 (DET1-PSD-LDA), except that it does not have the averaging and debounce blocks of DET1. This design intends to extract subject specific ERD/ERS frequency bands that lead to more discrimination between the two classes, that is, the left- and right-hand movements. As in DET1, the stepwise linear discriminant analysis (LDA) method is employed to select the subject specific ERD/ERS frequency bands and bipolar EEG channels. We have evaluated a similar design of DET2 when the inputs were monopolar EEG channels. Preliminary analysis of the data shows that using bipolar electrodes yields better performances. As such, we used bipolar electrodes as input to the system and did not further evaluate the overall performance of the 3-state brain-computer interface using monopolar electrodes.

Two designs of a 3-state self-paced BCI system are evaluated. The first design uses the combination of DET1-LF-1NN and DET2-PSD-LDA and the second one uses the combination of DET1-PSD-LDA followed by DET2-PSD-LDA.

4. EVALUATION

The designed 3-state self-paced BCI first detects whether or not a movement is performed. If a movement is detected, then the system classifies it as one of two classes, the right-hand (IC1) or the left-hand (IC2) extension classes. If the system does not detect a movement, the output reports an inactive state.

We use 80% randomly chosen trials (about 120 trials) to train the 3-state self-paced BCI system and use the remaining data to evaluate the performance of the system. We repeat this procedure five times and report the mean performance of the system. The ability of the subjects to control the 3-state BCI system is evaluated using three performance measures. At a fixed false positive rate, these measures report the correct detection rates of the right- and the left-hand extensions (from the ongoing EEG), respectively. These three measures are as follows.

(1) The percentage of correct right-hand movement detection during IC states (i.e., the true positive rate for right-hand movement, TP_R) calculated using (1) below:

$$TP_R = \frac{\text{number of correctly detected right movements}}{\text{total number of right movements}}. \quad (1)$$

(2) The percentage of correct left-hand movement detection during IC states (true positives of left-hand movements, TP_L) calculated using (2) below:

$$TP_L = \frac{\text{number of correctly detected left movements}}{\text{total number of left movements}}. \quad (2)$$

(3) The percentage of false switch activations during NC states (false positives, FPs) calculated using (3) below:

$$FP = \frac{\text{number of false activations}}{\text{total number of the system's decisions during NC state}}. \quad (3)$$

Table 2: Mean percentages of true positives (TP_{IC}) at fixed false positive rate of 1% for the two designs of DET1.

DET1 Design	Subject 1	Subject 2	Subject 3	Subject 4	Average
DET1-LF-1NN	50.1	38.4	56.5	71.0	54.0
DET1-PSD-LDA	38.2	54.7	60.2	60.3	53.4

Note that the system make a decision every 1/16th of a second.

A TP is identified if the BCI system is activated at least once in a response window, that is, a time window spanning 0.25 seconds before the time of movement till 0.5 seconds after it, a method similar to that employed in [4, 5, 7, 23, 24]. FPs are assessed in the periods outside the response window as explained above. Periods during which ocular artifacts occurred are blocked from analysis.

We also report the overall true positive and false positive rates of DET1 (regardless of the type of movement). We refer to these measures as TP_{IC} and FP_{IC}. The TP_{IC} is the percentage of correct detection of a movement whether it is a right-hand or a left-hand one. Thus it reflects the performance of the system if used as a 2-state self-paced BCI. We report this measure to compare the findings of this study with our latest 2-state self-paced BCI as stated in goal (1) of this study.

5. RESULTS

The mean performance of DET1 (TP_{IC}) in detecting the presence of hand movements, regardless of the type of movement, from the background EEG is shown in Table 2. This table shows the TP rates at a fixed FP rate of 1% for the two designs of DET1. As we are interested in low false positive rates, we do not report the performance of the system for higher false positive rates. For higher false positive rates (e.g., FP > 3%) the true positive rate is almost 100%. As shown in the last column of Table 2, the mean performance of DET1-LF-1NN is slightly better than DET1-PSD-LDA. For subject 2, the mean true positive rate of DET1-PSD-LDA is more than 15% higher than that of DET1-PSD-1NN with significance level of $P < .03$ using "paired t-test". For subject 3, however, the differences between the performances of DET1-PSD-LDA and DET1-PSD-1NN are not significant at the significance level of 0.05. In the rest of the two subjects, the mean true positive rates of DET1-LF-1NN outperform DET1-PSD-LDA by more than 10% with significance levels of $P < .02$ through the use of "paired t-test".

Table 3 shows the mean performance of the whole 3-state self-paced BCI for the two proposed designs (i.e., <DET1-LF-1NN + DET2-PSD-LDA> and <DET1-PSD-LDA + DET2-PSD-LDA>) at a fixed false positive rate of 1%.

On average, 36% of the right- and left-hand extensions of the 4 subjects are correctly identified by the 3-state <DET1-LF-1NN + DET2-PSD-LDA> design (for a false positive rate of 1%). As shown in Table 3, <DET1-LF-1NN + DET2-PSD-LDA> outperforms <DET1-PSD-LDA + DET2-PSD-LDA> in three of the tested subjects.[1]

Table 4 shows the best performing 3-state self-paced BCI design for each individual subject. As the last column of Table 4 shows, the average performance of the 3-state system achieves an overall true positive rate of 40.1% (at false positive rate of 1%). If used as a 2-state BCI its average true positive is 58.1%.

6. DISCUSSION

The proposed 3-state self-paced BCI was specifically designed to support NC state. This system was tested in a specific experimental paradigm and on NC state data that were supposed to be the most difficult one as they were surrounded by IC state data. However, a more thorough study is needed to investigate the performance of the system under different experimental paradigms and on different sets of NC state data, for example, when the person perform different mental tasks except for the IC task. This study would provide a better estimate of the performance of a self-paced BCI system in a real-world application.

The performance of DET1-LF-1NN and DET1-PSD-LDA in detecting the presence of a movement (regardless of its type) yielded average true positive rates of 54% and 53.4% at false positive (FP) rate of 1%, respectively. In the meantime, as shown in the third column of Table 4, the average TP_{IC} rate for the best performing design across the subjects was 58.1% at false positive rate of 1%. In other words, if the current system was used as a 2-state self-paced BCI, the true positive rate would be 58.1% at false positive of 1%. In comparison, the results of the latest 2-state self-paced BCI [11] for four able-bodied subjects yielded an average true positive rate of 41% at the same false positive rate of 1%. Thus, when used as a 2-state system the proposed BCI performs significantly better than the 2-state self-paced BCI system in [11]. It should be noted that while this 2-state self-paced brain computer interface detects finger flexions [11], DET1 of the 3-state self-paced BCI detects the presence of a left- or a right-hand extension movement. This improvement should be the result of using hand extension movements instead of a finger flexion one. It should be noted however that direct comparison of the current system with [11] is not completely accurate as the data and experimental paradigms used in testing the two systems were different; a more thorough study is needed to verify these findings. Verifying these results on a very large subject pool would eventually provide a better neurophysiological source for controlling current 2-state self-paced BCIs.

As shown in Table 2, the overall performance of the 3-state BCI varies across the subjects and depends on the type of the design used. Such performance variability across different designs and subjects has also been observed in other

[1] Note that <DET1-LF-1NN + DET2-PSD-LDA> indicates a design of a 3-state BCI that uses DET1-LF-1NN design for DET1 and DET2-PSD-LDA design for DET2. A similar description applies to <DET1-PSD-1NN + DET2-PSD-LDA> design as well.

Table 3: Mean percentages of right and left true positives (TP_R and TP_L) of the two proposed 3-state brain-computer interfaces (when false positive rate is set at 1%). The TP_R and TP_L value of the best design combination for each subject is highlighted.

3-state BCI Design structure	Subject 1		Subject 2		Subject 3		Subject 4		Average
	TP_R	TP_L	TP_R	TP_L	TP_R	TP_L	TP_R	TP_L	
<DET1-LF-1NN + DET2-PSD-LDA>[1]	**30.6**	**32.6**	16.1	33.4	**30.5**	**36.7**	**53.3**	**54.7**	36.0
<DET1-PSD-LDA + DET2-PSD-LDA>	19.5	22.2	**35.6**	**47.0**	30.1	34.3	37.4	45.2	33.9

Table 4: Best design combination for each subject together with the performances of the 2-state and 3-state systems (at false positive of 1%), where A = <DET1-LF-1NN + DET2-PSD-LDA> and B = <DET1-PSD-LDA + DET2-PSD-LDA>.

Subject	Best design	2-state BCI	3-state BCI		
		TP_{IC}	TP_R	TP_L	Average TP ($TP_{3\text{-state}}$)
Subject 1	A	50.1	30.6	32.6	31.6
Subject 2	B	54.7	35.6	47	41.3
Subject 3	A	60.2	30.5	36.7	33.6
Subject 4	A	71.0	53.3	54.7	54
Average	—	58.1	37.5	42.8	40.1

BCI systems (e.g., [24, 25]). Given the variable performance of subjects across the two designs, an approach that can select a suitable design and adapt to each subject is expected to achieve better detection rates. Significant gains may also be achieved from the combination of several single designs if these designs provide complementary information for the classification task. Several studies have demonstrated some evidence of existing independent features related to movement tasks that could be used to achieve better classification accuracies [26–28].

Subject 4 yielded the best right and left true positive rates (TP_R and TP_L) of 53.3% and 54.7% at false positive rate of 1%, respectively. Although DET1's true positive rate in detecting the presence of a movement (TP_{IC}) for subject 3 was the second best, overall the system has poor performance in differentiation between right and left movements. The following reasons might have caused the poor performance related to this subject.

(a) This subject did not generate significantly differentiable ERD/ERS patterns for the left- and right-hand movements. Many factors such as task complexity, effort and attention during the task can also contribute to the quality of the ERD/ERS patterns [15]. Other studies such as [29] have reported some subjects who poorly performed (classification rates of close to chance) compared to the rest of the subjects.

(b) In the experimental paradigm used in this study, no feedback during the performed tasks was provided to the subjects. While we adopted this paradigm to simulate a more natural mode of control, this may have caused a lower performance in some subjects.

(c) No subject prescreening and prior training was performed before the sessions.

Previous findings [17, 30] show that spinal-cord-injured (SCI) subjects can operate a self-paced BCI with almost the same results as able-bodied subjects. Thus, able-bodied subjects using a real movement are good predictors of the controllability of our proposed BCI system by SCI subjects using an attempted movement. It should be noted, however, that the findings of this study should be confirmed on our target population (i.e., individuals with motor disabilities) in future studies.

7. CONCLUSION

This study introduced and evaluated two designs of a 3-state self-paced brain-computer interface based on movement related potentials. This 3-state self-paced brain-computer interface is the first of its kind in its capability in (1) supporting the NC state, and (2) generating low false positive rates. While the true positive rate of the latest 2-state self-paced BCI is 41% (at FP = 1%) [11], the best average true positive rate of the proposed 3-state system is 40.1% (at FP = 1%). These results show that the 3-state system performs almost the same as the latest 2-state self-paced BCI [11] with the advantage of providing more control options than a 2-state system.

This preliminary study was performed to examine the feasibility of a 3-state "self-paced" brain-computer interface design. Although the results are promising, more improvements are needed in both of its components, that for detecting a movement and that for differentiating between two movements. The true positive rate of the system is reported at a false positive rate of 1%. Even a false positive rate of 1% is still not suitable for real-world applications as it corresponds to an average of one false activation every six seconds and may cause excessive user frustration. Use of more efficient feature extraction and classification methods, subject training, providing online feedback during the performed task, and verifying the results on a large number of subjects are in the scope of our future directions to improve these results.

REFERENCES

[1] S. G. Mason, A. Bashashati, M. Fatourechi, K. F. Navarro, and G. E. Birch, "A comprehensive survey of brain interface technology designs," *Annals of Biomedical Engineering*, vol. 35, no. 2, pp. 137–169, 2007.

[2] J. R. Wolpaw, "Brain-computer interfaces (BCIs) for communication and control: a mini-review," *Supplements to Clinical Neurophysiology*, vol. 57, pp. 607–613, 2004.

[3] A. Bashashati, M. Fatourechi, R. K. Ward, and G. E. Birch, "A survey of signal processing algorithms in brain-computer interfaces based on electrical brain signals," *Journal of Neural Engineering*, vol. 4, no. 2, pp. R32–R57, 2007.

[4] S. G. Mason and G. E. Birch, "A brain-controlled switch for asynchronous control applications," *IEEE Transactions on Biomedical Engineering*, vol. 47, no. 10, pp. 1297–1307, 2000.

[5] E. Yom-Tov and G. F. Inbar, "Detection of movement-related potentials from the electro-encephalogram for possible use in a brain-computer interface," *Medical and Biological Engineering and Computing*, vol. 41, no. 1, pp. 85–93, 2003.

[6] S. P. Levine, J. E. Huggins, S. L. BeMent, et al., "A direct brain interface based on event-related potentials," *IEEE Transactions on Rehabilitation Engineering*, vol. 8, no. 2, pp. 180–185, 2000.

[7] G. Townsend, B. Graimann, and G. Pfurtscheller, "Continuous EEG classification during motor imagery-simulation of an asynchronous BCI," *IEEE Transactions on Neural Systems and Rehabilitation Engineering*, vol. 12, no. 2, pp. 258–265, 2004.

[8] R. Scherer, G. R. Müller, C. Neuper, B. Graimann, and G. Pfurtscheller, "An asynchronously controlled EEG-based virtual keyboard: improvement of the spelling rate," *IEEE Transactions on Biomedical Engineering*, vol. 51, no. 6, pp. 979–984, 2004.

[9] R. Scherer, F. Lee, A. Schlogl, R. Leeb, H. Bischot, and G. Pfurtscheller, "Towards self-paced brain-computer communication: navigation through virtual worlds," to appear in *IEEE Transactions on Biomedical Engineering*.

[10] J. D. R. Millán and J. Mouriño, "Asynchronous BCI and local neural classifiers: an overview of the adaptive brain interface project," *IEEE Transactions on Neural Systems and Rehabilitation Engineering*, vol. 11, no. 2, pp. 159–161, 2003.

[11] A. Bashashati, S. Mason, R. K. Ward, and G. E. Birch, "An improved asynchronous brain interface: making use of the temporal history of the LF-ASD feature vectors," *Journal of Neural Engineering*, vol. 3, no. 2, pp. 87–94, 2006.

[12] A. Stancák Jr. and G. Pfurtscheller, "Event-related desynchronisation of central beta-rhythms during brisk and slow self-paced finger movements of dominant and nondominant hand," *Cognitive Brain Research*, vol. 4, no. 3, pp. 171–183, 1996.

[13] S. Slobounov, J. Johnston, H. Chiang, and W. Ray, "Movement-related EEG potentials are force or end-effector dependent: evidence from a multi-finger experiment," *Clinical Neurophysiology*, vol. 113, no. 7, pp. 1125–1135, 2002.

[14] G. H. Yue, J. Z. Liu, V. Siemionow, V. K. Ranganathan, T. C. Ng, and V. Sahgal, "Brain activation during human finger extension and flexion movements," *Brain Research*, vol. 856, no. 1-2, pp. 291–300, 2000.

[15] G. Pfurtscheller and F. H. Lopes da Silva, "Event-related EEG/MEG synchronization and desynchronization: basic principles," *Clinical Neurophysiology*, vol. 110, no. 11, pp. 1842–1857, 1999.

[16] A. Bashashati, M. Fatourechi, R. K. Ward, and G. E. Birch, "User customization of the feature generator of an asynchronous brain interface," *Annals of Biomedical Engineering*, vol. 34, no. 6, pp. 1051–1060, 2006.

[17] J. F. Borisoff, S. G. Mason, A. Bashashati, and G. E. Birch, "Brain-computer interface design for asynchronous control applications: improvements to the LF-ASD asynchronous brain switch," *IEEE Transactions on Biomedical Engineering*, vol. 51, no. 6, pp. 985–992, 2004.

[18] P. Welch, "The use of fast Fourier transform for the estimation of power spectra: a method based on time averaging over short, modified periodograms," *IEEE Transactions on Audio and Electroacoustics*, vol. 15, no. 2, pp. 70–73, 1967.

[19] P. A. Lachenbruch, *Discriminant Analysis*, Hafner Press, New York, NY, USA, 1975.

[20] G. Pfurtscheller and A. Aranibar, "Evaluation of event-related desynchronization (ERD) preceding and following voluntary self-paced movement," *Electroencephalography and Clinical Neurophysiology*, vol. 46, no. 2, pp. 138–146, 1979.

[21] G. Pfurtscheller, C. Neuper, C. Andrew, and G. Edlinger, "Foot and hand area mu rhythms," *International Journal of Psychophysiology*, vol. 26, no. 1–3, pp. 121–135, 1997.

[22] M. Pregenzer and G. Pfurtscheller, "Frequency component selection for an EEG-based brain to computer interface," *IEEE Transactions on Rehabilitation Engineering*, vol. 7, no. 4, pp. 413–419, 1999.

[23] G. E. Birch, P. D. Lawrence, and R. D. Hare, "Single-trial processing of event-related potentials using outlier information," *IEEE Transactions on Biomedical Engineering*, vol. 40, no. 1, pp. 59–73, 1993.

[24] B. Graimann, J. E. Huggins, S. P. Levine, and G. Pfurtscheller, "Toward a direct brain interface based on human subdural recordings and wavelet-packet analysis," *IEEE Transactions on Biomedical Engineering*, vol. 51, no. 6, pp. 954–962, 2004.

[25] G. R. Müller-Putz, R. Scherer, C. Brauneis, and G. Pfurtscheller, "Steady-state visual evoked potential (SSVEP)-based communication: impact of harmonic frequency components," *Journal of Neural Engineering*, vol. 2, no. 4, pp. 123–130, 2005.

[26] G. Dornhege, B. Blankertz, G. Curio, and K.-R. Müller, "Boosting bit rates in non-invasive EEG single-trial classifications by feature combination and multi-class paradigms," *IEEE Transactions on Biomedical Engineering*, vol. 51, no. 6, pp. 993–1002, 2004.

[27] G. Dornhege, B. Blankertz, G. Curio, and K.-R. Müller, "Combining features for BCI," in *Proceedings of the 6th Annual Neural Information Processing Systems Conference (NIPS '02)*, S. Becker, S. Thrun, and K. Obermayer, Eds., vol. 15 of *Advances in Neural Information Processing Systems*, pp. 1115–1122, British Columbia, Canada, December 2003.

[28] C. Babiloni, F. Carducci, F. Cincotti, et al., "Human movement-related potentials vs desynchronization of EEG alpha rhythm: a high-resolution EEG study," *NeuroImage*, vol. 10, no. 6, pp. 658–665, 1999.

[29] B. Blankertz, G. Dornhege, M. Krauledat, et al., "The Berlin brain-computer interface: EEG-based communication without subject training," *IEEE Transactions on Neural Systems and Rehabilitation Engineering*, vol. 14, no. 2, pp. 147–152, 2006.

[30] G. E. Birch, Z. Bozorgzadeh, and S. G. Mason, "Initial online evaluations of the LF-ASD brain-computer interface with able-bodied and spinal-cord subjects using imagined voluntary motor potentials," *IEEE Transactions on Neural Systems and Rehabilitation Engineering*, vol. 10, no. 4, pp. 219–224, 2002.

Hindawi Publishing Corporation
Computational Intelligence and Neuroscience
Volume 2007, Article ID 82069, 10 pages
doi:10.1155/2007/82069

Research Article

Online Artifact Removal for Brain-Computer Interfaces Using Support Vector Machines and Blind Source Separation

Sebastian Halder,[1] Michael Bensch,[2] Jürgen Mellinger,[1] Martin Bogdan,[2,3] Andrea Kübler,[1] Niels Birbaumer,[1,4] and Wolfgang Rosenstiel[2]

[1] *Institute of Medical Psychology and Behavioral Neurobiology, University of Tübingen, Gartenstr. 29, 72074 Tübingen, Germany*
[2] *Wilhelm-Schickard Institute for Computer Engineering, University of Tübingen, Sand 13, 72076 Tübingen, Germany*
[3] *Computer Engineering, Institute of Computer Science, Faculty of Mathematics and Computer Science, University of Leipzig, Johannisgasse 26, 04103 Leipzig, Germany*
[4] *National Institutes of Health (NIH), National Institute of Neurological Disorders and Stroke (NINDS), Human Cortical Physiology Section, Bethesda, MD 20892, USA*

Correspondence should be addressed to Sebastian Halder, halder@informatik.uni-tuebingen.de

Received 16 February 2007; Revised 31 May 2007; Accepted 23 August 2007

Recommended by Andrzej Cichocki

We propose a combination of blind source separation (BSS) and independent component analysis (ICA) (signal decomposition into artifacts and nonartifacts) with support vector machines (SVMs) (automatic classification) that are designed for online usage. In order to select a suitable BSS/ICA method, three ICA algorithms (JADE, Infomax, and FastICA) and one BSS algorithm (AMUSE) are evaluated to determine their ability to isolate electromyographic (EMG) and electrooculographic (EOG) artifacts into individual components. An implementation of the selected BSS/ICA method with SVMs trained to classify EMG and EOG artifacts, which enables the usage of the method as a filter in measurements with online feedback, is described. This filter is evaluated on three BCI datasets as a proof-of-concept of the method.

1. INTRODUCTION

Since the discovery of the human electroencephalogram (EEG) activity in 1929 by Hans Berger [1], EEG measurements were mainly used for medical reasons or for research in the area of brain function. In the past 15 years, applications have been developed allowing the use of EEG activity as a nonmuscular communication channel or as an aid in motor restoration after paralysis, so-called brain-computer interfaces (BCIs) [2]. The idea is to provide completely paralyzed patients with a rudimentary communication channel by classifying the EEG signal (currently with information transfer rates between 10–25 bits/min [2]). Further progress of BCI systems depends on the development of new training methods for patients, the identification of signals best suited for voluntary control, and the removal of noise interfering with these signals.

Noise includes artifacts (we define any noncentral nervous system (CNS) signal recorded by the EEG to be an artifact) introduced either by the subject himself or by an external source. Artifacts in EEG recordings can be caused by eye blinks, eye movement, muscle and cardiac noise, as well as nonbiological sources (e.g., power-line noise). A problem arises if the artifacts generated by the subject are used to control the BCI system, because this violates the definition of a BCI as a nonmuscular communication channel. Furthermore, subjects with degenerative diseases would eventually lose this ability. For instance, these artifacts could be a voluntary or involuntary blinks or muscle contractions when the task is presented. Additionally, involuntary muscle or ocular activity might obscure the actual EEG signal, obstructing measurement of the features used to control the system. Electromyographic (EMG) activity tends to overlap EEG from 8 Hz upwards, whereas electrooculographic (EOG) activity

overlaps in the range 0–12 Hz (e.g., the μ-rhythm has a frequency of 8–12 Hz). An overview of the effect of EMG on BCI training sessions is given in [3].

A supervisor can detect artifacts visually by analyzing the topographic and spectral properties of a signal. Unfortunately, the contaminated sections cannot just be rejected, due to the data loss this implies (blinks occur with a frequency of about 20 per minute and a duration between 50 and 500 milliseconds [4, 5]). Additionally, if the recordings are very long, the process of manual artifact rejection implies a significant increase in the time needed to fully process a dataset. Automating rejection would speed up this process but still cause the same amount of data loss. Therefore, the only feasible approach is to remove artifacts without affecting the remaining EEG data.

A comprehensive review of numerous artifact removal techniques and their application in BCI studies can be found in [6]. For example, a simple approach is highpass filtering the data to remove EOG and lowpass filtering the data to remove EMG artifacts, see, for example, [7]. This method will remove any brain signals of interest in the same frequency range. If a reliable reference channel is available, for example, an EOG recording, regression in the time, or frequency domain can be performed [8, 9]. The disadvantage of this method is that EOG recordings often contain brain signals which would inevitably also be removed. Nonetheless, it has been shown that this is preferable over artifact rejection methods because of the reduced amount of data loss [10].

An alternative approach is to use blind source separation (BSS), which is based on estimating the underlying sources (components) that compose the signals measured with the EEG. Ideally, the estimated components contain either artifacts or EEG activity. It is then possible to remove artifacts by elimination of the corresponding components. Makeig was one of the first to demonstrate the possibility of applying ICA methods to perform BSS on EEG data [11].

Artifacts were successfully isolated into a few output components and removed from the data. Advantages of using ICA to remove EOG artifacts from EEG data, instead of rejection- or regression-based techniques, have been shown in several studies, indicating that the percentage of brain signal that is removed with the EOG is reduced [12, 13]. EOG artifact removal on the basis of isolation into independent components (ICs) using BSS has been demonstrated in [14]. Another approach employs the second order statistics based "algorithm for multiple unknown signals extraction (AMUSE)" to detect EEG artifacts in sleep studies [15, 16].

In this paper, we propose an artifact removal method that removes artifacts whilst causing only minimal data loss and it is applicable in online environments and has no need for user interaction. This filter is implemented by using BSS/ICA algorithms in conjunction with support vector machine (SVM) classification and is based on an online capable design. The use of BSS/ICA algorithms minimizes data loss as the artifacts are isolated into ICs, automatic classification of these ICs with SVMs makes user interaction unnecessary, and the online capable design of the artifact filter provides a continuous stream of data in online settings. To make an objective selection of the algorithm being in the filter, possible, three ICA algorithms and one BSS algorithm are evaluated to determine their artifact isolation capabilities. An SVM is trained to classify artifacts on the basis of ICs extracted from data recorded for this purpose. Finally, we demonstrate the functionality of the filter using existing BCI data recorded from healthy and paralyzed participants.

2. METHODS

As a data model we assume a linear mixture of brain signals and artifact signals. This model corresponds to the model underlying BSS/ICA algorithms. As far as this model is accurate, artifacts can be removed from the EEG signal with an artifact removal matrix. This matrix is continuously updated and is calculated from SVM classification results on ICs determined with BSS/ICA.

A comparison to determine the best algorithm for the isolation of artifacts was conducted before training the SVMs. This comparison was limited to four algorithms which were selected because they cover the various principles of IC estimation employed in BSS algorithms. AMUSE [16] is a BSS method restricted to second-order statistics, JADE [17] a tensorial ICA method, Infomax [18] is based on maximum likelihood estimation, and FastICA [19] on the maximization of nongaussianity. After the selection of the best performing algorithms, SVMs were trained with artifact data recorded specifically for this purpose. A discussion of the filter design and the methods to achieve online functionality follows.

All of the BSS/ICA algorithms are contained in EEGLAB [20] and/or ICALAB [21].

2.1. BSS evaluation

2.1.1. Method of BSS evaluation

The method that was used to evaluate the performance of the four BSS algorithms is discussed here. All algorithms were evaluated by mixing a known artifact component with an artifact-free background EEG signal, re-extracting the known component and measuring the correlation of the extracted components and the introduced artifact components, as done in [24].

EEG data recorded while the subject was performing no particular task was cleaned of blinks and other obvious artifacts by removing the corresponding sections using EEGLAB and then used as background $\mathbf{B}_{\text{orig}}$. To obtain the first artifact source, an EMG recording was made on the forearm of a subject. This ensures that no CNS signals are contained in this artifact component. We assume that the spectral properties of an EMG signal generated at the forearm are comparable to those generated by muscles located on the head, for example, jaw muscles. This assumption seems to be a feasible tradeoff considering that it ensures that no CNS signals are contained in the EMG signal. The mixing matrix is constructed from jaw muscle recordings so that the spatial pattern is also as similar as possible to a real-jaw muscle recording. To ensure the availability of an EOG artifact component free of CNS signals, 20 blinks from channel Fp1 (see Figure 2 for electrode location) of an artifact recording were extracted,

Table 1: EEG recording parameters.

	EEG recording parameters
Amplifier	16 channel biosignal (gtec, Graz, Austria)
Sampling frequency	160 Hz
Highpass filter	0.01 Hz
Lowpass filter	70 Hz
Notch filter	50 Hz
Electrode placements	16 channel subset of 10–20 systems (see Figure 2) [22]
Ground	Left mastoid (A1)
Reference	Right mastoid (A2)
Electrode material	Ag/AgCl
Recording software	BCI2000 [23]

averaged, and then added to a zero baseline signal with varying gaps and a random multiplication factor ranging from 0.5 to 1.5.

Let $\mathbf{W}$ be the unmixing matrix obtained using BSS/ICA, and the mixing matrix $\mathbf{A}$ its inverse. A mixing matrix $\mathbf{A}$ was created for each of the two artifact signals $\mathbf{y}_{\text{art}}$ by averaging over the mixing matrices calculated by the four algorithms for each artifact type. Thus, the mixing matrix for the EMG artifact was created by averaging mixing matrices calculated using BSS/ICA for jaw muscle artifacts and the mixing matrix for the EOG artifact by averaging mixing matrices calculated using BSS/ICA for eye blinks. The artifact signals $\mathbf{y}_{\text{art}}$ were multiplied with the corresponding column i of these matrices and then added back to the background data $\mathbf{B}_{\text{orig}}$, which yields the mixed signal $\mathbf{B}'$:

$$\mathbf{B}' = \mathbf{B}_{\text{orig}} + \mathbf{A}_i \mathbf{y}_{\text{art}}. \quad (1)$$

After re-extraction, the component $\mathbf{y}_{\text{extr}}$, showing the maximum correlation with the introduced signal, was assumed to be the introduced artifact signal. This component was then removed from $\mathbf{B}'$ to obtain $\mathbf{B}_{\text{clean}}$. The correlation between $\mathbf{B}_{\text{org}}$ and $\mathbf{B}_{\text{clean}}$ as well as $\mathbf{y}_{\text{art}}$ and $\mathbf{y}_{\text{extr}}$ was calculated as performance measure. For space reasons and because both measures allowed the same conclusions, only the results for the correlation between $\mathbf{y}_{\text{art}}$ and $\mathbf{y}_{\text{extr}}$ are shown in detail. The background signal had a length of 16714 samples recorded with the settings shown in Table 1. A sliding window was moved over the data with a length of 480 and an overlap of 240 samples. Each of these 480 sample segments was tested with the above procedure.

AMUSE and JADE were run with default parameters. Infomax was run with a limit of 32, 64, and 128 iterations to restrict runtime to less than two seconds and to analyze the influence of the number of iterations on runtime and quality. The weight matrix computed in the previous step was passed to the algorithm as an initial guess. A learning rate of 0.001 was used. FastICA was run with a maximum number of iterations of 100, 200, and 400. "Approach" was set to "symmetric," as described in [25]. This causes the program to calculate all components in parallel, which is faster than a serial calculation if all components are to be estimated. The hyperbolic tangent function was chosen as "nonlinearity." "Stabilization" was turned on, which prevents the program from getting stuck at certain points by halving the step size μ. Again the previous weight matrix was used as an initial guess. Without a restriction on the number of iterations, Infomax and FastICA tended to have a very high variance in computation time to convergence.

2.1.2. BSS evaluation results

The performance of Infomax, JADE, AMUSE, and FastICA, determined using the evaluation method presented in the previous section, is shown here. The parameters stated in Section 2.1.1 were used.

Runtimes are shown only for the EOG signal because they did not differ for the two artifact types (see Figure 1). AMUSE has a runtime lower by a factor of 50 compared to the second fastest algorithm, which is Infomax (with 32 iterations). JADE is the slowest algorithm and also exhibits the greatest variance. This excludes it from any application in online environments where a reliable runtime is vital to achieve optimal performance. The extraction of the artificially generated EOG artifact is also performed best by the AMUSE algorithm and worst by the JADE algorithm. Infomax does not perform as well as AMUSE, but it is clearly better than FastICA.

The performance of AMUSE drops for the extraction of the EMG signal. Infomax performs best with this type of artifact.

The data shows that no algorithm is optimal for both types of artifacts. Since the runtime of AMUSE is lower by a factor of 50, it is possible to employ both algorithms. This has the additional advantage that only AMUSE will run if EOG artifacts only are to be removed. Therefore, we decided to use AMUSE in combination with Infomax. This is realized by creating an $\mathbf{R}$ (4) for each of the algorithms. These matrices are then combined by multiplication and applied to the data.

2.2. Support vector machine training

2.2.1. Training data

The artifacts recorded for SVM training and how the training of the SVMs was conducted are discussed in this section.

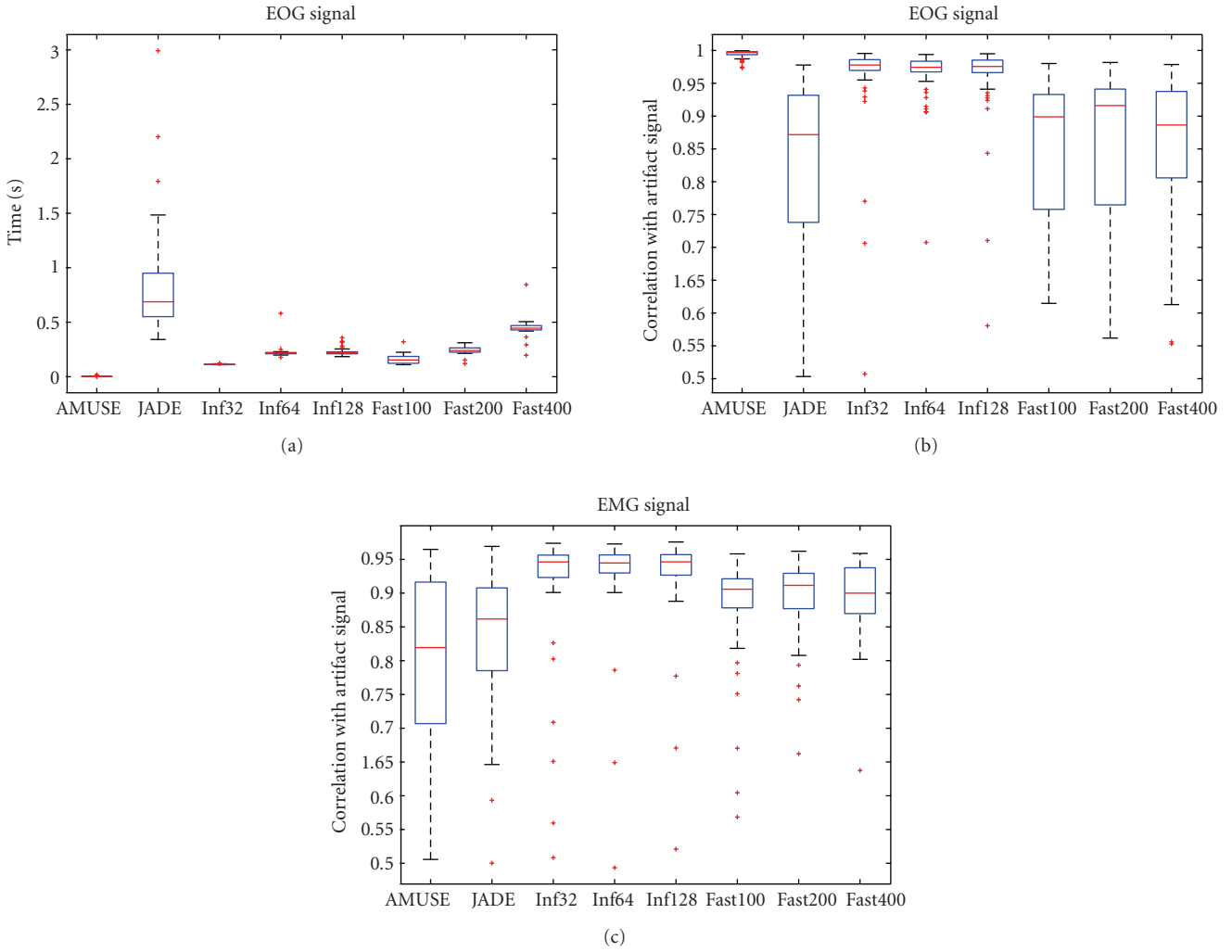

Figure 1: Boxplots showing times needed for extraction and EOG/EMG artifact extraction performance.

Four kinds of artifacts (jaw muscles, forehead movement, eye blinks, and eye movement), each recorded with four different subjects, were recorded to train the SVMs to classify various EEG artifacts. All recordings were made with the settings shown in Table 1.

The instructions to generate artifacts were presented to the subjects in random order, 40 times for each artifact type. Each presentation lasted 3 seconds. In total, this resulted in 19200 samples per artifact. These recordings were then split into blocks of 480 samples (i.e., 3 seconds), which were used to train the SVMs (at lengths lower than 300 samples, the classification rates began to deteriorate probably due to the fact that this is not sufficient for the BSS/ICA algorithms to perform separation on). This resulted in a training dataset with 2560 components per artifact. Every component was labeled by hand as either "artifact" or "nonartifact" by an expert. ICs containing EOG artifacts were mostly unambiguous. EMG artifacts tended to contaminate most ICs with varying degrees of intensity. Labeling every IC with only traces of EMG as artifact would result in too much of the nonartifact EEG data being removed. Therefore, only those ICs with strong EMG or no EEG were labeled as artifacts. The SVMs were all trained with an equal number of artifacts and nonartifacts (which were randomly selected from the set of available nonartifacts).

An RBF kernel [26] was used to classify the data based on their power spectral density (PSD) and the topography of the ICs (based on elements of the mixing matrix calculated with BSS/ICA). The PSD was calculated using Welch's method [27] and split into 16 frequency bins ranging from 1.6 Hz to 80 Hz. The corresponding columns in the mixing matrix were used as the remaining 16 elements. This results in a feature vector which is the concatenation of spectrum and topography.

Figure 2 shows the difference between the topography of eye blinking and horizontal eye movement ICs. The eye blinking artifacts project most strongly on the frontal electrodes Fp1 and Fp2, whereas horizontal eye movement artifacts have a very distinct projection, in which electrodes on different hemispheres have a different polarity. The topography of EMG artifacts depends strongly on the muscles used, but they all show a characteristic power spectrum. An EMG

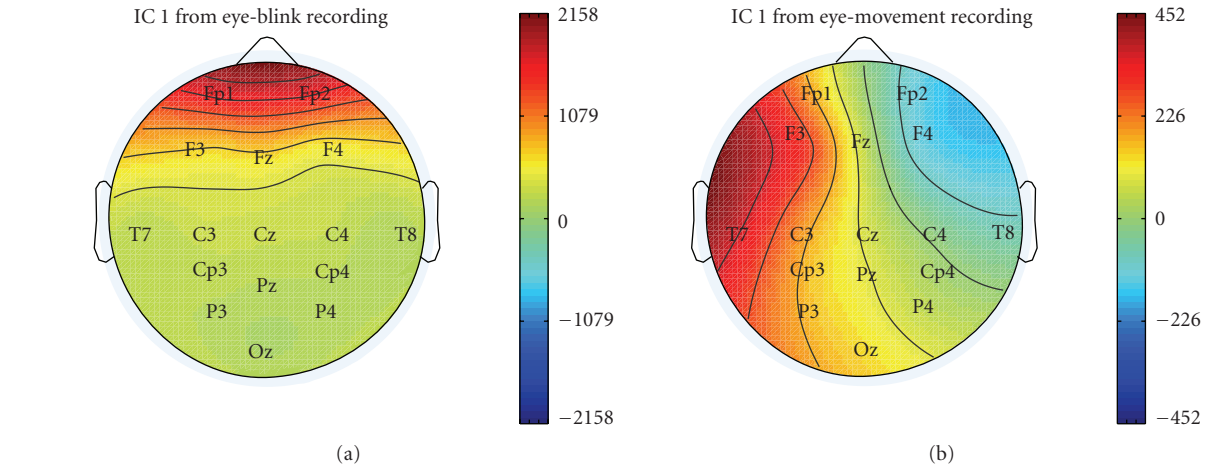

Figure 2: Topographic plots illustrating the differences in the features used for classification. The topographies of two ICs containing eye blinks (left) and eye movement (right) are shown.

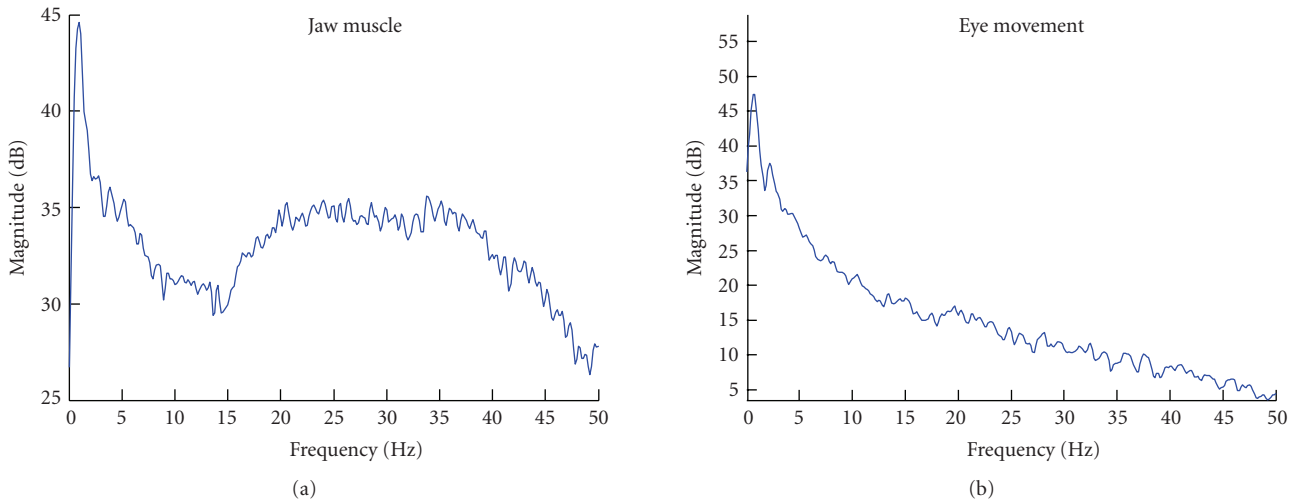

Figure 3: Power spectra showing the differences in the features used for classification, in this case of an IC containing jaw muscle contraction (a) and eye movement (b).

power spectrum of a jaw muscle artifact is shown next to an eye movement power spectrum in Figure 3.

2.2.2. *Support vector machine classification performance*

Classification rates of the SVMs for EOG and EMG artifacts using the features discussed in the previous section are briefly presented in the following section. The most apparent difference between EOG and EMG artifacts is that EMG artifacts contaminate a much higher percentage of the ICs than EOG artifacts (see Table 2). This is due to the fact that EMG artifacts are composed of multiple sources. These sources tend to be isolated into individual ICs, which leaves fewer components for the signal of interest. Additionally, traces of muscle activity remain in most of the components, varying in their intensity. That means that there is no hyperplane that clearly separates EMG and non-EMG components. This is reflected in the percentage of contaminated ICs and the percentage of correctly classified ICs during 20-fold cross validation (CV). Nevertheless, all classification rates lie above 90%, even above 99% in the case of EOG artifacts.

2.3. *Implementation*

The artifact filter is implemented using Matlab and integrated into the BCI2000 [23] software using an available Matlab interface. It consists of two major components. The first uses the signal data contained in buffer $\mathbf{Z}_{\mathrm{ICA}}$ and applies BSS/ICA to calculate the unmixing matrix $\mathbf{W}$. Application of $\mathbf{W}$ to $\mathbf{Z}_{\mathrm{ICA}}$ yields the corresponding sources $\mathbf{S}$:

$$\mathbf{S} = \mathbf{W}\mathbf{Z}_{\mathrm{ICA}}. \tag{2}$$

Table 2: SVM training summary showing the percentage of independent components (ICs) that are contaminated by artifacts in the particular artifact dataset and the percentage of ICs classified correctly as artifact and nonartifact when using 20-fold crossvalidation (CV). Additionally, channel capacity calculated using the Blahut-Arimoto algorithm [28, 29] and the parameters C (error penalty) and γ (kernel parameter of RBF kernel) used to train the SVMs are shown.

Artifact	% ICs	% correct (CV)	Channel capacity	C/γ
Eye blink	6.40	99.39	0.8141	2000/0.0005
Eye movement	5.15	99.62	0.9373	2/0.5
Jaw muscle	52.34	92.26	0.6308	8/0.5
Forehead	19.34	91.51	0.6043	2/0.5

Then the SVMs are used to classify the sources $\mathbf{S}$. We use the probability estimates p (values between zero and one, i.e., the probability that a component is not an artifact) of the SVM instead of classification results (zero or one) to construct a removal matrix. Probability estimates are calculated according to [30]. This avoids oscillation between removal and retainment in case of ambiguous components. Especially muscle artifacts are not cleanly isolated into single components, and those which contain only weak contamination might suffer from this problem when binary classification is used. p is used to construct a diagonal matrix $\mathbf{D}$ using the output of the SVMs for each of the four artifact types:

$$\begin{aligned} D_{ii} &= p_i, \quad i = 1,\ldots,N, \\ D_{ij} &= 0, \quad \forall\, i \neq j,\ i = 1,...,N,\ j = 1,\ldots,N, \end{aligned} \tag{3}$$

with N being the number of ICs.

$\mathbf{D}$ is combined with the unmixing matrix $\mathbf{W}$ and the mixing matrix $\mathbf{A}$, as shown in (4), to create the removal matrix $\mathbf{R}$ that is applied to the current output sample σ_i from buffer $\mathbf{Z}_{\text{sig}}$ in the second component of the artifact filter (5) which yields a sample σ_i' reconstructed out of BSS/ICA components weighted according to the probability estimates p of the SVM:

$$\mathbf{R} = \mathbf{ADW}, \tag{4}$$

$$\sigma_i' = \mathbf{R}\sigma_i. \tag{5}$$

The matrix $\mathbf{R}$ must be applied to every sample that passes through the filter. In a sequential approach in which the calculation of $\mathbf{R}$ takes $t_{\mathbf{R}} > 0$ this will prevent continuous output in online scenarios. Therefore the calculation of $\mathbf{R}$ and the application of $\mathbf{R}$ to the current output sample σ_i must be performed in separate threads.

$\mathbf{R}$ must include mixing and unmixing matrices from AMUSE and Infomax. $\mathbf{D}$ must be calculated for each of the four SVMs (eye movement, eye blinks, jaw muscle and forehead muscle artifacts). All matrices are then combined by multiplication as shown in (6) and applied to the data.

$$\begin{aligned} \mathbf{R} = {} & \mathbf{A}_{\text{AMUSE}}\mathbf{D}_{\text{EOG1}}\mathbf{D}_{\text{EOG2}}\mathbf{W}_{\text{AMUSE}} \\ & \times \mathbf{A}_{\text{Infomax}}\mathbf{D}_{\text{EMG1}}\mathbf{D}_{\text{EMG2}}\mathbf{W}_{\text{Infomax}}. \end{aligned} \tag{6}$$

Additionally, it must be taken into account that the calculation of the unmixing matrix $\mathbf{W}$ using the BSS/ICA algorithm is based on more than one sample. Therefore, the data that are used for the calculation, that is, $\mathbf{Z}_{\text{ICA}}$, must be representative of the sample σ_i that the removal matrix $\mathbf{R}$ is applied to. If simply the last n samples of the data are used, newly occurring artifacts might not have a strong enough impact on the SVM to be classified as such, which would lead to the artifact not being removed from σ_i. Conversely, artifacts in the buffer which contaminate most of the samples, but not the newest sample, will cause the SVM to classify a component of σ_i as an artifact which is in fact artifact-free. Hence, the incoming samples have to be delayed by half of the number of samples $k_{\mathbf{Z}_{\text{ICA}}}$ in buffer $\mathbf{Z}_{\text{ICA}}$ that contains the data for the BSS/ICA. This does not mean that a new sample arrives only every $k_{\mathbf{Z}_{\text{ICA}}}/2$ samples but that the whole recording is shifted by this amount and the samples still arrive with the same interval.

It is inevitable that the same matrix is used for several samples as the time $t_{\mathbf{R}}$, needed for the calculation of $\mathbf{R}$, is greater than the time represented by one sample of the data.

3. RESULTS

The artifact filter is applied offline to three BCI datasets to evaluate the effect on determination coefficient plots and subject performance. It is shown that application of the filter increases performance in cases where artifacts randomly interfere with the control signal and decreases performance when artifacts are used to control the BCI. Additionally, the online functionality of the filter is discussed.

3.1. Offline analysis of BCI data

The data analyzed originate from μ-rhythm (i.e., a BCI controlled using imagined movement/planning) training sessions recorded with the settings shown in Table 1 during a BCI evaluation project [31] (none of the datasets was used during the training of the SVMs). The control a user has over the BCI can be evaluated with determination coefficient (Pearson product-moment correlation coefficient, r^2) values as those plotted in Figure 4. A higher value indicates modulation of the signal in a certain channel at a certain frequency in correspondence with the required task. In this case, the modulation of the signal was used to control the movement of a cursor to either the top or the bottom of the screen. Artifacts either increase or decrease the determination coefficient value at certain frequency ranges. If the artifact correlates with the task (mostly due to the attempt to control the BCI with muscle activity or an involuntary muscle contraction while trying to perform the mental task), it will increase the value, and if it does not (due to involuntary

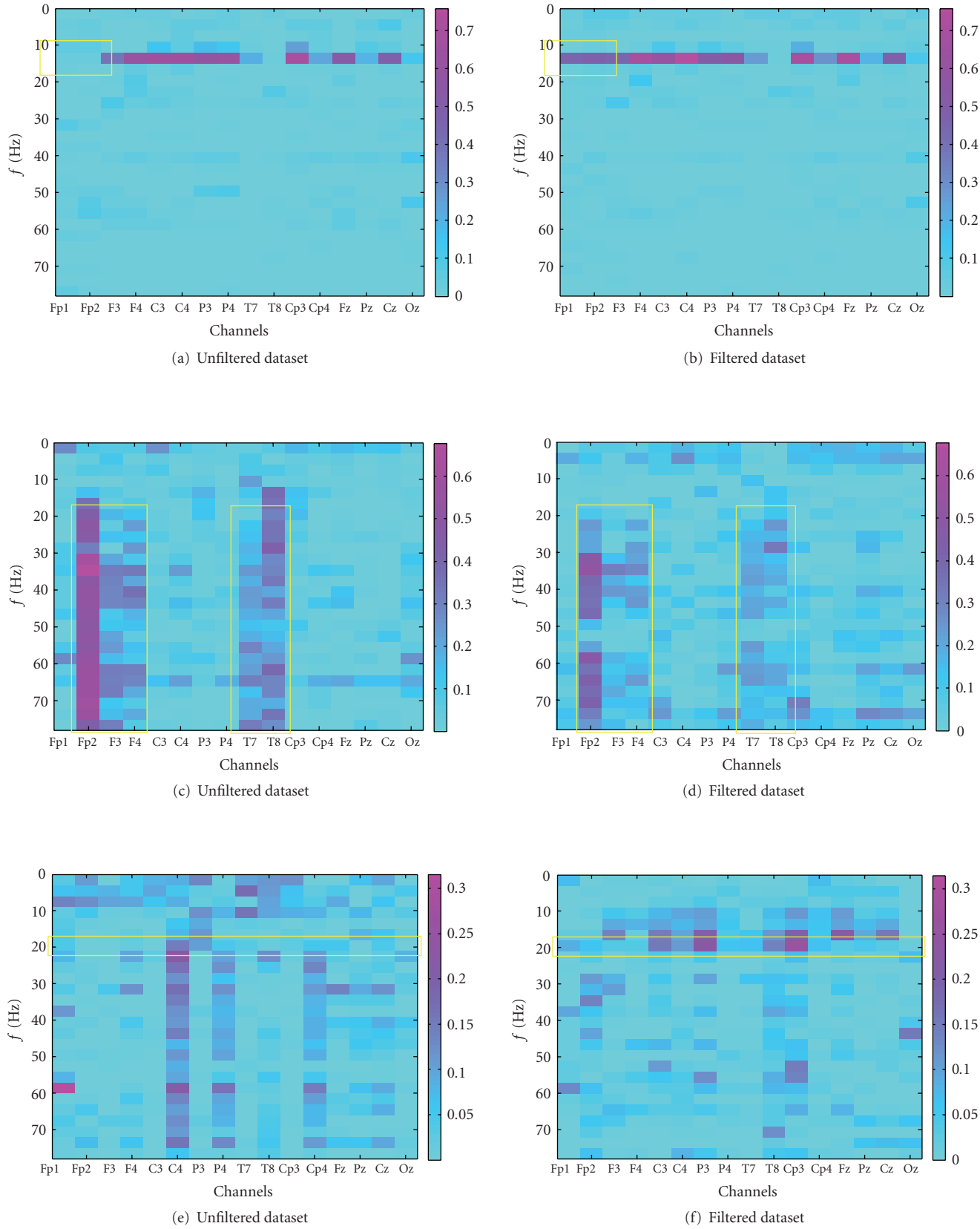

(a) Unfiltered dataset

(b) Filtered dataset

(c) Unfiltered dataset

(d) Filtered dataset

(e) Unfiltered dataset

(f) Filtered dataset

FIGURE 4: Determination coefficient (r^2) plots showing the correlation with a given task before (left) and after (right) filtering the signal. The first pair of plots (a) and (b) shows the effect of removing eye blinks uncorrelated with the task. The second pair (c) and (d) shows the removal of correlated muscle activity. The third pair (e) and (f) shows the effect of removing uncorrelated muscle activity. Regions of interest are marked with yellow boxes.

muscle spasms), it will decrease the determination coefficient value. In the former case, removal can be expected to decrease performance; in the latter, an increased or unchanged performance can be expected. This is what is intended since using artifacts to control a BCI violates the definition of it as being a nonmuscular communication channel. Plots 4(a) and 4(b) in Figure 4 show the effect of EOG artifact removal on data, which were recorded from a healthy subject presented 23 targets over 120 seconds, 22 of which were correctly chosen. Both of the frontal channels, Fp1 and Fp2, were contaminated with eye blinks. Since the blinks are uncorrelated with target location, this will have a negative influence on the determination coefficient value. As expected, the right plot, which shows the determination coefficient plot of the filtered data, has a visibly increased determination coefficient value on the frontal channels. On Fp1 the r^2 value increased from 0.0772 to 0.4539, and on Fp2 from 0.0929 to 0.4775. The maximum r^2 value increases from 0.7006 to 0.7585. This increase occurs in the same frequency range as the horizontal band of high determination coefficient values which existed previously, which is an indication of identical source (see box in 4(a) and 4(b)). Such a horizontal pattern is typical of successful μ-rhythm modulation. Because the control signal was not influenced significantly on the other electrodes, no increase in hit rate occurred.

In contrast to the top two plots, plots 4(c) and 4(d) show data from a subject that used muscle artifacts to control the BCI. This is reflected in the plot by the vertical structures (which indicate signals with a broad spectrum) that correlate with the task (which indicates that these signals were generated intentionally). Such patterns are visible on channels 2, 3, 4, 9, and 10 (see box in 4(c) and 4(d)). In total, 34 targets were presented, 29 of which were hit (85%). The filter does not entirely remove the EMG artifacts due to the previously described problem of muscle artifacts contaminating too many ICs. Nevertheless, the effect of the artifacts is significantly reduced, in particular below 20 Hz. Additionally, the absolute amplitude of the correlation of the EMG signals with the task was decreased visibly by the application of the filter (the maximum r^2 value decreases from 0.6777 to 0.5208). The removal led to a decrease of the simulated hit rate from 85% to 73%. The final case that is presented (see Figures 4(e) and 4(f)) also shows some contamination by EMG artifacts, even though not as strongly as the previous data. The subject was presented 34 targets, 17 of which were hit resulting in a hit-rate of 50%. The interesting fact about this dataset is that the removal of the EMG artifact reveals a horizontal structure in the range of 20 Hz (see box 4(e) and 4(f)). This indicates that there was some brain activity that was superimposed by EMG and could therefore not be used to control the BCI. The strongest increase of the determination coefficient value is based around electrode CP3 (channel 11), supporting this claim. On this channel, the maximum r^2 increases from 0.1204 to 0.2598. Additionally, this electrode was determined to be the most discriminative in initial screening sessions with the subject. The simulated performance of the subject increased from 50% to 74%.

3.2. Online functionality

The performance of the filter was tested by applying it to raw data and classifying it again. The data obtained are identical to the data that would have been obtained if the filter had been used in an online recording with the same settings. Of course, an arbitrary amount of time is available for the artifact filter in an offline setting. Therefore, the quality of artifact removal is potentially higher. Thus, the interval at which the removal matrix is updated was set to 5 sample blocks, which would be realistic in an online environment. Since the data was recorded with 8 samples per block at 160 Hz, this allows for 250 milliseconds per update.

The application of the removal matrix takes about 2.6 milliseconds per sample block. The calculation of a new removal matrix takes 145 milliseconds using both AMUSE and Infomax on the basis of 480 samples[1]. This is fast enough to update the removal matrix every five sample blocks with the above settings.

Using the BCI2000, several P300 recordings were made to ensure that running the filter would not have a negative impact on performance.

4. DISCUSSION

A filter that removes artifacts from EEG signals used in BCI systems was described. The data presented in this paper shows that the implementation of an online artifact filter using blind source separation and support vector machines is possible. This is achieved by delaying output by a constant amount between one and two seconds and by calculating and applying the removal matrix in two separate threads. Infomax was found to be the best ICA method to decompose EEG signals contaminated with myographic artifacts, but it had problems producing components which were completely free of contamination (especially if the myographic artifacts were very strong, as jaw muscle contraction). The second-order statistics-based algorithm AMUSE produced a very clean decomposition of recordings containing ocular artifacts, both eye movements and blinking. In turn, it was possible to train SVMs to recognize these artifacts with very high accuracy, because no contamination remained in the other components, making it easier to determine a separating hyperplane. Correspondingly, muscle artifacts could not be classified with such a high accuracy. The application of our artifact filter to BCI data demonstrates the usefulness of the technique. Performance increases were achieved in the case of uncorrelated muscle and ocular activity task. Additionally, a decrease in performance was apparent if the filter was applied to data in which the subject used muscle artifacts to control the BCI. Unfortunately, the removal was not complete, allowing some control of muscles of the BCI to remain. In future experiments, this might be improved by using more EEG channels which increase the number of ICs and therefore the chance that an EMG

[1] Using an AMD Athlon X2 4400+ with 2 GB RAM.

subspace can be isolated from the EEG subspace. Additionally, the method could be adapted for use with alternative BSS methods which are particularly suited to isolate EMG artifacts, for example, the canonical correlation analysis (CCA) method demonstrated in [32]. The CCA would be used instead of one of the ICA algorithms employed in this paper and be automated by using the available SVMs.

The feasibility of using ICA as a preprocessing technique for artifact detection has been shown in [33]. Performance increased for all presented artifact detection types after ICA preprocessing. It was noted though, that no performance increase was found when applying ICA to data contaminated with muscle artifacts. This is another indication that an alternative BSS or ICA algorithm should be used before classifying the data with SVMs.

Automated artifact removal techniques have been presented previously. For example, an automated regression analysis-based EOG removal method was presented in [34]. While being easy to apply it still suffers from the drawbacks of EEG-contaminated EOG channels (even though this was addressed by mounting the EOG electrodes in the proximity of the eyes and only calculating the regression coefficients from large EOG artifacts). Moreover, it is not possible to extend such a method to remove EMG artifacts.

Artifact isolation and removal using BSS/ICA algorithms automated by combination with SVMs or some other automatic classifier were already shown in [35]. While the applicability of the method presented in [35] is also restricted to ocular artifacts, we demonstrated a method based on the combination of BSS/ICA algorithms and SVMs that uses artifact features (topography and spectrum) that are available for all artifact types. Furthermore, we presented a design for online settings. A comparable method suitable for online use presented in [36], also not applied to EMG artifacts, depends on static models of artifact and brain signal topographies that do not adapt if the artifact changes, as the unmixing matrix calculated with BSS/ICA does. The method presented in [36] offers the advantage of having no delay and a reduced computational complexity.

We demonstrated that it is possible to implement an online-automated artifact removal technique on the basis of BSS/ICA and SVMs and illustrated the ameliorating effect on BCI performance.

ACKNOWLEDGMENTS

This work was supported by the Deutsche Forschungsgemeinschaft SFB550/TB5 and Grant no. Ro1030/12-1 as well as the National Institutes of Health, USA.

REFERENCES

[1] H. Berger, "Über das Elektroenzephalogramm des Menschen," *Archiv für Psychiatrie und Nervenkrankheiten*, vol. 87, pp. 527–570, 1929.

[2] J. R. Wolpaw, N. Birbaumer, D. J. McFarland, G. Pfurtscheller, and T. M. Vaughan, "Brain-computer interfaces for communication and control," *Clinical Neurophysiology*, vol. 113, no. 6, pp. 767–791, 2002.

[3] D. J. McFarland, W. A. Sarnacki, T. M. Vaughan, and J. R. Wolpaw, "Brain-computer interface (BCI) operation: signal and noise during early training sessions," *Clinical Neurophysiology*, vol. 116, no. 1, pp. 56–62, 2005.

[4] M. Iwasaki, C. Kellinghaus, A. V. Alexopoulos, et al., "Effects of eyelid closure, blinks, and eye movements on the electroencephalogram," *Clinical Neurophysiology*, vol. 116, no. 4, pp. 878–885, 2005.

[5] P. P. Caffier, U. Erdmann, and P. Ullsperger, "Experimental evaluation of eye-blink parameters as a drowsiness measure," *European Journal of Applied Physiology*, vol. 89, no. 3-4, pp. 319–325, 2003.

[6] M. Fatourechi, A. Bashashati, R. K. Ward, and G. E. Birch, "EMG and EOG artifacts in brain-computer interface systems: a survey," *Clinical Neurophysiology*, vol. 118, no. 3, pp. 480–494, 2007.

[7] J. S. Barlow, "EMG artifact minimization during clinic EEG recordings by special analog filtering," *Electroencephalography and Clinical Neurophysiology*, vol. 58, no. 2, pp. 161–174, 1984.

[8] T. Elbert, W. Lutzenberger, B. Rockstroh, and N. Birbaumer, "Removal of ocular artifacts from the EEG—a biophysical approach to the EOG," *Electroencephalography and Clinical Neurophysiology*, vol. 60, no. 5, pp. 455–463, 1985.

[9] R. J. Croft and R. J. Barry, "Removal of ocular artifact from the EEG: a review," *Neurophysiologie Clinique*, vol. 30, no. 1, pp. 5–19, 2000.

[10] R. J. Croft and R. J. Barry, "Issues relating to the subtraction phase in EOG artefact correction of the EEG," *International Journal of Psychophysiology*, vol. 44, no. 3, pp. 187–195, 2002.

[11] S. Makeig, A. J. Bell, T.-P. Jung, and T. J. Sejnowski, "Independent component analysis of electroencephalographic data," in *Advances in Neural Information Processing Systems*, vol. 8, pp. 145–151, The MIT Press, Cambridge, Mass, USA, 1996.

[12] R. N. Vigário, "Extraction of ocular artefacts from EEG using independent component analysis," *Electroencephalography and Clinical Neurophysiology*, vol. 103, no. 3, pp. 395–404, 1997.

[13] T.-P. Jung, S. Makeig, M. Westerfield, J. Townsend, E. Courchesne, and T. J. Sejnowski, "Removal of eye activity artifacts from visual event-related potentials in normal and clinical subjects," *Clinical Neurophysiology*, vol. 111, no. 10, pp. 1745–1758, 2000.

[14] C. A. Joyce, I. F. Gorodnitsky, and M. Kutas, "Automatic removal of eye movement and blink artifacts from EEG data using blind component separation," *Psychophysiology*, vol. 41, no. 2, pp. 313–325, 2004.

[15] S. Romero, M. A. Mañanas, S. Clos, S. Gimenez, and M. J. Barbanoj, "Reduction of EEG artifacts by ICA in different sleep stages," in *Proceedings of the 25th Annual International Conference of the IEEE Engineering in Medicine and Biology Society (EMBS '03)*, vol. 3, pp. 2675–2678, Cancun, Mexico, September 2003.

[16] L. Tong, R.-W. Liu, V. C. Soon, and Y.-F. Huang, "Indeterminacy and identifiability of blind identification," *IEEE Transactions on Circuits and Systems*, vol. 38, no. 5, pp. 499–509, 1991.

[17] J.-F. Cardoso, "High-order contrasts for independent component analysis," *Neural Computation*, vol. 11, no. 1, pp. 157–192, 1999.

[18] S. Makeig, T.-P. Jung, A. J. Bell, D. Ghahremani, and T. J. Sejnowski, "Blind separation of auditory event-related brain responses into independent components," *Proceedings of the National Academy of Sciences of the United States of America*, vol. 94, no. 20, pp. 10979–10984, 1997.

[19] A. Hyvärinen and E. Oja, "A fast fixed-point algorithm for independent component analysis," *Neural Computation*, vol. 9, no. 7, pp. 1483–1492, 1997.

[20] A. Delorme and S. Makeig, "EEGLAB: an open source toolbox for analysis of single-trial EEG dynamics including independent component analysis," *Journal of Neuroscience Methods*, vol. 134, no. 1, pp. 9–21, 2004.

[21] A. Cichocki, S. Amari, K. Siwek, et al., "ICALAB Toolboxes," http://www.bsp.brain.riken.jp/ICALAB.

[22] H. H. Jasper, "The 10-20 electrode system of the international federation," *Electroencephalography and Clinical Neurophysiology*, vol. 10, pp. 371–375, 1958.

[23] G. Schalk, D. J. McFarland, T. Hinterberger, N. Birbaumer, and J. R. Wolpaw, "BCI2000: a general-purpose brain-computer interface (BCI) system," *IEEE Transactions on Biomedical Engineering*, vol. 51, no. 6, pp. 1034–1043, 2004.

[24] N. J. Knight, "Signal fraction analysis and artifact removal in EEG," M.S. thesis, Colorado State University, Fort Collins, Colo, USA, 2004, http://www.cs.colostate.edu/eeg/publications/natethesis.pdf.

[25] A. Hyvärinen, "Fast and robust fixed-point algorithms for independent component analysis," *IEEE Transactions on Neural Networks*, vol. 10, no. 3, pp. 626–634, 1999.

[26] C.-C. Chang and C.-J. Lin, "LIBSVM: a library for support vector machines," http://www.csie.ntu.edu.tw/~cjlin/libsvm, 2001.

[27] P. D. Welch, "The use of fast Fourier transform for the estimation of power spectra: a method based on time averaging over short, modified periodograms," *IEEE Transactions on Audio and Electroacoustics*, vol. 15, no. 2, pp. 70–73, 1967.

[28] S. Arimoto, "An algorithm for computing the capacity of arbitrary discrete memoryless channels," *IEEE Transactions on Information Theory*, vol. 18, no. 1, pp. 14–20, 1972.

[29] R. E. Blahut, " Computation of channel capacity and rate-distortion functions," *IEEE Transactions on Information Theory*, vol. 18, no. 4, pp. 460–473, 1972.

[30] T.-F. Wu, C.-J. Lin, and R. C. Weng, "Probability estimates for multi-class classification by pairwise coupling," *Journal of Machine Learning Research*, vol. 5, pp. 975–1005, 2004.

[31] A. Kübler, F. Nijboer, J. Mellinger, et al., "Patients with ALS can use sensorimotor rhythms to operate a brain-computer interface," *Neurology*, vol. 64, no. 10, pp. 1775–1777, 2005.

[32] W. De Clercq, A. Vergult, B. Vanrumste, W. Van Paesschen, and S. Van Huffel, "Canonical correlation analysis applied to remove muscle artifacts from the electroencephalogram," *IEEE Transactions on Biomedical Engineering*, vol. 53, no. 12, part 1, pp. 2583–2587, 2006.

[33] A. Delorme, T. Sejnowski, and S. Makeig, "Enhanced detection of artifacts in EEG data using higher-order statistics and independent component analysis," *NeuroImage*, vol. 34, no. 4, pp. 1443–1449, 2007.

[34] A. Schlögl, C. Keinrath, D. Zimmermann, R. Scherer, R. Leeb, and G. Pfurtscheller, "A fully automated correction method of EOG artifacts in EEG recordings," *Clinical Neurophysiology*, vol. 118, no. 1, pp. 98–104, 2007.

[35] L. Shoker, S. Sanei, and J. Chambers, "Artifact removal from electroencephalograms using a hybrid BSS-SVM algorithm," *IEEE Signal Processing Letters*, vol. 12, no. 10, pp. 721–724, 2005.

[36] N. Ille, P. Berg, and M. Scherg, "Artifact correction of the ongoing EEG using spatial filters based on artifact and brain signal topographies," *Journal of Clinical Neurophysiology*, vol. 19, no. 2, pp. 113–124, 2002.

Hindawi Publishing Corporation
Computational Intelligence and Neuroscience
Volume 2007, Article ID 25487, 10 pages
doi:10.1155/2007/25487

Review Article

fMRI Brain-Computer Interface: A Tool for Neuroscientific Research and Treatment

Ranganatha Sitaram,[1] Andrea Caria,[1] Ralf Veit,[1,2] Tilman Gaber,[1,2] Giuseppina Rota,[1,3] Andrea Kuebler,[1] and Niels Birbaumer[1,4]

[1] *Institute of Medical Psychology and Behavioral Neurobiology, Eberhard-Karls-University of Tübingen, 72074 Tübingen, Germany*
[2] *Max Planck Institute for Biological Cybernetics, P.O. Box 21 69, 72076 Tübingen, Germany*
[3] *Institute for Natural Language Processing, University of Stuttgart, 70174 Stuttgart, Germany*
[4] *National Institute of Health (NIH), NINDS, Human Cortical Physiology, Bethesda, MD 20892-1428, USA*

Correspondence should be addressed to Ranganatha Sitaram, sitaram.ranganatha@uni-tuebingen.de

Received 28 February 2007; Revised 2 August 2007; Accepted 18 September 2007

Recommended by Shangkai Gao

Brain-computer interfaces based on functional magnetic resonance imaging (fMRI-BCI) allow volitional control of anatomically specific regions of the brain. Technological advancement in higher field MRI scanners, fast data acquisition sequences, preprocessing algorithms, and robust statistical analysis are anticipated to make fMRI-BCI more widely available and applicable. This noninvasive technique could potentially complement the traditional neuroscientific experimental methods by varying the activity of the neural substrates of a region of interest as an independent variable to study its effects on behavior. If the neurobiological basis of a disorder (e.g., chronic pain, motor diseases, psychopathy, social phobia, depression) is known in terms of abnormal activity in certain regions of the brain, fMRI-BCI can be targeted to modify activity in those regions with high specificity for treatment. In this paper, we review recent results of the application of fMRI-BCI to neuroscientific research and psychophysiological treatment.

1. INTRODUCTION

Brain-computer interfaces (BCIs) enable control of computers and of external devices with regulation of brain activity alone (Birbaumer et al. [1], Donoghue [2], Wolpaw et al. [3], Nicolelis [4], Wolpaw and McFarland [5], Hochberg and Donoghue [6]). Two different traditions of BCI research have dominated the field: invasive BCI, based on animal studies and realized with implanted electrodes, and noninvasive BCI, primarily using electroencephalography (EEG). Invasive multielectrode BCIs in animals enabled execution of reaching, grasping, and force control from spike patterns and extracellular field potentials. Clinical applications have been derived predominantly from noninvasive approaches: communication for the completely paralyzed and locked-in patients using slow cortical potentials, sensorimotor rhythm, and the P300 event-related potential, and restoration of movement and cortical reorganization in high spinal cord lesions and chronic stroke.

EEG-BCIs have certain drawbacks. Mainly, EEG provides only a low spatial resolution and ambiguous localization of neuronal activity, since underlying electric sources need to be reconstructed from the distribution of electric potentials across the scalp (Weiskopf et al. [7]). A BCI based on real-time fMRI allows for noninvasive recording of neuronal activity across the entire brain with relatively high spatial resolution and moderate temporal resolution (in the range of millimeters and seconds, resp.). Unlike EEG-BCI, fMRI-BCI allows brain activity in very specific parts of cortical and subcortical regions of the brain, for example, the left anterior insula, to be extracted and used for online feedback (Caria et al. [8]). However, major disadvantages of fMRI-BCI are its high cost and complexity of development and usage. With the wide-spread use of MRI systems in the clinics and research centres, and the emergence of real-time fMRI data processing and analysis tools such as turbo-brain voyager (Brain Innovations, Maastricht, The Netherlands) and TurboFIRE (Sefan Posse, NM, USA), fMRI-BCI might become more accessible in the future.

Despite the fact that BOLD is an indirect measure, there is growing evidence for a strong correlation between the BOLD signal and electrical brain activity. Studies have characterized the relationship between localized increases in neuronal activity and the corresponding increase in BOLD (Logothetis et al. [9], Shmuel et al. [10]), making it possible to interpret positive functional responses in terms of neural changes. These results constitute a convincing basis for using fMRI in BCI studies. With innovations in high-performance magnetic resonance scanners and computers, and developments in techniques for faster acquisition, processing and analysis of MR images, real-time fMRI has recently become a possibility. With improvements in real-time fMRI, a novel type of noninvasive fMRI-BCI has emerged.

Studies that have been reported so far (Yoo and Jolesz [11], Posse et al. [12], Weiskopf et al. [13], DeCharms et al. [14], Weiskopf et al. [15], Yoo et al. [16], DeCharms et al. [17], Sitaram et al. [18], Caria et al. [19], Rota et al. [20], Veit et al. [21]) have demonstrated that human subjects using real-time fMRI can learn voluntary self-regulation of localized brain regions. These studies manipulated different cortical and subcortical areas, namely, supplementary motor area (SMA) (Wagner and Barrett [22], Weiskopf et al. [15], Sitaram et al. [18]), sensorimotor area (Yoo and Jolesz [11], DeCharms et al. [14], Yoo et al. [16]), posterior part of the superior temporal gyrus (Yoo et al. [16]), medial superior frontal gyrus (Yoo et al. [16]), parahippocampal place area (PPA) (Weiskopf et al. [15]), the anterior cingulate cortex (ACC) (Weiskopf et al. [13], temporal gyrus (Yoo et al. [16]), medial superior frontal gyrus (Yoo et al. [16]), parahippocampal place area (PPA) (Weiskopf et al. [15]), the anterior cingulate cortex (ACC) (Weiskopf et al. [13], Yoo et al. [16], Caria et al. [19]), insula (Veit et al. [21]), Broca's area (Rota et al. [20]), and amygdale (Posse et al. [12]). Importantly, these studies have reported evidence for behavioral modifications that accompany self-regulation training.

FMRI-BCI is a general system employing real-time fMRI technology that enables various applications including training to self-regulate activity in precisely specified regions of the brain to study plasticity and functional reorganization, application of the knowledge so derived in psychophysiological treatement, quality assurance of neuroimaging data, presurgical patient assessment and teaching of brain imaging methods (Weiskopf et al. [7]). In the context of a self-regulation experiment, fMRI-BCI can extract BOLD activity from voxels in one or more regions of interest (ROIs) in the brain to compute average activity in the ROIs, or correlation coefficient of activity between ROIs, or any other function that could be used to provide feedback to the participant. However, fMRI-BCI need not necessarily function based on self-regulation of brain activity alone. There has recently been much progress in the detection and discrimination of mental states using fMRI data (Haynes and Rees [23]). Although much of the research work has focussed on offline pattern classification of brain states using machine learning techniques, there are also attempts to develop online classification (Laconte et al. [24]). With this approach the participant does not have to be trained to regulate activity in the brain. On the contrary, the system learns to recognize the patterns of activity that spontaneously occur in a participant's brain. This new approach promises applications such as lie detection, and detection of cognitive, perceptual, and emotional states for neuroscientific research and clinical treatment. The output from such a system could also be used for communication and the control of external devices.

Section 2 presents the general architecture of an fMRI-BCI system and its components. Section 3 paints a picture of potential applications of this emerging approach for neuroscientific research. Section 4 describes possible applications in psychophysiological treatment. Section 5 offers concluding remarks.

2. ARCHITECTURE OF fMRI-BCI

An fMRI-BCI system is a closed-loop system that can be depicted as shown in Figure 1. It has the following major components: (1) the participant, (2) signal acquisition, (3) signal analysis, (4) signal feedback. The last 3 components are usually executed on separate computers for optimizing the system performance, and are connected by a local area network (LAN).

Localized brain activity is measured by fMRI using the BOLD effect which is the vascular response to neural activity. FMRI signals are usually acquired by echo planar imaging (EPI). Our experiments are conducted using a 3T whole body scanner (Trio, Siemens, Erlangen, Germany) with standard head coil. EPI sequence parameters used are repetition time TR = 1.5 seconds, echo time TE = 45 milliseconds, flip angle = 70°, 16 slices, bandwidth 1.3 KHz/pixel, $\mathrm{FOV_{PE}}$ = 210, $\mathrm{FOV_{RO}}$ = 210, image matrix = 64 × 64, voxel size 3 × 3 × 5 $\mathrm{mm^3}$. Images are reconstructed, distortion corrected, and averaged on the magnetic resonance scanner computer. The signal analysis component is implemented in our work using turbo-brain voyager (Brain Innovations, Maastricht, The Netherlands) (Goebel [25]). The signal analysis component retrieves reconstructed images, and performs data preprocessing (including 3D motion correction) and statistical analysis. The time series of selected regions of interest are then exported to the custom-made visualization software which provides feedback to the subject using either a video projection or MRI compliant goggles.

Feedback is presented with a delay that depends on the time involved for image acquisition and processing. A short delay is critical (the best achieved so far is about 1.3 seconds in our lab) for volitional control. The advantage of fMRI in comparison to EEG is its superior spatial specificity and resolution. Most studies so far have used the BOLD signal from static regions of interest (ROIs) from one or multiple EPI slices of the human brain for feedback. ROI is chosen by drawing a rectangular area on the functional map computed in the signal analysis software (e.g., TBV). To improve selection of ROIs, functional maps could be coregistered with previously acquired anatomical scans of the subject. Studies have also used differential feedback (Weiskopf et al. [13], Weiskopf et al. [15]) between two ROIs to subtract out global signal changes. Specificity of the signal can be further improved by

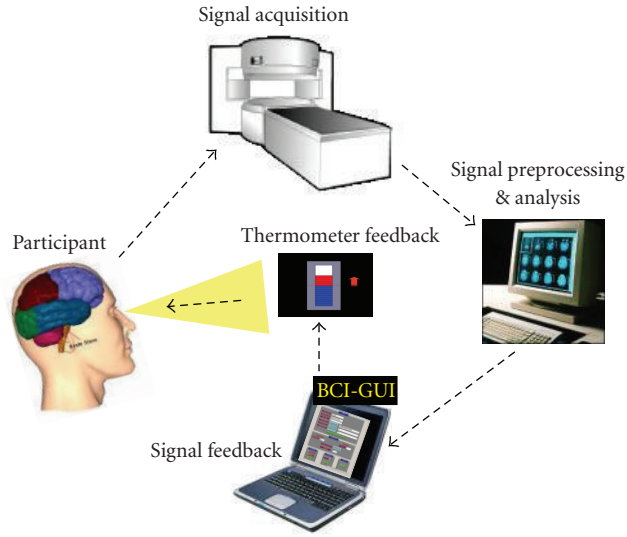

Figure 1: An fMRI-BCI system is a closed-loop system that has the following major components: (1) signal acquisition, (2) signal analysis, (3) signal feedback, and (4) the participant. The first 3 components are usually executed on separate computers for optimizing the system performance, and are connected together by a local area network (LAN). Spatially localized brain activity is measured by fMRI using the BOLD effect which is the neurovascular response to electric brain activity. Usually, echo planar imaging (EPI) sequences are applied to acquire functional images when the subject is performing a mental task or imagery. Images are reconstructed, distortion corrected, and averaged by the signal acquisition component. The signal analysis component retrieves the data, and performs data preprocessing, such as including 3D motion correction, and statistical analysis. The signal time series of interactively selectable regions of interest are then exported to the custom-made visualization software (signal feedback component) which provides feedback to the subject using video projection.

designing a protocol that includes bidirectional control, that is, both increase and decrease of the BOLD activity in the ROI. General effects of arousal and attention caused by the demands of the task or the state of the subject are thus canceled out leaving only the effects of increase or decrease of the signal.

Average BOLD values from ROIs are computed by the signal analysis software and stored in a continuously updated file to be retrieved in real-time by the signal feedback component. In our work, we have developed a custom software called "BCI-GUI" that provides a graphical user interface to configure the fMRI-BCI experiment, enter user input, choose one among a variety of feedback modalities, present feedback to the subject in real-time, and report experimental results as graphs and charts at the end of the feedback session (see Figure 2).

Many feedback modalities, such as verbal, visual, auditory, olfactory, tactile, and a combination of these, are possible. However, most studies have used visual feedback. A variety of visualization methods have been employed by different researchers to indicate the required level of activation over time. Scrolling time series graphs and curves of BOLD activation of the ROI is a computationally fast yet effective method to provide immediate information to the subject (Weiskopf et al. [13], DeCharms et al. [14], Weiskopf et al. [15]). Sitaram et al. (Sitaram et al. [18]) introduced the thermometer type of feedback that shows a snap-shot of brain activity as variations of the thermometer. Positive BOLD activity with respect to baseline activity can be shown in one color (red) to differentiate negative BOLD activity (blue). Sitaram et al. also introduced virtual reality (VR) for feedback (Sitaram et al. [18]) (Figure 3).

3. fMRI-BCI APPLICATION TO NEUROSCIENTIFIC RESEARCH

3.1. Background

There are two general approaches in neuroscience for studying the interaction between brain and behavior. The first category involves the manipulation of the neural substrate and the observation of behavior as a dependent variable (Moonen and Bandettini [26], Feinberg and Farah [27]). The effects of stimulation and lesions of brain areas are studied with this approach. The second approach is less intrusive in nature, manipulating behavior as an independent variable and neural function as a dependent variable, constituting the psychophysiological approach.

fMRI-BCI is in a unique position to combine both approaches. It is a manipulative approach, as the subject is trained to voluntarily change the activity in a particular region of the brain as an independent variable to observe the changes in behavior. It realizes also the psychophysiological perspective as it incorporates experimental paradigms with neural response as the dependent variable. Using the EEG neurofeedback and BCI approaches, studies on slow cortical potentials (SCPs) reported behavioral effects on lexical processing, motor action, and musical performance (Rockstroh et al. [28], Pulvermuller et al. [29], Egner and Gruzelier [30]). FMRI-BCI has the advantage of targeting a localized brain

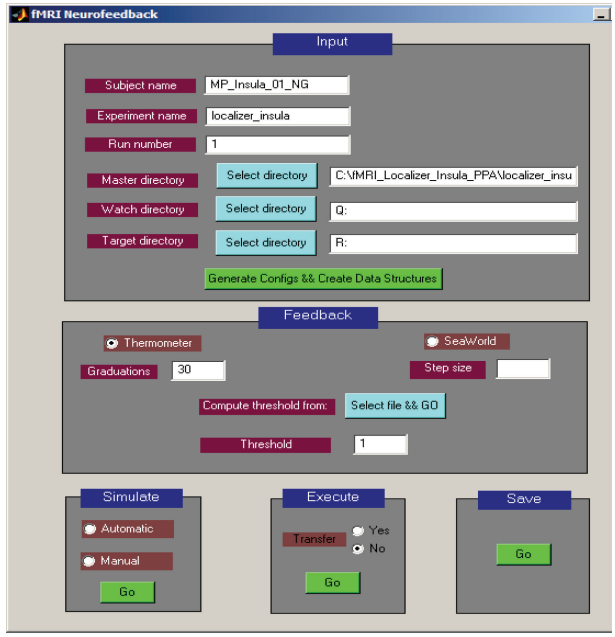

Figure 2: "BCI-GUI" is a software tool with a graphical user interface to configure the fMRI-BCI experiment, enter user input and protocol parameters, choose one among a variety of feedback modalities, present feedback to the subject in real-time, and report experimental results as graphs and charts at the end of the feedback session. The software is extensible, allowing development of additional preprocessing, analysis, and feedback methods. Modifications to the system can be tested offline by simulating fMRI data before bringing it to the MRI scanner.

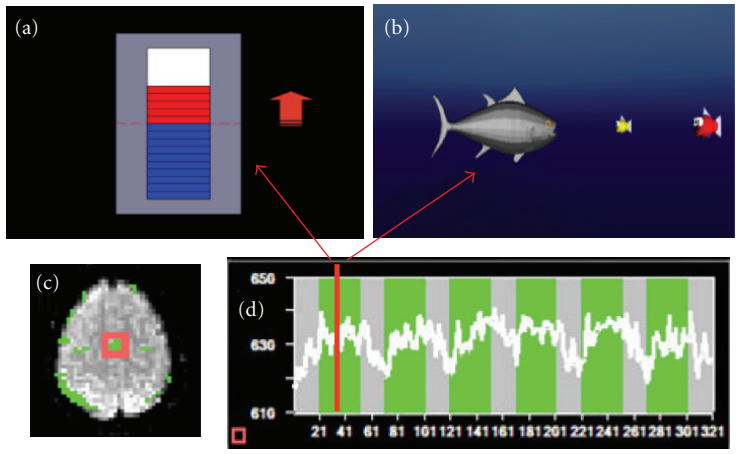

Figure 3: An important criterion in successfully training subjects to self-regulate their BOLD response is the feedback. (a) shows the thermometer feedback that gives regularly updated snap shot of brain activity as graduations in the thermometer. Positive BOLD activity with respect to baseline activity can be shown in one color (red) to differentiate negative BOLD activity (blue). Using this feedback the subject has an intuitive grasp of increasing or decreasing the thermometer graduations during self-regulation. (b) shows an exemplar virtual reality environment for feedback. A well-designed virtual reality feedback system can enhance the efficacy of training subjects to self-regulate a localized brain region. Volunteers have to control a 3D animated character, a fish in water, by self-regulating their BOLD response to carry out a task of moving the fish towards a food item (a smaller fish) and eating it. (c) shows the localization of supplementary motor area (SMA) as the region of interest (ROI). (d) shows a participant's time series of self-regulation of BOLD response from SMA after 3 training sessions.

region, with high spatial resolution and a reasonable temporal resolution. BOLD feedback with a latency of less than 1.3-second interval has been achieved (Weiskopf et al. [13]). We discuss below fMRI-BCI applications in emotional processing, language processing, pain processing and pain perception, motor control, sensory perception, and aversive conditioning.

3.2. *Emotional processing*

Weiskopf et al. (Weiskopf et al. [13]) used fMRI-BCI to study the effect of volitional control of anterior cingulated cortex (ACC) on emotional processing. From previous anatomical and functional studies two major subdivisions of the ACC are distinguished, which subserve two distinct types

of functions. The dorsal ACC is called the "cognitive division" (ACcd) and the rostral-ventral "affective" division (ACad). Due to its involvement in different functional networks, physiological self-regulation was applied to study cognitive and emotional parameters, for example, emotional valence and arousal, dependent on the differential activation of the two subdivisions. In this study, two continuously updated curves were presented to the subject depicting BOLD activity in ACcd and ACad. During blocks of 60-second duration, subjects were instructed to move both curves upwards (alternating 60 seconds rest and 60 seconds up-regulation). The subject was instructed to use his own strategy for voluntary BOLD regulation. The subject reported that he used the imagery of winter landscapes, engaging in snowboarding and social interactions during up-regulation, and attending to the feedback curve without performing any specific imagery during the rest blocks. An improved control of the rostral-ventral affective subdivision was observed during training. Subsequent testing of the affective state using self-assessment Manikin (SAM) (Bradley and Lang [31]) showed an increase in valence and arousal during the up-regulation of BOLD in the ACad only.

In a recent study (Caria et al. [32], Figure 4), we investigated whether healthy subjects could voluntarily gain control over right anterior insular activity. Subjects were provided with continuously updated information of the target ROI's level of activation by the thermometer feedback. All participants were able to successfully regulate BOLD—magnitude in the right anterior insular cortex within three sessions of four blocks each. Training resulted in a significantly increased activation cluster in the anterior portion of the right insula across sessions. An increased activity was also found in the left anterior insula but the percent signal change was lower than in the target ROI. Two different control conditions intended to assess the effects of nonspecific feedback and mental imagery demonstrated that the training effect was not due to unspecific activations or non-feedback-guided strategies. Both control groups showed no enhanced activation across the sessions which confirmed our main hypothesis that rtfMRI feedback is area specific. The increased activity in the right anterior insula during training demonstrates that the effects observed are functionally specific and self-regulation of right anterior insula only is achievable. This is the first group study demonstrating that volitional control of an emotional area can be learned by training with an fMRI-BCI. We are presently conducting further studies to understand the behavioral effects of volitional control of insula.

3.3. Neuroplasticity of motor systems

Study of neuroplasticity and functional reorganization for recovery after neurological diseases such as stroke is of relevance. Real-time fMRI feedback could be used to successively reactivate affected regions of the brain. Sitaram et al. (Sitaram et al. [18]) trained 4 healthy volunteers to control the BOLD response of the SMA. Offline analysis showed significant activation of the SMA with training. Further, with training there was a distinct reduction in activation in the surrounding areas, indicating that volitional control training focuses activity in the region-of-interest (Figure 5).

3.4. Language processing

Rota et al. (Rota et al. [20]) explored human capacity for differential self-regulation of the BOLD activity recorded locally in Broca's area (BA 45). The linguistic task used to localize the ROI (BA 45) was previously shown to activate the inferior frontal gyrus (Dogil et al. [33]). The task consisted of reading and manipulating the syntactic structure of German sentences. Four healthy volunteers were trained with a thermometer feedback of activity from the ROI for a total of 12 sessions in a 3T Siemens Trio with the following EPI parameters: TR 1.5 seconds, TE 45 milliseconds, flip angle = 70°, 16 slices, bandwidth 1.3 KHz/pixel, voxel size $3 \times 3 \times 5$ mm^3. For behavioral assessment of the effect of feedback training, two linguistic tests were performed by the volunteers immediately before and after the feedback sessions. The two tests involved grammatical judgement and emotional prosody identification. Their results showed that up-regulation of the right BA 45 correlated with emotional prosody identification.

3.5. Visual perception

Tong et al. (Tong et al. [34]) used fMRI to study binocular rivalry when a face and a house were presented to different eyes. As the retinal stimulation remained constant, subjects perceiving changes from house to face were accompanied by increasing activity in the fusiform face area (FFA) and decreasing activity in the parahippocampal place area (PPA), while subjects perceiving changes from face to house was seen during opposite pattern of responses. Although correlations have been found between increased brain activities in certain regions during reported conscious perception, as summarized above, a definite causal link has not been established. Is the firing activity of these neurons merely covarying with the percept? Are these cells really the central players in the percept? How tight is the link between the onset and strength of activity and the behavior on a trial-to-trial basis? We propose that fMRI-BCI can be applied to clarify these issues.

There are 3 stages to our proposed experiment: pretest, volitional control training, and posttest. In the pretest, the subject observes the rival images of houses and faces presented separately and simultaneously to the two eyes, and to press a button to indicate the changing percepts. This stage will establish the frequency and duration of the percepts. During the volitional control training, the subject's brain regions considered to be implicated in the one of the percepts (ROI) are localized. The subject is then trained in several sessions to self-regulate the ROI (i.e., FFA). During training, the subject is conditioned to decrease (or increase) the BOLD activity of the ROI of the face area. In the posttest, the binocular rivalry task is presented again to measure frequency and duration of the changing percept. If the subject has been successfully trained to self-regulate the BOLD activity in FFA, one may expect a significant change in the

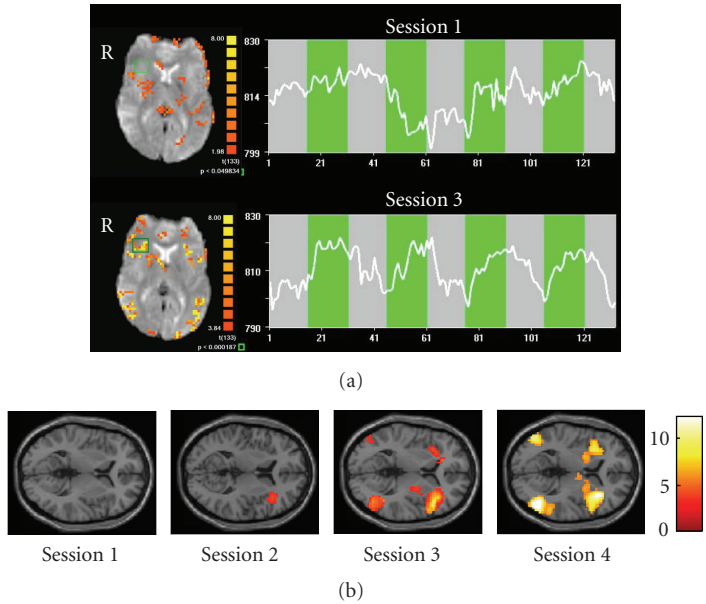

(a)

(b)

Figure 4: (a) Single subject statistical maps (left) and BOLD time-courses (right) of the right anterior insula in the first (upper) and in the last sessions (lower). The selected region of interest is delineated by the green box. The time course of the BOLD activity (white line) is related to the ROI selected and is showing the progress during the regulation blocks (green) and the baseline blocks (grey). Number of volumes is along the x-axis and magnitude of the signal is along the y-axis. (b) Random effects analysis on the experimental group confirmed an increased BOLD magnitude in the right anterior insular cortex over time course. SPM2 analysis of the single sessions showed no significant activation during the first session in the target area; a significant activation cluster ($t = 4.50$; $P = .001$ uncorrected) during the second session (MNI coordinates: 39,33,0); and a highly significant activation cluster ($t = 10.23$; $P < .001$ uncorrected) during the third session located (MNI coordinates: 36,26,6) (Caria et al. [32]).

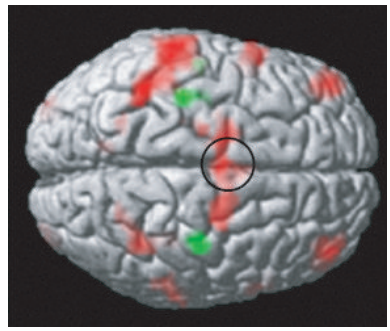

Overlay of localization and up-regulation

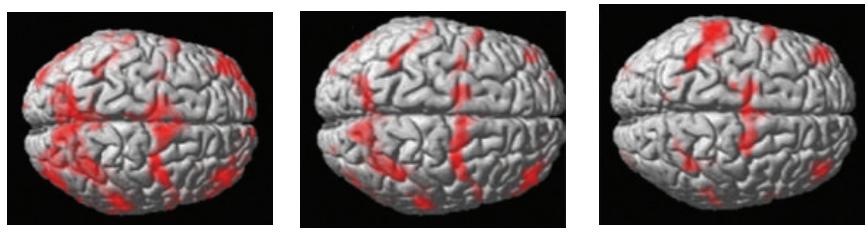

Start session Midsession Last session

Figure 5: Study of neuroplasticity and functional reorganization is of much research interest. Real-time fMRI feedback could be used to successively reactivate affected regions of the brain. (a)-(d) show results of offline analysis in terms of functional activity superimposed on the anatomical structure of a healthy volunteer trained to self-regulate supplementary motor area (SMA). (a) shows significant activity around the SMA during the functional localization session when the volunteer carried out self-paced finger tapping task. (b)-(d) show brain activity during the first, middle, and last session of self-regulation training. With increased training there was a distinct reduction in activation in other areas, indicating that self-regulation training focuses on activity in the region-of-interest.

perception of faces. This establishes the causal link between conscious perception of the image and the brain activity in the corresponding region.

4. fMRI-BCI APPLICATION TO PSYCHOPHYSIOLOGICAL TREATMENT

4.1. Background

Behavior medicine focuses on the application of learning theories to the treatment of medical disorders. To give an example: patients with attention-deficit and hyperactivity disorder (ADHD) (Fuchs et al. [35]) were treated with self-regulation of 12–15 Hz EEG brain activity. Epilepsy patients were trained to suppress epileptic activity by self-regulation of slow cortical potentials (SCP) (Kotchoubey et al. [36]). If the neurobiological basis of the disorder is known in terms of abnormal activity in a certain region of the brain, fMRI-BCI can be targeted to those regions with greater specificity for treatment. Many types of disorders, namely, memory disorders, chronic pain, motor disorders, psychopathy, social phobia, depression, emotional disturbances, anxiety, and posttraumatic disorder might be treated with fMRI-BCI.

4.2. Stroke rehabilitation

A potential clinical application of fMRI-BCI is the rehabilitation of the victims of motor disorders. Hemiparesis (paralysis or weakness affecting one side of the body) is a common neurological deficit after stroke (Kato et al. [37]). Recent studies have suggested that the recovery after stroke is facilitated by the reorganization of cortical motor areas in both damaged and nondamaged hemispheres. Despite the potential of recovery, relearning of the movement of the disabled arm does not occur spontaneously. A treatment modality consists of successive reinforcement of the elements of the required behavior to activate the neural network involved in arm movement (Dobkin [38]). This might be achieved by training patients first to learn to reactivate the premotor area, and then in a stepwise fashion the primary motor cortex, basal ganglia, and cerebellum. The reorganization of the brain regions could be assisted with fMRI-BCI. Yoo and Jolesz reported successful modification of motor function in response to real-time fMRI feedback (Yoo and Jolesz [11]). Scharnowski et al. (Scharnowski et al. [39]) trained volunteers to differentially self-regulate SMA and PPA in four sessions, and then tested for effects on reaction times in a bimanual motor task. An increase of activity in the SMA only correlated with a speeded response.

We are exploring a new approach to assist movement restoration in stroke victims using fMRI-BCI. There is evidence for motor recovery and cortical reorganization after stroke when patients undergo treatment involving mental practice and mental imagery (de Vries and Mulder [40]). These results indicate that enhancing neural activity in the motor cortex is bilateral to the lesion (target ROI) while simultaneously inhibiting activity in the motor cortex contralateral (secondary ROI) to the lesion may help in stroke rehabilitation. This means that the fMRI-BCI training should aim to increase activity in the target ROI while maintaining a negative correlation with the activity in the secondary ROI. In order to achieve this, we compute online a feedback value proportional to the product of the negative correlation coefficient of the activation time courses for the specified number of time points (e.g., last 10 time points) of the two ROIs, and the magnitude of the activation in the target ROI. The feedback value computed is presented to the subject as thermometer bars or a dial indicating positive to negative correlation. Subjects can be trained to increase the bars of the thermometer to enhance activation in the ipsilesion area while inhibiting the contralesion area. Our preliminary results with 2 healthy volunteers who were provided feedback of motor imagery have shown that subjects could be trained to enhance activity in the target ROI in counter-correlation with the activity in the contralesion hemisphere. Our future work is aimed at establishing the behavioral effect of this enhanced activity and the suitability of this method for stroke therapy.

4.3. Treating chronic pain

Chronic pain is one of the most frequent clinical problems. Chronic pain can be substantially affected by cognitive and emotional processes (DeCharms et al. [17]). Subregions within rostral ACCr in association with other brain regions are implicated to be involved in the perception of pain. Hence, it is possible that by altering the activity in the rACC, pain perception might be accordingly varied. Indeed, Maeda et al. (Maeda et al. [41]) reported a substantial decrease of symptoms in chronic pain patients by training patients to self-regulate ACC. A further report from the same group (DeCharms et al. [17]), involving 16 healthy volunteers and 12 chronic pain patients, indicates the potential application of real-time fMRI for treating chronic pain. Subjects were able to learn to control activation in the rostral anterior cingulate cortex (rACC), a region involved in pain perception and regulation. The authors reported that if subjects deliberately induced increases or decreases of rACC fMRI activation, there was a corresponding change in the perception of pain caused by an applied noxious thermal stimulus. Control experiments showed that this effect was not observed after training without real-time fMRI feedback, or using feedback from a different region, or sham feedback derived from a different subject. Chronic pain patients were also trained to control activation in rACC and reported decreases in the ongoing level of chronic pain after training.

4.4. Treating emotional disorders

Emotional regulation training for patients suffering from depression, anxiety, posttraumatic disorder, and other emotional disturbances might be another application of fMRI-BCI. Experiments by Caria et al. (Phan et al. [42]) have shown that the emotional system can also be self-regulated. In another study (Posse et al. [12]) subjects were trained to self-regulate their amygdala activation by a strategy of self-induced sadness. Behavioral tests showed that the subjects' emotional ratings correlated with their activity in amygdala, substantiating the earlier findings that amygdala is involved

in negative emotions (Anders et al. [43]). Weiskopf et al., (Weiskopf et al. [13]), Caria et al., (Caria et al. [19]), Veit et al., (Veit et al. [21]) have reported that volitional control of ACC and insula correlated with changes in emotional valence and arousal.

4.5. Psychopathy and social phobia

Criminal psychopathy is a major problem encountered by society. Psychopaths form only 15–30% of prison population, but they commit 50% more crime than nonpsychopaths (Viding [44], Viding [45]). The brain regions and neural mechanisms of the disorder are not well understood. A psychopath is characterized by poverty of affect and lack of shame, superficially charming, manipulative, and shows irresponsible behavior. Previous studies have implicated orbitofrontal cortex, amygdala, anterior insula, anterior parietal cortex and anterior cingulated cortex (Brennan and Raine [46], Blair [47], LeDoux [48]). Our studies (Veit et al. [21], Birbaumer et al. [49]) have shown that a hypoactive frontolimbic circuit may represent the neural correlate of psychopathic behavior, whereas an overactive frontolimbic system may underlie social fear. Increased activation in the emotionally relevant areas such as amygdala, anterior insula, and medial frontal cortex may lead to improved aversive conditioning. A real-time fMRI system for the specific treatment of criminal psychopathy is currently under development. Criminal psychopaths are trained to self-regulate their BOLD activity in localized brain areas implicated in the disorder, such as, anterior insula and amygdala. Behavioral effects of this training are investigated by conducting aversive delay conditioning and other behavioral tests before and after treatment.

5. DISCUSSION

Brain-computer interfaces based on fMRI enable real-time conditioning of circumscribed brain regions to learn volitional control of those regions. This is an emerging field of intense research excitement. Technological advancement in higher field MRI scanners, data acquisition sequences and image reconstruction techniques, preprocessing algorithms to correct for artefacts, more intelligent and robust analysis and interpretation methods, and faster feedback and visualization technology are anticipated to make fMRI-BCI widely available and applicable. Examples of such future developments are z-shimming sequence adapted for fMRI-BCI to correct for magnetic inhomogeneity differences; connectivity analysis, for example, using dynamic causal modelling (Friston et al. [50]) incorporating a whole network of neural activity instead of just one local ROI; support vector and other machine learning and pattern classification approaches (LaConte et al. [51], Mourão-Miranda et al. [52]); independent component analysis (Esposito et al. [53]) for extracting BOLD response of interest; motion compensation (Thesen et al. [54]) for head motion artefact removal; and augmented virtual worlds for more immersive feedback. Anticipated developments in dedicated purpose MRI scanners (such as those of ONI Medical Systems, Inc, Wilmington, Mass, USA) that offer high-field performance at a low-price compared to whole body scanners can make fMRI-BCI applications more user-friendly, affordable and hence widely accessible.

There are certain limitations to the current fMRI-BCIs that future research would have to overcome. Conventional neuroimaging methods seek to find out how a particular perceptual or cognitive state is encoded in brain activity by measuring brain activity from many thousands of locations repeatedly, but then analyzing each location separately (univariate analysis). If the responses at any brain location differ between two states, then it is possible to use measurements of the activity at that location to determine or decode the state. However, it is often difficult to find individual locations where the difference between conditions is large enough to allow for efficient decoding. In contrast to the conventional analysis, recent work shows that neuroimaging may be improved by taking into account the spatial pattern of brain activity (Haynes and Rees [23]). Pattern-based methods use considerably more information for detecting the current state from measurements of brain activity. LaConte et al. (Laconte et al. [24]) have reported probably the first implementation of real-time multivariate classification that could be applied to fMRI-BCI. With such improvements, FMRI-BCI has the potential of establishing itself as a tool for certain types of neuroscientific research and experimentation, and also as an aid for psychophysiological treatment.

ACKNOWLEDGMENTS

This work was supported by grants from the SFB 437 "Kriegserfahrungen" of the Deutsche Forschungsgemeinschaft (DFG), the Marie Curie Host Fellowship for Early Stage Researchers Training, and the National Institute of Health (NIH). The authors are indebted to M. Erband W. Grodd for technical assistance in data acquisition and helpful discussions. They also thank Dr. Roopashree Dwarkanathfor comments on the text.

REFERENCES

[1] N. Birbaumer, N. Ghanayim, T. Hinterberger, et al., "A spelling device for the paralysed," *Nature*, vol. 398, no. 6725, pp. 297–298, 1999.

[2] J. P. Donoghue, "Connecting cortex to machines: recent advances in brain interfaces," *Nature Neuroscience*, vol. 5, pp. 1085–1088, 2002.

[3] J. R. Wolpaw, N. Birbaumer, D. J. McFarland, G. Pfurtscheller, and T. M. Vaughan, "Brain-computer interfaces for communication and control," *Clinical Neurophysiology*, vol. 113, no. 6, pp. 767–791, 2002.

[4] M. A. L. Nicolelis, "Brain-machine interfaces to restore motor function and probe neural circuits," *Nature Reviews Neuroscience*, vol. 4, no. 5, pp. 417–422, 2003.

[5] J. R. Wolpaw and D. J. McFarland, "Control of a two-dimensional movement signal by a noninvasive brain-computer interface in humans," *Proceedings of the National Academy of Sciences of the United States of America*, vol. 101, no. 51, pp. 17849–17854, 2004.

[6] L. R. Hochberg and J. P. Donoghue, "Sensors for brain-computer interfaces: options for turning thought into action," *IEEE Engineering in Medicine and Biology Magazine*, vol. 25, no. 5, pp. 32–38, 2006.

[7] N. Weiskopf, R. Sitaram, O. Josephs, et al., "Real-time functional magnetic resonance imaging: methods and applications," *Magnetic Resonance Imaging*, vol. 25, no. 6, pp. 989–1003, 2007.

[8] A. Caria, R. Veit, R. Sitaram, et al., "Regulation of anterior insular cortex activity using real-time fMRI," *NeuroImage*, vol. 35, no. 3, pp. 1238–1246, 2007.

[9] N. K. Logothetis, J. Pauls, M. Augath, T. Trinath, and A. Oeltermann, "Neurophysiological investigation of the basis of the fMRI signal," *Nature*, vol. 412, no. 6843, pp. 150–157, 2001.

[10] A. Shmuel, M. Augath, A. Oeltermann, and N. K. Logothetis, "Negative functional MRI response correlates with decreases in neuronal activity in monkey visual area V1," *Nature Neuroscience*, vol. 9, no. 4, pp. 569–577, 2006.

[11] S.-S. Yoo and F. A. Jolesz, "Functional MRI for neurofeedback: feasibility study on a hand motor task," *NeuroReport*, vol. 13, no. 11, pp. 1377–1381, 2002.

[12] S. Posse, D. Fitzgerald, K. Gao, et al., "Real-time fMRI of temporolimbic regions detects amygdala activation during single-trial self-induced sadness," *NeuroImage*, vol. 18, no. 3, pp. 760–768, 2003.

[13] N. Weiskopf, R. Veit, M. Erb, et al., "Physiological self-regulation of regional brain activity using real-time functional magnetic resonance imaging (fMRI): methodology and exemplary data," *NeuroImage*, vol. 19, no. 3, pp. 577–586, 2003.

[14] R. C. DeCharms, K. Christoff, G. H. Glover, J. M. Pauly, S. Whitfield, and J. D. E. Gabrieli, "Learned regulation of spatially localized brain activation using real-time fMRI," *NeuroImage*, vol. 21, no. 1, pp. 436–443, 2004.

[15] N. Weiskopf, F. Scharnowski, R. Veit, R. Goebel, N. Birbaumer, and K. Mathiak, "Self-regulation of local brain activity using real-time functional magnetic resonance imaging (fMRI)," *Journal of Physiology*, vol. 98, no. 4–6, pp. 357–373, 2004.

[16] S.-S. Yoo, T. Fairneny, N.-K. Chen, et al., "Brain-computer interface using fMRI: spatial navigation by thoughts," *NeuroReport*, vol. 15, no. 10, pp. 1591–1595, 2004.

[17] R. C. DeCharms, F. Maeda, G. H. Glover, et al., "Control over brain activation and pain learned by using real-time functional MRI," *Proceedings of the National Academy of Sciences of the United States of America*, vol. 102, no. 51, pp. 18626–18631, 2005.

[18] R. Sitaram, A. Caria, R. Veit, T. Gaber, A. Kuebler, and N. Birbaumer, "Real-time fMRI based brain-computer interface enhanced by interactive virtual worlds," in *Proceedings of the 45th Annual Meeting Society for Psychophysiological Research*, Lisbon, Portugal, 2005.

[19] A. Caria, R. Veit, T. Gaber, R. Sitaram, A. Kuebler, and N. Birbaumer, "Can we learn to increase our emotional involvement? real-time fMRI of anterior cingulate cortex during emotional processing," in *Human Brain Mapping*, Florence, Italy, June 2006.

[20] G. Rota, R. Sitaram, R. Veit, N. Weiskopf, N. Birbaumer, and G. Dogil, " fMRI-neurofeedback for operant conditioning and neural plasticity investigation: a study on the physiological self-induced regulation of the BA 45," in *Proceedings of the Cognitive Neuroscience Conference*, San Francisco, Calif, USA, 2006.

[21] R. Veit, H. Flor, M. Erb, et al., "Brain circuits involved in emotional learning in antisocial behavior and social phobia in humans," *Neuroscience Letters*, vol. 328, no. 3, pp. 233–236, 2002.

[22] C. H. Wagner and M. L. Barrett, Published online by PsycExtra, 2004.

[23] J.-D. Haynes and G. Rees, "Decoding mental states from brain activity in humans," *Nature Reviews Neuroscience*, vol. 7, no. 7, pp. 523–534, 2006.

[24] S. M. Laconte, S. J. Peltier, and X. P. Hu, "Real-time fMRI using brain-state classification," in *Human Brain Mapping*, 2006.

[25] R. Goebel, "Cortex-based real-time fMRI," *NeuroImage*, vol. 13, no. 6, p. 129, 2001.

[26] C. T. W. Moonen and P. A. Bandettini, Eds., *Functional MRI*, Springer, Berlin, Germany, 2000.

[27] T. E. Feinberg and M. J. Farah, Eds., *Behavioral Neurology and Neuropsychology*, McGraw-Hill, New York, NY, USA, 2nd edition, 2003.

[28] B. Rockstroh, T. Elbert, N. Birbaumer, and W. Lutzenberger, "Biofeedback-produced hemispheric asymmetry of slow cortical potentials and its behavioural effects," *International Journal of Psychophysiology*, vol. 9, no. 2, pp. 151–165, 1990.

[29] F. Pulvermüller, B. Mohr, H. Schleichert, and R. Veit, "Operant conditioning of left-hemispheric slow cortical potentials and its effect on word processing," *Biological Psychology*, vol. 53, no. 2-3, pp. 177–215, 2000.

[30] T. Egner and J. H. Gruzelier, "Ecological validity of neurofeedback: modulation of slow wave EEG enhances musical performance," *NeuroReport*, vol. 14, no. 9, pp. 1221–1224, 2003.

[31] M. M. Bradley and P. J. Lang, "Measuring emotion: the self-assessment manikin and the semantic differential," *Journal of Behavior Therapy and Experimental Psychiatry*, vol. 25, no. 1, pp. 49–59, 1994.

[32] A. Caria, R. Veit, R. Sitaram, M. Lotze, N. Weiskopf, W. Grodd, and N. Birbaumer, "Regulation of anterior insular cortex activity using real-time fMRI," *Neuroimage*, vol. 35, no. 3, pp. 1238–1246, 2007.

[33] G. Dogil, I. Frese, H. Haider, D. RÖhm, and W. Wokurek, "Where and how does grammatically geared processing take place-and why is broca's area often involved. A coordinated fMRI/ERBP study of language processing," *Brain and Language*, vol. 89, no. 2, pp. 337–345, 2004.

[34] F. Tong, K. Nakayama, J. T. Vaughan, and N. Kanwisher, "Binocular rivalry and visual awareness in human extrastriate cortex," *Neuron*, vol. 21, no. 4, pp. 753–759, 1998.

[35] T. Fuchs, N. Birbaumer, W. Lutzenberger, J. H. Gruzelier, and J. Kaiser, "Neurofeedback treatment for attention-deficit/hyperactivity disorder in children: a comparison with methylphenidate," *Applied Psychophysiology Biofeedback*, vol. 28, no. 1, pp. 1–12, 2003.

[36] B. Kotchoubey, U. Strehl, C. Uhlmann, et al., "Modification of slow cortical potentials in patients with refractory epilepsy: a controlled outcome study," *Epilepsia*, vol. 42, no. 3, pp. 406–416, 2001.

[37] H. Kato, M. Izumiyama, H. Koizumi, A. Takahashi, and Y. Itoyama, "Near-infrared spectroscopic topography as a tool to monitor motor reorganization after hemiparetic stroke: a comparison with functional MRI," *Stroke*, vol. 33, no. 8, pp. 2032–2036, 2002.

[38] B. H. Dobkin, "Functional MRI: a potential physiologic indicator for stroke rehabilitation interventions," *Stroke*, vol. 34, no. 5, pp. e23–e28, 2003.

[39] F. Scharnowski, N. Weiskopf, K. Mathiak, et al., "Self-regulation of the BOLD signal of supplementary motor area (SMA) and parahippocampal place area (PPA): fMRI-neurofeedbackand its behavioural consequences," in *Proceedings of 10th International Conference on Functional Mapping of the Human Brain*, Budapest, Hungary, 2004.

[40] S. de Vries and T. Mulder, "Motor imagery and stroke rehabilitation: a critical discussion," *Journal of Rehabilitation Medicine*, vol. 39, no. 1, pp. 5–13, 2007.

[41] F. Maeda, "Learning to explicitly control activation in a localized brain region through real-time fMRI feedback based training, with result impact on pain perception," in *Proceedings of the Society for Neuroscience*, pp. 601–604, Washington, DC, USA, 2004.

[42] K. L. Phan, D. A. Fitzgerald, K. Gao, G. J. Moore, M. E. Tancer, and S. Posse, "Real-time fMRI of cortico-limbic brain activity during emotional processing," *NeuroReport*, vol. 15, no. 3, pp. 527–532, 2004.

[43] S. Anders, M. Lotze, M. Erb, W. Grodd, and N. Birbaumer, "Brain activity underlying emotional valence and arousal: a response-related fMRI study," *Human Brain Mapping*, vol. 23, no. 4, pp. 200–209, 2004.

[44] E. Viding, "On the nature and nurture of antisocial behavior and violence," *Annals of the New York Academy of Sciences*, vol. 1036, pp. 267–277, 2004.

[45] E. Viding, "Annotation: understanding the development of psychopathy," *Journal of Child Psychology and Psychiatry and Allied Disciplines*, vol. 45, no. 8, pp. 1329–1337, 2004.

[46] P. A. Brennan and A. Raine, "Biosocial bases of antisocial behavior: psychophysiological, neurological, and cognitive factors," *Clinical Psychology Review*, vol. 17, no. 6, pp. 589–604, 1997.

[47] R. J. R. Blair, "Neurobiological basis of psychopathy," *British Journal of Psychiatry*, vol. 182, pp. 5–7, 2003.

[48] J. LeDoux, "The emotional brain, fear, and the amygdala," *Cellular and Molecular Neurobiology*, vol. 23, no. 4-5, pp. 727–738, 2003.

[49] N. Birbaumer, R. Veit, M. Lotze, et al., "Deficient fear conditioning in psychopathy: a functional magnetic resonance imaging study," *Archives of General Psychiatry*, vol. 62, no. 7, pp. 799–805, 2005.

[50] K. J. Friston, L. Harrison, and W. Penny, "Dynamic causal modelling," *NeuroImage*, vol. 19, no. 4, pp. 1273–1302, 2003.

[51] S. LaConte, S. Strother, V. Cherkassky, J. Anderson, and X. Hu, "Support vector machines for temporal classification of block design fMRI data," *NeuroImage*, vol. 26, no. 2, pp. 317–329, 2005.

[52] J. Mourão-Miranda, A. L. W. Bokde, C. Born, H. Hampel, and M. Stetter, "Classifying brain states and determining the discriminating activation patterns: support vector machine on functional MRI data," *NeuroImage*, vol. 28, no. 4, pp. 980–995, 2005.

[53] F. Esposito, E. Seifritz, E. Formisano, et al., "Real-time independent component analysis of fMRI time-series," *NeuroImage*, vol. 20, no. 4, pp. 2209–2224, 2003.

[54] S. Thesen, O. Heid, E. Mueller, and L. R. Schad, "Prospective acquisition correction for head motion with image-based tracking for real-time fMRI," *Magnetic Resonance in Medicine*, vol. 44, no. 3, pp. 457–465, 2000.

Hindawi Publishing Corporation
Computational Intelligence and Neuroscience
Volume 2007, Article ID 56986, 8 pages
doi:10.1155/2007/56986

Research Article

Modern Electrophysiological Methods for Brain-Computer Interfaces

Rolando Grave de Peralta Menendez,[1,2] Quentin Noirhomme,[1] Febo Cincotti,[3] Donatella Mattia,[3] Fabio Aloise,[3] and Sara González Andino[1]

[1] *Electrical Neuroimaging Group, Department of Clinical Neurosciences, Geneva University Hospital, 1211 Geneva, Switzerland*
[2] *Neurodynamics Laboratory, Department of Psychiatry and Clinical Psychobiology, University of Barcelona, 08035 Barcelona, Catalonia, Spain*
[3] *Neurofisiopatologia Clinica, Fondazione Santa Lucia, 00179 Roma, Italy*

Correspondence should be addressed to Rolando Grave de Peralta Menendez, rolando.grave@hcuge.ch

Received 15 February 2007; Revised 6 July 2007; Accepted 18 September 2007

Recommended by Andrzej Cichocki

Modern electrophysiological studies in animals show that the spectrum of neural oscillations encoding relevant information is broader than previously thought and that many diverse areas are engaged for very simple tasks. However, EEG-based brain-computer interfaces (BCI) still employ as control modality relatively slow brain rhythms or features derived from preselected frequencies and scalp locations. Here, we describe the strategy and the algorithms we have developed for the analysis of electrophysiological data and demonstrate their capacity to lead to faster accurate decisions based on linear classifiers. To illustrate this strategy, we analyzed two typical BCI tasks. (1) Mu-rhythm control of a cursor movement by a paraplegic patient. For this data, we show that although the patient received extensive training in mu-rhythm control, valuable information about movement imagination is present on the untrained high-frequency rhythms. This is the first demonstration of the importance of high-frequency rhythms in imagined limb movements. (2) Self-paced finger tapping task in three healthy subjects including the data set used in the BCI-2003 competition. We show that by selecting electrodes and frequency ranges based on their discriminative power, the classification rates can be systematically improved with respect to results published thus far.

1. INTRODUCTION

Development of direct brain-computer interfaces (BCI) is a novel and very interesting field of research, aimed at building an alternative communication channel between men and machines that do not rely on physiological output pathways. EEG-based BCI stems from decades of research on electrophysiological correlates of brain activity. As such, it is mostly based on methods developed for traditional analysis of scalp signals. Such techniques resulted were beneficial in the earliest states of EEG-based BCI and speeded up initial developments. However, when compared with the accelerated progresses achieved with implanted devices, a certain impasse becomes evident [1]. Few attempts have been made to incorporate results obtained in electrophysiological studies in animals within this field. For instance, EEG-based BCI is mostly characterized by the use of regions (i.e., electrodes locations) and frequency bands defined from average evoked potentials (e.g., P300), and thus mainly determined by the EEG low-frequency components [2]. Such a priori preselection of a few electrodes based on results of ERPs is at odds with recent experimental findings showing substantial learning induced modification of neural activity within a single session [3, 4] or the involvement of a distributed brain network in even the simplest motor tasks.

EEG analysis aiming to answer basic neurophysiological questions has benefited from analysis procedures that rely upon the broad spectrum analysis of single trials either based on scalp-recorded signals or noninvasive estimates of local field potentials (eLFPs) [5–7]. Such procedures offer an alternative to traditional electrophysiological analysis using trials averaging and/or single maps (or set of maps) analysis able to unveil new neural mechanisms. The application of these methods to paradigms used for standard ERP analysis

demonstrated that short EEG windows (500 milliseconds) following a single stimulus presentation are enough to identify the category of the visual stimuli and the brain regions involved in their processing [8]. Even shorter time windows (200 milliseconds) were sufficient to predict the laterality of the impending hand responses in simple visuomotor reaction-time tasks [9]. Later study demonstrated the importance of neural oscillations above 100 Hz for the decoding of movement laterality. Parallel studies based on invasive recordings in animals and humans confirmed the importance of such largely unexplored frequency band in movement control [10, 11]. In practice, the use of features derived from the broad band spectral analysis of the signals reduces the importance of the preselected pattern recognition algorithm allowing for implementations based on simpler and faster classifiers.

Previously described procedures have been incorporated in a Matlab-based environment for the analysis of both online (near real-time) and offline EEG data. This platform, dubbed as Geneva Brain-Computer Interface (GBCI), contains the novel methods proposed for the analysis of single trials, based on broad spectrum exploration of the EEG or ELFPs derived from it, that is, based on sound electrophysiological and biophysical information together with simple and fast classification algorithms.

In this paper, we illustrate the application of these principles to three different data sets. The first data set consisted in EEG recordings from a paraplegic patient suffering from complete traumatic spinal cord injury. In the experiment, the patient attempts to control the movement of a cursor on the screen through imagined movements of the limbs and self control of the mu-rhythm. The second and the third data sets correspond to EEG data recorded from healthy subjects performing a self-paced finger tapping task. The second data set (two subjects) was recorded at our lab and the third data set is a courtesy of Blankertz and colleagues [12, 13]. Latest data set constitutes a good reference to evaluate the advantages of the proposed procedures since it has been analyzed by many different groups on the framework of the BCI competition 2003 [13].

2. MATERIAL AND METHODS

2.1. Data recording

The first data set (referred from now on as MI) was acquired from a subject (male, 42 years old, suffering from paraplegia due to complete traumatic spinal cord injury at level of T10. EEG signals were collected by 61 sintered-silver electrodes mounted on a cap according to the extended 10–20 system, amplified and digitized at 1000 samples per second (BrainAmp, Brain Products GmbH, Gilching, Germany). The subject seated relaxed at his own wheelchair while performing the experiment. The task consisted in moving a cursor towards a target as soon as the latter appeared on any of the four sides of the screen. The instructions received at the beginning of the training in order to move the cursor were to concentrate on kinesthetic imagination of movement of his hands (cursor up), his feet (cursor down), his right or left hand (cursor right or left, resp.). At the time of recording, the subject had automated control of his mu-rhythm, thus he reported that he only sporadically had to imagine movements. Nevertheless, during acquisition, the experimenter made sure that no overt limb movement was present and that EEG potentials were not contaminated by EMG or EOG. In addition, EEG recordings were reviewed offline by an expert electroencephalographer to remove epochs contaminated by EOG and EMG artifacts. EMG and EOG control was based on the monitoring of all border (e.g., T7, O1) and frontopolar channels, respectively.

Only correct trials of the (two) classes composed by right and left cursor movements linked to lateralization of the mu-rhythm were analyzed. The data set was acquired in four sessions recorded in different days, and consisted of about 240 trials (120 for each class, resp.). Each trial, starting at target appearance, ended when the cursor either hit the target (correct) or moved to the wrong side of the screen (incorrect). Trial duration ranged between 2 to 10 seconds. We here restrict the analysis to the one second window starting one second after target appearance.

The second data set (referred from now on as ENG) corresponds to two different subjects (ENG1 and ENG2) performing a self-paced finger tapping paradigm identical to the one used for the BCI-2003 competition (see below). EEG was recorded from 64 electrodes disposed in standard (10/10) system using a sampling frequency of 512 Hz. A total of 240 epochs (120 for each hand) of 500 milliseconds were selected for analysis per subject. To avoid EMG contamination, epochs ended 146 milliseconds before key press.

The third EEG data set (referred from now on as BCI) is the self-paced finger task of the BCI-2003 competition [12]. It was recorded from a healthy subject seated in a normal chair, relaxed arms resting on the table, and fingers in the standard typing position at the computer keyboard. The task was to press keys with either the index or the little finger of either the left or the right hand in self-chosen order and timing. A total of 416 epochs of 500 milliseconds were selected for analysis. To avoid EMG contamination, epochs ended 130 milliseconds before key press. The training set was composed by 316 epochs randomly selected and the remaining 100 epochs were used as the test set. Twenty eight electrodes disposed in standard (10/20) system were used for the EEG recording at 1000 Hz.

2.2. Feature extraction

Practical experience on EEG-based BCI indicates that subjects can learn to control specific frequency rhythms as to provide control of neuroprosthetic devices [14–17]. Nonetheless, electrophysiological recordings in animals show that oscillatory activity at frequency bands hardly explored on human EEG encode relevant neurophysiological information [18]. Indeed, very high-frequency oscillation above 100 Hz, sometimes called epsilon oscillations [19], correlate with motor intentions [9]. We therefore use as feasible physiological features all frequency oscillations identified from the power spectral density (PSD) of the EEG. To select from the whole PSD the range of oscillations and sensors that better

encode the mental commands specific to each task, we use a mathematical algorithm (the Discriminative Power) described below (see Section 3.3).

We computed the PSD using modern multitaper methods [20]. These methods have shown to be particularly well suited for spectral analysis of short segments of noisy data, and have been successfully applied to the analysis of neuronal recordings in behaving animals [21]. Specifically, the PSD was estimated using 7 Slepian data tapers to reduce the variance. Each EEG window was multiplied by eachof the tapers, and the Fourier componentswere then computed via Fast Fourier Transform (FFT). The power spectral density was then computed by taking square of the modulus of the FFT from 0 to Nyquist frequency (i.e., half of the frequency sampling).

2.3. Feature selection

Features were selected on the basis of their Discriminative power (DP) [19]. This measure provides an estimate of the percentage of true positives that can be obtained classifying with each single feature given that the number of false positive is set to zero. By definition, the DP does not consider interaction between features and might be affected by extreme values (outliers). However, in practice, these outliers are very unlikely. If outliers are indeed present, they can be identified and removed by simple exploration of the training or learning set.

To compute the DP, we denote by a (b) the feature vector for class A (B), that is, a vector formed by the feature values over all trials in class A (B). By swapping vectors a and b, we can always assume that $a_{\min}$ = {minimum of a} $\leq$ $b_{\min}$ = {minimum of b}. If $b_{\max}$ ={maximum of b} $\leq$ $a_{\max}$ = {maximum of a} (i.e., one condition contains the other), then DP = 0; otherwise,

$$\mathrm{DP} = \frac{\mathrm{card}\{a < b_{\min}\} + \mathrm{card}\{b > a_{\max}\}}{\mathrm{card}\{a\} + \mathrm{card}\{b\}} * 100, \qquad (1)$$

where card $\{\cdot\}$ stands for the number of elements in a set.

Given the matrix composed by the DP for all sensors and frequencies, we define the set of the best N features as the highest N entries of this matrix. Plotting the maximum DP for each column (i.e., all sensors confounded) as a function of the column index (frequency) yields a very informative plot summarizing the behavior of each frequency over the whole electrode space (see Figures 1, 2, 3, and 4).

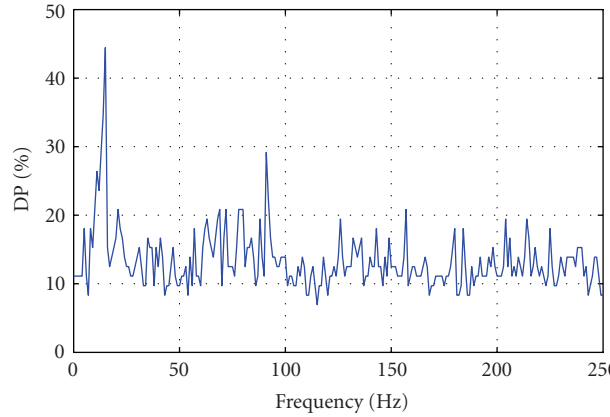

Figure 1: Discriminative power (DP) versus frequency for the MI data set (paraplegic patient). The panel represents the plot of maximum DP (best discrimination between left and right cursor movements) as a function of frequency. Although the trained mu-rhythm provides the best discrimination in this patient, significant contribution to the discrimination (higher than 20% of trials) is observed for very fast frequency oscillation (peaks at 69, 72, 78–80, 91, and 157 Hz).

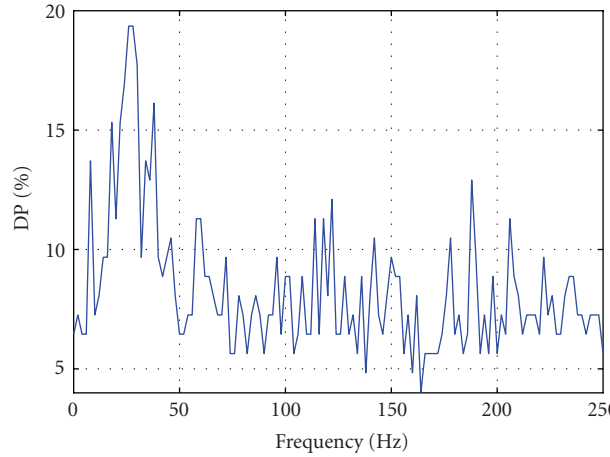

Figure 2: Discriminative power (DP) versus frequency for the ENG1 data set. The panel represents the plot of maximum DP (best discrimination between left and right finger tappings) as a function of frequency. Peaks (DP >12) are seen at alpha, beta, and gamma bands but also for very high-frequency bands (122 and 188 Hz).

2.4. Support vector machine classifiers

For the sake of simplicity and speed, we used a linear classifier: the linear proximal support vector machine (PSVM) developed and implemented in [22]. As described by Mangasarian and Wild [23], " ... a standard support vector machine with a linear classifier, is given by a plane midway between two parallel bounding planes that bound two disjoint half spaces each containing points mostly of class 1 or 2. In another somewhat less standard approach, the proximal support vector classification, two parallel planes are generated such that each plane is closest to one of two data sets to be classified and such that the two planes are as far apart as possible. The classifying plane is again midway between the parallel proximal planes." Since these planes are determined by the unconstrained minimization of a quadratic function, the PSVM formulation leads to a very fast and efficient algorithm.

2.5. Crossvalidation procedure

The performance was evaluated with a 10-fold crossvalidation method where the data set is divided into ten subsets. Each subset is used once as test set while the complementary

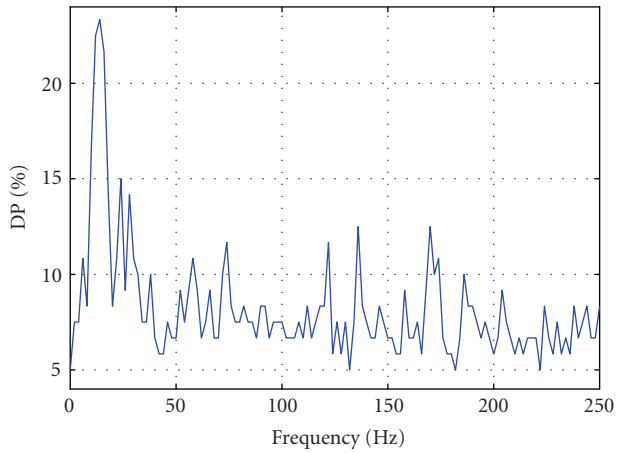

Figure 3: Discriminative power (DP) versus frequency for the ENG2 data set. The panel represents the plot of maximum DP (best discrimination between left and right finger tappings) as a function of frequency. Peaks (DP > 12) are observed at classical frequency bands (alpha and beta) as well as epsilon oscillations (136 Hz and 170 Hz).

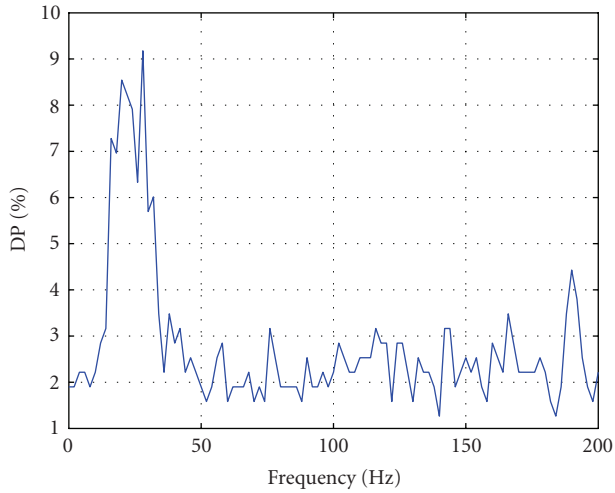

Figure 4: Discriminative power (DP) versus frequency for the BCI data set (BCI 2003). The panel represents the plot of maximum DP (best discrimination between left and right finger tapping) as a function of frequency. Discrimination is maximal over the beta/low gamma band with little discrimination for the ultra-fast frequency oscillations.

nine subsets are used as training sets to select the features and compute the classifier. Consequently, every data point (i.e., trial) is a member of the test set only once and a member of the training set nine times.

The correct classification (CC in %) rates reported here indicate the percentage of trials on the test set correctly assigned to its original class by the classifier. Unless otherwise specified, it corresponds to the CC value averaged over the 10 folds.

3. RESULTS

3.1. Results for MI data: mu-rhythm lateralization

Our goal in the analysis of this data set was to explore the possible role of high-frequency rhythms in a task where the subject has received training on mu-rhythm control. We considered two different strategies of analysis. First, to evaluate the generalization of the model independent of the recording session, we pooled the data from the four experimental sessions into one single data set.

Figure 1 shows a typical distribution of the maximum (over electrodes) DP values observed as a function of frequency on the training set. Significant contribution is observed all over the frequency axis with main peaks (higher than 20%) at 11–15, 69, 72, 78–80, 91, and 157 Hz.

The proportion of correct classification (CC%) for each fold was 75, 79, 83, 87, 87, 91, 83, 75, 83, and 75 with an average CC value of 82%. The differences observed between folds (from 75 to 91) suggest that the features and the classifier of a randomly selected part of the data might not be good enough to describe the full variability of the underlying process. Changes on the internal state of the subject such as motivation, attention, or switches on strategy between sessions might explain such results.

To further evaluate this aspect, we carried out a second analysis where each session was submitted separately to a 10-fold crossvalidation. The 10-fold averaged CC% results for the four sessions were 73, 86, 81, and 73, suggesting that the strategy used is not equally efficient for all sessions or that in addition the data is not homogeneous from session to session. Nevertheless, comparison with previous analysis suggests that a global model with features derived from all sessions together is more efficient than separate models for each session. More importantly, the DP plot in Figure 1 shows the importance of high frequencies for differentiating between conditions and should be then considered on any model of this data.

3.2. Results for ENG data: self-paced finger tapping

Through the analysis of this data set, we would like to illustrate the strategy and methods described before that rely on the single assumption that the EEG oscillatory activity contains the information needed to correctly classify the single trials into one of the two classes. Following the precept that scalp locations and frequencies should be selected on the basis of their capability to discriminate between classes, we computed for each electrode and each single trial the PSD as described in Section 2.2 and applied the 10-fold crossvalidation procedure described in Section 2.5

Figures 2 and 3 show typical distributions of the maximum (over electrodes) DP as a function of frequency for subjects ENG1 and ENG2, respectively. These are the results obtained over the training set. Significant contribution is observed at low (<50 Hz) and very high (>150 Hz) frequencies.

A discussion about the best approaches to select the optimal number of features is out of the scope of this paper that basically aims to stress the importance of minimizing

Table 1

Number of features	CC% for ENG1	CC% for ENG2
50	74	79
80	78	81
100	79	80
150	77	82

assumptions when exploring the encoding value of EEG oscillatory activity. Thus, for the sake of simplicity, and just as a matter of example, we present in Table 1 the crossvalidation result (CC%) for some predefined number of features for both subjects.

By selecting the number of features from this table, we can obtain classification values comparable with or better than most (13 out of 15) results submitted to the BCI-2003 competition [13] for a similar task. A direct comparison using the data set included in the competition is presented in next section.

3.3. Results for BCI data: self-paced finger tapping

Based on the definition given by the organizers of the competition, we used the training set to compute the DP for all frequencies and all electrodes. The maximum DP over the electrodes as a function of the frequency is depicted in Figure 4. Surprisingly, the discriminative power maxima were observed for frequencies below 40 Hz although the frequency sampling of the data set was 1000 Hz. The differences with subjects ENG1 and ENG2 (see Figures 2 and 3) in terms of both frequencies and DP values are striking. As obvious from the plot, the features selected with the DP measure belong to the low frequencies 0–40 Hz for this subject. The DP selected the higher entries from the DP matrix composed by the 28 electrodes (rows) and the 40 frequencies (columns). To select the number of features, we explored the classification results on the training set as a function of the number of features.

Figure 5 depicts the percentage (%) of correct classification (CC) on the training set and the test set as a function of the number of features. To be compatible with the information available at the time of the competition, we selected the number of features based only on the training set. For the number of features [10, 20, 40, 60, 70, 80, 100, 120, 150, 180, 200], we obtained CC values of [64, 68, 72, 81, 80, 83, 84, 86, 88, 89, 89], respectively. The final number of features was selected as 180, corresponding to the value where the CC first stabilizes (reaches a plateau) at a value of 89%. Note that, as happens with linear interpolation procedures, the CC might still increase with the number of features and attain a new plateau for a higher number of features. Nonetheless, for this number of features, the CC is 87% for the test set outperforming the best results obtained thus far for this data (i.e., best results are marked as a horizontal dotted line in Figure 5). The plot of the CC for the test set indicates that there are better solutions using only 60 or 70 features. At these points, performance on the test set attains 88% and 89%, respectively.

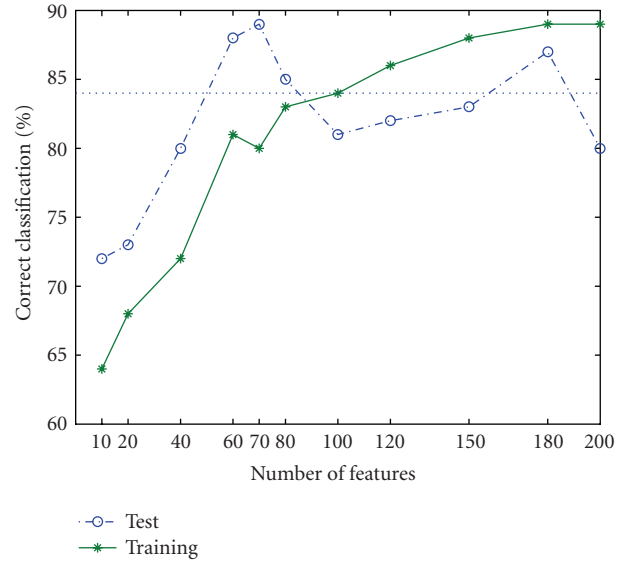

Figure 5: Selecting the number of features for the BCI data set. The picture depicts the percentage (%) of correct classification (CC) on the training set (continuous trace) and the test set (discontinuous trace) as a function of the number of features. The number of features (180) is defined as the beginning of the first plateau, that is, where increasing the number of features does not increase CC on the training set.

4. DISCUSSION AND CONCLUSIONS

The most impressive results obtained thus far in the brain control of neuroprosthetic devices have been probably those based on highly invasive recordings of action potentials within the motor cortex of monkeys [24]. In this study, Chapin et al. [24] demonstrated accurate control of a robotic arm through the decoding of the information contained on the spike trains. However, the tradeoff invasiveness/benefits of invasive approaches remains to be evaluated in practice. At this stage, noninvasive control modalities might offer a safer and cheaper alternative for patients. Of substantial interest for the community of researchers dealing with noninvasive BCI such as the EEG is the finding that very high-frequency oscillations are significantly correlated to the tuning of simultaneously recorded single units. This would imply that while synaptic activity will mainly contribute to the EEG lower frequencies [25], the EEG epsilon oscillations might contain significant power from action potentials. This finding is not exclusive to the motor cortex but seems to hold true for the inferotemporal cortex as well [26]. This finding is highly promissory since recent theoretical [27] as well as experimental studies [9, 28, 29] provide evidences that such very high-frequency oscillations are readily observable by scalp EEG recordings. This would imply that scalp EEG might constitute a more accurate BCI control modality than previously thought. To take practical advantage of these developments, we have to develop the analysis techniques that

are able to separate such weak signals from the background noise and the algorithms required to readily interpret the mental commands from these signals. Importantly, very fast rhythms develop over short temporal windows and appear to constitute a crucial element for ultra-fast synaptic transmission [30]. Later finding would imply that the analysis windows required to detect low frequency (e.g., ≤ 40 Hz) cortical potentials might be replaced by shorter temporal windows needed for high frequencies (e.g., 150 Hz). This could increase the efficiency of noninvasive BCI systems.

In this paper, we have described how simple analysis techniques can be exploited to face the new challenges introduced by the need to analyze such broad band signals to extract their more informative features on individual basis. We used the multitaper spectral method as a way to provide more robust spectral estimates. This was combined with the Discriminative power measure which is enormously simple and still provides substantial information about the rhythms that better differentiate between the studied classes. Importantly, such feature selection alternatives can be entered into a linear classifier to fulfill the requirements of real-time control of neuroprosthetic devices.

The analysis of the finger tapping task data from the two subjects (ENG data) confirms the presence and the importance of high frequencies on the EEG. While the higher discrimination is observed for relatively low-frequency ranges (<50 Hz), the presence of peaks for gamma and epsilon (>100 Hz) frequency ranges is systematic. We hypothesize that it is the complementary character of the high and low frequencies that allow for good classification results using so simple procedures (i.e., linear classifiers). Nevertheless, further analyses are needed to confirm this conjecture.

On the light of the experimental results described above, the DP results obtained for the BCI-2003 finger tapping task are slightly surprising. Rhythms providing the best differentiation between tapping hands were limited to frequencies below 40 Hz. This is in clear contradiction with evidence from direct intracortical recordings in epileptic patients which indicate that the encoding of different motor actions might involve rhythms up to 180 Hz [31]. Similar conclusions have been obtained in monkey studies that demonstrate significant cosine tuning of very fast oscillations in both 2D and 3D center-out reaching tasks [10]. The DP plots of Figure 4 are also at odds with the results shown on Figures 2 and 3. In general, the DP values observed in this subject were lower than the ones we obtained for the ENG data and with a remarkably flat DP profile, that is, the DP was very similar for all frequencies with DP differences rarely surpassing 2%.

Despite the lack of oscillatory activity over 40 Hz, we obtained for this data set a correct classification rate of 87%. This rate constitutes a slight improvement in performance when compared with rates previously achieved for the same data set. The improvement is however noticeable if one considers the simplicity of the procedures employed for feature selection and the fact that results are based on very simple and fast (linear) classifiers.

The BCI data discussed here has been analyzed by several authors. The best rate obtained in the competition was 84% [13]. Posterior attempts [32] failed to improve these results despite combining source localization algorithms and more complex tools than the ones employed here. One possible explanation is the use of cumbersome preprocessing algorithms (spatial filtering, region of interests, etc.) aiming to substitute the classifier. Note that such preprocessing steps are likely to imply a heavier computational load than the simple linear classifier used here. A second aspect likely to influence their results is the selection of an inverse solution which is extremely sensitive to noise. According to our previous experience with inverse solutions, a sound regularization strategy is required to achieve good classification results on short single trials analysis windows [8, 33]. Nevertheless, we have observed that for the case of simple tasks like finger tapping or error-related negativity, resorting to inverse solutions is not needed since the scalp EEG contains all the information required for categorization of the single trials. The use of an inverse solution adds little information while introducing unnecessary computational load. This is probably why the classification rates in this study go beyond the results of Congedo et al. [32].

In the case of the paraplegic patients, we observed better classification accuracy when features were selected from the pooling of sessions. However, classification rates were not considerably reduced when features and classifier were computed for each session separately. While the most discriminative oscillations were observed within the mu-band that the subject has been trained to control, substantial discrimination was observed for the fast (gamma) and ultra-fast (above 100 Hz) rhythms. Considering the purported relationship observed between such oscillations and action potentials, we could interpret this result as an evidence of sustained action potential activity in the presence of imagined limb movements. In any case, these results show that training a given rhythm does not suppress the importance of self-generated oscillatory activity for the performance of imagined movements. To our knowledge, this is the first evidence of modulation of ultra-fast rhythms during imagined limb movements in a paraplegic patient.

This study illustrates that EEG-based BCI systems might considerably benefit from the experience gathered from animal electrophysiology. Rather than increasing the computational burden, broad band spectral analysis and individualized feature selection facilitate the use of simpler feature selection algorithms and linear classifiers. The observed modulation of ultra-fast frequency of oscillations in the paraplegic patient paves the way for studies aiming to clarify the functional role of these rhythms. If the relationship between single-unit activity and ultra-fast oscillations is confirmed, we might be able to provide a faster and finer control of neuroprosthetic devices in the future using noninvasive modalities.

ACKNOWLEDGMENTS

This work has been supported by the Swiss National Science Foundation Grant IM2.MI on brain-machines interfaces and the European IST Program FET Projects FP6-003758 (MAIA) and FP6-IST-027140 (BACS). This paper only reflects the authors' views and funding agencies are

not liable for any use that may be made of the information contained herein. We acknowledge the contribution of two anonymous reviewers for their constructive comments and suggestions.

REFERENCES

[1] M. A. Lebedev and M. A. L. Nicolelis, "Brain-machine interfaces: past, present and future," *Trends in Neurosciences*, vol. 29, no. 9, pp. 536–546, 2006.

[2] J. R. Wolpaw, N. Birbaumer, D. J. McFarland, G. Pfurtscheller, and T. M. Vaughan, "Brain-computer interfaces for communication and control," *Clinical Neurophysiology*, vol. 113, no. 6, pp. 767–791, 2002.

[3] J. N. Sanes and J. P. Donoghue, "Plasticity and primary motor cortex," *Annual Review of Neuroscience*, vol. 23, pp. 393–415, 2000.

[4] M. Graziano, "The organization of behavioral repertoire in motor cortex," *Annual Review of Neuroscience*, vol. 29, pp. 105–134, 2006.

[5] S. L. González Andino, M. M. Murray, J. J. Foxe, and R. Grave de Peralta Menendez, "How single-trial electrical neuroimaging contributes to multisensory research," *Experimental Brain Research*, vol. 166, no. 3-4, pp. 298–304, 2005.

[6] R. Grave de Peralta Menendez, S. González Andino, L. Perez, P. W. Ferrez, and J. D. R. Millán, "Non-invasive estimation of local field potentials for neuroprosthesis control," *Cognitive Processing*, vol. 6, no. 1, pp. 59–64, 2005.

[7] S. L. González Andino, C. M. Michel, G. Thut, T. Landis, and R. Grave de Peralta Menendez, "Prediction of response speed by anticipatory high-frequency (gamma band) oscillations in the human brain," *Human Brain Mapping*, vol. 24, no. 1, pp. 50–58, 2005.

[8] S. L. González Andino, R. Grave de Peralta Menendez, A. Khateb, A. J. Pegna, G. Thut, and T. Landis, "A glimpse into your vision," *Human Brain Mapping*, vol. 28, no. 7, pp. 614–624, 2006.

[9] S. L. Gonzalez, R. Grave de Peralta Menendez, G. Thut, J. D. R. Millán, P. Morier, and T. Landis, "Very high frequency oscillations (VHFO) as a predictor of movement intentions," *NeuroImage*, vol. 32, no. 1, pp. 170–179, 2006.

[10] J. Rickert, S. Cardoso de Oliveira, E. Vaadia, A. Aertsen, S. Rotter, and G. Mehring, "Encoding of movement direction in different frequency ranges of motor cortical local field potentials," *Journal of Neuroscience*, vol. 25, no. 39, pp. 8815–8824, 2005.

[11] E. C. Leuthardt, K. J. Miller, G. Schalk, R. P. N. Rao, and J. G. Ojemann, "Electrocorticography-based brain computer interface—the seattle experience," *IEEE Transactions on Neural Systems and Rehabilitation Engineering*, vol. 14, no. 2, pp. 194–198, 2006.

[12] B. Blankertz, G. Dornhege, C. Schäfer, et al., "Boosting bit rates and error detection for the classification of fast-paced motor commands based on single-trial EEG analysis," *IEEE Transactions on Neural Systems and Rehabilitation Engineering*, vol. 11, no. 2, pp. 127–131, 2003.

[13] B. Blankertz, K.-R. Müller, G. Curio, et al., "The BCI competition 2003: progress and perspectives in detection and discrimination of EEG single trials," *IEEE Transactions on Biomedical Engineering*, vol. 51, no. 6, pp. 1044–1051, 2004.

[14] J. R. Wolpaw and D. J. McFarland, "Control of a two-dimensional movement signal by a noninvasive brain-computer interface in humans," *Proceedings of the National Academy of Sciences of the United States of America*, vol. 101, no. 51, pp. 17849–17854, 2004.

[15] J. D. R. Millán, M. Franzé, J. Mouriño, F. Cincotti, and F. Babiloni, "Relevant EEG features for the classification of spontaneous motor-related tasks," *Biological Cybernetics*, vol. 86, no. 2, pp. 89–95, 2002.

[16] J. D. R. Millán, F. Renkens, J. Mouriño, and W. Gerstner, "Noninvasive brain-actuated control of a mobile robot by human EEG," *IEEE Transactions on Biomedical Engineering*, vol. 51, no. 6, pp. 1026–1033, 2004.

[17] N. Birbaumer, A. Kubler, N. Ghanayim, et al., "The thought translation device (TTD) for completely paralyzed patients," *IEEE Transactions on Rehabilitation Engineering*, vol. 8, no. 2, pp. 190–193, 2000.

[18] A. Bragin, J. Engel Jr., C. L. Wilson, I. Fried, and G. Buzsáki, "High-frequency oscillations in human brain," *Hippocampus*, vol. 9, no. 2, pp. 137–142, 1999.

[19] W. J. Freeman, "Definitions of state variables and state space for brain-computer interface—part 1: multiple hierarchical levels of brain function," *Cognitive Neurodynamics*, vol. 1, no. 1, pp. 3–14, 2007.

[20] D. J. Thomson, "Spectrum estimation and harmonic analysis," *Proceedings of the IEEE*, vol. 70, no. 9, pp. 1055–1096, 1982.

[21] B. Pesaran, J. S. Pezaris, M. Sahani, P. P. Mitra, and R. A. Andersen, "Temporal structure in neuronal activity during working memory in macaque parietal cortex," *Nature Neuroscience*, vol. 5, no. 8, pp. 805–811, 2002.

[22] G. Fung and O. L. Mangasarian, "Proximal support vector machine classifiers," in *Proceedings of the 7th ACM SIGKDD International Conference on Knowledge Discovery and Data Mining (KDD '01)*, pp. 77–86, San Francisco, Calif, USA, August 2001.

[23] O. L. Mangasarian and E. W. Wild, "Multisurface proximal support vector machine classification via generalized eigenvalues," *IEEE Transactions on Pattern Analysis and Machine Intelligence*, vol. 28, no. 1, pp. 69–74, 2006.

[24] J. K. Chapin, K. A. Moxon, R. S. Markowitz, and M. A. L. Nicolelis, "Real-time control of a robot arm using simultaneously recorded neurons in the motor cortex," *Nature Neuroscience*, vol. 2, no. 7, pp. 664–670, 1999.

[25] A. B. Schwartz, X. T. Cui, D. J. Weber, and D. W. Moran, "Brain-controlled interfaces: movement restoration with neural prosthetics," *Neuron*, vol. 52, no. 1, pp. 205–220, 2006.

[26] G. Kreiman, C. P. Hung, A. Kraskov, R. Q. Quiroga, T. Poggio, and J. J. DiCarlo, "Object selectivity of local field potentials and spikes in the macaque inferior temporal cortex," *Neuron*, vol. 49, no. 3, pp. 433–445, 2006.

[27] S. Murakami and Y. Okada, "Contributions of principal neocortical neurons to magnetoencephalography and electroencephalography signals," *Journal of Physiology*, vol. 575, no. 3, pp. 925–936, 2006.

[28] S. N. Baker, G. Curio, and R. N. Lemon, "EEG oscillations at 600 Hz are macroscopic markers for cortical spike bursts," *Journal of Physiology*, vol. 550, no. 2, pp. 529–534, 2003.

[29] G. Curio, "Linking 600 Hz "spikelike" EEG/MEG wavelets ('σ-bursts') to cellular substrates: concepts and caveats," *Journal of Clinical Neurophysiology*, vol. 17, no. 4, pp. 377–396, 2000.

[30] D. Schmitz, S. Schuchmann, A. Fisahn, et al., "Axo-axonal coupling: a novel mechanism for ultrafast neuronal communication," *Neuron*, vol. 31, no. 5, pp. 831–840, 2001.

[31] E. C. Leuthardt, G. Schalk, J. R. Wolpaw, J. G. Ojemann, and D. W. Moran, "A brain-computer interface using electrocorticographic signals in humans," *Journal of Neural Engineering*, vol. 1, no. 2, pp. 63–71, 2004.

[32] M. Congedo, F. Lotte, and A. Lécuyer, "Classification of movement intention by spatially filtered electromagnetic inverse solutions," *Physics in Medicine and Biology*, vol. 51, no. 8, pp. 1971–1989, 2006.

[33] R. G. Grave de Peralta Menendez, S. González Andino, L. Perez, P. W. Ferrez, and J. D. R. Millán, "Non-invasive estimation of local field potentials for neuroprosthesis control," *Cognitive Processing*, vol. 6, no. 1, pp. 59–64, 2005.

Hindawi Publishing Corporation
Computational Intelligence and Neuroscience
Volume 2007, Article ID 57180, 11 pages
doi:10.1155/2007/57180

Research Article

Classifying EEG for Brain-Computer Interface: Learning Optimal Filters for Dynamical System Features

Le Song[1] and Julien Epps[2]

[1] *School of Information Technologies, The University of Sydney, N.S.W. 2006, Australia*
[2] *National ICT Australia, Locked Bag 9013 Alexandria, N.S.W. 1435, Australia*

Correspondence should be addressed to Le Song, lesong@it.usyd.edu.au

Received 19 February 2007; Accepted 27 May 2007

Recommended by Andrzej Cichocki

Classification of multichannel EEG recordings during motor imagination has been exploited successfully for brain-computer interfaces (BCI). In this paper, we consider EEG signals as the outputs of a networked dynamical system (the cortex), and exploit synchronization features from the dynamical system for classification. Herein, we also propose a new framework for learning optimal filters automatically from the data, by employing a Fisher ratio criterion. Experimental evaluations comparing the proposed dynamical system features with the CSP and the AR features reveal their competitive performance during classification. Results also show the benefits of employing the spatial and the temporal filters optimized using the proposed learning approach.

1. INTRODUCTION

A brain-computer interface (BCI) is a communication system that relies on the brain rather than the body for control and feedback [1]. Ideally, it should run in a servo mode, allowing the subjects to initiate the communication anytime and anywhere without resorting to external stimuli or triggers. Such an interface not only offers a promising prosthetic device for those severely paralyzed, but also signifies a radically new technology for the general public. Current BCI research is still in its early stage and the emphasis is placed on the design of algorithms to decode a prespecified set of brain states. This involves three main aspects.

Brain states

Only brain states consciously controllable by the subjects are suitable for BCI. Besides, these states should generate distinct, repeatable, and measurable patterns whenever accessed. Among the most commonly used brain states are imaginations of body movements (motor imaginations). Motor imaginations can reliably change the neural activities over sensorimotor cortices. Depending on the part of the body imagined moving, these changes exhibit distinct spatial distributions [2]. Recognition of these patterns can then be translated into control signals, as is the case in this study.

Recording devices

Motor imaginations can be recorded by both electroencephalography (EEG) and magnetoencephalography (MEG). EEG remains the most popular way to record BCI signals and will be the focus of this study. It measures scalp electrical activities diffused from the cortex. Compared to MEG, it is portable and inexpensive. However, EEG can only measure blurred cortical activities due to the diffusion of the skull and the skin. Thus, EEG is normally used for studying cortical patches in the centimeter scale. Furthermore, EEG signals are contaminated by noise from various sources, such as muscle activities and power line interference. Spatial and temporal filters are commonly applied before any further analysis [3, 4].

Decoding algorithms

Prefiltered EEG signals still contain considerable noise, which poses a challenge for its decoding. Statistical machine learning (ML) techniques have been introduced into BCI to combat these variations. Techniques like artificial neural networks, support vector machine (SVM) [5], and Linear Discriminant Analysis [4] have been employed to learn patterns from training EEG signals and then classify new EEG signals. This strategy often results in increased decoding success and

significant shortening of subject training time (from several months down to several days). The most prominent examples include the Berlin BCI [4], the MPI BCI [6], and the Graz BCI [7].

Apart from the classifiers, these ML-based BCIs also differ in the features they extract from EEG signals. The most successfully used features include autoregressive (AR) coefficients [6, 8] and common spatial patterns (CSP) [4, 7]. In this paper, we will employ a novel type of feature based explicitly on the neurophysiology of EEG signals instead. Basically, we consider EEG signals as the outputs of a networked dynamical system. The nodes of this system consist of cortical patches, while the links correspond to neural fibers. A large and complex system like this often generates interesting collective dynamics, such as synchronization in the activities of the nodes, and they result in the change of EEG patterns measured on the scalp. These features from the collective dynamics of the system can be employed for classification [9, 10]. This will be elaborated in Section 2.

To recover the cortical dynamics from the EEG signals, subject-specific spatial and temporal filtering is usually needed [4, 11]. Instead of manually tuning these filters, we propose a common framework in Section 3 to learn them from the data. Our basic idea is to optimize the filters so that the separability of the two classes is improved. Experimental results show that the learned filters not only reduce the classification errors of the dynamical system (DS) features, but also extract physically meaningful information from the EEG signals. Comparisons are also made between the DS features with the learned filters and the CSP and the AR features with manually tuned filters. These comparisons together with further comparisons to other filter learning methods, such as the CSSP [12] and CSSSP [4] methods, demonstrate the competitive performance of our method (Section 4). Finally, the conclusion is given in Section 6.

2. DYNAMICAL SYSTEM FEATURES

The cortex is a highly folded sheet of neurons (≈100 billion neurons) and they self-organize into clusters. These neuronal clusters not only tightly connect with their neighbors, but also communicate with distal clusters through neural fibers. Each cluster is often associated with certain aspect of information processing. The collaboration of these clusters achieves the normal functioning of the brain. In this section, we will first describe a simple mathematical model of the cortex, and then show how it leads to dynamical system features related to motor imaginations.

2.1. Mathematical model of the cortex

Typically, a neuronal cluster will generate electrical oscillations. It has been modeled as an oscillator with phase θ and output s. Its dynamics are governed by a simple phase model [13]:

$$\begin{aligned} s &= f(\theta), \\ \dot{\theta} &= \omega + g(t), \end{aligned} \tag{1}$$

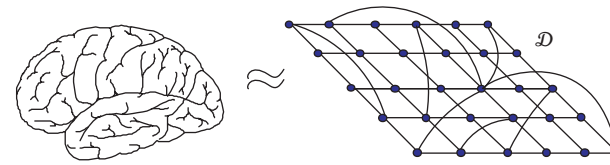

Figure 1: Networked dynamical system model of the cortex.

where ω is the intrinsic frequency of the oscillation and f is a function 2π-periodic in θ. $g(t)$ is the input to the oscillator. $g(t)$ will accelerate the oscillation if it assumes positive values, and slow it down if negative.

The whole cortex can then be modeled as a networked dynamical system $\mathcal{D}$, as shown in Figure 1. Each node in the system represents a neuronal cluster and each link a neural interaction. The input, $g(t)$, to each neuronal cluster now consists of two parts: influence from other clusters and modulation by subcortical structures [2]. Suppose that the links of the network are represented as an adjacency matrix $\mathbf{G}$ ($\mathbf{G}_{ij} = 1$ if node i and j are connected; $\mathbf{G}_{ij} = 0$ otherwise). Then, the dynamics of a node i take a more specific form:

$$\dot{\theta}_i = \omega_i + \sum_j \epsilon_{ij}\mathbf{G}_{ij}(s_j - s_i) + h_i(t), \tag{2}$$

where s_i and s_j denote the outputs from node i and j, respectively, $\sum_j \epsilon_{ij}\mathbf{G}_{ij}(s_j - s_i)$ represents the influence from other nodes, and $h_i(t)$ is the subcortical input. Note that there is an added parameter ϵ_{ij} in (2), which controls the strength of the influence from node j to i.

2.2. Desynchronization of neuronal clusters

Two properties of the network of oscillators in (2) are of particular interest to BCI [13].

(i) Without the input $h(t)$, all nodes will settle down into an oscillation of the same frequency ω_0, if the network is connected and the influence ϵ is sufficiently strong (mutual synchronization).

(ii) If the input $h_i(t)$ to node i is sufficiently strong and oscillates at a frequency ω_0, node i will then be forced to oscillate in the same frequency ω_0 (forced synchronization).

These two properties explain well the spatial distribution of the EEG signals during motor imaginations [2].

(i) If no imagination is carried out, the neuronal clusters in the idle sensorimotor cortex tend to synchronize with each other and oscillate in the frequency range of 8–26 Hz (EEG α and β rhythm). The spatial summation of this unison is a strong α (and/or β) rhythm in EEG signals.

(ii) If the subject is actively engaged in motor imaginations, the associated neuronal clusters will be strongly modulated by the subcortical structures. The dynamics of these clusters will then stray away from their former synchronous state. This results in a decrease of α (and/or β) power in EEG signals.

This phenomenon is called event-related desynchronization (ERD) in the neuroscience literature. Depending on the part of the body imagined moving, neuronal clusters at different locations will be active. These clusters desynchronize with other clusters, and the spatial distribution of the desynchronization will be different as the imagination contents change. ERD suggests that the strength of the synchronization between neuronal clusters can be used as features for classification [9, 10].

2.3. Features for motor imaginations

An EEG electrode measures mostly the activities of the neuronal cluster directly underneath it (we will qualify this in Section 3). Suppose that the pairwise synchronization of the measured neuronal clusters can be computed from EEG signals and organized into a matrix $\mathbf{S}$ ($\mathbf{S}$ is symmetric with entry $\mathbf{S}_{ij}$ for clusters i and j). Each entry in $\mathbf{S}$ is a dynamical system feature and the similarity between two EEG signals can then be quantified in terms of these features as follows:

$$k(\mathbf{S}, \widetilde{\mathbf{S}}) = \mathrm{Tr}\left((\mathbf{S} \circ \mathbf{A})^{\mathsf{T}}(\widetilde{\mathbf{S}} \circ \mathbf{A})\right), \tag{3}$$

where $\mathbf{A}$ is a weighting matrix, $\mathrm{Tr}(\cdot)$ computes the trace of a matrix, and $\circ$ represents element-wise matrix product. Essentially, this measure transforms EEG trials into synchronization features and then computes their similarity based on these features. Since we will use a SVM classifier for our later experiments, $k(\cdot, \cdot)$ can be interpreted as a kernel between EEG trials.

Preliminary analysis of our motor imagination data set (this data set is further explained in Section 4) indicates that the synchronization in our data appears to be either inphase ($\theta_i - \theta_j = 0$) or antiphase ($\theta_i - \theta_j = \pi$). These two types of synchronization can be well detected simply using the covariance. Therefore, classifying EEG signals using the DS features consists of three steps.

(i) Filter EEG signals. This is the step where filter learning techniques are applied. For our method, filters are learned for individual channels. Hence, EEG signals from different channels are filtered differently.

(ii) Compute the entries of $\mathbf{S}$ and apply $\mathbf{A}$. In this paper, $\mathbf{S}$ is simply the sample covariance matrix, and this is computed for each trial separately. Each entry in $\mathbf{S}$ is a DS feature, and the matrix $\mathbf{A}$ is mainly used for selecting the features. For instance, by setting 20 entries of $\mathbf{A}$ (in (3)) to 1 and all others to 0, then only 20 features are used for later classification.

(iii) Compute the kernel $k(\cdot, \cdot)$ (in (3)) for pairs of trials, form the kernel matrix $\mathbf{K}$, and pass it to SVM for classification. The entry in $\mathbf{K}$ corresponding to trial $\mathbf{S}$ and $\widetilde{\mathbf{S}}$ is simply $k(\mathbf{S}, \widetilde{\mathbf{S}})$ (as in (3)).

3. LEARNING OPTIMAL FILTERS

Filtering EEG signals is important for later classifications. Due to the diffusion of the skull and skin, an EEG electrode actually measures a mixture of signals from several neuronal clusters. Spatial filters, such as a Laplacian filter, are usually applied to concentrate the signals to a single neuronal cluster. Furthermore, EEG signals are contaminated by various noises, such as electrical signals from muscle movements. Our interest lies in oscillation in the frequency range of 8–26 Hz (α and β rhythm). Bandpass filtering is usually needed to suppress other signals.

As previous BCI researchers have experienced [4], the optimal filters for each subject are very different, and it is quite inconvenient to manually choose these filters. Attempts have been made to learn these filters from the training EEG data. Pioneering works have been reported in [4, 12], where FIR (temporal) filters are learned for the CSP features to improve the separability of the two classes. Our work is inspired by their ideas, but our approach is different in two aspects. First, our approach is directed to the dynamical system features. Second, we have proposed a common framework for the learning of both the spatial and the temporal filters. In the following sections, the common framework is first described before it is specialized into the spatial and the temporal filter learning.

3.1. New framework

Our filter learning framework involves three steps: (i) quantify the quality of a feature using the Fisher ratio; (ii) express the Fisher ratio using the filter parameters; (iii) and then maximize the Fisher ratio with respect to the filter parameters. Given the data and the filter parameter $\mathbf{a}$, our framework can be formulated mathematically as follows

$$\max_{\mathbf{a}} Q(\mathbf{a}) = \frac{\left(\mu_+(\mathbf{a}) - \mu_-(\mathbf{a})\right)^2}{\sigma_+^2(\mathbf{a}) + \sigma_-^2(\mathbf{a})}, \tag{4}$$

where Q is the fisher ratio, μ the mean value of a feature, and σ its standard deviation (the subscripts + and − restrict computation to positive and negative classes, resp.). Higher values of Q usually indicate better separation of the two classes. This learning framework can be applied to various problems. However, only local optimum can be guaranteed for the solution, since Q is in general not convex in terms of $\mathbf{a}$. This is also the case in learning the filters for the DS features. To find an optimal solution efficiently, we will employ the subspace optimization technique.

The filter learning is performed on each pair of EEG electrodes separately. For a pair, two filters are learned, one for each electrode. Suppose that the parameters of the two filters are $\mathbf{a}$ and $\mathbf{b}$, respectively. It turns out that for both the spatial and the temporal filtering, Q assumes a form biquadratic in $\mathbf{a}$ and $\mathbf{b}$. For instance, if $\mathbf{b}$ is fixed, Q becomes the quotient between $\mathbf{a}^{\mathsf{T}}\mathbf{V}(\mathbf{b})\mathbf{a}$ and $\mathbf{a}^{\mathsf{T}}\mathbf{W}(\mathbf{b})\mathbf{a}$, where $\mathbf{V}(\mathbf{b})$ and $\mathbf{W}(\mathbf{b})$ are matrices quadratic in $\mathbf{b}$. The optimal $\mathbf{a}$ can then be obtained by solving the following constrained optimization problem:

$$\max_{\mathbf{a}} \mathbf{a}^{\mathsf{T}}\mathbf{V}(\mathbf{b})\mathbf{a}, \quad \text{s.t. } \mathbf{a}^{\mathsf{T}}\mathbf{W}(\mathbf{b})\mathbf{a} + \gamma\mathbf{b}^{\mathsf{T}}\mathbf{b}\mathbf{a}^{\mathsf{T}}\mathbf{a} = c. \tag{5}$$

Note that the additional term $\gamma\mathbf{b}^{\mathsf{T}}\mathbf{b}\mathbf{a}^{\mathsf{T}}\mathbf{a}$ does not originate from Q. It is a regularized product of the norms of $\mathbf{a}$ and $\mathbf{b}$, and the strength of this regularization is controlled by γ.

Input: random initial values of $\mathbf{a}$ and $\mathbf{b}$
Output: optimized value of $\mathbf{a}$ and $\mathbf{b}$
(1) **repeat**
(2) $\tilde{\mathbf{a}} \leftarrow \mathbf{a}$
(3) $\tilde{\mathbf{b}} \leftarrow \mathbf{b}$
(4) compute $\mathbf{V}(\mathbf{a})$, $\mathbf{W}(\mathbf{a})$, $\widetilde{\mathbf{V}}(\mathbf{a})$, and $\widetilde{\mathbf{W}}(\mathbf{a})$
(5) $\mathbf{b} \leftarrow$ eigenvector of $\widetilde{\mathbf{V}}(\mathbf{a})\mathbf{b} = \lambda\widetilde{\mathbf{W}}(\mathbf{a})\mathbf{b}$
(6) compute $\mathbf{V}(\mathbf{b})$, $\mathbf{W}(\mathbf{b})$, $\widetilde{\mathbf{V}}(\mathbf{b})$, and $\widetilde{\mathbf{W}}(\mathbf{b})$
(7) $\mathbf{a} \leftarrow$ eigenvector of $\widetilde{\mathbf{V}}(\mathbf{b})\mathbf{a} = \lambda\widetilde{\mathbf{W}}(\mathbf{b})\mathbf{a}$
(8) **until** $\|\mathbf{a} - \tilde{\mathbf{a}}\|^2 < \varepsilon$ and $\|\mathbf{b} - \tilde{\mathbf{b}}\|^2 < \varepsilon$

Algorithm 1: Learning optimal filter $\mathbf{a}$ and $\mathbf{b}$.

Using the Lagrange multiplier method (let the multiplier be λ), the optimal $\mathbf{a}$ can be derived from the following generalized eigenvector problem:

$$\widetilde{\mathbf{V}}(\mathbf{b})\mathbf{a} = \lambda\widetilde{\mathbf{W}}(\mathbf{b})\mathbf{a}, \tag{6}$$

where

$$\begin{aligned}\widetilde{\mathbf{V}}(\mathbf{b}) &= \mathbf{V}(\mathbf{b}) + \mathbf{V}(\mathbf{b})^{\mathsf{T}},\\ \widetilde{\mathbf{W}}(\mathbf{b}) &= \mathbf{W}(\mathbf{b}) + \mathbf{W}(\mathbf{b})^{\mathsf{T}} + 2\gamma\mathbf{b}^{\mathsf{T}}\mathbf{b}\mathbf{I}.\end{aligned} \tag{7}$$

The optimal $\mathbf{a}$ is then the generalized eigenvector corresponding to the largest eigenvalue. Similarly, $\mathbf{b}$ can be optimized by fixing $\mathbf{a}$. Local maxima can then be found by optimizing $\mathbf{a}$ and $\mathbf{b}$ alternately (Algorithm 1). In our experiments, the solution usually changes very little after two iterations, and henceforth only two iterations are used. To specialize this algorithm into the learning of the spatial and the temporal filters, we only need to derive the exact forms of $\mathbf{V}(\mathbf{a})$, $\mathbf{W}(\mathbf{a})$, $\mathbf{V}(\mathbf{b})$, and $\mathbf{W}(\mathbf{b})$ for these two cases, respectively.

3.2. Learning spatial filters

Studies show that the spherical spline Laplacian filter is useful for the study of cortical dynamics [14]. This method models the shape of the head as a unit sphere and uses orthogonal bases on the sphere to spatially interpolate EEG signals [3]. The filtering is then achieved by computing the analytical Laplacian of the interpolation function. This filters only high-passes EEG signals, and is unable to emphasize interesting signals in the middle frequency range [11] (also see Figure 2). This section will start with a reformulation of the spherical spline Laplacian filter, which leads to a class of spatial filters. The exact forms of $\mathbf{V}(\mathbf{a})$, $\mathbf{W}(\mathbf{a})$, $\mathbf{V}(\mathbf{b})$, and $\mathbf{W}(\mathbf{b})$ are then derived.

For square integrable functions on a sphere, the Legendre polynomials $p_n(\cdot)$ evaluated at $\cos\theta$ constitute a set of orthogonal bases. The parameter n is the degree of the polynomial and it controls the spatial frequency of a basis. A p_n with larger n will generally represent higher spatial frequency. θ is the latitudinal (zonal) angle. In this study, a maximum of $n = 20$ is used for the interpolation of EEG signals (due to the low spatial variation of EEG signals).

Suppose that a position on the unit sphere is $\mathbf{e}$, and the position of the ith EEG electrode is $\mathbf{e}_i$. Let $\cos(\mathbf{e}, \mathbf{e}_i)$ denote the cosine of the angle between $\mathbf{e}$ and $\mathbf{e}_i$, we can construct a matrix $\mathbf{P}(\mathbf{e})$ with entries:

$$\left(\mathbf{P}(\mathbf{e})\right)_{in} = \frac{1}{4\pi}\frac{2n+1}{\left(n(n+1)\right)^4}p_n\left(\cos\left(\mathbf{e}, \mathbf{e}_i\right)\right), \tag{8}$$

where i ranges through the index of the electrodes, and $n = 1 \cdots 20$. Then, EEG signals at position $\mathbf{e}$ can be interpolated as follows:

$$\mathbf{u}(\mathbf{e}) = \mathbf{c}_0 + \mathbf{C}^{\mathsf{T}}\mathbf{P}(\mathbf{e})\mathbf{1}, \tag{9}$$

where $\mathbf{u}(\mathbf{e})$ is a vector with each dimension corresponding to a time point. $\mathbf{1}$ is a vector of all ones. $\mathbf{c}_0$ (a vector of the same size as $\mathbf{u}(\mathbf{e})$) and $\mathbf{C}^{\mathsf{T}}$ (a matrix with 20 columns and the same number of rows as $\mathbf{u}(\mathbf{e})$) are the interpolation coefficients estimated from actual EEG signals. The solution of these coefficients can be found using two constraints [3]: (i) the interpolated function has to pass the actual EEG measurements; (ii) $\mathbf{C}^{\mathsf{T}} \cdot \mathbf{1} = \mathbf{0}$. Our formulation in (9) is equivalent to (1) in Perrin's original formulation [3]. The difference is that (9) describes the interpolation for each time point of a time series rather than that of a single time point. Our reformulation simply stacks separate interpolation for each time point into a matrix notation. This provides us with insight to how spatial filtering is performed.

Spatial filtering of EEG signals can then be achieved by simply removing the DC component $\mathbf{c}_0$ and reweighting other frequency components (the bases). Suppose that the filter (weighting) is $\mathbf{a}$. Thus, spatial filtering can be computed as follows:

$$\tilde{\mathbf{u}}(\mathbf{e}_i) = \mathbf{C}^{\mathsf{T}}\mathbf{P}(\mathbf{e}_i)(\mathbf{1} \circ \mathbf{a}) = \mathbf{C}^{\mathsf{T}}\mathbf{P}(\mathbf{e}_i)\mathbf{a}. \tag{10}$$

The spherical spline Laplacian filter can be obtained by simply setting entries of $\mathbf{a}$ to $-n(n+1)$ (equivalent to [3, equation (5)]). With formula (10), other types of filtering can also be implemented by varying $\mathbf{a}$. For example, a bell-shaped bandpass filter can be obtained by setting the entries of $\mathbf{a}$ to $\exp(-\kappa n(n+1))n(n+1)$ (κ is a parameter controlling the width and the peak). These two filters are illustrated in Figure 2. Note that the weights in the figures are normalized into the range between 0 and 1.

Suppose that filter $\mathbf{a}$ and $\mathbf{b}$ are applied to electrode $\mathbf{e}_i$ and $\mathbf{e}_j$, respectively, the covariance between the two filtered EEG signals can then be computed as

$$\mathsf{cov}^{ij} = \frac{1}{l}\tilde{\mathbf{u}}(\mathbf{e}_i)^{\mathsf{T}}\tilde{\mathbf{u}}(\mathbf{e}_j) = \frac{1}{l}\mathbf{a}^{\mathsf{T}}\mathbf{P}^{\mathsf{T}}(\mathbf{e}_i)\mathbf{C}\mathbf{C}^{\mathsf{T}}\mathbf{P}(\mathbf{e}_j)\mathbf{b}, \tag{11}$$

where l is the number of time points. Further, denote $\tilde{\mathbf{C}}^{ij} = \mathbf{P}^{\mathsf{T}}(\mathbf{e}_i)\mathbf{C}\mathbf{C}^{\mathsf{T}}\mathbf{P}(\mathbf{e}_j)$. (Since the following derivations are the same for each pair of electrodes, the superscripts ij are dropped henceforth for convenience.) Then, μ_+ in (4) can be computed as follows:

$$\mu_+ = \frac{1}{m}\sum_{k\in+}\mathsf{cov}_k = \mathbf{a}^{\mathsf{T}}\left(\frac{1}{ml}\sum_{k\in+}\tilde{\mathbf{C}}_k\right)\mathbf{b} = \mathbf{a}^{\mathsf{T}}\mathbf{D}_+\mathbf{b}, \tag{12}$$

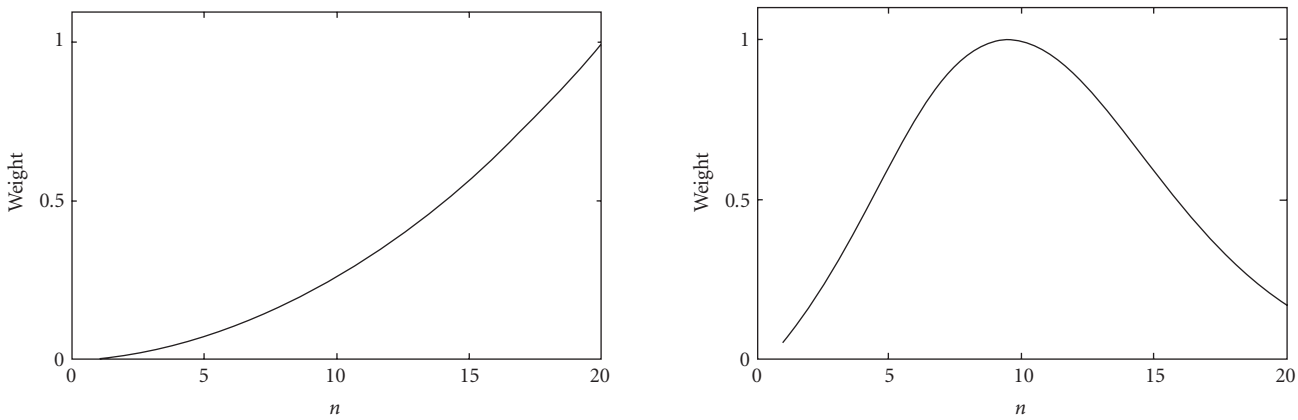

Figure 2: (a) Spherical spline Laplacian filter and (b) a bell-shaped filter.

where $k \in +$ means that the index ranges through all m trials in the positive class. (Suppose that the negative class also has m trials). The variance σ_+ can be computed as follows:

$$(\sigma_+)^2 = \frac{1}{m}\sum_{k\in+}(\mathrm{cov}_k - \mu_+)^2 = \mathbf{a}^{\mathsf{T}}\mathbf{E}_+(\mathbf{b})\mathbf{a}, \tag{13}$$

where

$$\mathbf{E}_+(\mathbf{b}) = \frac{1}{m^2 l^2}\left(\left(\sum_{k\in+}\widetilde{\mathbf{C}}_k\right)\mathbf{b}\right)^2 - \frac{1}{ml^2}\sum_{k\in+}(\widetilde{\mathbf{C}}_k\mathbf{b})^2. \tag{14}$$

Similarly, $\mu_- = \mathbf{a}^{\mathsf{T}}\mathbf{D}_-\mathbf{b}$ and $(\sigma_-)^2 = \mathbf{a}^{\mathsf{T}}\mathbf{E}_-(\mathbf{b})\mathbf{a}$. $\mathbf{V}(\mathbf{b})$ and $\mathbf{W}(\mathbf{b})$ can then be derived as follows:

$$\begin{aligned}(\mu_+ - \mu_-)^2 &= \mathbf{a}^{\mathsf{T}}(\mathbf{D}_+\mathbf{b} - \mathbf{D}_-\mathbf{b})^2\mathbf{a} = \mathbf{a}^{\mathsf{T}}\mathbf{V}(\mathbf{b})\mathbf{a},\\ (\sigma_+)^2 + (\sigma_-)^2 &= \mathbf{a}^{\mathsf{T}}(\mathbf{E}_+(\mathbf{b}) + \mathbf{E}_-(\mathbf{b}))\mathbf{a} = \mathbf{a}^{\mathsf{T}}\mathbf{W}(\mathbf{b})\mathbf{a}.\end{aligned} \tag{15}$$

Since $\mathbf{a}$ and $\mathbf{b}$ are symmetric, $\mathbf{V}(\mathbf{a})$ and $\mathbf{W}(\mathbf{a})$ can be derived analogously by exchanging the positions of $\mathbf{a}$ and $\mathbf{b}$ and transposing $\widetilde{\mathbf{C}}_k$ in (12)–(15). Substituting $\mathbf{V}(\mathbf{a})$, $\mathbf{W}(\mathbf{a})$, $\mathbf{V}(\mathbf{b})$, and $\mathbf{W}(\mathbf{b})$ into Algorithm 1 will then produce the optimal filters.

3.3. Learning temporal filters

Unlike [4] that formulated the learning of the temporal filters in the time domain (FIR filter), our formulation works directly in the frequency domain. The basic idea of our approach is to place weighting directly on the complex coefficients of the discrete Fourier transformation (DFT).

Weighting the frequency components of an EEG signal $\mathbf{u}(\mathbf{e}_i)$ will transform it to

$$\widetilde{\mathbf{u}}(\mathbf{e}_i) = \mathcal{F}^{-1}(\mathcal{F}(\mathbf{u}(\mathbf{e}_i)) \circ \mathbf{a}), \tag{16}$$

where $\mathbf{a}$ is the filter (weighting), and $\mathcal{F}$ represents the forward DFT ($\mathcal{F}^{-1}$, the inverse DFT). Suppose that filters $\mathbf{a}$ and $\mathbf{b}$ are applied to EEG electrodes $\mathbf{e}_i$ and $\mathbf{e}_j$, respectively. The covariance of the filtered signals can then be computed as follows:

$$\begin{aligned}\mathrm{cov} &= \frac{1}{l}\widetilde{\mathbf{u}}(\mathbf{e}_i)^{\mathsf{T}}\widetilde{\mathbf{u}}(\mathbf{e}_j)\\ &= \frac{1}{l}(\mathcal{F}^{-1}(\mathcal{F}(\mathbf{u}(\mathbf{e}_i)) \circ \mathbf{a}))^{\mathsf{T}}(\mathcal{F}^{-1}(\mathcal{F}(\mathbf{u}(\mathbf{e}_i)) \circ \mathbf{b})).\end{aligned} \tag{17}$$

(Note that the superscripts are dropped for convenience.) Computation (17) is inefficient, since two forward and inverse DFTs are needed. The computation, however, can be reduced using the correlation theorem. This theorem states that the covariance between two signals $\mathbf{u}(\mathbf{e}_i)$ and $\mathbf{u}(\mathbf{e}_j)$ is equal to $(\mathcal{F}(\mathbf{u}(\mathbf{e}_i)))^*\mathcal{F}(\mathbf{u}(\mathbf{e}_j))$ ($*$ denotes conjugate transpose). Thus, (17) can be simplified to:

$$\mathrm{cov} = \frac{1}{l}\mathbf{a}^{\mathsf{T}}\mathrm{Diag}((\mathcal{F}(\mathbf{u}(\mathbf{e}_i)))^* \circ \mathcal{F}(\mathbf{u}(\mathbf{e}_j)))\mathbf{b}, \tag{18}$$

where $\mathrm{Diag}(\cdot)$ transforms its vector argument into a diagonal matrix. Formula (18) requires only two DFT computations, and hence it is more efficient.

The derivations for $\mathbf{V}(\mathbf{a})$, $\mathbf{W}(\mathbf{a})$, $\mathbf{V}(\mathbf{b})$, and $\mathbf{W}(\mathbf{b})$ become straightforward if we compare (18) with (11). By setting $\widetilde{\mathbf{C}}^{ij} = \mathrm{Diag}((\mathcal{F}(\mathbf{u}(\mathbf{e}_i)))^* \circ \mathcal{F}(\mathbf{u}(\mathbf{e}_j)))$, they can be obtained from (12)–(15). Substituting these matrices into Algorithm 1 produces the optimal filters.

4. RESULTS AND COMPARISON

The dynamical system (DS) features and the filter learning approach are evaluated using data set IVa from the Berlin BCI group [8]. This data set contains EEG signals (118 channels, sampled at 100 Hz) for five healthy subjects (labeled "aa," "al," "av," "aw" and "ay," resp.). During the recordings, they were prompted by visual cues to imagine for 3.5 seconds

Table 1: Averaged dynamical system features (DS) and common spatial patterns (CSP) for five subjects ("aa," "al," "av," "aw," and "ay") over three-time windows (0–0.5 second, 0.5–2.5 seconds, and 3.5–4.0 seconds) during the motor imagination. The top 20 most discriminative DS features are shown as edges connecting the corresponding electrodes (dots). The most discriminative CSPs for right-hand imagination are plotted as color maps.

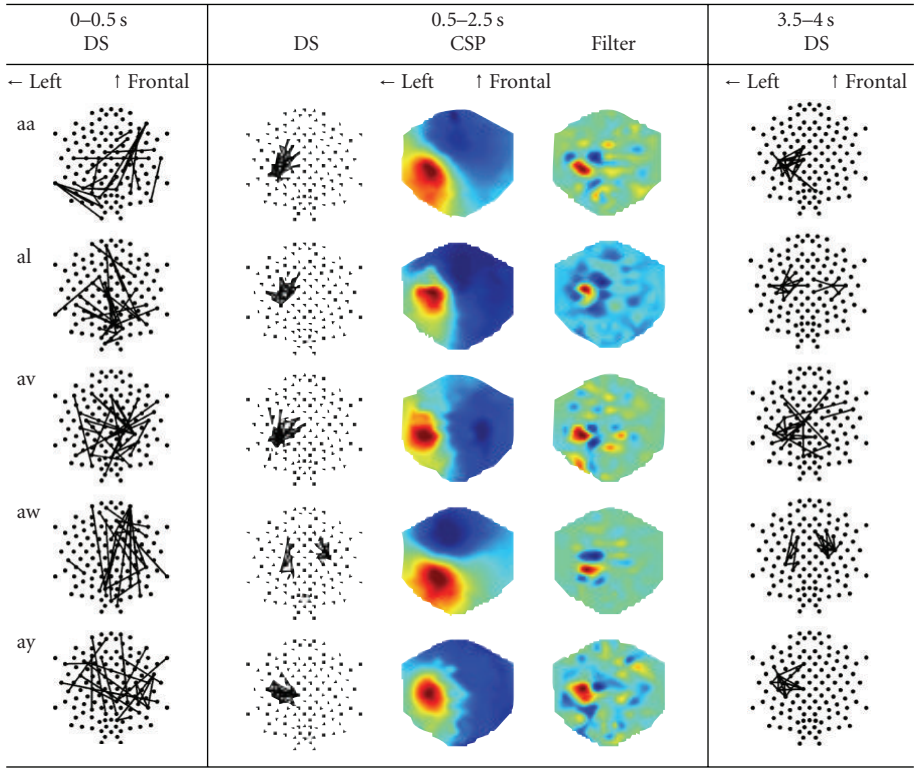

either right-hand (the positive class) or right-foot movements (the negative class). Our classification analysis will focus on the data between 0.5 seconds and 2.5 seconds (i.e., 200 time points for each channel), since in an online BCI setting a sliding window seldom exceeds 2 seconds [4]. For convenience, the period between 0 s and 1 s of a trial is called imagination preparation stage, and the period between 3.5 seconds and 4.0 seconds is called postimagination stage. Each type of imagination was carried out 140 times. Thus, there are 280 labeled trials in total for each subject (note: each trial is a multivariate time series of 118 dimensions). The task is to classify the type of the imagination for each trial in an offline fashion.

Two sets of experiments were conducted in our evaluations. They are designed to reveal two major aspects: (i) using DS features for classification, and (ii) learning spatial and temporal filters. We will first describe procedures common to these experiments. All our classifications are carried out using SVM and the errors are obtained from 10×10 fold cross-validation. An identical temporal prefiltering (bandpass between 8–40 Hz) is applied to all subjects. In the case of the DS features, an identical spatial prefiltering (a bell-shaped bandpass filter $\exp(-\kappa n(n+1))n(n+1)$ with $\kappa = 0.01$) is also applied for all subjects. Furthermore, only the top 20 DS features (in terms of their Fisher ratios) are used for classification.

4.1. Dynamical system features

4.1.1. Where are the discriminative dynamical system features?

The dynamical system (DS) features during motor imagination (0.5–2.5 s) are scored by Fisher ratio for each fold of the cross-validation, and these scores are further averaged over the folds. The top 20 most discriminative DS features are plotted in the second column of Table 1. For comparison, typical common spatial patterns (CSPs) for the right-hand imagination (corresponding to the smallest generalized eigenvalues) are also shown beside the DS features.

For four of the five subjects ("aa," "al," "av," and "ay"), the DS features share clear pattern across the subjects—they tightly concentrate on the area in charge of right-hand imagination (left motor cortex, hand region in the Homunculus). This phenomenon can be well explained by the theory of event-related desynchronization (ERD): as the hand region in the left motor cortex is actively engaged in imagination, its neuronal activities deviate from those of the neighboring cortices; and such localized spatial discordance results in the tight cluster of the DS features.

Furthermore, the typical common spatial patterns (CSP) also show nice agreement with the DS features. The areas of the ERD correspond to the peaks in the CSPs.

Table 2: Classification errors (%) of the CSP, the AR, and the DS features with optimized filters.

Sb	CSP	AR	DS + S + T
aa	**8.5 ± 5.4**	10.5 ± 6.0	*9.5 ± 5.7*
al	**0.8 ± 1.8**	*1.6 ± 2.5*	2.7 ± 3.1
av	29.1 ± 8.2	*23.3 ± 7.6*	**21.5 ± 7.6**
aw	**3.1 ± 2.8**	7.7 ± 3.8	6.5 ± 4.5
ay	**5.3 ± 3.8**	9.5 ± 4.4	*8.5 ± 5.0*

Table 3: Classification errors (%) of the combinations of the CSP, the AR, and the DS features.

Sb	CSP + AR	CSP + DS	AR + DS	ALL
aa	*7.6 ± 5.0*	**7.3 ± 5.1**	7.7 ± 4.7	**7.3 ± 4.9**
al	1.6 ± 2.3	**0.9 ± 1.9**	1.6 ± 2.5	*1.5 ± 2.2*
av	22.3 ± 7.4	22.5 ± 7.8	**21.4 ± 7.4**	*21.6± 7.1*
aw	3.5 ± 3.2	**2.8 ± 3.1**	5.2 ± 3.8	*3.4 ± 3.2*
ay	8.9 ± 4.6	**5.5 ± 4.3**	9.1 ± 4.6	*8.7 ± 4.5*

Beside the similarity also revealed in the figures is the difference of the DS features across subjects. Especially for subject "aw," half of the DS features locate in the contralateral hand region. A plausible explanation is that the subject may have imagined movements of both hands.

4.1.2. How do dynamical system features evolve over time?

The top 20 DS features in the imagination preparation stage (0–0.5 s) and the postimagination stage (3.5–4.0 s) are scored similarly and plotted, respectively, in the first and the third column of Table 1. These figures provide us an idea of the evolution of the DS features over time.

During the preparation stage, the DS features scatter around the whole scalp. They mostly connect distal regions of the brain; other than that, no clear pattern is shared across subjects. In fact, these DS features provide classifications only slightly better than random (the errors are not reported). This implies that the DS features within this period do not contain useful information for classification.

During the imagination, tight clusters of DS features are formed and they lead to good classification. Then, as the subjects are signaled to stop their imaginations (3.5–4.0 s), the clusters start to diffuse into wider areas of the brain. Such trend is most clearly revealed in subject "av," where parts of the DS features are replaced by long range connections across hemispheres of the brain.

The formation and the dissolution of clusters over the course of an imagination present a unique characteristic for the DS features. Potentially, such pattern can be exploited for online detection of motor imagination.

4.1.3. Dynamical system features are competitive

The DS features obtained with learned filters were compared to the CSP and the AR features obtained with manually chosen parameters. The parameters for the CSP features (filtering frequency, selected channels, and the number of projection subspaces) and the AR features (filtering frequency, selected channels, and the order of the AR model) were tuned according to the winning entry of BCI competition III [15]. The results are shown in Table 2.

Overall, the CSP features perform the best, the DS features follow, and the AR features produce lower accuracy. Furthermore, the DS features often obtain the best (highlighted in bold) or the second best place (highlighted in italic). Especially for subject "av," the DS features outperform the CSP features by 6%. It is important to note that the parameters for the CSP and AR features have been tuned manually and intensively, while the results for the DS features are obtained with exactly the same starting parameters. This shows the usefulness of the DS features and our filter learning approach.

4.1.4. Dynamical system features extract complementary information

The CSP, AR, and DS features are computed differently from the EEG signals. An interesting question is whether they complement each other during classification. To investigate this, we combine more than two types of features (CSP + AR, CSP + DS, AR + DS, and ALL three) using the META scheme described by [8]. The classifications of the combined features are presented in Table 3. The combination with the smallest error for each subject is highlighted in bold and the second place in italic. Furthermore, we surround an error with a box, if it is the smallest ever (in Tables 2 and 3) for a subject.

The DS features indeed complement the CSP and the AR features, as is evidenced by the further reduction of errors in subject, "aa," "av," and "aw." The reduction, however, is not large (the largest being around 1% for subject "aa"). Furthermore, the combination of all three types of features does not necessarily further reduce the errors. This happens when the best features have already extracted almost all information about the separability of the two classes. Additional features may only provide redundant or even conflicting information for the classification. This is very likely in our case since we have optimized each type of features intensively. Finally, our results suggest that the combination of the CSP and the DS features performs the best, and the DS features complement the CSP features better than the AR features.

4.2. Learned filters

4.2.1. Learned filters improve classification

For each pair of EEG electrodes (equivalent to a DS feature), the optimal spatial and temporal filters were learned sequentially. In Table 4, we present the classification errors using the following: (i) the DS features without the spatial and the temporal filter optimization (DS column); (ii) the DS features only with the spatial filter optimization (DS + S column); (iii) the DS features only with the temporal filter optimization (DS + T column); (iv) the DS features with both the

Table 4: Classification errors (%) of the DS features before and after applying the learned filters.

Sb	DS	DS + S	DS + T	DS + S + T
aa	16.7 ± 7.2	14.6 ± 7.0	**9.7 ± 5.7**	9.5 ± 5.7
al	3.7 ± 3.3	**3.2 ± 3.2**	3.6 ± 3.4	2.7 ± 3.1
av	27.3 ± 7.9	25.1 ± 8.0	**21.4 ± 7.9**	21.5 ± 7.6
aw	13.1 ± 6.0	12.1 ± 5.7	**7.5 ± 4.4**	6.2 ± 4.5
ay	11.0 ± 5.3	**9.6 ± 5.0**	9.7 ± 5.1	8.5 ± 5.0

spatial and the temporal filter optimization (DS + S + T column). Note that for all four comparisons prefilters have already been applied in both temporal and spatial domains.

The results demonstrate that both the learned spatial and temporal filters improve the classification (DS + S and DS + T columns). Although there is no absolute winner in the two types of filters, when applied separately, the temporal filters outperform the spatial filters in general (the winning filter for each subject is highlighted in bold). Especially for subjects "aa" and "aw," the temporal filters reduce about 5% more errors than the spatial filters.

The combined application of the learned filters almost always further reduces the errors (only subject "av" slightly violates this rule). The maximum reduction is around 7% (for subject, "aa" and "aw"). The errors obtained (DS + S + T column) are now lower than 10% for 4 of the 5 subjects (except "av"). It seems that the learned filters help less for some subjects ("al" and "ay"). The reason can be that the prefiltering is already near the optimal solution.

The classification for subject "av" has the largest error. Our preliminary studies indicate that the most responsive frequency range of this subject shifts above 26 Hz (contrary to the usual 8–26 Hz). While most energy in the EEG signals concentrates below 26 Hz, this makes it difficult to extract good features for the subject.

4.2.2. Learned filters extract meaningful information

Several details related to Section 4.2.1 are clarified here. The spatial and the temporal filters can be interpreted as weighting in the corresponding frequency domain. We have further restricted them to be polynomial models in our experiments. The results in Table 4 are obtained with polynomial functions of degree 6 (for both the spatial and the temporal filter learnings). The regularization parameters γ for the spatial and the temporal filters are 10^{-7} and 10^{-13}, respectively. For the case of the temporal filter, a bell-shaped prefilter is also applied ($-\exp(-\kappa n(n+1))n(n+1)$ with $\kappa = 0.001$ for all subjects). Note that the filters are always learned in pairs, that is, one for each channel in a pair. We will illustrate the learned filters in two ways.

The first way is the joint effect of the bell-shaped prefilter and a learned filter from a single channel. Since the learned filter is always applied after the prefiltering, we will show the shape of the prefilter, the learned filter, and their multiplication in one picture (Figures 3(a) and 4(a)).

The second way is the joint effect of the overall filtering from two channels. Since a DS feature is bilinear in the filters applied to the two channels, our optimization in Algorithm 1 only has exact control over their multiplicative effect. Therefore, we will illustrate the filtering effects for two channels and their multiplication in one picture (Figures 3(b) and 4(b)).

Figure 3(a) shows a learned spatial filter (thin line, bow-shaped) and the prefilter (thin line, bell-shaped) for one channel. Although both filters are simple, their multiplicative effect creates a double-peak characteristics (dotted line). This is equivalent to emphasizing the frequency contributions under these two peaks. The overall effect of the learned filters from two channels (dotted lines in Figure 3(b)) is also double peaked (thick line in Figure 3(b)). We believe that these peaks are somehow related to the electrode spacing on the scalp. It is likely that the learned filters weight the information from the actual electrodes more heavily than that from the interpolated positions.

For the temporal filters, we will interpret the learned filters in terms of their effects on the power spectrum. Hence, only the absolute values of the weighting are displayed. The final filter for an example channel (dotted line in Figure 4(a); it is the multiplication of a prefilter and a learned filter, both in thin lines) does not appear to emphasize the motor imagination signals (i.e., ERD in 8–26 Hz). The meaning, however, becomes clearer when we examine the filters from two channels together. In Figure 4(b), the filters from two channels are shown in dotted lines and their multiplication in thick line. The multiplication creates the strongest peak within 10–18 Hz, and a second strongest peak within 18–28 Hz. This corresponds well to the most responsive frequency range of the motor imaginations.

Note that one can *not* simply replace individual filters, $\mathbf{a}$ and $\mathbf{b}$, from a pair of electrodes by the square root of their multiplication. This is because the two filters $\mathbf{a}$ and $\mathbf{b}$ always appear in the form of $\mathbf{ba}^{\mathsf{T}}$ in the objective and the constraint of (5). For instance, one can show that according to (15)

$$\mathbf{a}\mathbf{V}(\mathbf{b})\mathbf{a} = \mathrm{Tr}\left(\left((\mathbf{D}_+ - \mathbf{D}_-)\mathbf{b}\mathbf{a}^{\mathsf{T}}\right)^2\right). \tag{19}$$

Therefore, only when two pairs of filters, $\mathbf{a}$ and $\mathbf{b}$ versus $\mathbf{a}'$ and $\mathbf{b}'$, produce the same outer product (i.e., $\mathbf{ba}^{\mathsf{T}} = \mathbf{b}'\mathbf{a}'^{\mathsf{T}}$), they can be equated with each other. In Figures 3(b) and 4(b), we only showed the diagonal of $\mathbf{ba}^{\mathsf{T}}$ to produce a concise summary of their joint filtering effect. One should keep in mind that the learned filters have further effect beyond what is visualized here.

4.2.3. Learned filters are competitive

The DS features obtained with the learned filters were compared to the CSP features produced by the CSSP [12] and the CSSSP [4] methods. These two methods are also designed to remove the manual filter tuning, and they have incorporated the filter learning into the original CSP method. The comparisons are presented in Table 5.

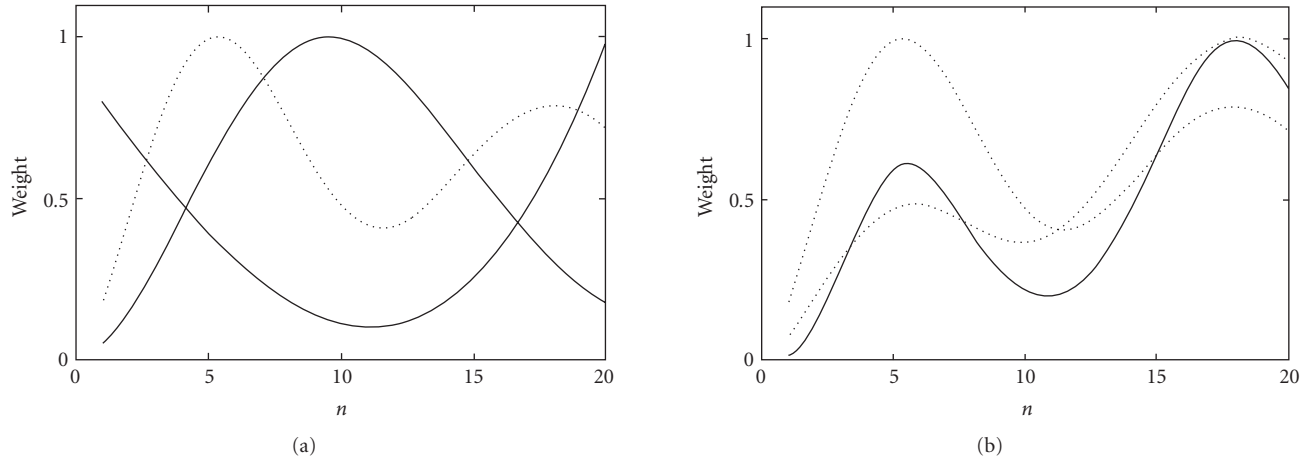

Figure 3: Illustration of spatial filters: (a) the prefilter (thin line, bell-shaped), a learned filter (thin line, bow-shaped), and their multiplication (dotted line); (b) learned filters from a pair of channels (dotted lines) and their multiplication (thick line).

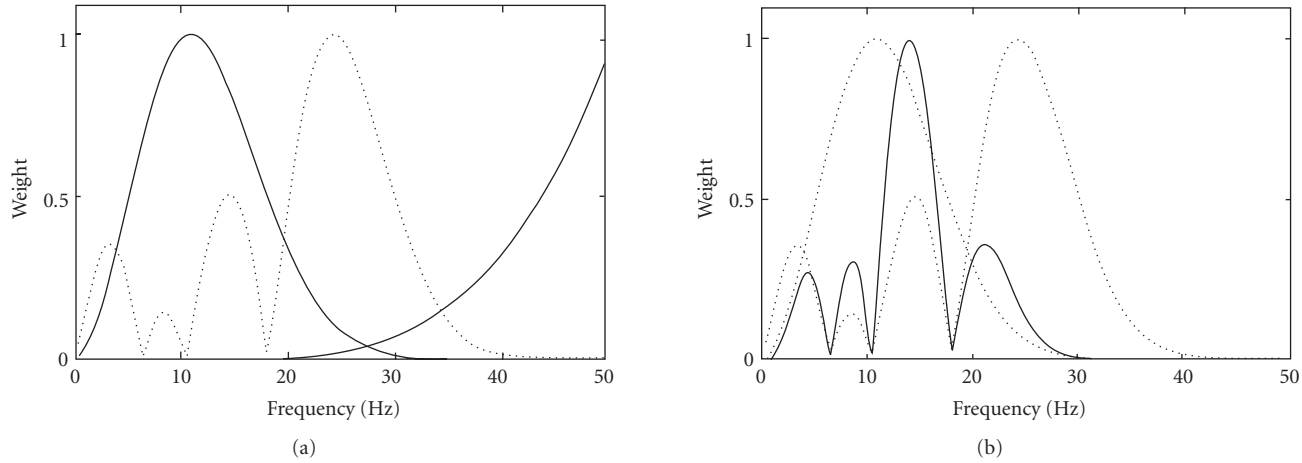

Figure 4: Illustration of temporal filters: (a) the pre-filter (thin line, bell-shaped), a learned filter (thin line, wedge-shaped), and their multiplication (dotted line); (b) learned filters from a pair of channels (dotted lines) and their multiplication (thick line).

Table 5: Classification errors (%) of the CSSP, the CSSSP, and the DS + S + T methods.

Sb	CSSP	CSSSP	DS + S + T
aa	14.6 ± 6.2	*11.6 ± 6.3*	**9.5 ± 2.1**
al	*2.3 ± 3.0*	**2.1 ± 2.7**	2.7 ± 3.1
av	32.6 ± 7.6	*31.8 ± 7.7*	**21.5 ± 7.6**
aw	**3.5 ± 3.3**	*6.5 ± 4.3*	*6.5 ± 4.5*
ay	**6.0 ± 3.9**	10.5 ± 5.7	*8.5 ± 5.0*

It can be seen that the three methods are quite competitive. Each method has its best performance in certain subjects. Notably, our method does the best in subject "av," outperforming the other two methods by about 10%. As mentioned earlier, the most responsive frequency range of "av" shifts above the normal α and β bands (8–26 Hz). This seems to suggest that for such BCI "abnormal," the DS features may be a better choice for the classification task.

5. DISCUSSION

5.1. Relation to other filter learning methods

In Section 4, a bell-shaped spatial filter is applied as a preprocessing for the DS features. Equivalently, this prefilter can be viewed as a weighting on the electrodes. Spatially, it resembles a Mexico hat, a positive peak surrounded by a ring of negative peaks (as illustrated in Figure 5(a)).

Our filter learning method further optimizes this prefilter by modifying its shape in the frequency domain (e.g., Figure 3(a)). After the optimization, the spatial influence of the resulting filter remains similar to the prefilter (Figure 5(b)). However, the separation between the positive and the negative peaks of the learned filter increases. This allows signals of lower spatial frequency to pass. Such adaptation helps the filter to extract more discriminative signals from the EEG signals.

An interesting observation is that the spatial filters obtained from the CSP method locally resemble the prefilter we

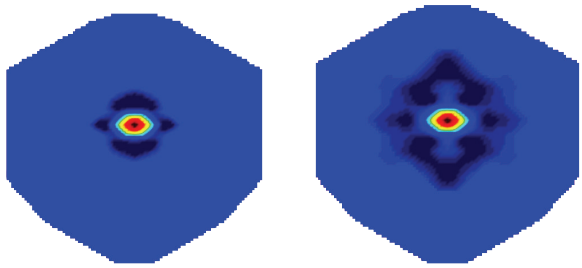

(a) (b)

Figure 5: (a) A bell-shaped spatial filter; (b) a learned spatial filter.

applied for the DS features. As shown in the middle column of Table 1, the filters learned by the CSP method emphasize the electrode directly above the neuronal cluster in charge of the imagination; at the same time, they suppress the contribution from adjacent electrodes.

While our filter learning method employs the prefilter as a prior knowledge and successively refines this knowledge locally, the CSP method arrives at similar results by computing a global filter instead. In the cases where this prior knowledge is accurate, we expect that better filters can be obtained by our method, which eventually leads to lower classification error (e.g., the classification error for subject "av" in Table 2).

5.2. Higher-order dynamical system features

In this paper, the covariance is used as a measure of dependence between different regions of the brain. Covariance, however, can only detect second-order dependence between the signals. Other more-powerful measures are needed if one wants to exploit higher-order dynamical system (DS) features of the brain.

Various measures have been explored in the literature. For instance, phase synchronization has also been employed as DS features for classifying BCI signals [9, 10]. Another example is the mutual information [13], but its use in BCI context remains unexplored. In all these cases, however, it is not yet clear how spatial and temporal filters can be learned automatically from the data.

6. CONCLUSION

In this paper, we exploited the collective dynamics of the cortex as features for BCI. We also proposed a framework for learning the optimal spatial and temporal filters during the extraction of these features. For 4 of the 5 subjects tested, our automated approach reduces classification errors to less than 10%. This performance is comparable to that of the CSP features obtained with manually tuned parameters. Further comparisons with other filter learning approaches also show the competitive performance of our method. Our results suggest that the dynamical system features combined with filter learning approach are very promising for BCI. More investigation is needed to fully demonstrate its advantage.

ACKNOWLEDGMENTS

The authors thank Ms. Yingxin Wu and the reviewers for useful comments. National ICT Australia is funded through the Australian Government's Backing Australia's Ability initiative, in part through the Australian Research Council. Earlier version of this paper appeared in ICML 2006 [16]. This version includes additional experimental results, a new discussion section and extended description of the method.

REFERENCES

[1] J. R. Wolpaw, N. Birbaumer, D. J. McFarland, G. Pfurtscheller, and T. M. Vaughan, "Brain-computer interfaces for communication and control," *Clinical Neurophysiology*, vol. 113, no. 6, pp. 767–791, 2002.

[2] G. Pfurtscheller and F. H. Lopes da Silva, "Event-related EEG/MEG synchronization and desynchronization: basic principles," *Clinical Neurophysiology*, vol. 110, no. 11, pp. 1842–1857, 1999.

[3] F. Perrin, J. Pernier, O. Bertrand, and J. F. Echallier, "Spherical splines for scalp potential and current density mapping," *Electroencephalography and Clinical Neurophysiology*, vol. 72, no. 2, pp. 184–187, 1989.

[4] G. Dornhege, B. Blankertz, M. Krauledat, F. Losch, G. Curio, and K.-R. Müller, "Optimizing spatio-temporal filters for improving brain-computer interfacing," in *Advances in Neural Information Processing Systems*, vol. 18, pp. 315–322, MIT Press, Cambridge, Mass, USA, 2006.

[5] K.-R. Müller, C. W. Anderson, and G. E. Birch, "Linear and nonlinear methods for brain-computer interfaces," *IEEE Transactions on Neural Systems and Rehabilitation Engineering*, vol. 11, no. 2, pp. 165–169, 2003.

[6] T. N. Lal, M. Schröder, N. J. Hill, et al., "A brain computer interface with online feedback based on magnetoencephalography," in *Proceedings of the 22nd International Conference on Machine Learning (ICML '05)*, pp. 465–472, Bonn, Germany, August 2005.

[7] H. Ramoser, J. Müller-Gerking, and G. Pfurtscheller, "Optimal spatial filtering of single trial EEG during imagined hand movement," *IEEE Transactions on Rehabilitation Engineering*, vol. 8, no. 4, pp. 441–446, 2000.

[8] G. Dornhege, B. Blankertz, G. Curio, and K.-R. Müller, "Boosting bit rates in noninvasive EEG single-trial classifications by feature combination and multiclass paradigms," *IEEE Transactions on Biomedical Engineering*, vol. 51, no. 6, pp. 993–1002, 2004.

[9] E. Gysels and P. Celka, "Phase synchronization for the recognition of mental tasks in a brain-computer interface," *IEEE Transactions on Neural Systems and Rehabilitation Engineering*, vol. 12, no. 4, pp. 406–415, 2004.

[10] L. Song, E. Gysels, and E. Gordon, "Phase synchrony rate for the recognition of motor imagery in brain-computer interface," in *Advances in Neural Information Processing Systems*, vol. 18, pp. 1265–1272, MIT Press, Cambridge, Mass, USA, 2006.

[11] L. Song and J. Epps, "Improving separability of EEG signals during motor imagery with an efficient circular Laplacian," in *Proceedings of IEEE International Conference on Acoustics, Speech, and Signal Processing (ICASSP '06)*, vol. 2, pp. 1048–1051, Toulouse, France, May 2006.

[12] S. Lemm, B. Blankertz, G. Curio, and K.-R. Müller, "Spatio-spectral filters for improving the classification of single trial EEG," *IEEE Transactions on Biomedical Engineering*, vol. 52, no. 9, pp. 1541–1548, 2005.

[13] A. Pikovsky, M. Rosenblum, J. Kurths, and B. Chirikov, *Synchronization: A Universal Concept in Nonlinear Sciences*, Cambridge University Press, Cambridge, UK, 2003.

[14] R. Srinivasan, P. L. Nunez, and R. B. Silberstein, "Spatial filtering and neocortical dynamics: estimates of EEG coherence," *IEEE Transactions on Biomedical Engineering*, vol. 45, no. 7, pp. 814–826, 1998.

[15] X. Gao, Z. Zhang, B. Hong, and S. Gao, http://ida.first.fraunhofer.de/projects/bci/competition_iii/results/berlin_IVa/YijunWang_desc.pdf

[16] L. Song and J. Epps, "Classifying EEG for brain-computer interfaces: learning optimal filters for dynamical system features," in *Proceedings of the 23rd International Conference on Machine Learning (ICML '06)*, pp. 857–864, Pittsburgh, Pa, USA, June 2006.

Hindawi Publishing Corporation
Computational Intelligence and Neuroscience
Volume 2007, Article ID 54925, 12 pages
doi:10.1155/2007/54925

Research Article

High-Resolution Movement EEG Classification

Jakub Šťastný and Pavel Sovka

Biosignal Laboratory, Department of Circuit Theory, Faculty of Electrotechnical Engineering, Czech Technical University in Prague, Technická 2, 16627 Prague, Czech Republic

Correspondence should be addressed to Jakub Šťastný, stastnj1@seznam.cz

Received 17 February 2007; Accepted 23 September 2007

Recommended by Andrzej Cichocki

The aim of the contribution is to analyze possibilities of high-resolution movement classification using human EEG. For this purpose, a database of the EEG recorded during right-thumb and little-finger fast flexion movements of the experimental subjects was created. The statistical analysis of the EEG was done on the subject's basis instead of the commonly used grand averaging. Statistically significant differences between the EEG accompanying movements of both fingers were found, extending the results of other so far published works. The classifier based on hidden Markov models was able to distinguish between movement and resting states (classification score of 94–100%), but it was unable to recognize the type of the movement. This is caused by the large fraction of other (nonmovement related) EEG activities in the recorded signals. A classification method based on advanced EEG signal denoising is being currently developed to overcome this problem.

1. INTRODUCTION

There are a great number of existing BCI prototypes all around the world. However, all of them suffer from one major drawback; the communication channel between a human brain and a computer is usually very slow working at a speed lower than 100 bits per minute. If we compare this communication channel with a standard keyboard computer interface allowing us to type texts at blazing speeds up to 1 kbit per minute, we can conclude that all these BCI devices are still not very suitable for the real computer control.

One possibility leading to higher data transfer lies in the recognition of more distinct brain states, which means transferring more bits per state via the communication channel (high-resolution EEG recognition), while keeping the average recognition score for the single states as high as possible. However, the currently existing systems recognize only few very different EEG phenomena (left/right- hand or finger movement [1–5], mental activities such as mental arithmetic, mental rotation, visual imagination [3, 4, 6, 7], conscious EEG rhythm control [8, 9], or event-related potentials [10–12], among others). Our research is targeted to the exploration of possibilities of the high-resolution movement recognition from the EEG signal. The movement-related EEG was selected because it is very natural to control anything with movement-related EEG as we usually control our surroundings in this way. It is well known that only imagination of the movement is sufficient [13, 14] to produce the desired brain activity pattern and last, but not the least, it is possible to change quickly the movement-related states of the brain compared , for example, to mental activities further increasing the interface transfer speed.

Our previous work showed that it is possible to distinguish right-shoulder and right-index finger movements easily from the EEG signal [15, 16] and classify the direction of the right-index finger movement on the basis of the EEG signal [17]. Movements performed at only one side of the body were used. This task is more complicated compared to differentiating only the left/right-hand movement or types of mental activities. The key requirement built into the classification system was to use changes in signal parameters rather than information stored in the difference of signal powers from different electrodes (extracted by means of appropriately defined spatial filters [18]), which lies in contrast with other existing systems. Encouraged by our previous result, we targeted our research to the development of a classification

method which is able to recognize the single-finger movements from the EEG signal. Finger movements were chosen owing to the results of other works [19, 20].

The second important finding we learnt from our experiments is that the individualities of experimental subjects cause great differences between their recorded brain activities. These differences nowadays obstruct the possibility of the BCI generalization (the usage of the system trained on one subject for the movement classification of another subject). This led us to the conclusion that an individual approach to the EEG statistical analysis will be selected instead of the commonly used grand averaging (see, e.g., [20, 21]).

Last, but not least, the developed classification scheme [16] allows us to do a movement-related EEG classification without any need of subject training, which is a great advantage compared to other systems.

Our current work deals with the right-index and little-finger flexion movement-related EEG analysis and classification. This contribution is organized as follows. The general properties of the movement-related EEG are introduced in Section 2. Further, the EEG recording experiment is described. Section 4 section is devoted to a simple preliminary analysis of the recorded EEG proving the validity of our database. The core of our work is described in Sections 5 and 6. First we analyze the EEG in an individual way to find subtle differences between movements, then the classification system description and classification results are introduced. Finally, several conclusions and future steps are drawn.

2. GENERAL PROPERTIES OF THE MOVEMENT-RELATED EEG

We deal with movement-related changes of the EEG in the spectral domain in our work. The following characteristic phenomena are observed in the short-time EEG spectrum around the time of a movement (see [20, 21]).

μ-rhythm event-related desynchronization (μERD) starts about 1 second prior to the movement onset (see Figures 1 and 4 with marked ERDs and interval II in Figure 2). μERD is usually localized to the C3/CP3 and C4/CP4 scalp areas [14, 20, 22] and it exhibits a contralateral preponderance; usually we see two foci over both sensorimotor cortices. μERD allows to differentiate not only the side of the body performing the movement but slow and fast movements as well [23]. The desynchronization accompanies even the mere motor imagery and it is present in most normal adults' EEG.

β-rhythm event-related desynchronization (βERD) has a diffuse character over the scalp central area, and it is more widespread than βERS [14, 24]. βERD is at least partially coupled to the μERD showing the desynchronization at the frequency of the second harmonic component of the μ-rhythm [25]. Although there might be some components related to the βERS in the β-band during the ERD, there is no known evidence that they somehow allow to distinguish between different types of movement.

β-rhythm event-related synchronization (βERS) is displayed by central β rhythms as a rebound in the form of a phasic synchronization [24] after the movement. βERS represents a postmovement rise of power in the β-band; the phenomenon is located about 1 second after the movement onset (see Figures 1 and 4 with marked ERSs, and Figure 2 for interval III). βERS is larger over the contralateral hemisphere [24] and it is focused slightly anteriorly of the largest μERD. It is known that βERS allows to distinguish various types of movements such as wrist/finger flexion movements [20], index finger extension/flexion movements [26], or distal/proximal movements [21]. The βERS differences between extension/flexion movements and distal/proximal movements were successfully used for movement classification [16, 17].

3. EEG RECORDING

The following paragraphs describe the EEG recording and postprocessing procedures and provide basic characteristics of experimental subjects.

3.1. Experimental subjects

Eight subjects took part in the experiment—7 men and 1 woman with average age of 24.5 years ($\sigma = 3.59$, see Table 1). None of them had a previous experience with such an experiment; all of them gave us an informed consent with the experiment and stated that they were healthy, without any known neurological problems, and were not under influence of any drug in the time of the experiment.

At first, we examined all the subjects on hand dominance. The [27] hand-dominance test consisting of three different tapping and drawing tasks was used. According to this test, four out of eight subjects were found to be right-handed, three as nonright-handed, and one as left-handed. The subjects with no significantly dominant hand were selected intentionally as the proposed system will work independently of the subject's handedness.

3.2. EEG recording setup

We used 41 unipolar scalp Ag/AgCl electrodes with 9 mm diameter placed symmetrically and equidistantly with 2.5 cm spacing [28] above both sensorimotor areas of the experimental subject (see Figure 3). Since the EEG changes in both time and space, the selection of appropriate EEG electrode representing movement is a crucial point for a successful classification of movements. As both movements are controlled primarily by the contralateral sensorimotor cortex, the most suitable electrodes are those overlying the contralateral sensorimotor hand area (electrode C3 and its surroundings) [14, 20]. The ground electrode was mounted on the nose, and impedances of all the electrodes were kept below 10 kΩ. The real exact positions of the scalp electrodes were measured with the help of the Isotrak II 3D scanner (manufactured by Polhemus, Colchester, Vermont, USA). In addition to the scalp electrodes, the following four bipolar channels were used: vertical and horizontal EOGs (electrodes placed horizontally and vertically along the subject's right eye), thumb EMG electrode placed on *thenar* recording the EMG of *musculus flexor pollicis brevis, m. opponens pollicis*, and *m. adductor pollicis*, and little-finger EMG electrode

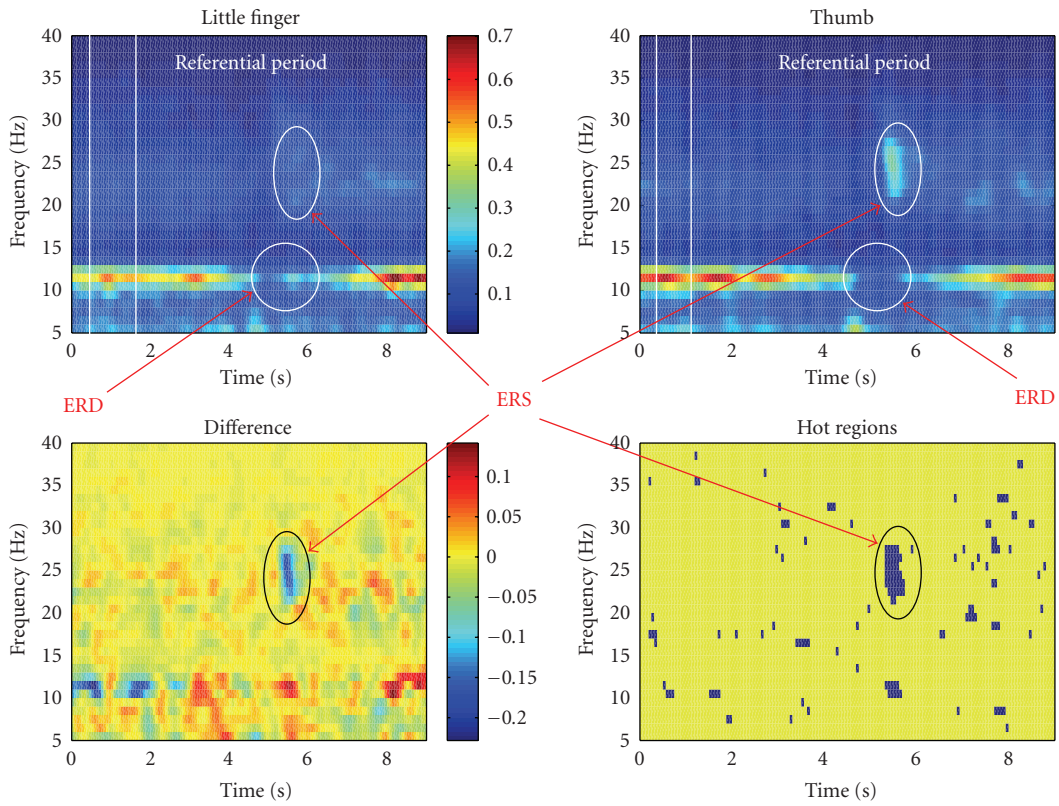

Figure 1: Example of the confidence intervals analysis (subject 1, electrode 4). The upper figures are the little-finger and thumb flexion PSD spectrograms. The time is biased to the movement onset—the movement was done in 0 second. Both figures share the same color scale. Lower left figure is the difference between both spectrograms. Some fluctuations can be seen at 11 Hz—μ-rhythm instabilities—and a difference in the βERS amplitudes is marked with a circle (positive difference = little-finger PSD which is at the given frequency and time instant larger than the thumb PSD). Finally, the lower right figure shows time-frequency combinations where the confidence intervals of both spectrograms are disjoint. Besides some random fluctuations, a clearly pronounced βERS region may be seen.

placed on *hypothenar* recording EMG of *m. flexor digiti minimi brevis* and *m. opponens digiti minimi*. The BrainScope EEG recording machine (manufactured by M&I, Prague, Czech Republic) was used for the EEG recording.

3.3. EEG recording procedure

The subject sat in a comfortable armchair in a silent and dim room with her/his right hand lying on the armrest in such a way so as she/he might freely perform the required thumb and little-finger movements. They were asked to keep their eyes closed and to avoid other movements than those asked for during the recording. Further, she/he was told to be as much relaxed as possible, but not to fall asleep. Before the recording was started, the subject was trained to perform the required movements properly.

The EEG was recorded in four blocks. The subject was performing the required self-paced voluntary movements during the first three blocks. The order and time between the movements were left at the subject's free will; no stimulation was used. This was to make the experimental procedure as much similar as possible to the real BCI usage. Two kinds of movements were performed during the recording—brisk flexions of the right thumb and the right little finger. Each of the three recording blocks contained about 30 movement; the blocks were separated by 10 minutes of rest.

During the fourth block, the resting EEG was recorded. We used this EEG as a referential one for false-movement detection rate estimation later on. The results of the experimental procedure were four blocks of about 15-minute-long EEG recordings per subject. The EEG was recorded with sampling rate of 256 Hz.

3.4. Data postprocessing

The first step was the temporal movement localization by means of visual inspection of EEG and EMG traces and by flagging the movement onsets. All the movements were found and tagged as either thumb or little finger. The resting period was tagged automatically by resting tag periodic insertion with 10-second period, with movement onset at the fifth second of the record.

Further we localized artifacts. Any movement or resting tag was changed into an artifact tag if any artifact was found in the 10-second-long epoch centred around the examined event. Also the EMG traces were checked and outliers were discarded.

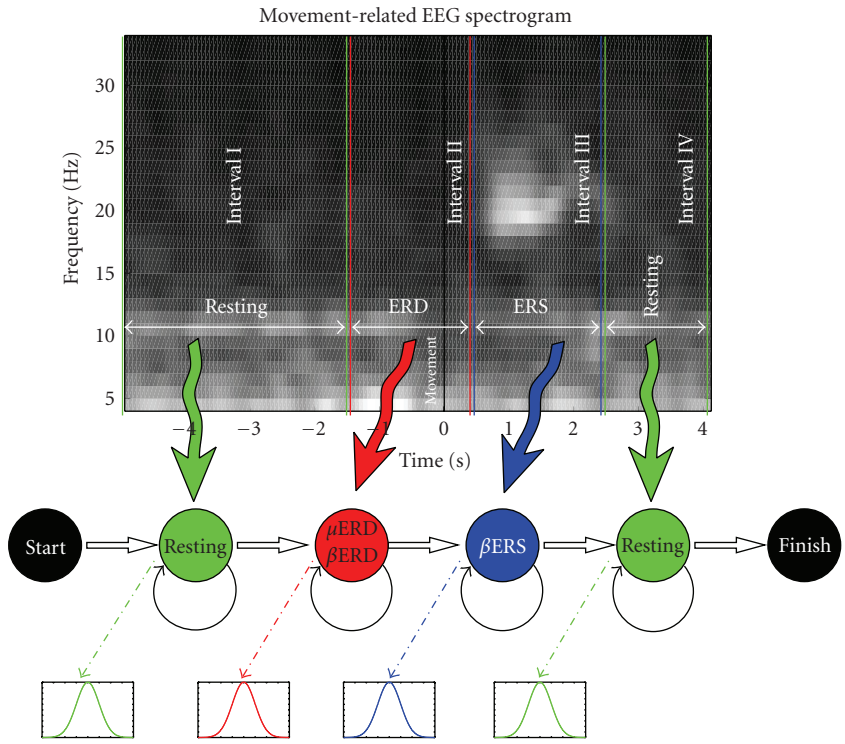

Figure 2: Used model architecture and its correspondence to the real EEG shape. The first and last emitting states model the resting period before and after the movement. The second emitting state holds the $\mu$and βERD characteristics, and the third one is related to the βERS.

Table 1: The list of the experimental subjects' characteristics. Positive dominance score means that the subject's right hand is more skilled than the lefthand. Right-handed subjects had the average score of 17.2, nonright-handed had 5.2, and left-handed had −10.

Subject number	Age (yrs)	Dominance score (–)	Dominant hand	Little-finger epochs	Thumb epochs	Resting epochs
1	26	24.18	Right	88	87	90
2	26	5.44	Nonright	55	60	56
3	25	7.92	Nonright	86	86	75
4	25	13.81	Right	94	89	95
5	30	−10.03	Left	66	85	93
6	25	2.29	Nonright	86	85	91
7	18	15.63	Right	83	70	105
8	21	15.92	Right	84	85	132

The last step of the postprocessing was the Laplacian filtration with the 8-neighboring-electrodes Laplacian filter [29, 30]. Prior to the Laplacian filtration, the sequential sampling nature of our EEG machine was compensated by quadratic interpolation to improve the Laplacian output signal-to-noise ratio [31].

Since we wanted to perform a single-trial offline analysis and classification, we divided the EEG into 10-second-long epochs centered at the movement, with resting tags having the movement onset in the fifth second of the movement epoch. The resulting numbers of epochs for each of the subjects are listed in Table 1.

4. VERIFICATION OF THE NEW EEG DATABASE

The next step was to check whether our EEG was valid. We checked whether the movement-related phenomena in the recorded EEG were in compliance with previously published works [20, 21, 26] dealing with similar databases.

A standard method was used to extract the ERD and ERS parameters [21, 26, 29]. First, the average spectrograms giving the time development of the EEG power spectral density (PSD) for each subject, electrode and type of movement were computed (frequency resolution of 1 Hz, time resolution of 200 milliseconds, with Blackman window used; see

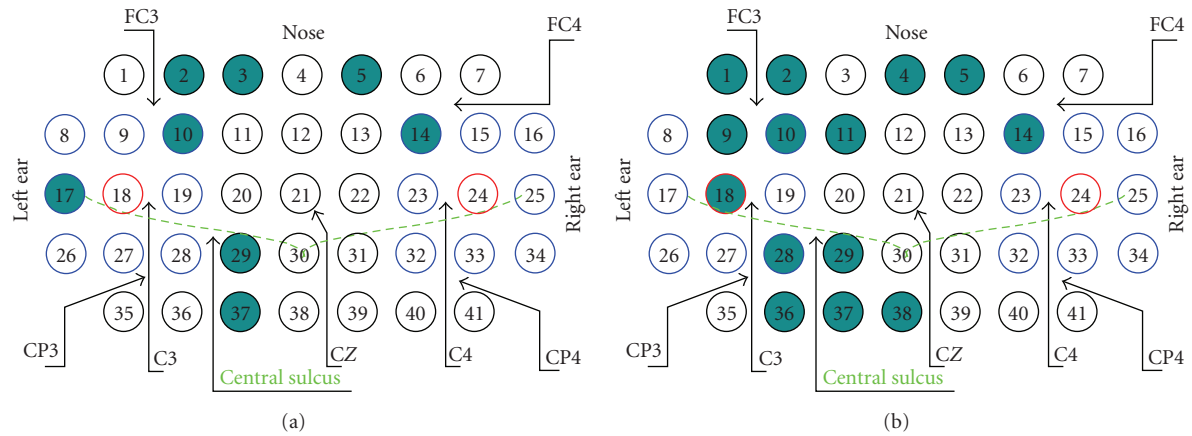

Figure 3: Localization of the electrodes allowing for the highest classification score and the real scalp electrode placement diagram. The 10–20 electrode positions C_3, C_4, and C_Z are denoted, and *central sulcus* is roughly localized. The electrode spacing is equidistant, 2.5 cm. Figures correspond to Table 5 (a) to the upper half: and (b) to the lower half; all the electrodes are shaded. Frontal locations (electrodes 1–16) correspond to the cases where the classifier distinguishes movement and resting EEG on the base of the βERS; classification on the parietal locations relies very likely more on the ERD. The best electrodes allowing to obtain the highest recognition score are placed contralaterally to the movement with the exception of electrode 5 (subject 8) and electrode 14 (subject 3 in Figure 3(a)) and electrodes 1 and 7 (in Figure 3(b)). All these subjects have a strong βERS present in the EEG and electrodes 5 and 14 are the anterior ones where the ERS is often present. The presence of the βERS thus allows the classifier to distinguish between resting and movement-related realizations here.

Table 2: The most reactive μERD spectral components' parameters for the single subjects, and contralateral and ipsilateral scalp sides.

		Contralateral hemisphere				
Subject number	Little-finger			Thumb		
	Electrode	frequency (Hz)	ERD (%)	Electrode	frequency (Hz)	ERD (%)
1	9	12	−87	9	13	−91
2	1	8	−95	1	8	−95
3	18	12	−87	18	12	−91
4	36	9	−79	30	9	−73
5	18	11	−88	18	12	−89
6	18	13	−93	18	13	−90
7	30	11	−72	30	10	−83
8	36	10	−62	36	10	−66
		Ipsilateral hemisphere				
Subject number	Little-finger			Thumb		
	Electrode	frequency (Hz)	ERD (%)	Electrode	frequency (Hz)	ERD (%)
1	24	11	−87	24	11	−91
2	7	8	−89	7	8	−93
3	24	12	−75	24	11	−84
4	33	10	−77	33	9	−72
5	24	11	−85	24	11	−88
6	24	12	−87	24	12	−88
7	24	11	−69	31	10	−75
8	32	11	−66	24	14	−69

Figure 1, e.g.). Averaging was done across all the realizations of the EEG belonging to one subject, movement, and electrode. Then the reference "resting" EEG power spectral density (PSD) (see Figure 1) was computed by averaging the PSDs belonging to time interval of 4.5−3.5 seconds before the movement onset. The average spectrograms were biased to this resting EEG giving a normalized course of the EEG PSD over time [29].

The most reactive frequencies for each of the subjects, electrodes, and type of movement were found in the μ- and β-bands—either the most attenuated one for ERD, or the most amplified one for ERS analysis. We performed

Table 3: The most reactive βERS spectral components' parameters for the single subjects and contralateral and ipsilateral scalp sides.

Contralateral hemisphere						
Subject number	Little-finger			Thumb		
	Electrode	frequency (Hz)	ERS (%)	Electrode	frequency (Hz)	ERS (%)
1	12	31	262	12	32	222
1	12	29	222	4	26	337
2	17	27	141	37	22	126
3	10	27	260	10	26	231
3	—	—	—	03	10	125
4	8	14	85	27	21	80
5	8	17	132	8	18	95
5	8	28	107	—	—	—
6	10	26	174	1	16	145
6	1	33	131	10	27	143
7	27	21	738	18	21	509
8	9	19	389	9	18	379
8	21	30	164	21	28	236
Ipsilateral hemisphere						
Subject number	Little-finger			Thumb		
	Electrode	frequency (Hz)	ERS (%)	Electrode	frequency (Hz)	ERS (%)
1	12	31	262	4	26	338
1	12	29	221	4	26	338
2	16	28	650	16	35	192
3	15	26	169	16	14	117
4	—	—	—	—	—	—
5	16	32	117	41	17	104
6	14	16	260	14	17	326
7	15	22	383	15	19	664
8	14	19	374	14	21	128
8	—	—	—	23	29	110

a separate analysis for contralateral as well as ipsilateral sides of the scalp.

μ-band ERD: the following average frequency and ERD attenuation on the contralateral scalp side were obtained (average value ± one sigma estimation): *for little-finger flexion,* $f_{\text{avg}} = 10.75 \pm 0.67$ Hz, $\text{ERD}_{\text{avg}} = -83.0 \pm 4.0\%$; *for thumb flexion,* $f_{\text{avg}} = 10.88 \pm 0.67$ Hz, $\text{ERD}_{\text{avg}} = -84.3 \pm 3.4\%$. There were no significant differences apparent either between the ERD central frequencies or between the average ERD amplitudes for both fingers. The averaged frequencies and amplitudes computed for the ipsilateral scalp side were as follows: for *little-finger flexion,* $f_{\text{avg}} = 10.75 \pm 0.65$ Hz, $\text{ERD}_{\text{avg}} = -79.4 \pm 3.2\%$; *for thumb flexion,* $f_{\text{avg}} = 10.75 \pm 0.65$ Hz, $\text{ERD}_{\text{avg}} = -82.5 \pm 3.2\%$. Again, no significant differences were obtained. In addition to these averaged values, we analyzed the average ERD time courses across all the subjects. No significant differences were found either. Detailed results per subject are listed in Table 2.

Our results were compared to previously published results of experiments with similar EEG databases.

(i) Work [20] compares the μERD properties of right-index finger, little-finger, and wrist movements. The authors analyzed only the EEG recorded on C3 and C4 positions compared to our coverage of the whole sensorimotor scalp area. No differences between the little-finger and index-finger ERDs were found, which is in compliance with our findings.

(ii) Works [22, 26] analyze μERD accompanying right-index finger brisk extensions and flexions. Although the authors chose different movements, we can at least compare the localization of the strongest ERD to our findings and see that we are in compliance with [26].

(iii) In compliance with other works (e.g., [22]), the contralateral μERD was found to be stronger than the ipsilateral one in 6 out of 8 subjects.

β-band ERS: the results of our βERS analysis—the most reactive ERS components over both hemispheres—are given in Table 3. For all of the subjects but 3 contralaterally and for subjects 3 and 8 ipsilaterally, two distinct reactive bands (upper and lower) were found. The ERSs of subjects 2 and 4 β were very weak. We computed the ensemble average parameters for contralateral hemisphere (*little-finger flexion:* $f_{\text{avg1}} = 22.8 \pm 1.8$ Hz, $\text{ERS}_{\text{avg1}} = 272 \pm 75\%$, $f_{\text{avg2}} = 18.0 \pm 4.5$ Hz, $\text{ERS}_{\text{avg2}} = 86 \pm 28\%$; *thumb flexion:* $f_{\text{avg1}} = 21.8 \pm 1.8$ Hz, $\text{ERS}_{\text{avg1}} = 223 \pm 53\%$, $f_{\text{avg2}} = 13.8 \pm 4.5$ Hz, $\text{ERS}_{\text{avg2}} = 104 \pm 45\%$) as well as ipsilateral hemisphere (*little-finger*

flexion: $f_{\text{avg}} = 22.9 \pm 2.7$ Hz, $\text{ERS}_{\text{avg}} = 156 \pm 38\%$; *thumb flexion:* $f_{\text{avg}} = 21.8 \pm 1.8$ Hz, $\text{ERS}_{\text{avg}} = 188 \pm 58\%$). It is obvious that there are no significant differences between either movement parameters. Further, in the grand average courses, no differences were found either.

Compared to other works the following can be concluded that

(i) work [20] did not find any significant difference between right-index finger and little-finger flexion βERSs (this is in compliance with our findings),

(ii) work [26] analyzes the βERS accompanying the right-index finger extension and flexion movement; the strongest ERS is localized 2.5 cm anteriorly and about 5–7.5 cm left from the Cz position; we found the strongest thumb and little-finger ERS locations roughly in the same area.

The results listed above clearly show that the database is usable for our experiments and contains reliable movement-related EEG. The analysis results of the most reactive EEG frequency components are in compliance with previously published works with similar EEG recordings. No systematic differences between the EEGs of both movements are apparent. Results summarized in Tables 2 and 3 show no common relation between the βERS and μERD of the thumb and little-finger flexions (e.g., ERS of the thumb is *not* always stronger than ERS of the little finger).

5. INDIVIDUAL EEG ANALYSIS

Our previous experiments with the EEG signal classification clearly showed that there are large differences in the EEG signals of different subjects. Although we usually observed the same phenomena in the EEG recordings of different subjects, the individual parameters were different. This observation led us to the conclusion that the standard approach to the movement-related EEG patterns analysis via grand averaging the ERS and ERD over all subjects would not be suitable for finding subtle differences between both movement-related types of the EEG. The grand averaging wipes out any individual EEG differences between both movements which are not systematic (i.e., the same trend occurred across all the subjects). That is why we did a deep statistical analysis of individual EEG patterns to find any statistically significant phenomena in the EEG allowing us to recognize the finger which performed the movement.

5.1. Method

For each of the subjects (subject $s = 1,\ldots,8$), electrodes (electrode $e = 1,\ldots,41$), types of the EEG (type m = *littel finger, thumb*), and realizations (realization $r = 1,\ldots,R(s,m)$; $R(s,m)$ is the number of realizations available for the given subject s and type of the EEG m), a spectrogram $\mathcal{S}_{s,e,m,r}[f,t]$ was computed. The frequency resolution was 1 Hz ($f = 0,\ldots,128$; frequency in Hz) and time resolution was 0.125 second ($t = 0,\ldots,72$; time in 1-second segments with 0.875-second overlap [16]). The spectrograms described the time development of the short-time EEG power spectra. Next, we computed the average spectrogram $\hat{\mathcal{S}}_{s,e,m}$ for the given subject s, electrode e, and type of the EEG m by averaging $\mathcal{S}_{s,e,m,r}$ across all available realizations $r = 1,\ldots,R(s,m)$ (see Figure 2). $\hat{\mathcal{S}}_{s,e,m}[f,t]$ describes the time development of the short-time EEG power spectral density (PSD). No referencing to the resting EEG referential period was applied here because we wanted to analyze exactly the same spectra as those which would be used for the classification later on.

As the PSD is χ^2-distributed [32] with degrees of freedom equal to two times the number of realizations ($2R(s,e,m)$), we can simply find the 95% confidence-level interval as

$$\frac{2R(s,e,m)\hat{\mathcal{S}}_{s,e,m}}{\chi^2_{2R(s,e,m),0.025}} \leq \hat{\mathcal{S}}_{s,e,m} \leq \frac{2R(s,e,m)\hat{\mathcal{S}}_{s,e,m}}{\chi^2_{2R(s,e,m),0.975}}. \quad (1)$$

We computed these confidence intervals for all the spectrograms and found out where there were disjoint for both types of movements. These areas were marked as "hot," and thus we devoted our attention to them (see Figure 1).

As the processed spectrograms were non-Gaussian and since we needed to analyze the single frequency bins of the spectrum, we applied Kruskal-Wallis nonparametric test (KWT) of equal population means to the computed spectrograms in the "hot" areas instead of the commonly used ANOVA which requires Gaussianity.

The KWT was applied to the precomputed PSD spectrograms giving us the confidence that the average PSD values really differed between subjects. The confidence was thresholded at the 95% confidence level, and regions in which the average values differed were found. Then we passed through all the subjects across all the electrodes by hand looking for these regions, and we tried to summarize and systematize this rather large amount of data. The results of this analysis are the subjects of the following paragraphs.

The results discussed below need not necessarily be in accordance with the results listed in Tables 2 and 3 which were achieved by an approach commonly used by neurologists relying on searching for the most reactive ERD and ERS components and comparing them. Instead, here we tried to locate as many statistically significant individual differences between both movements as possible.

5.2. β-band ERS

The β-rhythm ERS analysis gave us the most valuable results. Our conclusions for the given experimental subjects are summarized in Table 4; it may be clearly seen that we did not obtain any systematical differences between the PSDs of both movements' EEGs. For subjects 1, 3, and 6, the ERS of the thumb flexion was stronger; for subjects 5 and 8, the little-finger flexion ERS was more pronounced; subject 7 showed both cases depending on the scalp location, and no significant differences were found for subjects 2 and 4. Note that the electrodes at which the ERSs are stronger for the thumb flexion are located more anteriorly compared to the electrodes with stronger little-finger ERSs (except subject 5, electrode 1). This is in compliance with the more lateral and anterior representation of the thumb compared to the more medial

Table 4: Statistically significant βERS spectral components for the single subjects, summary of the analysis. The location column gives the location of the found components in terms of our electrode numbers, see Figure 3.

Subject number	Movement with stronger βERS	Parameters (time, frequency)	Location (electrode)
1	Thumb	0.5–1 sec, 26-27 Hz	**2**, 3, **4**, **5**, 9, 10, **18**, 19, 24
2		No significant differences	
3	Thumb	0.375–0.875 s, 25–29 Hz	**14**
4		No significant differences	
5	Little	1.250–1.625 s, 16–20 Hz	1, **29**, 31
6	Thumb	0.25–1.125 s, 20–27 Hz	6, 23
7	Thumb	1–1.5 s, 17–23 Hz	5, **7**, **15**, **16**, 24
	Little	1–1.5 s, 17–23 Hz	36, 37, 38, 39
8	Little	1.5–2.0 s, 20–24 Hz	15

localization of the little finger in the M1 and S1 areas [19]. Interestingly, this trend did not appear in the most reactive ERS analysis (see Table 3), where the strongest ERS courses for both fingers were often found at the same electrode.

In the later classification experiments, we reached a significant level of the movement-resting EEG discrimination on some of the electrodes mentioned in Table 4 (marked with boldface). This fact implies that there must be strong statistically significant differences between the resting EEGs and movement-related EEG realizations as well. Our examination here shows statistically significant differences between both movements. All these findings imply that it should be possible to discriminate the movements after some suitable EEG postprocessing.

Some more differences were found in addition to these listed above, but they marked only changes in duration or bandwidth of the ERS between both movements. We did not list them here because they are outside the scope of this paper.

5.3. μ-band ERD

Although the μERD parameters are believed not to be dependent on the type of the movements [20], we analyzed the μERD behavior with the test mentioned above. We discovered the following phenomena:

(i) for subject 4, the little-finger μERD around the movement onset was found to be stronger than the thumb μERD at some of the locations (electrodes 20, 21, 25, 27, 29),

(ii) finally we found some differences in the length of μERD of both movements.

5.4. β-band ERD

We also briefly examined ERD in β-band in order not to neglect anything which might be helpful or interesting. We found significant differences in the βERDs with one subject—subject no. 1, electrodes 9, 10, and 26, where the thumb-related βERD was significantly stronger than the little-finger flexion-related one. The frequency of the most reactive βERD component was 25–26 Hz. The βERD was observed in the same band as the βERS. The βERD frequency band did not contain the frequency of the μERD second harmonic component, and thus it was not related to the ongoing μERD.

6. CLASSIFICATION

The next step was to test the possibility of a single-trial offline classification. The following paragraphs describe the classification paradigm, parameterization, and results.

We intentionally always used only one electrode for the EEG classification. Our target was to squeeze as much information as possible from only one signal source, without utilizing any information stored in differences between signals from different electrodes.

6.1. Classifier

The used classification system is based on Hidden Markov models (HMM) [16, 33]. The HMMs —although nearly not used for EEG classification—have several advantages:

utilization of the context information: the system uses the temporary context of the EEG to improve the classification score,

physiological compatibility: the selected model architecture matches the underlying physiological process, it is even possible to segment the EEG with the help of the HMM classifier [16, 34],

ease of the interpretation: it is quite simple to interpret the contents of the trained model. This is a big advantage compared to, for example, some kinds of neural networks, where the implementation of the trained system is not so straightforward,

ability to model the EEG: we are able to generate synthetic realizations of the EEG for testing of various algorithms.

The used models have the left-to-right, no skips architecture which captures the sequence of the movement-related EEG phases (see Figure 2) with 4 emitting states modelling the four significant phases of movement-related EEG [16, 21] (resting EEG, desynchronization, post-movement synchronization, resting EEG) generating p-dimensional Gaussian random processes (p is equal to the number of used EEG

Table 5: EEG-based movement classification, the best results from the overall classification score and minimalization of false positive movement detection points of view. The meanings of the table fields are as follows: *Subj. no.* = number of the subject, *Scalp loc.* = scalp position which gave the best classification score, *Fingers correct* = weighed classification score for both fingers, correct classification, *Fingers wrg.* = weighed classification score for both fingers, thumb classified as little finger and vice versa, *Fingers ign.* = percentage of finger movements classified as resting EEG—ignored movements, *Fingers false* = false positive detection, percentage of resting EEG realizations classified as movement, *Resting* = classification score of resting EEG, *Total* = overall classification score, weighed average of the single scores, *Parameters* = parameterization used to get the best results.

Results sorted according to overall classification score								
Subj. no.	Scalp loc.	Fingers corr. [%]	Fingers wrg. [%]	Fingers ign. [%]	Fingers false [%]	Resting [%]	Total [%]	Parameters used
1	2	56.1	42.3	1.6	11.4	88.6	67.3	FFT+Δ
2	3	57.8	41.2	1.1	8.5	91.5	68.8	FFT
3	14	51.4	44.4	4.1	1.3	98.7	65.7	AR
4	37	52.9	42.7	4.4	0.0	100.0	68.8	AR
5	29	51.6	48.4	0.0	0.0	100.0	70.0	AR
6	10	53.8	42.8	3.4	28.3	71.7	60.0	FFT+Δ
7	17	57.7	39.4	2.9	1.9	98.1	74.2	AR
8	5	48.8	51.0	0.1	0.4	99.6	70.9	AR
Results sorted according to false positive detections								
Subj. no.	Scalp loc.	Fingers corr. [%]	Fingers wrg. [%]	Fingers ign. [%]	Fingers false [%]	Resting [%]	Total [%]	Parameters used
1	14	35.1	40.2	24.7	0.8	99.2	57.1	AR+Δ
2	1	49.4	46.1	4.5	0.0	100.0	65.8	AR+Δ
3	1	23.4	24.6	52.0	0.3	99.7	46.4	FFT
4	37	52.9	42.7	4.4	0.0	100.0	68.8	AR
5	29	51.6	48.4	0.0	0.0	100.0	70.0	AR
6	1	28.3	34.2	37.5	4.9	94.1	51.2	FFT+Δ
7	18	53.8	45.7	0.5	0.0	100.0	72.7	AR
8	5	48.8	51.0	0.1	0.4	99.6	70.9	AR

features, per the Parameterization paragraph below) with diagonal covariance matrices. The used classification system was the same as in our other EEG BCI works [16, 34, 35] built around the Hidden Markov Toolkit [36]. The classification experiment consisted of the following steps performed for all the subjects, electrodes, and types of parameterization:

(1) EEG was parameterized with a selected algorithm,
(2) the randomization procedure was applied to mitigate the effect of the small training and testing set (only $\approx$ 100 realizations per movement, person, and electrode). Each classification experiment was run for 16 times with different (and random) division of EEG realizations between the disjunctive training (75% of realizations) and testing (25% of realizations) sets. The number of runs was selected to get 99% probability that any of the realizations is used for testing. This helps us to get reliable results independent on the concrete selected training and testing EEG realizations [34],
(3) models were trained (initialization followed by Baum-Welch reestimation) on the training set,
(4) classification accuracy was tested,
(5) the average classification scores were computed for all the EEG types across the 16 performed experiments.

6.2. EEG parameterization

Our previous results [15] showed that the best results are reachable either with a pure FFT linear spectrum or with AR model coefficients combined with Δ parameters. The Δ parameters (although not used with EEG signal processing) are able to improve the classification score significantly [15]. This is a result of emphasizing the movement-related spectral changes which allows the classifier to better capture the underlying signal statistics. In all cases, we extracted the features from a sliding window of 1 sec length; step of the window was chosen as 200 ms [16]. We utilized the following parameterizations:

linear spectrum: FFT amplitude spectrum covering 5–40 Hz band with spectral resolution of 1 Hz. The k-th feature vector consisted of 36 parameters $F_k = (f_k[1], \ldots, f_k[36])$ where k is the time index,

linear spectrum + Δ coefficients: additional 36 $\Delta f_k[i]$ coefficients were added to the already computed linear spectrum. The following polynomial approximation of the first derivative common in speech processing was used [36]

$$\Delta f_k[i] = \frac{\sum_{l=1}^{3} l\left(f_{k+l}[i] - f_{k-l}[i]\right)}{2\sum_{l=1}^{3} l^2}, \tag{2}$$

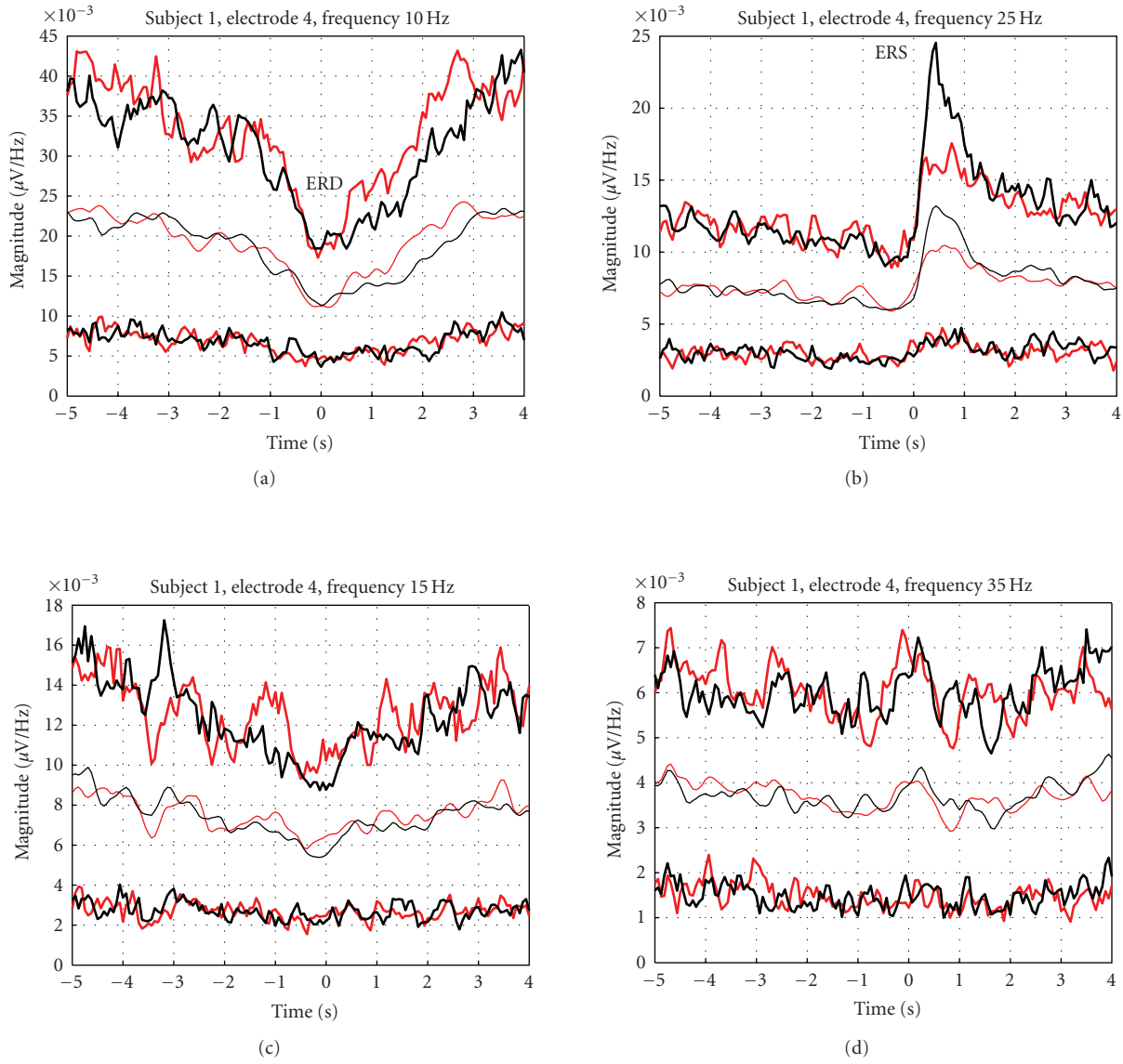

FIGURE 4: Confidence intervals computed for the selected frequency components (subject 1, electrode 4); see also Figure 1. Black:thumb flexion; red:little-finger flexion; thin lines:average courses of the indicated spectral components; thick lines:boundaries containing 75 % of the real EEG realizations.

AR coefficients: 8th order AR model coefficients [15] were used; the feature vector had 8 coefficients here. The EEG was decimated by factor 2 before the coefficients were computed to cover the important low-frequency part of the spectrum better,

AR coefficients + Δ coefficients: 8 first-order derivative approximations (2) were computed and the feature vector was extended to 16 values.

6.3. Results

The complete classification was run with all these parameters covering all the scalp electrodes. The results were sorted according to two criteria:

(1) overall classification score computed as a weighed average of the little finger, thumb and resting EEG classification scores. This number tells us how good it is possible to discriminate the single types of EEG at the given electrode and for the given subject,

(2) false movement rate detection which is a probability measure of a movement detection when the subject is actually resting.

The best results selected according to these criteria for each of the subjects are listed in Table 5. It may be seen that it is possible to distinguish between movement-related and resting EEG and to find an electrode and parameterization which minimizes the possibility of false movement detection for any of the subjects. On the other hand, the classifier

was not able to distinguish between the thumb and little finger EEG. Some of the movements are always ignored (less than 10%) recognizing them as resting EEG; however, the thumb—little finger discrimination—failed. Figure 3 with the localization of the electrodes summarizes the best performances from the classification score point of view.

Subsequent analysis of the recognized movements showed that—although the mean values of the movement-related EEG spectra are significantly statistically different—the real time courses of the movement-related EEG are heavily buried in the non-movement related activity, see Figure 4.

7. CONCLUSIONS, NEXT STEPS

In this work, a detailed finger movement-related EEG statistical analysis and result of classification experiment were presented.

The movement-related EEG was analyzed in an individual way searching for as statistically significant phenomena as possible instead of the commonly used analysis of the strongest EEG component. This approach is in contrast with the method used by [20, 21, 26] and others, where the strongest ERDs and ERSs are found first and their statistical significance is checked afterwards.

We found statistically significant differences between both types of movement-related EEG signals. The differences in the β and μERD parameters were present, although not very important. More interestingly, we discovered significant differences in the βERS courses, their characters being highly individually dependent. These results are promising from the classification point of view. No such results of finger movement-related EEG analysis have been published yet. In addition to this, our analysis covered the whole EEG frequency band (5–30 Hz) and both sensorimotor areas extending the results of [20], where only EEG recorded from C3/C4 positions and only signal powers in 10–12 Hz, 16–20 Hz and 20–24 Hz bands were examined.

Our classification paradigm was only partially successful—we were able to distinguish the movement-related and resting EEG, but the movements were not distinguished from each other. This was attributed to the fact that the movement-related spectral EEG courses are masked by other on-going EEG activities not related to the movement. Thanks to the individual analysis results we believe it will be able to separate and successfully classify both movements with the help of an advanced denoising approach.

In our recent work [37] we showed that it is possible to separate movement-related EEG sources and non-movement related EEG activity with the help of the independent component analysis (ICA). Now we have been working on the integration of an ICA-based denoising procedure into our classification system. This approach should help us to increase the classification score by means of EEG separation into meaningful sources.

Next step will be to combine the developed method with the left/right limb movement recognition to double the number of recognized states—to increase the brain-computer channel data rate.

ACKNOWLEDGMENTS

The authors thank Professor Andrej Stančák for his invaluable comments and help. Further, they would like to thank Jiří Vrána and Josef Mlynář for their help with data recording. In addition, grateful thanks go to all the experimental subjects. This work has been supported by the research program Transdisciplinary Research in Biomedical Engineering II no. MSM6840770012 of the Czech Technical University in Prague.

REFERENCES

[1] L. Pickup, "Machine learning approaches for brain-computer interfacing," Tech. Rep. PARG-02-01, Pattern Analysis and Machine Leraning Group, Robotics Research Group, Department of engineering science, University of Oxford, Oxford, UK, May 2002.

[2] B. Blankertz, G. Dornhege, M. Krauledat, et al., "The Berlin brain-computer interface: EEG-based communication without subject training," *IEEE Transactions on Neural Systems and Rehabilitation Engineering*, vol. 14, no. 2, pp. 147–152, 2006.

[3] W. D. Penny and S. J. Roberts, "Experiments with an EEG-based computer interface," Tech. Rep., Department of Electrical Engineering, Imperial College, London, UK, July 1999.

[4] W. D. Penny, S. J. Roberts, and M. J. Stokes, "EEG-based communication: a pattern recognition approach," in *Brain-Computer Interface Technology: Theory and Practice. First International Meeting*, Rensselaerville, NY, USA, May 1999.

[5] A. Schlögl, K. Lugger, and G. Pfurtscheller, "Using adaptive autoregressive parameters for a brain-computer interface equipment," in *Proceedings of the 19th International Conference of the IEEE Engineering in Medicine and Biology Society (EMBS '97)*, pp. 1533–1535, Chicago, Ill, USA, October-Novermber 1997.

[6] C. W. Anderson, E. A. Stolz, and S. Shasunder, "Discriminating mental tasks using EEG represented by AR model," in *Proceedings of IEEE 17th Annual Conference on Engineering in Medicine and Biology Society (IEMBS '95)*, vol. 2, pp. 875–876, Montreal, Quebec, Canada, September 1995.

[7] C. W. Anderson and Z. Sijerčíc, "Classification of EEG signals from four subjects during five mental tasks," in *Solving Engineering Problems with Neural Networks: Proceedings of the Conference on Engineering Applications in Neural Networks (EANN '96)*, pp. 407–414, Turku, Finland, June 1996.

[8] J. R. Wolpaw, N. Birbaumer, D. J. McFarland, G. Pfurtscheller, and T. M. Vaughan, "Brain-computer interfaces for communication and control," *Clinical Neurophysiology*, vol. 113, no. 6, pp. 767–791, 2002.

[9] J. R. Wolpaw, D. J. McFarland, and T. M. Vaughan, "Brain-computer interface research at the Wadsworth Center," *IEEE Transactions on Rehabilitation Engineering*, vol. 8, no. 2, pp. 222–226, 2000.

[10] J. D. Bayllis and D. H. Ballard, "Recognizing evoked potentials in a virtual environment," in *Advances in Neural Information Processing Systems 12*, vol. 12, pp. 3–9, Denver, Colo, USA, November-December 2000.

[11] G. Schalk, J. R. Wolpaw, D. J. McFarland, and G. Pfurtscheller, "EEG-based communication:presence of an error potential," *Clinical Neurophysiology*, vol. 111, no. 12, pp. 2138–2144, 2000.

[12] U. Hoffman, J.-M Versin, K. Deserens, and T. Ebrahimi, "An efficient P300-based brain computer interface for disabled subjects," preprint, 2007, http://bci.epfl.ch/efficientp300bci.html.

[13] W. D. Penny, S. J. Roberts, and M. J. Stokes, "Imagined hand movements identified from the EEG μ-rhythm," Tech. Rep., Department of Electrical Engineering, Imperial College, London, UK, August 1998.

[14] D. J. McFarland, L. A. Miner, T. M. Vaughan, and J. R. Wolpaw, "μ and β rhythm topographies during motor imagery and actual movements," *Brain Topography*, vol. 12, no. 3, pp. 177–186, 2000.

[15] J. Šťastný, J. Zejbrdlich, and P. Sovka, "Optimal parameterization selection for the brain-computer interface," in *Proceedings of the 4th WSEAS International Conference of Applications of Electrical Engineering* , pp. 300–304, Prague, Czech Republic, March 2005.

[16] J. Šťastný, P. Sovka, and A. Stančák, "EEG signal classification," in *Proceedings of the 23rd Annual International Conference of the IEEE Engineering in Medicine and Biology Society*, vol. 2, pp. 2020–2023, Istanbul, Turkey, October 2001.

[17] J. Doležal, J. Šťastný, and P. Sovka, "Recognition of direction of finger movement from EEG signal using markov models," in *Proceedings of the 3rd European Medical&Biological Engineering Conference (EMBEC '05)*, vol. 11, pp. 1492-1–1492-6, Prague, Czech Republic, November 2005.

[18] H. Ramoser, J. Müller-Gerking, and G. Pfurtscheller, "Optimal spatial filtering of single trial EEG during imagined hand movement," *IEEE Transactions on Rehabilitation Engineering*, vol. 8, no. 4, pp. 441–446, 2000.

[19] P. Hluštík, A. Solodkin, R. P. Gullapalli, D. C. Noll, and S. L. Small, "Somatotopy in human primary motor and somatosensory hand representations revisited," *Cerebral Cortex*, vol. 11, no. 4, pp. 312–321, 2001.

[20] G. Pfurtscheller, K. Zalaudek, and C. Neuper, "Event-related beta synchronization after wrist, finger and thumb movement," *Electroencephalography and Clinical Neurophysiology - Electromyography and Motor Control*, vol. 109, no. 2, pp. 154–160, 1998.

[21] A. Stančák, B. Feige, C. H. Lücking, and R. Kristeva-Feige, "Oscillatory cortical activity and movement-related potentials in proximal and distal movements," *Clinical Neurophysiology*, vol. 111, no. 4, pp. 636–650, 2000.

[22] A. Stančák and G. Pfurtscheller, "The effects of handedness and type of movement on the contralateral preponderance of μ-rhythm desynchronisation," *Electroencephalography and Clinical Neurophysiology*, vol. 99, no. 2, pp. 174–182, 1996.

[23] A. Stančák, A. Riml, and G. Pfurtscheller, "The effects of external load on movement-related changes of the senorimotor EEG rhythms," *Electroencephalography and Clinical Neurophysiology*, vol. 102, no. 6, pp. 495–504, 1997.

[24] G. Pfurtscheller, A. Stančák, and C. Neuper, "Post-movement beta synchronization: a correlate of an idling motor area?" *Electroencephalography and Clinical Neurophysiology*, vol. 98, no. 4, pp. 281–293, 1996.

[25] G. Pfurtscheller, A. Stančák, and G. Edlinger, "On the existence of different types of central β rhythms below 30 Hz," *Electroencephalography and Clinical Neurophysiology*, vol. 102, no. 4, pp. 316–325, 1997.

[26] A. Stančák, "Event-related desynchronization of the μ-rhythm in extension and flexion finger movements," in *11th International Congress of Electromyography and Clinical Neurophysiology*, Supplements to Clinical Neurophysiology, 53, pp. 636–650, Prague, Czech Republic, September 2000.

[27] H. J. Steingrüber and G. A. Lieuert, *Hand-Dominanztest*, Hogrefe, 2nd edition, 1976.

[28] R. Srinivasan, "Methods to improve the spatial resolution of EEG," *International Journal of Bioelectromagnetism*, vol. 1, no. 1, pp. 102–111, 1999.

[29] G. Pfurtscheller, *Digital Biosignal Processing*, chapter 17, Elsevier Science, Amsterdam, The Netherlands, 2nd edition, 1991.

[30] B. Hjorth, "An on-line transformation of EEG scalp potentials into orhtogonal source derivations," *Electroencephalography and Clinical Neurophysiology*, vol. 39, no. 5, pp. 526–530, 1975.

[31] J. Šťastný and P. Sovka, "The 3D surface Laplacian filtration with integrated sampling error compensation," *Signal Processing*, vol. 87, no. 1, pp. 51–60, 2007.

[32] J. Uhlíř and P. Sovka, *Digital Signal Processing*, Czech Technical University, Prague, Czech Republic, 2nd edition, 2002.

[33] L. R. Rabiner, "A tutorial on hidden markov models and selected applications in speech recognition," *Proceedings of the IEEE*, vol. 77, no. 2, pp. 257–286, 1989.

[34] J. Šťastný, P. Sovka, and A. Stančák, "EEG signal classification: introduction to the problem," *Radioengineering*, vol. 12, no. 3, pp. 51–55, 2003.

[35] J. Šťastný, P. Sovka, and A. Stančák, "EEG signal classification and segmentation by means of hidden markov models," in *Proceedings of 16th Biennial International EURASIP Conference on Analysis of Biomedical Signals and Images (BIOSIGNAL '02)*, pp. 415–417, Brno, Czech Republic, June 2002.

[36] S. J. Young, *HTK Reference Manual*, Cambridge University Engineering Department, Cambridge, UK, 1993.

[37] O. Konopka, J. Šťastný, and P. Sovka, "Movement-related EEG separation using independent component analysis," in *Proceedings of the 3rd European Medical & Biological Engineering Conference (EMBEC '05)* , vol. 11, pp. 1471-1–1471-6, Prague, Czech Republic, Novermber 2006.